Advancing High-Throughput Experimentation for Reaction Discovery and Development

by

Andrew Outlaw

A dissertation submitted in partial fulfillment
of the requirements for the degree of
Doctor of Philosophy
(Medicinal Chemistry)
in the University of Michigan
2025

Doctoral Committee:

Associate Professor Timothy A. Cernak, Chair
Professor Pavel Nagorny
Associate Professor Alison R.H. Narayan
Associate Professor Jonathan Z. Sexton

Andrew D. Outlaw

anoutlaw@umich.edu

ORCID iD: 0009-0007-0087-3791

© Andrew D. Outlaw 2025

Dedication

This dissertation is dedicated to my friends, family, and all who have supported me on this journey. It wouldn't have been possible without you.

Acknowledgements

Most importantly, I would like to thank my advisor, Dr. Tim Cernak for all of his hard work and assistance in making these projects a reality. I have learned a tremendous amount and had so many opportunities to work with such amazing scientists thanks to him. I have gained so much valuable experience as a scientist and as a person. It's hard to think of myself as the same person that I was before my time in his lab. All of my connections, progress, and achievements made at U of M wouldn't have been possible without his encouragement and support.

I would also like to make special mention of all the amazing coworkers I have had the chance to interact with over the last several years. They have each taught me something and made my stay in Tim's lab all the better. I especially thank Doctors Andrew McGrath, Bo Mahjour, Chris Audu, Haiyan Huang, Di Wang, Ruheng Zhao, Santanu Singha, Sandip Das, (soon-to-be) Dr. Yu-Ting Kao, as well as Nikolaos Tripolitsiotis and Carl Mauro.

I would like to extend my gratitude to my committee members Dr. Pavel Nagorny, Dr. Jonny Sexton, and Dr. Alison Narayan who have provided very helpful feedback on these projects and have been very understanding with rescheduling meeting dates.

As well, Dr. Allen Schoffstall helped inspire me to pursue my chemistry education, from my first organic chemistry class all the way to applying for graduate school. He has helped me figure out what I want to do in life while also just being an amazing person to talk to.

I am incredibly grateful to my mother who always puts in 110% effort into everything and worked hard to raise my brother, sister, and I. Even when I am on the other side of the country, she makes sure I know she supports me.

Finally, to my partner Chun-Yi Tsai who has given me tremendous support in these last few months of job hunting and finishing my PhD studies. I am incredibly grateful and hope I can repay you someday soon when it is your time to defend. I look forward to our future together.

Table of Contents

Dedication ii

Acknowledgements iii

List of Tables vii

List of Figures ix

List of Spectra xvi

Abstract xxii

Chapter 1 Accelerating Synthesis with High-Throughput Experimentation 1

1.1 Introduction to High-Throughput Experimentation (HTE) and Automation 1

1.2 Hardware Implementation in HTE 3

1.2.1 Automation 4

1.3 Software Implementation in HTE 6

1.3.1 Design of Experiments (DoE) and Reaction Array Planning 6

1.3.2 Data Processing and Visualization 8

1.4 High-Throughput Analytical Methods 9

1.4.1 Chromatographic and Spectrometric Methods 9

1.4.2 Colorimetric and Fluorometric Methods 12

1.5 Limitations of Modern HTE 15

1.6 References 16

Chapter 2 Development of Late-Stage Saturation (LSS) 27

2.1 Introduction to Arene Saturation 27

2.2 Late-Stage Saturation (LSS) 28

2.2.1 Chemoinformatic Analysis of Saturated Druglike Space 30
2.3 Optimization of the LSS Reaction 31
2.3.1 Screening of Metals, Reductants, and Solvents 31
2.3.2 Substrate Scope Evaluation 31
2.3.3 Optimization of Miniaturized LSS 34
2.3.4 Nanoscale Substrate Scope Study in 1,536-Well Plate Format 35
2.3.5 Direct-to-Microsomal Stability Assay Comparison of Saturated Drugs 37
2.4 Conclusions and Future Work 38
2.5 Experimental Section for the LSS Reaction 39
2.5.1 General Methods 39
2.5.2 Procedures for the LSS Reaction 41
2.5.3 Procedure for LSS in 1,536-Well Plate Format 71
Microtiter Plate Sealing Studies 74
2.5.4 Procedure for Microsomal Stability Assay 152
2.5.5 Measurement of $LogP_{o/w}$ 157
2.6 Spectra 160
2.7 References 222
Chapter 3 FRET for Reaction Development 228
3.1 Introduction 228
3.2 Reaction Deconvolution with FRET 228
3.3 Development of FRET Pairs 229
3.3.1 Perylene–BODIPY (sp^2-sp^3) Amine-Acid Pair 230
3.3.2 Perylene-BODIPY (sp^3-sp^3) Amine-Acid Pair 231
3.3.3 Effects of Linker Length 233
3.4 Comparison of UPLC–MS and FRET Analysis Platforms 234

3.5 Conclusions and Future Work 237
3.6 Experimental Section for the FRET Platform 240
3.6.1 General Methods 240
3.6.2 Procedures for Synthesis of FRET Dyes 241
3.6.3 Photophysical Studies on Perylene and BODIPY Dyes 250
3.6.4 Procedure for Nanoscale Amine-Acid Screen 261
3.6.5 Procedure for Nanoscale Pyridinium Salt-Acid Screen 266
3.7 Spectra 275
3.8 References 299
Chapter 4 Development of Diverse Amine-Acid Couplings 302
4.1 Introduction to Amine-Acid Couplings 302
4.2 Enabling the Functionalization of Amines 302
4.2.1 α-Functionalization and Rearrangement of Pyridinium Salts 303
4.3 Applying Diverse Amine-Acid Couplings to Fluorescein 305
4.4 Conclusions and Future Work 310
4.5 Experimental Section for Amine-Acid Couplings 310
4.5.1 General Methods 310
4.5.2 Procedures for the Synthesis and Reaction of Pyridinium Salts 312
4.5.3 Procedures for Fluorescein Couplings 313
4.5.4 HTE Screening for Fluorescein Alkyl Amine 315
4.5.5 HTE Screening for Fluorescein Benzoxazole 318
4.6 Spectra 321
4.7 References 328

List of Tables

Table 2-1 Recipe for 96-well comparison screen of arene reduction conditions 68

Table 2-2 The effect of DMSO and water as an additive on reactions using aminacrine **7**. NMR yields represent the overall yield of mono- and di-reduced products **20** and **21**. 70

Table 2-3 SMILES strings and yields for all substrates used in 1,536-well LSS screen across both 3.5 equivalents and 7.0 equivalents of reductant 151

Table 2-4 Recipe for 24-Well LSS Screen for Microsomal Stability Studies 154

Table 2-5 Comparison of %remaining of parent arene compounds after 60 minutes of exposure to human liver microsomes. Determined by LC-MS integration of parent compound relative to caffeine internal standard. 156

Table 2-6 RP-HPLC separation conditions of compounds 158

Table 2-7 Standard equation and linearity of compounds (n = 7) 159

Table 3-1 Concentrations of reagent stock solutions prepared for the 96-well fluorescence poisoning experiment and the volumes they are dosed into the appropriate reaction wells. 256

Table 3-2 Concentrations of reagent stock solutions prepared for 1,536-well plate amide coupling experiment and the volumes they are dosed into the appropriate reaction wells. Each stock solution is made in triplicate at the same concentration and dosed at the same volume, only differing by solvent (one in DMF, DMSO, and diglyme). 263

Table 3-3 List of reagents that are dosed to all five 1,536 plates in the same locations per plate. 268

Table 3-4 Metals used in the first of five 1,536 well reaction plates in the pyridinium salt-acid screening campaign. 269

Table 3-5 Metals used in the second of five 1,536 well reaction plates in the pyridinium salt-acid screening campaign. 269

Table 3-6 Metals used in the third of five 1,536 well reaction plates in the pyridinium salt-acid screening campaign. 270

Table 3-7 Metals used in the fourth of five 1,536 well reaction plates in the pyridinium salt-acid screening campaign. 271

Table 3-8 Metals used in the fifth of five 1,536 well reaction plates in the pyridinium salt-acid screening campaign. 272

Table 4-1 Reagents used in Fluorescein Alkyl Amine Screen. 317

Table 4-2 Reagents used in Fluorescein Benzoxazole Screen. 319

List of Figures

Figure 1-1 Example of stock solution preparation in 1-dram vials for dosing into the corresponding glass microvials of a 24- or 96-well aluminum heating block. 2

Figure 1-2 Cronin's Chemputer platform for automated synthesis with modules for reaction, filtration, separation, and evaporation connected by a series of interconnected ports to transfer between modules. Chemputer's two-step synthesis of organic oxidant DMP from digitization of literature procedures to automated execution. 5

Figure 1-3 EDBO+ Optimization of a) Mitsunobu reaction and b) Deoxyfluorination reaction of benzylic alcohols. Initial conditions shown in red are the starting point for Bayesian Optimization. 7

Figure 1-4 a) The chemists' experimental plan can translate directly into the b) high-throughput experiment planning and execution via phactor. From reagent selection to analytical data storage, phactor directly generates heatmaps for cheminformatic analysis. c) The general workflow, from inputting reagent selection into phactor to receiving a human-readable experiment layout for either manual or automated screening. Input of analytical data, such as from UPLC-MS, allows for direct analysis within the phactor platform. 8

Figure 1-5 Accelerated Serendipity approach to screening of random chemical space. Two substrates from the substrate pool are dosed to each well in the reaction plate followed by dosing of a selected catalyst system to the whole plate. GC-MS analysis of well containing amine **D** and nitrile **E** identified an α-arylation reaction. 10

Figure 1-6 Depiction of the Snap Deconvolution technique, where pooled substrates are subjected to transition metal catalysis in triplicate 96-well plate experiments. Each separate 96-well plate uses the same catalysts, but a different pool of substrates with unique mass handles is used (represented by blue balls). If High-Resolution Mass Spectrometry identifies corresponding product masses in all three plates, reactivity is confirmed. 11

Figure 1-7 The use of conjugated ferrocene dyes to colorimetrically analyze a hydrosilation reaction. As reaction progresses, the conjugated linker is saturated and the dye color diminishes which can be visually distinguished. 12

Figure 1-8 The use of fluorogenic dyes containing an intramolecular aldehyde quencher. Upon reaction of the aldehyde functionality fluorescence is restored and can be directly quantitated using fluorescence plate reading. 13

Figure 1-9 Three applications of Hartwig's FRET assay to screening palladium-catalyzed reaction conditions. First used to analyze high-throughput Mizoroki-Heck couplings, then α-arylation of cyanoacetates, and finally amine arylation conditions. 14

Figure 2-1 Comparison between the existing approach of Late-stage functionalization and the proposed approach of Late-stage saturation for modifying drug molecules. The overall drug properties of LSF analogues are often decreased due to the large increase in molecular weight, while LSS can markedly change physicochemical properties, while maintaining overall drug-likeness since only 6 hydrogen atoms are installed. 28

Figure 2-2 Examples of saturated matched pairs of molecules with dramatically modified drug properties..... 29

Figure 2-3 A) Cheminformatic workflow for analyzing the ChEMBL database. B) Identification of 9704 matched pairs from >1.5 million aromatic drugs. C) Kernel density of the fraction of sp^3 atoms showing the change in this property upon performing a virtual LSS (green) of the aromatic drugs (gray) in the ChEMBL database..... 30

Figure 2-4 Aromatic drugs transformed to saturated drugs by LSS: production of saturated drugs with distinct medicinal properties. Extent of saturation can be controlled by equivalents of the $B_2(OH)_4$ reductant. 32

Figure 2-5 Examples of LSS on mono-aromatic system containing drugs..... 32

Figure 2-6 Examples of LSS on multi-aromatic system containing drugs. For naphthalene-containing examples like Nabumetone **52** and (*S*)-Naproxen-OMe **55**, multiple regioisomeric products are isolatable..... 33

Figure 2-7 Step-economic synthesis of lead compounds empowered by LSS concept. 34

Figure 2-8 A library of 768 pharmaceutically relevant complex molecules stored in wet DMSO were subjected to LSS using $[Rh(COD)OH]_2$, $B_2(OH)_4$ in ethylene glycol. Selections of miniaturized reactions were confirmed on ~50 mg scale in ethanol to obtain isolated yields. *Yields shown in square brackets were obtained using ethylene glycol as solvent. 36

Figure 2-9 Predicted properties for Cinacalcet, Prilocaine, and their LSS-analogues **51** and **27.** Calculated properties, Fsp^3, TPSA, CYP inhibition, and LD_{50} along with experimental $LogP_{o/w}$ values are predicted to remain constant or improve upon saturation. $LogP_{o/w}$ values were determined from the experimental shake-flask method. 37

Figure 2-10 Microsomal stability data obtained for 24 LSS reaction mixtures showing the change in microsomal stability following saturation of various drugs. %Change indicates the increase or decrease in metabolic stability of the saturated drug compared to its arene precursor upon exposure to human liver microsomes for 60 minutes. 38

Figure 2-11 Reagents and 96-well plate set up for arene reduction conditions. 69

Figure 2-12 High-throughput 96-well screen to interrogate mild late-stage saturation conditions on drug substrates, propranolol, gemfibrozil, and ketoprofen under mild autoclave-free hydrogenation conditions. cod = 1,5-cyclooctadiene, TFE = 1,1,1-trifluoroethanol, Et. Gl. = ethylene glycol. 70

Figure 2-13 Calibration Curve for GC-MS Response to DMSO 71

Figure 2-14 Residual DMSO in 384-Well Plates Following First (A), Second (B), and Third (C) Evaporation Cycles 73

Figure 2-15 384-well plate split into 4 quadrants according to solvent along with color mapping for each added reagent. 74

Figure 2-16 384-well plate dosed with solvents, catalyst, and reductant (Top). Foil seal after heating well plate at 50°C for 24 hours (Bottom). 75

Figure 2-17 A) Heat map for 1,536-well plate experiment colored by percent conversion determined from UPLC-MS ionization peak area for 768 substrates subjected to two different reductant equivalents. B) Yield and chemical space distributions of 1,536-well plate experiment separated by equivalents of reductant used. 78

Figure 2-18 Example mass spectra from 1,536-well LSS experiment. Showing integration and calculation of percent conversion of the parent arene drugs used in the screen to saturated drugs. 81

Figure 2-19 Reagents and Grid of Screen for Microsomal Stability Studies 155

Figure 2-20 Difference in metabolic stability of 20 drugs determined before and after late-stage saturation. Ordered by increasing metabolic stability of saturated congener relative to its unsaturated parent material 157

Figure 3-1 A) Equation for efficiency of FRET energy transfer, $\mathbf{E_{FRET}}$. Inter-dye separation distance is represented by **r**. Förster distance, $\mathbf{R_0}$, is proportional to the overlap of the emission band of one dye and the absorption band of the second dye as well as the molecular orientation between the two dyes. B) FRET is observable between the fluorescently labelled substrates when their with reaction handles, **X** and **Y**, couple together. 229

Figure 3-2 Depiction of the Perylene **84** and BODIPY **85** fluorophores. Normalized absorption and emission spectra of the two fluorophores are shown along with the spectral overlap required for FRET shaded as the orange curve. 229

Figure 3-3 Two-step synthesis formylation and coupling step to synthesize Perylene aryl amine **87**. One-step synthesis of BODIPY acid **88** from dimethyl pyrrole and glutaric anhydride 230

Figure 3-4 Coupling of sp^2 Perylene amine **87** with sp^3 BODIPY acid **88** to FRET-active amide **89**. The ratio of fluorescence at 510 / 460 nm reveals a 9.1-fold increase in fluorescence for the amide coupled dyes over the uncoupled dyes. All dyes are 10 μM in DMSO. Uncoupled

fluorescence is reported from well containing 10 μM of both free amine and acid present. Excitation λ = 430 nm. 231

Figure 3-5 Synthesis of Perylene alkyl amine **91**. Initial attempts at Sonogashira coupling and reduction failed to fully reduce the appended alkyne in appreciable yields. Alternate Mizoroki-Heck coupling followed by cobalt-assisted nitrile reduction enabled synthesis of **91** on multi-gram scale. 232

Figure 3-6 Coupling of sp^3 Perylene amine **91** with sp^3 BODIPY acid **88** to alkyl amide **93**. The Fluorescence ratio at 510 / 460 nm gives an 11.6-fold increase for the amide over the uncoupled dyes. All dyes are 10 μM in DMSO. Uncoupled fluorescence is from well containing 10 μM of both free amine and acid present. Excitation λ = 430 nm. 232

Figure 3-7 Synthesis of Perylene amines with extended linkers through Friedel-Crafts Acylation and reduction steps. Newly synthesized amines coupling with BODIPY **88** towards new FRET pairs **96a-c**. 233

Figure 3-8 Fluorescence for extended-linker amides **96a-c** compared to previous 3-carbon amide **93**. Maximal 94.2 signal-to-noise of coupled amide relative to uncoupled amine/acid pair is reported from the 6-carbon linker of amide **96a**. Longer linker distances decrease FRET efficiency. All dyes are 10 μM in DMSO. Uncoupled fluorescence is reported from well containing 10 μM of both free amine and acid present. Excitation λ = 430 nm. Y-axis is plotted on a logarithmic scale. 234

Figure 3-9 a) Trends in decreasing fluorescence at 460 nm with increasing mole fraction of amide **96a**. A constant final concentration of 10 μM of amine+acid+amide is maintained while mole fraction of amide increases relative to decreasing mole fraction of amine+acid. b) Comparison of LCMS and FRET assay yields in the amide coupling of **95a** and **88** across varied equivalents of amide-coupling reagent HATU. 235

Figure 3-10 High-throughput 1,536-well plate screen of amide coupling conditions on optimized FRET dyes. Comparison of FRET platform relative to traditional UPLC–MS assay yields. 236

Figure 3-11 Comparison of LC–MS Assay Yields vs Ratiometric FRET analysis of 1,536-well amide coupling experiment. Each set of quadruplicate wells is averaged and displayed as a single point. The y-axis is displayed on a logarithmic scale with the average of negative controls displayed as the horizontal blue line at y = 0.826. Coefficient of determination of the log-scaled data is additionally displayed. 237

Figure 3-12 Normalized absorption and emission spectra of 10 μM **87** in DMSO. Excitation λ = 300 nm, λ max abs. = 447 nm, λ max em. = 455 nm..... 250

Figure 3-13 Normalized absorption and emission spectra of 10 μM **88** in DMSO. Excitation λ = 300 nm, λ max abs. = 499 nm, λ max em. = 512 nm..... 251

Figure 3-14 Normalized absorption and emission spectra of 10 μM **89** in DMSO. Excitation λ = 300 nm, λ max abs. = 498 nm, λ max em. = 512 nm..... 251

Figure 3-15 Normalized absorption and emission spectra of 10 μM **91** in DMSO. Excitation λ = 300 nm, λ max abs. = 447 nm, λ max em. = 456 nm..... 252

Figure 3-16 Normalized absorption and emission spectra of 10 μM **93** in DMSO. Excitation λ = 300 nm, λ max abs. = 499 nm, λ max em. = 512 nm..... 252

Figure 3-17 Normalized absorption and emission spectra of 10 μM **95a** in DMSO. Excitation λ = 300 nm, λ max abs. = 447 nm, λ max em. = 457 nm..... 253

Figure 3-18 Normalized absorption and emission spectra of 10 μM **96a** in DMSO. Excitation λ = 300 nm, λ max abs. = 500 nm, λ max em. = 512 nm..... 253

Figure 3-19 Normalized absorption and emission spectra of 10 μM **95b** in DMSO. Excitation λ = 300 nm, λ max abs. = 447 nm, λ max em. = 458 nm..... 254

Figure 3-20 Normalized absorption and emission spectra of 10 μM **96b** in DMSO. Excitation λ = 300 nm, λ max abs. = 499 nm, λ max em. = 512 nm..... 254

Figure 3-21 Normalized absorption and emission spectra of 10 μM **95c** in DMSO. Excitation λ = 300 nm, λ max abs. = 447 nm, λ max em. = 457 nm..... 255

Figure 3-22 Normalized absorption and emission spectra of 10 μM **96c** in DMSO. Excitation λ = 300 nm, λ max abs. = 499 nm, λ max em. = 512 nm..... 255

Figure 3-23 Grid of 96-well screen subjecting pure C3 amide **93** to various transition metal catalyzed conditions. Metals are allocated by row and ligands by column. Colored well outlines correlates to one of four different acid/base/reductant/oxidant additives. 257

Figure 3-24 Initial fluorescence of 96-well poisoning study taken at t = 0 hrs. 257

Figure 3-25 Final fluorescence of 96-well poisoning study taken at t = 24 hrs. Excitation λ = 430 nm, emission λ = 510 nm. 4% decrease in average plate fluorescence was noted relative to the initial data..... 258

Figure 3-26 Titration of increasing mole fraction of FRET-active amide **96a** (0 to 1.0 mole fraction). Decreasing fluorescence at 460 nm was used to plot the resulting linear trend line below..... 260

Figure 3-27 Titration of uncoupled amine **95a** and acid **88** with increasing mole fraction of amide **96a**. The lower fluorescence at 460 nanometers for amide **96a** results from energy transfer between the linked Perylene and BODIPY dyes. 260

Figure 3-28 Calibration Curve for Assay yield determination of amide coupling yields by LC–MS..... 264

Figure 3-29 Heatmap from LC–MS analysis of the 1,536-well amide coupling of FRET dyes. Colored by increasing assay yield. Columns 1, 2, 17, 18, 33, and 34 are positive and negative controls..... 264

Figure 3-30 Heatmap from fluorescence analysis of the 1,536-well amide coupling of FRET dyes. Colored by the increasing fluorescence ratio at 510 nm / 460 nm. Columns 1, 2, 17, 18, 33, and 34 are positive and negative controls. 265

Figure 3-31 Comparison of LC–MS Assay Yields vs Ratiometric FRET analysis of 1,536-well amide coupling experiment. The y-axis is displayed on a logarithmic scale and R^2 value is representative of fitting the log-value data to a linear trend. 265

Figure 3-32 Layout for each of the five 1,536-well reaction plates in the nanoscale pyridinium salt-acid screening campaign. In each plate the substrate, control, ligand, and additives dosed are identical between plates. The only variable is the identity of metals dosed to each column of each plate. Columns 1 and 25 represent positive and negative controls, respectively, which only received amide **96a** (+ control) or uncoupled dyes **95a-pyridinium salt** and **88** (- neg control). 267

Figure 3-33 Heatmap of Fluorescence detected at at 510nm / 460 nm for Plate 1 from the nanoscale pyridinium salt-acid FRET screen. Excitation λ = 430 nm. 272

Figure 3-34 Heatmap of Fluorescence detected at at 510nm / 460 nm for Plate 2 from the nanoscale pyridinium salt-acid FRET screen. Excitation λ = 430 nm. 273

Figure 3-35 Heatmap of Fluorescence detected at at 510nm / 460 nm for Plate 3 from the nanoscale pyridinium salt-acid FRET screen. Excitation λ = 430 nm. 273

Figure 3-36 Heatmap of Fluorescence detected at at 510nm / 460 nm for Plate 4 from the nanoscale pyridinium salt-acid FRET screen. Excitation λ = 430 nm. 274

Figure 3-37 Heatmap of Fluorescence detected at at 510nm / 460 nm for Plate 5 from the nanoscale pyridinium salt-acid FRET screen. Excitation λ = 430 nm. 274

Figure 3-38 Identified Pummerer-type rearrangement from wells containing [Ir(cod)Cl_2] and triethyl silane. Showcased on a model acid substrate. 275

Figure 4-1 Synthesis of model pyridinium salt **99** from benzyl amine **97** and pyrylium salt **98**. The proposed reactivity would engage the α-position of the pyridinium salt via deprotonation and subsequent capture by an electrophile. 303

Figure 4-2 Optimization of pyridinium salt deprotonation conditions to enable C–C bond formation with benzaldehyde. 304

Figure 4-3 Lewis Acid screening for rearranged aldehyde product **102** that results from migration of phenyl ring and loss of triphenyl pyridine **103**. Yields of **102** are reported as the alcohol resulting from $NaBH_4$ reduction of the aldehyde. 304

Figure 4-4 Application of diverse amine-acid couplings to the derivatization of the bioimaging dye Fluorescein **104** with *p*-toluidine **105**. 305

Figure 4-5 Fluorescein's equilibrium between closed **106** and open **104** forms can be shut off by protection and reduction of the tricyclic xanthene core. Reduced Fluorescein diacetate **107** can be directly used in coupling with *p*-toluidine **105**. 306

Figure 4-6 HTE Screen for Fluorescein Alkyl Amine **108**. Each row was dosed with a different phosphine ligand, every two rows a different platinum catalyst, and rows alternate between phenylsilane and diphenylsilane reductants. 306

Figure 4-7 Proposed scheme for amidation of Fluorescein followed by oxidative cyclization of its amide motif. 307

Figure 4-8 HTE Screen for Fluorescein Benzoxazole **110** from Fluorescein Amide **109**. Each row was dosed with a different acid, each column with a different oxidant, and all wells received 50 mol% 1-iodo-4-nitrobenzene additive. 307

Figure 4-9 Complete library of 12 Fluorescein analogues accessed from coupling of Fluorescein **104** or reduced Fluorescein diacetate **107** with *p*-toluidine **105**. 308

Figure 4-10 Kernel Density Estimate plots showing the range of physicochemical properties of the Fluorescein analogue library. The grey line in each plot indicates the value of Fluorescein carboxylic acid. Height of each peak represents the frequency of occurrence for each value. MW = molecular weight, LOGP = calculated log(partition coefficient), HBA/D = h-bond acceptor/donor count, PSA = polar surface area, ROTB = rotatable bond count, FC = formal charge at pH 7.4, QED = quantitative estimate of drug likeness. Values are computed using RDKit. 309

Figure 4-11 Calibration Curve for Fluorescein Alkyl Amine 316

Figure 4-12 Grid of 24-Well Fluorescein Alkyl Amine Screen 317

Figure 4-13 Heatmap for Fluorescein Alkyl Amine Screen 318

Figure 4-14 Calibration Curve for Fluorescein Benzoxazole 319

Figure 4-15 Grid of 24-Well Fluorescein Biaryl Ether Screen 320

Figure 4-16 Heatmap for Fluorescein Benzoxazole Screen 320

List of Spectra

Spectrum 2-1 ^{1}H NMR of compound 20 160

Spectrum 2-2 ^{1}H NMR of compound 21 160

Spectrum 2-3 ^{13}C NMR of compound 21 161

Spectrum 2-4 ^{1}H NMR of compound 23 161

Spectrum 2-5 ^{13}C NMR of compound 23 162

Spectrum 2-6 ^{1}H NMR of compound 25 162

Spectrum 2-7 ^{13}C NMR of compound 25 163

Spectrum 2-8 ^{1}H NMR of compound 27 163

Spectrum 2-9 ^{13}C NMR of compound 27 164

Spectrum 2-10 ^{1}H NMR of compound 29a..... 165

Spectrum 2-11 ^{13}C NMR of compound 29a 165

Spectrum 2-12 ^{1}H NMR of compound 29b 166

Spectrum 2-13 ^{13}C NMR of compound 29b 166

Spectrum 2-14 ^{1}H NMR of compound 31 167

Spectrum 2-15 ^{13}C NMR of compound 31 167

Spectrum 2-16 ^{1}H NMR of compound 33 168

Spectrum 2-17 ^{13}C NMR of compound 33 169

Spectrum 2-18 ^{1}H NMR of compound 35 170

Spectrum 2-19 ^{13}C NMR of compound 35 171

Spectrum 2-20 ^{1}H NMR of compound 35’ 172

Spectrum 2-21 ^{13}C NMR of compound 35’ 173

Spectrum 2-22 ^{1}H NMR of compound 37 174
Spectrum 2-23 ^{13}C NMR of compound 37 175
Spectrum 2-24 ^{1}H NMR of compound 38 176
Spectrum 2-25 ^{13}C NMR of compound 38 177
Spectrum 2-26 ^{1}H NMR of compound 39 177
Spectrum 2-27 ^{13}C NMR of compound 39 178
Spectrum 2-28 ^{19}F NMR of compound 39 178
Spectrum 2-29 ^{1}H NMR of compound 40 179
Spectrum 2-30 ^{13}C NMR of compound 40 180
Spectrum 2-31 ^{1}H NMR of compound 41 181
Spectrum 2-32 ^{13}C NMR of compound 41 182
Spectrum 2-33 ^{1}H NMR of compound 42 183
Spectrum 2-34 ^{13}C NMR of compound 42 184
Spectrum 2-35 ^{19}F NMR of compound 42 185
Spectrum 2-36 ^{1}H NMR of compound 43 185
Spectrum 2-37 ^{13}C NMR of compound 43 186
Spectrum 2-38 ^{1}H NMR of compound 43’ 187
Spectrum 2-39 ^{13}C NMR of compound 43’ 188
Spectrum 2-40 ^{1}H NMR of compound 44 189
Spectrum 2-41 ^{13}C NMR of compound 44 190
Spectrum 2-42 ^{1}H NMR of compound 45 190
Spectrum 2-43 ^{13}C NMR of compound 45 191
Spectrum 2-44 ^{1}H NMR of compound 46 191
Spectrum 2-45 ^{13}C NMR of compound 46 192
Spectrum 2-46 ^{1}H NMR of compound 47 193

Spectrum 2-47 ^{13}C NMR of compound 47 194
Spectrum 2-48 ^{1}H NMR of compound 48 195
Spectrum 2-49 ^{13}C NMR of compound 48 196
Spectrum 2-50 ^{1}H NMR of compound 49 197
Spectrum 2-51 ^{13}C NMR of compound 49 197
Spectrum 2-52 ^{1}H NMR of compound 50 198
Spectrum 2-53 ^{13}C NMR of compound 50 198
Spectrum 2-54 ^{1}H NMR of compound 51 199
Spectrum 2-55 ^{13}C NMR of compound 51 199
Spectrum 2-56 ^{19}F NMR of compound 51 200
Spectrum 2-57 ^{1}H NMR of compound 53 200
Spectrum 2-58 ^{13}C NMR of compound 53 201
Spectrum 2-59 ^{1}H NMR of compound 54 202
Spectrum 2-60 ^{13}C NMR of compound 54 203
Spectrum 2-61 ^{1}H NMR of compound 56 204
Spectrum 2-62 ^{13}C NMR of compound 56 205
Spectrum 2-63 ^{1}H NMR of compound 57 206
Spectrum 2-64 ^{13}C NMR of compound 57 206
Spectrum 2-65 ^{1}H NMR of compound 59 207
Spectrum 2-66 ^{13}C NMR of compound 59 207
Spectrum 2-67 ^{1}H NMR of compound 62 208
Spectrum 2-68 ^{13}C NMR of compound 62 208
Spectrum 2-69 ^{1}H NMR of compound 67 209
Spectrum 2-70 ^{13}C NMR of compound 67 209
Spectrum 2-71 ^{1}H NMR of compound 69 210

Spectrum 2-72 ^{13}C NMR of compound 69 210
Spectrum 2-73 ^{1}H NMR of compound 71 211
Spectrum 2-74 ^{1}H NMR of compound 71 211
Spectrum 2-75 ^{1}H NMR of compound 74 212
Spectrum 2-76 ^{13}C NMR of compound 74 212
Spectrum 2-77 ^{1}H NMR of compound 74' 213
Spectrum 2-78 ^{13}C NMR of compound 74' 213
Spectrum 2-79 ^{1}H NMR of compound 77 214
Spectrum 2-80 ^{1}H NMR of compound 79 214
Spectrum 2-81 ^{13}C NMR of compound 79 215
Spectrum 2-82 ^{1}H NMR of compound 80 215
Spectrum 2-83 ^{13}C NMR of compound 80 216
Spectrum 2-84 ^{1}H NMR of compound 81 217
Spectrum 2-85 ^{13}C NMR of compound 81 218
Spectrum 2-86 ^{1}H NMR of compound 82 219
Spectrum 2-87 ^{13}C NMR of compound 82 220
Spectrum 2-88 ^{1}H NMR of compound 83 221
Spectrum 2-89 ^{13}C NMR of compound 83 222
Spectrum 3-1 ^{1}H NMR of compound 86 275
Spectrum 3-2 ^{13}C NMR of compound 86 276
Spectrum 3-3 ^{1}H NMR of compound 87 277
Spectrum 3-4 ^{13}C NMR of compound 87 278
Spectrum 3-5 ^{1}H NMR of compound 88 279
Spectrum 3-6 ^{13}C NMR of compound 88 280
Spectrum 3-7 ^{19}F NMR of compound 88 281

Spectrum 3-8 ^{1}H NMR of compound 89 282
Spectrum 3-9 ^{13}C NMR of compound 89 283
Spectrum 3-10 ^{1}H NMR of compound 91 284
Spectrum 3-11 ^{13}C NMR of compound 91 285
Spectrum 3-12 ^{1}H NMR of compound 93 286
Spectrum 3-13 ^{13}C NMR of compound 93 287
Spectrum 3-14 ^{1}H NMR of compound 95a 288
Spectrum 3-15 ^{13}C NMR of compound 95a 289
Spectrum 3-16 ^{1}H NMR of compound 96a 290
Spectrum 3-17 ^{1}H NMR of compound 96a 291
Spectrum 3-18 ^{13}C NMR of compound 95b 292
Spectrum 3-19 ^{13}C NMR of compound 95b 293
Spectrum 3-20 ^{1}H NMR of compound 96b 294
Spectrum 3-21 ^{13}C NMR of compound 96b 295
Spectrum 3-22 ^{1}H NMR of compound 95c 296
Spectrum 3-23 ^{13}C NMR of compound 95c 297
Spectrum 3-24 ^{1}H NMR of compound 96c 298
Spectrum 3-25 ^{13}C NMR of compound 96c 299
Spectrum 4-1 ^{1}H NMR of compound 102 321
Spectrum 4-2 ^{13}C NMR of compound 102 322
Spectrum 4-3 ^{1}H NMR of compound 108a 323
Spectrum 4-4 ^{13}C NMR of compound 108a 324
Spectrum 4-5 ^{1}H NMR of compound 108b 325
Spectrum 4-6 ^{13}C NMR of compound 108b 326
Spectrum 4-7 ^{1}H NMR of compound 110 327

Spectrum 4-8 ^{13}C NMR of compound 110 328

Abstract

Drug discovery is largely bottlenecked by the speed of chemical synthesis. High-Throughput Experimentation (HTE) is a critical technique that enables chemists to generate orders of magnitude more chemical information from their experiments than traditional synthetic methods. Here, we demonstrate the HTE-enabled expansion of drug-like chemical space in the development of new reactions that directly leverage the most prevalent medicinal chemistry substrates: arenes, carboxylic acids, and amines.

While sp^2-carbon-rich fragments are increasingly facile to synthesize using high-quality cross-coupling reactions, the products are flat and lipophilic which can decrease their odds of becoming marketed drugs. To expand chemical space accessible from ubiquitous aromatic motifs, we have developed a late-stage rhodium-catalyzed arene saturation protocol amenable to a host of densely functionalized drug leads and marketed drugs. This method has been successfully applied to the saturation of several hundred drug-like substrates in 1,536-well plate format and a 24-well direct-to-biology microsomal stability assessment of drug metabolism directly on crude reaction mixtures. Proven competent across a range of pharmaceutically relevant arenes, the reported method enables rapid exploration of three-dimensional chemical space in hopes of improved clinical outcomes.

In parallel, this work demonstrates new ways in which medicinal chemists can combine the two most abundant functional groups in drug discovery, amines and carboxylic acids, in ways beyond that of the traditional amide bond. While amines and acids are incredibly abundant chemical feedstocks, medicinal chemists almost exclusively combine the two to form an amide bond. However, there are increasing reports on unique ways to combine these two functionalities towards products with other bond arrangements and diverse properties to compliment the venerable amide coupling.

To enable the rapid exploration of amine–acid coupling space, we have developed a high-throughput reaction analysis platform based on Fluorescence Resonance Energy Transfer (FRET) that gives a reaction readout at rapid pace. This technology enables the accurate analysis

of 1,536-well plate amine-acid couplings over 300-fold faster than ultra-performance liquid chromatography-mass spectrometry (UPLC–MS) analysis. Finally, these studies are complimented by the development of several unorthodox amine–acid couplings on the derivatization of the bioimaging dye, fluorescein. Various coupling modes between the acid functionality on fluorescein and the model amine, *p*-toluidine, are engaged through a variety of amine and acid-activation techniques to produce diverse and interesting fluorescent dyes. Collectively, these studies serve to showcase the power of HTE in reaction development and help further bolster the amine–acid coupling toolbox.

Chapter 1 Accelerating Synthesis with High-Throughput Experimentation

1.1 Introduction to High-Throughput Experimentation (HTE) and Automation

Traditionally, reaction discovery and optimization have relied on serial experimentation, wherein chemists iterate through reaction parameters one at a time. In contrast, High-Throughput Experimentation (HTE) is the practice of conducting parallel miniaturized experiments in microtiter plates or microvials. Borne from biological high-throughput screening (HTS) techniques,[1] HTE enables chemists to rapidly execute tens to hundreds to thousands of chemical reactions in systematically varied conditions. Employing microtiter plates or microvial arrays for reaction setup allows chemists to simultaneously explore a range of reaction variables such as catalysts, ligands, bases, solvents, and additives while consuming only milligram to microgram quantities of potentially precious materials.[2] The systematic nature of HTE allows chemists to more easily interrogate the interplay between combinations of reagents to either drive reaction optimization or to develop large libraries of molecules. As a result, a well-executed high-throughput experiment can vastly accelerate the rate of research beyond that of traditional benchtop experimentation.

A modern HTE workflow begins with the mapping of reaction parameters to an array. For example, a 96-well array might evaluate four catalysts, six ligands, two solvents, and two bases simultaneously to achieve 96 distinct conditions in a single experiment. A variety of software systems help facilitate the design of miniaturized experiments, the simplest being an Excel spreadsheet. Once a plan is made, the preparation and dosing of stock solutions into the appropriate wells or vials in the reaction array is then carried out by manual pipetting or automated liquid handling robotics. Each well will typically range from volumes of 1–100 μL and concentrations near 0.1 molar once all stock solutions are dosed to the appropriate wells (Figure 1-1). The reaction plate can then be sealed and heated to the desired temperature until ready for analysis. An appropriate analytical method, typically LC–MS or GC–MS, can then be used to gather data from the screen and better inform later rounds of experimentation.

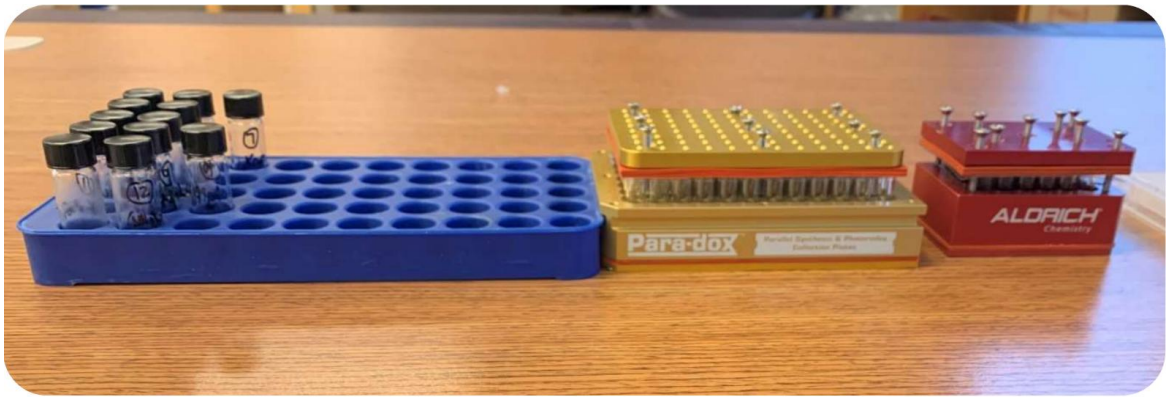


Figure 1-1 Example of stock solution preparation in 1-dram vials for dosing into the corresponding glass microvials of a 24- or 96-well aluminum heating block.

While high-throughput biological assays have been in practice since at least the 1980's,[3] high-throughput methods in chemistry have been much less widely adopted. Early reports of solid-phase peptide synthesis in well plate format mark some of the first applications of high-throughput chemistry.[4–7] In the 1990's and 2000's HTE began to see more widescale adoption as successful reports of combinatorial small molecule synthesis arose.[8–13] In a modern outlook, HTE is seeing successful implementation in a variety of industrial and academic settings, notable academic examples being the University of Pennsylvania and Princeton which house dedicated HTE facilities for students. Since its inception, the scope of chemistry amenable to HTE has broadened considerably. Early implementations were constrained to aqueous conditions reminiscent of the biological applications HTE was derived from. Modern applications encompass photoredox catalysis[14–16], electrochemistry,[17–19] transition metal-mediated transformations,[20–23] and even enzymatic chemistry.[24–27]

The potential of HTE to accelerate reaction discovery and optimization is particularly evident in modern pharmaceutical and agrochemical development. Late-stage functionalization (LSF) of complex molecules is often bottlenecked by the availability of precious late-stage intermediates. In these scenarios, HTE is routinely used to optimize reactivity or build libraries of derivatives on these complex scaffolds with minimal material usage.[2,28–34] By combinatorially screening catalyst, ligand, solvent, additive combinations in parallel, chemists can identify promising reaction conditions directly on advanced intermediates. Increasing reports from both industrial and academic groups have showcased the power of HTE to optimize C–N, C–C, and C–O bond formations, hydrogenations, and oxidative couplings under conditions relevant to medicinal chemistry.[17,35–46] As well, the potential for increased data generation afforded by HTE

has driven significant interest in building machine learning models and structure-reactivity relationships for predictive chemistry applications. [47–51]

While high-throughput chemistry has seen an uptick in popularity in recent years, there are still several factors impeding its more widescale adoption.[52–54] The engineering challenges associated with miniaturized scale chemistry is perhaps the most burdensome. The reliance on stock solution for transferring reagents into microvials or well plates means that heterogenous reactions often perform poorly or inconsistently compared to traditional weighing of solid reagents. The miniaturization down to microliter scale reactions also poses several problems regarding compatibility of chemical reagents with hardware and robotics that occasionally renders a reaction unsuitable for HTE. Another point of discourse surrounding HTE is the prohibitively expensive hardware and automation required to carry out some of the more miniaturized scale experiments. In response to these concerns, there have been great strides in recent years to combat these points and make HTE a more robust and accessible practice for all. In the following sections we will discuss common hardware and software implementations as well as improvements made to HTE infrastructure in recent years.

1.2 **Hardware Implementation in HTE**

The successful execution of high-throughput experimentation relies on carefully chosen engineering infrastructure that enables reliable and reproducible miniaturized reactions. Unlike the homogeneous aqueous assays used in biological high-throughput screening, chemical HTE presents unique challenges due to the diversity of solvents, reagents, temperatures, and atmospheric conditions employed in synthetic transformations. These constraints have driven significant innovation in hardware design, reaction vessels, liquid handling systems, environmental control, and specialized reactors for photochemical, electrochemical, and heterogenous catalytic experiments.

Most often, HTE reactions are facilitated by the preparation and dosing of reagent stock solutions into the corresponding vials or wells of a reaction array. For small- to medium-scale screens (24 or 96 wells), glass shell vials housed in aluminum heating blocks are the most common configuration. These glass vials easily accommodate a range of organic solvents and temperatures without warping which is a concern with plastic microtiter plates. These setups can be readily integrated with hot plates, stir plates, or tumble stirrers to provide uniform heating and mixing. Commercial systems such as the Unchained Labs Junior[29] or Analytical Sales &

Services HTE reactor blocks[22,23,29] have standardized the use of these blocks while facilitating reaction temperatures from –15 °C to >150 °C.

When considering 384- or 1,536-well experiments, polypropylene or cyclic olefin copolymer (COC) plates are most frequently used. Chemical compatibility must be taken into account when considering plastic well plates as nonpolar hydrocarbon-based solvents often degrade the plastic and cause swelling, especially at elevated temperatures. Glass plates provide superior chemical resistance but are prohibitively expensive and fragile in 384- and 1536-well formats. Additionally, solvent selection must be limited to non-volatile, high boiling solvents to prevent evaporation when working with ultra-miniaturized setups. Reactions done at ~100 µL volumes in glass vials can be executed in traditional solvent systems without issue. Ultra-miniaturized experiments at ~1 µL are typically limited to solvents such as dimethyl sulfoxide (DMSO), N,N-dimethyl formamide (DMF), N-Methyl-2-pyrrolidone (NMP), or ethylene glycol.

While many of these solvents dissolve a wide range of organic reagents, slurries of undissolved materials can also cause problems with stock solution dosing on miniaturized scale. Heterogenous mixtures can still be slurry loaded into 24- and 96-well screens using wide-bore pipette tips. However, this problem doesn't have a clear-cut solution on more miniaturized scales. Specialized engineering solutions such as centrifugal evaporation can enable dosing of inorganic reagents in aqueous solutions to an entire well plate, followed by evaporation and reconstitution in the intended reaction solvent.[31] As well, ChemBeads have been developed as another solution to dosing insoluble reagents. Reagents pre-adsorbed to glass beads can be directly portioned into 24- and 96-well screens at nanomole scale precision.[55] While ChemBeads don't currently offer a solution for solid dispensing into 1,536-well format, they do provide an innovative direction for solid dosing in HTE that may yet prove adaptable into ultra-miniaturized formats.

1.2.1 ***Automation***

As HTE relies heavily on the repetitive dosing of stock solutions, implementation of robotics and automation in high-throughput workflows has helped to alleviate operator burden and accelerate experiment turnaround times. While automation is most associated with 384- and 1,536-well plate experimentation, owing to the impracticality of manual dosing nanoliter volumes, even conventional benchtop workflows are increasingly becoming automated. We will first discuss the more traditional HTE-tailored automation platforms. Commercially available

systems such as the STP Labtech Mosquito,[2,32,49,56] Labcyte Echo,[57,58] Opentrons OT-2,[59] Thermo Matrix,[60] and Chemspeed SWING[61,62] robots can dispense nanoliter to microliter volumes with high accuracy. The Mosquito system, for example, employs positive displacement pipetting with disposable tips to handle solution dosing, while the Labcyte Echo utilizes acoustic droplet ejection (ADE) to transfer nanoliter droplets via ultrasonic pulses. ADE-based systems excels at setting up of thousands of reactions per hour without physical contact between pipette and reagent but are particularly limited to aqueous and DMSO-based solutions. For laboratories seeking cost-effective solutions, open-source platforms such as the Opentrons OT-2 are sufficiently capable of accurate dosing in 24, 96, or 384-well plate formats. Additionally, 3D printing capabilities can further extend the ability of the OT-2 robot to dose into more custom labware setups. Additionally, many of these instruments comfortably fit into glovebox setups to enable inert atmosphere chemistry.

Regarding automation of more traditional tasks, both industrial and academic efforts have been made towards "self-driving" lab ecosystems capable of experiment design, execution, and analysis with minimal human intervention. A notable academic example being the Cronin group's Chemputer platform that utilizes the chemical markup language, XDL (Experimental Description Language) to digitize and execute multi-step synthetic operations such as mixing, heating, or filtering directly from a literature procedure.[63] For example, the common oxidizing agent Dess-Martin Periodinane (DMP) was prepared via feeding a two-step literature process into their system. Including multiple reagent addition, heating and filtration steps, they were able to synthesize DMP in a 52% yield (Figure 1-2).

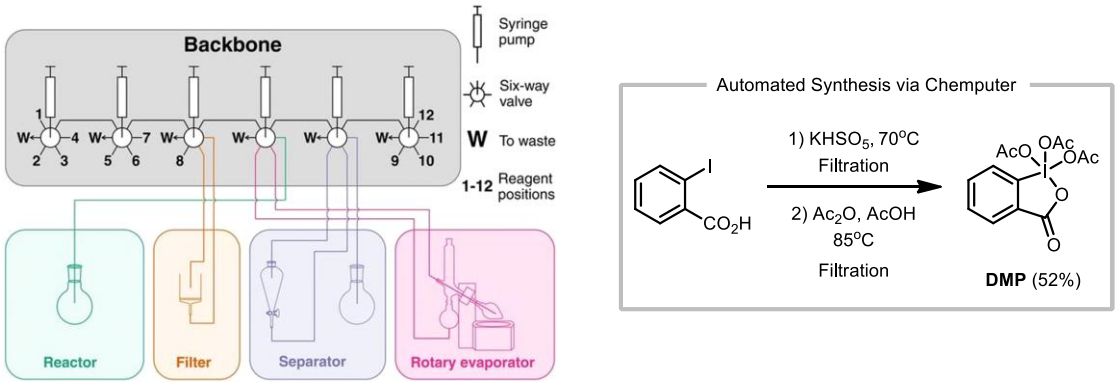


Figure 1-2 Cronin's Chemputer platform for automated synthesis with modules for reaction, filtration, separation, and evaporation connected by a series of interconnected ports to transfer between modules. Chemputer's two-step synthesis of organic oxidant DMP from digitization of literature procedures to automated execution.

The pharmaceutical industry is also increasingly engaged in automating routine workflows. For instance, AbbVie,[64] Eli Lilly,[65] and AstraZeneca[66] all are building up their automated lab ecosystems for streamlined library synthesis and optimization efforts. AbbVie showcased the synthesis, purification, and bioassay testing of 55 novel polycomb protein EED binders in a 45-hour turnaround time with their fully hands-off robotics platform.[67] Remote cloud labs, such as Strateos and Emerald Cloud Lab, offer their automation facilities as a commercial service. Researchers can send materials to these automation facilities while remotely accessing their robotics platforms to execute and analyze experiments in a range of high-throughput formats. The increasing demand for rapid drug development pipelines is certainly a positive indicator that automation will take an increasing role in the future of the pharmaceutical industry. The following section will examine the software infrastructure that integrates with these physical platforms and their role in the collection and analysis of HTE-generated data libraries.

1.3 **Software Implementation in HTE**

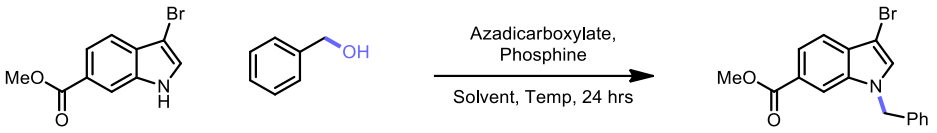
The physical infrastructure of HTE is what fundamentally enables the miniaturization and execution of chemical reactions. Meanwhile, the software layer is what allows for the rapid turnaround time in data compiling and deconvolution to draw chemical insight and inform future experiments. Software tools in HTE serve multiple roles: experimental design, instrument control, data capture, analysis, and storage. The software layer can be thought of as bridging the gap between the chemist's conceptual design, the execution of thousands of reactions, and finally the interpretation of those reactions. We will first discuss software that assists in the planning of high-throughput chemistry followed by systems that tie into data processing and analysis.

1.3.1 ***Design of Experiments (DoE) and Reaction Array Planning***

Some of the earliest methods to plan HTE experiments relied on custom Excel macros and spreadsheets to generate reaction matrices and dosing instructions, but these tools were highly user-dependent and lacked standardization.[29] To overcome these limitations, commercial and academic software platforms have been developed that integrate experiment design with laboratory hardware and analytical data streams. Examples include ACD/Labs Katalyst D2D, Unchained Labs LEA, and academic solutions such as Phactor™ developed by our lab. These tools automate the construction of multidimensional arrays by allowing users to define what variables are being screened, such as catalysts, ligands, or solvents, and then map all possible permutations to the experimental plate.

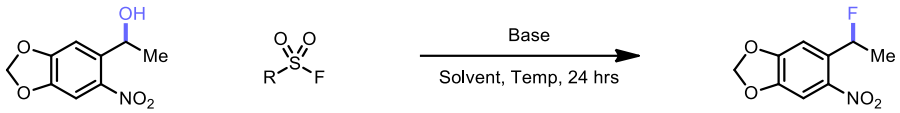
Design of experiments (DoE) algorithms are increasingly integrated into these systems, enabling chemists to sample reaction space more efficiently than through exhaustive enumeration. Fractional factorial and response surface algorithms[68] allow the software to select a subset of conditions that maximizes information gain while minimizing the total number of experiments needing to be run. In 2021, the Doyle group reported on a streamlined framework for the popular Bayesian optimization algorithm that allows chemists to easily integrate DoE models into everyday reaction optimization work.[50] Their Experimental Design by Bayesian Optimization (EDBO) package was able to outperform human intuition in both reducing the number of experiments needed to improve reaction efficiency as well as consistency across multiple different reaction types. Demonstrated towards the optimization of Mitsunobu chemistry as well as deoxyfluorination of benzylic alcohols, EDBO was able to improve reaction yields from 60% to 99% for the Mitsunobu reaction and from 36% to 69% for the deoxyfluorination reaction (Figure 1-3).

a



AD (equiv.)	Phosphine (equiv.)	Solvent (M)	Temperature (°C)	Yield
DIAD (1.1)	PPh_3 (1.1)	THF (0.1)	25	60%
ADDP (1.9)	$P(Ph)_2Me$ (1.9)	THF (0.2)	25	99%
DMAD (1.9)	$P(Ph)_2Me$ (1.9)	MeCN (0.15)	45	99%
ADDP (1.9)	$P(Ph)_2Me$ (1.9)	THF (0.15)	45	99%

b



R (equiv.)	Base (equiv.)	Solvent (M)	Temperature (°C)	Yield
PyFluor (1.1)	DBU (2.0)	THF (0.5)	20	36%
4-CF_3-Ph (1.9)	BTMG (1.9)	$PhCF_3$ (0.5)	20	69%
3,5-dCF_3-Ph (1.1)	BTMG (1.9)	PhMe (0.1)	60	69%
4-NO_2-Ph (1.9)	BTMG (1.9)	PhMe (0.1)	20	68%

Figure 1-3 EDBO+ Optimization of a) Mitsunobu reaction and b) Deoxyfluorination reaction of benzylic alcohols. Initial conditions shown in red are the starting point for Bayesian Optimization.

1.3.2 ***Data Processing and Visualization***

As HTE campaigns generate anywhere from tens to thousands of data points per run, data management is a critical component of the workflow. Each reaction produces a combination of raw analytical data (i.e. chromatograms, spectra) and metadata (i.e. reagent identities, concentrations, temperature, time, and solvent). Effective software infrastructure captures this raw analytical data to facilitate interpretation and downstream analysis. Several platforms have been developed to streamline this process. ACD Katalyst D2D, Spotfire, and Virscidian all provide platforms for data collection and management along with chromatographic deconvolution and peak integration. Tools such as Phactor[69] and MZMine[70] handle large-scale data imports from LC–MS and GC–MS instruments. Developed by the Cernak lab, Phactor is tailored for end-to-end integration of design, execution, and analysis of HTE experiments. It allows for direct design of reaction arrays that can be linked directly to robotic instructions and analytical outputs along with ultimate generation of data visualizations such as heat maps or correlation plots from the compiled data (Figure 1-4).

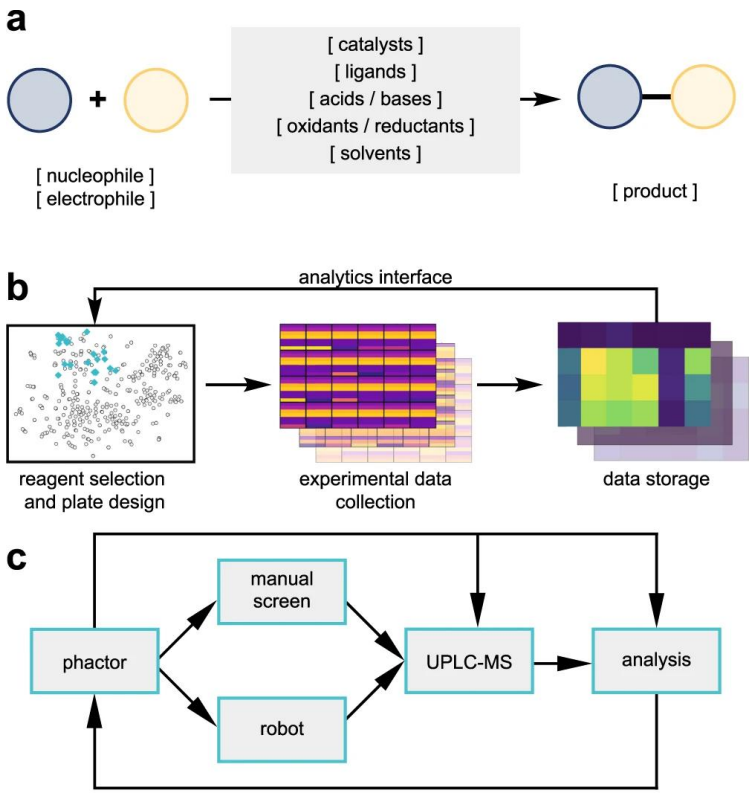


Figure 1-4 a) The chemists' experimental plan can translate directly into the b) high-throughput experiment planning and execution via phactor. From reagent selection to analytical data storage, phactor directly generates heatmaps for cheminformatic analysis. c) The general workflow, from inputting reagent selection into phactor to receiving a human-readable experiment layout for either manual or automated screening. Input of analytical data, such as from UPLC-MS, allows for direct analysis within the phactor platform.

These tools facilitate experiment planning, inventory management, metadata capture, and automated data visualization, establishing a foundation for machine-readable and shareable chemical data. Stemming from the ability to rapidly produce and interpret massive libraries of HTE data, machine learning (ML) algorithms have become increasingly popular to model and predict chemical trends. For example, the Aspuru-Guzik, Sigman, and Doyle groups have demonstrated the correlation of chemical descriptors with reaction performance can help elucidate trends in chemical reactivity that would otherwise be difficult to discern.[49,71,72] Importantly, the success of these approaches depends on the fidelity of the data generated during each experimental cycle, emphasizing the need for robust analytical and metadata capture. In the following section, we will turn our focus towards the analytical methods being employed in HTE and their ability to provide high quality data.

1.4 **High-Throughput Analytical Methods**

As previously mentioned, one of the main draws of high-throughput chemistry is the ability to systematically explore vast swaths of chemical and reaction space for the rapid identification and optimization of chemical transformations. However, the growing capability to conduct reactions at high throughput has shifted the experimental bottleneck downstream. While an HTE chemist can execute hundreds or thousands of reaction mixtures within a day, conventional analytical techniques such as UPLC–MS can process only a fraction of these samples in comparable time. As a result, the throughput of analysis has become the rate-limiting step in the experimental workflow. Significant research has been done to alleviate the burden of reaction analysis and there are many reviews on the current state of the field and limitations.[73–75] However, there is still a great demand for a universal reaction analysis technique that matches the scale and speed of modern HTE has driven significant research in developing new high-throughput analytical techniques.

1.4.1 ***Chromatographic and Spectrometric Methods***

The most widely adopted solution for analysis of high-throughput experiments is ultra-performance liquid chromatography-mass spectrometry, which combines rapid chromatographic separation with mass-based identification of products and side products. Modern UPLC–MS systems can achieve sample analysis times of one to two minutes per well, enabling the analysis of 96-well plates within a few hours. On the other hand, a 1,536-well plate experiment can take upwards of two days for data collection, drastically slowing down development turnaround

times. Innovations such as MISER (Multiple Injections in a Single Experimental Run),[2] MALDI–TOF–MS (Matrix-Assisted Laser Desorption/Ionization Time-Of-Flight Mass Spectrometry),[76] and NL–ADE–MS (Neutral Loss Acoustic Droplet Ejection Mass Spectrometry)[77] has cut analytical runtimes down to ~1 to 2 seconds per sample using custom instrumentation systems. While these methods pave significant ground in improving analytical turnaround times, they also have notable limitations such as expensive and specialized equipment or provide only limited reaction data that can impede identification of side product formation or starting material conversion.

Alternate lower-throughput methods have been developed that simply seek to better facilitate untargeted reaction discovery. In 2011, the MacMillan group reported on their "Accelerated Serendipity" technique to expedite the discovery of "serendipitous" or seemingly random chemical reactions.[78] Applied to high-throughput photoredox chemistry, they dosed pairwise combinations of their selected substrate pool into a 96-well plate followed by templating of a designated catalytic system (i.e. catalyst, ligand, additive, solvent) to the whole plate. Each 96-well screen representing a single catalytic system applied to all possible combinations of their substrates. Downstream GC–MS data collection and comparison to an NIST mass spectral library enabled them to identify the α-functionalization of N,N-dimethylaniline by 1,4-dicyanobenzene to form the corresponding α-aryl amine **1** (Figure 1-5). Later investigation of the reaction conditions identified $Ir(ppy)_3$ as a higher performing catalyst, achieving α-arylation of a variety of amines in 78-98% yields.

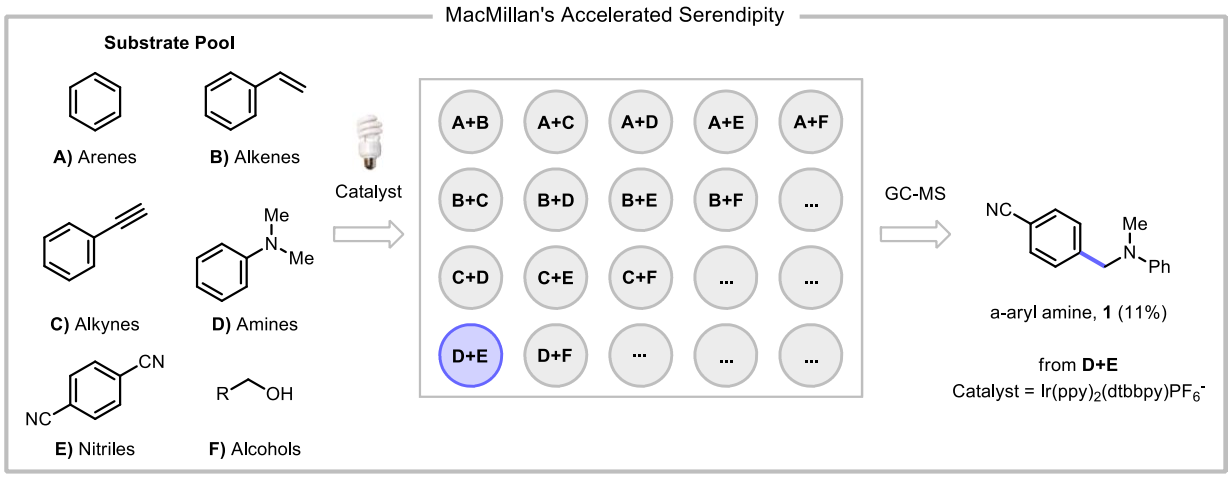


Figure 1-5 Accelerated Serendipity approach to screening of random chemical space. Two substrates from the substrate pool are dosed to each well in the reaction plate followed by dosing of a selected catalyst system to the whole plate. GC-MS analysis of well containing amine **D** and nitrile **E** identified an α-arylation reaction.

Further work in the space of high-throughput untargeted reaction discovery aimed to expand on the concept of accelerated serendipity using a carefully chosen substrate pools to better facilitate the deconvolution of complex reaction data. Hartwig and co-workers introduced the concept of "Snap Deconvolution" which leverages a unique substrate pooling technique to better facilitate the analysis of high-throughput experiments.[79] Creation of three different substrate pools that vary from the other substrate pools by a unique mass handle enables more confident determination of reactivity. For example, the three pools each containing either octylamine, decylamine, or dodecylamine would yield the same reaction product, but differing by 28 amu between the three reaction pools. High-resolution mass spectrometry can then identify the appropriate product masses from all three reactions to verify reaction is occurring between the expected substrates. From a series of 96-well screens on various transition metal catalysts, they were able to identify both a novel nickel-catalyzed alkyne hydroallylation reaction and a novel nickel-catalyzed alkyne diarylation reaction by their snap deconvolution method (Figure 1-6).

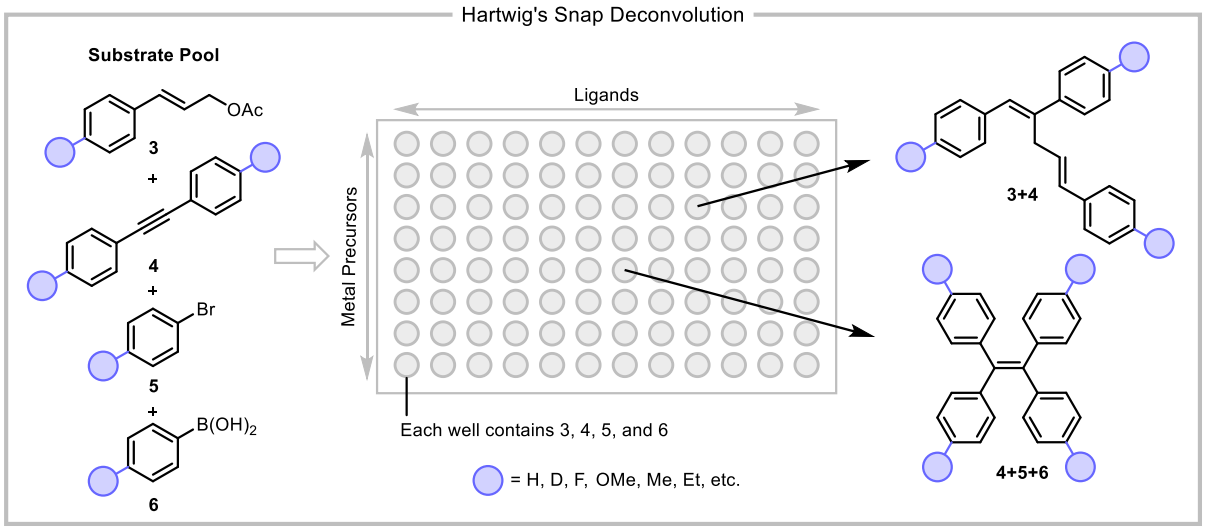


Figure 1-6 Depiction of the Snap Deconvolution technique, where pooled substrates are subjected to transition metal catalysis in triplicate 96-well plate experiments. Each separate 96-well plate uses the same catalysts, but a different pool of substrates with unique mass handles is used (represented by blue balls). If High-Resolution Mass Spectrometry identifies corresponding product masses in all three plates, reactivity is confirmed.

Collectively, these chromatographic and spectrometric platforms represent the current state of the art in high-throughput reaction analysis. However, they are not without their own limitations, either on the range of compatible substrates, requirements for high-end instrumentation, with sacrificing experimental throughput or the breadth of analytical data.

There is of course no definitive answer for what analytical method works best for all applications, but it is certain there is demand for faster and more reliable reaction analysis.

1.4.2 ***Colorimetric and Fluorometric Methods***

Despite the dominance of chromatographic and spectrometric techniques, a wide variety of colorimetric and fluorimetric methods have also been developed for high-throughput environments. Their direct outputs, such as an observable color change or direct fluorescence reading, can provide a rapid initial greenlight for reaction success, then allowing for more comprehensive analysis on those select reaction wells. These optical signals provide little structural data themselves but allow chemists to rapidly determine whether a transformation has occurred without exhaustive spectral analysis. Although these methods have not yet achieved the same level of standardization or generality as LC–MS or GC–MS, current research has established their validity in the rapid monitoring chemical transformations.

One of the earliest examples is the Crabtree group's colorimetric hydrogenation assay, which employed highly conjugated ferrocene dyes to visualize a hydrogenation reaction.[80] A designer substrate is used that links ferrocene to an N-alkyl pyridinium salt via either an alkene or imine (**7**). The highly conjugated pi-system is broken as metal-catalyzed hydrosilation progresses and the alkene/imine linker is hydrogenated (**8**, Figure 1-7). A camera enables recording of the loss of color as hydrogenation occurs to determine the most efficient metal catalysts for hydrogenation. While this system is highly convenient, it can be prone to error if a colored catalyst is added or if the hydrogenated product still retains color.

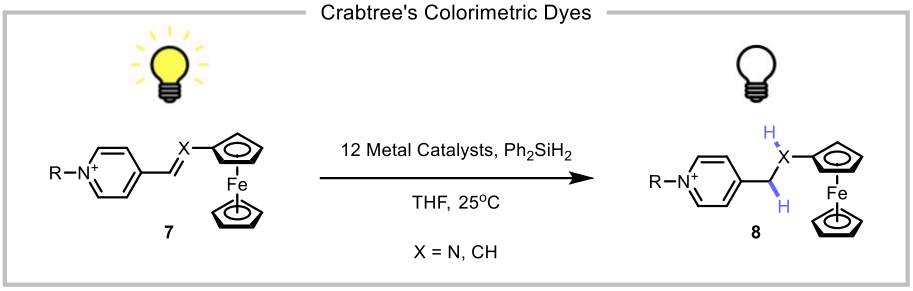


Figure 1-7 The use of conjugated ferrocene dyes to colorimetrically analyze a hydrosilation reaction. As reaction progresses, the conjugated linker is saturated and the dye color diminishes which can be visually distinguished.

Later work by the Barbas' lab demonstrated the fluorimetric analysis of an Aldol condensation using a fluorescent probe that is initially quenched by an aldehyde present on the same molecule.[81] Upon condensation of aldehyde **9** with acetone, an immediate signal is observable by fluorescent plate reading as the aldehyde is converted to the corresponding β-

hydroxy ketone (**10**, Figure 1-8). Alternate modifications of the aldehyde quencher such as indium-catalyzed allylation or sodium cyanoborohydride reduction to an alcohol revealed the same restoration of fluorescence to the appended pi-system. This system presents a highly quantitative approach to fluorometric reaction analysis, wherein the magnitude of fluorescence can be measured and correlated with reaction progress. Though only showcased on benchtop scale, the system can reasonably be appended to more a high-throughput format and is likely tolerable of replacing the aldehyde with alternate quenching functionalities. A similar application by the Buchwald group enables detection of boronic acids which are typically difficult to monitor.[82] A fluorescence turn-on mechanism occurs through reaction of a custom coumarin dye with any boronic acid present in a reaction mixture to produce a fluorescent solution when held up to a handheld UV lamp.

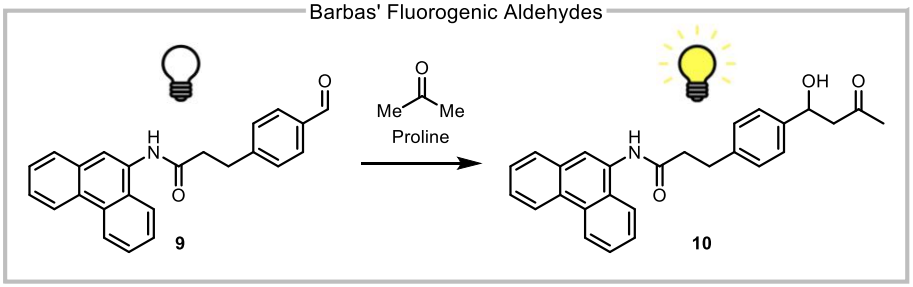


Figure 1-8 The use of fluorogenic dyes containing an intramolecular aldehyde quencher. Upon reaction of the aldehyde functionality fluorescence is restored and can be directly quantitated using fluorescence plate reading.

As a last case study, we will look at a series of papers from the Hartwig group, initially published in 2001. They looked at the application of Fluorescence Resonance Energy Transfer (FRET) to the exploration of a series of palladium–catalyzed coupling reactions. Here, we will give a brief description of FRET as Chapter 3 will have a more detailed look at developing FRET for high-throughput chemistry. To briefly discuss the concept, FRET is a complex mechanism by which energy is transferred between two dyes in close spatial proximity (1-10 nanometers).[83] These dyes must also have overlapping spectral properties such that the fluorescence emission band of one dye overlaps with the excitation band of the other dye. As a result of the distance dependence, FRET can be used as a benchmark to indicate successful coupling of fluorescently labelled substrates that would otherwise not undergo FRET when uncoupled.

Here we will discuss the Hartwig's group results in the application of FRET towards screening conditions for room temperature Mizoroki−Heck couplings.[84] Their method relies on

the quenching of the initially fluorescent dansyl dye **11** by a coupled azodye **12** (Figure 1-9). As a result, the successfully coupled substrates have lower fluorescence than that of the uncoupled starting materials. In the screening of phosphine ligands for Heck reactions, they were able to identify 15 new ligands capable of generating at least 70% yield on initial screening. The authors also note that traditional LC–MS analysis showed only one of these conditions produced results more than 10% different by the FRET assay yield.

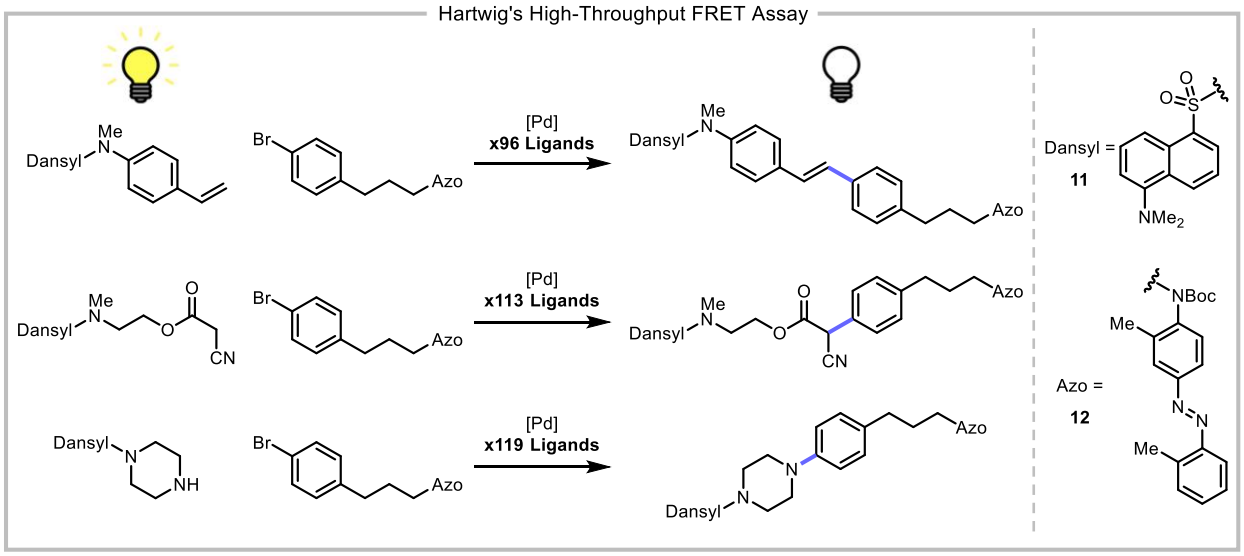


Figure 1-9 Three applications of Hartwig's FRET assay to screening palladium-catalyzed reaction conditions. First used to analyze high-throughput Mizoroki-Heck couplings, then α-arylation of cyanoacetates, and finally amine arylation conditions.

Following these results, the authors went on to test the application of the same FRET assay in screening conditions for the arylation of cyanoacetates.[85] Expanding their ligand library to include 113 various phosphine, N-heterocyclic carbene (NHC), and nitrogen–based ligands, 12 of these reported results greater than 20% yield of the desired α-arylated product. Assay yields were lower this time around due to the starting cyanoacetate reportedly undergoing partial hydrolysis during reaction. Further optimization of conditions at benchtop scale enabled their best ligand, tri-*tert*-butylphosphine, to give a final α–arylation yield of 90%.

In the last study, their dansyl dye was modified with a piperazine ring to enable optimization of C–N coupling conditions.[86] Their 119-ligand library was screened in duplicate reactions towards the coupling of their dansyl and azo dyes. From their duplicate experiments, 16 of the 119 reaction conditions had greater than 30% variation between experiments. The authors surmised that variations in the aliquots taken from each reaction likely accounted for this

difference in yield. Another important note is the detection of two false-positive hits, wherein promiscuous or chemically unstable ligands appeared to either react directly with the dyes or act as fluorescence quenchers. A final four ligands were looked at as having notably lower yields in their FRET assay than expected by previous literature reports. From control experiments, the interaction of the azodye with those particular metal-ligand combinations was found responsible for the ~40% lower yields. Beyond these outliers, several bulky phosphine and NHC ligands reported yields above 60% for palladium-catalyzed C–N coupling.

Collectively, these studies provide a solid basis for both colorimetric and fluorometric methods in the rapid analysis of high-throughput experiments. While there exist several nuances to these systems, they provide a complimentary approach to the more traditional chromatographic and spectrometric approaches used in HTE analysis.

1.5 **Limitations of Modern HTE**

Despite its profound impact on modern chemistry, high-throughput experimentation remains an evolving practice with several technical and analytical limitations that impede its more widescale adoption. The most frequent concern users have when approaching HTE is whether the time invested to ensure accurate setup, execution, and analysis of your reaction will take longer than engaging in slower but simpler preparative-scale experiments. Additionally, the expense of materials and robotics platforms is a significant issue regarding how accessible HTE is to many academic labs.

Between considerations of solvent volatility and compatibility with plastic components, homogeneity of slurries, reaction atmosphere or pressure requirements, execution of more exotic reaction setups can present a significant hurdle on miniaturized scale. Many of these problems are more manageable at 24, 96, or even 384-well formats, however the reproducibility and performance tend to suffer as the reaction scale decreases, especially 1,536-well format. Replicate reactions or experiments can be carried out to determine the reliability of a method but require sacrificing additional materials or limit the breadth of unique conditions that can be tested.

Despite these limitations, the trajectory of HTE points toward increasing integration of automation and high-throughput techniques, both in academia and industry. Many of the current challenges to HTE implementation can be overcome as more precise, reliable, and accessible instrumentation is developed in the near future.

1.6 **References**

(1) Maier, W. F. Early Years of High-Throughput Experimentation and Combinatorial Approaches in Catalysis and Materials Science. *ACS Comb. Sci.* **2019**, *21* (6), 437–444. https://doi.org/10.1021/acscombsci.8b00189.

(2) Santanilla, A. B.; Regalado, E. L.; Pereira, T.; Shevlin, M.; Bateman, K.; Campeau, L.-C.; Schneeweis, J.; Berritt, S.; Shi, Z.-C.; Nantermet, P.; Liu, Y.; Helmy, R.; Welch, C. J.; Vachal, P.; Davies, I. W.; Cernak, T.; Dreher, S. D. Nanomole-Scale High-Throughput Chemistry for the Synthesis of Complex Molecules. *Science* **2015**. https://doi.org/10.1126/science.1259203.

(3) Pereira, D. A.; Williams, J. A. Origin and Evolution of High Throughput Screening. *Br. J. Pharmacol.* **2007**, *152* (1), 53–61. https://doi.org/10.1038/sj.bjp.0707373.

(4) Takátsy, G. The Use of Spiral Loops in Serological and Virological Micro-Methods. 1955. *Acta Microbiol. Immunol. Hung.* **2003**, *50* (4), 369–382; discussion 382-383. https://doi.org/10.1556/AMicr.50.2003.4.5.

(5) Merrifield, R. B.; Stewart, J. Morrow.; Jernberg, Nils. Instrument for Automated Synthesis of Peptides. *Anal. Chem.* **1966**, *38* (13), 1905–1914. https://doi.org/10.1021/ac50155a057.

(6) Schnorrenberg, G.; Gerhardt, H. Fully Automatic Simultaneous Multiple Peptide Synthesis in Micromolar Scale - Rapid Synthesis of Series of Peptides for Screening in Biological Assays. *Tetrahedron* **1989**, *45* (24), 7759–7764. https://doi.org/10.1016/S0040-4020(01)85791-4.

(7) Geysen, H. M.; Meloen, R. H.; Barteling, S. J. Use of Peptide Synthesis to Probe Viral Antigens for Epitopes to a Resolution of a Single Amino Acid. *Proc. Natl. Acad. Sci.* **1984**, *81* (13), 3998–4002. https://doi.org/10.1073/pnas.81.13.3998.

(8) Maier, W. F. Early Years of High-Throughput Experimentation and Combinatorial Approaches in Catalysis and Materials Science. *ACS Comb. Sci.* **2019**, *21* (6), 437–444. https://doi.org/10.1021/acscombsci.8b00189.

(9) Bunin, B. A.; Ellman, J. A. A General and Expedient Method for the Solid-Phase Synthesis of 1,4-Benzodiazepine Derivatives. *J. Am. Chem. Soc.* **1992**, *114* (27), 10997–10998. https://doi.org/10.1021/ja00053a067.

(10) Reetz, M. T. Combinatorial and Evolution-Based Methods in the Creation of Enantioselective Catalysts. *Angew. Chem. Int. Ed.* **2001**, *40* (2), 284–310.

https://doi.org/10.1002/1521-3773(20010119)40:2%253C284::AID-ANIE284%253E3.0.CO;2-N.

(11) Chun, S.; Xu, J.; Cheng, J.; Ding, L.; Winograd, N.; Fenniri, H. Spectroscopically Encoded Resins for High Throughput Imaging Time-of-Flight Secondary Ion Mass Spectrometry. *J. Comb. Chem.* **2006**, *8* (1), 18–25. https://doi.org/10.1021/cc050086y.

(12) Balkenhohl, F.; von dem Bussche-Hünnefeld, C.; Lansky, A.; Zechel, C. Combinatorial Synthesis of Small Organic Molecules. *Angew. Chem. Int. Ed. Engl.* **1996**, *35* (20), 2288–2337. https://doi.org/10.1002/anie.199622881.

(13) Ding, K.; Du, H.; Yuan, Y.; Long, J. Combinatorial Chemistry Approach to Chiral Catalyst Engineering and Screening: Rational Design and Serendipity. *Chem. – Eur. J.* **2004**, *10* (12), 2872–2884. https://doi.org/10.1002/chem.200305707.

(14) Sun, A. C.; Steyer, D. J.; Allen, A. R.; Payne, E. M.; Kennedy, R. T.; Stephenson, C. R. J. A Droplet Microfluidic Platform for High-Throughput Photochemical Reaction Discovery. *Nat. Commun.* **2020**, *11* (1), 6202. https://doi.org/10.1038/s41467-020-19926-z.

(15) González-Esguevillas, M.; Fernández, D. F.; Rincón, J. A.; Barberis, M.; de Frutos, O.; Mateos, C.; García-Cerrada, S.; Agejas, J.; MacMillan, D. W. C. Rapid Optimization of Photoredox Reactions for Continuous-Flow Systems Using Microscale Batch Technology. *ACS Cent. Sci.* **2021**, *7* (7), 1126–1134. https://doi.org/10.1021/acscentsci.1c00303.

(16) Gesmundo, N. J.; Sarris, K.; Sawicki, J. W.; Wang, Y.; Radosevich, A. J.; Pan, J. Y. High-Throughput Experimentation for Photoredox Cross-Couplings Using the Automated Photoredox Optimization Reactor. *React. Chem. Eng.* **2025**. https://doi.org/10.1039/D5RE00241A.

(17) Rein, J.; Annand, J. R.; Wismer, M. K.; Fu, J.; Siu, J. C.; Klapars, A.; Strotman, N. A.; Kalyani, D.; Lehnherr, D.; Lin, S. Unlocking the Potential of High-Throughput Experimentation for Electrochemistry with a Standardized Microscale Reactor. *ACS Cent. Sci.* **2021**. https://doi.org/10.1021/acscentsci.1c00328.

(18) Becker, R.; Weber, K.; Pfeiffer, T. V.; Kranendonk, J. van; Schouten, K. J. A Scalable High-Throughput Deposition and Screening Setup Relevant to Industrial Electrocatalysis. *Catalysts* **2020**, *10* (10), 1165. https://doi.org/10.3390/catal10101165.

(19) Mo, Y.; Rughoobur, G.; Nambiar, A. M. K.; Zhang, K.; Jensen, K. F. A Multifunctional Microfluidic Platform for High-Throughput Experimentation of Electroorganic Chemistry.

Angew. Chem. Int. Ed. **2020**, *59* (47), 20890–20894. https://doi.org/10.1002/anie.202009819.

(20) Silva, J. D. J.; Ferreira, M. A. B.; Fedorov, A.; Sigman, M. S.; Copéret, C. Molecular-Level Insight in Supported Olefin Metathesis Catalysts by Combining Surface Organometallic Chemistry, High Throughput Experimentation, and Data Analysis. *Chem. Sci.* **2020**, *11* (26), 6717–6723. https://doi.org/10.1039/D0SC02594A.

(21) Douthwaite, J. L.; Zhao, R.; Shim, E.; Mahjour, B.; Zimmerman, P. M.; Cernak, T. Formal Cross-Coupling of Amines and Carboxylic Acids to Form Sp3–Sp2 Carbon–Carbon Bonds. *J. Am. Chem. Soc.* **2023**, *145* (20), 10930–10937. https://doi.org/10.1021/jacs.2c11563.

(22) Shen, Y.; Mahjour, B.; Cernak, T. Development of Copper-Catalyzed Deaminative Esterification Using High-Throughput Experimentation. *Commun. Chem.* **2022**, *5* (1), 83. https://doi.org/10.1038/s42004-022-00698-0.

(23) Zhang, Z.; Cernak, T. The Formal Cross-Coupling of Amines and Carboxylic Acids to Form Sp3–Sp3 Carbon–Carbon Bonds. *Angew. Chem. Int. Ed.* **2021**, *60* (52), 27293–27298. https://doi.org/10.1002/anie.202112454.

(24) Burns, M.; Martinez, C. A.; Vanderplas, B.; Wisdom, R.; Yu, S.; Singer, R. A. A Chemoenzymatic Route to Chiral Intermediates Used in the Multikilogram Synthesis of a Gamma Secretase Inhibitor. *Org. Process Res. Dev.* **2017**, *21* (6), 871–877. https://doi.org/10.1021/acs.oprd.7b00096.

(25) Savile, C. K.; Janey, J. M.; Mundorff, E. C.; Moore, J. C.; Tam, S.; Jarvis, W. R.; Colbeck, J. C.; Krebber, A.; Fleitz, F. J.; Brands, J.; Devine, P. N.; Huisman, G. W.; Hughes, G. J. Biocatalytic Asymmetric Synthesis of Chiral Amines from Ketones Applied to Sitagliptin Manufacture. *Science* **2010**, *329* (5989), 305–309. https://doi.org/10.1126/science.1188934.

(26) Champagne, S. E.; Chiang, C.-H.; Gemmel, P. M.; Brooks, C. L. I.; Narayan, A. R. H. Biocatalytic Stereoselective Oxidation of 2-Arylindoles. *J. Am. Chem. Soc.* **2024**, *146* (4), 2728–2735. https://doi.org/10.1021/jacs.3c12393.

(27) Hernández-Meléndez, J. R.; Paton, A. E.; Perkins, J. C.; Yang, D.; Chiang, C.-H.; Narayan, A. R. H. Ancestral Sequence Reconstruction to Accelerate Non-Heme Iron-

Dependent Biocatalyst Engineering. *ACS Cent. Sci.* **2025**. https://doi.org/10.1021/acscentsci.5c01137.

(28) Cernak, T.; Dykstra, K. D.; Tyagarajan, S.; Vachal, P.; Krska, S. W. The Medicinal Chemist's Toolbox for Late Stage Functionalization of Drug-like Molecules. *Chem. Soc. Rev.* **2016**, *45* (3), 546–576. https://doi.org/10.1039/C5CS00628G.

(29) Mennen, S. M.; Alhambra, C.; Allen, C. L.; Barberis, M.; Berritt, S.; Brandt, T. A.; Campbell, A. D.; Castañón, J.; Cherney, A. H.; Christensen, M.; Damon, D. B.; Eugenio de Diego, J.; García-Cerrada, S.; García-Losada, P.; Haro, R.; Janey, J.; Leitch, D. C.; Li, L.; Liu, F.; Lobben, P. C.; MacMillan, D. W. C.; Magano, J.; McInturff, E.; Monfette, S.; Post, R. J.; Schultz, D.; Sitter, B. J.; Stevens, J. M.; Strambeanu, I. I.; Twilton, J.; Wang, K.; Zajac, M. A. The Evolution of High-Throughput Experimentation in Pharmaceutical Development and Perspectives on the Future. *Org. Process Res. Dev.* **2019**, *23* (6), 1213–1242. https://doi.org/10.1021/acs.oprd.9b00140.

(30) Friis, S. D.; Johansson, M. J.; Ackermann, L. Cobalt-Catalysed C–H Methylation for Late-Stage Drug Diversification. *Nat. Chem.* **2020**, *12* (6), 511–519. https://doi.org/10.1038/s41557-020-0475-7.

(31) Liu, D.-H.; Pflüger, P. M.; Outlaw, A.; Lückemeier, L.; Zhang, F.; Regan, C.; Rashidi Nodeh, H.; Cernak, T.; Ma, J.; Glorius, F. Late-Stage Saturation of Drug Molecules. *J. Am. Chem. Soc.* **2024**, *146* (17), 11866–11875. https://doi.org/10.1021/jacs.4c00807.

(32) Gesmundo, N. J.; Sauvagnat, B.; Curran, P. J.; Richards, M. P.; Andrews, C. L.; Dandliker, P. J.; Cernak, T. Nanoscale Synthesis and Affinity Ranking. *Nature* **2018**, *557* (7704), 228–232. https://doi.org/10.1038/s41586-018-0056-8.

(33) Greshock, T. J.; Moore, K. P.; McClain, R. T.; Bellomo, A.; Chung, C. K.; Dreher, S. D.; Kutchukian, P. S.; Peng, Z.; Davies, I. W.; Vachal, P.; Ellwart, M.; Manolikakes, S. M.; Knochel, P.; Nantermet, P. G. Synthesis of Complex Druglike Molecules by the Use of Highly Functionalized Bench-Stable Organozinc Reagents. https://doi.org/10.1002/anie.201604652.

(34) Ichiishi, N.; Moore, K. P.; Wassermann, A. M.; Wolkenberg, S. E.; Krska, S. W. Reducing Limitation in Probe Design: The Development of a Diazirine-Compatible Suzuki–Miyaura Cross Coupling Reaction. *ACS Med. Chem. Lett.* **2019**, *10* (1), 56–61. https://doi.org/10.1021/acsmedchemlett.8b00403.

(35) Rohrbach, S.; Šiaučiulis, M.; Chisholm, G.; Pirvan, P.-A.; Saleeb, M.; Mehr, S. H. M.; Trushina, E.; Leonov, A. I.; Keenan, G.; Khan, A.; Hammer, A.; Cronin, L. Digitization and Validation of a Chemical Synthesis Literature Database in the ChemPU. *Science* **2022**, *377* (6602), 172–180. https://doi.org/10.1126/science.abo0058.

(36) Steiner, S.; Wolf, J.; Glatzel, S.; Andreou, A.; Granda, J. M.; Keenan, G.; Hinkley, T.; Aragon-Camarasa, G.; Kitson, P. J.; Angelone, D.; Cronin, L. Organic Synthesis in a Modular Robotic System Driven by a Chemical Programming Language. *Science* **2019**, *363* (6423), eaav2211. https://doi.org/10.1126/science.aav2211.

(37) Boga, S. B.; Christensen, M.; Perrotto, N.; Krska, S. W.; Dreher, S.; Tudge, M. T.; Ashley, E. R.; Poirier, M.; Reibarkh, M.; Liu, Y.; Streckfuss, E.; Campeau, L.-C.; Ruck, R. T.; Davies, I. W.; Vachal, P. Selective Functionalization of Complex Heterocycles via an Automated Strong Base Screening Platform. *React. Chem. Eng.* **2017**, *2* (4), 446–450. https://doi.org/10.1039/C7RE00057J.

(38) Fu, J.; Vaughn, Z.; Nolting, A. F.; Gao, Q.; Yang, D.; Schuster, C. H.; Kalyani, D. Diastereoselective Reductive Etherification Via High-Throughput Experimentation: Access to Pharmaceutically Relevant Alkyl Ethers. *J. Org. Chem.* **2023**, *88* (19), 13454–13465. https://doi.org/10.1021/acs.joc.3c00822.

(39) Burger, B.; Maffettone, P. M.; Gusev, V. V.; Aitchison, C. M.; Bai, Y.; Wang, X.; Li, X.; Alston, B. M.; Li, B.; Clowes, R.; Rankin, N.; Harris, B.; Sprick, R. S.; Cooper, A. I. A Mobile Robotic Chemist. *Nature* **2020**, *583* (7815), 237–241. https://doi.org/10.1038/s41586-020-2442-2.

(40) Godfrey, A. G.; Masquelin, T.; Hemmerle, H. A Remote-Controlled Adaptive Medchem Lab: An Innovative Approach to Enable Drug Discovery in the 21st Century. *Drug Discov. Today* **2013**, *18* (17), 795–802. https://doi.org/10.1016/j.drudis.2013.03.001.

(41) Chatterjee, S.; Guidi, M.; Seeberger, P. H.; Gilmore, K. Automated Radial Synthesis of Organic Molecules. *Nature* **2020**, *579* (7799), 379–384. https://doi.org/10.1038/s41586-020-2083-5.

(42) Tanaka, Y.; Fuse, S.; Tanaka, H.; Doi, T.; Takahashi, T. An Efficient Synthesis of a Cyclic Ether Key Intermediate for 9-Membered Masked Enediyne Using an Automated Synthesizer. *Org. Process Res. Dev.* **2009**, *13* (6), 1111–1121. https://doi.org/10.1021/op9002455.

(43) Douthwaite, J. L.; Houde, D. J.; Pardo, E. H.; Moran, M. S.; Baird, J.; Meyer, S. R.; Mahjour, B.; Zhao, Q.; Larrow, J. F.; Juang, Y.-P.; Han, C. K.; Kelley, B.; Dunstan, D. R.; Billings, K. J.; Mader, M. M.; Taylor, A. M.; Sexton, J. Z.; Boezio, A. A.; Cernak, T. Nanoscale Direct-to-Biology Optimization of Cdk2 Inhibitors. ChemRxiv April 17, 2025. https://doi.org/10.26434/chemrxiv-2025-4fr3l.

(44) Mahjour, B.; Zhang, R.; Shen, Y.; McGrath, A.; Zhao, R.; Mohamed, O. G.; Lin, Y.; Zhang, Z.; Douthwaite, J. L.; Tripathi, A.; Cernak, T. Rapid Planning and Analysis of High-Throughput Experiment Arrays for Reaction Discovery. *Nat. Commun.* **2023**, *14* (1), 3924. https://doi.org/10.1038/s41467-023-39531-0.

(45) Friedfeld, M. R.; Shevlin, M.; Hoyt, J. M.; Krska, S. W.; Tudge, M. T.; Chirik, P. J. Cobalt Precursors for High-Throughput Discovery of Base Metal Asymmetric Alkene Hydrogenation Catalysts. *Science* **2013**, *342* (6162), 1076–1080. https://doi.org/10.1126/science.1243550.

(46) Izquierdo-Ferrer, J.; Bellizzi, M. E.; Tu, N.; Bogdan, A.; Wang, Y. A Miniaturized Chemical High Throughput Experimentation Plate to Enable Late-Stage Oxidation Screening and Scale-Up. *ACS Med. Chem. Lett.* **2025**, *16* (6), 916–924. https://doi.org/10.1021/acsmedchemlett.5c00175.

(47) Lin, D.-Z.; Pan, K.-J.; Li, Y.; Charles B.; Zhang, L.; Jayarapu, K. N.; Li, T.; Tran, J. V.; Goddard, W. A.; Luo, Z.; Liu, Y. A High-Throughput Experimentation Platform for Data-Driven Discovery in Electrochemistry. *Sci. Adv.* **2025**, *11* (14), eadu4391. https://doi.org/10.1126/sciadv.adu4391.

(48) Foppa, L.; Sutton, C.; Ghiringhelli, L. M.; De, S.; Löser, P.; Schunk, S. A.; Schäfer, A.; Scheffler, M. Learning Design Rules for Selective Oxidation Catalysts from High-Throughput Experimentation and Artificial Intelligence. *ACS Catal.* **2022**, *12* (4), 2223–2232. https://doi.org/10.1021/acscatal.1c04793.

(49) Ahneman, D. T.; Estrada, J. G.; Lin, S.; Dreher, S. D.; Doyle, A. G. Predicting Reaction Performance in C–N Cross-Coupling Using Machine Learning. *Science* **2018**, *360* (6385), 186–190. https://doi.org/10.1126/science.aar5169.

(50) Shields, B. J.; Stevens, J.; Li, J.; Parasram, M.; Damani, F.; Alvarado, J. I. M.; Janey, J. M.; Adams, R. P.; Doyle, A. G. Bayesian Reaction Optimization as a Tool for Chemical Synthesis. *Nature* **2021**, *590* (7844), 89–96. https://doi.org/10.1038/s41586-021-03213-y.

(51) Ickes, A. R.; Liles, J. P.; Borlinghaus, N.; Henle, J.; Swiatowiec, R.; Prakash Kaushik, N.; Braje, W. M.; Harper, K. C.; Shekhar, S.; Sigman, M. S. Leveraging Data Science to Elucidate Ligand Features for Pd-Catalyzed Enantioretentive N-Arylations of Cyclic α-Substituted Amines in Aqueous Media. *J. Am. Chem. Soc.* **2025**, *147* (32), 28981–28992. https://doi.org/10.1021/jacs.5c07224.

(52) Caldentey, X.; Romero, E. High-Throughput Experimentation as an Accessible Technology for Academic Organic Chemists in Europe and Beyond. *Chemistry–Methods* **2023**, *3* (5), e202200059. https://doi.org/10.1002/cmtd.202200059.

(53) Dingerdissen, U.; Linke, D. Scopes and Limitations of High Throughput Preparation and Screening Tools. In *Studies in Surface Science and Catalysis*; Gaigneaux, E. M., Devillers, M., De Vos, D. E., Hermans, S., Jacobs, P. A., Martens, J. A., Ruiz, P., Eds.; Scientific Bases for the Preparation of Heterogeneous Catalysts; Elsevier, 2006; Vol. 162, pp 1–12. https://doi.org/10.1016/S0167-2991(06)80884-0.

(54) Gaunt, M. J.; Janey, J. M.; Schultz, D. M.; Cernak, T. Myths of High-Throughput Experimentation and Automation in Chemistry. *Chem* **2021**, *7* (9), 2259–2260. https://doi.org/10.1016/j.chempr.2021.08.012.

(55) Tu, N. P.; Dombrowski, A. W.; Goshu, G. M.; Vasudevan, A.; Djuric, S. W.; Wang, Y. High-Throughput Reaction Screening with Nanomoles of Solid Reagents Coated on Glass Beads. *Angew. Chem. Int. Ed.* **2019**, *58* (24), 7987–7991. https://doi.org/10.1002/anie.201900536.

(56) Uehling, M. R.; King, R. P.; Krska, S. W.; Cernak, T.; Buchwald, S. L. Pharmaceutical Diversification via Palladium Oxidative Addition Complexes. *Science* **2019**, *363* (6425), 405–408. https://doi.org/10.1126/science.aac6153.

(57) Wang, Y.; Shaabani, S.; Ahmadianmoghaddam, M.; Gao, L.; Xu, R.; Kurpiewska, K.; Kalinowska-Tluscik, J.; Olechno, J.; Ellson, R.; Kossenjans, M.; Helan, V.; Groves, M.; Dömling, A. Acoustic Droplet Ejection Enabled Automated Reaction Scouting. *ACS Cent. Sci.* **2019**, *5* (3), 451–457. https://doi.org/10.1021/acscentsci.8b00782.

(58) Shaabani, S.; Xu, R.; Ahmadianmoghaddam, M.; Gao, L.; Stahorsky, M.; Olechno, J.; Ellson, R.; Kossenjans, M.; Helan, V.; Dömling, A. Automated and Accelerated Synthesis of Indole Derivatives on a Nano-Scale. *Green Chem.* **2019**, *21* (2), 225–232. https://doi.org/10.1039/C8GC03039A.

(59) Mahjour, B.; Zhang, R.; Shen, Y.; McGrath, A.; Zhao, R.; Mohamed, O. G.; Lin, Y.; Zhang, Z.; Douthwaite, J. L.; Tripathi, A.; Cernak, T. Rapid Planning and Analysis of High-Throughput Experiment Arrays for Reaction Discovery. *Nat. Commun.* **2023**, *14* (1), 3924. https://doi.org/10.1038/s41467-023-39531-0.

(60) Lin, S.; Dikler, S.; Blincoe, W. D.; Ferguson, R. D.; Sheridan, R. P.; Peng, Z.; Conway, D. V.; Zawatzky, K.; Wang, H.; Cernak, T.; Davies, I. W.; DiRocco, D. A.; Sheng, H.; Welch, C. J.; Dreher, S. D. Mapping the Dark Space of Chemical Reactions with Extended Nanomole Synthesis and MALDI-TOF MS. *Science* **2018**, *361* (6402), eaar6236. https://doi.org/10.1126/science.aar6236.

(61) Boga, S. B.; Christensen, M.; Perrotto, N.; Krska, S. W.; Dreher, S.; Tudge, M. T.; Ashley, E. R.; Poirier, M.; Reibarkh, M.; Liu, Y.; Streckfuss, E.; Campeau, L.-C.; Ruck, R. T.; Davies, I. W.; Vachal, P. Selective Functionalization of Complex Heterocycles via an Automated Strong Base Screening Platform. *React. Chem. Eng.* **2017**, *2* (4), 446–450. https://doi.org/10.1039/C7RE00057J.

(62) Christensen, M.; Yunker, L. P. E.; Adedeji, F.; Häse, F.; Roch, L. M.; Gensch, T.; dos Passos Gomes, G.; Zepel, T.; Sigman, M. S.; Aspuru-Guzik, A.; Hein, J. E. Data-Science Driven Autonomous Process Optimization. *Commun. Chem.* **2021**, *4* (1), 112. https://doi.org/10.1038/s42004-021-00550-x.

(63) Mehr, S. H. M.; Craven, M.; Leonov, A. I.; Keenan, G.; Cronin, L. A Universal System for Digitization and Automatic Execution of the Chemical Synthesis Literature. *Science* **2020**, *370* (6512), 101–108. https://doi.org/10.1126/science.abc2986.

(64) Baranczak, A.; Tu, N. P.; Marjanovic, J.; Searle, P. A.; Vasudevan, A.; Djuric, S. W. Integrated Platform for Expedited Synthesis–Purification–Testing of Small Molecule Libraries. *ACS Med. Chem. Lett.* **2017**, *8* (4), 461–465. https://doi.org/10.1021/acsmedchemlett.7b00054.

(65) *Lilly launches new robotic laboratory - Journal for Clinical Studies*. https://journalforclinicalstudies.com/lilly-launches-new-robotic-laboratory/ (accessed 2025-11-02).

(66) *The AstraZeneca iLab*. https://www.astrazeneca.com/content/astraz/r-d/our-technologies/ilab.html (accessed 2025-11-02).

(67) Baranczak, A.; Tu, N. P.; Marjanovic, J.; Searle, P. A.; Vasudevan, A.; Djuric, S. W. Integrated Platform for Expedited Synthesis–Purification–Testing of Small Molecule Libraries. *ACS Med. Chem. Lett.* **2017**, *8* (4), 461–465. https://doi.org/10.1021/acsmedchemlett.7b00054.

(68) Alben, K. T. Books and Software: Design, Analyze, and Optimize with Design-Expert. *Anal. Chem.* **2002**, *74* (7), 222 A-223 A. https://doi.org/10.1021/ac0219703.

(69) Mahjour, B.; Zhang, R.; Shen, Y.; McGrath, A.; Zhao, R.; Mohamed, O. G.; Lin, Y.; Zhang, Z.; Douthwaite, J. L.; Tripathi, A.; Cernak, T. Rapid Planning and Analysis of High-Throughput Experiment Arrays for Reaction Discovery. *Nat. Commun.* **2023**, *14* (1), 3924. https://doi.org/10.1038/s41467-023-39531-0.

(70) Schmid, R.; Heuckeroth, S.; Korf, A.; Smirnov, A.; Myers, O.; Dyrlund, T. S.; Bushuiev, R.; Murray, K. J.; Hoffmann, N.; Lu, M.; Sarvepalli, A.; Zhang, Z.; Fleischauer, M.; Dührkop, K.; Wesner, M.; Hoogstra, S. J.; Rudt, E.; Mokshyna, O.; Brungs, C.; Ponomarov, K.; Mutabdžija, L.; Damiani, T.; Pudney, C. J.; Earll, M.; Helmer, P. O.; Fallon, T. R.; Schulze, T.; Rivas-Ubach, A.; Bilbao, A.; Richter, H.; Nothias, L.-F.; Wang, M.; Orešič, M.; Weng, J.-K.; Böcker, S.; Jeibmann, A.; Hayen, H.; Karst, U.; Dorrestein, P. C.; Petras, D.; Du, X.; Pluskal, T. Integrative Analysis of Multimodal Mass Spectrometry Data in MZmine 3. *Nat. Biotechnol.* **2023**, *41* (4), 447–449. https://doi.org/10.1038/s41587-023-01690-2.

(71) *Univariate classification of phosphine ligation state and reactivity in cross-coupling catalysis*. https://doi.org/10.1126/science.abj4213.

(72) Gensch, T.; dos Passos Gomes, G.; Friederich, P.; Peters, E.; Gaudin, T.; Pollice, R.; Jorner, K.; Nigam, A.; Lindner-D'Addario, M.; Sigman, M. S.; Aspuru-Guzik, A. A Comprehensive Discovery Platform for Organophosphorus Ligands for Catalysis. *J. Am. Chem. Soc.* **2022**, *144* (3), 1205–1217. https://doi.org/10.1021/jacs.1c09718.

(73) Murray, B. E.; Penabad, L. I.; Kennedy, R. T. Advances in Coupling Droplet Microfluidics to Mass Spectrometry. *Curr. Opin. Biotechnol.* **2023**, *82*, 102962. https://doi.org/10.1016/j.copbio.2023.102962.

(74) Morato, N. M.; Le, M. T.; Holden, D. T.; Graham Cooks, R. Automated High-Throughput System Combining Small-Scale Synthesis with Bioassays and Reaction Screening. *SLAS Technol.* **2021**, *26* (6), 555–571. https://doi.org/10.1177/24726303211047839.

(75) J. Welch, C. High Throughput Analysis Enables High Throughput Experimentation in Pharmaceutical Process Research. *React. Chem. Eng.* **2019**, *4* (11), 1895–1911. https://doi.org/10.1039/C9RE00234K.

(76) Lin, S.; Dikler, S.; Blincoe, W. D.; Ferguson, R. D.; Sheridan, R. P.; Peng, Z.; Conway, D. V.; Zawatzky, K.; Wang, H.; Cernak, T.; Davies, I. W.; DiRocco, D. A.; Sheng, H.; Welch, C. J.; Dreher, S. D. Mapping the Dark Space of Chemical Reactions with Extended Nanomole Synthesis and MALDI-TOF MS. *Science* **2018**, *361* (6402), eaar6236. https://doi.org/10.1126/science.aar6236.

(77) Hu, M.; Yang, L.; Twarog, N.; Ochoada, J.; Li, Y.; Vrettos, E. I.; Torres-Hernandez, A. X.; Martinez, J. B.; Bhatia, J.; Young, B. M.; Price, J.; McGowan, K.; Nguyen, T. H.; Shi, Z.; Anyanwu, M.; Rimmer, M. A.; Mercer, S.; Rankovic, Z.; Shelat, A. A.; Blair, D. J. Continuous Collective Analysis of Chemical Reactions. *Nature* **2024**, *636* (8042), 374–379. https://doi.org/10.1038/s41586-024-08211-4.

(78) McNally, A.; Prier, C. K.; MacMillan, D. W. C. Discovery of an α-Amino C–H Arylation Reaction Using the Strategy of Accelerated Serendipity. *Science* **2011**, *334* (6059), 1114–1117. https://doi.org/10.1126/science.1213920.

(79) *Snap deconvolution: An informatics approach to high-throughput discovery of catalytic reactions*. https://doi.org/10.1126/science.aan1568.

(80) Cooper, A. C.; McAlexander, L. H.; Lee, D.-H.; Torres, M. T.; Crabtree, R. H. Reactive Dyes as a Method for Rapid Screening of Homogeneous Catalysts. *J. Am. Chem. Soc.* **1998**, *120* (38), 9971–9972. https://doi.org/10.1021/ja9818607.

(81) Tanaka, F.; Mase, N.; Barbas, C. F. Design and Use of Fluorogenic Aldehydes for Monitoring the Progress of Aldehyde Transformations. *J. Am. Chem. Soc.* **2004**, *126* (12), 3692–3693. https://doi.org/10.1021/ja049641a.

(82) Barder, T. E.; Buchwald, S. L. Benchtop Monitoring of Reaction Progress via Visual Recognition with a Handheld UV Lamp: In Situ Monitoring of Boronic Acids in the Suzuki−Miyaura Reaction. *Org. Lett.* **2007**, *9* (1), 137–139. https://doi.org/10.1021/ol062802q.

(83) Sahoo, H. Förster Resonance Energy Transfer – A Spectroscopic Nanoruler: Principle and Applications. *J. Photochem. Photobiol. C Photochem. Rev.* **2011**, *12* (1), 20–30. https://doi.org/10.1016/j.jphotochemrev.2011.05.001.

(84) Stambuli, J. P.; Stauffer, S. R.; Shaughnessy, K. H.; Hartwig, J. F. Screening of Homogeneous Catalysts by Fluorescence Resonance Energy Transfer. Identification of Catalysts for Room-Temperature Heck Reactions. *J. Am. Chem. Soc.* **2001**, *123* (11), 2677–2678. https://doi.org/10.1021/ja0058435.

(85) Stauffer, S. R.; Beare, N. A.; Stambuli, J. P.; Hartwig, J. F. Palladium-Catalyzed Arylation of Ethyl Cyanoacetate. Fluorescence Resonance Energy Transfer as a Tool for Reaction Discovery. *J. Am. Chem. Soc.* **2001**, *123* (19), 4641–4642. https://doi.org/10.1021/ja0157402.

(86) Stauffer, S. R.; Hartwig, J. F. Fluorescence Resonance Energy Transfer (FRET) as a High-Throughput Assay for Coupling Reactions. Arylation of Amines as a Case Study. *J. Am. Chem. Soc.* **2003**, *125* (23), 6977–6985. https://doi.org/10.1021/ja034161p.

Chapter 2 Development of Late-Stage Saturation (LSS)

2.1 Introduction to Arene Saturation

The available methods of chemical synthesis have arguably contributed to the prevalence of aromatic rings, such as benzene, toluene, xylene, or pyridine, in modern pharmaceuticals. Many such sp^2-carbon-rich fragments are now easy to synthesize using high-quality cross-coupling reactions that click together an ever-expanding menu of commercially available building blocks, but the products are flat and lipophilic, decreasing their odds of becoming marketed drugs. Converting flat aromatic molecules into saturated analogues with a higher fraction of sp^3 carbons could improve their medicinal properties and facilitate the invention of safe, efficacious, metabolically stable, and soluble medicines. In this chapter, we show that aromatic and heteroaromatic drugs can be readily saturated under exceptionally mild rhodium-catalyzed hydrogenation, acid-mediated reduction, or photocatalyzed-hydrogenation conditions, converting sp^2 carbon atoms into sp^3 carbon atoms and leading to saturated molecules with improved medicinal properties. These methods are productive in diverse pockets of chemical space, producing complex saturated pharmaceuticals bearing a variety of functional groups and three-dimensional architectures

The hydrogenation of arenes has evolved continuously since Sabatier and Senderens' seminal report in 1901.[87] We[88–90] and others[91–96] have explored increasingly robust and selective protocols for arene saturation. Recently, developments in mild hydrogenation from our lab,[90] Dou,[95] and Du[96] have enabled reduction of simple benzene or heteroaromatic substrates using boron-derived reductants in alcoholic solvents without the need for additional hydrogen gas. These operationally simple conditions obviate the need for gas handling in a high-pressure autoclave, facilitating adoption in diverse industrial, academic, and discovery settings. While these preliminary studies on simple substrates demonstrate that arenes containing select functional groups can be successfully saturated, no study has demonstrated the mild saturation of drugs or other complex molecules, which can be particularly useful in the exploration of new chemical and druglike space.

This section adapts content from: *J. Am. Chem. Soc.* **2024**, *146*, 17, 11866–11875

2.2 **Late-Stage Saturation (LSS)**

Medicines require a balance of properties to ensure their safety and efficacy. Aromatic molecules are comparatively easy to access synthetically, but a high degree of aromaticity has been shown to correlate with unfavorable outcomes such as poor solubility, selectivity, and metabolic stability.[97,98] To address this issue, many recent reaction methods have sought to increase access to saturated molecules via de novo synthesis.[99,100] Meanwhile, strategic advances in chemical synthesis now enable modification of complex molecular structures at a late stage for the navigation of chemical space and property space. As mentioned in the prior chapter, late-stage functionalization (LSF)[101] decorates the periphery of complex molecules while emerging skeletal editing techniques[102] manipulate shape and property space by altering a molecule's backbone.[101,103–105] Herein, we consider that late-stage saturation (LSS), where aromatic rings of complex drug substrates are saturated by dearomative hydrogenation, could be a valuable addition to the drug hunter's toolbox (Figure 2-1).

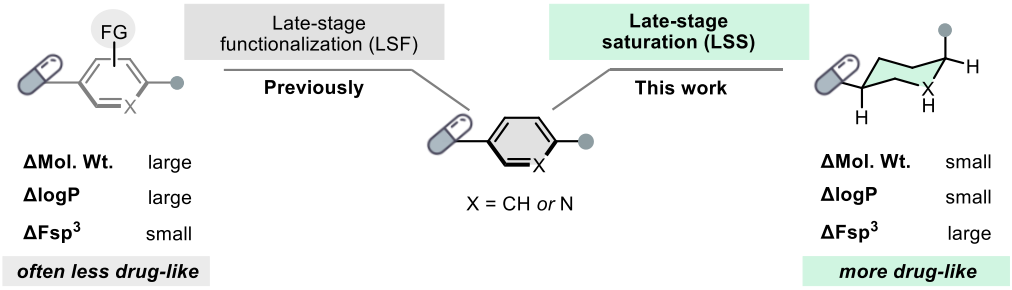


Figure 2-1 Comparison between the existing approach of Late-stage functionalization and the proposed approach of Late-stage saturation for modifying drug molecules. The overall drug properties of LSF analogues are often decreased due to the large increase in molecular weight, while LSS can markedly change physicochemical properties, while maintaining overall drug-likeness since only 6 hydrogen atoms are installed.

Most drugs contain at least one aromatic moiety, with benzene (74.4%) and pyridine (10.8%) rings accounting for the vast majority of aromatic 6-membered rings in drugs in the PubChem database.[106] Escaping from flat aromatic structures toward saturated molecules with a higher fraction of sp3 atoms (Fsp^3) has been invoked as a drug design strategy to improve clinical outcomes,[97,98] solubility,[107] selectivity for target proteins, and efficacy.[108] Drug candidates with a high Fsp^3 are desirable, yet the chemical synthesis of saturated analogues, potentially with multiple stereocenters, is often less facile than stitching together aromatic building blocks. Recognizing that the three most popular reactions used in pharmaceutical research—the amide coupling, Suzuki coupling, and Buchwald–Hartwig coupling[109]—can easily click together aromatic building blocks, LSS would be a powerful complementary method. A

successful LSS strategy would require mild reaction conditions with high functional group tolerance and robust substrate scope to be impactful while obviating the need for autoclaves or other special hydrogenation equipment to facilitate adoption by medicinal chemists in diverse academic and industrial settings. Drug discovery campaigns often seek to "escape from flatland" toward analogues with a higher Fsp^3.[97,98,107,108] As an example (Figure 2-2), the partially saturated lead compound **14** is a SARS-CoV M^{pro} inhibitor that is more than twice as active as its aromatic congener **13**.[110,111] Similarly, a saturation-induced potency increase was observed between TNKS1 inhibitors **15** and **16**, wherein other drug properties including plasma stability and aqueous solubility simultaneously improved upon saturation.[112] Furthermore, several approved drugs have a saturated analogue with an entirely different medicinal use. For instance, methamphetamine (**17**) is a scheduled substance and stimulant, while its saturated analogue, propylhexedrine (**18**), is a topical vasoconstrictor. Aminacrine (**19**) is a topical antiseptic while its partially saturated congener, tacrine (**20**), is approved to treat dementia.

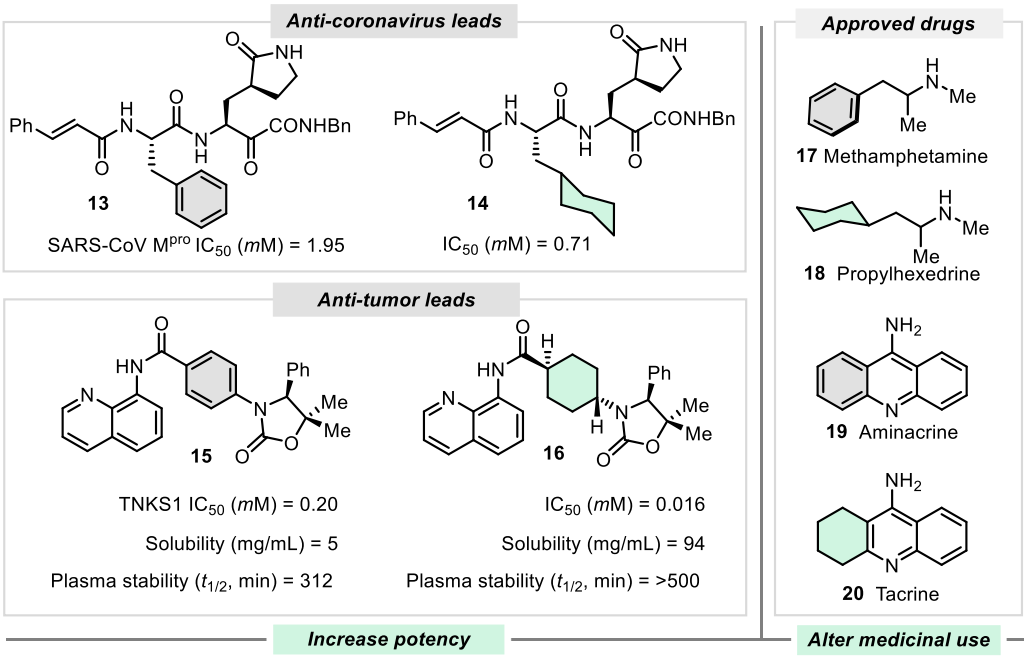


Figure 2-2 Examples of saturated matched pairs of molecules with dramatically modified drug properties.

2.2.1 ***Chemoinformatic Analysis of Saturated Druglike Space***

To statistically explore the direct impact of saturation on aromatic drugs, a cheminformatic analysis on the ChEMBL database of 2.1 M druglike molecules[113] highlighted the impact of the LSS strategy (Figure 2-3). First, virtual compounds were filtered to include only substrates having 6- membered aromatic rings, leaving over 1.5 M compounds, and highlighting that current bioactive molecular space consists mainly of planar, C(sp^2)-rich compounds. Next, in silico saturation on each aromatic ring, resulting in a virtual library of saturated products. A matched-pair analysis identified 9,704 pairs of compounds in ChEMBL for which there was an aromatic compound and an exact analogue wherein the only structural change was saturation of the aromatic ring. Most pairs (88.0%) comprised benzene-cyclohexyl analogues, with the second-most popular pyridine-piperidine analogue pairing accounting for a much smaller proportion of the library (5.9%). This is somewhat surprising since drugs containing piperidine rings are twice as prevalent as those containing pyridine.[114]
This discrepancy may be explained by a follow-up observation that most saturated drugs among the 9704 pairs were accessed by resource-intensive total synthesis, challenging their facile production and highlighting the need for a practical LSS technology.

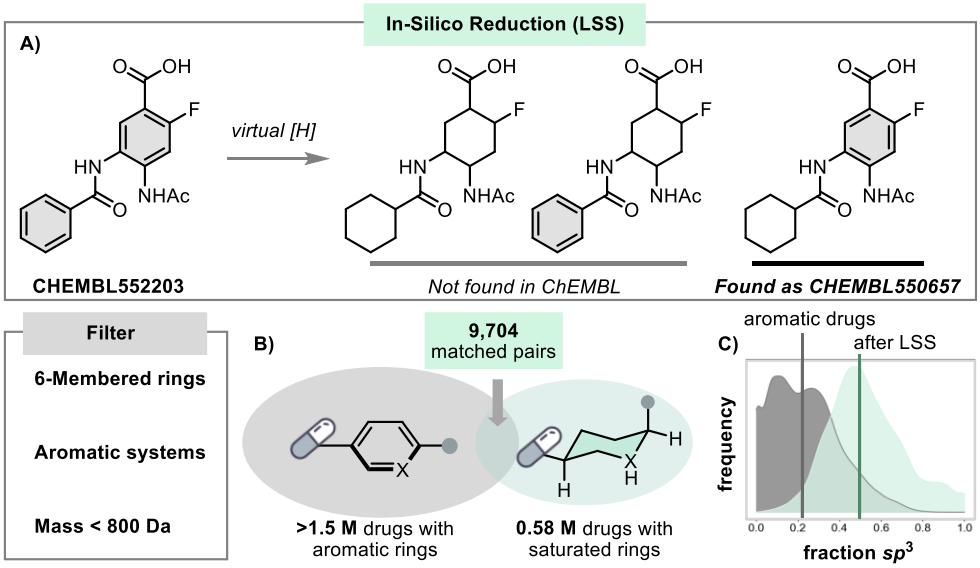


Figure 2-3 A) Cheminformatic workflow for analyzing the ChEMBL database. B) Identification of 9704 matched pairs from >1.5 million aromatic drugs. C) Kernel density of the fraction of sp^3 atoms showing the change in this property upon performing a virtual LSS (green) of the aromatic drugs (gray) in the ChEMBL database.

Specifically, we concluded from these data that a method to reduce benzene and pyridine rings would be one of the most impactful starting points for LSS. Also, LSS can in principle

access multiple regio- and stereoisomers, and this combinatorial explosion of permutations is a viable computational approach to generate ultra-large virtual libraries, which can increase the quality of lead compounds in computer-aided drug discovery.[115] Although the reduction of benzenoid rings will lead to a considerable increase in Fsp^3 and a modest predicted contribution to partition coefficient (Log *P*), the saturation of heteroarenes may have a dramatic impact on compound properties, as for instance when the reduction of a pyridine ring generates a piperidine that is several orders of magnitude more basic and with an additional hydrogen bond donor.

2.3 **Optimization of the LSS Reaction**

2.3.1 ***Screening of Metals, Reductants, and Solvents***

To explore if mild arene hydrogenation conditions could achieve LSS on drugs, I performed an HTE reaction array surveying rhodium catalysts, boron-derived reductants at various stoichiometries, and alcohol solvents using the drugs propranolol, gemfibrozil, and ketoprofen as substrates. Among the 96 reactions surveyed, $[Rh(COD)OH]_2$, $B_2(OH)_4$ in ethanol and $[Rh(COD)Cl]_2$, $NH_3{\cdot}BH_3$ in 1,1,1-trifluoroethanol exhibited the best performance, reducing propranolol in 85% and 67% assay yield, respectively. In general, increasing the amount of reductant led to increased levels of LSS. Importantly, the solvents n-butanol and ethylene glycol, which were included as high-boiling solvents for the application of reaction miniaturization at nanomole scale,[116–118] exhibited good performance using $[Rh(COD)OH]_2$, $B_2(OH)_4$, with nearly identical results obtained using ethanol or ethylene glycol for the three drugs tested. These latter conditions in ethylene glycol suggested potential translation of LSS to drug compounds acquired from pharmaceutical compound collections in 96-, 384-, or 1536-well plates.

2.3.2 ***Substrate Scope Evaluation***

Starting on the traditional scale, we explored LSS for a variety of drugs using ethanol or ethylene glycol as a solvent. Accordingly, **19** was reduced to give saturation product **20** in 50% yield along with doubly saturated product **21** in 15% yield. By increasing the amount of $B_2(OH)_4$ from 3 to 7 equiv, **21** became predominant (Figure 2-4). This change in chemoselectivity is attributed to an increase in available H_2.[90,95] This observation highlights the ability to access

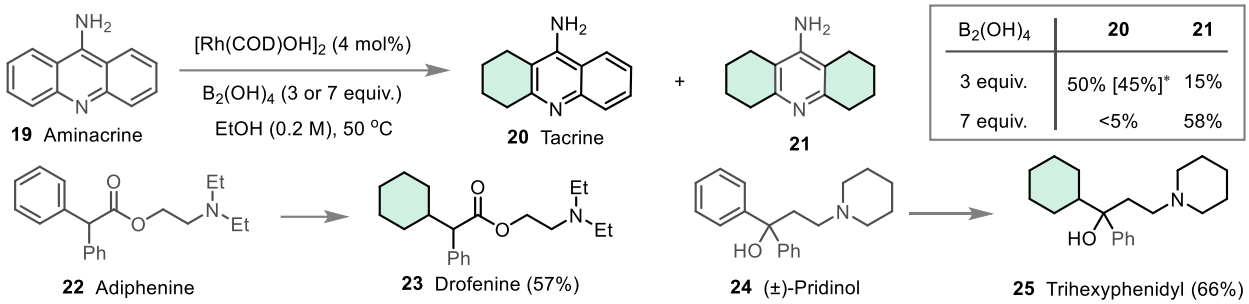


Figure 2-4 Aromatic drugs transformed to saturated drugs by LSS: production of saturated drugs with distinct medicinal properties. Extent of saturation can be controlled by equivalents of the $B_2(OH)_4$ reductant.

diverse saturated analogues in chemical space through simple modification of reaction conditions. Next, adiphenine (**22**) and pridinol (**24**) were successfully reduced to furnish the saturated drugs drofenine (**23**) and trihexyphenidyl (**25**), respectively. A variety of other arene-containing pharmaceuticals were readily reduced to provide the saturated drug analogues in good to excellent yields (Figure 2-5 and 2-6). Several examples highlight the remarkable functional group tolerance, for instance, primidone gave **44** in 96% yield despite the presence of two unprotected N−H bonds while (*R*)-tolterodine gave **41** even though a free phenol and basic amine were present. Remarkably, atorvastatin could be submitted to the reaction as its calcium salt, producing **48** in 56% yield. Free carboxylic acids (**29, 39, 49**), fluorine (**39**) and trifluoromethyl (**42**) were well tolerated. Densely functionalized alkaloids such as midostaurin were viable substrates, giving **50** in 55% yield. The calcium-modulating drug (*R*)-cinacalcet was readily reduced to give **51**, a compound with generally superior calculated physicochemical and pharmacokinetic properties compared to the starting material. Interestingly, reduction of nabumetone (**52**) and (*S*)-naproxen-OMe (**55**) gave regioisomers **53**−**54** and **56**− **57**, respectively.

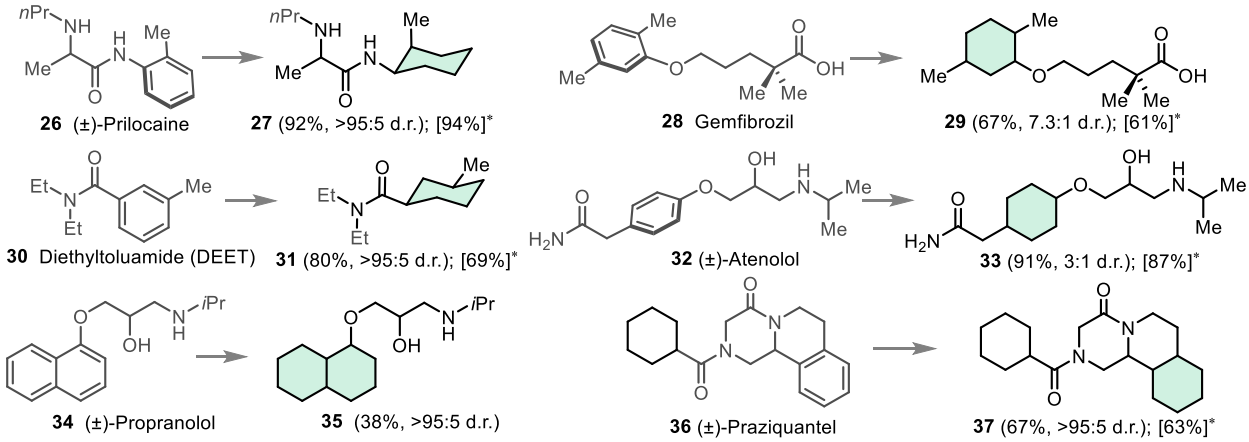


Figure 2-5 Examples of LSS on mono-aromatic system containing drugs.

While this example highlights the opportunity to produce a diversity of saturated analogues in a single reaction, we observed very high regio- and diastereoselectivity for most substrates. General chemoselectivity trends emerged. Under the Rh-catalyzed hydrogenation, the less-substituted (i.e., **39**−**43, 79**) or less-electron-rich (i.e., **78**) benzene rings are more prone to be reduced. Further, pyridines, which generally have lower aromatic resonance energy than benzenes, are typically more easily reduced (i.e., **80**−**83**).

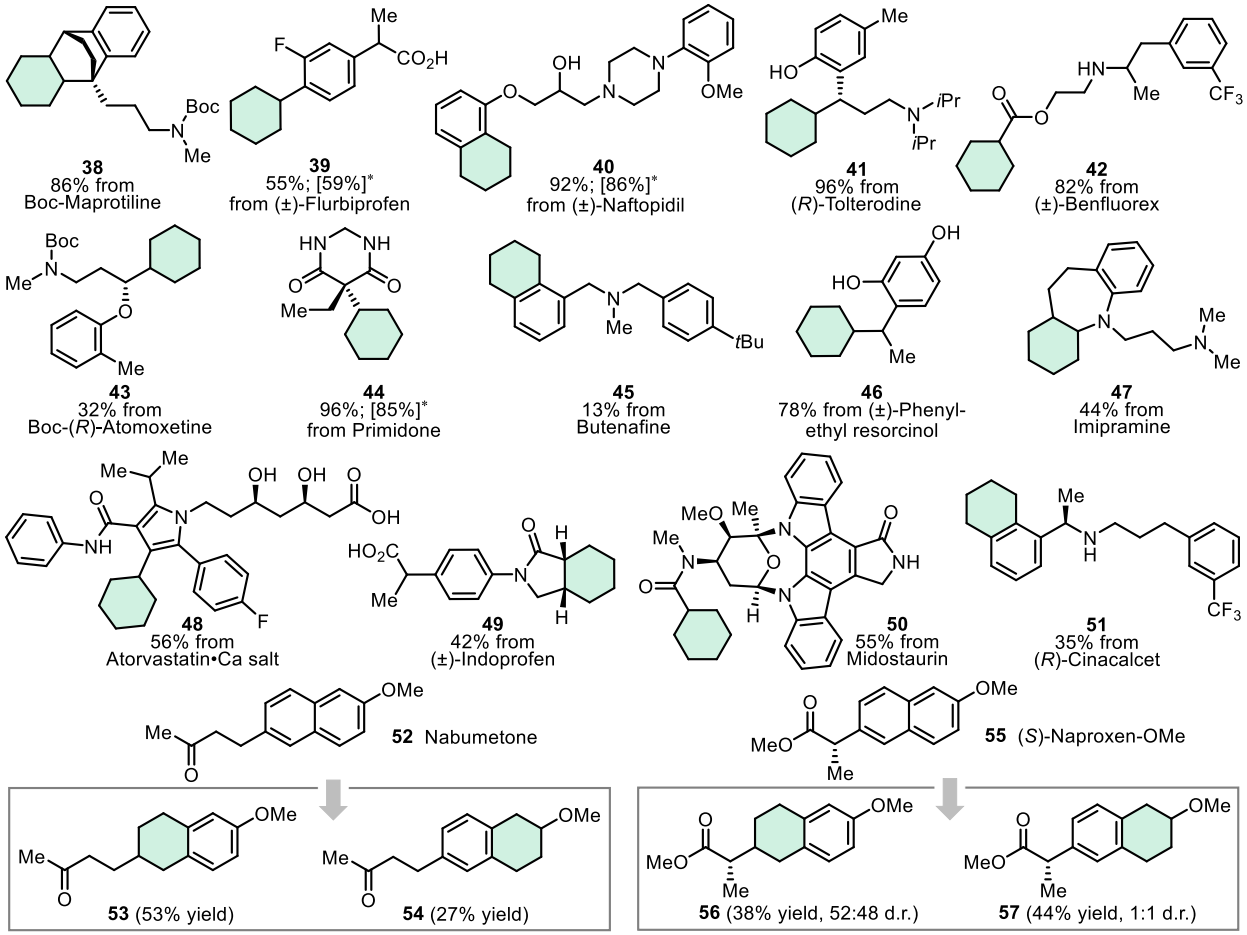


Figure 2-6 Examples of LSS on multi-aromatic system containing drugs. For naphthalene-containing examples like Nabumetone **52** and (*S*)-Naproxen-OMe **55**, multiple regioisomeric products are isolatable.

Furthermore, LSS can dramatically improve synthetic efficiency and complement retrosynthetic strategies (Figure 2-7). For example, compound **59**, an inhibitor for chemotactic activation of neutrophils, has been conventionally obtained by a 7-step linear synthesis from **58**.[119] In contrast, the commercial drug ketoprofen **60** can be directly saturated to afford **59** in a single step. Similarly, the anti-inflammatory agent **62** was previously synthesized in 13 steps from **61**,[120] while LSS logic provided **62** directly from commercial cicloprofen (**63**) in 59% yield.

The status quo to access saturated analogues by total synthesis is exemplified in the production of **66** (aromatic) and **67** (aliphatic)[121] in 6 steps each from **64** and **65**, whereas LSS converts **66** to **67** in 1-step and 46% yield with no protection of the carboxylic acid needed. While we have generally observed excellent regioselectivity in our studies, product mixtures are occasionally obtained. The synthesis of separable analogues **69** and **71** from commercially available biprofen (**70**) showcases how LSS can more expediently explore three-dimensional chemical space, compared to the production of **69** alone from **68**.[122] Additional applications of LSS to shortcut *de novo* syntheses are shown for leads **74** and **77**.[123,124]

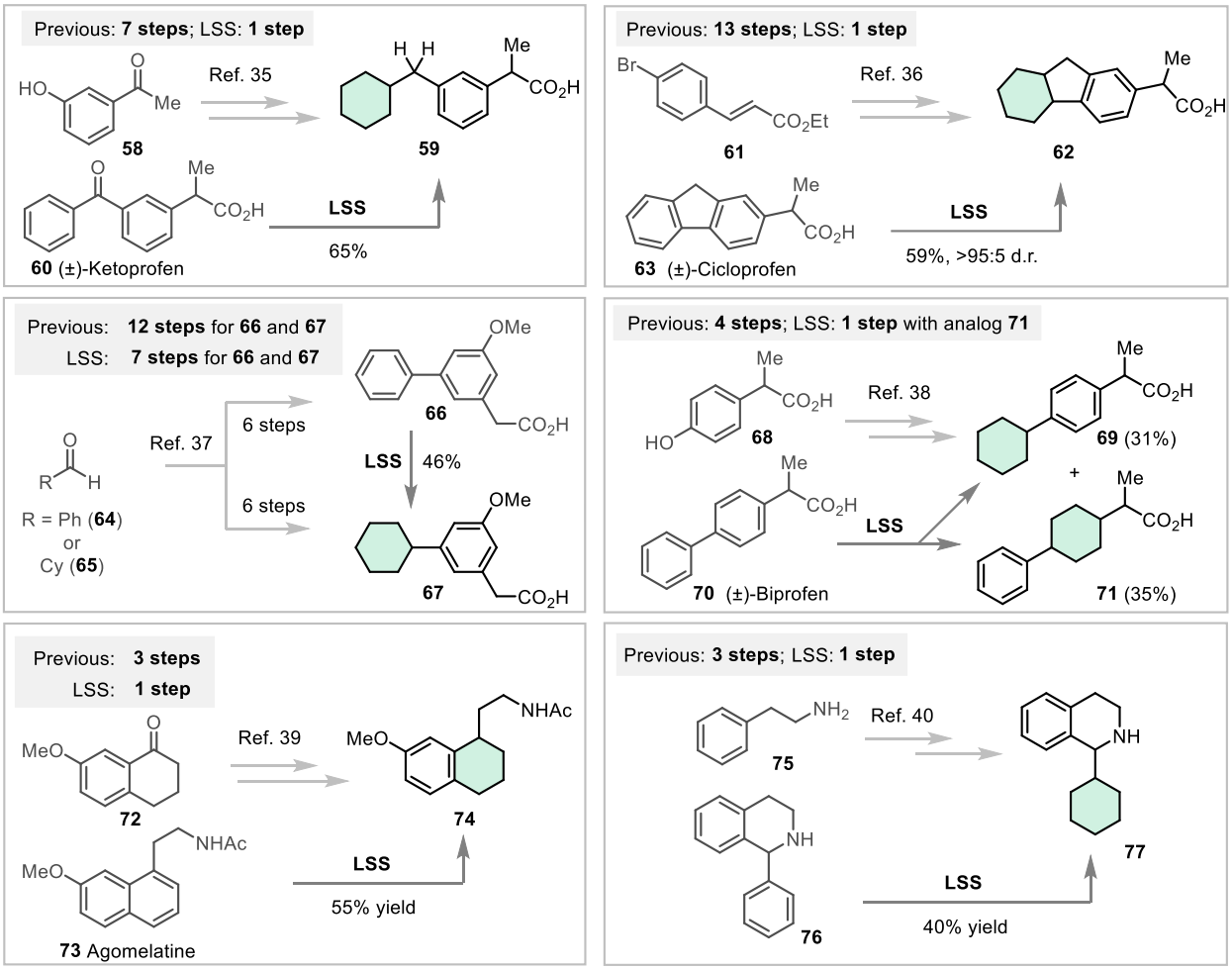


Figure 2-7 Step-economic synthesis of lead compounds empowered by LSS concept.

2.3.3 Optimization of Miniaturized LSS

Next, I tested the impact of DMSO and water poisoning on the reaction. Pharmaceutical compound collections are available in high chemical diversity and are typically formatted in microtiter plates for rapid delivery to biochemical or cellular high-throughput screening

campaigns. However, drugs in physical libraries are generally available in <10 mg amounts and are commonly stored in DMSO, which is most often wet owing to non-anhydrous storage and handling conditions. While wet DMSO is a suitable stock solution for many miniaturized bioassays, both DMSO and water are extreme inhibitors of most transition-metal-catalyzed reactions, often poisoning reactions when present in trace amounts. Studying the impact of DMSO and water on the present Rh-catalyzed hydrogenation, it was revealed that stoichiometric but not excess amounts of these additives were tolerated. Collectively, the finding that the protocol tolerated trace DMSO or water suggested that direct access to pharmaceutical compound collections via LSS could be possible to enable deep chemical space exploration and medicinal property optimization on a traditional (~50 mg) scale in ethanol or miniaturized (~50 μg) scale in ethylene glycol.

2.3.4 ***Nanoscale Substrate Scope Study in 1,536-Well Plate Format***

Miniaturization of reactions via ultraHTE[116,117] can be impactful for advancing medicinal chemistry, particularly via modern direct-to-biology approaches.[117] We acquired a library of drugs from The University of Michigan Drug Discovery Center that had been stored in DMSO for many months, with no special precautions taken to exclude ambient moisture. Since the LSS protocol tolerates traces of, but not an excess of, DMSO and water, we reformatted a library of 768 drugs from DMSO solutions into a 384-well microtiter source plate and removed volatiles by centrifugal evaporation. The residues were reconstituted in ethylene glycol, then transferred to a 1536-well reaction plate along with $[Rh(COD)OH]_2$ (4 mol%) and $B_2(OH)_4$ (3.5 or 7.0 equiv). The plate containing 1536 reaction mixtures was then sealed and heated at 50 °C for 24 h. Analysis of the conversion to product by ultraperformance liquid chromatography−mass spectrometry (UPLC−MS) showed product formation for 690 of the 768 drugs. The conversion to product was generally good to excellent (Figure 2-8), with an average saturation conversion of 42.9% over the 1536 reactions. The stoichiometry of $B_2(OH)_4$ (3.5 versus 7.0 equiv) had a modest impact on reaction conversion. The performance of the LSS protocol on such a broad diversity of pharmaceutically relevant molecules is exceptional, especially when compared to

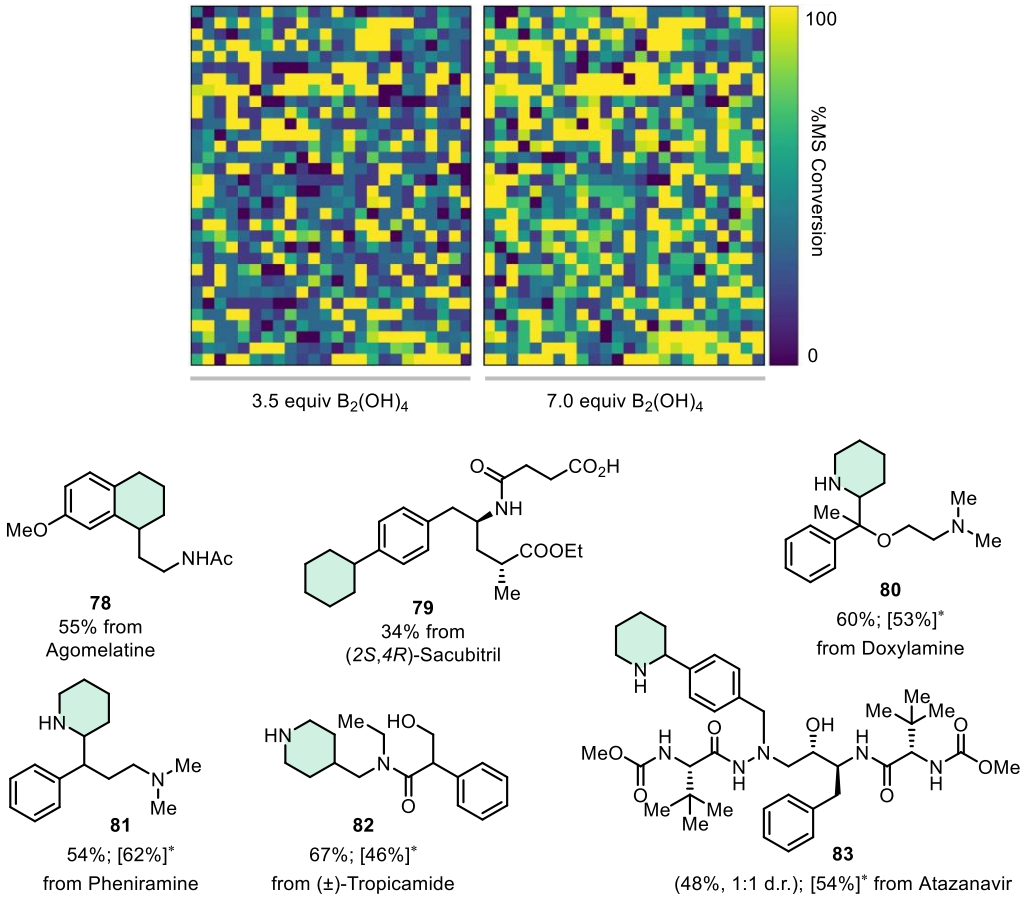
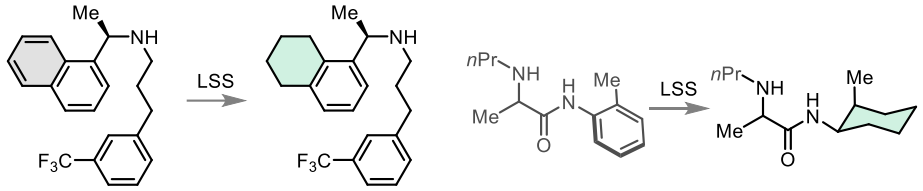


Figure 2-8 A library of 768 pharmaceutically relevant complex molecules stored in wet DMSO were subjected to LSS using $[Rh(COD)OH]_2$, $B_2(OH)_4$ in ethylene glycol. Selections of miniaturized reactions were confirmed on ~50 mg scale in ethanol to obtain isolated yields. *Yields shown in square brackets were obtained using ethylene glycol as solvent.

other miniaturized high-throughput reaction campaigns on pharmaceuticals and natural products.[56,116–118] A cheminformatic analysis showed no obvious pockets of chemical space where substrates did not yield the saturated product. The fact that the Rh-catalyzed LSS protocol was agnostic of reaction scale was further verified by comparing reaction performance from reactions run on an ~50 μg scale in ethylene glycol to reactions run on a ~50 mg scale in ethanol or ethylene glycol for 34 drugs, and the correlation of UPLC-MS conversion from the miniaturized reactions to isolated yields from reactions performed on a traditional scale was excellent. A sampling of the isolated products (**78**–**83**) is shown in Figure 2-8. It is worth noting that the pyridine-containing drugs were also tolerated well to give the piperidine congeners **80**–**83**. To our knowledge, this represents the first successful application of a transition-metal-catalyzed reaction to a library of drugs reconstituted from wet DMSO.

2.3.5 *Direct-to-Microsomal Stability Assay Comparison of Saturated Drugs*

Increasing the three-dimensionality of pharmaceuticals is expected to modulate their overall properties, and calculations on cinacalcet and prilocaine alongside their saturated congeners **51** and **27** highlight some potential differences (Figure 2-9). The measured octanol−water partition coefficient (Log *P*) of several drugs and their saturated congeners suggests that LSS is a viable strategy to modulate hydrophilicity, with most drugs showing a slight increase in Log *P* upon saturation.



	(*R*)-Cinacalcet	**51**	(±)-Prilocaine	**27**
Fraction C(sp^3)	27%	**45%**	46%	**92%**
TPSA ($Å^2$)	12.0	12.0	41.1	41.1
$LogP_{o/w}$	5.84	5.90	2.34	2.33
CYP1A2 inhibition	Yes	**No**	Yes	**No**
CYP2C19 inhibition	Yes	**No**	No	No
CYP2D6 inhibition	Yes	Yes	Yes	**No**
$LD_{50}(Log_{mol/kg})$	0.260	**0.349**	0.830	0.846

Figure 2-9 Predicted properties for Cinacalcet, Prilocaine, and their LSS-analogues **51** and **27.** Calculated properties, Fsp^3, TPSA, CYP inhibition, and LD_{50} along with experimental $LogP_{o/w}$ values are predicted to remain constant or improve upon saturation. $LogP_{o/w}$ values were determined from the experimental shake-flask method.

A final experiment was performed to merge LSS with microsomal stability testing in a direct-to-biology[117] format. Here, 24 drugs were saturated and, following reaction quenching and metal scavenging, directly transferred an incubation with human liver microsomes. While most drugs exhibited little change or a modest decrease in microsomal stability upon saturation, several drugs, most notably flurbiprofen congener **39** exhibited an increase in stability (Figure 2-10). Given the well-documented benefits of increasing a pharmaceutical's Fsp^3,[97,98,107,108] this ability to saturate and in situ demonstrate improved metabolic stability could be beneficial to drug discovery efforts.

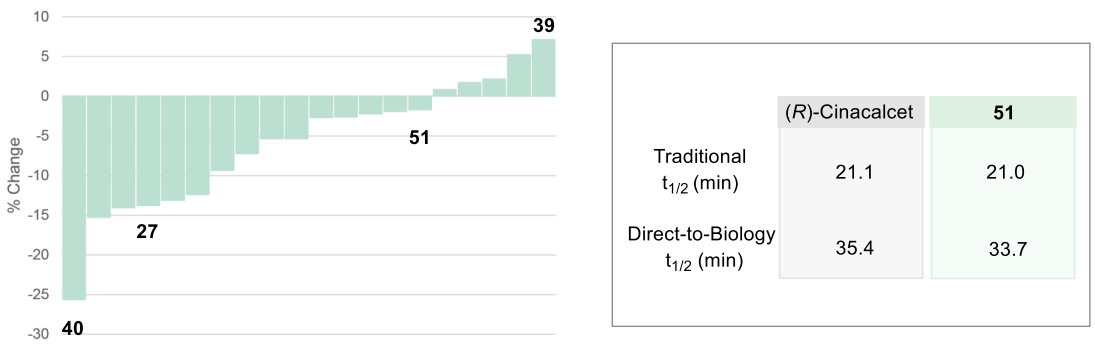


Figure 2-10 Microsomal stability data obtained for 24 LSS reaction mixtures showing the change in microsomal stability following saturation of various drugs. %Change indicates the increase or decrease in metabolic stability of the saturated drug compared to its arene precursor upon exposure to human liver microsomes for 60 minutes.

2.4 **Conclusions and Future Work**

Our results highlight the potential to convert aromatic drugs to their saturated congeners in a rapid and user-friendly format. A growing body of evidence suggests that three-dimensional molecules have medicinal properties superior to those of their flat aromatic analogues. Nonetheless, cross-coupling of aromatic building blocks, commercially available in high diversity, is a robust technology with considerable user adoption, making the production of flat drugs quite facile. The saturation of such aromatic molecules at a late stage as described here will allow for rapid exploration of three-dimensional chemical space toward improved clinical outcomes and other diverse applications.

We envision that further development of this system can enable an even broader range of applications beyond those reported herein. Poisoning of the rhodium precatalyst is one of the predominant factors contributing to low yielding saturation reactions. We envision work can be done to identify alternate precatalysts less prone to chelation by promiscuous functional groups such as highly basic amines. Otherwise, precatalysts able to rapidly form an activated catalyst could circumvent the ~60 minute incubation period $[Rh(Cod]OH]_2$ requires to form catalytically active rhodium nanoparticles.

Another direction for future work is the development of a more tunable fully homogenous catalytic system that doesn't rely on the formation of heterogeneous rhodium nanoparticles to engage with hydrogen gas. While we have demonstrated a range of diverse substrates that are efficiently reduced by rhodium nanoparticles, we have also encountered a host of sterically encumbered and electron-deficient arenes that pose a problem for our system. Fully soluble transfer hydrogenation systems derived from existing cobalt and nickel systems may be

able to better facilitate hydrogenation on sterically hindered or electronically deactivated substrates. The ability to tune both the steric and electronic properties of soluble metal-ligand complexes is indeed highly attractive in this regard.

2.5 **Experimental Section for the LSS Reaction**

For further details on the Glorius and Ma groups' chemoinformatic analysis of matched pairs and analysis of the PubChem and ChEMBL libraries that was conducted in this work, please see the supporting information of: *J. Am. Chem. Soc.* **2024**, *146*, 17, 11866–11875. The chemoinformatic analysis and computational property prediction work for this project was conducted by: De-Hai Liu, Philipp M. Pflüger, Lukas Lückemeier, Fuhao Zhang, Jiajia Ma, and Frank Glorius. Compound synthesis and reaction optimization was done by: De-Hai Liu, Andrew Outlaw, Lukas Lückemeier, and Fuhao Zhang. High-throughput screening and microsomal stability work was conducted by: Andrew Outlaw, Hamid Rashidi Nodeh, Clinton Regan, and Tim Cernak.

2.5.1 ***General Methods***

Unless otherwise noted, all reactions were carried out under an atmosphere of argon or nitrogen in dried glassware. Reaction temperatures are referred to as the ones of the heating/cooling media (heating block, cryogenic bath), unless otherwise stated. Dry solvents were either purchased from ACROS Organics or Adamas (H2O < 50 ppm), stored under activated molecular sieves, withdrawn under positive argon pressure or purified using a custom-made SPS purification system (activated alumina columns) and transferred under argon. Solvents for flash column chromatography (petroleum ether, EtOAc, CH_2Cl_2) were purchased of technical grade and purified by atmospheric pressure distillation or purchased of reagent grade (MeOH) and used without additional purification. Reagents were purchased from Sigma-Aldrich, ACROS Organics, TCI, Adamas, Bidepharm and used without additional purification, unless otherwise stated. Reaction setup involving dosing of substrates and reagents into the 1,536-well plate experiment were set up in an MBraun LABmaster Pro Glove Box (H2O level <0.1 ppm, O2 level <0.1 ppm). Transferring and dosing of 384 and 1,536-well plates was conducted using an SPT Labtech Mosquito liquid handling robot and the corresponding mosquito software to develop dosing and mixing procedures. Glass 1-dram (Fisherbrand™ parts No. 03-339-21B) or 2-dram vials (Fisherbrand™ parts No. 03-339-21D) were used as reaction vessels, fitted with screwcaps with Teflon-coated silicone septa (CG-4910-02), and magnetic stir bars (Fisher Scientific #14-

513-93 or #14-513-65). Microtiter plate evaporation was performed using a Genevac HT-4X Series II centrifugal evaporator with vacuum pump controller (Genevac #70-0938), BOC Edwards XDS-5 dry scroll pump (Edwards #A724-01-104), and side-bridge swing attachments for well plate evaporation. Vacuum plot capacity: 2.3 L. Vacuum control range: 1-1000 mbar. Standard evaporation method listed below: 40°C internal chamber temperature, 1 mbar chamber vacuum, very low rotor speed, 2 hours runtime.

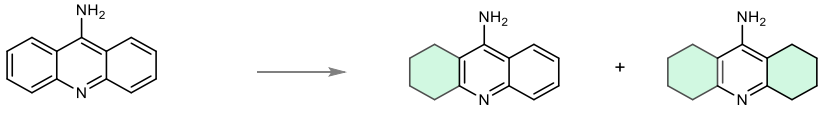
Proton nuclear magnetic resonance (^{1}H NMR) spectra were recorded on a Varian MR-500 MHz, or Varian MR-400 MHz spectrometer and chemical shifts are reported in parts per million (ppm) using the solvent residual peak as an internal standard ($CDCl_3$ at 7.26 ppm, DMSO-d_6 at 2.50 ppm, D_2O at 4.80). Data are reported using the abbreviations: app = apparent, s = singlet, d = doublet, t = triplet, q = quartet, m = multiplet, comp = complex, br = broad. Coupling constant(s) are reported in Hz. Proton-decoupled carbon nuclear magnetic resonance spectra (^{13}C NMR) spectra were recorded on a Varian MR-500 MHz or Varian MR-400 MHz spectrometer and chemical shifts are reported in ppm using the solvent as an internal standard ($CDCl_3$ at 77.16 ppm, DMSO-d_6 at 39.52 ppm). High resolution mass spectrometry data (HRMS) was obtained on a Micromass AutoSpec Ultima Magnetic Sector instrument. Reaction analysis was typically performed by thin-layer chromatography (TLC) on silica gel 60 F_{254} glass plates (Fisher Scientific #S07876) and visualized using ultraviolet light (254 nm) or potassium permanganate ($KMnO_4$) stain; or using a Waters I-class ACQUITY UPLC-MS (Waters Corporation, Milford, MA, USA) equipped with in-line photodiode array detector (PDA) and QDa mass detector (ESI positive ionization mode). 0.1 µL sample injections were taken from acetonitrile solutions of reaction mixtures or products (~1 mg/mL). A partial loop injection mode was used with the needle placement at 1.0 mm from bottom of the wells and a 0.2 µL air gap at pre-aspiration and post-aspiration. Column used: Waters Cortecs UPLC C18+ column, 2.1mm · 50 mm with (Waters #186007114) with Waters Cortecs UPLC C18+ VanGuard Pre-column 2.1mm · 5 mm (Waters #186007125), Mobile Phase A: 0.1 % formic acid in Optima LC/MSgrade water, Mobile Phase B: 0.1% formic acid in Optima LC/MS-grade MeCN. Flow rate: 0.8 mL/min. Column temperature: 45 °C. The PDA sampling rate was 20 points/sec. The QDa detector monitored m/z 150-750 with a scan time of 0.06 seconds and a cone voltage of 30 V. The PDA detector range was between 210 nm – 400 nm with a resolution of 1.2 nm. 1-minute and 2-minute methods were used. The method gradients are as follows: 0 min: 0.8 mL/ min, 95%

0.1% formic acid in water/ 5% 0.1% formic acid in acetonitrile; 1.5 min: 0.8 mL/ min, 0.1% 0.1% formic acid in water/ 99.9% 0.1% formic acid in acetonitrile; 1.91 min: 0.8 mL/min, 95% 0.1% formic acid in water/ 5% 0.1% formic acid in acetonitrile. Flash chromatography was performed on silica gel (230 – 400 Mesh, Grade 60) under a positive pressure of air.

2.5.2 ***Procedures for the LSS Reaction***

General Procedure

A dried 5 or 10 mL Schlenk tube was charged with the starting material drug or lead compound, $B_2(OH)_4$ (3-7 equivalents) and $[Rh(COD)OH]_2$ (2.5-5 mol%) in ethanol (0.1 M) under nitrogen or argon atmosphere. The reaction mixture was stirred vigorously at 50-80 ℃ until the full conversion of the starting material. Afterwards, the reaction was quenched by saturated aqueous $NaHCO_3$ and extracted with CH_2Cl_2 or EtOAc (10 mL x 3). The organic phases were combined and concentrated under reduced pressure. The product was obtained by flash chromatography on silica gel (petroleum ether/EtOAc, petroleum ether/Et_2O or CH_2Cl_2/MeOH, optionally, with NH_3 (7.0 M in MeOH) as additive). Note, in case the substrate drug was a carboxylic acid, the reaction mixture was concentrated and subjected to the column chromatography directly.



19 Aminacrine　　20 Tacrine　　21

According to the general procedure, a mixture of **aminacrine** (38.8 mg, 0.20 mmol, 1.0 equiv.), $B_2(OH)_4$ (54.0 mg, 0.60 mmol, 3.0 equiv.) and $[Rh(COD)OH]_2$ (3.7 mg, 4.0 mol%, 0.008 mmol) in EtOH (1.0 mL, 0.2 M) was stirred under nitrogen atmosphere for 26 hours at 50 ℃ to afford **tacrine** as a yellow solid (19.9 mg, 50% yield) and the second product **21** (6.0 mg, 15% yield). Under an alternative condition with $B_2(OH)_4$ (113.3 mg, 1.4 mmol, 7.0 equiv.) and $[Rh(COD)OH]_2$ (3.7 mg, 4.0 mol%, 0.008 mmol), **7** (23.3 mg, 58% yield) was afforded whereas tacrine was not obtained.

Purification conditions: NH_3 (7.0 M solution in MeOH)/CH_2Cl_2 = 1:50 to 1:20

R_f(tacrine) = 0.7 in NH_3(7.0 M solution in MeOH)/CH_2Cl_2 = 1:10.

R_f(**9**) = 0.5 in NH_3(7.0 M solution in MeOH)/CH_2Cl_2 = 1:10.

Analytical data of **tacrine**:

^{1}H NMR (400 MHz, $CDCl_3$) δ 7.89 (d, *J* = 8.8 Hz, 1H), 7.73 (d, *J* = 8.4 Hz, 1H), 7.59 - 7.53 (m, 1H), 7.39 - 7.33 (m, 1H), 4.84 (br, 2H), 3.02 (t, *J* = 6.0 Hz, 2H), 2.59 (t, *J* = 6.0 Hz, 2H), 1.98 - 1.87 (m, 4H)

HRMS (ESI, *m*/*z*) calcd for $C_{13}H_{15}N_2^+$ $[M+H]^+$: 199.1235, found: 199.1237.

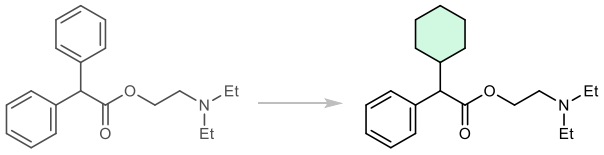
All other analtical data is consistent with previous reports.

Analytical data of **21**:

^{1}H NMR (400 MHz, $CDCl_3$) δ 4.70 (br, 2H), 2.86 - 2.77 (m, 4H), 2.44 - 2.36 (m, 4H), 1.86 - 1.73 (m, 8H).

^{13}C NMR (100 MHz, $CDCl_3$) δ 151.5, 151.1, 113.2, 30.8, 22.9, 22.4.

HRMS (ESI, *m*/*z*) calcd for $C_{13}H_{19}N_2^+$ $[M+H]^+$: 203.1548, found: 203.1549



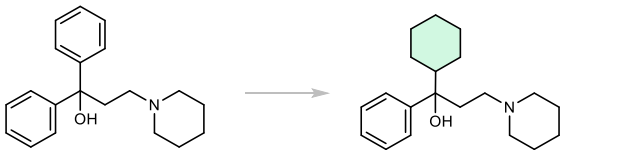
22 Adipheine **23 Drofenine** (57% yield)

According to the general procedure, a mixture of **adiphenine** (62.3 mg, 0.2 mmol, 1.0 equiv.), $B_2(OH)_4$ (107.5 mg, 1.2 mmol, 6.0 equiv.) and $[Rh(COD)OH]_2$ (3.7 mg, 4.0 mol%, 0.008 mmol) in in *i*-PrOH/EtOH (v/v = 9:1, 1.0 mL) was stirred under nitrogen atmosphere for 24 hours at 80 °C to afford **drofenine** as a colorless oil (36.4 mg, 57% yield).

^{1}H NMR (400 MHz, $CDCl_3$) δ 7.35 - 7.24 (m, 4H), 7.27 - 7.18 (m, 1H), 4.20 - 4.04 (m, 2H), 3.22 (d, *J* = 10.8 Hz, 1H), 2.64 (t, *J* = 6.0 Hz, 2H), 2.50 (q, *J* = 7.2 Hz, 4H), 2.01 (qt, *J* = 11.2, 3.2 Hz, 1H), 1.87 - 1.79 (m, 1H), 1.78 - 1.68 (m, 1H), 1.67 - 1.53 (m, 2H), 1.36 - 1.24 (m, 2H), 1.19 - 1.02 (m, 3H), 0.97 (t, *J* = 7.2 Hz, 6H), 0.73 (qd, *J* = 12.4, 3.6 Hz, 1H).

^{13}C NMR (100 MHz, $CDCl_3$) δ 174.0, 138.0, 128.7, 128.5, 127.2, 62.9, 59.0, 51.1, 47.6, 41.1, 32.1, 30.5, 26.4, 26.12, 26.09, 12.0.

HRMS (ESI, *m*/*z*) calcd for $C_{20}H_{32}NO_2^+$ $[M+H]^+$:318.2428, found: 318.2433



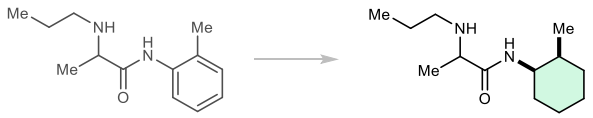
24 (±)-Pridinol **25 Trihexyphenidyl** (66% yield)

According to the general procedure, a mixture of **(±)-pridinol** (59.1 mg, 0.20 mmol, 1.0 equiv.), $B_2(OH)_4$ (80.6 mg, 0.9 mmol, 4.5 equiv.) and $[Rh(COD)OH]_2$ (3.7 mg, 4.0 mol%, 0.008 mmol) in EtOH (1.0 mL, 0.2 M) was stirred under nitrogen atmosphere for 36 hours at 80 ℃ to afford **trihexyphenidyl** as a white solid (39.8 mg, 66% yield).

Purification conditions: Acetone/petroleum ether = 1:8 to 1:4.

R_f = 0.4 in Acetone/petroleum ether = 1:3.

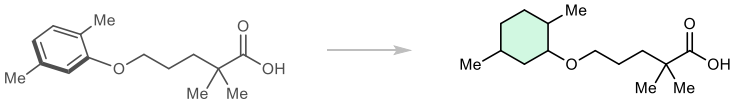
^{1}H NMR (400 MHz, $CDCl_3$) δ 7.39 (d, *J* = 7.6 Hz, 2H), 7.30 (t, *J* = 7.6 Hz, 2H), 7.18 (t, *J* = 7.2 Hz, 1H), 2.64 - 2.37 (br, 1H), 2.35 - 2.18 (m, 3H), 2.15 - 1.92 (m, 3H), 1.80 - 1.68 (m, 2H), 1.65 - 1.49 (m, 7H), 1.46 - 1.34 (m, 2H), 1.32 - 1.12 (m, 3H), 1.12 - 0.97 (m, 4H). ^{13}C NMR (100 MHz, $CDCl_3$) δ 147.0, 127.7, 126.3, 125.8, 79.8, 55.5, 54.4, 49.1, 33.1, 27.2, 27.0, 26.9, 26.8, 26.6, 25.9, 24.1. HRMS (ESI, *m*/*z*) calcd for $C_{20}H_{32}NO^+$ $[M+H]^+$: 302.2478, found: 302.2482.



26 (±)-Prilocaine **27** (92% yield, >95:5 d.r.)

According to the general procedure, a mixture of **(±)-prilocaine** (44.0 mg, 0.2 mmol, 1.0 equiv.), $B_2(OH)_4$ (107.5 mg, 1.2 mmol, 6.0 equiv.) and $[Rh(COD)OH]_2$ (3.6 mg, 4 mol%, 0.0080 mmol) in EtOH (1.0 mL, 0.2 M) was stirred under argon atmosphere for 14 hours at 50 ℃ to afford **27** as a colorless oil (41.0 mg, 92% yield, >95:5 d.r.).

^{1}H NMR (400 MHz, $CDCl_3$, mixture of diastereomers) δ 7.53 (br, 1H), 4.03-3.96 (m, 1H), 3.12 (qd, *J* = 6.9, 1.9 Hz, 1H), 2.63-2.57 (m, 1H), 2.52 - 2.42 (m, 1H), 1.84 - 1.73 (m, 1H), 1.68 - 1.59 (m, 2H), 1.56 - 1.43 (m, 5H), 1.37 - 1.16 (m, 7H), 0.94 - 0.91 (m, 3H), 0.84 (t, *J* = 7.1 Hz, 3H). ^{13}C NMR (101 MHz, $CDCl_3$, mixture of diastereomers) δ 174.6, 58.9, 58.8, 50.8, 50.7, 48.6, 48.4, 34.1, 34.1, 30.4, 30.3, 30.2, 24.2, 23.7, 23.7, 22.0, 22.0, 20.5, 20.4, 17.2, 17.0, 11.9, 11.9. HRMS (ESI, *m*/*z*) calcd for $C_{13}H_{27}N_2O$ $[M+H]^+$: 227.2123, found: 227.2120.



28 Gemfibrozil

Isolated diastereomers:
29a (59% yield), **29b** (8% yield)

According to the general procedure, a mixture of **gemfibrozil** (100.1 mg, 0.4 mmol, 1.0 equiv.), $B_2(OH)_4$ (161.4 mg, 1.8 mmol, 4.5 equiv.) and $[Rh(COD)OH]_2$ (4.6 mg, 2.5 mol%, 0.010 mmol) in EtOH (2.0 mL, 0.2 M) was stirred under argon atmosphere for 14 hours at 50 °C to afford **29a** (60.6 mg, 59% yield) and **29b** (8.2 mg, 8% yield) as colorless oil.

Analytical data of **29a**:

^{1}H NMR (400 MHz, $CDCl_3$) δ 3.48 - 3.43 (m, 1H), 3.35 - 3.27 (m, 2H), 2.14 (m, 1H), 1.64 - 1.52 (m, 6H), 1.47 - 1.31 (m, 3H), 1.20 (s, 6H), 1.15 - 1.02 (m, 2H), 0.91 (d, J = 6.4 Hz, 3H), 0.86 (d, J = 7.1 Hz, 3H).

^{13}C NMR (151 MHz, $CDCl_3$) δ 184.5, 80.0, 68.1, 42.1, 37.1, 35.3, 32.0, 30.6, 30.4, 28.7, 25.8, 25.07, 25.06, 22.5, 11.2.

HRMS (ESI, *m*/*z*) calcd for $C_{15}H_{28}O_3Na^+$ $[M+Na]^+$: 279.1931, found: 279.1930.

Analytical data of **29b**:

^{1}H NMR (400 MHz, $CDCl_3$) δ 3.53 - 3.47 (m, 1H), 3.28 (m, 1H), 3.25 - 3.20 (m, 1H), 1.91 (dq, J = 13.6, 3.3 Hz, 1H), 1.65 - 1.59 (m, 4H), 1.57 - 1.50 (m, 3H), 1.42 - 1.33 (m, 3H), 1.21 (s, 6H), 0.93 - 0.84 (m, 8H). ^{13}C NMR (151 MHz, $CDCl_3$) δ 183.0, 78.7, 69.2, 42.0, 38.3, 37.3, 36.4, 35.0, 29.0, 26.0, 25.9, 25.2, 25.1, 22.6, 18.5. HRMS (ESI, *m*/*z*) calcd for $C_{15}H_{28}O_3Na^+$ $[M+Na]^+$: 279.1931, found: 279.1931.



30 Diethyltoluamide (DEET)

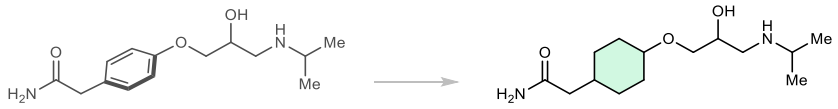
31 (80%, >95:5 d.r.)

According to the general procedure, a mixture of **diethyltoluamide** (38.3 mg, 0.20 mmol, 1.0 equiv.), $B_2(OH)_4$ (107.5 mg, 1.20 mmol, 6.0 equiv.) and $[Rh(COD)OH]_2$ (3.7 mg, 4.0 mol%, 0.008 mmol) in EtOH (1.0 mL, 0.2 M) was stirred under nitrogen atmosphere for 40 hours at 50 °C to afford **31** as a white oil (31.7 mg, 80% yield, >95:5 d.r.).

Purification conditions: petroleum ether/EtOAc = 10:1 to 6:1.

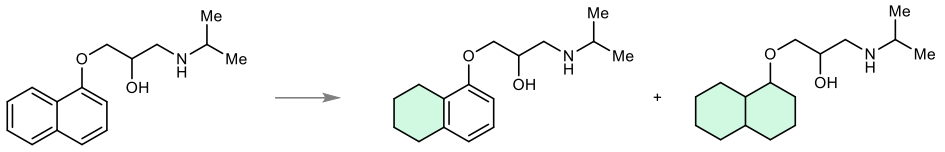
R_f = 0.5 in petroleum ether/EtOAc (2.5:1).

^{1}H NMR (400 MHz, $CDCl_3$) δ 3.39 - 3.27 (m, 4H), 2.42 (tt, *J* = 12.0, 4.0 Hz, 1H), 1.82 - 1.75 (m, 1H), 1.69 - 1.60 (m, 3H), 1.52 - 1.35 (m, 2H), 1.33 - 1.24 (m, 2H), 1.17 (t, *J* = 8.0 Hz, 3H), 1.08 (t, *J* = 8.0 Hz, 3H), 0.98 - 0.93 (m, 1H), 0.90 (d, *J* = 6.4 Hz, 3H).
^{13}C NMR (100 MHz, $CDCl_3$) δ 175.5, 41.8, 40.8, 40.2, 38.2, 34.6, 32.4, 29.3, 25.9, 22.8, 15.1, 13.3. HRMS (ESI, *m*/*z*) calcd for $C_{12}H_{24}NO$ $[M+H]^+$: 198.1858, found: 198.1855.



32 (±)-Atenolol **33** (91% yield, 3:1 d.r.)

According to the general procedure, a mixture of **(±)-atenolol** (53.3 mg, 0.2 mmol, 1.0 equiv.), $B_2(OH)_4$ (89.6 mg, 1.0 mmol, 5.0 equiv.) and $[Rh(COD)OH]_2$ (2.3 mg, 2.5 mol%, 0.005 mmol) in EtOH (1.0 mL, 0.2 M) was stirred under argon atmosphere for 14 hours at 50 °C to afford **33** as a colorless oil (49.3 mg, 91% yield, 3:1 d.r.).
^{1}H NMR (600 MHz, $CDCl_3$, mixture of diastereomers) δ 5.97 - 5.73 (m, 2H), 3.79 (m, 1H), 3.50 (m, 1H, major), 3.47 - 3.44 (m, 1H, minor), 3.41 - 3.33 (m, 2H, major; m, 1H, minor), 3.19 - 3.14 (m, 1H, minor), 2.82 - 2.70 (m, 4H), 2.60 - 2.54 (m, 1H), 2.08 (d, *J* = 7.1 Hz, 2H, major), 2.05 (d, *J* = 7.1 Hz, 2H, minor), 2.01 - 1.99 (m, 2H, minor), 1.85 - 1.70 (m, 3H), 1.51 - 1.48 (m, 2H, major), 1.45 - 1.41 (m, 2H, major), 1.34 - 1.28 (m, 2H, major), 1.26 - 1.19 (m, 2H, minor), 1.05 - 1.03 (m, 6H), 1.00 - 0.93 (m, 1H, minor). ^{13}C NMR (151 MHz, $CDCl_3$, mixture of diastereomers) δ 175.2 (major), 175.0 (minor), 78.6, 74.1, 71.0 (minor), 70.8 (major), 69.26 (minor), 69.24 (major), 49.9 (major), 49.8 (minor), 48.95 (minor), 48.94 (major), 43.1 (minor), 43.0 (major), 34.5, 34.00 (major), 31.9, 31.9, 31.1, 29.3, 29.2, 27.1 (major), 22.96 (minor), 22.93 (major), 22.90 (major). HRMS (ESI, *m*/*z*) calcd for $C_{14}H_{29}N_2O_3$ $[M+H]^+$: 273.2173, found: 273.2171.



According to the general procedure, a mixture of **(±)-propranolol** (51.9 mg, 0.2 mmol, 1.0 equiv.), $B_2(OH)_4$ (80.6 mg, 0.9 mmol, 4.5 equiv.) and $[Rh(COD)OH]_2$ (2.3 mg, 2.5 mol%, 0.005 mmol) in EtOH (1.0 mL, 0.2 M) was stirred under argon atmosphere for 14 hours at 50 ℃ to afford **35'** (43.1 mg, 83% yield) as colorless oil.

Under an alternative condition with $B_2(OH)_4$ (113.3 mg, 1.4 mmol, 7.0 equiv.) and $[Rh(COD)OH]_2$ (4.6 mg, 5 mol%, 0.01 mmol), **35'** (25.1 mg, 41% yield) and **35** (19.9 mg, 38% yield, >95:5 d.r.) were afforded as colorless oil.

Analytical data of **35'**:

^{1}H NMR (400 MHz, $CDCl_3$) δ 9.49 (br, 1H), 8.48 (br, 1H), 7.01 (m, 1H), 6.70 (d, J = 7.7 Hz, 1H), 6.56 (d, J = 8.1 Hz, 1H), 4.62 (m, 1H), 4.06 (dd, J = 9.6, 4.2 Hz, 1H), 3.93 (dd, J = 9.6, 6.1 Hz, 1H), 3.48 (m, 1H), 3.32 (m, 1H), 3.18 (m, 1H), 2.72 (t, J = 5.9 Hz, 2H), 2.62 (t, J = 6.1 Hz, 2H) 1.81 - 1.66 (m, 4H), 1.50 - 1.47 (m, 6H).

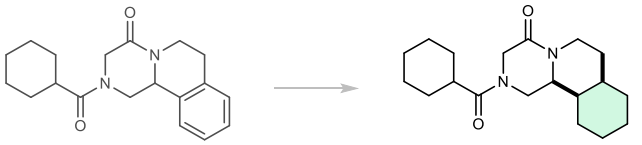
^{13}C NMR (101 MHz, $CDCl_3$) δ 155.9, 138.9, 126.1, 125.9, 122.3, 107.9, 69.5, 66.0, 51.6, 48.5, 29.7, 23.2, 22.9, 19.2, 19.1.

HRMS (ESI, *m*/*z*) calcd for $C_{16}H_{26}NO_2^+$ $[M+H]^+$: 264.1958, found: 264.1956.

Analytical data of **35**:

^{1}H NMR (400 MHz, $CDCl_3$, mixture of diastereomers) δ 3.87 - 3.81 (m, 1H), 3.57 - 3.47 (m, 1H), 3.44 - 3.36 (m, 1H), 3.30 (dt, J = 11.5, 4.6 Hz, 1H), 2.87 - 2.77 (m, 2H), 2.64 (ddd, J = 11.9, 7.8, 1.7 Hz, 1H), 2.54 (br, 2H), 2.05 - 1.96 (m, 1H), 1.80 - 1.76 (m, 2H), 1.70 - 1.66 (m, 1H), 1.63 - 1.54 (m, 3H), 1.53 - 1.29 (m, 6H), 1.27 - 1.14 (m, 3H), 1.10 (d, J = 6.3 Hz, 6H).

^{13}C NMR (101 MHz, $CDCl_3$, mixture of diastereomers) δ 81.7, 81.6, 70.73, 70.69, 69.3, 49.91, 49.90, 49.08, 49.06, 39.97, 39.89, 35.8, 32.1, 26.78, 26.73, 26.5, 25.01, 24.49, 22.96, 22.93, 21.7, 19.6. HRMS (ESI, *m*/*z*) calcd for $C_{16}H_{32}NO_2^+$ $[M+H]^+$: 270.2428, found: 270.2426.

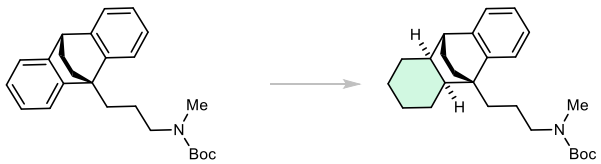


36 (±)-Praziquantel **37** (67% yield, >95:5 d.r.)

According to the general procedure, a mixture of **(±)-praziquantel** (62.4 mg, 0.2 mmol, 1.0 equiv.), $B_2(OH)_4$ (80.6 mg, 0.9 mmol, 4.5 equiv.) and $[Rh(COD)OH]_2$ (4.6 mg, 5 mol%, 0.010 mmol) in EtOH (1.0 mL, 0.2 M) was stirred under argon atmosphere for 14 hours at 50 ℃ to afford **37** as a colorless oil (42.5 mg, 67% yield, >95:5 d.r.).

^{1}H NMR (400 MHz, $CDCl_3$) δ 4.75-4.72 (m, 1H), 4.19 (d, *J* = 17.3 Hz, 1H), 4.07 - 4.00 (m, 2H), 3.54 (dd, *J* = 13.9, 5.6 Hz, 1H), 3.39 (td, *J* = 5.1, 3.0 Hz, 1H), 2.55 (dt, *J* = 12.0, 6.2 Hz, 1H), 2.39 (tt, *J* = 11.6, 3.5 Hz, 1H), 1.92 - 1.66 (m, 10H), 1.57 - 1.18 (m, 12H).

^{13}C NMR (101 MHz, $CDCl_3$) δ 174.4, 164.4, 58.3, 49.1, 43.1, 41.2, 41.1, 40.7, 35.9, 31.6, 29.3, 28.8, 25.96, 25.92, 25.8, 25.7, 24.5, 20.5, 19.9. HRMS (ESI, *m*/*z*) calcd for $C_{19}H_{30}N_2O_2Na^+$ $[M+Na]^+$: 341.2199, found: 341.2200.



Boc-Maprotiline **39** (86% yield)

According to the general procedure, a mixture of **Boc-Maprotiline** (75.4mg, 0.20 mmol, 1.0 equiv.), $B_2(OH)_4$ (80.6 mg, 0.9 mmol, 4.5 equiv.) and $[Rh(COD)OH]_2$ (3.7 mg, 4.0 mol%, 0.008 mmol) in EtOH (1.0 mL, 0.2 M) was stirred under nitrogen atmosphere for 48 hours at 80 ℃ to afford **39** as a white solid (66.5 mg, 86% yield, >95:5 d.r.)

Purification conditions: petroleum ether/CH_2Cl_2 = 5:1 to 2:1.

R_f = 0.3 in petroleum ether/ CH_2Cl_2 = 1:1

^{1}H NMR (400 MHz, $CDCl_3$) δ 7.24 - 7.08 (m, 4H), 3.31 (br, 2H), 2.91 (s, 3H), 2.70 - 2.65 (m, 1H), 2.06 - 1.94 (m, 1H), 1.90 - 1.55 (m, 8H), 1.54 - 1.44 (m, 11H), 1.43 - 1.24 (m, 5H), 1.23 - 1.10 (m, 2H). ^{13}C NMR (100 MHz, $CDCl_3$, mixture of rotamers) δ 155.99, 155.97, 146.2, 145.9, 143.8, 143.0, 125.6, 125.6, 125.4, 125.3, 123.4, 122.7, 121.6, 79.3, 79.3, 41.6, 41.1, 40.1, 40.1, 39.9, 39.4, 37.6, 34.6, 34.5, 30.6, 30.2, 30.0, 28.6, 27.2, 24.8, 23.0, 20.9, 20.6, 20.11, 20.09, 19.7, 18.9. HRMS (ESI, *m*/*z*) calcd for $C_{25}H_{37}NO_2Na^+$ $[M+Na]^+$: 406.2717, found: 406.2715.



(±)-Flurbiprofen **39** (55% yield)

According to the general procedure, a mixture of **(±)-flurbiprofen** (48.8 mg, 0.20 mmol, 1.0 equiv.), $B_2(OH)_4$ (80.6 mg, 0.90 mmol, 4.5 equiv.) and $[Rh(COD)OH]_2$ (2.4 mg, 2.5 mol%, 0.008 mmol) in EtOH (3.0 mL, 0.07 M) was stirred under nitrogen atmosphere for 40 hours at 50 ℃ to afford **39** as a colorless oil (27.5 mg, 55% yield).

Purification conditions: petroleum ether/acetone = 30:1 to 5:1.

R_f = 0.25 in petroleum ether/acetone = 3:1.

^{1}H NMR (400 MHz, $CDCl_3$) δ 7.17 (t, *J* = 7.6 Hz, 1H), 7.03 (dd, *J* = 8.0, 2.0 Hz, 1H), 6.98 (dd, *J* = 11.6, 2.0 Hz, 1H), 3.69 (q, *J* = 7.2 Hz, 1H), 2.88 - 2.76 (m, 1H), 1.83 (d, *J* = 8.8 Hz, 4H), 1.75 (d, *J* = 13.6 Hz, 1H), 1.49 (d, *J* = 6.8 Hz, 3H), 1.45 - 1.34 (m, 4H), 1.30 - 1.23 (m, 1H).

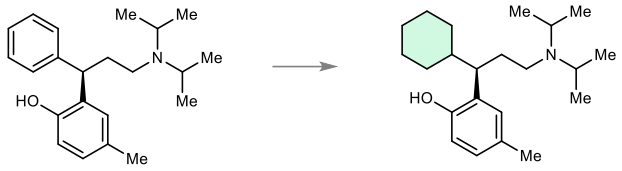
^{13}C NMR (100 MHz, $CDCl_3$) δ 180.1, 160.68 (d, *J* = 243.0 Hz), 139.0 (d, *J* = 8.0 Hz), 133.7 (d, *J* = 15.0 Hz), 127.96.0 (d, *J* = 5.0 Hz), 123.4 (d, *J* = 3.0 Hz), 114.6 (d, *J* = 24.0 Hz), 44.8, 37.10, 37.09, 33.1, 27.0, 26.3, 18.1. ^{19}F NMR (376 MHz, $CDCl_3$) δ -118.98. HRMS (ESI, *m*/*z*) calcd for $C_{15}H_{19}O_2FNa^+$ $[M+Na]^+$: 273.1267, found: 273.1262.



(±)-Naftopidil **40** (92% yield)

According to the general procedure, a mixture of **(±)-naftopidil** (78.50 mg, 0.2 mmol, 1.0 equiv.), $B_2(OH)_4$ (80.6 mg, 0.9 mmol, 4.5 equiv.) and $[Rh(COD)OH]_2$ (2.3 mg, 2.5 mol%, 0.005 mmol) in EtOH (1.0 mL, 0.2 M) was stirred under argon atmosphere for 14 hours at 50 ℃ to afford **40** as a colorless oil (72.0 mg, 92% yield).

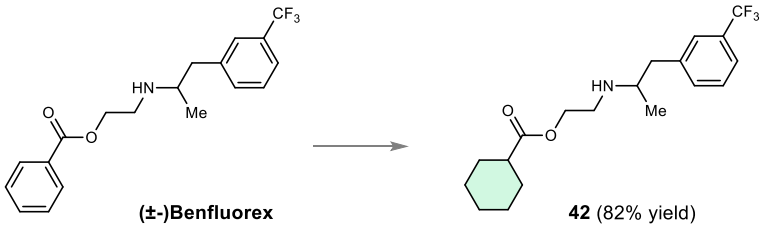
^{1}H NMR (400 MHz, $CDCl_3$) δ 7.09 - 7.01 (m, 2H), 6.98 - 6.93 (m, 2H), 6.89 (d, *J* = 7.8 Hz, 1H), 6.73 (d, *J* = 7.7 Hz, 1H), 6.67 (d, *J* = 8.1 Hz, 1H), 4.23 - 4.18 (m, 1H), 4.05 (dd, *J* = 9.4, 5.1 Hz, 1H), 3.99 (dd, *J* = 9.6, 5.0 Hz, 1H), 3.88 (s, 3H), 3.57 (br, 1H), 3.15 (m, 4H), 3.04 - 2.89 (m, 2H), 2.78 - 2.69 (m, 8H), 1.80 - 1.75 (m, 4H). ^{13}C NMR (101 MHz, $CDCl_3$) δ 156.4, 152.3, 141.2, 138.7, 126.2, 125.7, 123.2, 121.8, 121.1, 118.32, 111.3, 107.9, 70.2, 65.8, 61.1, 55.4, 53.7, 50.7, 29.7, 23.2, 22.89, 22.86. HRMS (ESI, *m*/*z*) calcd for $C_{24}H_{33}N_2O_3^+$ $[M+H]^+$: 397.2486, found: 397.2483.



(*R*)-Tolterodine **41** (96% yield)

According to the general procedure, a mixture of **(*R*)-tolterodine** (65.1 mg, 0.2 mmol, 1.0 equiv.), $B_2(OH)_4$ (80.6 mg, 0.9 mmol, 4.5 equiv.) and $[Rh(COD)OH]_2$ (2.3 mg, 2.5 mol%, 0.005 mmol) in EtOH (1.0 mL, 0.2 M) was stirred under argon atmosphere for 14 hours at 50 ℃ to afford **41** (63.4 mg, 96% yield) as colorless oil.

^{1}H NMR (400 MHz, Methanol-d_4) δ 6.89 - 6.96 (m, 2H), 6.69 (d, J = 8.0 Hz, 1H), 3.65 - 3.54 (m, 2H), 2.94 (ddd, J = 13.8, 12.1, 5.6 Hz, 1H), 2.76 - 2.60 (m, 2H), 2.23 (s, 3H), 2.19 - 2.00 (m, 3H), 1.82 - 1.75 (m, 1H), 1.73 - 1.62 (m, 3H), 1.44 - 1.41 (m, 1H), 1.32 - 1.22 (m, 13H), 1.18 - 1.12 (m, 2H), 1.01 (qd, J = 12.4, 3.6 Hz, 1H), 0.90 - 0.79 (m, 1H). ^{13}C NMR (101 MHz, Methanol-d_4) δ 154.5, 130.5, 129.9, 129.2, 128.9, 116.3, 56.2, 42.7, 32.54, 32.50, 31.2, 27.7, 27.5, 27.4, 20.7, 17.9. HRMS (ESI, *m*/*z*) calcd for $C_{22}H_{38}NO^+$ $[M+H]^+$: 332.2948, found: 332.2946.



(±-)Benfluorex **42** (82% yield)

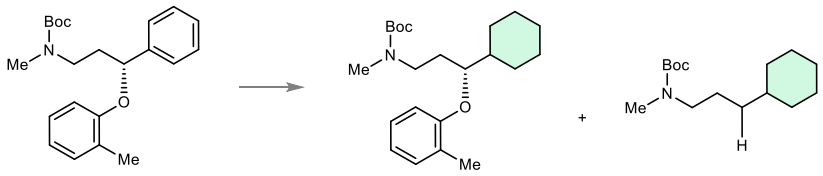
According to the general procedure, a mixture of (±)-**benfluorex** (70.3 mg, 0.20 mmol, 1.0 equiv.), $B_2(OH)_4$ (107.5 mg, 1.20 mmol, 6.0 equiv.) and $[Rh(COD)OH]_2$ (3.7 mg, 4.0 mol%, 0.008 mmol) in i-PrOH/EtOH (*v*/*v* = 9:1, 1.0 mL) was stirred under nitrogen atmosphere for 24 hours at 50 ℃ to afford **42** as a colorless oil (58.6 mg, 82% yield).

Purification conditions: CH_2Cl_2/MeOH = 50 to 30:1.

R_f = 0.4 in CH_2Cl_2/MeOH = 20 :1

^{1}H NMR (400 MHz, $CDCl_3$) δ 7.47 (d, J = 7.6 Hz, 1H), 7.44 (s, 1H), 7.42 - 7.35 (m, 2H), 4.19 - 4.12 (m, 1H), 4.11 - 4.04 (m, 1H), 2.99 - 2.86 (m, 2H), 2.82 - 2.78 (m, 1H) 2.77 - 2.73 (m, 1H), 2.69 (dd, J = 13.2, 6.4 Hz, 1H), 2.17 (tt, J = 11.2, 3.6 Hz, 1H), 1.80 - 1.65 (m, 4H), 1.65 - 1.57 (m, 1H), 1.37 - 1.13 (m, 6H), 1.07 (d, J = 6.4 Hz, 3H). ^{13}C NMR (100 MHz, $CDCl_3$) δ 176.0,

140.3, 132.8, 132.8, 130.83 (q, J = 32.0 Hz), 128.9, 126.0 (q, J = 3.7 Hz), 124.2 (q, J = 271.0 Hz), 123.23 (q, J = 3.9 Hz), 63.7, 54.1, 45.7, 43.5, 43.1, 29.0, 29.0, 25.8, 25.5, 25.5, 20.2. ^{19}F NMR (376 MHz, $CDCl_3$) δ -62.6. HRMS (ESI, *m*/*z*) calcd for Chemical Formula: $C_{19}H_{27}F_3NO_2^+$ $[M+H]^+$:358.1988, found: 358.1993.



Boc-(*R*)-Atomoxetine **43** (32% yield) **43'** (58% yield)

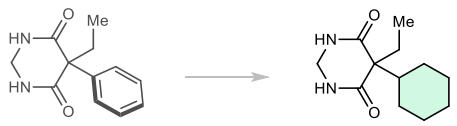
According to the general procedure, a mixture of **Boc-(*R*)-atomoxetine** (71.1 mg, 0.2 mmol, 1.0 equiv.), $B_2(OH)_4$ (164.6 mg, 1.8 mmol, 9.0 equiv.) and $[Rh(COD)OH]_2$ (2.3 mg, 2.5 mol%, 0.005 mmol) in EtOH (1.0 mL, 0.2 M) was stirred under argon atmosphere for 14 hours at 50 °C to afford **43** (23.4 mg, 32% yield) and **43´**(29.6 mg, 58% yield) as colorless oil.

Analytical data of **43**:

^{1}H NMR (600 MHz, $CDCl_3$) δ 7.13-7.09 (m, 2H), 6.80 (t, J = 7.4 Hz, 1H), 6.76 (d, J = 8.2 Hz, 1H), 4.13 (m, 1H), 3.34-3.23 (m, 2H), 2.79 (s, 3H), 2.22 (s, 3H), 1.88-1.85 (m, 2H), 1,80-1.66 (m, 6H), 1.41 (s, 9H), 1.26-1.19 (m, 2H), 1.17-1.11 (m, 3H). ^{13}C NMR (151 MHz, $CDCl_3$) δ 156.4, 155.7, 130.8, 127.3, 126.6, 119.8, 111.6, 79.3, 78.6, 45.9, 40.5, 34.3, 28.6, 28.4, 26.6, 26.3, 26.2, 16.5. HRMS (ESI, *m*/*z*) calcd for $C_{22}H_{35}NO_3Na^+$ $[M+ Na]^+$: 384.2511, found: 384.2509.

Analytical data of **43´**:

^{1}H NMR (600 MHz, $CDCl_3$) δ 3.15 (m, 2H), 2.82 (s, 3H), 1.72-1.64 (m, 5H), 1.52-1.46 (m, 2H), 1.44 (s, 9H), 1.24-1.17 (m, 3H), 1.16-1.11 (m, 3H), 0.93-0.82 (m, 2H). ^{13}C NMR (151 MHz, $CDCl_3$) δ 156.0, 79.2, 37.4, 34.5, 34.2, 33.5, 28.64, 28.62, 26.8, 26.5, 25.2. HRMS (ESI, *m*/*z*) calcd for $C_{15}H_{29}NO_2Na^+$ $[M+ Na]^+$: 278.1931, found: 278.2123.

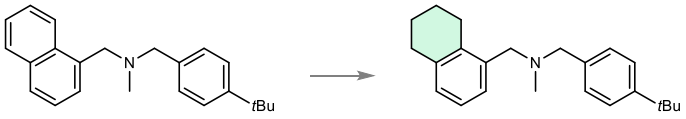


Primidone **44** (96% yield)

According to the general procedure, a mixture of **primidone** (43.6 mg, 0.2 mmol, 1.0 equiv.), $B_2(OH)_4$ (80.6 mg, 0.9 mmol, 4.5 equiv.) and $[Rh(COD)OH]_2$ (2.3 mg, 2.5 mol%, 0.005 mmol)

in EtOH (1.0 mL, 0.2 M) was stirred under argon atmosphere for 14 hours at 50 ℃ to afford **44** as a colorless oil (43.1 mg, 96% yield).

^{1}H NMR (600 MHz, Methanol-d_4) δ 4.64 (d, J = 10.9 Hz, 1H), 4.44 (d, J = 10.9 Hz, 1H), 1.91 (q, J = 7.6, 7.2 Hz, 2H), 1.86 (m, 1H), 1.81 - 1.77 (m, 4H), 1.65 (d, J = 12.6 Hz, 1H), 1.27 - 1.19 (m, 4H), 1.17 - 1.11 (m, 1H), 0.79 (t, J = 7.1 Hz, 3H). ^{13}C NMR (151 MHz, Methanol-d_4) δ 174.1, 60.6, 51.9, 47.0, 29.8, 27.9, 27.4, 26.3, 10.0. HRMS (ESI, m/z) calcd for $C_{12}H_{21}N_2O_2^+$ $[M+H]^+$: 225.1597, found: 225.1598.



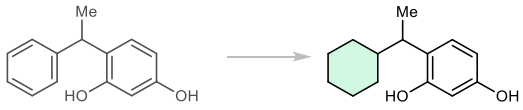
Butenafine **45** (13% yield)

According to the general procedure, a mixture of **butenafine** (63.4 mg, 0.20 mmol, 1.0 equiv.), $B_2(OH)_4$ (80.6 mg, 0.90 mmol, 4.5 equiv.) and $[Rh(COD)OH]_2$ (2.4 mg, 2.5 mol%, 0.001 mmol) in EtOH (1.0 mL, 0.2 M) was stirred under nitrogen atmosphere for 16 hours at 50 ℃ to afford **45** as a yellow oil (8.6 mg, 13% yield).

Purification conditions: CH_2Cl_2/MeOH = 200:1 to 80:1.

Rf = 0.5 in CH_2Cl_2/MeOH) = 50:1.

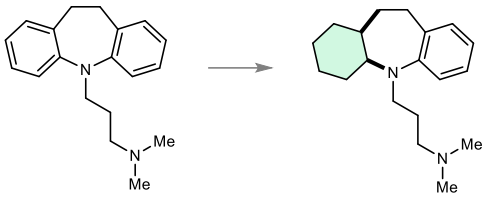
^{1}H NMR (400 MHz, $CDCl_3$) δ 7.33 (d, J = 8.4 Hz, 2H), 7.26 (d, J = 8.0 Hz, 2H), 7.18 (d, J = 7.2 Hz, 1H), 7.06 (t, J = 7.6 Hz, 1H), 6.98 (d, J = 7.6 Hz, 1H), 3.47 (d, J = 14.0 Hz, 4H), 2.79 (t, J = 6.0 Hz, 4H), 2.15 (s, 3H), 1.84 - 1.74 (m, 4H), 1.31 (s, 9H). ^{13}C NMR (100 MHz, $CDCl_3$) δ 150.0, 137.5, 136.6, 128.9, 128.4, 127.5, 125.9, 125.2, 125.0, 61.9, 59.8, 42.2, 34.6, 31.5, 30.3, 26.0, 23.4, 23.0. HRMS (ESI, m/z) calcd for $C_{23}H_{32}N^+$ $[M+H]^+$: 322.2535, found: 322.2537.



(±)-Phenylethyl resorcinol **46** (78% yield)

According to the general procedure, a mixture of **(±)-phenylethyl resorcinol** (42.8 mg, 0.2 mmol, 1.0 equiv.), $B_2(OH)_4$ (143.3 mg, 1.6 mmol, 8.0 equiv.) and $[Rh(COD)OH]_2$ (3.6 mg, 4 mol%, 0.0080 mmol) in EtOH (1.0 mL, 0.2 M) was stirred under nitrogen atmosphere for 14 hours at 50 ℃ to afford **46** as a colorless oil (34.5 mg, 78% yield).

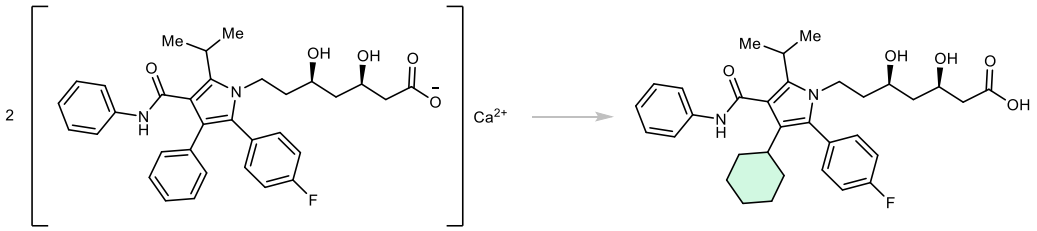
^{1}H NMR (400 MHz, $CDCl_3$) δ 6.94 (d, *J* = 8.3 Hz, 1H), 6.39 (dd, *J* = 8.4, 2.4 Hz, 1H), 6.30 (d, *J* = 2.5 Hz, 1H), 5.22 (br, 1H), 5.04 (br, 1H), 2.69 (p, *J* = 7.2 Hz, 1H), 2.09 - 1.85 (m, 2H), 1.76 - 1.72 (m, 1H), 1.68 - 1.56 (m, 2H), 1.52 - 1.49 (m, 1H), 1.45 - 1.36 (m, 1H), 1.18 (d, *J* = 7.0 Hz, 3H), 1.15 - 1.10 (m, 2H), 0.99 - 0.85 (m, 2H). ^{13}C NMR (101 MHz, $CDCl_3$) δ 154.1, 154.0, 128.9, 125.4, 107.9, 102.9, 43.6, 37.7, 31.5, 30.6, 29.8, 26.70, 26.67, 18.1. HRMS (ESI, *m*/*z*) calcd for $C_{14}H_{20}O_2Na^+$ $[M+Na]^+$: 243.1361, found: 243.1355.



Imipramine **47** (44% yield)

According to the general procedure, a mixture of **imipramine** (56.0 mg, 0.2 mmol, 1.0 equiv.), $B_2(OH)_4$ (80.6 mg, 0.9 mmol, 4.5 equiv.) and $[Rh(COD)OH]_2$ (4.6 mg, 5 mol%, 0.010 mmol) in EtOH (1.0 mL, 0.2 M) was stirred under argon atmosphere for 14 hours at 50 ℃ to afford **47** as a colorless oil (24.9 mg, 44% yield, >95:5 d.r.).

^{1}H NMR (400 MHz, $CDCl_3$) δ 7.13 - 7.07 (m, 2H), 6.92 - 6.85 (m, 2H), 3.47 - 3.37 (m, 1H), 3.27 - 3.12 (m, 2H), 2.98 - 2.85 (m, 2H), 2.75 - 2.56 (m, 8H), 2.14 - 1.96 (m, 3H), 1.68 - 1.51 (m, 5H), 1.36 - 1.09 (m, 4H), 0.78 (m, 1H). ^{13}C NMR (151 MHz, acetone-*d*$_6$, mixture of diastereomers) δ 148.6, 137.8, 129.8, 128.8, 126.5, 126.2, 122.7, 121.7, 120.7, 119.9, 62.1, 55.5, 50.0, 41.8, 33.8, 32.6, 31.9, 26.4, 26.2, 24.0, 23.5, 20.4. HRMS (ESI, *m*/*z*) calcd for $C_{19}H_{31}N_2^+$ $[M+H]^+$: 287.2482, found: 287.2480.

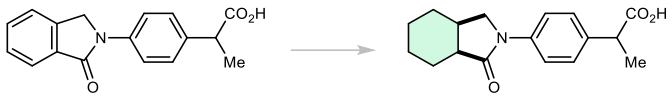


Atorvastatin Calcium Trihydrate **48** (56% yield)

According to the general procedure, a solution of Atorvastatin Calcium Trihydrate (120.9 mg, 0.1 mmol, 0.5 equiv.), $B_2(OH)_4$ (125.5 mg, 1.4 mmol, 7.0 equiv.) and $[Rh(COD)OH]_2$ (3.7 mg, 4.0 mol%, 0.005 mmol) in EtOH (1.0 mL, 0.2 M) was stirred under argon atmosphere for 24 hours at 50 ℃ to afford **48** (31.8 mg, 56% yield) as colorless oil.

Analytical data of **48**:

^{1}H NMR (500 MHz, $CDCl_3$) δ 7.18 - 7.05 (m, 7H), 6.98 (t, *J* = 8.6 Hz, 2H), 4.11 (dt, *J* = 14.3, 6.9 Hz, 2H), 3.96 (dt, *J* = 14.6, 7.2 Hz, 1H), 3.79 - 3.62 (m, 2H), 3.39 (p, *J* = 7.0 Hz, 1H), 2.45 (d, *J* = 3.2 Hz, 2H), 1.69 - 1.61 (m, 2H), 1.59 - 1.41 (m, 12H), 1.41 - 1.20 (m, 4H), 1.14 (d, *J* = 14.5 Hz, 1H), 1.00 (d, *J* = 10.8 Hz, 1H), 0.77 (t, *J* = 11.8 Hz, 2H). ^{13}C NMR (500 MHz, $CDCl_3$) δ 167.9, 165.9, 163.6, 138.8, 134.4, 132.8, 130.1, 128.8, 128.2, 127.9, 126.1, 121.9, 116.8, 115.6, 115.5, 69.6, 69.1, 49.0, 41.9, 41.3, 40.6, 37.1, 31.9, 26.9, 25.4, 24.5, 22.7, 22.2. HRMS (ESI, *m*/*z*) calcd for $C_{33}H_{42}N_2O_5F^+$ $[M+H]^+$: 565.3078, found: 564.3965.



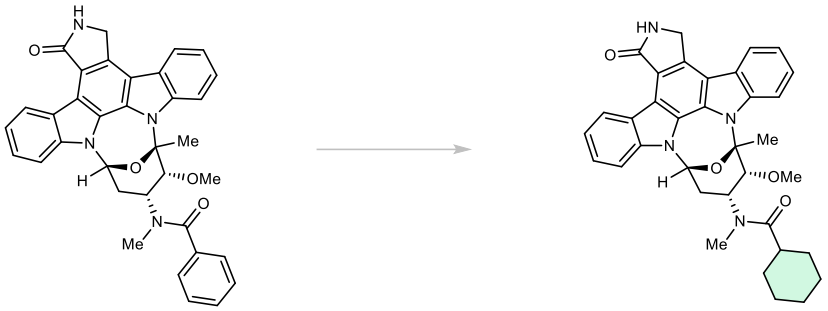
(±)-Indoprofen **49** (42% yield)

According to the general procedure, a mixture of **(±)-indoprofen** (56.9 mg, 0.20 mmol, 1.0 equiv.), $B_2(OH)_4$ (107.5 mg, 1.20 mmol, 6.0 equiv.) and $[Rh(COD)OH]_2$ (3.7 mg, 4.0 mol%, 0.008 mmol) in EtOH (3.0 mL, 0.07 M) was stirred under nitrogen atmosphere for 40 hours at 50 ℃ to afford **49** as a white oil (23.5 mg, 42% yield, >95:5 d.r.).

Purification conditions: petroleum ether/EtOAc = 30:1 to 5:1.

R_f = 0.3 in petroleum ether/EtOAc (1.5:1).

^{1}H NMR (400 MHz, $CDCl_3$) δ 7.59 (d, *J* = 8.4 Hz, 2H), 7.30 (d, *J* = 8.4 Hz, 2H), 3.81 (dd, *J* = 9.6, 6.0 Hz, 1H), 3.70 (q, *J* = 7.2 Hz, 1H), 3.36 (dd, *J* = 9.6, 2.0 Hz, 1H), 2.71 - 2.63 (m, 1H), 2.47 - 2.38 (m, 1H), 2.15 - 2.06 (m, 1H), 1.80 - 1.71 (m, 1H), 1.64 - 1.51 (m, 3H), 1.48 (d, *J* = 7.8 Hz, 3H), 1.33 - 1.23 (m, 3H). ^{13}C NMR (100 MHz, $CDCl_3$) δ 179.8, 175.5, 139.3, 135.9, 128.1, 119.9, 52.8, 44.9, 43.5, 32.2, 28.0, 23.7, 23.6, 22.9, 18.3. HRMS (ESI, *m*/*z*) calcd for $C_{17}H_{22}NO_3^+$ $[M+H]^+$: 288.1600, found: 288.1596.



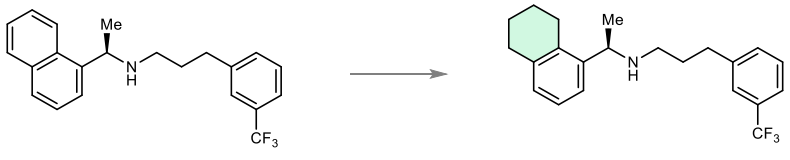
Midostaurin **50** (55% yield)

According to the general procedure, a mixture of **midostaurin** (114.0 mg, 0.20 mmol, 1.0 equiv.), $B_2(OH)_4$ (107.5 mg, 1.2 mmol, 6.0 equiv.) and $[Rh(COD)OH]_2$ (3.7 mg, 4.0 mol%, 0.008 mmol) in EtOH (1.0 mL, 0.2 M) was stirred under nitrogen atmosphere for 48 hours at 80 °C to afford **50** as a white solid (63.3 mg, 55% yield)

Purification conditions: petroleum ether/Acetone = 10:1 to 4:1.

R_f = 0.3 in petroleum ether/Acetone = 5:1

^{1}H NMR (400 MHz, $CDCl_3$) δ 9.47 (d, *J* = 8.0 Hz, 1H), 7.84 (d, J = 7.6 Hz, 1H), 7.72 (d, *J* = 8.8 Hz, 1H), 7.44 (q, *J* = 8.0 Hz, 2H), 7.37 (t, *J* = 7.6 Hz, 1H), 7.30 (t, *J* = 7.6 Hz, 1H), 7.20 (d, *J* = 8.0 Hz, 1H), 7.13 (br, 1H), 6.62 (dd, *J* = 8.0, 5.6 Hz, 1H), 5.19 - 5.09 (m, 1H), 4.96 (s, 2H), 3.99 (d, *J* = 2.0 Hz, 1H), 2.86 (s, 3H), 2.58 - 2.49 (m, 2H), 2.49 - 2.45 (m, 3H), 2.42 (s, 3H), 1.87 - 1.77 (m, 3H), 1.73 (d, *J* = 15.2 Hz, 3H), 1.66 - 1.45 (m, 2H), 1.31 - 1.23 (m, 3H). ^{13}C NMR (100 MHz, $CDCl_3$) δ 177.1, 173.5, 138.7, 136.6, 132.6, 130.5, 126.9, 126.3, 125.4, 125.0, 124.7, 123.7, 121.5, 120.5, 120.1, 119.3, 116.3, 114.6, 112.4, 107.8, 94.7, 84.9, 82.5, 60.6, 48.9, 46.1, 41.5, 31.3, 29.3, 29.2, 28.2, 25.95, 25.91, 25.85. HRMS (ESI, *m/z*) calcd for $C_{35}H_{36}N_4NaO_4^+$ $[M+Na]^+$: 599.2629, found: 599.2631.



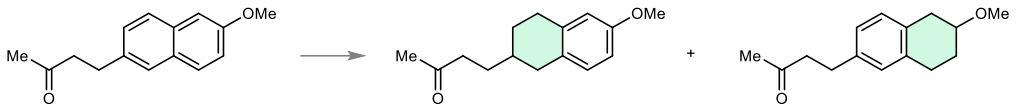
(*R*)-Cinacalcet **51** (35% yield)

According to the general procedure, a mixture of **(*R*)-Cinacalcet** (71.4 mg, 0.20 mmol, 1.0 equiv.), $B_2(OH)_4$ (107.5 mg, 1.20 mmol, 6.0 equiv.) and $[Rh(COD)OH]_2$ (3.7 mg, 4.0 mol%, 0.008 mmol) in EtOH (1.0 mL, 0.2 M) was stirred under nitrogen atmosphere for 48 hours at 50 °C to afford **51** as a colorless oil (25.4 mg, 35% yield).

Purification conditions: CH_2Cl_2/NH_3(7.0 M solution in MeOH) = 500:1 to 200:1.

R_f = 0.25 in CH_2Cl_2/NH_3(7.0 M solution in MeOH) = 200:1.

^{1}H NMR (400 MHz, $CDCl_3$) δ 7.38 - 7.32 (m, 2H), 7.31 - 7.23 (m, 2H), 7.22 - 7.17 (m, 1H), 7.06 (t, *J* = 7.6 Hz, 1H), 6.90 (d, *J* = 7.6 Hz, 1H), 3.98 (q, *J* = 6.4 Hz, 1H), 2.73 (t, *J* = 6.4 Hz, 2H), 2.69 - 2.54 (m, 4H), 2.52 - 2.39 (m, 2H), 1.78 - 1.66 (m, 7H), 1.22 (d, *J* = 6.8 Hz, 3H). ^{13}C NMR (100 MHz, $CDCl_3$) δ 143.2, 137.5, 134.3, 131.91, 131.90, 130.72 (q, *J* = 31.9 Hz), 128.5, 128.0, 125.9, 125.20 (q, *J* = 3.7 Hz), 124.4 (q, *J* = 282 Hz), 122.79 (q, *J* = 3.8 Hz), 122.5, 77.5, 77.2, 76.8, 52.8, 47.2, 33.5, 31.8, 30.5, 25.9, 23.5, 23.2, 22.8. ^{19}F NMR (376 MHz, $CDCl_3$) δ -62.52. HRMS (ESI, *m*/*z*) calcd for $C_{22}H_{27}F_3N^+$ $[M+H]^+$: 362.2096, found: 362.2095.



52 Nabumetone **53** (53% yield) **54** (27% yield)

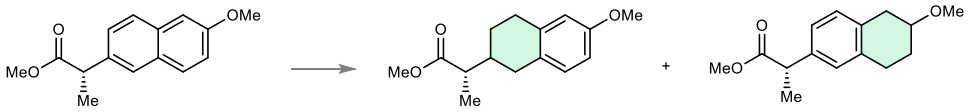
According to the general procedure, a mixture of **nabumetone** (45.7 mg, 0.2 mmol, 1.0 equiv.), $B_2(OH)_4$ (53.7 mg, 0.6 mmol, 3.0 equiv.) and $[Rh(COD)OH]_2$ (2.3 mg, 2.5 mol%, 0.005 mmol) in EtOH (1.0 mL, 0.2 M) was stirred under argon atmosphere for 14 hours at 50 ℃ to afford **53** (24.5 mg, 53% yield) and **54** (12.4 mg, 27% yield) as colorless oil.

Analytical data of **53**:

^{1}H NMR (600 MHz, $CDCl_3$) δ 6.96 (d, *J* = 8.4 Hz, 1H), 6.68 (d, *J* = 8.5 Hz, 1H), 6.61 (s, 1H), 3.77 (s, 3H), 2.81-2.74 (m, 3H), 2.54 (t, *J* = 6.8 Hz, 2H), 2.35 (dd, *J* = 16.2, 9.4 Hz, 1H), 2.17 (s, 3H), 1.94-1.87 (m, 1H), 1.69-1.63 (m, 3H), 1,42-1.35 (m, 1H). ^{13}C NMR (151 MHz, $CDCl_3$) δ 209.2, 157.7, 137.8, 130.0, 128.5, 113.5, 112.0, 55.4, 41.5, 35.3, 34.2, 30.3, 30.0, 29.5, 29.4. HRMS (ESI, *m*/*z*) calcd for $C_{15}H_{20}O_2Na^+$ $[M+Na]^+$: 255.1355, found: 255.1354.

Analytical data of **54**:

^{1}H NMR (600 MHz, $CDCl_3$) δ 7.04 - 6.97 (m, 1H), 6.93 (d, *J* = 8.1 Hz, 1H), 6.91 (s, 1H), 3.67 - 3.63 (m, 1H), 3.42 (s, 3H), 3.04 (dd, *J* = 16.4, 4.8 Hz, 1H), 2.92 - 2.87 (m, 1H), 2.84 - 2.81 (m, 2H), 2.77 - 2.72 (m, 4H), 2.14 (s, 3H), 2.08 - 2.05 (m, 1H), 1.85 - 1.78 (m, 1H). ^{13}C NMR (151 MHz, $CDCl_3$) δ 208.2, 138.6, 136.3, 132.4, 129.7, 128.5, 125.9, 75.9, 56.0, 45.5, 34.9, 30.2, 29.5, 27.8, 27.0. HRMS (ESI, *m*/*z*) calcd for $C_{15}H_{20}O_2Na^+$ $[M+Na]^+$: 255.1355, found: 255.1355.



55 (*S*)-**Naproxen**-OMe **56** (38% yield) **57** (44% yield)

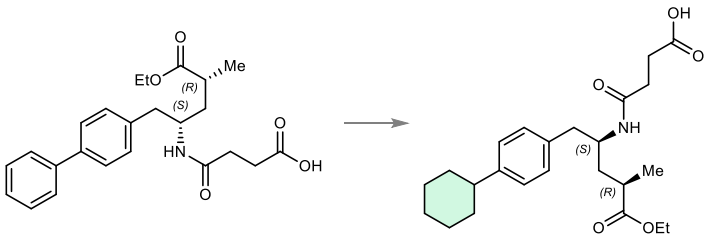
According to the general procedure, a mixture of **(*S*)-Naproxen-OMe** (48.8 mg, 0.2 mmol, 1.0 equiv.), $B_2(OH)_4$ (80.6 mg, 0.9 mmol, 4.5 equiv.) and $[Rh(COD)OH]_2$ (2.3 mg, 2.5 mol%, 0.005 mmol) in EtOH (1.0 mL, 0.2 M) was stirred under argon atmosphere for 14 hours at 50 ℃ to afford **56** (18.6 mg, 38% yield, 52:48 d.r.) and **57** (21.7 mg, 44% yield, 50:50 d.r.) as white solid.

Analytical data of **56**:

^{1}H NMR (599 MHz, $CDCl_3$, mixture of diastereomers) δ 6.97 (m, 1H), 6.68 (m, 1H), 6.62 (s, 1H), 3.77 (s, 3H), 3.70 (s, 3H), 2.83 - 2.68 (m, 3H), 2.51 - 2.42 (m, 2H), 2.14 - 1.81 (m, 2H), 1.48 - 1.39 (m, 1H), 1.23 - 1.21 (m, 3H). ^{13}C NMR (151 MHz, $CDCl_3$, mixture of diastereomers) δ 176.63, 176.56, 157.60, 157.56, 137.46, 137.37, 129.99, 129.94, 128.12, 127.98, 113.31, 113.30, 112.01, 111.96, 55.23, 55.22, 51.44, 44.66, 44.42, 37.67, 37.61, 32.99, 31.91, 29.56, 29.47, 27.64, 26.19, 14.28, 14.12. HRMS (ESI, *m*/*z*) calcd for $C_{15}H_{20}O_3Na^+$ $[M+Na]^+$: 271.1304, found: 271.1304.

Analytical data of **57**:

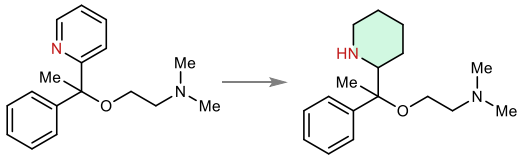
^{1}H NMR (599 MHz, $CDCl_3$, mixture of diastereomers) δ 7.04 (d, J = 1.2 Hz, 2H), 7.01 (s, 1H), 3.67-3.62 (m, 5H), 3.42 (s, 3H), 3.05 (dd, J = 16.3, 4.9 Hz, 1H), 2.92 (dq, J = 16.5, 5.5 Hz, 1H), 2.76 (dd, J = 16.3, 7.4 Hz, 2H), 2.18 - 1.99 (m, 1H), 1.86 - 1.78 (m, 1H), 1.47 (d, J = 7.1 Hz, 3H). ^{13}C NMR (151 MHz, $CDCl_3$, mixture of diastereomers) δ 175.31, 175.29, 138.26, 138.24, 136.48, 136.47, 133.55, 133.54, 129.88, 129.87, 127.69, 127.65, 125.12, 125.07, 75.84, 56.00, 52.14, 45.19, 45.17, 34.98, 34.97, 27.74, 27.73, 26.99, 26.97, 18.81, 18.79. HRMS (ESI, *m*/*z*) calcd for $C_{15}H_{20}O_3Na^+$ $[M+Na]^+$: 271.1304, found: 271.1304.



(2*S, 4R*)-Sacubitril **79** (34% yield)

According to the general procedure, a mixture of **(*2S, 4R*)-Sacubitril** (82.3 mg, 0.20 mmol, 1.0 equiv.), $B_2(OH)_4$ (107.5 mg, 1.20 mmol, 6.0 equiv.) and $[Rh(COD)OH]_2$ (3.7 mg, 4.0 mol%, 0.008 mmol) in EtOH (1.0 mL, 0.2 M) was stirred under nitrogen atmosphere fo 48 hours at 80 ℃ to afford **79** as a white solid (28.5 mg, 34% yield).

Purification conditions: Reverse-phase column chromatography ($MeCN/H_2O$ = 1:5 to 1.5:1) on SepaBean machine (Santai Technology Inc., China) equipped with C18-bonded SepaFlash columns. R_f= 0.4 in petroleum ether/acetone = 4:1 (the mixture of product and byproducts). ^1H NMR (400 MHz, $CDCl_3$) δ 7.11 (d, *J* = 8.0 Hz, 2H), 7.06 (d, *J* = 8.0 Hz, 2H), 5.93 - 5.83 (m, 1H), 4.24 - 4.14 (m, 1H), 4.10 (q, *J* = 7.2 Hz, 2H), 2.75 (d, *J* = 6.4 Hz, 2H), 2.64 - 2.57 (m, 2H), 2.56 - 2.38 (m, 4H), 1.95 - 1.78 (m, 5H), 1.73 (d, *J* = 12.4 Hz, 1H), 1.53 - 1.42 (m, 1H), 1.42 - 1.31 (m, 4H), 1.21 (t, *J* = 7.2 Hz, 4H), 1.13 (d, *J* = 7.2 Hz, 3H). ^{13}C NMR (100 MHz, $CDCl_3$) δ 176.6, 176.4, 172.0, 146.5, 134.7, 129.5, 127.0, 60.7, 48.9, 44.3, 40.5, 37.4, 36.6, 34.6, 31.0, 30.0, 27.0, 26.3, 17.7, 14.3. HRMS (ESI, *m/z*) calcd for $C_{24}H_{35}NO_5Na^+$ $[M+ Na]^+$: 440.2413, found: 440.2418.

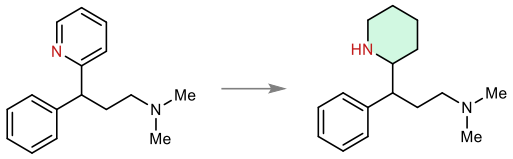


Doxylamine **80** (60% yield)

According to the general procedure, a mixture of **doxylamine** (54.0 mg, 0.20 mmol, 1.0 equiv.), $B_2(OH)_4$ (107.5 mg, 1.20 mmol, 6.0 equiv.) and $[Rh(COD)OH]_2$ (3.7 mg, 4.0 mol%, 0.008 mmol) in EtOH (1.0 mL, 0.2 M) was stirred under nitrogen atmosphere for 48 hours at 80 ℃ to afford **80** as a yellow oil (33.2 mg, 60% yield, major diastereoisomer).

Purification conditions: Reverse-phase column chromatography (MeOH/H_2O = 1:9 to 1.5:1) on SepaBean machine (Santai Tech-nology Inc., China) equipped with C18-bonded SepaFlash columns. R_f = 0.2 in NH_3(7.0 M solution in MeOH)/CH_2Cl_2 = 1:10.

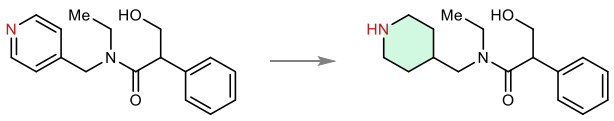
^{1}H NMR (400 MHz, $CDCl_3$) δ 7.32 - 7.24 (m, 4H), 7.21 - 7.16 (m, 1H), 3.34 (dt, *J* = 9.6, 6.4 Hz, 1H), 3.07 (dt, *J* = 9.6, 6.0 Hz, 1H), 2.94 - 2.89 (m, 1H), 2.52 (dd, *J* = 11.2, 2.0 Hz, 1H), 2.48 - 2.35 (m, 3H), 2.17 (s, 6H), 1.69 (d, *J* = 10.0 Hz, 2H), 1.54 (s, 3H), 1.45 - 1.41 (m, 1H), 1.32 - 1.13 (m, 2H), 1.12 - 1.01 (m, 1H). ^{13}C NMR (100 MHz, $CDCl_3$) δ 143.4, 128.2, 127.2, 127.1, 80.9, 66.9, 60.5, 59.6, 47.6, 46.0, 26.9, 26.2, 25.0, 18.9. HRMS (ESI, *m/z*) calcd for $C_{17}H_{29}N_2O^+$ $[M+H]^+$: 277.2280, found: 277.2281.



Pheniramine **81** (54% yield)

According to the general procedure, a mixture of **pheniramine** (48.0 mg, 0.2 mmol, 1.0 equiv.), $B_2(OH)_4$ (107.5 mg, 1.2 mmol, 6.0 equiv.) and $[Rh(COD)OH]_2$ (3.7 mg, 4 mol%, 0.008 mmol) in EtOH (1.0 mL, 0.2 M) was stirred under nitrogen atmosphere for 36 hours at 50 °C to afford **81** (26.7 mg, 54% yield, major diastereoisomer) as colorless oil.

^{1}H NMR (400 MHz, $CDCl_3$) δ 7.32 - 7.28 (m, 2H), 7.23 - 7.19 (m, 3H), 2.97 - 2.94 (m, 1H), 2.67 - 2.58 (m, 2H), 2.50 (td, J = 11.8, 2.9 Hz, 1H), 2.21 - 2.14 (m, 7H), 2.07 - 1.99 (m, 1H), 1.97 - 1.91 (m, 2H), 1.84 - 1.81 (m, 1H), 1.73 - 1.64 (m, 1H), 1.59 - 1.56 (m, 1H), 1.45 - 1.25 (m, 4H). ^{13}C NMR (101 MHz, $CDCl_3$) δ 142.5, 128.7, 128.5, 126.8, 61.5, 58.1, 50.2, 47.0, 45.3, 29.7, 29.5, 25.9, 24.8. HRMS (ESI, *m/z*) calcd for $C_{16}H_{27}N_2^+$ $[M+H]^+$: 247.2174, found: 247.2171.

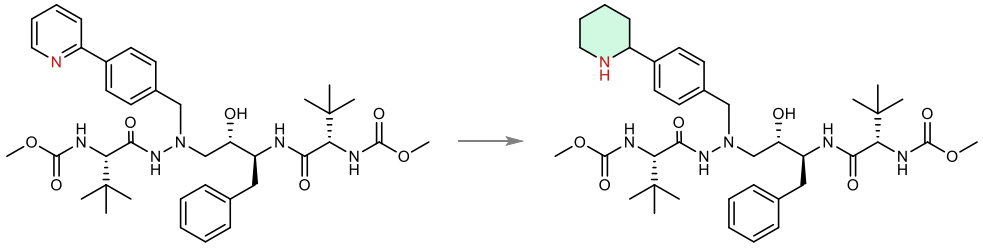


(±)-Tropicamide **82** (67% yield)

According to the general procedure, a mixture of **(±)-tropicamide** (56.9 mg, 0.20 mmol, 1.0 equiv.), $B_2(OH)_4$ (107.5 mg, 1.20 mmol, 6.0 equiv.) and $[Rh(COD)OH]_2$ (3.7 mg, 4.0 mol%, 0.008 mmol) in EtOH (1.0 mL, 0.2 M) was stirred under nitrogen atmosphere for 48 hours at 80 °C to afford **82** as a colorless oil (39.1 mg, 67% yield).

Purification conditions: Reverse-phase column chromatography ($MeOH/H_2O$ = 1:9 to 1.5:1) on SepaBean machine (Santai Tech-nology Inc., China) equipped with C18-bonded SepaFlash columns. R_f = 0.2 in NH_3(7.0 M solution in MeOH)/CH_2Cl_2 = 1:6.

^{1}H NMR (400 MHz, $CDCl_3$, mixture of rotamer) δ 7.32 - 7.27 (m, 2H, major; m, 2H, minor), 7.25 - 7.18 (m, 3H, major; m, 3H, minor), 4.06 - 3.96 (m, 1H, major; m, 1H, minor), 3.93 - 3.87 (m, 1H, major; m, 1H, minor), 3.75 - 3.64 (m, 1H, major; m, 1H, minor), 3.39 (dd, *J* = 13.6, 7.2 Hz, 1H), 3.27 (dq, *J* = 14.4, 7.2 Hz, 1H), 3.13 - 2.83 (m, 6H, major; m, 6H, minor), 2.74 (dd, *J* = 14.8, 6.4 Hz, 1H, minor), 2.57 - 2.42 (m, 2H, major; m, 2H, minor), 1.87 - 1.74 (m, 1H), 1.68 - 1.61 (m, 1H, minor), 1.60 - 1.40 (m, 2H, major; m, 2H, minor), 1.19 - 1.09 (m, 1H, major; m, 1H, minor), 1.06 (t, *J* = 7.2 Hz, 3H, minor), 0.93 (t, *J* = 7.2 Hz, 3H). ^{13}C NMR (100 MHz, $CDCl_3$) δ 172.7(major), 172.5(minor), 136.8(major), 136.7(minor), 129.1(minor), 129.0(major), 128.1(major), 128.0(minor), 127.52(major), 127.46(minor), 66.1(minor), 66.0(major), 52.7(minor), 52.0(major), 51.8(minor), 50.9(major), 46.2(minor), 46.1(major), 42.8(major), 41.4(minor), 36.1(minor), 34.9(major), 31.1(major), 30.9(minor), 13.6(major), 12.3(minor). HRMS (ESI, *m*/*z*) calcd for $C_{17}H_{27}N_2O_2^+$ $[M+H]^+$: 291.2073, found: 291.2073.



Atazanavir **83** (48% yield, 1:1 d.r.)

According to the general procedure, a mixture of **atazanavir** (140.9 mg, 0.20 mmol, 1.0 equiv.), $B_2(OH)_4$ (107.5 mg, 1.20 mmol, 6.0 equiv.) and $[Rh(COD)OH]_2$ (3.7 mg, 4.0 mol%, 0.008 mmol) in EtOH (1.0 mL, 0.2 M) was stirred under nitrogen atmosphere for 48 hours at 50 ℃ to afford **83** as a white solid (69.0 mg, 48% yield, 1:1 d.r.).

Purification conditions: CH_2Cl_2/NH_3(7.0 M solution in MeOH) = 50:1 to 20:1.

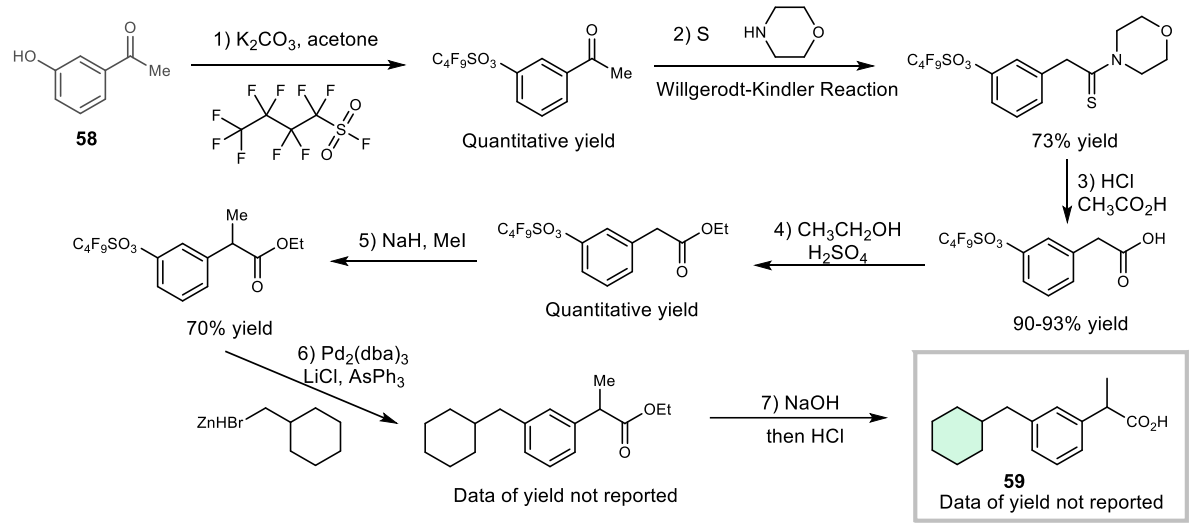
R_f = 0.3 in CH_2Cl_2/NH_3(7.0 M solution in MeOH) = 15:1.

^{1}H NMR (400 MHz, $CDCl_3$) δ 7.30 - 7.24 (m, 5H), 7.22 - 7.18 (m, 4H), 7.15 - 7.10 (m, 1H), 6.63 (d, *J* = 9.2 Hz, 1H), 5.47 (dd, *J* = 22.0, 9.2 Hz, 2H), 4.98 (br, 1H), 4.06 (q, *J* = 8.4 Hz, 1H), 3.98 (d, *J* = 14.0 Hz, 1H), 3.87 - 3.84 (m, 2H), 3.69 - 3.56 (m, 9H), 3.19 (d, *J* = 11.2 Hz, 1H), 2.93 (d,

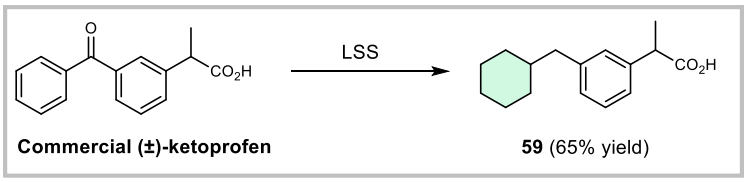
J = 7.6 Hz, 2H), 2.86 - 2.75 (m, 2H), 2.58 (d, *J* = 12.4 Hz, 1H), 2.53 - 2.29 (m, 1H), 1.92 - 1.84 (m, 1H), 1.74 (d, *J* = 8.8 Hz, 1H), 1.69 - 1.62 (m, 1H), 1.60 - 1.43 (m, 3H), 0.88 (s, 9H), 0.72 (s, 9H). ^{13}C NMR (100 MHz, $CDCl_3$) δ 171.0, 170.8, 157.0 (2C), 144.9, 138.2, 134.7, 129.4, 129.1, 128.3, 126.9, 126.3, 67.5, 63.6, 62.3, 62.1, 62.1, 61.4, 61.2, 52.5, 52.4, 52.1, 47.7, 38.8, 34.3, 34.0, 26.7, 26.3, 25.8, 25.4. HRMS (ESI, *m*/*z*) calcd for $C_{38}H_{59}N_6O_7^+$ $[M+H]^+$: 711.4445, found: 711.4449.

Step-Economic Synthesis of Lead Compounds

a) Previous 7-step synthesis of **59** from compound **58** in WO203043625A1, 2003



b) This work: single-step synthesis of **59**



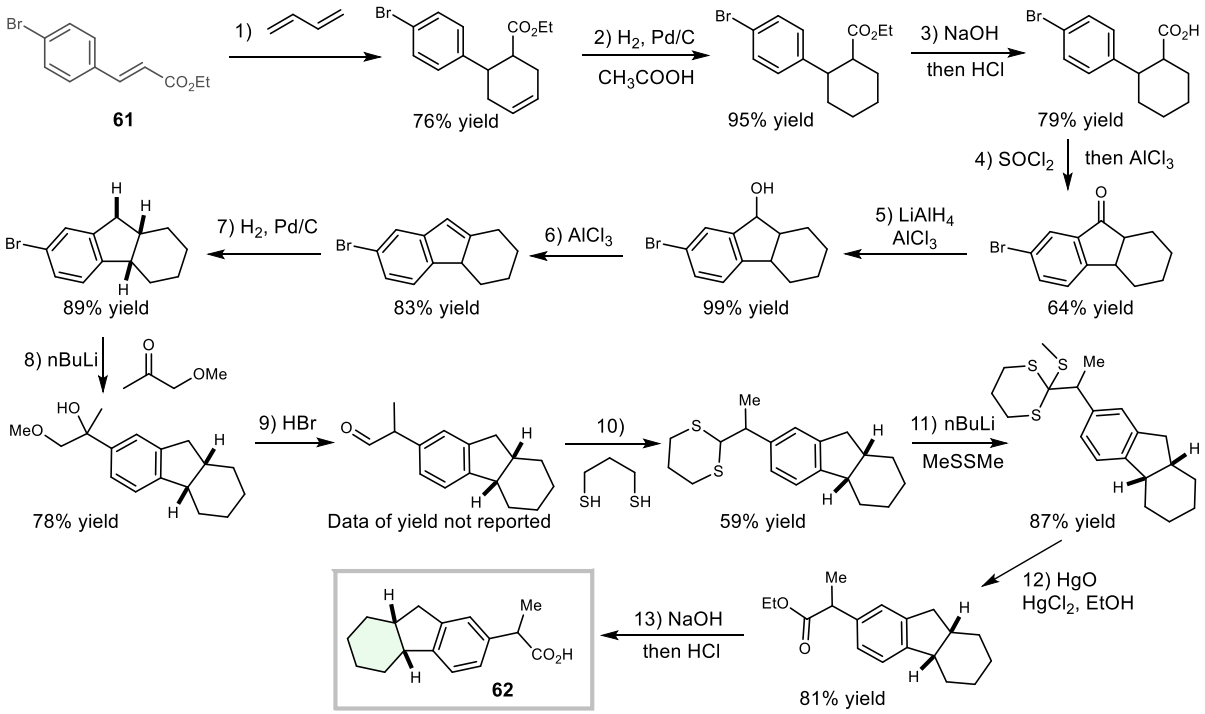
According to the general procedure, a mixture of commercial **(±)-ketoprofen** (50.8 mg, 0.20 mmol, 1.0 equiv.), $B_2(OH)_4$ (80.6 mg, 0.9 mmol, 4.5 equiv.) and $[Rh(COD)OH]_2$ (2.4 mg, 2.5 mol%, 0.005 mmol) in EtOH (1.0 mL, 0.2 M) was stirred under nitrogen atmosphere for 16 hours at 50 ℃ to afford **59** as a white oil (32.3 mg, 65% yield).

Purification conditions: petroleum ether/EtOAc = 10:1 to 5:1.

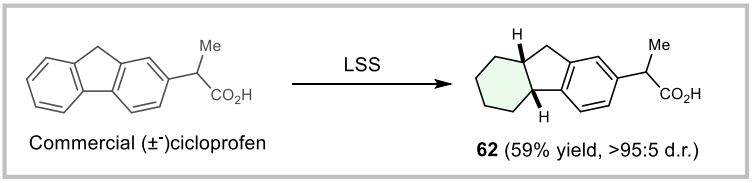
R_f(**59**) = 0.4 in petroleum ether/EtOAc (3:1).

^{1}H NMR (400 MHz, $CDCl_3$) δ 7.23 (t, *J* = 7.6 Hz, 1H), 7.14 (d, *J* = 7.6 Hz, 1H), 7.08 (s, 1H), 7.05 (d, *J* = 7.6 Hz, 1H), 3.71 (q, *J* = 7.2 Hz, 1H), 2.47 (d, *J* = 6.8 Hz, 2H), 1.73 - 1.61 (m, 5H), 1.51 (d, *J* = 7.2 Hz, 4H), 1.23 - 1.11 (m, 3H), 1.00 - 0.88 (m, 2H). ^{13}C NMR (100 MHz, $CDCl_3$) δ 180.7, 142.0, 139.6, 128.7, 128.4, 128.4, 124.9, 45.5, 44.2, 39.8, 33.3, 26.7, 26.4, 18.3. HRMS (ESI, *m*/*z*) calcd for $C_{16}H_{22}O_2Na^+$ $[M+Na]^+$: 269.1517, found: 269.1514.

a) Previous 13-step synthesis of **62** from compound **61** in J. Med. Chem. 1977, 20, 726



b) This work: single-step synthesis of **62**



According to the general procedure, a mixture of commercial **(±)-cicloprofen** (47.7 mg, 0.20 mmol, 1.0 equiv.), $B_2(OH)_4$ (164.6 mg, 1.8 mmol, 9.0 equiv.) and $[Rh(COD)OH]_2$ (4.8 mg, 5.0 mol%, 0.01 mmol) in EtOH (1.0 mL, 0.2 M) was stirred under nitrogen atmosphere for 48 hours at 80 °C to afford **62** as a white solid (28.8 mg, 59% yield, >95:5 d.r.).

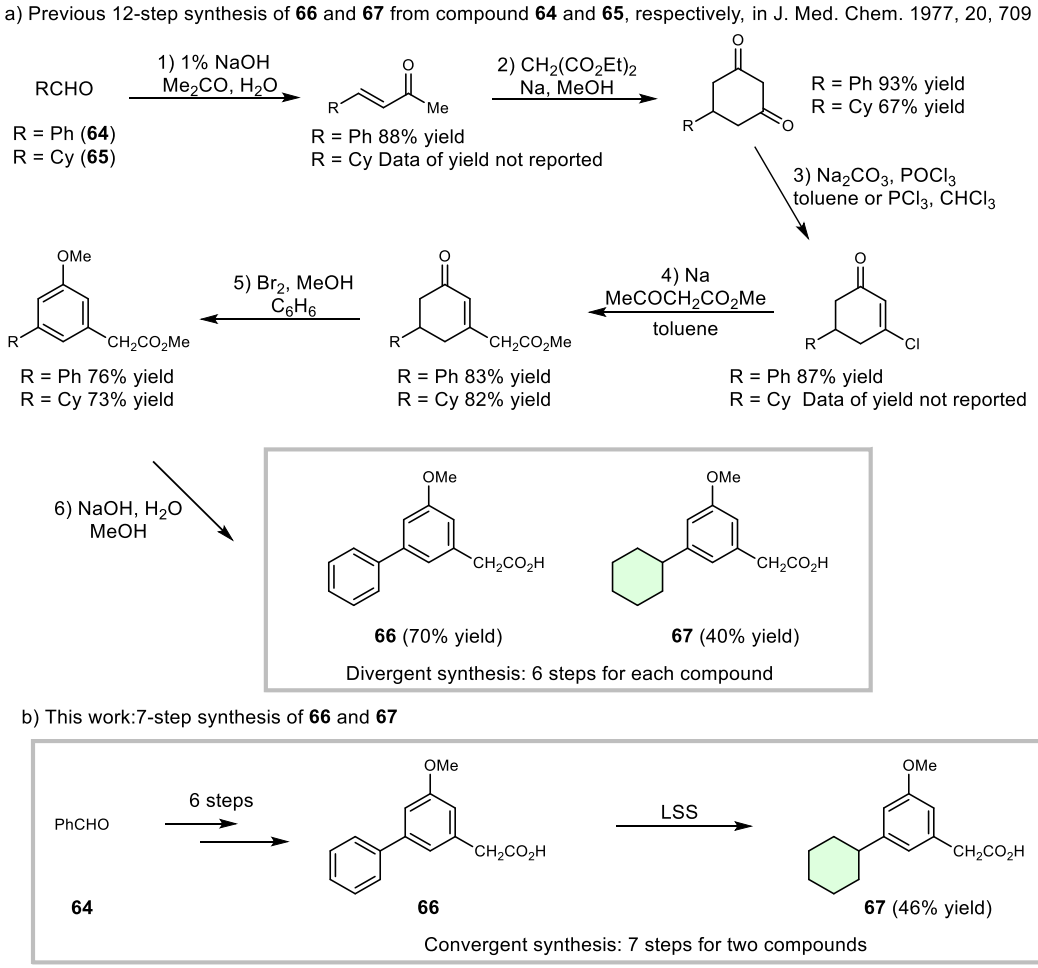
Purification conditions: petroleum ether/acetone = 20:1 to 8:1.

R_f(**62**) = 0.4 in petroleum ether/acetone = 3:1.

^{1}H NMR (400 MHz, $CDCl_3$) δ 7.18 (s, 1H), 7.13 - 7.07 (m, 2H), 3.71 (q, *J* = 7.2 Hz, 1H), 3.05 (q, *J* = 6.0 Hz, 1H), 2.82 (dd, *J* = 15.2, 6.4 Hz, 1H), 2.57 (dd, *J* = 15.2, 4.4 Hz, 1H), 2.48 - 2.38 (m, 1H), 1.87 - 1.70 (m, 2H), 1.60 - 1.52 (m, 1H), 1.50 (d, *J* = 7.2 Hz, 3H), 1.47 - 1.28 (m, 5H).

^{13}C NMR (100 MHz, $CDCl_3$, mixture of diastereomers) δ 180.6, 146.4, 144.5, 137.7, 125.6, 125.4 124.6, 124.4, 123.12, 123.10, 45.5, 43.8, 40.0, 37.55, 37.52, 28.0, 27.4, 23.9, 22.7, 18.5.

HRMS (ESI, *m*/*z*) calcd for $C_{16}H_{20}O_2Na^+$ $[M+Na]^+$: 267.1361, found: 267.1359.

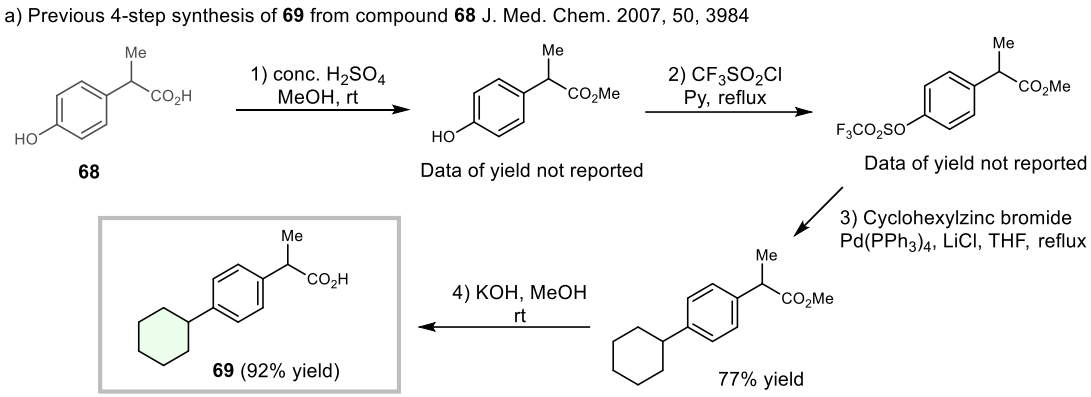


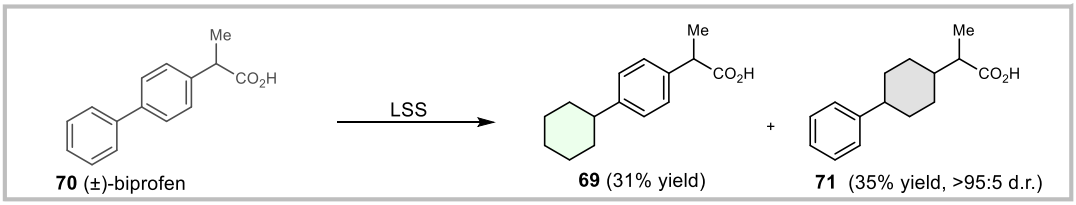
According to the general procedure, a mixture of **66** (48.4 mg, 0.20 mmol, 1.0 equiv.), $B_2(OH)_4$ (164.6 mg, 1.8 mmol, 9.0 equiv.) and $[Rh(COD)OH]_2$ (4.8 mg, 5.0 mol%, 0.01 mmol) in EtOH (1.0 mL, 0.2 M) was stirred under nitrogen atmosphere for 26 hours at 80 ℃ to afford **67** as a yellow solid (22.8 mg, 46% yield).

Purification conditions: petroleum ether/acetone = 20:1 to 6:1.

R_f = 0.35 in petroleum ether/acetone = 3:1.

^{1}H NMR (400 MHz, $CDCl_3$) δ 6.73 (s, 1H), 6.68 (d, *J* = 10.0 Hz, 2H), 3.80 (s, 3H), 3.60 (s, 2H), 2.52 - 2.42 (m, 1H) ,1.92 - 1.80 (m, 4H), 1.75 (d, *J* = 12.4 Hz, 1H), 1.46 - 1.32 (m, 4H), 1.31 - 1.19 (m, 1H). ^{13}C NMR (100 MHz, $CDCl_3$) δ 177.9, 159.9, 150.2, 134.4, 120.7, 112.2, 111.9, 55.3, 44.7, 41.4, 34.5, 27.0, 26.3. HRMS (ESI, m/z) calcd for $C_{15}H_{20}O_3Na^+$ $[M+Na]^+$: 271.1310, found: 271.1310.





According to the general procedure, a mixture of **(±)-biprofen** (45.3 mg, 0.20 mmol, 1.0 equiv.), $B_2(OH)_4$ (107.5 mg, 1.20 mmol, 6.0 equiv.) and $[Rh(COD)OH]_2$ (3.7 mg, 4.0 mol%, 0.008 mmol) in EtOH (1.0 mL, 0.2 M) was stirred under nitrogen atmosphere for 48 hours at 80 ℃ to afford **69** as a white solid (14.5 mg, 31% yield) and **71** as a white solid (16.3 mg, 35% yield, >95:5 d.r.).Purification conditions: Reverse-phase column chromatography ($MeOH/H_2O$ = 1:4 to 2:1) on SepaBean machine (Santai Technology Inc., China) equipped with C18-bonded SepaFlash columns. R_f= 0.4 in petroleum ether/ acetone = 4:1 (the mixture of **69** and **71**).

Analytical data of **69:**

^{1}H NMR (400 MHz, $CDCl_3$) δ 7.24 (d, *J* = 8.0 Hz, 2H), 7.16 (d, *J* = 8.0 Hz, 2H), 3.71 (q, *J* = 7.2 Hz, 1H), 2.52 - 2.44 (m, 1H), 1.90 - 1.79 (m, 4H), 1.78 - 1.71 (m, 1H), 1.50 (d, *J* = 7.2 Hz, 3H), 1.45 - 1.32 (m, 4H), 1.29 - 1.18 (m, 1H). ^{13}C NMR (100 MHz, $CDCl_3$) δ 180.5, 147.4, 137.2, 127.6, 127.2, 45.0, 44.3, 34.5, 27.0, 26.3, 18.2. HRMS (ESI, *m*/*z*) calcd for $C_{15}H_{20}O_2Na^+$ $[M+Na]^+$: 255.1361, found: 255.1359.

Analytical data of **71:**

^{1}H NMR (400 MHz, $CDCl_3$) δ 7.30 - 7.27 (m, 2H), 7.24 - 7.21 (m, 2H), 7.20 - 7.14 (m, 1H), 2.76 - 2.60 (m, 2H), 1.97 - 1.59 (m, 9H), 1.19 (d, *J* = 6.8 Hz, 3H). ^{13}C NMR (100 MHz, $CDCl_3$) δ 183.2, 146.8, 128.4, 127.1, 126.9, 126.0, 42.8, 40.5, 36.7, 29.1, 29.0, 28.9, 26.7, 15.5. HRMS (ESI, *m*/*z*) calcd for $C_{15}H_{20}O_2Na^+$ $[M+Na]^+$: 255.1361, found: 255.1356.

According to the general procedure, a mixture of **agomelatine** (48.6 mg, 0.2 mmol, 1.0 equiv.), $B_2(OH)_4$ (80.6 mg, 0.9 mmol, 4.5 equiv.) and $[Rh(COD)OH]_2$ (2.3 mg, 2.5 mol%, 0.005 mmol) in EtOH (1.0 mL, 0.2 M) was stirred under argon atmosphere for 14 hours at 50 ℃ to afford **74** (27.0 mg, 55% yield) and **74´**(12.9 mg, 26% yield) as colorless oil.

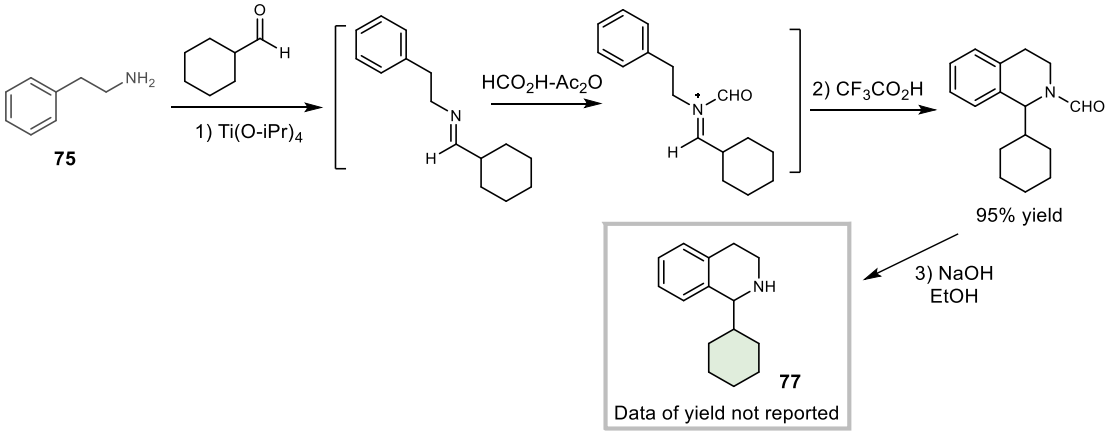
Analytical data of **74**:

^{1}H NMR (400 MHz, $CDCl_3$) δ 6.98 - 6.96 (m, 1H), 6.69 - 6.66 (m, 2H), 5.58 (br, 1H), 3.77 (s, 3H), 3.41 - 3.29 (m, 2H), 2.83 - 2.77 (m, 1H), 2.74 - 2.61 (m, 2H), 1.96 (s, 3H), 1.91 - 1.62 (m, 6H). ^{13}C NMR (101 MHz, $CDCl_3$) δ 170.2, 157.7, 141.4, 130.1, 129.4, 113.5, 111.9, 55.4, 37.9, 36.6, 35.8, 28.9, 27.7, 23.5, 20.2. HRMS (ESI, *m*/*z*) calcd for $C_{15}H_{21}NO_2Na^+$ $[M+Na]^+$: 270.1465, found: 270.1461.

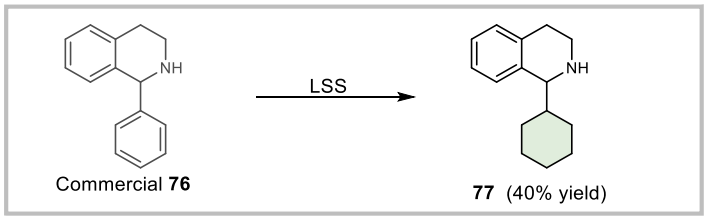
Analytical data of **74´**:

^{1}H NMR (400 MHz, $CDCl_3$) δ 7.10 - 7.06 (m, 1H), 7.00 - 6.96 (m, 2H), 5.67 (br, 1H), 3.72 - 3.66 (m, 1H), 3.52 - 3.41 (m, 5H), 3.04 (dd, *J* = 16.6, 5.1 Hz, 1H), 2.94 (dt, *J* = 16.8, 6.0 Hz, 1H), 2.80 (t, *J* = 7.1 Hz, 2H), 2.71 (dd, *J* = 16.5, 7.1 Hz, 1H), 2.12 - 2.03 (m, 2H), 1.96 (s, 3H), 1.85 - 1.76 (m, 1H). ^{13}C NMR (101 MHz, $CDCl_3$) δ 170.4, 137.3, 136.9, 133.1, 127.4, 127.0, 126.0, 76.1, 56.1, 39.61, 32.59, 32.4, 27.4, 27.2, 23.4. HRMS (ESI, *m*/*z*) calcd for $C_{15}H_{21}NO_2Na^+$ $[M+Na]^+$: 270.1465, found: 270.1461.

a) Previous 3-step synthesis of **77** from compound **75** in E. J. Med. Chem. 2009, 44, 4034



b) This work: single-step synthesis of **77**



According to the general procedure, a mixture of **76** (41.8 mg, 0.20 mmol, 1.0 equiv.), $B_2(OH)_4$ (107.5 mg, 1.20 mmol, 6.0 equiv.) and $[Rh(COD)OH]_2$ (3.7 mg, 4.0 mol%, 0.008 mmol) in EtOH (1.0 mL, 0.2 M) was stirred under nitrogen atmosphere for 26 hours at 50 °C to afford **77** as a colorless oil (17.2 mg, 40% yield).

Purification conditions: NH_3(7.0 M solution in MeOH)/CH_2Cl_2 = 1:50 to 1:25

R_f = 0.5 in NH_3(7.0 M solution in MeOH)/CH_2Cl_2 = 1:10.

^{1}H NMR (400 MHz, $CDCl_3$) δ 7.19 - 7.03 (m, 4H), 3.91 (br, 1H), 3.32 - 3.22 (m, 1H), 2.98 - 2.89 (m, 1H), 2.88 - 2.78 (m, 1H), 2.73 - 2.63 (m, 1H), 1.98 - 1.88 (m, 1H), 1.83 (d, *J* = 11.6 Hz, 1H), 1.72 - 1.64 (m, 3H), 1.45 - 1.25 (m, 4H), 1.21 - 1.03 (m, 3H). HRMS (ESI, *m*/*z*) calcd for $C_{15}H_{22}N^+$ $[M+H]^+$: 216.1752, found: 216.1750.

All the other data is consistent with previous reports.

Procedure for Arene Reduction Screen

Stock solutions, or suspensions, were prepared as shown in the heatmap preparation table. In an inert atmosphere glovebox, reagents were weighed and dissolved or suspended in anhydrous solvent to achieve their listed concentrations in the associated table. Stock solutions of reagents were stirred until either a clear solution or a uniform slurry was achieved. A 96-well aluminum microvial plate (Analytical Sales & Services #96960) was equipped with oven-dried shell vials (Analytical Sales & Services cat. no. 884001) and then moved into the glovebox.. All stock solutions except for $[Rh(COD)OH]_2$ and $[Rh(cod)Cl]_2$ were prepared in DCM and dosed into the appropriate well locations using single channel micropipetters, then blown down under a stream of nitrogen. After complete removal of solvent from each well, the rhodium catalyst solutions were added last to achieve the final reaction volume (100 μL) and solvent composition for each well. A parylene-coated stir dowel (Analytical Sales & Services #13258) was then added to each vial. The microvial plate was sealed, removed from the glove box, and stirred on a tumble stirrer with heating to 50°C for 24 hours. The reactions were quenched by opening the reaction block and adding 100 μL saturated aqueous $NaHCO_3$ solution and 400 μL EtOAc. Reactions were extracted by resealing the plate and shaking manually. From each reaction, a 40 μL aliquot of the quenched reaction mixture was added into a 96- well polypropylene collection plate (Analytical Sales & Services cat. no. 17P687). The solvent was evaporated by blowing nitrogen down on the analytical plate. An acetonitrile solution of caffeine as internal standard (0.05 mg/mL, 800 μL) was added, and mixed by pipetting up and down. The reactions were then analyzed by UPLC-MS. The assay yields were produced by measuring the MS Ionization Peak Area of the desired product relative to the starting material. The reaction data points for the 96-well screen are deposited on github: https://github.com/cernak-lab/late_stage_saturation

Reagents	C_{stock} (M)	V_{dose} (µL)	Wells
Propranolol	0.198	50	A1-A4, B1-B4, C1-C4, D1-D4, E1-E4, F1-F4, G1-G4, H1-H4
Gemfibrozil	0.198	50	A5-A8, B5-B8, C5-C8, D5-D8, E5-E8, F5-F8, G5-G8, H5-H8
Ketoprofen	0.198	50	A9-A12, B9-B12, C9-C12, D9-D12, E9-E12, F9-F12, G9-G12, H9-H12
$B_2(OH)_4$ (3.5 equiv)	0.693	50	Rows: A, B, E, F Columns:1, 2, 5, 6, 9, 10
$B_2(OH)_4$ (7.0 equiv)	1.386	50	Rows: A, B, E, F Columns: 3, 4, 7, 8, 11, 12
BH_3NH_3 (1.5 equiv)	0.297	50	Rows: C, D, G, H Columns: 1, 2, 5, 6, 9, 10
BH_3NH_3 (3.0 equiv)	0.594	50	Rows: C, D, G, H Columns: 3, 4, 7, 8, 11, 12
$[Rh(COD)OH]_2$ (in EtOH)	0.004	100	Rows: A, C Columns: 1, 3, 5, 7, 9, 11
$[Rh(cod)Cl]_2$ (in EtOH)	0.002	100	Rows: E, G Columns: 1, 3, 5, 7, 9, 11
$[Rh(COD)OH]_2$ (in TFE)	0.004	100	Rows: A, C Columns: 2, 4, 6, 8, 10, 12
$[Rh(cod)Cl]_2$ (in TFE)	0.002	100	Rows: E, G Columns: 2, 4, 6, 8, 10, 12
$[Rh(COD)OH]_2$ (in n-BuOH)	0.004	100	Rows: B, D Columns: 1, 3, 5, 7, 9, 11
$[Rh(cod)Cl]_2$ (in n-BuOH)	0.002	100	Rows: F, H Columns: 1, 3, 5, 7, 9, 11
$[Rh(COD)OH]_2$ (in Ethylene Glycol)	0.004	100	Rows: B, D Columns: 2, 4, 6, 8, 10, 12
$[Rh(cod)Cl]_2$ (in Ethylene Glycol)	0.002	100	Rows: F, H Columns: 2, 4, 6, 8, 10, 12

Table 2-1 Recipe for 96-well comparison screen of arene reduction conditions

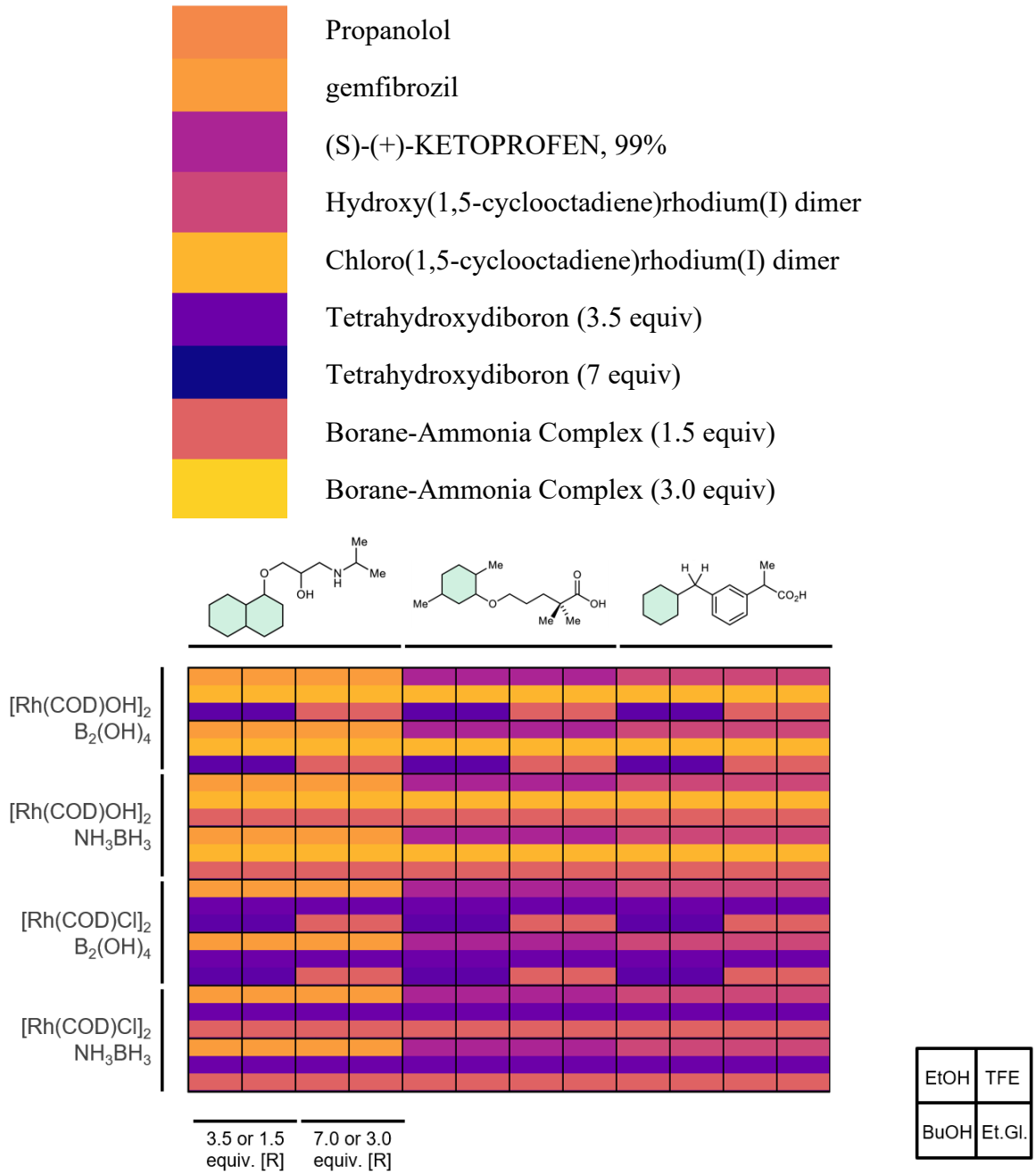


Figure 2-11 Reagents and 96-well plate set up for arene reduction conditions.

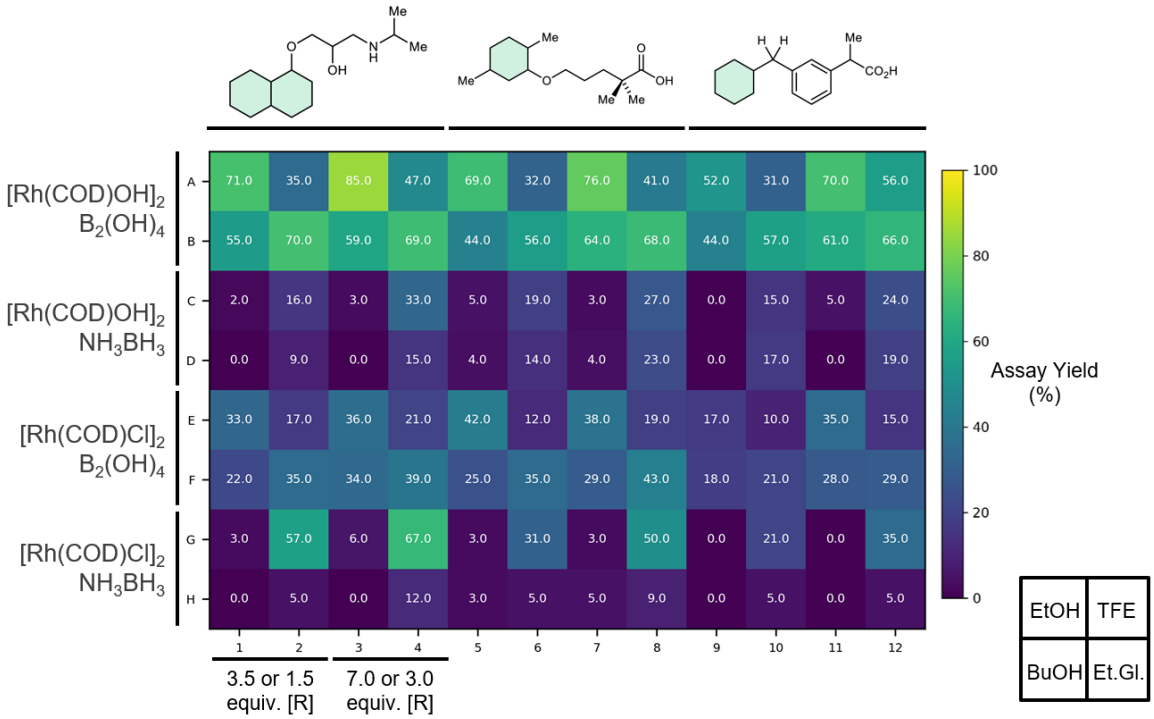


Figure 2-12 High-throughput 96-well screen to interrogate mild late-stage saturation conditions on drug substrates, propranolol, gemfibrozil, and ketoprofen under mild autoclave-free hydrogenation conditions. cod = 1,5-cyclooctadiene, TFE = 1,1,1-trifluoroethanol, Et. Gl. = ethylene glycol.

Additive	NMR Yield
None	60%
DMSO (0.10 eq)	57%
DMSO (0.10 eq) in EtOH	58%
DMSO (0.25 eq)	52%
DMSO (5% vol.)	N.R.
DMSO (100% vol.)	N.R.
Water (5% vol.)	56%

Table 2-2 The effect of DMSO and water as an additive on reactions using aminacrine **7**. NMR yields represent the overall yield of mono- and di-reduced products **20** and **21**.

2.5.3 ***Procedure for LSS in 1,536-Well Plate Format***

An investigation on the ability to directly translate drug library stock solutions in wet DMSO into the LSS reaction revealed several challenges. Titrating in stoichiometric quantities of DMSO into the saturation of aminacrine **x** revealed inhibition of the rhodium catalytic cycle. Additional attempts to miniaturize the LSS reaction in HTE compatible solvents such as butanol or pentanol revealed compatibility issues between many alcohol solvents and the well plate seals used to cover 384 and 1,536-well plates. Finally, validation of a mass spectrum-based analytical method was carried out to ensure accurate quantitation of saturated drug products was possible. In turn, each of these problems were addressed as described below.

Removal of DMSO from Drug Library Stock Solutions

To quantitate DMSO remaining after evaporation and reconstitution cycles of solutions of drug library samples, GC-MS analysis was used to detect residual DMSO in 384-well plate format that could inhibit catalytic activity in rhodium-catalyzed hydrogenation. Initially, a standard calibration curve was produced from GCMS response to DMSO (0.1 mM to 30 mM) in methanol. A standard solution of 100 mM DMSO in methanol was used to prepare solutions of 30 mM, 20 mM, 10 mM, 1 mM, and 0.1 mM DMSO via serial dilution. The standard samples ranging from 30 to 0.1 mM DMSO were run in triplicate to produce a calibration curve of mass spectrometer response to DMSO across relevant concentration ranges that would impede rhodium-catalysed hydrogenation.

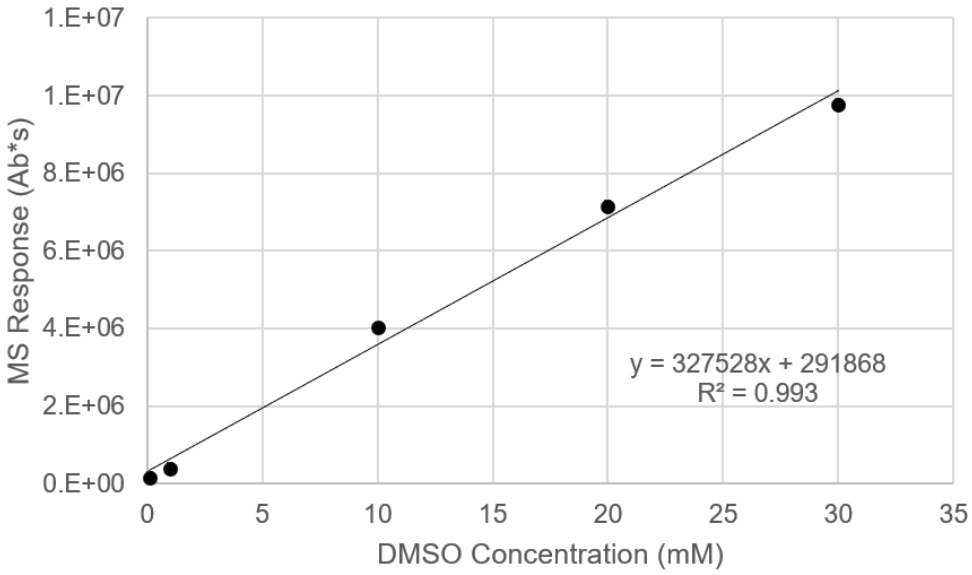
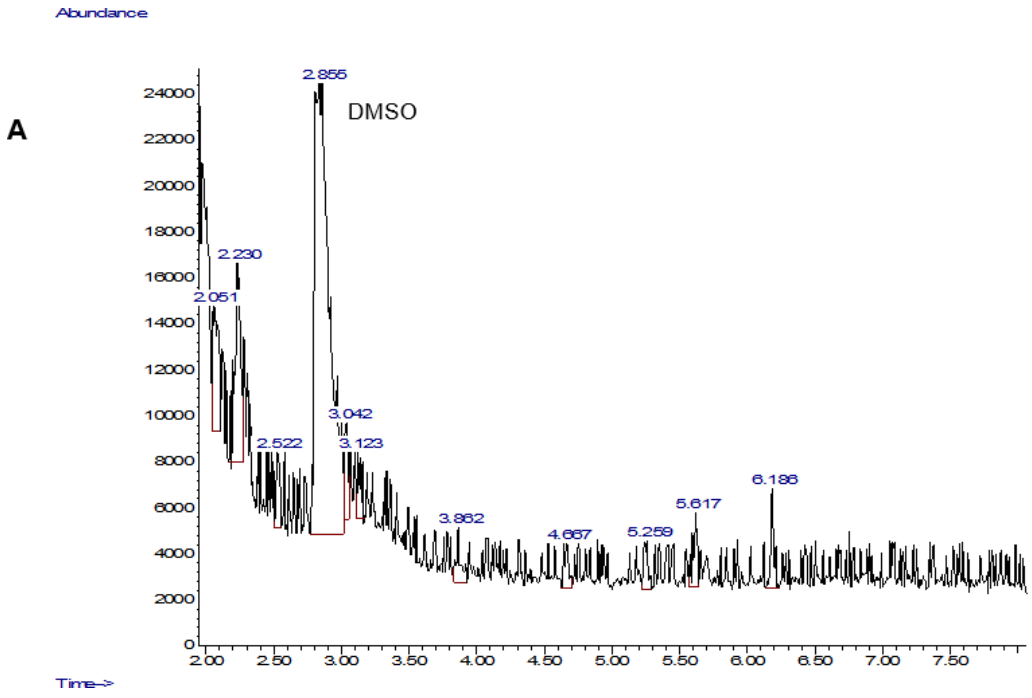


Figure 2-13 Calibration Curve for GC-MS Response to DMSO

To test efficiency of DMSO removal in well plate format, a single 384-well microtiter plate was filled with DMSO (30 µL per well) and the plate was subjected to a 2-hour evaporation cycle using a Genevac HT-4X. To three selected wells, 30 µL of methanol was added then transferred to the appropriate GC-MS analytical vials pre-filled with 1.0 mL of methanol. The first round of samples were analyzed in triplicate using a standard calibration curve to determine DMSO concentrations after one round of evaporation. The process was then repeated a second and third time, by portioning 30 µL of ethanol to all wells in the 384-well plate, subjecting the plate to a 2-hour evaporation cycle, and selecting three new wells to aliquot into analytical vials for GCMS analysis. By the end of the third evaporation cycle no detectable DMSO concentrations were evident in the 384-well plate samples.



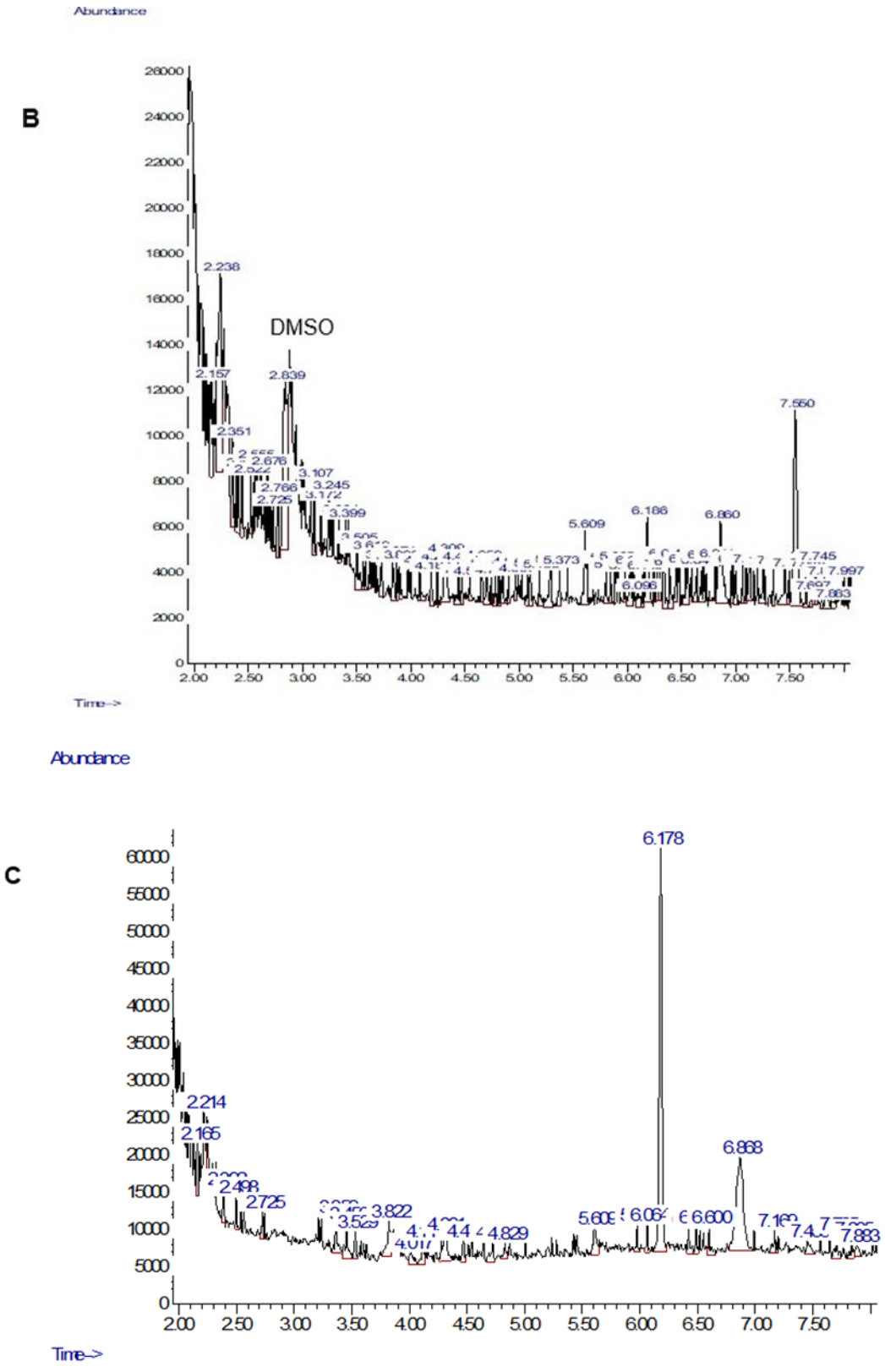


Figure 2-14 Residual DMSO in 384-Well Plates Following First (A), Second (B), and Third (C) Evaporation Cycles

Microtiter Plate Sealing Studies

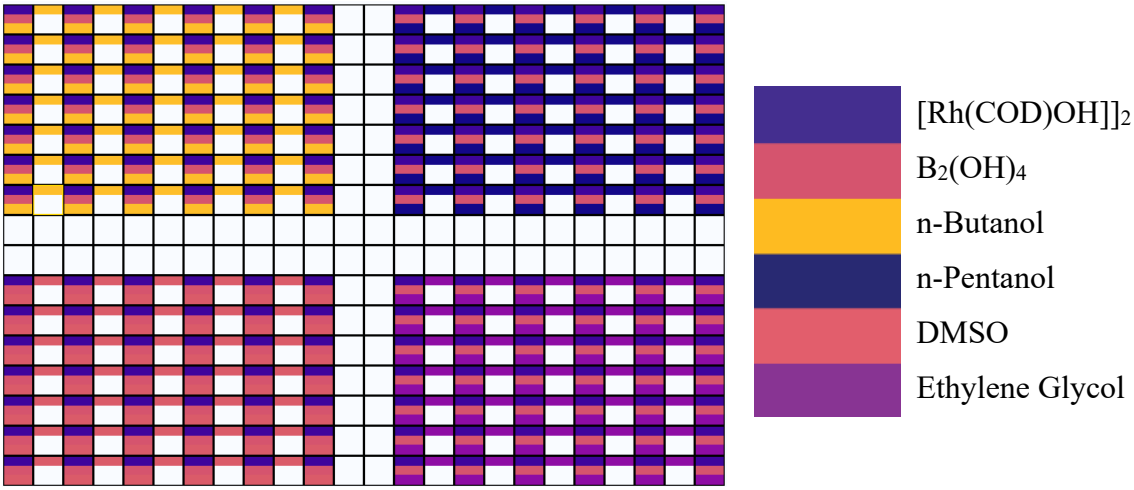


Figure 2-15 384-well plate split into 4 quadrants according to solvent along with color mapping for each added reagent.

Solvent effects on well plate sealing integrity were determined from subjecting a series of alcohol-based solvents to model reaction conditions (50°C for 24 hours) in 384-well plate format. A single 384-well microtiter plate was portioned into quadrants. To each quarter a different HTE-viable solvent was allocated (n-Butanol, n-Pentanol, DMSO, or Ethylene Glycol). 76 wells were allocated per solvent with 30 µL pure solvent added to each well. Two rows/columns were left empty between each quadrant. Four 0.1 M stock solutions of $[Rh(COD)OH]]_2$ and four 0.1 M stock solutions of $B_2(OH)_4$ were freshly prepared by dissolving the corresponding reagent (91 mg Rh or 18 mg $B_2(OH)_4$) in one of the four corresponding solvents (2.0 mL). From these eight total stock solutions, 10 µL Rh stock solution and 10 µL $B_2(OH)_4$ stock solution were added to each well previously dosed with solvent. Butanol-containing stock solutions were allocated to the top left of the plate, pentanol to the top right, DMSO to the bottom left, and ethylene glycol to the bottom right.

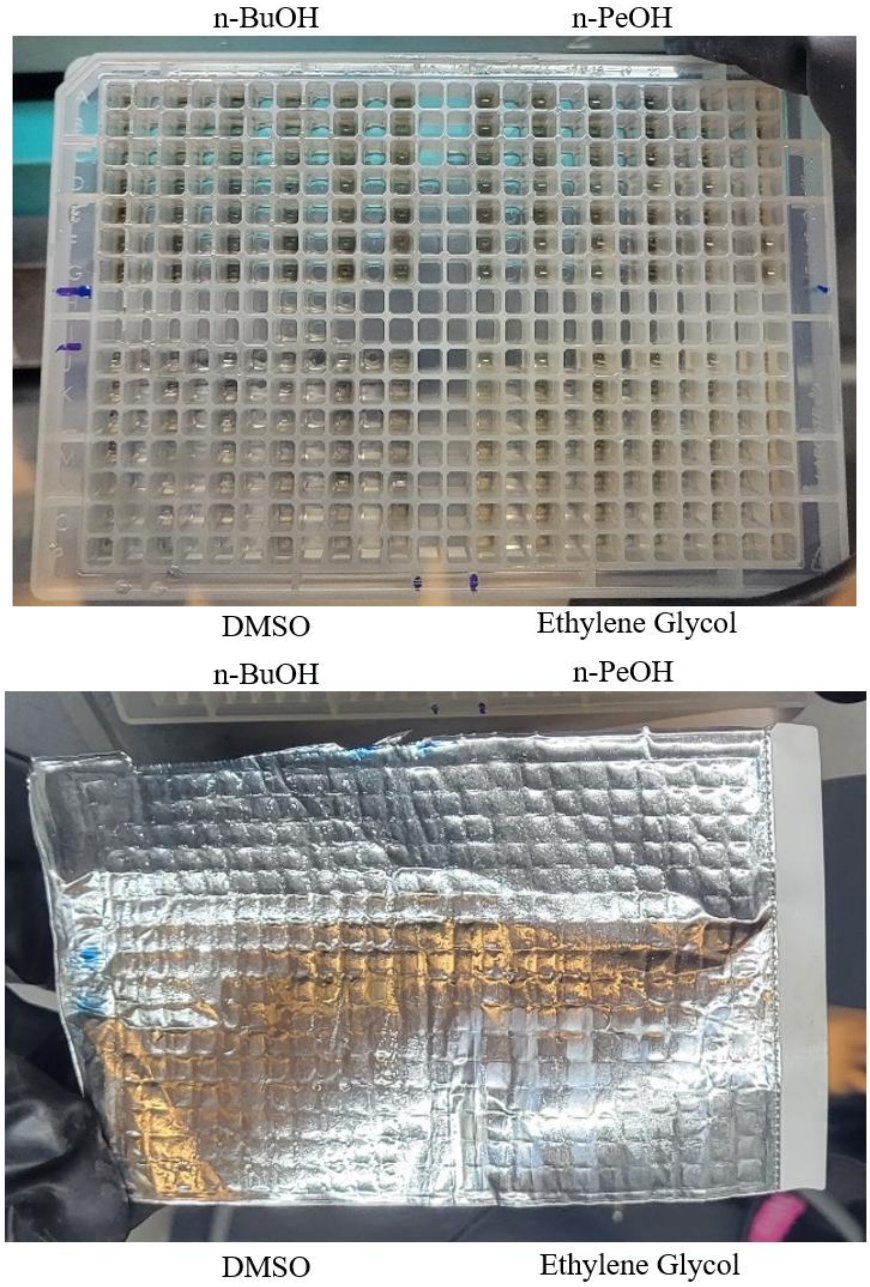
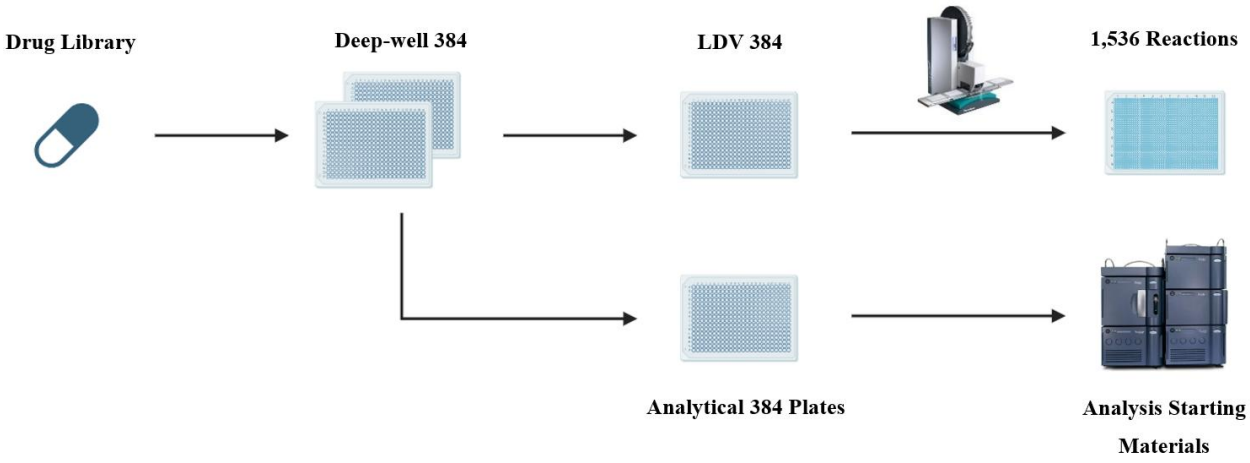


Figure 2-16 384-well plate dosed with solvents, catalyst, and reductant (Top). Foil seal after heating well plate at 50°C for 24 hours (Bottom).

Significant loss of seal was observed for n-Butanol and n-Pentanol quadrants due to solvent deposition on the surface of the foil seal. Moderate solvent evaporation was also observed in the n- Butanol and n-Pentanol wells due to poor sealing over the heating period. The seal over DMSO and Ethylene Glycol wells remained intact post experiment with little to no solvent deposition or evaporation. From these results Ethylene Glycol was used for further HTE studies due to its low volatility and compatibility with HTE workflow.

Procedure for 1,536-well plate experiment



Samples of 734 druglike compounds in 5mM DMSO were sourced from the Dart Neurosciences collection, courtesy of the Center for Chemical Genomics at the University of Michigan Ann Arbor. The workflow for the 1,536-well experiment is outlined above (figure drawn in BioRender) To verify the ionization intensity and purity of the starting materials by UPLC-MS, 6 µL of each sample were transferred into two 384-well microtiter plates (Analytical Sales part No. 38435) using an SPT Labtech mosquito® liquid handling robot. An additional 24 µL of 1.25 mM caffeine in DMSO was then transferred into each well using multi-channel micropipettes to achieve a final concentration of 1 mM analyte and caffeine. The plates containing starting materials were then analyzed by UPLC- MS to determine ionization intensity relative to the caffeine internal standard prior to reaction. Following, another 27 µL of the original DMSO stock solutions were transferred into two low-dead volume (LDV) 384-well microtiter source plates (Greiner Bio-One part No. 784201) for evaporation and reconstitution of starting materials. The plates were subject to solvent evaporation using a GeneVac HT-4X centrifugal evaporator until wells reached dryness after a two-hour evaporation cycle. Then, 30 µL aliquots of ethanol were added to each well and a second two-hour evaporation cycle was carried out. A final cycle of ethanol addition and evaporation was carried out once more to ensure complete DMSO removal from the samples. The samples were then reconstituted up to 20 mM by addition of 6.75 µL of anhydrous ethylene glycol to each well. Samples of the 34 starting materials reduced by rhodium catalysis in the prior Experimental section were also included in the library collection as 20 mM stock solutions in anhydrous ethylene glycol and 6.75 µL of each sample was transferred into the remaining wells in the low-dead volume 384-well source plates. From these 384- well source plates, 4 µL was transferred into the corresponding 2 wells in a

1,536 well reaction plate via mosquito (2 μL per reaction plate well, Analytical Sales part No. 15020). The first 384 well source plate was mapped to columns 1-12 and 25-36 of the 1,536-well reaction plate while the second 384- well source plate was mapped to columns 13-24 and 37-48 of the 1,536-well reaction plate. The 1,536-well reaction plate was subjected to a two-hour evaporation cycle to remove solvent. Stock solutions of B2(OH)4 (70 mM and 140 mM) in anhydrous ethylene glycol along with [Rh(COD)OH]2 (0.8 mM) in anhydrous ethylene glycol were prepared separately and transferred into a third 384-well source plate via multichannel pipetting. From this source plate, 1 μL of 70 mM B2(OH)4 was aliquoted into wells in columns 1-24 and 1 μL of 140 mM B2(OH)4 was aliquoted into wells in columns 25-48 of the 1,536-well reaction plate. After subjecting the 1,536-well reaction plate to a four-hour solvent evaporation cycle to achieve dryness, 1 μL of rhodium catalyst stock solution was aliquoted into each well in the 1,536-well reaction plate, utilizing dispense mixing in triplicate to homogenize reaction well solutions.

After dosing and mixing, the reaction plate was sealed with foil sealing tape (ThermoFisher part No. 232699) and centrifuged (Fisher Scientific Mini Plate Spinner) on full speed for ~1 minute. The reaction plate was then placed inside the plate heating apparatus (Eppendorf ThermoMixer C with Eppendorf ThermoTop attachment) to heat at 50°C for 24 hours. The foil seal was removed the reaction wells were quenched by addition of 2 μL of caffeine (120 mM) in DMSO, and the reaction plate centrifuged to settle and particulates. Reaction aliquots of 1 μL were then transferred into four 384-well microtiter plates pre-filled with 29 μL of HPLC-grade DMSO per well for analysis. The plates were then analyzed by UPLC-MS and results processed and visualized as described in the Supplementary Methods section. The output data is available on github (https://github.com/cernak-lab/late_stage_saturation). Example UPLC-MS traces and calculations of percent conversion for several wells from the 1,536-well experiment are shown below along with SMILES strings and yields for all compounds used.

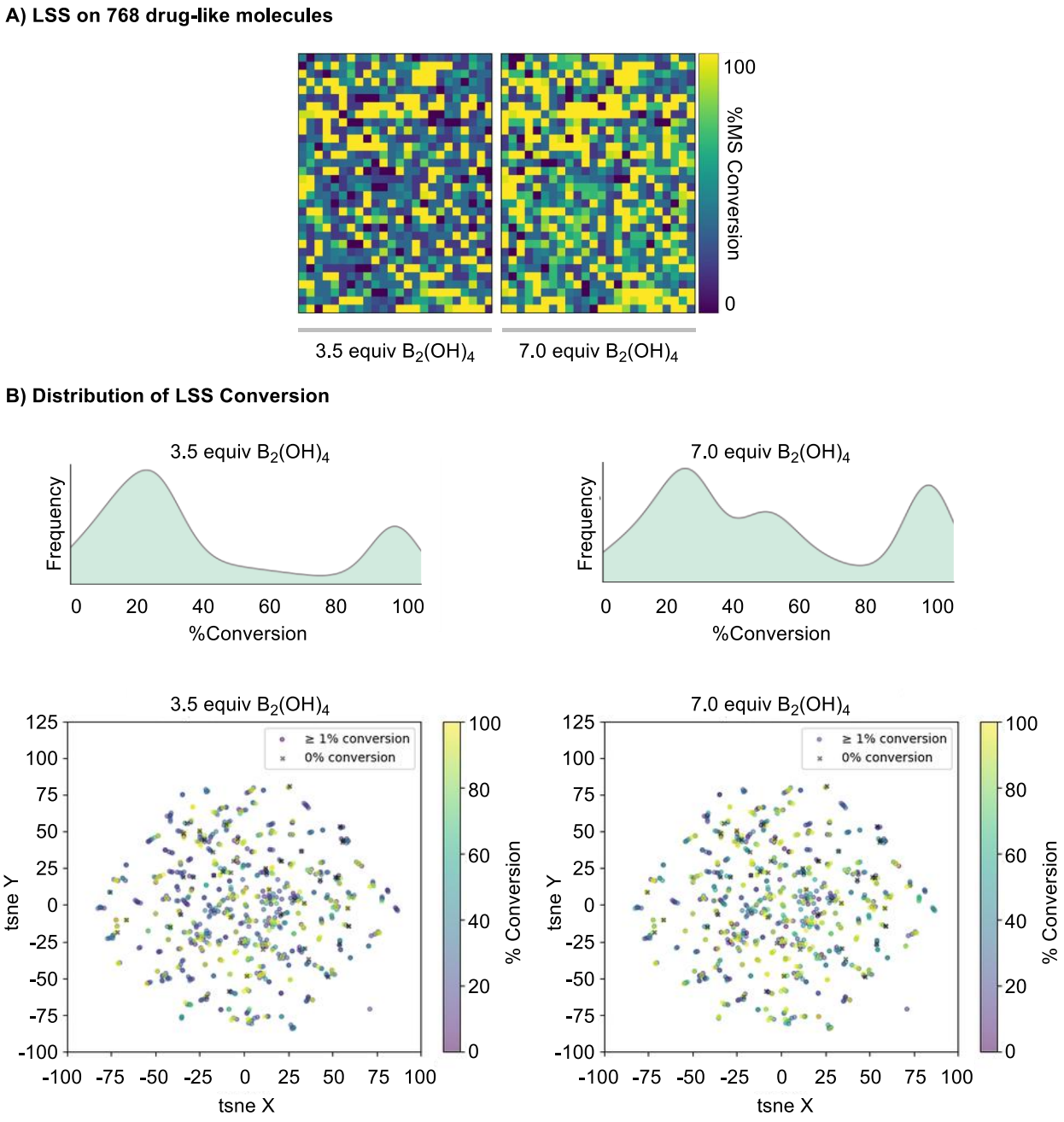
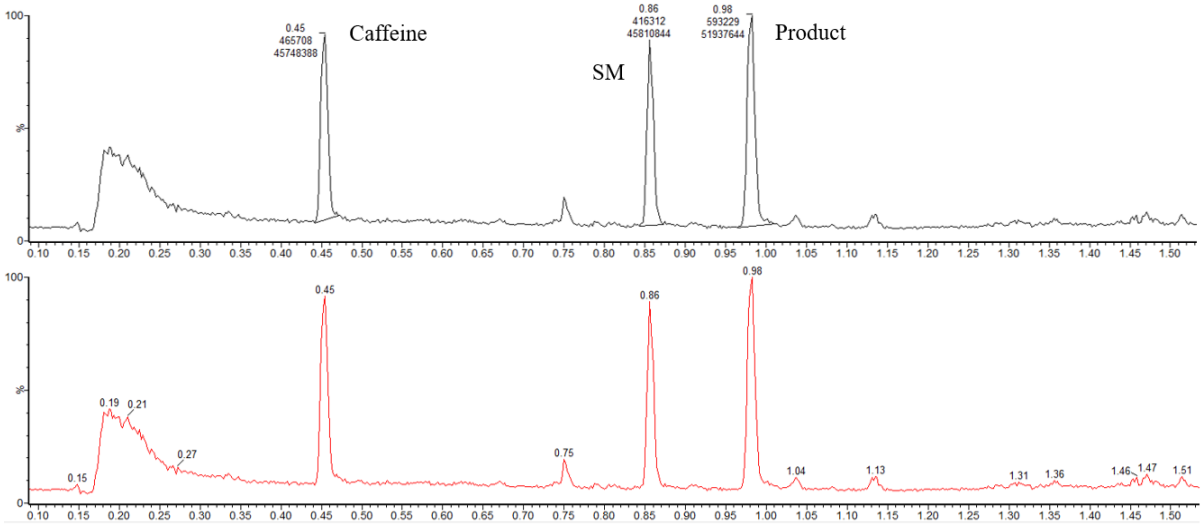


Figure 2-17 A) Heat map for 1,536-well plate experiment colored by percent conversion determined from UPLC-MS ionization peak area for 768 substrates subjected to two different reductant equivalents. B) Yield and chemical space distributions of 1,536-well plate experiment separated by equivalents of reductant used.

Well A28

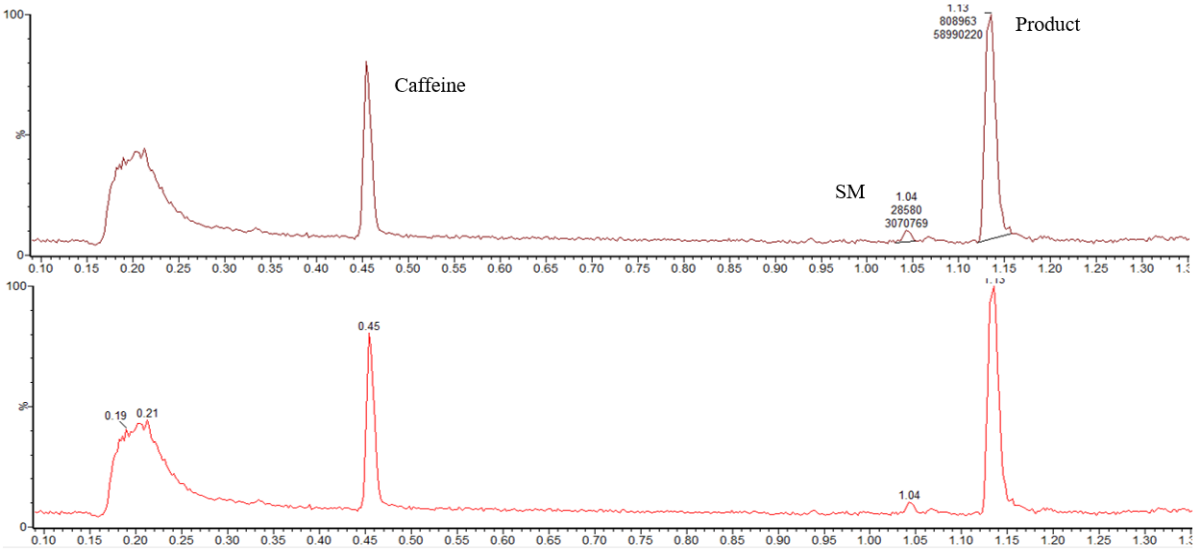


$$\%Conversion_{Product}^{MS} = 100 \times \left(\frac{\text{Area}_{\text{product}}}{Area_{sm} + Area_{product}}\right)$$

$$\%Conversion_{Product}^{MS} = 100 \times \left(\frac{51937644 \text{ counts}}{45810844\ counts + 51937644\ counts}\right)$$

$$\%Conversion_{Product}^{MS} = \mathbf{53.1}\%$$

Well B34

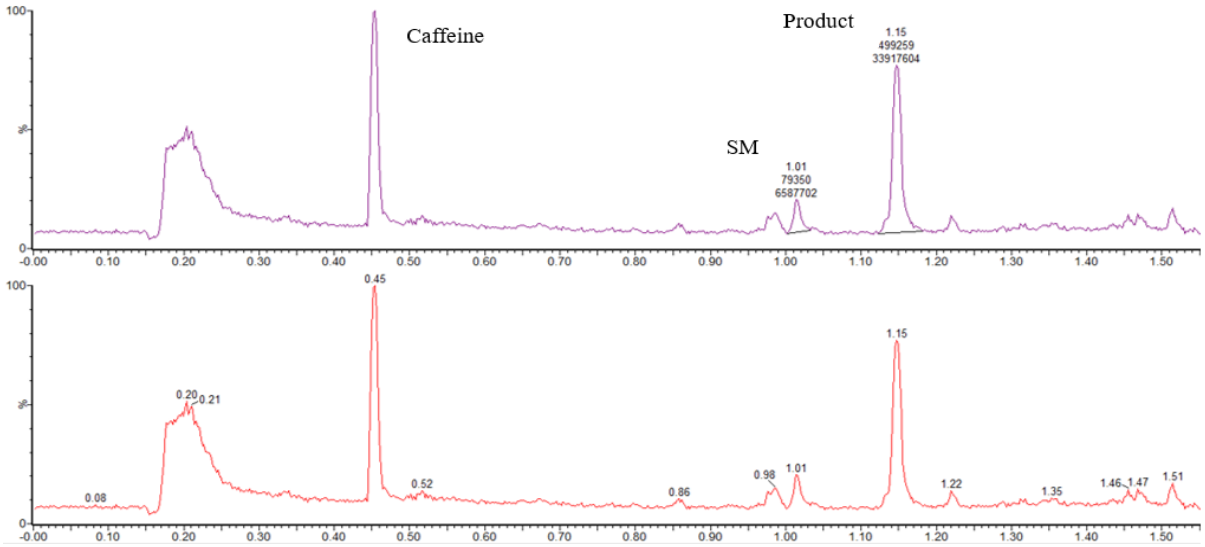


$$\%Conversion_{Product}^{MS} = 100 \times \left(\frac{\text{Area}_{\text{product}}}{Area_{sm} + Area_{product}}\right)$$

$$\%Conversion_{Product}^{MS} = 100 \times \left(\frac{58990220 \text{ counts}}{3070769\ counts + 58990220\ counts}\right)$$

$$\%Conversion_{Product}^{MS} = \mathbf{95.1}\%$$

Well T32



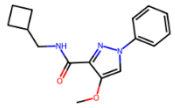
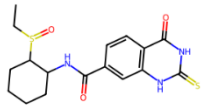
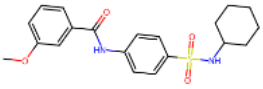
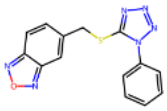
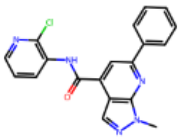
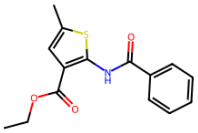
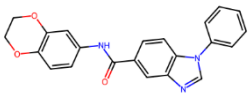
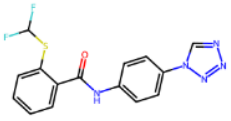
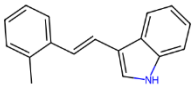
$$\%Conversion_{Product}^{MS} = 100 \times \left(\frac{\text{Area}_{\text{product}}}{Area_{sm} + Area_{product}}\right)$$

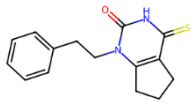
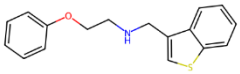
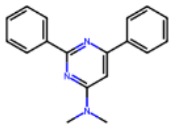
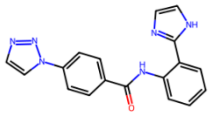
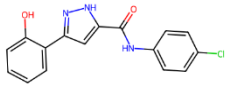
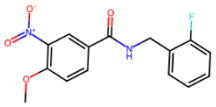
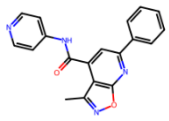
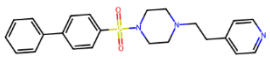
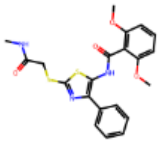
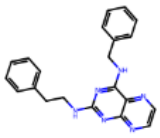
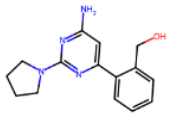
$$\%Conversion_{Product}^{MS} = 100 \times \left(\frac{33917604 \text{ counts}}{6587702\ counts + 33917604\ counts}\right)$$

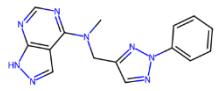
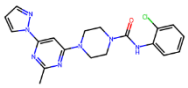
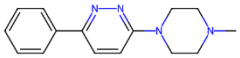
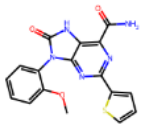
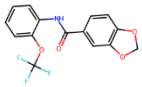
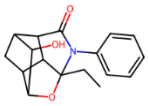
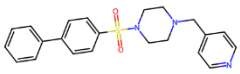
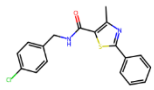
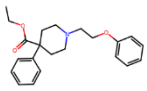
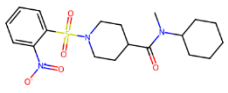
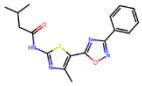
$$\%Conversion_{Product}^{MS} = \mathbf{83.7}\%$$

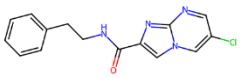
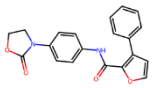
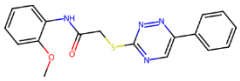
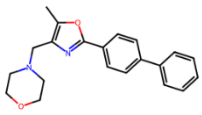
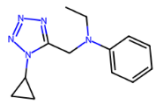
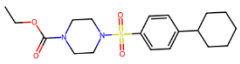
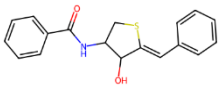
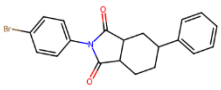
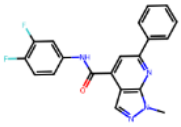
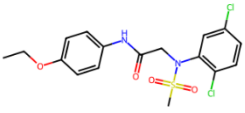
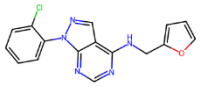
Figure 2-18 Example mass spectra from 1,536-well LSS experiment. Showing integration and calculation of percent conversion of the parent arene drugs used in the screen to saturated drugs.

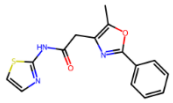
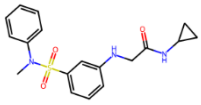
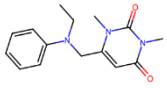
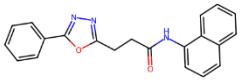
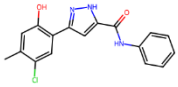
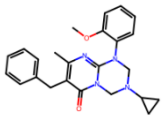
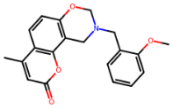
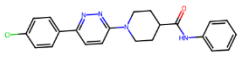
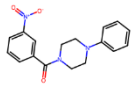
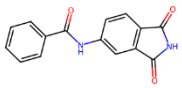
SMILES strings for substrates in 1,536-well LSS experiment

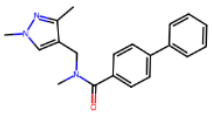
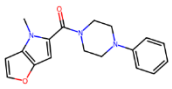
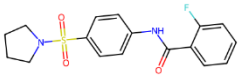
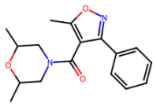
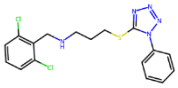
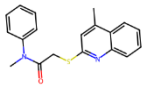
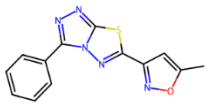
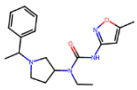
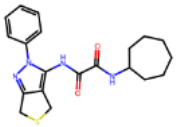
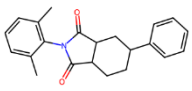
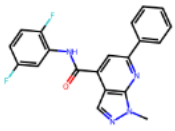
Wells	Structure	SMILES String	%Conversion 3.5 eq. (7.0 eq.) $B_2(OH)_4$
A1/ A25		COC1=CN(N=C1C(=O)NCC2CCC2)C3=CC=CC=C3	35 (34)
A2/ A26		CCS(=O)C1CCCCC1NC(=O)C2=CC3=C(C=C2)C(=O)NC(=S)N3	0 (0)
A3/ A27		COC1=CC=CC(=C1)C(=O)NC2=CC=C(C=C2)S(=O)(=O)NC3CCCCC3	22 (0)
A4/ A28		C1=CC=C(C=C1)N2C(=NN=N2)SCC3=CC4=NON=C4C=C3	27 (53)
A5/ A29		CN1C2=C(C=N1)C(=CC(=N2)C3=CC=CC=C3)C(=O)NC4=C(N=CC=C4)Cl	6 (21)
A6/ A30		CCOC(C1=C(NC(C2=CC=CC=C2)=O)SC(C)=C1)=O	23 (27)
A7/ A31		C1COC2=C(O1)C=CC(=C2)NC(=O)C3=CC4=C(C=C3)N(C=N4)C5=CC=CC=C5	89 (94)
A8/ A32		C1=CC=C(C(=C1)C(=O)NC2=CC=C(C=C2)N3C=NN=N3)SC(F)F	27 (50)
A9/ A33		CC1=CC=CC=C1C=CC2=CNC3=CC=CC=C32	22 (52)

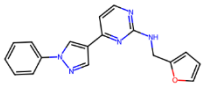
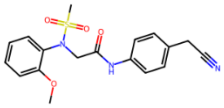
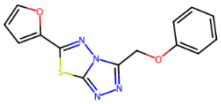
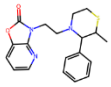
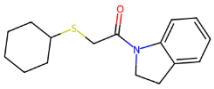
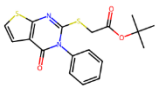
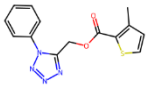
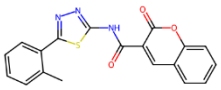
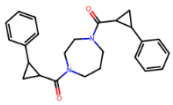
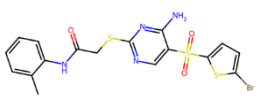
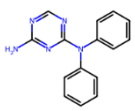
A10/ A34		C1CC2=C(C1)N(C(=O)NC2=S)CCC3=CC=CC=C3	57 (53)
A11/ A35		C1=CC=C(C=C1)OCCNCC2=CSC3=CC=CC=C32	11 (10)
A12/ A36		CN(C)C1=NC(=NC(=C1)C2=CC=CC=C2)C3=CC=CC=C3	18 (88)
A13/ A37		C1=CC=C(C(=C1)C2=NC=CN2)NC(=O)C3=CC=C(C=C3)N4C=CN=N4	88 (93)
A14/ A38		C1=CC=C(C(=C1)C2=NNC(=C2)C(=O)NC3=CC=C(C=C3)Cl)O	11 (70)
A15/ A39		COC1=C(C=C(C=C1)C(=O)NCC2=CC=CC=C2F)[N+](=O)[O-]	2 (21)
A16/ A40		CC1=NOC2=C1C(=CC(=N2)C3=CC=CC=C3)C(=O)NC4=CC=NC=C4	7 (19)
A17/ A41		C1CN(CCN1CCC2=CC=NC=C2)S(=O)(=O)C3=CC=C(C=C3)C4=CC=CC=C4	21 (30)
A18/ A42		CNC(=O)CSC1=NC(=C(S1)NC(=O)C2=C(C=CC=C2OC)OC)C3=CC=CC=C3	16 (32)
A19/ A43		C1=CC=C(C=C1)CCNC2=NC3=NC=CN=C3C(=N2)NCC4=CC=CC=C4	16 (22)
A20/ A44		C1CCN(C1)C2=NC(=CC(=N2)N)C3=CC=CC=C3CO	24 (17)

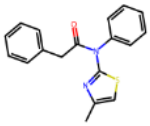
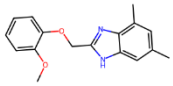
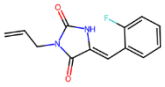
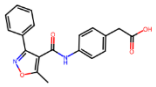
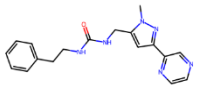
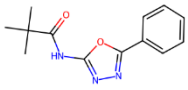
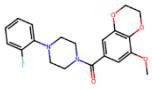
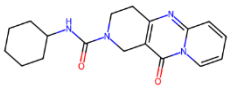
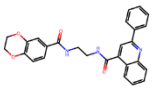
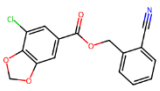
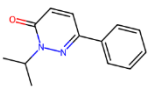
A21/ A45		CN(CC1=NN(N=C1)C2=CC=CC=C2)C3=NC=NC4=C3C=NN4	11 (25)
A22/ A46		CC1=NC(=CC(=N1)N2CCN(CC2)C(=O)NC3=CC=CC=C3Cl)N4C=CC=N4	34 (79)
A23/ A47		CN1CCN(CC1)C2=NN=C(C=C2)C3=CC=CC=C3	22 (20)
A24/ A48		COC1=CC=CC=C1N2C3=NC(=NC(=C3NC2=O)C(=O)N)C4=CC=CS4	23 (22)
B1/ B25		C1OC2=C(O1)C=C(C=C2)C(=O)NC3=CC=CC=C3OC(F)(F)F	0 (49)
B2/ B26		CCC12C3C4CC(C(O)C4O2)C3C(N1C5=CC=CC=C5)=O	20 (0)
B3/ B27		C1CN(CCN1CC2=CC=NC=C2)S(=O)(=O)C3=CC=C(C=C3)C4=CC=CC=C4	90 (88)
B4/ B28		CC1=C(SC(=N1)C2=CC=CC=C2)C(=O)NCC3=CC=C(C=C3)Cl	32 (36)
B5/ B29		CCOC(=O)C1(CCN(CC1)CCOC2=CC=CC=C2)C3=CC=CC=C3	79 (81)
B6/ B30		CN(C1CCCCC1)C(=O)C2CCN(CC2)S(=O)(=O)C3=CC=CC=C3[N+](=O)[O-]	27 (22)
B7/ B31		CC1=C(SC(=N1)NC(=O)CC(C)C)C2=NC(=NO2)C3=CC=CC=C3	40 (39)

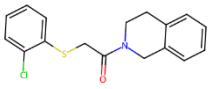
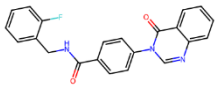
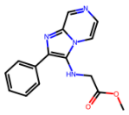
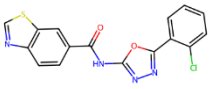
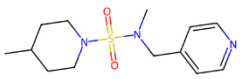
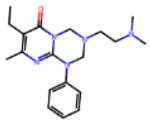
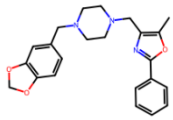
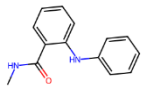
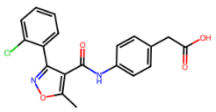
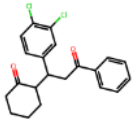
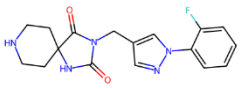
B8/ B32		C1=CC=C(C=C1)CCNC(=O)C2=CN3C=C(C=NC3=N2)Cl	10 (45)
B9/ B33		C1COC(=O)N1C2=CC=C(C=C2)NC(=O)C3=C(C=CO3)C4=CC=CC=C4	6 (49)
B10/ B34		COC1=CC=CC=C1NC(=O)CSC2=NC=C(N=N2)C3=CC=CC=C3	81 (95)
B11/ B35		CC1=C(N=C(O1)C2=CC=C(C=C2)C3=CC=CC=C3)CN4CCOCC4	26 (31)
B12/ B36		CCN(C1=CC=CC=C1)CC2=NN=NN2C3CC3	18 (22)
B13/ B37		CCOC(=O)N1CCN(CC1)S(=O)(=O)C2=CC=C(C=C2)C3CCCCC3	25 (63)
B14/ B38		C1C(C(C(=CC2=CC=CC=C2)S1)O)NC(=O)C3=CC=CC=C3	33 (63)
B15/ B39		C1CC2C(CC1C3=CC=CC=C3)C(=O)N(C2=O)C4=CC=C(C=C4)Br	46 (28)
B16/ B40		CN1C2=C(C=N1)C(=CC(=N2)C3=CC=CC=C3)C(=O)NC4=CC(=C(C=C4)F)F	94 (96)
B17/ B41		CCOC1=CC=C(C=C1)NC(=O)CN(C2=C(C=CC(=C2)Cl)Cl)S(=O)(=O)C	90 (97)
B18/ B42		C1=CC=C(C(=C1)N2C3=NC=NC(=C3C=N2)NCC4=CC=CO4)Cl	92 (92)

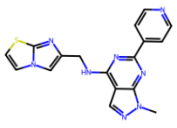
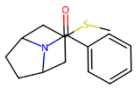
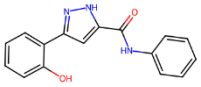
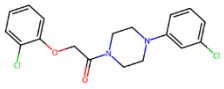
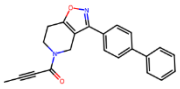
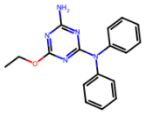
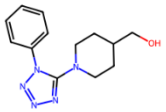
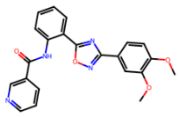
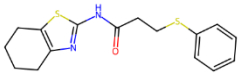
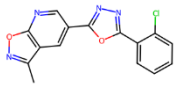
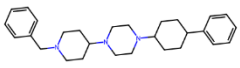
B19/ B43		C1=CC=C(C(=C1)C2=NN3C(=NN=C3S2)C4=CN=CC=C4)Br	92 (94)
B20/ B44		CC1=C(N=C(O1)C2=CC=CC=C2)CC(=O)NC3=NC=CS3	12 (13)
B21/ B45		CN(C1=CC=CC=C1)S(=O)(=O)C2=CC=CC(=C2)NCC(=O)NC3CC3	11 (19)
B22/ B46		CCN(CC1=CC(=O)N(C(=O)N1C)C)C2=CC=CC=C2	52 (40)
B23/ B47		C1=CC=C(C=C1)C2=NN=C(O2)CCC(=O)NC3=CC=CC4=CC=CC=C43	25 (93)
B24/ B48		CC1=CC(=C(C=C1Cl)C2=NNC(=C2)C(=O)NC3=CC=CC=C3)O	7 (44)
C1/ C25		CC1=C(C(=O)N2CN(CN(C2=N1)C3=CC=CC=C3OC)C4CC4)CC5=CC=CC=C5	74 (70)
C2/ C26		CC1=CC(=O)OC2=C1C=CC3=C2CN(CO3)CC4=CC=CC=C4OC	23 (43)
C3/ C27		C1CN(CCC1C(=O)NC2=CC=CC=C2)C3=NN=C(C=C3)C4=CC=C(C=C4)Cl	11 (50)
C4/ C28		C1CN(CCN1C2=CC=CC=C2)C(=O)C3=CC(=CC=C3)[N+](=O)[O-]	0 (4)
C5/ C29		C1=CC=C(C=C1)C(=O)NC2=CC3=C(C=C2)C(=O)NC3=O	29 (52)

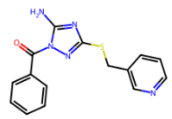
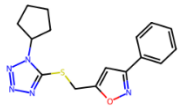
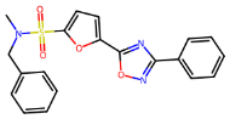
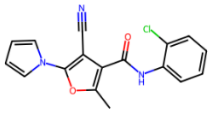
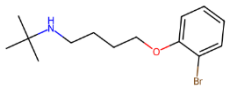
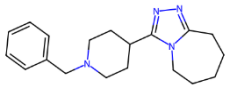
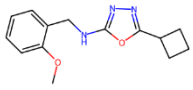
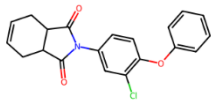
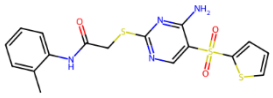
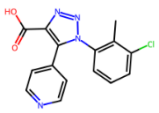
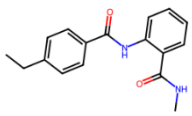
C6/ C30		CC1=NN(C=C1CN(C)C(=O)C2=CC=C(C=C2)C3=CC=CC=C3)C	32 (31)
C7/ C31		CN1C2=C(C=C1C(=O)N3CCN(CC3)C4=CC=CC=C4)OC=C2	50 (96)
C8/ C32		C1CCN(C1)S(=O)(=O)C2=CC=C(C=C2)NC(=O)C3=CC=CC=C3F	8 (26)
C9/ C33		CC1CN(CC(O1)C)C(=O)C2=C(ON=C2C3=CC=CC=C3)C	91 (89)
C10/ C34		C1=CC=C(C=C1)N2C(=NN=N2)SCCCNCC3=C(C=CC=C3Cl)Cl	31 (31)
C11/ C35		CC1=CC(=NC2=CC=CC=C12)SCC(=O)N(C)C3=CC=CC=C3	28 (63)
C12/ C36		CC1=CC(C2=NN3C(C4=CC=CC=C4)=NN=C3S2)=NO1	93 (95)
C13/ C37		CCN(C1CCN(C1)C(C)C2=CC=CC=C2)C(=O)NC3=NOC(=C3)C	20 (23)
C14/ C38		C1CCCC(CC1)NC(=O)C(=O)NC2=C3CSCC3=NN2C4=CC=CC=C4	26 (15)
C15/ C39		CC1=C(C(=CC=C1)C)N2C(=O)C3CCC(CC3C2=O)C4=CC=CC=C4	95 (88)
C16/ C40		CN1C2=C(C=N1)C(=CC(=N2)C3=CC=CC=C3)C(=O)NC4=C(C=CC(=C4)F)F	94 (98)

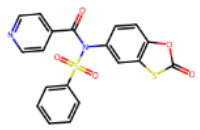
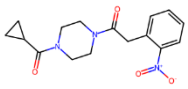
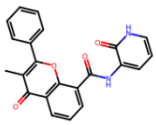
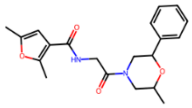
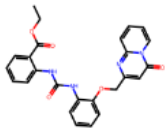
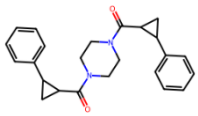
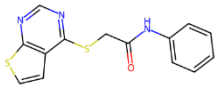
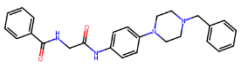
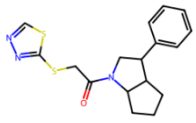
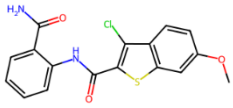
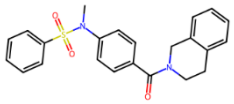
C17/ C41		C1=CC=C(C=C1)N2C=C(C=N2)C3=NC(=NC=C3)NCC4=CC=CO4	96 (97)
C18/ C42		COC1=CC=CC=C1N(CC(=O)NC2=CC=C(C=C2)CC#N)S(=O)(=O)C	16 (42)
C19/ C43		C1=CC=C(C=C1)OCC2=NN=C3N2N=C(S3)C4=CC=CO4	29 (21)
C20/ C44		CC1C(N(CCS1)CCN2C3=C(C=CC=N3)OC2=O)C4=CC=CC=C4	36 (39)
C21/ C45		C1CCC(CC1)SCC(=O)N2CCC3=CC=CC=C32	51 (47)
C22/ C46		CC(C)(C)OC(=O)CSC1=NC2=C(C=CS2)C(=O)N1C3=CC=CC=C3	12 (32)
C23/ C47		CC1=C(SC=C1)C(=O)OCC2=NN=NN2C3=CC=CC=C3	28 (25)
C24/ C48		CC1=CC=CC=C1C2=NN=C(S2)NC(=O)C3=CC4=CC=CC=C4OC3=O	26 (19)
D1/ D25		C1CN(CCN(C1)C(=O)C2CC2C3=CC=CC=C3)C(=O)C4CC4C5=CC=CC=C5	21 (20)
D2/ D26		CC1=CC=CC=C1NC(=O)CSC2=NC=C(C(=N2)N)S(=O)(=O)C3=CC=C(S3)Br	91 (92)
D3/ D27		C1=CC=C(C=C1)N(C2=CC=CC=C2)C3=NC=NC(=N3)N	24 (63)

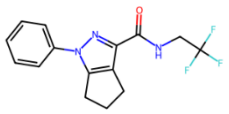
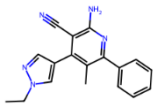
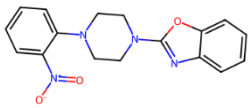
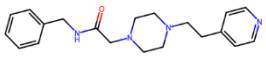
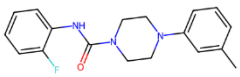
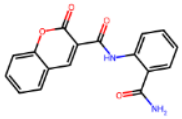
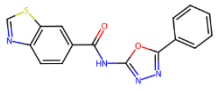
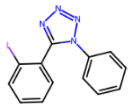
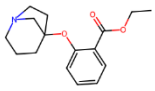
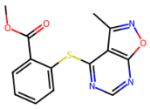
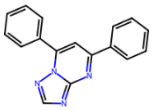
D4/ D28		CC1=CSC(=N1)N(C2=CC=CC=C2)C(=O)CC3=CC=CC=C3	89 (97)
D5/ D29		CC1=CC(=C2C(=C1)NC(=N2)COC3=CC=CC=C3OC)C	91 (90)
D6/ D30		C=CCN1C(=O)C(=CC2=CC=CC=C2F)NC1=O	31 (64)
D7/ D31		CC1=C(C(=NO1)C2=CC=CC=C2)C(=O)NC3=CC=C(C=C3)CC(=O)O	38 (21)
D8/ D32		CN1C(=CC(=N1)C2=NC=CN=C2)CNC(=O)NCCC3=CC=CC=C3	88 (95)
D9/ D33		CC(C)(C)C(=O)NC1=NN=C(O1)C2=CC=CC=C2	19 (15)
D10/ D34		COC1=CC(=CC2=C1OCCO2)C(=O)N3CCN(CC3)C4=CC=CC=C4F	95 (95)
D11/ D35		C1CCC(CC1)NC(=O)N2CCC3=C(C2)C(=O)N4C=CC=CC4=N3	14 (31)
D12/ D36		C1COC2=C(O1)C=CC(=C2)C(=O)NCCNC(=O)C3=CC(=NC4=CC=CC=C43)C5=CC=CC=C5	57 (52)
D13/ D37		C1OC2=C(O1)C(=CC(=C2)C(=O)OCC3=CC=CC=C3C#N)Cl	13 (18)
D14/ D38		CC(C)N1C(=O)C=CC(=N1)C2=CC=CC=C2	28 (0)

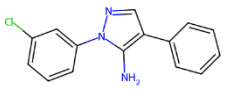
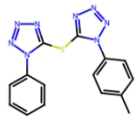
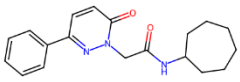
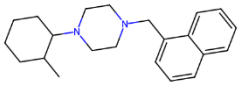
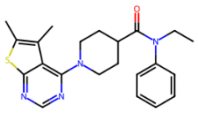
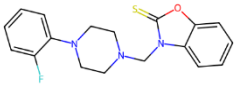
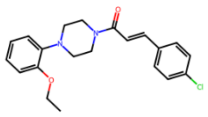
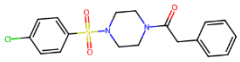
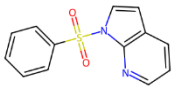
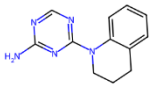
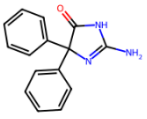
D15/ D39		C1CN(CC2=CC=CC=C21)C(=O)CSC3=CC=CC=C3Cl	89 (97)
D16/ D40		C1=CC=C(C(=C1)CNC(=O)C2=CC=C(C=C2)N3C=NC4=CC=CC=C4C3=O)F	89 (90)
D17/ D41		COC(=O)CNC1=C(N=C2N1C=CN=C2)C3=CC=CC=C3	79 (91)
D18/ D42		C1=CC=C(C(=C1)C2=NN=C(O2)NC(=O)C3=CC4=C(C=C3)N=CS4)Cl	12 (44)
D19/ D43		CC1CCN(CC1)S(=O)(=O)N(C)CC2=CC=NC=C2	27 (27)
D20/ D44		CCC1=C(N=C2N(CN(CN2C1=O)CCN(C)C)C3=CC=CC=C3)C	28 (10)
D21/ D45		CC1=C(N=C(O1)C2=CC=CC=C2)CN3CCN(CC3)CC4=CC5=C(C=C4)OCO5	0 (26)
D22/ D46		CNC(=O)C1=CC=CC=C1NC2=CC=CC=C2	32 (15)
D23/ D47		CC1=C(C(=NO1)C2=CC=CC=C2Cl)C(=O)NC3=CC=C(C=C3)CC(=O)O	27 (23)
D24/ D48		C1CCC(=O)C(C1)C(CC(=O)C2=CC=CC=C2)C3=CC(=C(C=C3)Cl)Cl	7 (10)
E1/ E25		C1CNCCC12C(=O)N(C(=O)N2)CC3=CN(N=C3)C4=CC=CC=C4F	72 (96)

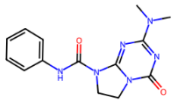
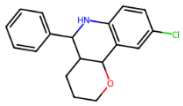
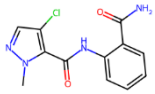
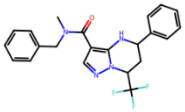
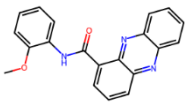
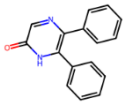
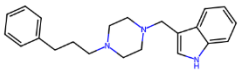
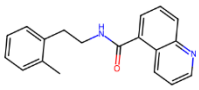
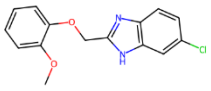
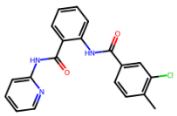
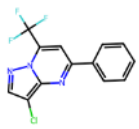
E2/ E26		CN1C2=NC(=NC(=C2C=N1)NCC3=CN4C=CSC4=N3)C5=CC=NC=C5	22 (13)
E3/ E27		CSC1CC2CCC(C1)N2C(=O)C3=CC=CC=C3	89 (95)
E4/ E28		C1=CC=C(C=C1)NC(=O)C2=CC(=NN2)C3=CC=CC=C3O	20 (28)
E5/ E29		C1CN(CCN1C2=CC(=CC=C2)Cl)C(=O)COC3=CC=CC=C3Cl	96 (93)
E6/ E30		CC#CC(=O)N1CCC2=C(C1)C(=NO2)C3=CC=C(C=C3)C4=CC=CC=C4	89 (91)
E7/ E31		CCOC1=NC(=NC(=N1)N(C2=CC=CC=C2)C3=CC=CC=C3)N	18 (21)
E8/ E32		C1CN(CCC1CO)C2=NN=NN2C3=CC=CC=C3	19 (49)
E9/ E33		COC1=C(C=C(C=C1)C2=NOC(=N2)C3=CC=CC=C3NC(=O)C4=CN=CC=C4)OC	26 (0)
E10/ E34		C1CCC2=C(C1)N=C(S2)NC(=O)CCSC3=CC=CC=C3	24 (27)
E11/ E35		CC1=NOC2=C1C=C(C=N2)C3=NN=C(O3)C4=CC=CC=C4Cl	34 (38)
E12/ E36		C1CC(CCC1C2=CC=CC=C2)N3CCN(CC3)C4CCN(CC4)CC5=CC=CC=C5	17 (22)

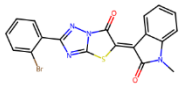
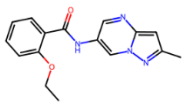
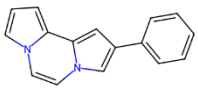
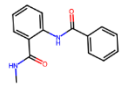
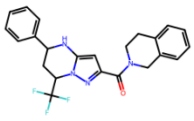
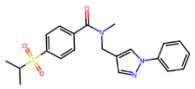
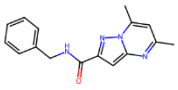
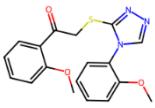
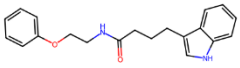
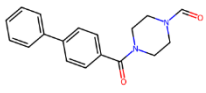
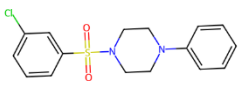
E13/ E37		C1=CC=C(C=C1)C(=O)N2C(=NC(=N2)SCC3=CN=CC=C3)N	26 (14)
E14/ E38		C1CCC(C1)N2C(=NN=N2)SCC3=CC(=NO3)C4=CC=CC=C4	27 (53)
E15/ E39		CN(CC1=CC=CC=C1)S(=O)(=O)C2=CC=C(O2)C3=NC(=NO3)C4=CC=CC=C4	24 (10)
E16/ E40		CC1=C(C(=C(O1)N2C=CC=C2)C#N)C(=O)NC3=CC=CC=C3Cl	28 (60)
E17/ E41		CC(C)(C)NCCCCOC1=CC=CC=C1Br	8 (25)
E18/ E42		C1CCC2=NN=C(N2CC1)C3CCN(CC3)CC4=CC=CC=C4	0 (18)
E19/ E43		COC1=CC=CC=C1CNC2=NN=C(O2)C3CCC3	16 (22)
E20/ E44		C1C=CCC2C1C(=O)N(C2=O)C3=CC(=C(C=C3)OC4=CC=CC=C4)Cl	25 (25)
E21/ E45		CC1=CC=CC=C1NC(=O)CSC2=NC=C(C(=N2)N)S(=O)(=O)C3=CC=CS3	34 (31)
E22/ E46		CC1=C(C=CC=C1Cl)N2C(=C(N=N2)C(=O)O)C3=CC=NC=C3	25 (11)
E23/ E47		CCC1=CC=C(C=C1)C(=O)NC2=CC=CC=C2C(=O)NC	17 (18)

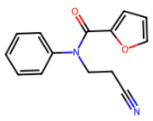
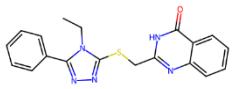
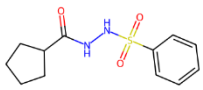
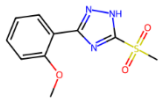
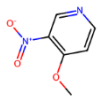
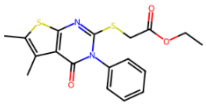
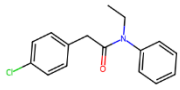
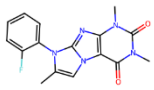
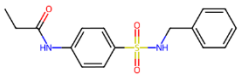
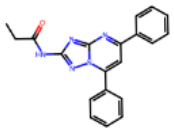
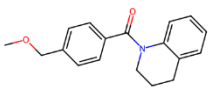
E24/ E48		C1=CC=C(C=C1)S(=O)(=O)N(C2=CC3=C(C=C2)OC(=O)S3)C(=O)C4=CC=NC=C4	8 (45)
F1/ F25		C1CC1C(=O)N2CCN(CC2)C(=O)CC3=CC=CC=C3[N+](=O)[O-]	26 (49)
F2/ F26		CC1=C(OC2=C(C1=O)C=CC=C2C(=O)NC3=CC=CNC3=O)C4=CC=CC=C4	8 (13)
F3/ F27		CC1CN(CC(O1)C2=CC=CC=C2)C(=O)CNC(=O)C3=C(OC(=C3)C)C	19 (20)
F4/ F28		CCOC(=O)C1=CC=CC=C1NC(=O)NC2=CC=CC=C2OCC3=CC(=O)N4C=CC=CC4=N3	17 (12)
F5/ F29		C1CN(CCN1C(=O)C2CC2C3=CC=CC=C3)C(=O)C4CC4C5=CC=CC=C5	7 (49)
F6/ F30		C1=CC=C(C=C1)NC(=O)CSC2=NC=NC3=C2C=CS3	96 (94)
F7/ F31		C1CN(CCN1CC2=CC=CC=C2)C3=CC=C(C=C3)NC(=O)CNC(=O)C4=CC=CC=C4	9 (27)
F8/ F32		C1CC2C(C1)N(CC2C3=CC=CC=C3)C(=O)CSC4=NN=CS4	0 (8)
F9/ F33		COC1=CC2=C(C=C1)C(=C(S2)C(=O)NC3=CC=CC=C3C(=O)N)Cl	0 (0)
F10/ F34		CN(C1=CC=C(C=C1)C(=O)N2CCC3=CC=CC=C3C2)S(=O)(=O)C4=CC=CC=C4	0 (51)

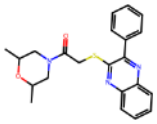
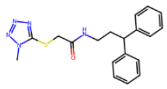
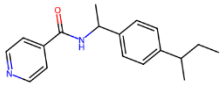
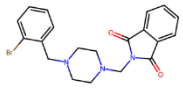
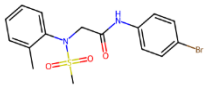
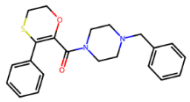
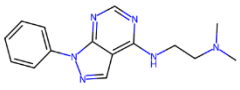
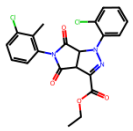
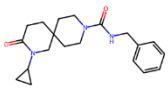
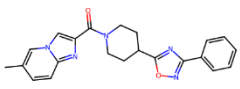
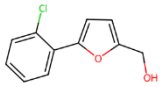
F11/ F35		C1CC2=C(C1)N(N=C2C(=O)NCC(F)(F)F)C3=CC=CC=C3	27 (10)
F12/ F36		CCN1C=C(C=N1)C2=C(C(=NC(=C2C#N)N)C3=CC=CC=C3)C	26 (0)
F13/ F37		C1CN(CCN1C2=CC=CC=C2[N+](=O)[O-])C3=NC4=CC=CC=C4O3	90 (91)
F14/ F38		C1CN(CCN1CCC2=CC=NC=C2)CC(=O)NCC3=CC=CC=C3	97 (93)
F15/ F39		CC1=CC(=CC=C1)N2CCN(CC2)C(=O)NC3=CC=CC=C3F	97 (97)
F16/ F40		C1=CC=C2C(=C1)C=C(C(=O)O2)C(=O)NC3=CC=CC=C3C(=O)N	11 (23)
F17/ F41		C1=CC=C(C=C1)C2=NN=C(O2)NC(=O)C3=CC4=C(C=C3)N=CS4	22 (45)
F18/ F42		C1=CC=C(C=C1)N2C(=NN=N2)C3=CC=CC=C3I	93 (89)
F19/ F43		CCOC(=O)C1=CC=CC=C1OC23CCCN(C2)CC3	10 (9)
F20/ F44		CC1=NOC2=C1C(=NC=N2)SC3=CC=CC=C3C(=O)OC	36 (80)
F21/ F45		C1=CC=C(C=C1)C2=CC(=NC3=NC=NN23)C4=CC=CC=C4	14 (11)

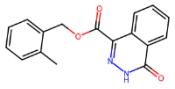
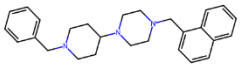
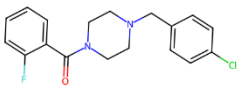
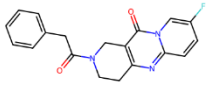
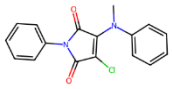
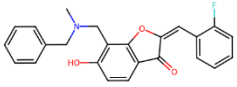
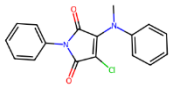
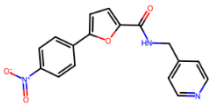
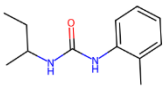
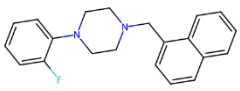
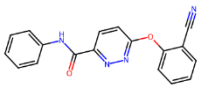
F22/ F46		C1=CC=C(C=C1)C2=C(N(N=C2)C3=CC(=CC=C3)Cl)N	90 (97)
F23/ F47		CC1=CC=C(C=C1)N2C(=NN=N2)SC3=NN=NN3C4=CC=CC=C4	29 (72)
F24/ F48		C1CCCC(CC1)NC(=O)CN2C(=O)C=CC(=N2)C3=CC=CC=C3	7 (20)
G1/ G25		CC1CCCCC1N2CCN(CC2)CC3=CC=CC4=CC=CC=C43	19 (19)
G2/ G26		CCN(C1=CC=CC=C1)C(=O)C2CCN(CC2)C3=C4C(=C(SC4=NC=N3)C)C	88 (91)
G3/ G27		C1CN(CCN1CN2C3=CC=CC=C3OC2=S)C4=CC=CC=C4F	91 (89)
G4/ G28		CCOC1=CC=CC=C1N2CCN(CC2)C(=O)C=CC3=CC=C(C=C3)Cl	21 (19)
G5/ G29		C1CN(CCN1C(=O)CC2=CC=CC=C2)S(=O)(=O)C3=CC=C(C=C3)Cl	12 (24)
G6/ G30		C1=CC=C(C=C1)S(=O)(=O)N2C=CC3=C2N=CC=C3	98 (97)
G7/ G31		C1CC2=CC=CC=C2N(C1)C3=NC=NC(=N3)N	7 (22)
G8/ G32		C1=CC=C(C=C1)C2(C(=O)NC(=N2)N)C3=CC=CC=C3	16 (13)

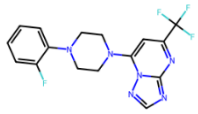
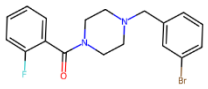
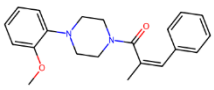
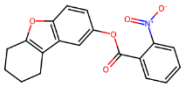
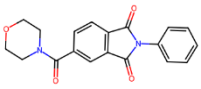
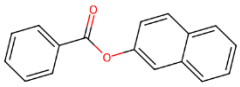
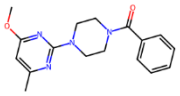
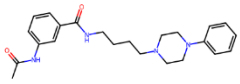
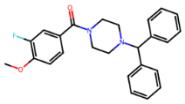
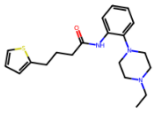
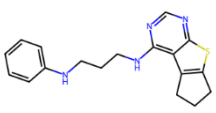
G9/ G33		CN(C)C1=NC(=O)N2CCN(C2=N1)C(=O)NC3=CC=CC=C3	98 (91)
G10/ G34		C1CC2C(NC3=C(C2OC1)C=C(C=C3)Cl)C4=CC=CC=C4	97 (85)
G11/ G35		CN1C(=C(C=N1)Cl)C(=O)NC2=CC=CC=C2C(=O)N	92 (97)
G12/ G36		CN(CC1=CC=CC=C1)C(=O)C2=C3NC(CC(N3N=C2)C(F)(F)F)C4=CC=CC=C4	88 (93)
G13/ G37		COC1=CC=CC=C1NC(=O)C2=CC=CC3=NC4=CC=CC=C4N=C32	5 (0)
G14/ G38		C1=CC=C(C=C1)C2=C(N=CC(=O)N2)C3=CC=CC=C3	91 (89)
G15/ G39		C1CN(CCN1CCCC2=CC=CC=C2)CC3=CNC4=CC=CC=C43	97 (98)
G16/ G40		CC1=CC=CC=C1CCNC(=O)C2=C3C=CC=NC3=CC=C2	20 (45)
G17/ G41		COC1=CC=CC=C1OCC2=NC3=C(N2)C=C(C=C3)Cl	95 (89)
G18/ G42		CC1=C(C=C(C=C1)C(=O)NC2=CC=CC=C2C(=O)NC3=CC=CC=N3)Cl	90 (97)
G19/ G43		C1=CC=C(C=C1)C2=NC3=C(C=NN3C(=C2)C(F)(F)F)Cl	21 (48)

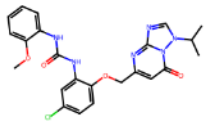
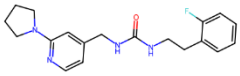
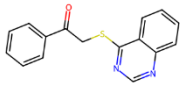
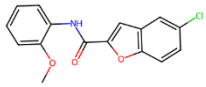
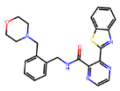
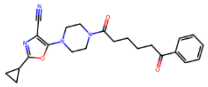
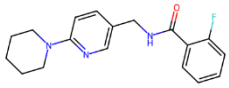
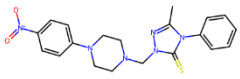
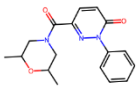
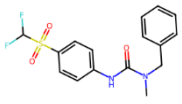
G20/ G44		CN1C2=CC=CC=C2C(=C3C(=O)N4C(=NC(=N4)C5=CC=CC=C5Br)S3)C1=O	21 (51)
G21/ G45		CCOC1=CC=CC=C1C(=O)NC2=CN3C(=CC(=N3)C)N=C2	92 (94)
G22/ G46		C1=CC=C(C=C1)C2=CN3C=CN4C=CC=C4C3=C2	95 (98)
G23/ G47		CNC(=O)C1=CC=CC=C1NC(=O)C2=CC=CC=C2	0 (27)
G24/ G48		C1CN(CC2=CC=CC=C21)C(=O)C3=NN4C(CC(NC4=C3)C5=CC=CC=C5)C(F)(F)F	91 (89)
H1/ H25		CC(C)S(=O)(=O)C1=CC=C(C=C1)C(=O)N(C)CC2=CN(N=C2)C3=CC=CC=C3	60 (98)
H2/ H26		CC1=CC(=NC2=CC(=NN12)C(=O)NCC3=CC=CC=C3)C	66 (65)
H3/ H27		COC1=CC=CC=C1C(=O)CSC2=NN=CN2C3=CC=CC=C3OC	89 (90)
H4/ H28		C1=CC=C(C=C1)OCCNC(=O)CCCC2=CNC3=CC=CC=C32	91 (98)
H5/ H29		C1CN(CCN1C=O)C(=O)C2=CC=C(C=C2)C3=CC=CC=C3	98 (93)
H6/ H30		C1CN(CCN1C2=CC=CC=C2)S(=O)(=O)C3=CC(=CC=C3)Cl	0 (25)

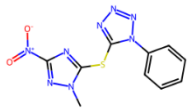
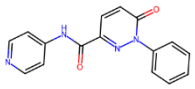
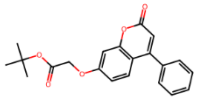
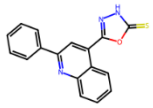
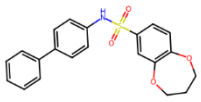
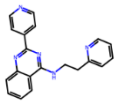
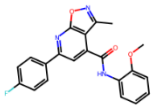
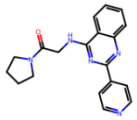
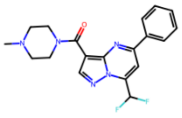
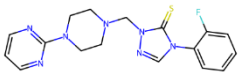
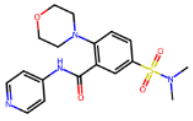
H7/ H31		C1=CC=C(C=C1)N(CCC#N)C(=O)C2=CC=CO2	29 (52)
H8/ H32		CCN1C(=NN=C1SCC2=NC3=CC=CC=C3C(=O)N2)C4=CC=CC=C4	98 (92)
H9/ H33		C1CCC(C1)C(=O)NNS(=O)(=O)C2=CC=CC=C2	97 (89)
H10/ H34		COC1=CC=CC=C1C2=NNC(=N2)S(=O)(=O)C	95 (88)
H11/ H35		COC1=C(C=NC=C1)[N+](=O)[O-]	43 (89)
H12/ H36		CCOC(CSC1=NC2=C(C(N1C3=CC=CC=C3)=O)C(C)=C(C)S2)=O	93 (91)
H13/ H37		CCN(C1=CC=CC=C1)C(=O)CC2=CC=C(C=C2)Cl	93 (90)
H14/ H38		CC1=CN2C3=C(N=C2N1C4=CC=CC=C4F)N(C(=O)N(C3=O)C)C	52 (93)
H15/ H39		CCC(=O)NC1=CC=C(C=C1)S(=O)(=O)NCC2=CC=CC=C2	89 (86)
H16/ H40		CCC(=O)NC1=NN2C(=CC(=NC2=N1)C3=CC=CC=C3)C4=CC=CC=C4	96 (96)
H17/ H41		COCC1=CC=C(C=C1)C(=O)N2CCCC3=CC=CC=C32	0 (11)

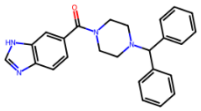
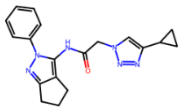
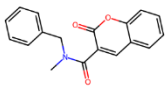
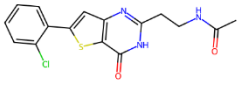
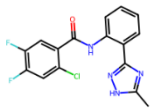
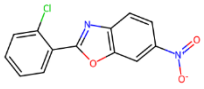
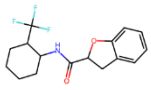
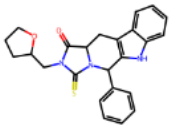
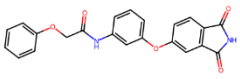
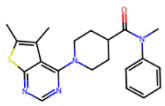
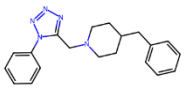
H18/ H42		CC1CN(CC(O1)C)C(=O)CSC2=NC3=CC=CC=C3N=C2C4=CC=CC=C4	0 (0)
H19/ H43		CN1C(=NN=N1)SCC(=O)NCCC(C2=CC=CC=C2)C3=CC=CC=C3	30 (36)
H20/ H44		CCC(C)C1=CC=C(C=C1)C(C)NC(=O)C2=CC=NC=C2	24 (12)
H21/ H45		C1CN(CCN1CC2=CC=CC=C2Br)CN3C(=O)C4=CC=CC=C4C3=O	92 (90)
H22/ H46		CC1=CC=CC=C1N(CC(=O)NC2=CC=C(C=C2)Br)S(=O)(=O)C	13 (10)
H23/ H47		C1CN(CCN1CC2=CC=CC=C2)C(=O)C3=C(SCCO3)C4=CC=CC=C4	26 (10)
H24/ H48		CN(C)CCNC1=C2C=NN(C2=NC=N1)C3=CC=CC=C3	93 (97)
I1/ I25		CCOC(=O)C1=NN(C2C1C(=O)N(C2=O)C3=C(C(=CC=C3)Cl)C)C4=CC=CC=C4Cl	91 (95)
I2/ I26		C1CC1N2CC3(CCC2=O)CCN(CC3)C(=O)NCC4=CC=CC=C4	20 (50)
I3/ I27		CC1=CN2C=C(N=C2C=C1)C(=O)N3CCC(CC3)C4=NC(=NO4)C5=CC=CC=C5	13 (43)
I4/ I28		C1=CC=C(C(=C1)C2=CC=C(O2)CO)Cl	91 (98)

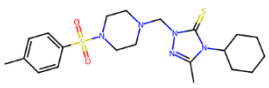
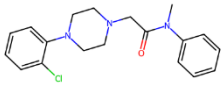
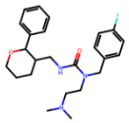
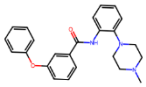
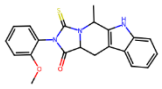
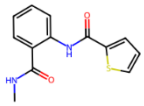
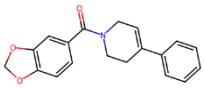
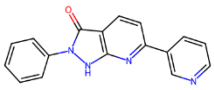
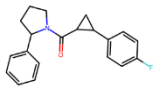
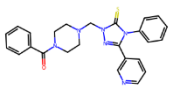
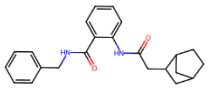
I5/ I29		CC1=CC=CC=C1COC(=O)C2=NNC(=O)C3=CC=CC=C32	23 (34)
I6/ I30		C1CN(CCC1N2CCN(CC2)CC3=CC=CC4=CC=CC=C43)CC5=CC=CC=C5	88 (97)
I7/ I31		C1CN(CCN1CC2=CC=C(C=C2)Cl)C(=O)C3=CC=CC=C3F	0 (28)
I8/ I32		C1CN(CC2=C1N=C3C=CC(=CN3C2=O)F)C(=O)CC4=CC=CC=C4	0 (7)
I9/ I33		CN(C1=CC=CC=C1)C2=C(C(=O)N(C2=O)C3=CC=CC=C3)Cl	29 (52)
I10/ I34		CN(CC1=CC=CC=C1)CC2=C(C=CC3=C2OC(=CC4=CC=CC=C4F)C3=O)O	17 (66)
I11/ I35		CN(C1=CC=CC=C1)C2=C(C(=O)N(C2=O)C3=CC=CC=C3)Cl	19 (14)
I12/ I36		C1=CC(=CC=C1C2=CC=C(O2)C(=O)NCC3=CC=NC=C3)[N+](=O)[O-]	23 (38)
I13/ I37		CCC(NC(NC1=CC=CC=C1C)=O)C	50 (51)
I14/ I38		C1CN(CCN1CC2=CC=CC3=CC=CC=C32)C4=CC=CC=C4F	15 (30)
I15/ I39		C1=CC=C(C=C1)NC(=O)C2=NN=C(C=C2)OC3=CC=CC=C3C#N	24 (6)

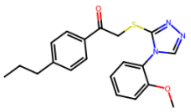
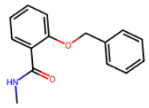
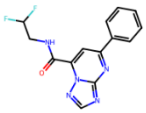
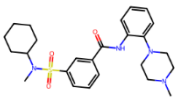
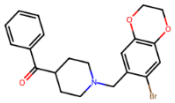
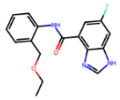
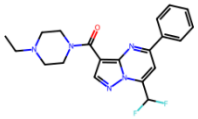
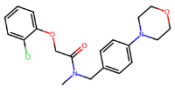
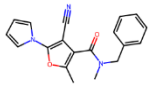
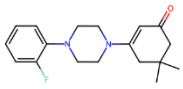
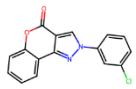
I16/ I40		C1CN(CCN1C2=CC=CC=C2F)C3=CC(=NC4=NC=NN34)C(F)(F)F	17 (19)
I17/ I41		C1CN(CCN1CC2=CC(=CC=C2)Br)C(=O)C3=CC=CC=C3F	0 (25)
I18/ I42		CC(=CC1=CC=CC=C1)C(=O)N2CCN(CC2)C3=CC=CC=C3OC	13 (52)
I19/ I43		C1CCC2=C(C1)C3=C(O2)C=CC(=C3)OC(=O)C4=CC=CC=C4[N+](=O)[O-]	0 (29)
I20/ I44		C1COCCN1C(=O)C2=CC3=C(C=C2)C(=O)N(C3=O)C4=CC=CC=C4	0 (0)
I21/ I45		C1=CC=C(C=C1)C(=O)OC2=CC3=CC=CC=C3C=C2	18 (0)
I22/ I46		CC1=CC(=NC(=N1)N2CCN(CC2)C(=O)C3=CC=CC=C3)OC	13 (64)
I23/ I47		CC(=O)NC1=CC=CC(=C1)C(=O)NCCCCN2CCN(CC2)C3=CC=CC=C3	29 (50)
I24/ I48		COC1=C(C=C(C=C1)C(=O)N2CCN(CC2)C(C3=CC=CC=C3)C4=CC=CC=C4)F	22 (28)
J1/ J25		CCN1CCN(CC1)C2=CC=CC=C2NC(=O)CCCC3=CC=CS3	93 (94)
J2/ J26		C1(NCCCNC2=C3C4=C(SC3=NC=N2)CCC4)=CC=CC=C1	26 (7)

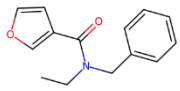
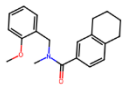
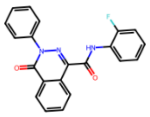
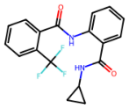
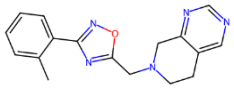
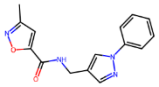
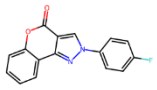
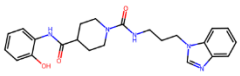
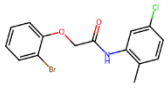
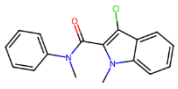
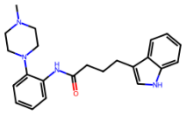
J3/ J27		CC(C)N1C=NC2=NC(=CC(=O)N21)COC3=C(C=C(C=C3)Cl)NC(=O)NC4=CC=CC=C4OC	12 (26)
J4/ J28		C1CCN(C1)C2=NC=CC(=C2)CNC(=O)NCCC3=CC=CC=C3F	88 (93)
J5/ J29		C1=CC=C(C=C1)C(=O)CSC2=NC=NC3=CC=CC=C32	11 (3)
J6/ J30		COC1=CC=CC=C1NC(=O)C2=CC3=C(O2)C=CC(=C3)Cl	11 (51)
J7/ J31		C1COCCN1CC2=CC=CC=C2CNC(=O)C3=NC=CN=C3C4=NC5=CC=CC=C5S4	31 (30)
J8/ J32		C1CC1C2=NC(=C(O2)N3CCN(CC3)C(=O)CCCCC(=O)C4=CC=CC=C4)C#N	25 (24)
J9/ J33		CC1=CC=CC=C1OCC(=O)NC2=C(C=CC(=C2)Cl)N3CCN(CC3)C	64 (65)
J10/ J34		C1CCN(CC1)C2=NC=C(C=C2)CNC(=O)C3=CC=CC=C3F	43 (87)
J11/ J35		CC1=NN(C(=S)N1C2=CC=CC=C2)CN3CCN(CC3)C4=CC=C(C=C4)[N+](=O)[O-]	6 (10)
J12/ J36		CC1CN(CC(O1)C)C(=O)C2=NN(C(=O)C=C2)C3=CC=CC=C3	96 (90)
J13/ J37		CN(CC1=CC=CC=C1)C(=O)NC2=CC=C(C=C2)S(=O)(=O)C(F)F	26 (11)

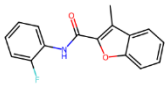
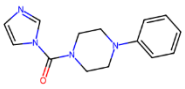
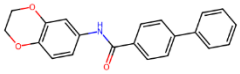
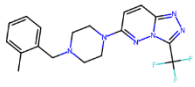
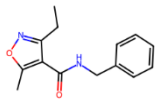
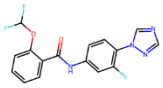
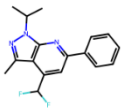
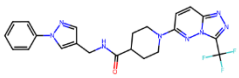
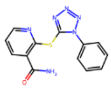
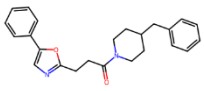
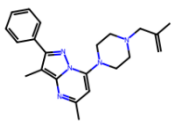
J14/ J38		CN1C(SC2=NN=NN2C3=CC=CC=C3)=NC([N+]([O-])=O)=N1	63 (94)
J15/ J39		C1=CC=C(C=C1)N2C(=O)C=CC(=N2)C(=O)NC3=CC=NC=C3	26 (43)
J16/ J40		CC(C)(C)OC(=O)COC1=CC2=C(C=C1)C(=CC(=O)O2)C3=CC=CC=C3	20 (26)
J17/ J41		C1=CC=C(C=C1)C2=NC3=CC=CC=C3C(=C2)C4=NNC(=S)O4	91 (90)
J18/ J42		C1COC2=C(C=C(C=C2)S(=O)(=O)NC3=CC=C(C=C3)C4=CC=CC=C4)OC1	21 (28)
J19/ J43		C1=CC=C2C(=C1)C(=NC(=N2)C3=CC=NC=C3)NCCC4=CC=CC=N4	14 (28)
J20/ J44		CC1=NOC2=C1C(=CC(=N2)C3=CC=C(C=C3)F)C(=O)NC4=CC=CC=C4OC	30 (27)
J21/ J45		C1CCN(C1)C(=O)CNC2=NC(=NC3=CC=CC=C32)C4=CC=NC=C4	88 (89)
J22/ J46		CN1CCN(CC1)C(=O)C2=C3N=C(C=C(N3N=C2)C(F)F)C4=CC=CC=C4	19 (44)
J23/ J47		C1CN(CCN1CN2C(=S)N(C=N2)C3=CC=CC=C3F)C4=NC=CC=N4	23 (18)
J24/ J48		CN(C)S(=O)(=O)C1=CC(=C(C=C1)N2CCOCC2)C(=O)NC3=CC=NC=C3	0 (19)

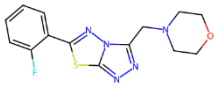
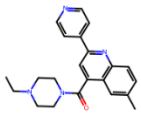
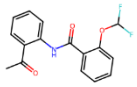
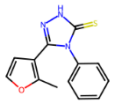
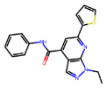
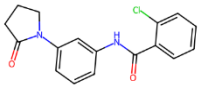
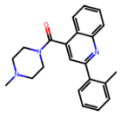
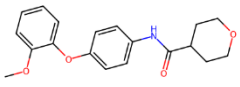
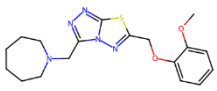
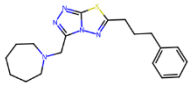
K1/ K25		C1CN(CCN1C(C2=CC=CC=C2)C3=CC=CC=C3)C(=O)C4=CC5=C(C=C4)N=CN5	12 (11)
K2/ K26		C1CC2=C(N(N=C2C1)C3=CC=CC=C3)NC(=O)CN4C=C(N=N4)C5CC5	26 (47)
K3/ K27		CN(CC1=CC=CC=C1)C(=O)C2=CC3=CC=CC=C3OC2=O	22 (0)
K4/ K28		CC(=O)NCCC1=NC2=C(C(=O)N1)SC(=C2)C3=CC=CC=C3Cl	91 (98)
K5/ K29		CC1=NC(=NN1)C2=CC=CC=C2NC(=O)C3=CC(=C(C=C3Cl)F)F	96 (89)
K6/ K30		C1=CC=C(C(=C1)C2=NC3=C(O2)C=C(C=C3)[N+](=O)[O-])Cl	14 (26)
K7/ K31		C1CCC(C(C1)C(F)(F)F)NC(=O)C2CC3=CC=CC=C3O2	92 (92)
K8/ K32		C1CC(OC1)CN2C(=O)C3CC4=C(C(N3C2=S)C5=CC=CC=C5)NC6=CC=CC=C46	88 (95)
K9/ K33		C1=CC=C(C=C1)OCC(=O)NC2=CC(=CC=C2)OC3=CC4=C(C=C3)C(=O)NC4=O	0 (0)
K10/ K34		CC1=C(SC2=NC=NC(=C12)N3CCC(CC3)C(=O)N(C)C4=CC=CC=C4)C	89 (93)
K11/ K35		C1CN(CCC1CC2=CC=CC=C2)CC3=NN=NN3C4=CC=CC=C4	30 (92)

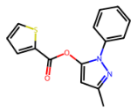
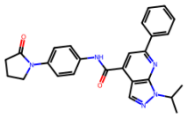
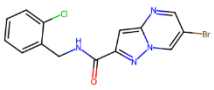
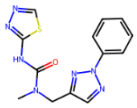
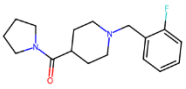
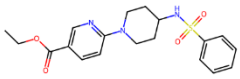
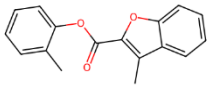
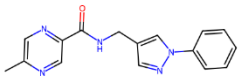
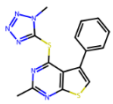
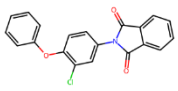
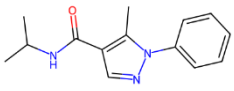
K12/ K36		CC1=CC=C(C=C1)S(=O)(=O)N2CCN(CC2)CN3C(=S)N(C(=N3)C)C4CCCCC4	24 (48)
K13/ K37		CN(C1=CC=CC=C1)C(=O)CN2CCN(CC2)C3=CC=CC=C3Cl	11 (22)
K14/ K38		CN(C)CCN(CC1=CC=C(C=C1)F)C(=O)NCC2CCCOC2C3=CC=CC=C3	9 (13)
K15/ K39		CN1CCN(CC1)C2=CC=CC=C2NC(=O)C3=CC(=CC=C3)OC4=CC=CC=C4	15 (44)
K16/ K40		CC1C2=C(CC3N1C(=S)N(C3=O)C4=CC=CC=C4OC)C5=CC=CC=C5N2	29 (7)
K17/ K41		CNC(=O)C1=CC=CC=C1NC(=O)C2=CC=CS2	34 (55)
K18/ K42		C1CN(CC=C1C2=CC=CC=C2)C(=O)C3=CC4=C(C=C3)OCO4	9 (48)
K19/ K43		C1=CC=C(C=C1)N2C(=O)C3=C(N2)N=C(C=C3)C4=CN=CC=C4	7 (18)
K20/ K44		C1CC(N(C1)C(=O)C2CC2C3=CC=C(C=C3)F)C4=CC=CC=C4	21 (18)
K21/ K45		C1CN(CCN1CN2C(=S)N(C(=N2)C3=CN=CC=C3)C4=CC=CC=C4)C(=O)C5=CC=CC=C5	34 (67)
K22/ K46		C1CC2CC1CC2CC(=O)NC3=CC=CC=C3C(=O)NCC4=CC=CC=C4	18 (59)

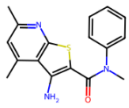
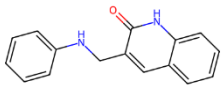
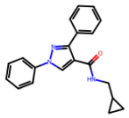
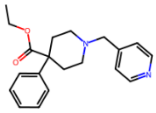
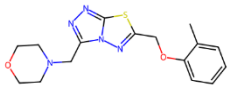
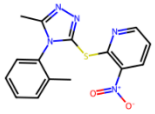
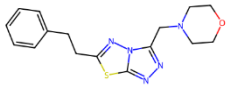
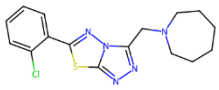
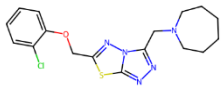
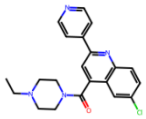
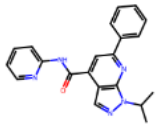
K23/ K47		CCCC1=CC=C(C=C1)C(=O)CSC2=NN=CN2C3=CC=CC=C3OC	12 (29)
K24/ K48		CNC(=O)C1=CC=CC=C1OCC2=CC=CC=C2	94 (94)
L1/ L25		C1=CC=C(C=C1)C2=NC3=NC=NN3C(=C2)C(=O)NCC(F)F	23 (14)
L2/ L26		CN1CCN(CC1)C2=CC=CC=C2NC(=O)C3=CC(=CC=C3)S(=O)(=O)N(C)C4CCCCC4	34 (43)
L3/ L27		C1CN(CCC1C(=O)C2=CC=CC=C2)CC3=CC4=C(C=C3Br)OCCO4	0 (6)
L4/ L28		CCOCC1=CC=CC=C1NC(=O)C2=C3C(=CC(=C2)F)NC=N3	25 (59)
L5/ L29		CCN1CCN(CC1)C(=O)C2=C3N=C(C=C(N3N=C2)C(F)F)C4=CC=CC=C4	17 (19)
L6/ L30		CN(CC1=CC=C(C=C1)N2CCOCC2)C(=O)COC3=CC=CC=C3Cl	23 (22)
L7/ L31		CC1=C(C(=C(O1)N2C=CC=C2)C#N)C(=O)N(C)CC3=CC=CC=C3	92 (94)
L8/ L32		CC1(CC(=CC(=O)C1)N2CCN(CC2)C3=CC=CC=C3F)C	95 (93)
L9/ L33		C1=CC=C2C(=C1)C3=NN(C=C3C(=O)O2)C4=CC(=CC=C4)Cl	80 (98)

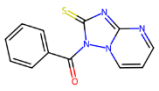
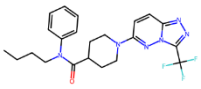
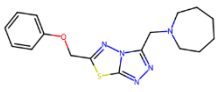
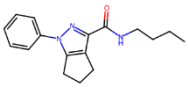
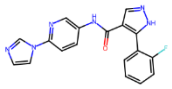
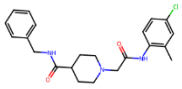
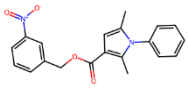
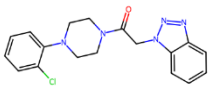
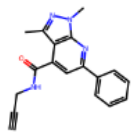
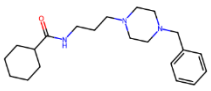
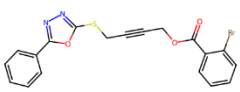
L10/ L34		CCN(CC1=CC=CC=C1)C(=O)C2=COC=C2	94 (97)
L11/ L35		CN(CC1=CC=CC=C1OC)C(=O)C2=CC3=C(CCCC3)C=C2	92 (90)
L12/ L36		C1=CC=C(C=C1)N2C(=O)C3=CC=CC=C3C(=N2)C(=O)NC4=CC=CC=C4F	20 (18)
L13/ L37		C1CC1NC(=O)C2=CC=CC=C2NC(=O)C3=CC=CC=C3C(F)(F)F	25 (30)
L14/ L38		CC1=CC=CC=C1C2=NOC(=N2)CN3CCC4=CN=CN=C4C3	91 (96)
L15/ L39		CC1=NOC(=C1)C(=O)NCC2=CN(N=C2)C3=CC=CC=C3	54 (93)
L16/ L40		C1=CC=C2C(=C1)C3=NN(C=C3C(=O)O2)C4=CC=C(C=C4)F	36 (36)
L17/ L41		C1CN(CCC1C(=O)NC2=CC=CC=C2O)C(=O)NCCCN3C=NC4=CC=CC=C43	8 (27)
L18/ L42		CC1=C(C=C(C=C1)Cl)NC(=O)COC2=CC=CC=C2Br	24 (45)
L19/ L43		CN1C2=CC=CC=C2C(=C1C(=O)N(C)C3=CC=CC=C3)Cl	93 (89)
L20/ L44		CN1CCN(CC1)C2=CC=CC=C2NC(=O)CCCC3=CNC4=CC=CC=C43	8 (20)

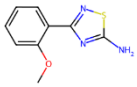
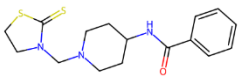
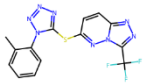
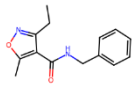
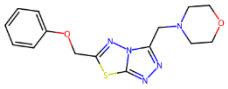
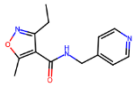
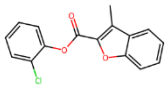
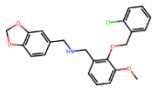
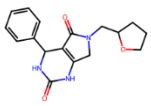
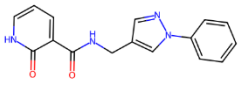
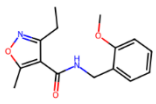
L21/ L45		CC1=C(OC2=CC=CC=C12)C(=O)NC3=CC=CC=C3F	96 (97)
L22/ L46		C1CN(CCN1C2=CC=CC=C2)C(=O)N3C=CN=C3	23 (47)
L23/ L47		C1COC2=C(O1)C=CC(=C2)NC(=O)C3=CC=C(C=C3)C4=CC=CC=C4	29 (42)
L24/ L48		CC1=CC=CC=C1CN2CCN(CC2)C3=NN4C(=NN=C4C(F)(F)F)C=C3	14 (17)
M1/ M25		CCC1=NOC(C)=C1C(NCC2=CC=CC=C2)=O	22 (56)
M2/ M26		C1=CC=C(C(=C1)C(=O)NC2=CC(=CC=C2)N3C=NC=N3)F)OC(F)F	33 (75)
M3/ M27		CC1=NN(C2=C1C(=CC(=N2)C3=CC=CC=C3)C(F)F)C(C)C	89 (96)
M4/ M28		C1CN(CCC1C(=O)NCC2=CN(N=C2)C3=CC=CC=C3)C4=NN5C(=NN=C5C(F)(F)F)C=C4	11 (0)
M5/ M29		C1=CC=C(C=C1)N2C(=NN=N2)SC3=C(C=CC=N3)C(=O)N	90 (68)
M6/ M30		C1CN(CCC1CC2=CC=CC=C2)C(=O)CCC3=NC=C(O3)C4=CC=CC=C4	73 (92)
M7/ M31		CC1=NC2=C(C(=NN2C(=C1)N3CCN(CC3)CC(=C)C)C4=CC=CC=C4)C	28 (25)

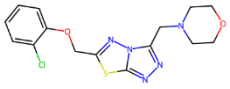
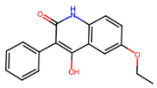
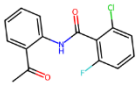
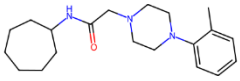
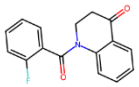
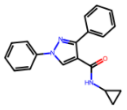
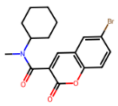
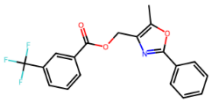
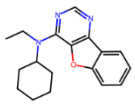
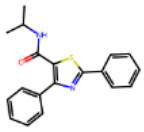
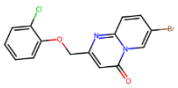
M8/ M32		C1COCCN1CC2=NN=C3N2N=C(S3)C4=CC=CC=C4F	18 (28)
M9/ M33		CCN1CCN(CC1)C(=O)C2=CC(=NC3=C2C=C(C=C3)C)C4=CC=NC=C4	12 (28)
M10/ M34		CC(=O)C1=CC=CC=C1NC(=O)C2=CC=CC=C2OC(F)F	23 (41)
M11/ M35		CC1=C(C2=NNC(N2C3=CC=CC=C3)=S)C=CO1	53 (98)
M12/ M36		CCN1C2=C(C=N1)C(=CC(=N2)C3=CC=CS3)C(=O)NC4=CC=CC=C4	30 (13)
M13/ M37		CC(C)NC(=O)C1=CN(N=C1C2=CC=CC=C2)C3=CC=CC=C3	28 (18)
M14/ M38		C1CC(=O)N(C1)C2=CC=CC(=C2)NC(=O)C3=CC=CC=C3Cl	62 (61)
M15/ M39		CC1=CC=CC=C1C2=NC3=CC=CC=C3C(=C2)C(=O)N4CCN(CC4)C	18 (66)
M16/ M40		COC1=CC=CC=C1OC2=CC=C(C=C2)NC(=O)C3CCOCC3	25 (0)
M17/ M41		COC1=CC=CC=C1OCC2=NN3C(=NN=C3S2)CN4CCCCCC4	49 (98)
M18/ M42		C1CCCN(CC1)CC2=NN=C3N2N=C(S3)CCCC4=CC=CC=C4	95 (91)

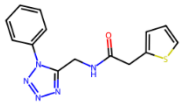
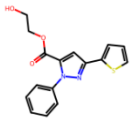
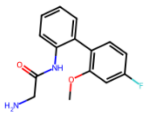
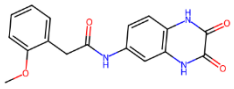
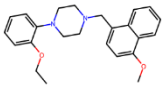
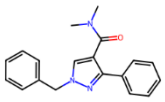
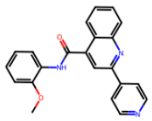
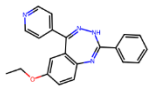
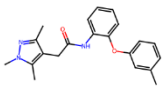
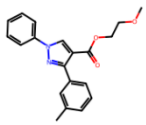
M19/ M43		CC1=NN(C(=C1)OC(=O)C2=CC=CS2)C3=CC=CC=C3	27 (57)
M20/ M44		CC(C)N1C2=C(C=N1)C(=CC(=N2)C3=CC=CC=C3)C(=O)NC4=CC=C(C=C4)N5CCCC5=O	23 (28)
M21/ M45		C1=CC=C(C(=C1)CNC(=O)C2=NN3C=C(C=NC3=C2)Br)Cl	88 (89)
M22/ M46		CN(CC1=NN(N=C1)C2=CC=CC=C2)C(=O)NC3=NN=CS3	24 (52)
M23/ M47		C1CCN(C1)C(=O)C2CCN(CC2)CC3=CC=CC=C3F	96 (98)
M24/ M48		CCOC(=O)C1=CN=C(C=C1)N2CCC(CC2)NS(=O)(=O)C3=CC=CC=C3	15 (46)
N1/ N25		CC1=CC=CC=C1OC(=O)C2=C(C3=CC=CC=C3O2)C	23 (28)
N2/ N26		CC1=CN=C(C=N1)C(=O)NCC2=CN(N=C2)C3=CC=CC=C3	46 (50)
N3/ N27		CC1=NC2=C(C(=CS2)C3=CC=CC=C3)C(=N1)SC4=NN=NN4C	24 (25)
N4/ N28		C1=CC=C(C=C1)OC2=C(C=C(C=C2)N3C(=O)C4=CC=CC=C4C3=O)Cl	33 (23)
N5/ N29		CC1=C(C=NN1C2=CC=CC=C2)C(=O)NC(C)C	25 (19)

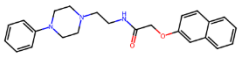
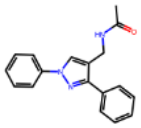
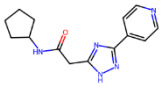
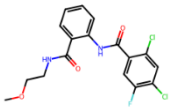
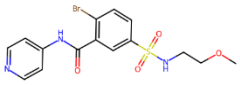
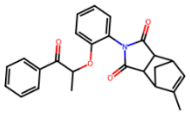
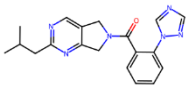
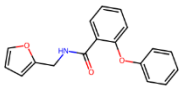
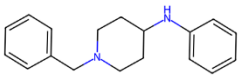
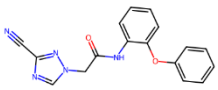
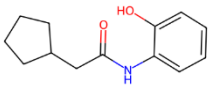
N6/ N30		CC1=CC(=NC2=C1C(=C(S2)C(=O)N(C)C3=CC=CC=C3)N)C	22 (0)
N7/ N31		C1=CC=C(C=C1)NCC2=CC3=CC=CC=C3NC2=O	25 (5)
N8/ N32		C1CC1CNC(=O)C2=CN(N=C2C3=CC=CC=C3)C4=CC=CC=C4	27 (10)
N9/ N33		CCOC(=O)C1(CCN(CC1)CC2=CC=NC=C2)C3=CC=CC=C3	41 (50)
N10/ N34		CC1=CC=CC=C1OCC2=NN3C(=NN=C3S2)CN4CCOCC4	0 (11)
N11/ N35		CC1=CC=CC=C1N2C(=NN=C2SC3=C(C=CC=N3)[N+](=O)[O-])C	93 (95)
N12/ N36		C1COCCN1CC2=NN=C3N2N=C(S3)CCC4=CC=CC=C4	21 (26)
N13/ N37		C1CCCN(CC1)CC2=NN=C3N2N=C(S3)C4=CC=CC=C4Cl	49 (90)
N14/ N38		C1CCCN(CC1)CC2=NN=C3N2N=C(S3)COC4=CC=CC=C4Cl	22 (54)
N15/ N39		CCN1CCN(CC1)C(=O)C2=CC(=NC3=C2C=C(C=C3)Cl)C4=CC=NC=C4	5 (9)
N16/ N40		CC(C)N1C2=C(C=N1)C(=CC(=N2)C3=CC=CC=C3)C(=O)NC4=CC=CC=N4	51 (57)

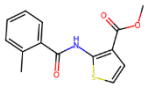
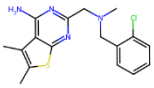
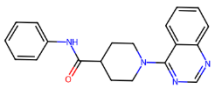
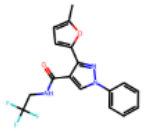
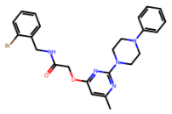
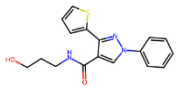
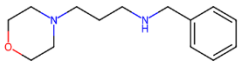
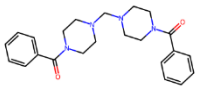
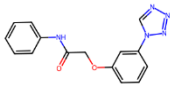
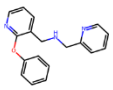
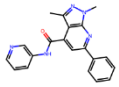
N17/ N41		C1=CC=C(C=C1)C(=O)N2C(=S)N=C3N2C=CC=N3	26 (13)
N18/ N42		CCCCN(C1=CC=CC=C1)C(=O)C2CCN(CC2)C3=NN4C(=NN=C4C(F)(F)F)C=C3	25 (26)
N19/ N43		C1CCCN(CC1)CC2=NN=C3N2N=C(S3)COC4=CC=CC=C4	15 (42)
N20/ N44		CCCCNC(=O)C1=NN(C2=C1CCC2)C3=CC=CC=C3	12 (23)
N21/ N45		C1=CC=C(C(=C1)C2=C(C=NN2)C(=O)NC3=CN=C(C=C3)N4C=CN=C4)F	23 (30)
N22/ N46		CC1=C(C=CC(=C1)Cl)NC(=O)CN2CCC(CC2)C(=O)NCC3=CC=CC=C3	11 (44)
N23/ N47		CC1=CC(=C(N1C2=CC=CC=C2)C)C(=O)OCC3=CC(=CC=C3)[N+](=O)[O-]	89 (90)
N24/ N48		C1CN(CCN1C2=CC=CC=C2Cl)C(=O)CN3C4=CC=CC=C4N=N3	28 (56)
O1/ O25		CC1=NN(C2=C1C(=CC(=N2)C3=CC=CC=C3)C(=O)NCC#C)C	46 (92)
O2/ O26		C1CCC(CC1)C(=O)NCCCN2CCN(CC2)CC3=CC=CC=C3	29 (7)
O3/ O27		C1=CC=C(C=C1)C2=NN=C(O2)SCC#CCOC(=O)C3=CC=CC=C3Br	14 (0)

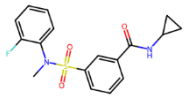
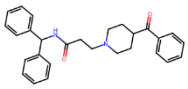
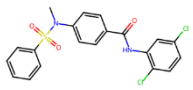
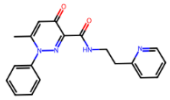
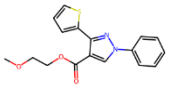
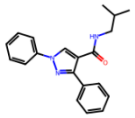
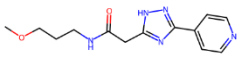
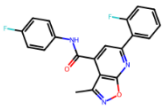
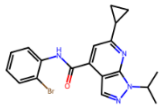
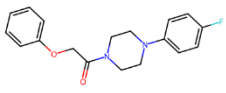
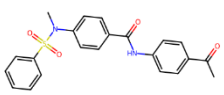
O4/ O28		COC1=CC=CC=C1C2=NSC(=N2)N	73 (97)
O5/ O29		C1CN(CCC1NC(=O)C2=CC=CC=C2)CN3CCSC3=S	92 (94)
O6/ O30		CC1=CC=CC=C1N2C(=NN=N2)SC3=NN4C(=NN=C4C(F)(F)F)C=C3	23 (35)
O7/ O31		CCC1=NOC(=C1C(=O)NCC2=CC=CC=C2)C	10 (47)
O8/ O32		C1COCCN1CC2=NN=C3N2N=C(S3)COC4=CC=CC=C4	82 (79)
O9/ O33		CCC1=NOC(=C1C(=O)NCC2=CC=NC=C2)C	0 (26)
O10/ O34		CC1=C(OC2=CC=CC=C12)C(=O)OC3=CC=CC=C3Cl	9 (19)
O11/ O35		COC1=CC=CC(=C1OCC2=CC=CC=C2Cl)CNCC3=CC4=C(C=C3)OCO4	0 (17)
O12/ O36		C1CC(OC1)CN2CC3=C(C2=O)C(NC(=O)N3)C4=CC=CC=C4	0 (26)
O13/ O37		C1=CC=C(C=C1)N2C=C(C=N2)CNC(=O)C3=CC=CNC3=O	72 (37)
O14/ O38		CCC1=NOC(=C1C(=O)NCC2=CC=CC=C2OC)C	16 (30)

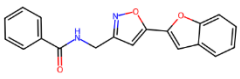
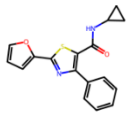
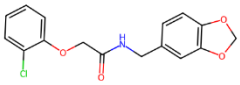
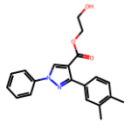
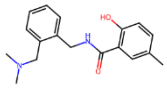
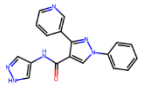
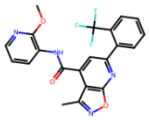
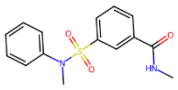
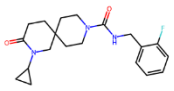
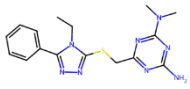
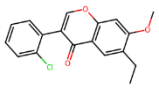
O15/ O39		C1COCCN1CC2=NN=C3N2N=C(S3)COC4=CC=CC=C4Cl	23 (7)
O16/ O40		CCOC1=CC2=C(C=C1)NC(=O)C(=C2O)C3=CC=CC=C3	16 (21)
O17/ O41		CC(=O)C1=CC=CC=C1NC(=O)C2=C(C=CC=C2Cl)F	88 (94)
O18/ O42		CC1=CC=CC=C1N2CCN(CC2)CC(=O)NC3CCCCCC3	89 (92)
O19/ O43		C1CN(C2=CC=CC=C2C1=O)C(=O)C3=CC=CC=C3F	17 (42)
O20/ O44		C1CC1NC(=O)C2=CN(N=C2C3=CC=CC=C3)C4=CC=CC=C4	23 (52)
O21/ O45		CN(C1CCCCC1)C(=O)C2=CC3=C(C=CC(=C3)Br)OC2=O	21 (47)
O22/ O46		CC1=C(N=C(O1)C2=CC=CC=C2)COC(=O)C3=CC(=CC=C3)C(F)(F)F	97 (92)
O23/ O47		CCN(C1CCCCC1)C2=NC=NC3=C2OC4=CC=CC=C43	0 (25)
O24/ O48		CC(C)NC(=O)C1=C(N=C(S1)C2=CC=CC=C2)C3=CC=CC=C3	0 (51)
P1/ P25		C1=CC=C(C(=C1)OCC2=CC(=O)N3C=C(C=CC3=N2)Br)Cl	66 (72)

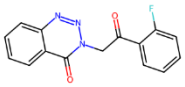
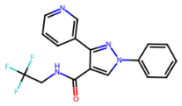
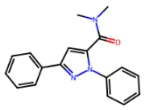
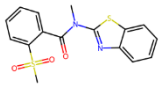
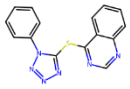
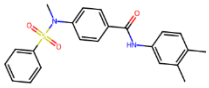
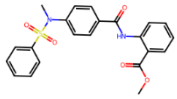
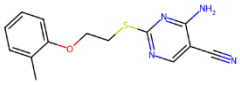
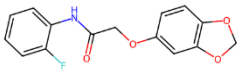
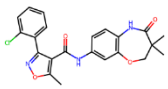
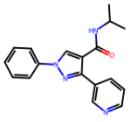
P2/ P26		O=C(CC1=CC=CS1)NCC2=NN=NN2C3=CC=CC=C3	97 (88)
P3/ P27		C1=CC=C(C=C1)N2C(=CC(=N2)C3=CC=CS3)C(=O)OCCO	19 (82)
P4/ P28		COC1=C(C=CC(=C1)F)C2=CC=CC=C2NC(=O)CN	21 (46)
P5/ P29		COC1=CC=CC=C1CC(=O)NC2=CC3=C(C=C2)NC(=O)C(=O)N3	0 (10)
P6/ P30		CCOC1=CC=CC=C1N2CCN(CC2)CC3=CC=C(C4=CC=CC=C34)OC	12 (14)
P7/ P31		CC1=CC(=NN1C2CN(C2)S(=O)(=O)NCC3=CC=CC=C3)C	27 (57)
P8/ P32		CN(C)C(=O)C1=CN(N=C1C2=CC=CC=C2)CC3=CC=CC=C3	18 (26)
P9/ P33		COC1=CC=CC=C1NC(=O)C2=CC(=NC3=CC=CC=C32)C4=CC=NC=C4	20 (46)
P10/ P34		CCOC1=CC2=C(C=C1)N=C(NN=C2C3=CC=NC=C3)C4=CC=CC=C4	13 (30)
P11/ P35		CC1=CC(=CC=C1)OC2=CC=CC=C2NC(=O)CC3=C(N(N=C3C)C)C	9 (25)
P12/ P36		CC1=CC(=CC=C1)C2=NN(C=C2C(=O)OCCOC)C3=CC=CC=C3	11 (18)

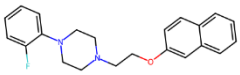
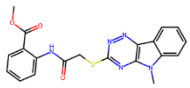
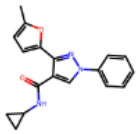
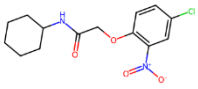
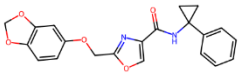
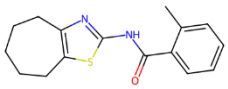
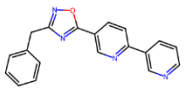
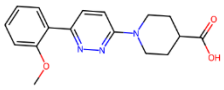
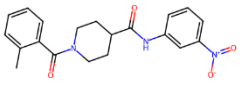
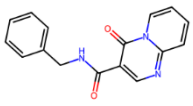
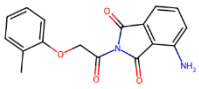
P13/ P37		C1CN(CCN1CCNC(=O)COC2=CC3=CC=CC=C3C=C2)C4=CC=CC=C4	15 (22)
P14/ P38		CC(=O)NCC1=CN(N=C1C2=CC=CC=C2)C3=CC=CC=C3	21 (11)
P15/ P39		C1CCC(C1)NC(=O)CC2=NC(=NN2)C3=CC=NC=C3	8 (0)
P16/ P40		COCCNC(=O)C1=CC=CC=C1NC(=O)C2=CC(=C(C=C2Cl)Cl)F	10 (0)
P17/ P41		COCCNS(=O)(=O)C1=CC(=C(C=C1)Br)C(=O)NC2=CC=NC=C2	95 (91)
P18/ P42		CC1=CC2CC1C3C2C(=O)N(C3=O)C4=CC=CC=C4OC(C)C(=O)C5=CC=CC=C5	22 (30)
P19/ P43		CC(C)CC1=NC=C2CN(CC2=N1)C(=O)C3=CC=CC=C3N4C=NC=N4	44 (90)
P20/ P44		C1=CC=C(C=C1)OC2=CC=CC=C2C(=O)NCC3=CC=CO3	12 (18)
P21/ P45		C1CN(CCC1NC2=CC=CC=C2)CC3=CC=CC=C3	0 (28)
P22/ P46		C1=CC=C(C=C1)OC2=CC=CC=C2NC(=O)CN3C=NC(=N3)C#N	26 (16)
P23/ P47		C1CCC(C1)CC(=O)NC2=CC=CC=C2O	16 (21)

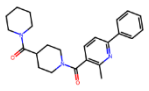
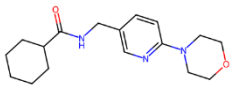
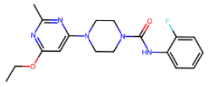
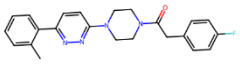
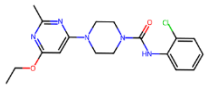
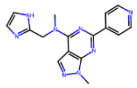
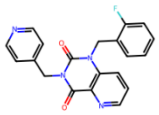
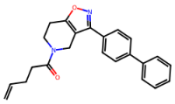
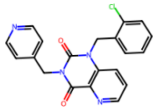
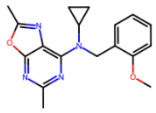
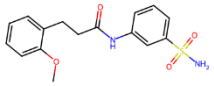
P24/ P48		CC1=CC=CC=C1C(=O)NC2=C(C=CS2)C(=O)OC	0 (23)
Q1/ Q25		CC1=C(SC2=NC(=NC(=C12)N)CN(C)CC3=CC=CC=C3Cl)C	94 (95)
Q2/ Q26		C1CN(CCC1C(=O)NC2=CC=CC=C2)C3=NC=NC4=CC=CC=C43	92 (97)
Q3/ Q27		CC1=CC=C(O1)C2=NN(C=C2C(=O)NCC(F)(F)F)C3=CC=CC=C3	25 (14)
Q4/ Q28		CC1=CC(=NC(=N1)N2CCN(CC2)C3=CC=CC=C3)OCC(=O)NCC4=CC=CC=C4Br	10 (22)
Q5/ Q29		C1=CC=C(C=C1)N2C=C(C(=N2)C3=CC=CS3)C(=O)NCCCO	32 (69)
Q6/ Q30		C1COCCN1CCCNCC2=CC=CC=C2	10 (23)
Q7/ Q31		C1CN(CCN1CN2CCN(CC2)C(=O)C3=CC=CC=C3)C(=O)C4=CC=CC=C4	26 (21)
Q8/ Q32		C1=CC=C(C=C1)NC(=O)COC2=CC=CC(=C2)N3C=NN=N3	37 (38)
Q9/ Q33		C1=CC=C(C=C1)OC2=C(C=CC=N2)CNCC3=CC=CC=N3	27 (63)
Q10/ Q34		CC1=NN(C2=C1C(=CC(=N2)C3=CC=CC=C3)C(=O)NC4=CN=CC=C4)C	0 (43)

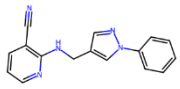
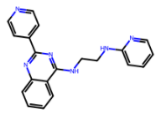
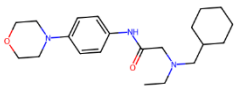
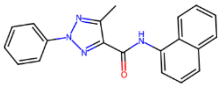
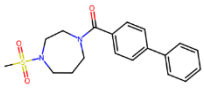
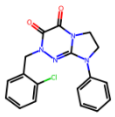
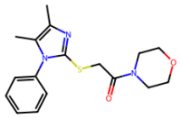
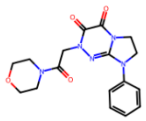
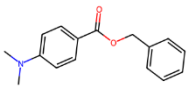
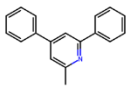
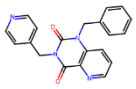
Q11/ Q35		CN(C1=CC=CC=C1F)S(=O)(=O)C2=CC=CC(=C2)C(=O)NC3CC3	0 (43)
Q12/ Q36		C1CN(CCC1C(=O)C2=CC=CC=C2)CCC(=O)NC(C3=CC=CC=C3)C4=CC=CC=C4	28 (43)
Q13/ Q37		CN(C1=CC=C(C=C1)C(=O)NC2=C(C=CC(=C2)Cl)Cl)S(=O)(=O)C3=CC=CC=C3	36 (37)
Q14/ Q38		CC1=CC(=O)C(=NN1C2=CC=CC=C2)C(=O)NCCC3=CC=CC=N3	20 (27)
Q15/ Q39		COCCOC(=O)C1=CN(N=C1C2=CC=CS2)C3=CC=CC=C3	13 (48)
Q16/ Q40		CC(C)CNC(=O)C1=CN(N=C1C2=CC=CC=C2)C3=CC=CC=C3	88 (92)
Q17/ Q41		COCCCNC(=O)CC1=NC(=NN1)C2=CC=NC=C2	24 (38)
Q18/ Q42		CC1=NOC2=C1C(=CC(=N2)C3=CC=CC=C3F)C(=O)NC4=CC=C(C=C4)F	25 (21)
Q19/ Q43		CC(C)N1C2=C(C=N1)C(=CC(=N2)C3CC3)C(=O)NC4=CC=CC=C4Br	10 (10)
Q20/ Q44		C1CN(CCN1C2=CC=C(C=C2)F)C(=O)COC3=CC=CC=C3	96 (91)
Q21/ Q45		CC(=O)C1=CC=C(C=C1)NC(=O)C2=CC=C(C=C2)N(C)S(=O)(=O)C3=CC=CC=C3	33 (38)

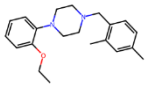
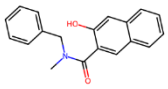
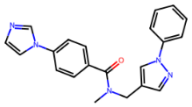
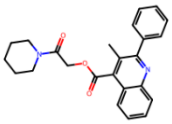
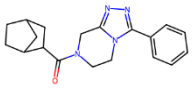
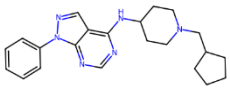
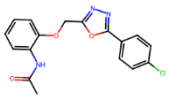
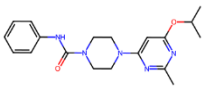
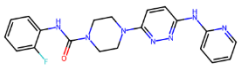
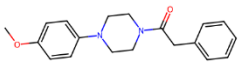
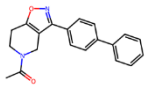
Q22/ Q46		C1=CC=C(C=C1)C(=O)NCC2=NOC(=C2)C3=CC4=CC=CC=C4O3	30 (15)
Q23/ Q47		C1CC1NC(=O)C2=C(N=C(S2)C3=CC=CO3)C4=CC=CC=C4	64 (89)
Q24/ Q48		C1OC2=C(O1)C=C(C=C2)CNC(=O)COC3=CC=CC=C3Cl	7 (14)
R1/ R25		CC1=C(C=C(C=C1)C2=NN(C=C2C(=O)OCCO)C3=CC=CC=C3)C	98 (93)
R2/ R26		CC1=CC(=C(C=C1)O)C(=O)NCC2=CC=CC=C2CN(C)C	46 (85)
R3/ R27		C1=CC=C(C=C1)N2C=C(C(=N2)C3=CN=CC=C3)C(=O)NC4=CNN=C4	27 (53)
R4/ R28		CC1=NOC2=C1C(=CC(=N2)C3=CC=CC=C3C(F)(F)F)C(=O)NC4=C(N=CC=C4)OC	29 (51)
R5/ R29		CNC(=O)C1=CC(=CC=C1)S(=O)(=O)N(C)C2=CC=CC=C2	7 (0)
R6/ R30		C1CC1N2CC3(CCC2=O)CCN(CC3)C(=O)NCC4=CC=CC=C4F	35 (36)
R7/ R31		CCN1C(=NN=C1SCC2=NC(=NC(=N2)N(C)C)N)C3=CC=CC=C3	0 (28)
R8/ R32		CCC1=CC2=C(C=C1OC)OC=C(C2=O)C3=CC=CC=C3Cl	16 (25)

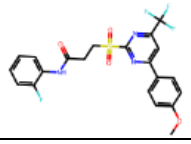
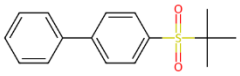
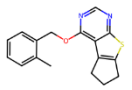
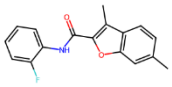
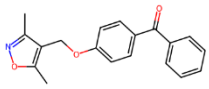
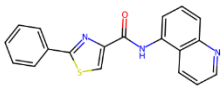
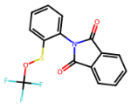
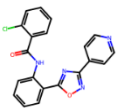
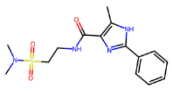
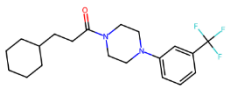
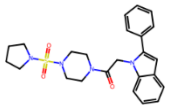
R9/ R33		C1=CC=C2C(=C1)C(=O)N(N=N2)CC(=O)C3=CC=CC=C3F	89 (92)
R10/ R34		C1=CC=C(C=C1)N2C=C(C(=N2)C3=CN=CC=C3)C(=O)NCC(F)(F)F	19 (8)
R11/ R35		CN(C)C(=O)C1=CC(=NN1C2=CC=CC=C2)C3=CC=CC=C3	25 (43)
R12/ R36		CN(C1=NC2=CC=CC=C2S1)C(=O)C3=CC=CC=C3S(=O)(=O)C	20 (48)
R13/ R37		C1=CC=C(C=C1)N2C(=NN=N2)SC3=NC=NC4=CC=CC=C43	25 (51)
R14/ R38		CC1=C(C=C(C=C1)NC(=O)C2=CC=C(C=C2)N(C)S(=O)(=O)C3=CC=CC=C3)C	31 (10)
R15/ R39		CN(C1=CC=C(C=C1)C(=O)NC2=CC=CC=C2C(=O)OC)S(=O)(=O)C3=CC=CC=C3	8 (17)
R16/ R40		CC1=CC=CC=C1OCCSC2=NC=C(C(=N2)N)C#N	68 (90)
R17/ R41		C1OC2=C(O1)C=C(C=C2)OCC(=O)NC3=CC=CC=C3F	97 (89)
R18/ R42		CC1=C(C(=NO1)C2=CC=CC=C2Cl)C(=O)NC3=CC4=C(C=C3)NC(=O)C(CO4)(C)C	29 (21)
R19/ R43		CC(C)NC(=O)C1=CN(N=C1C2=CN=CC=C2)C3=CC=CC=C3	11 (8)

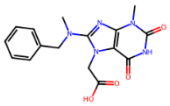
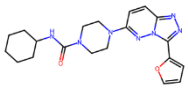
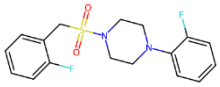
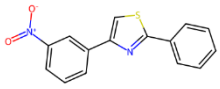
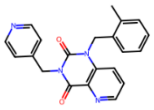
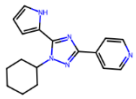
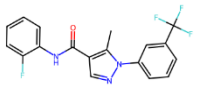
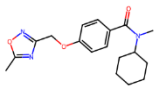
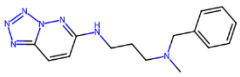
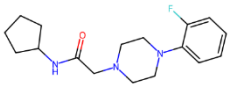
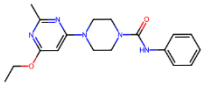
R20/ R44		C1CN(CCN1CCOC2=CC3=CC=CC=C3C=C2)C4=CC=CC=C4F	41 (45)
R21/ R45		CN1C2=CC=CC=C2C3=C1N=C(N=N3)SCC(=O)NC4=CC=CC=C4C(=O)OC	30 (18)
R22/ R46		CC1=CC=C(O1)C2=NN(C=C2C(=O)NC3CC3)C4=CC=CC=C4	15 (50)
R23/ R47		C1CCC(CC1)NC(=O)COC2=C(C=C(C=C2)Cl)[N+](=O)[O-]	32 (63)
R24/ R48		C1CC1(C2=CC=CC=C2)NC(=O)C3=COC(=N3)COC4=CC5=C(C=C4)OCO5	89 (94)
S1/ S25		CC1=CC=CC=C1C(=O)NC2=NC3=C(S2)CCCCC3	39 (41)
S2/ S26		C1=CC=C(C=C1)CC2=NOC(=N2)C3=CN=C(C=C3)C4=CN=CC=C4	13 (41)
S3/ S27		COC1=CC=CC=C1C2=NN=C(C=C2)N3CCC(CC3)C(=O)O	34 (77)
S4/ S28		CC1=CC=CC=C1C(=O)N2CCC(CC2)C(=O)NC3=CC(=CC=C3)[N+](=O)[O-]	26 (45)
S5/ S29		O=C(C1=CN=C2C=CC=CN2C1=O)NCC3=CC=CC=C3	0 (27)
S6/ S30		CC1=CC=CC=C1OCC(=O)N2C(=O)C3=C(C2=O)C(=CC=C3)N	22 (36)

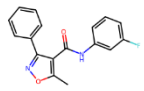
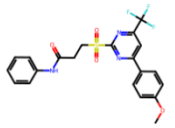
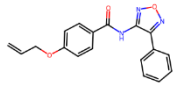
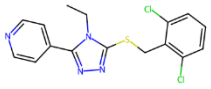
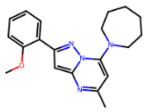
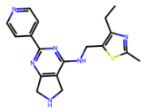
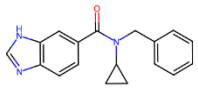
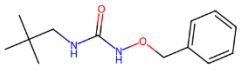
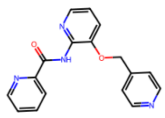
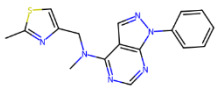
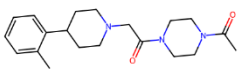
S7/ S31		CC1=C(C=CC(=N1)C2=CC=CC=C2)C(=O)N3CCC(CC3)C(=O)N4CCCCC4	11 (27)
S8/ S32		C1CCC(CC1)C(=O)NCC2=CN=C(C=C2)N3CCOCC3	21 (40)
S9/ S33		CCOC1=NC(=NC(=C1)N2CCN(CC2)C(=O)NC3=CC=CC=C3F)C	88 (47)
S10/ S34		CC1=CC=CC=C1C2=NN=C(C=C2)N3CCN(CC3)C(=O)CC4=CC=C(C=C4)F	4 (29)
S11/ S35		CCOC1=NC(=NC(=C1)N2CCN(CC2)C(=O)NC3=CC=CC=C3Cl)C	20 (8)
S12/ S36		CN1C2=C(C=N1)C(=NC(=N2)C3=CC=NC=C3)N(C)CC4=NC=CN4	95 (93)
S13/ S37		C1=CC=C(C(=C1)CN2C3=C(C(=O)N(C2=O)CC4=CC=NC=C4)N=CC=C3)F	28 (37)
S14/ S38		C=CCCC(=O)N1CCC2=C(C1)C(=NO2)C3=CC=C(C=C3)C4=CC=CC=C4	14 (23)
S15/ S39		C1=CC=C(C(=C1)CN2C3=C(C(=O)N(C2=O)CC4=CC=NC=C4)N=CC=C3)Cl	51 (90)
S16/ S40		CC1=NC(=C2C(=N1)OC(=N2)C)N(CC3=CC=CC=C3OC)C4CC4	0 (28)
S17/ S41		COC1=CC=CC=C1CCC(=O)NC2=CC(=CC=C2)S(=O)(=O)N	24 (27)

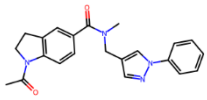
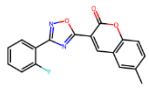
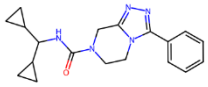
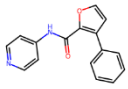
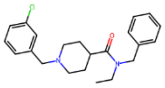
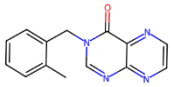
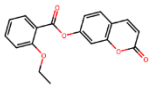
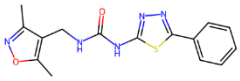
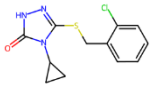
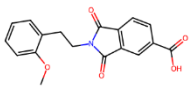
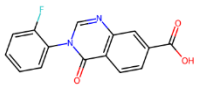
S18/ S42		C1=CC=C(C=C1)N2C=C(C=N2)CNC3=C(C=CC=N3)C#N	25 (48)
S19/ S43		C1=CC=C2C(=C1)C(=NC(=N2)C3=CC=NC=C3)NCCNC4=CC=CC=N4	94 (96)
S20/ S44		CCN(CC1CCCCC1)CC(=O)NC2=CC=C(C=C2)N3CCOCC3	21 (22)
S21/ S45		CC1=NN(N=C1C(=O)NC2=CC=CC3=CC=CC=C32)C4=CC=CC=C4	27 (25)
S22/ S46		CS(=O)(=O)N1CCCN(CC1)C(=O)C2=CC=C(C=C2)C3=CC=CC=C3	0 (0)
S23/ S47		C1CN2C(=O)C(=O)N(N=C2N1C3=CC=CC=C3)CC4=CC=CC=C4Cl	28 (59)
S24/ S48		CC1=C(N(C(=N1)SCC(=O)N2CCOCC2)C3=CC=CC=C3)C	5 (28)
T1/ T25		C1CN2C(=O)C(=O)N(N=C2N1C3=CC=CC=C3)CC(=O)N4CCOCC4	16 (30)
T2/ T26		CN(C)C1=CC=C(C=C1)C(=O)OCC2=CC=CC=C2	89 (97)
T3/ T27		CC1=CC(=CC(=N1)C2=CC=CC=C2)C3=CC=CC=C3	91 (91)
T4/ T28		C1=CC=C(C=C1)CN2C3=C(C(=O)N(C2=O)CC4=CC=NC=C4)N=CC=C3	25 (27)

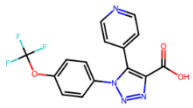
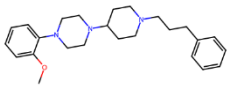
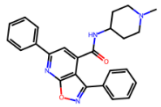
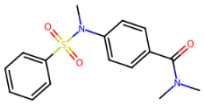
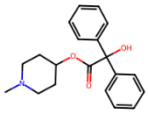
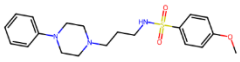
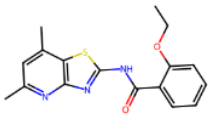
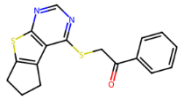
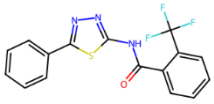
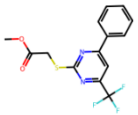
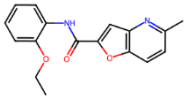
T5/ T29		CCOC1=CC=CC=C1N2CCN(CC2)CC3=C(C=C(C=C3)C)C	12 (43)
T6/ T30		CN(CC1=CC=CC=C1)C(=O)C2=CC3=CC=CC=C3C=C2O	94 (91)
T7/ T31		CN(CC1=CN(N=C1)C2=CC=CC=C2)C(=O)C3=CC=C(C=C3)N4C=CN=C4	39 (78)
T8/ T32		CC1=C(C2=CC=CC=C2N=C1C3=CC=CC=C3)C(=O)OCC(=O)N4CCCCC4	95 (84)
T9/ T33		C1CC2CC1CC2C(=O)N3CCN4C(=NN=C4C5=CC=CC=C5)C3	10 (25)
T10/ T34		C1CCC(C1)CN2CCC(CC2)NC3=C4C=NN(C4=NC=N3)C5=CC=CC=C5	41 (43)
T11/ T35		CC(=O)NC1=CC=CC=C1OCC2=NN=C(O2)C3=CC=C(C=C3)Cl	21 (53)
T12/ T36		CC1=NC(=CC(=N1)OC(C)C)N2CCN(CC2)C(=O)NC3=CC=CC=C3	18 (31)
T13/ T37		C1CN(CCN1C2=NN=C(C=C2)NC3=CC=CC=N3)C(=O)NC4=CC=CC=C4F	6 (28)
T14/ T38		COC1=CC=C(C=C1)N2CCN(CC2)C(=O)CC3=CC=CC=C3	19 (18)
T15/ T39		CC(=O)N1CCC2=C(C1)C(=NO2)C3=CC=C(C=C3)C4=CC=CC=C4	95 (92)

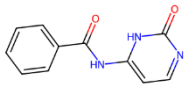
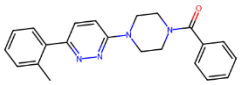
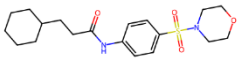
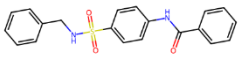
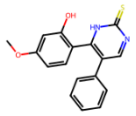
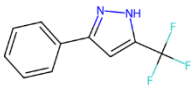
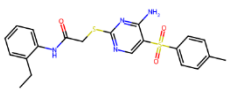
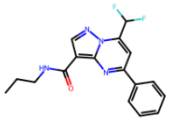
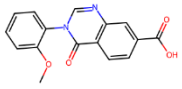
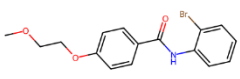
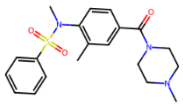
T16/ T40		COC1=CC=C(C=C1)C2=CC(=NC(=N2)S(=O)(=O)CCC(=O)NC3=CC=CC=C3F)C(F)(F)F	90 (95)
T17/ T41		CC(C)(C)S(=O)(=O)C1=CC=C(C=C1)C2=CC=CC=C2	27 (50)
T18/ T42		CC1=CC=CC=C1COC2=C3C4=C(CCC4)SC3=NC=N2	57 (96)
T19/ T43		CC1=CC2=C(C=C1)C(=C(O2)C(=O)NC3=CC=CC=C3F)C	24 (43)
T20/ T44		CC1=C(C(=NO1)C)COC2=CC=C(C=C2)C(=O)C3=CC=CC=C3	94 (89)
T21/ T45		C1=CC=C(C=C1)C2=NC(=CS2)C(=O)NC3=CC=CC4=C3C=CC=N4	22 (11)
T22/ T46		C1=CC=C2C(=C1)C(=O)N(C2=O)C3=CC=CC=C3SOC(F)(F)F	26 (60)
T23/ T47		C1=CC=C(C(=C1)C2=NC(=NO2)C3=CC=NC=C3)NC(=O)C4=CC=CC=C4Cl	15 (55)
T24/ T48		CC1=C(N=C(N1)C2=CC=CC=C2)C(=O)NCCS(=O)(=O)N(C)C	24 (25)
U1/ U25		C1CCC(CC1)CCC(=O)N2CCN(CC2)C3=CC=CC(=C3)C(F)(F)F	39 (14)
U2/ U26		C1CCN(C1)S(=O)(=O)N2CCN(CC2)C(=O)CN3C4=CC=CC=C4C=C3C5=CC=CC=C5	41 (50)

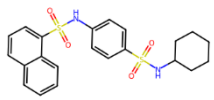
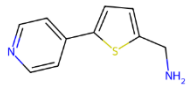
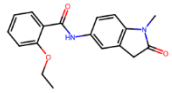
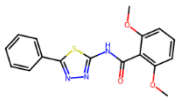
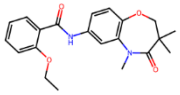
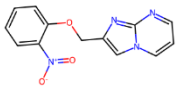
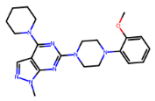
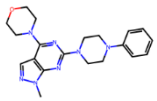
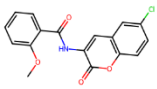
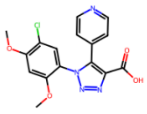
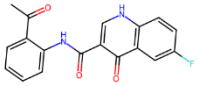
U3/ U27		CN1C2=C(C(=O)NC1=O)N(C(=N2)N(C)CC3=CC=CC=C3)CC(=O)O	56 (94)
U4/ U28		C1CCC(CC1)NC(=O)N2CCN(CC2)C3=NN4C(=NN=C4C5=CC=CO5)C=C3	39 (34)
U5/ U29		C1CN(CCN1C2=CC=CC=C2F)S(=O)(=O)CC3=CC=CC=C3F	29 (6)
U6/ U30		C1=CC=C(C=C1)C2=NC(=CS2)C3=CC(=CC=C3)[N+](=O)[O-]	14 (59)
U7/ U31		CC1=CC=CC=C1CN2C3=C(C(=O)N(C2=O)CC4=CC=NC=C4)N=CC=C3	14 (26)
U8/ U32		C1CCC(CC1)N2C(=NC(=N2)C3=CC=NC=C3)C4=CC=CN4	46 (47)
U9/ U33		CC1=C(C=NN1C2=CC=CC(=C2)C(F)(F)F)C(=O)NC3=CC=CC=C3F	97 (97)
U10/ U34		CC1=NC(=NO1)COC2=CC=C(C=C2)C(=O)N(C)C3CCCCC3	59 (57)
U11/ U35		CN(CCCNC1=NN2C(=NN=N2)C=C1)CC3=CC=CC=C3	61 (58)
U12/ U36		C1CCC(C1)NC(=O)CN2CCN(CC2)C3=CC=CC=C3F	18 (28)
U13/ U37		CCOC1=NC(=NC(=C1)N2CCN(CC2)C(=O)NC3=CC=CC=C3)C	95 (96)

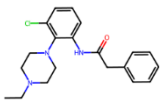
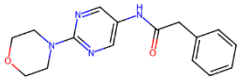
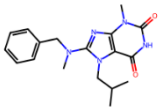
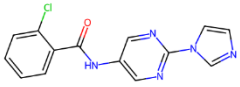
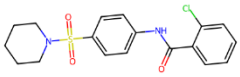
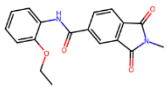
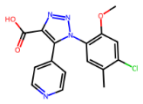
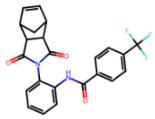
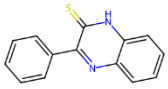
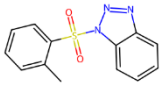
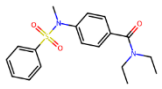
U14/ U38		CC1=C(C(=NO1)C2=CC=CC=C2)C(=O)NC3=CC(=CC=C3)F	4 (24)
U15/ U39		COC1=CC=C(C=C1)C2=CC(=NC(=N2)S(=O)(=O)CCC(=O)NC3=CC=CC=C3)C(F)(F)F	28 (34)
U16/ U40		C=CCOC1=CC=C(C=C1)C(=O)NC2=NON=C2C3=CC=CC=C3	96 (91)
U17/ U41		CCN1C(=NN=C1SCC2=C(C=CC=C2Cl)Cl)C3=CC=NC=C3	90 (72)
U18/ U42		CC1=NC2=CC(=NN2C(=C1)N3CCCCCC3)C4=CC=CC=C4OC	0 (51)
U19/ U43		CCC1=C(SC(=N1)C)CNC2=NC(=NC3=C2CNC3)C4=CC=NC=C4	22 (22)
U20/ U44		C1CC1N(CC2=CC=CC=C2)C(=O)C3=CC4=C(C=C3)N=CN4	20 (22)
U21/ U45		CC(C)(C)CNC(=O)NOCC1=CC=CC=C1	91 (90)
U22/ U46		C1=CC=NC(=C1)C(=O)NC2=C(C=CC=N2)OCC3=CC=NC=C3	10 (12)
U23/ U47		CC1=NC(=CS1)CN(C)C2=NC=NC3=C2C=NN3C4=CC=CC=C4	74 (81)
U24/ U48		CC1=CC=CC=C1C2CCN(CC2)CC(=O)N3CCN(CC3)C(=O)C	15 (27)

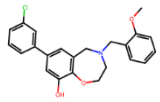
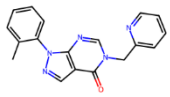
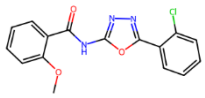
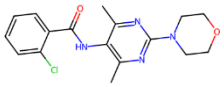
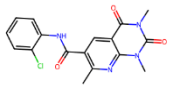
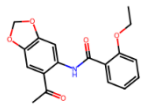
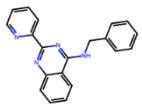
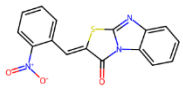
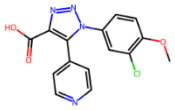
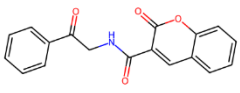
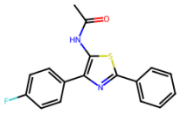
V1/ V25		CC(=O)N1CCC2=C1C=CC(=C2)C(=O)N(C)CC3=CN(N=C3)C4=CC=CC=C4	23 (43)
V2/ V26		CC1=CC2=C(C=C1)OC(=O)C(=C2)C3=NC(=NO3)C4=CC=CC=C4F	13 (0)
V3/ V27		C1CC1C(C2CC2)NC(=O)N3CCN4C(=NN=C4C5=CC=CC=C5)C3	45 (52)
V4/ V28		C1=CC=C(C=C1)C2=C(OC=C2)C(=O)NC3=CC=NC=C3	96 (91)
V5/ V29		CCN(CC1=CC=CC=C1)C(=O)C2CCN(CC2)CC3=CC(=CC=C3)Cl	9 (27)
V6/ V30		CC1=CC=CC=C1CN2C=NC3=NC=CN=C3C2=O	23 (56)
V7/ V31		CCOC1=CC=CC=C1C(=O)OC2=CC3=C(C=C2)C=CC(=O)O3	95 (94)
V8/ V32		CC1=C(C(=NO1)C)CNC(=O)NC2=NN=C(S2)C3=CC=CC=C3	23 (18)
V9/ V33		C1CC1N2C(=O)NN=C2SCC3=CC=CC=C3Cl	5 (49)
V10/ V34		COC1=CC=CC=C1CCN2C(=O)C3=C(C2=O)C=C(C=C3)C(=O)O	10 (55)
V11/ V35		C1=CC=C(C(=C1)N2C=NC3=C(C2=O)C=CC(=C3)C(=O)O)F	0 (13)

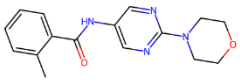
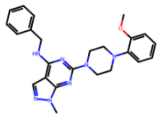
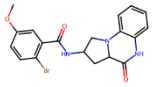
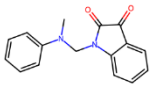
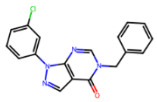
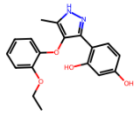
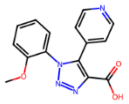
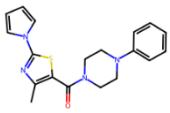
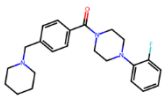
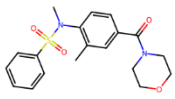
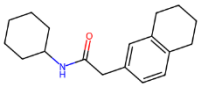
V12/ V36		C1=CC(=CC=C1N2C(=C(N=N2)C(=O)O)C3=CC=NC=C3)OC(F)(F)F	25 (24)
V13/ V37		COC1=CC=CC=C1N2CCN(CC2)C3CCN(CC3)CCCC4=CC=CC=C4	31 (68)
V14/ V38		CN1CCC(CC1)NC(=O)C2=CC(=NC3=C2C(=NO3)C4=CC=CC=C4)C5=CC=CC=C5	16 (26)
V15/ V39		CN(C)C(=O)C1=CC=C(C=C1)N(C)S(=O)(=O)C2=CC=CC=C2	27 (46)
V16/ V40		CN1CCC(CC1)OC(=O)C(C2=CC=CC=C2)(C3=CC=CC=C3)O	46 (87)
V17/ V41		COC1=CC=C(C=C1)S(=O)(=O)NCCCN2CCN(CC2)C3=CC=CC=C3	28 (22)
V18/ V42		CCOC1=CC=CC=C1C(=O)NC2=NC3=C(S2)C(=CC(=N3)C)C	13 (9)
V19/ V43		C1CC2=C(C1)SC3=C2C(=NC=N3)SCC(=O)C4=CC=CC=C4	32 (75)
V20/ V44		C1=CC=C(C=C1)C2=NN=C(S2)NC(=O)C3=CC=CC=C3C(F)(F)F	17 (20)
V21/ V45		COC(=O)CSC1=NC(=CC(=N1)C(F)(F)F)C2=CC=CC=C2	26 (0)
V22/ V46		CCOC1=CC=CC=C1NC(=O)C2=CC3=C(O2)C=CC(=N3)C	5 (40)

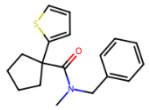
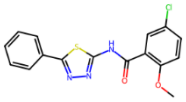
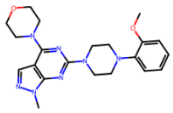
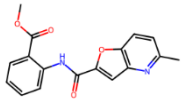
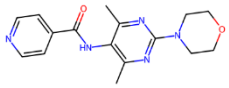
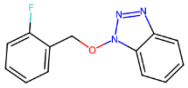
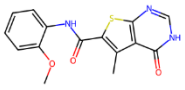
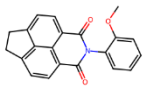
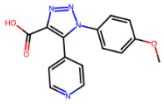
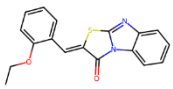
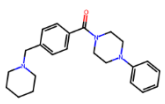
V23/ V47		C1=CC=C(C=C1)C(=O)NC2=CC=NC(=O)N2	18 (24)
V24/ V48		CC1=CC=CC=C1C2=NN=C(C=C2)N3CCN(CC3)C(=O)C4=CC=CC=C4	22 (11)
W1/ W25		C1CCC(CC1)CCC(=O)NC2=CC=C(C=C2)S(=O)(=O)N3CCOCC3	34 (90)
W2/ W26		C1=CC=C(C=C1)CNS(=O)(=O)C2=CC=C(C=C2)NC(=O)C3=CC=CC=C3	14 (30)
W3/ W27		COC1=CC(=C(C=C1)C2=C(C=NC(=S)N2)C3=CC=CC=C3)O	19 (4)
W4/ W28		C1=CC=C(C=C1)C2=NNC(=C2)C(F)(F)F	23 (24)
W5/ W29		CCC1=CC=CC=C1NC(=O)CSC2=NC=C(C(=N2)N)S(=O)(=O)C3=CC=C(C=C3)C	0 (22)
W6/ W30		CCCNC(=O)C1=C2N=C(C=C(N2N=C1)C(F)F)C3=CC=CC=C3	11 (9)
W7/ W31		COC1=CC=CC=C1N2C=NC3=C(C2=O)C=CC(=C3)C(=O)O	28 (48)
W8/ W32		COCCOC1=CC=C(C=C1)C(=O)NC2=CC=CC=C2Br	97 (93)
W9/ W33		CC1=C(C=CC(=C1)C(=O)N2CCN(CC2)C)N(C)S(=O)(=O)C3=CC=CC=C3	45 (44)

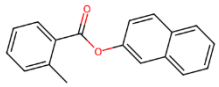
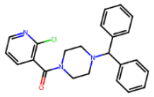
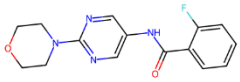
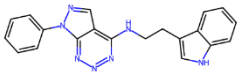
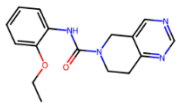
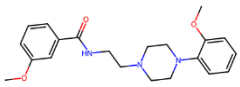
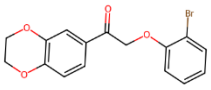
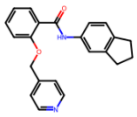
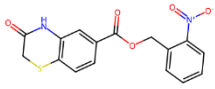
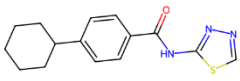
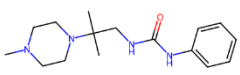
W10/ W34		C1CCC(CC1)NS(=O)(=O)C2=CC=C(C=C2)NS(=O)(=O)C3=CC=CC4=CC=CC=C43	22 (50)
W11/ W35		C1=CN=CC=C1C2=CC=C(S2)CN	96 (87)
W12/ W36		CCOC1=CC=CC=C1C(=O)NC2=CC3=C(C=C2)N(C(=O)C3)C	23 (45)
W13/ W37		COC1=C(C(=CC=C1)OC)C(=O)NC2=NN=C(S2)C3=CC=CC=C3	12 (15)
W14/ W38		CCOC1=CC=CC=C1C(=O)NC2=CC3=C(C=C2)OCC(C(=O)N3C)(C)C	21 (17)
W15/ W39		C1=CC=C(C(=C1)[N+](=O)[O-])OCC2=CN3C=CC=NC3=N2	16 (45)
W16/ W40		CN1C2=C(C=N1)C(=NC(=N2)N3CCN(CC3)C4=CC=CC=C4OC)N5CCCCC5	13 (15)
W17/ W41		CN1C2=C(C=N1)C(=NC(=N2)N3CCN(CC3)C4=CC=CC=C4)N5CCOCC5	25 (49)
W18/ W42		COC1=CC=CC=C1C(=O)NC2=CC3=C(C=CC(=C3)Cl)OC2=O	23 (42)
W19/ W43		COC1=CC(=C(C=C1N2C(=C(N=N2)C(=O)O)C3=CC=NC=C3)Cl)OC	20 (18)
W20/ W44		CC(=O)C1=CC=CC=C1NC(=O)C2=CNC3=C(C2=O)C=C(C=C3)F	92 (98)

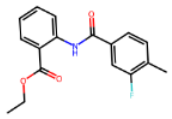
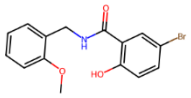
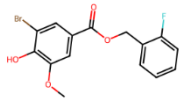
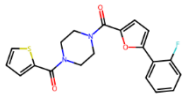
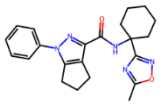
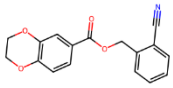
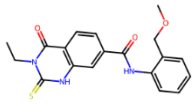
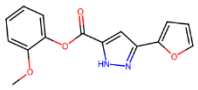
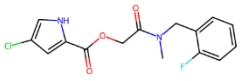
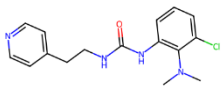
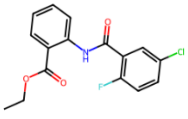
W21/ W45		CCN1CCN(CC1)C2=C(C=CC=C2Cl)NC(=O)CC3=CC=CC=C3	25 (45)
W22/ W46		C1COCCN1C2=NC=C(C=N2)NC(=O)CC3=CC=CC=C3	92 (92)
W23/ W47		CC(C)CN1C2=C(N=C1N(C)CC3=CC=CC=C3)N(C(=O)NC2=O)C	60 (88)
W24/ W48		C1=CC=C(C(=C1)C(=O)NC2=CN=C(N=C2)N3C=CN=C3)Cl	5 (22)
X1/ X25		C1CCN(CC1)S(=O)(=O)C2=CC=C(C=C2)NC(=O)C3=CC=CC=C3Cl	96 (96)
X2/ X26		CCOC1=CC=CC=C1NC(=O)C2=CC3=C(C=C2)C(=O)N(C3=O)C	14 (21)
X3/ X27		CC1=CC(=C(C=C1Cl)OC)N2C(=C(N=N2)C(=O)O)C3=CC=NC=C3	93 (94)
X4/ X28		C1C2C=CC1C3C2C(=O)N(C3=O)C4=CC=CC=C4NC(=O)C5=CC=C(C=C5)C(F)(F)F	22 (44)
X5/ X29		C1=CC=C(C=C1)C2=NC3=CC=CC=C3NC2=S	48 (45)
X6/ X30		CC1=CC=CC=C1S(=O)(=O)N2C3=CC=CC=C3N=N2	62 (62)
X7/ X31		CCN(CC)C(=O)C1=CC=C(C=C1)N(C)S(=O)(=O)C2=CC=CC=C2	0 (21)

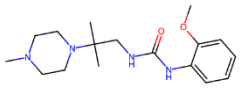
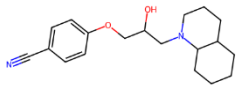
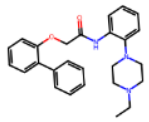
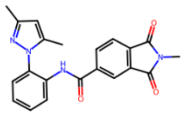
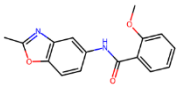
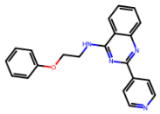
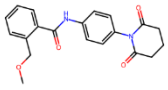
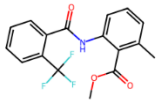
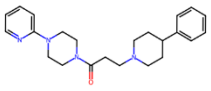
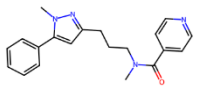
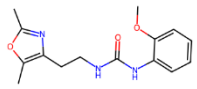
X8/ X32		COC1=CC=CC=C1CN2CCOC3=C(C2)C=C(C=C3O)C4=CC(=CC=C4)Cl	4 (47)
X9/ X33		CC1=CC=CC=C1N2C3=C(C=N2)C(=O)N(C=N3)CC4=CC=CC=N4	96 (93)
X10/ X34		COC1=CC=CC=C1C(=O)NC2=NN=C(O2)C3=CC=CC=C3Cl	8 (42)
X11/ X35		CC1=C(C(=NC(=N1)N2CCOCC2)C)NC(=O)C3=CC=CC=C3Cl	18 (23)
X12/ X36		CC1=C(C=C2C(=N1)N(C(=O)N(C2=O)C)C)C(=O)NC3=CC=CC=C3Cl	53 (90)
X13/ X37		CCOC1=CC=CC=C1C(=O)NC2=CC3=C(C=C2C(=O)C)OCO3	28 (10)
X14/ X38		C1=CC=C(C=C1)CNC2=NC(=NC3=CC=CC=C32)C4=CC=CC=N4	20 (19)
X15/ X39		C1=CC=C(C(=C1)C=C2C(=O)N3C4=CC=CC=C4N=C3S2)[N+](=O)[O-]	93 (89)
X16/ X40		COC1=C(C=C(C=C1)N2C(=C(N=N2)C(=O)O)C3=CC=NC=C3)Cl	11 (30)
X17/ X41		C1=CC=C(C=C1)C(=O)CNC(=O)C2=CC3=CC=CC=C3OC2=O	18 (39)
X18/ X42		CC(=O)NC1=C(N=C(S1)C2=CC=CC=C2)C3=CC=C(C=C3)F	82 (47)

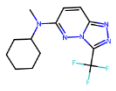
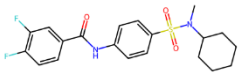
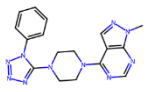
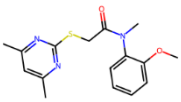
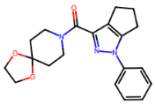
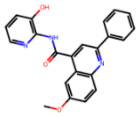
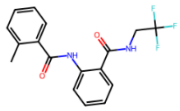
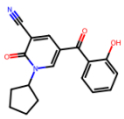
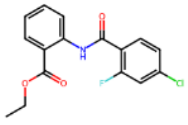
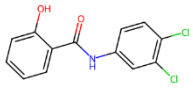
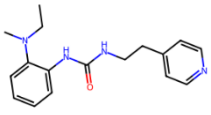
X19/ X43		CC1=CC=CC=C1C(=O)NC2=CN=C(N=C2)N3CCOCC3	16 (5)
X20/ X44		CN1C2=NC(=NC(=C2C=N1)NCC3=CC=CC=C3)N4CCN(CC4)C5=CC=CC=C5OC	8 (45)
X21/ X45		COC1=CC(=C(C=C1)Br)C(=O)NC2CC3C(=O)NC4=CC=CC=C4N3C2	91 (98)
X22/ X46		CN(CN1C2=CC=CC=C2C(=O)C1=O)C3=CC=CC=C3	22 (45)
X23/ X47		C1=CC=C(C=C1)CN2C=NC3=C(C2=O)C=NN3C4=CC(=CC=C4)Cl	15 (18)
X24/ X48		CCOC1=CC=CC=C1OC2=C(NN=C2C3=C(C=C(C=C3)O)O)C	11 (26)
Y1/ Y25		COC1=CC=CC=C1N2C(=C(N=N2)C(=O)O)C3=CC=NC=C3	12 (12)
Y2/ Y26		CC1=C(C(N2CCN(C3=CC=CC=C3)CC2)=O)SC(N4C=CC=C4)=N1	14 (0)
Y3/ Y27		C1CCN(CC1)CC2=CC=C(C=C2)C(=O)N3CCN(CC3)C4=CC=CC=C4F	89 (91)
Y4/ Y28		CC1=C(C=CC(=C1)C(=O)N2CCOCC2)N(C)S(=O)(=O)C3=CC=CC=C3	28 (18)
Y5/ Y29		C1CCC(CC1)NC(=O)CC2=CC3=C(CCCC3)C=C2	24 (29)

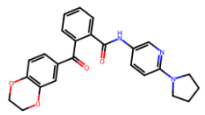
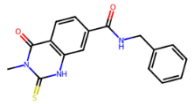
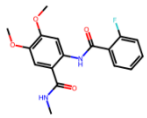
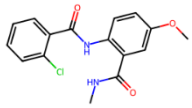
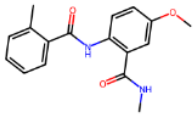
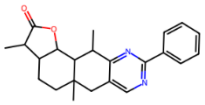
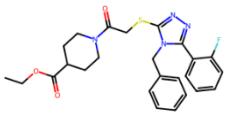
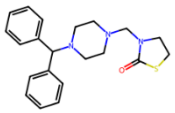
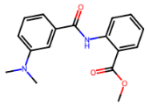
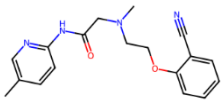
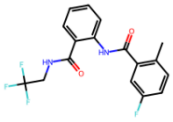
Y6/ Y30		CN(CC1=CC=CC=C1)C(=O)C2(CCCC2)C3=CC=CS3	38 (28)
Y7/ Y31		COC1=C(C=C(C=C1)Cl)C(=O)NC2=NN=C(S2)C3=CC=CC=C3	10 (21)
Y8/ Y32		CN1C2=C(C=N1)C(=NC(=N2)N3CCN(CC3)C4=CC=CC=C4OC)N5CCOCC5	15 (63)
Y9/ Y33		CC1=NC2=C(C=C1)OC(=C2)C(=O)NC3=CC=CC=C3C(=O)OC	17 (24)
Y10/ Y34		CC1=C(C(=NC(=N1)N2CCOCC2)C)NC(=O)C3=CC=NC=C3	26 (22)
Y11/ Y35		C1=CC=C(C(=C1)CON2C3=CC=CC=C3N=N2)F	62 (57)
Y12/ Y36		CC1=C(SC2=C1C(=O)NC=N2)C(=O)NC3=CC=CC=C3OC	22 (23)
Y13/ Y37		COC1=CC=CC=C1N2C(=O)C3=C4C(=CC=C5C4=C(CC5)C=C3)C2=O	0 (17)
Y14/ Y38		COC1=CC=C(C=C1)N2C(=C(N=N2)C(=O)O)C3=CC=NC=C3	18 (28)
Y15/ Y39		CCOC1=CC=CC=C1C=C2C(=O)N3C4=CC=CC=C4N=C3S2	79 (92)
Y16/ Y40		C1CCN(CC1)CC2=CC=C(C=C2)C(=O)N3CCN(CC3)C4=CC=CC=C4	25 (43)

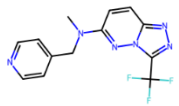
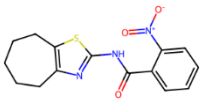
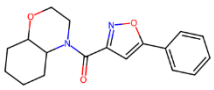
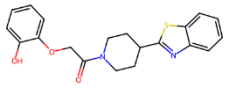
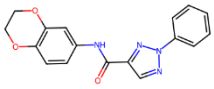
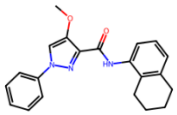
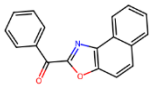
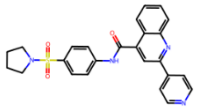
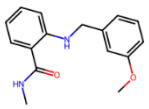
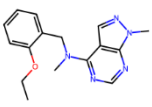
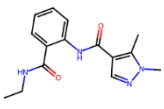
Y17/ Y41		CC1=CC=CC=C1C(=O)OC2=CC3=CC=CC=C3C=C2	14 (27)
Y18/ Y42		C1CN(CCN1C(C2=CC=CC=C2)C3=CC=CC=C3)C(=O)C4=C(N=CC=C4)Cl	11 (29)
Y19/ Y43		C1COCCN1C2=NC=C(C=N2)NC(=O)C3=CC=CC=C3F	93 (97)
Y20/ Y44		C1=CC=C(C=C1)N2C3=NN=NC(=C3C=N2)NCCC4=CNC5=CC=CC=C54	17 (34)
Y21/ Y45		CCOC1=CC=CC=C1NC(=O)N2CCC3=NC=NC=C3C2	8 (24)
Y22/ Y46		COC1=CC=CC(=C1)C(=O)NCCN2CCN(CC2)C3=CC=CC=C3OC	27 (55)
Y23/ Y47		C1COC2=C(O1)C=CC(=C2)C(=O)COC3=CC=CC=C3Br	70 (82)
Y24/ Y48		C1CC2=C(C1)C=C(C=C2)NC(=O)C3=CC=CC=C3OCC4=CC=NC=C4	0 (19)
Z1/ Z25		C1C(=O)NC2=C(S1)C=CC(=C2)C(=O)OCC3=CC=CC=C3[N+](=O)[O-]	25 (22)
Z2/ Z26		C1CCC(CC1)C2=CC=C(C=C2)C(=O)NC3=NN=CS3	90 (92)
Z3/ Z27		CC(C)(CNC(=O)NC1=CC=CC=C1)N2CCN(CC2)C	22 (29)

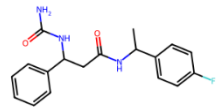
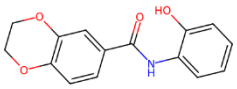
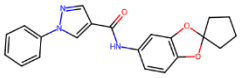
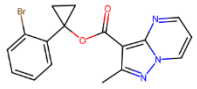
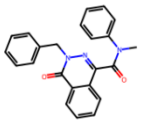
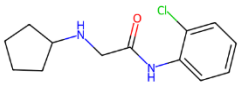
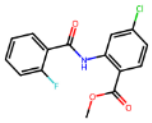
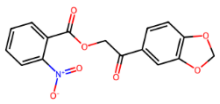
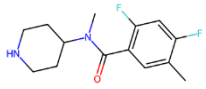
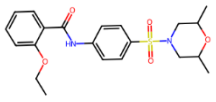
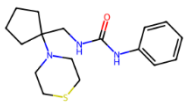
Z4/ Z28		CCOC(=O)C1=CC=CC=C1NC(=O)C2=CC(=C(C=C2)C)F	22 (10)
Z5/ Z29		COC1=CC=CC=C1CNC(=O)C2=C(C=CC(=C2)Br)O	32 (29)
Z6/ Z30		COC1=C(C(=CC(=C1)C(=O)OCC2=CC=CC=C2F)Br)O	27 (25)
Z7/ Z31		C1CN(CCN1C(=O)C2=CC=C(O2)C3=CC=CC=C3F)C(=O)C4=CC=CS4	28 (51)
Z8/ Z32		CC1=NC(=NO1)C2(CCCCC2)NC(=O)C3=NN(C4=C3CCC4)C5=CC=CC=C5	28 (49)
Z9/ Z33		C1COC2=C(O1)C=CC(=C2)C(=O)OCC3=CC=CC=C3C#N	20 (32)
Z10/ Z34		CCN1C(=O)C2=C(C=C(C=C2)C(=O)NC3=CC=CC=C3COC)NC1=S	97 (94)
Z11/ Z35		COC1=CC=CC=C1OC(=O)C2=CC(=NN2)C3=CC=CO3	10 (19)
Z12/ Z36		CN(CC1=CC=CC=C1F)C(=O)COC(=O)C2=CC(=CN2)Cl	27 (31)
Z13/ Z37		CN(C)C1=C(C=CC=C1Cl)NC(=O)NCCC2=CC=NC=C2	54 (90)
Z14/ Z38		CCOC(=O)C1=CC=CC=C1NC(=O)C2=C(C=CC(=C2)Cl)F	18 (11)

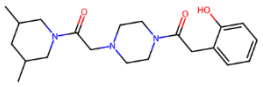
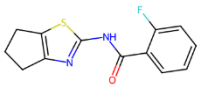
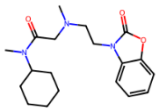
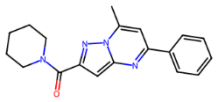
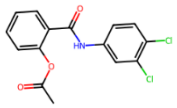
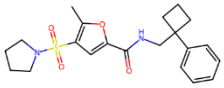
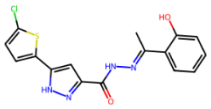
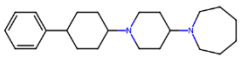
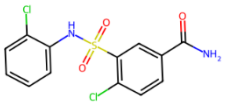
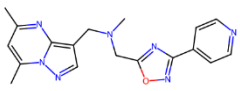
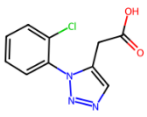
Z15/ Z39		CC(C)(CNC(=O)NC1=CC=CC=C1OC)N2CCN(CC2)C	15 (25)
Z16/ Z40		C1CCC2C(C1)CCCN2CC(COC3=CC=C(C=C3)C#N)O	25 (36)
Z17/ Z41		CCN1CCN(CC1)C2=CC=CC=C2NC(=O)COC3=CC=CC=C3C4=CC=CC=C4	43 (46)
Z18/ Z42		CC1=CC(=NN1C2=CC=CC=C2NC(=O)C3=CC4=C(C=C3)C(=O)N(C4=O)C)C	27 (20)
Z19/ Z43		CC1=NC2=C(O1)C=CC(=C2)NC(=O)C3=CC=CC=C3OC	26 (27)
Z20/ Z44		C1=CC=C(C=C1)OCCNC2=NC(=NC3=CC=CC=C32)C4=CC=NC=C4	26 (34)
Z21/ Z45		COCC1=CC=CC=C1C(=O)NC2=CC=C(C=C2)N3C(=O)CCCC3=O	94 (97)
Z22/ Z46		CC1=C(C(=CC=C1)NC(=O)C2=CC=CC=C2C(F)(F)F)C(=O)OC	94 (93)
Z23/ Z47		C1CN(CCC1C2=CC=CC=C2)CCC(=O)N3CCN(CC3)C4=CC=CC=N4	15 (32)
Z24/ Z48		CN1C(=CC(=N1)CCCN(C)C(=O)C2=CC=NC=C2)C3=CC=CC=C3	22 (41)
AA1/ AA25		CC1=C(N=C(O1)C)CCNC(=O)NC2=CC=CC=C2OC	24 (6)

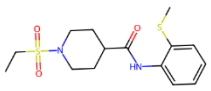
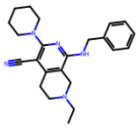
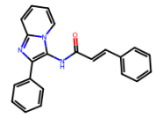
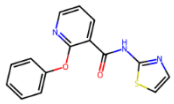
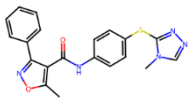
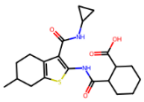
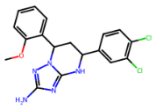
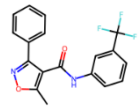
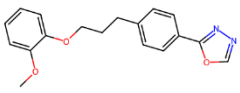
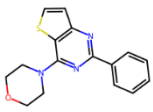
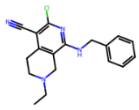
AA2/ AA26		CN(C1CCCCC1)C2=NN3C(=NN=C3C(F)(F)F)C=C2	0 (47)
AA3/ AA27		CN(C1CCCCC1)S(=O)(=O)C2=CC=C(C=C2)NC(=O)C3=CC(=C(C=C3)F)F	42 (38)
AA4/ AA28		CN1C2=C(C=N1)C(=NC=N2)N3CCN(CC3)C4=NN=NN4C5=CC=CC=C5	13 (23)
AA5/ AA29		CC1=CC(=NC(=N1)SCC(=O)N(C)C2=CC=CC=C2OC)C	12 (23)
AA6/ AA30		C1CC2=C(C1)N(N=C2C(=O)N3CCC4(CC3)OCCO4)C5=CC=CC=C5	8 (0)
AA7/ AA31		COC1=CC2=C(C=C1)N=C(C=C2C(=O)NC3=C(C=CC=N3)O)C4=CC=CC=C4	10 (52)
AA8/ AA32		CC1=CC=CC=C1C(=O)NC2=CC=CC=C2C(=O)NCC(F)(F)F	0 (27)
AA9/ AA33		C1CCC(C1)N2C=C(C=C(C2=O)C#N)C(=O)C3=CC=CC=C3O	0 (17)
AA10/ AA34		CCOC(=O)C1=CC=CC=C1NC(=O)C2=C(C=C(C=C2)Cl)F	16 (8)
AA11/ AA35		C1=CC=C(C(=C1)C(=O)NC2=CC(=C(C=C2)Cl)Cl)O	22 (22)
AA12/ AA36		CCN(C)C1=CC=CC=C1NC(=O)NCCC2=CC=NC=C2	95 (98)

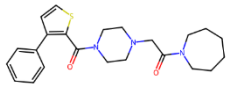
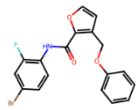
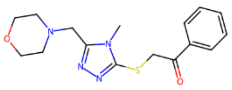
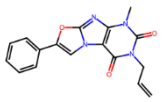
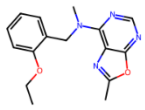
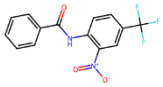
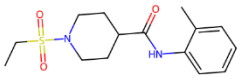
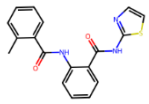
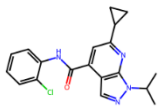
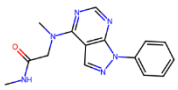
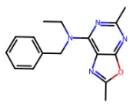
AA13/ AA37		C1CCN(C1)C2=NC=C(C=C2)NC(=O)C3=CC=CC=C3C(=O)C4=CC5=C(C=C4)OCCO5	18 (42)
AA14/ AA38		CN1C(=O)C2=C(C=C(C=C2)C(=O)NCC3=CC=CC=C3)NC1=S	96 (47)
AA15/ AA39		CNC(=O)C1=CC(=C(C=C1NC(=O)C2=CC=CC=C2F)OC)OC	97 (93)
AA16/ AA40		CNC(=O)C1=C(C=CC(=C1)OC)NC(=O)C2=CC=CC=C2Cl	34 (39)
AA17/ AA41		CC1=CC=CC=C1C(=O)NC2=C(C=C(C=C2)OC)C(=O)NC	10 (47)
AA18/ AA42		CC1C2CCC3(CC4=CN=C(N=C4C(C3C2OC1=O)C)C5=CC=CC=C5)C	31 (19)
AA19/ AA43		CCOC(=O)C1CCN(CC1)C(=O)CSC2=NN=C(N2CC3=CC=CC=C3)C4=CC=CC=C4F	75 (79)
AA20/ AA44		C1CN(CCN1CN2CCSC2=O)C(C3=CC=CC=C3)C4=CC=CC=C4	15 (27)
AA21/ AA45		CN(C)C1=CC=CC(=C1)C(=O)NC2=CC=CC=C2C(=O)OC	21 (53)
AA22/ AA46		CC1=CN=C(C=C1)NC(=O)CN(C)CCOC2=CC=CC=C2C#N	39 (40)
AA23/ AA47		CC1=C(C=C(C=C1)F)C(=O)NC2=CC=CC=C2C(=O)NCC(F)(F)F	97 (91)

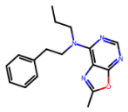
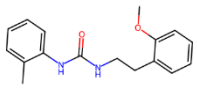
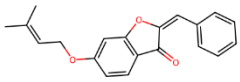
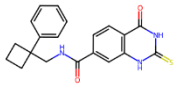
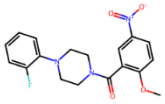
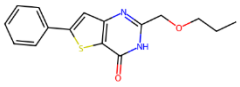
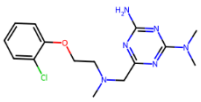
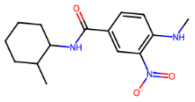
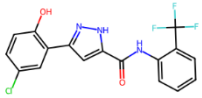
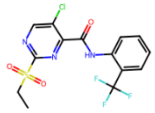
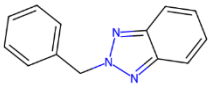
AA24/ AA48		CN(CC1=CC=NC=C1)C2=NN3C(=NN=C3C(F)(F)F)C=C2	93 (96)
AB1/ AB25		C1CCC2=C(CC1)SC(=N2)NC(=O)C3=CC=CC=C3[N+](=O)[O-]	44 (27)
AB2/ AB26		C1CCC2C(C1)N(CCO2)C(=O)C3=NOC(=C3)C4=CC=CC=C4	19 (0)
AB3/ AB27		C1CN(CCC1C2=NC3=CC=CC=C3S2)C(=O)COC4=CC=CC=C4O	24 (49)
AB4/ AB28		C1COC2=C(O1)C=CC(=C2)NC(=O)C3=NN(N=C3)C4=CC=CC=C4	79 (97)
AB5/ AB29		COC1=CN(N=C1C(=O)NC2=CC=CC3=C2CCCC3)C4=CC=CC=C4	98 (89)
AB6/ AB30		C1=CC=C(C=C1)C(=O)C2=NC3=C(O2)C=CC4=CC=CC=C43	13 (23)
AB7/ AB31		C1CCN(C1)S(=O)(=O)C2=CC=C(C=C2)NC(=O)C3=CC(=NC4=CC=CC=C43)C5=CC=NC=C5	17 (47)
AB8/ AB32		CNC(=O)C1=CC=CC=C1NCC2=CC(=CC=C2)OC	14 (23)
AB9/ AB33		CCOC1=CC=CC=C1CN(C)C2=NC=NC3=C2C=NN3C	52 (92)
AB10/ AB34		CCNC(=O)C1=CC=CC=C1NC(=O)C2=C(N(N=C2)C)C	21 (14)

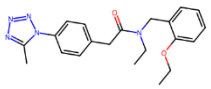
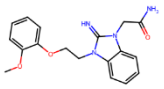
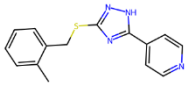
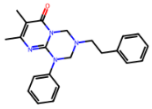
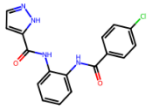
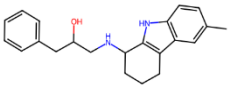
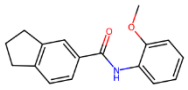
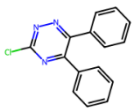
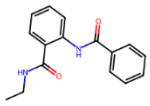
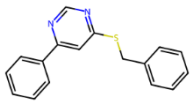
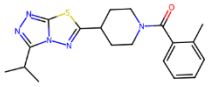
AB11/ AB35		CC(C1=CC=C(C=C1)F)NC(=O)CC(C2=CC=CC=C2)NC(=O)N	26 (48)
AB12/ AB36		C1COC2=C(O1)C=CC(=C2)C(=O)NC3=CC=CC=C3O	39 (21)
AB13/ AB37		C1CCC2(C1)OC3=C(O2)C=C(C=C3)NC(=O)C4=CN(N=C4)C5=CC=CC=C5	95 (93)
AB14/ AB38		CC1=NN2C=CC=NC2=C1C(=O)OC3(CC3)C4=CC=CC=C4Br	29 (22)
AB15/ AB39		CN(C1=CC=CC=C1)C(=O)C2=NN(C(=O)C3=CC=CC=C32)CC4=CC=CC=C4	25 (22)
AB16/ AB40		C1CCC(C1)NCC(=O)NC2=CC=CC=C2Cl	90 (88)
AB17/ AB41		COC(=O)C1=C(C=C(C=C1)Cl)NC(=O)C2=CC=CC=C2F	94 (90)
AB18/ AB42		C1OC2=C(O1)C=C(C=C2)C(=O)COC(=O)C3=CC=CC=C3[N+](=O)[O-]	89 (91)
AB19/ AB43		CC1=CC(=C(C=C1F)F)C(=O)N(C)C2CCNCC2	25 (28)
AB20/ AB44		CCOC1=CC=CC=C1C(=O)NC2=CC=C(C=C2)S(=O)(=O)N3CC(OC(C3)C)C	10 (47)
AB21/ AB45		C1CCC(C1)(CNC(=O)NC2=CC=CC=C2)N3CCSCC3	14 (26)

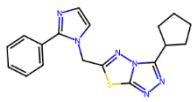
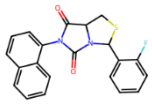
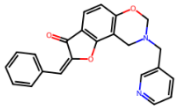
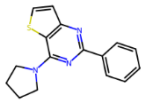
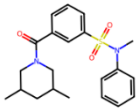
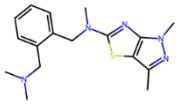
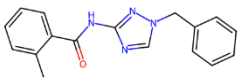
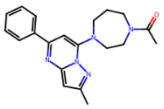
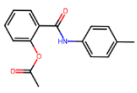
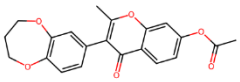
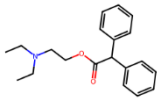
AB22/ AB46		CC1CC(CN(C1)C(=O)CN2CCN(CC2)C(=O)CC3=CC=CC=C3O)C	38 (40)
AB23/ AB47		C1CC2=C(C1)SC(=N2)NC(=O)C3=CC=CC=C3F	16 (28)
AB24/ AB48		CN(CCN1C2=CC=CC=C2OC1=O)CC(=O)N(C)C3CCCCC3	14 (30)
AC1/ AC25		CC1=CC(=NC2=CC(=NN12)C(=O)N3CCCCC3)C4=CC=CC=C4	94 (88)
AC2/ AC26		CC(=O)OC1=CC=CC=C1C(=O)NC2=CC(=C(C=C2)Cl)Cl	80 (36)
AC3/ AC27		CC1=C(C=C(O1)C(=O)NCC2(CCC2)C3=CC=CC=C3)S(=O)(=O)N4CCCC4	25 (13)
AC4/ AC28		CC(=NNC(=O)C1=NNC(=C1)C2=CC=C(S2)Cl)C3=CC=CC=C3O	25 (48)
AC5/ AC29		C1CCCN(CC1)C2CCN(CC2)C3CCC(CC3)C4=CC=CC=C4	49 (98)
AC6/ AC30		C1=CC=C(C(=C1)NS(=O)(=O)C2=C(C=CC(=C2)C(=O)N)Cl)Cl	19 (58)
AC7/ AC31		CC1=CC(=NC2=C(C=NN12)CN(C)CC3=NC(=NO3)C4=CC=NC=C4)C	4 (43)
AC8/ AC32		C1=CC=C(C(=C1)N2C(=CN=N2)CC(=O)O)Cl	27 (29)

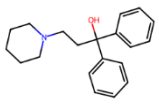
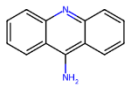
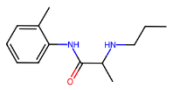
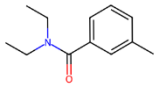
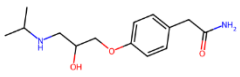
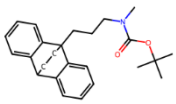
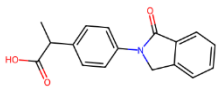
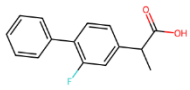
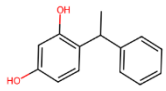
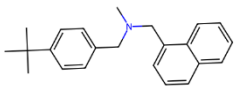
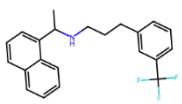
AC9/ AC33		CCS(=O)(=O)N1CCC(CC1)C(=O)NC2=CC=CC=C2SC	8 (47)
AC10/ AC34		CCN1CCC2=C(C1)C(=NC(=C2C#N)N3CCCCC3)NCC4=CC=CC=C4	35 (90)
AC11/ AC35		C1=CC=C(C=C1)C=CC(=O)NC2=C(N=C3N2C=CC=C3)C4=CC=CC=C4	22 (0)
AC12/ AC36		C1=CC=C(C=C1)OC2=C(C=CC=N2)C(=O)NC3=NC=CS3	20 (18)
AC13/ AC37		CC1=C(C(=NO1)C2=CC=CC=C2)C(=O)NC3=CC=C(C=C3)SC4=NN=CN4C	22 (20)
AC14/ AC38		CC1CCC2=C(C1)SC(=C2C(=O)NC3CC3)NC(=O)C4CCCCC4C(=O)O	94 (97)
AC15/ AC39		COC1=CC=CC=C1C2CC(NC3=NC(=NN23)N)C4=CC(=C(C=C4)Cl)Cl	28 (0)
AC16/ AC40		CC1=C(C(=NO1)C2=CC=CC=C2)C(=O)NC3=CC=CC(=C3)C(F)(F)F	49 (57)
AC17/ AC41		COC1=CC=CC=C1OCCCC2=CC=C(C=C2)C3=NN=CO3	20 (11)
AC18/ AC42		C1COCCN1C2=NC(=NC3=C2SC=C3)C4=CC=CC=C4	11 (54)
AC19/ AC43		CCN1CCC2=C(C1)C(=NC(=C2C#N)Cl)NCC3=CC=CC=C3	30 (59)

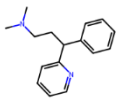
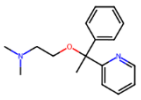
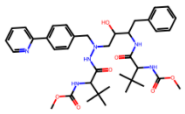
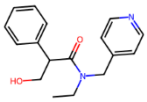
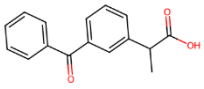
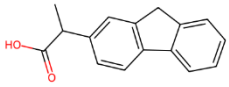
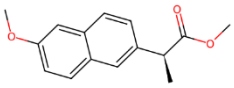
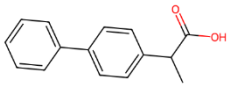
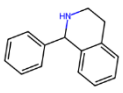
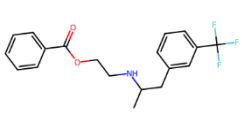
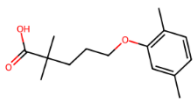
AC20/ AC44		C1CCCN(CC1)C(=O)CN2CCN(CC2)C(=O)C3=C(C=CS3)C4=CC=CC=C4	29 (24)
AC21/ AC45		C1=CC=C(C=C1)OCC2=C(OC=C2)C(=O)NC3=C(C=C(C=C3)Br)F	29 (25)
AC22/ AC46		CN1C(=NN=C1SCC(=O)C2=CC=CC=C2)CN3CCOCC3	65 (35)
AC23/ AC47		CN1C2=C(C(=O)N(C1=O)CC=C)N3C=C(OC3=N2)C4=CC=CC=C4	25 (15)
AC24/ AC48		CCOC1=CC=CC=C1CN(C)C2=C3C(=NC=N2)OC(=N3)C	12 (18)
AD1/ AD25		C1=CC=C(C=C1)C(=O)NC2=C(C=C(C=C2)C(F)(F)F)[N+](=O)[O-]	26 (60)
AD2/ AD26		CCS(=O)(=O)N1CCC(CC1)C(=O)NC2=CC=CC=C2C	57 (92)
AD3/ AD27		CC1=CC=CC=C1C(=O)NC2=CC=CC=C2C(=O)NC3=NC=CS3	24 (28)
AD4/ AD28		CC(C)N1C2=C(C=N1)C(=CC(=N2)C3CC3)C(=O)NC4=CC=CC=C4Cl	28 (48)
AD5/ AD29		CNC(=O)CN(C)C1=NC=NC2=C1C=NN2C3=CC=CC=C3	42 (96)
AD6/ AD30		CCN(CC1=CC=CC=C1)C2=C3C(=NC(=N2)C)OC(=N3)C	12 (20)

AD7/ AD31		CCCN(CCC1=CC=CC=C1)C2=C3C(=NC=N2)OC(=N3)C	40 (20)
AD8/ AD32		CC1=CC=CC=C1NC(=O)NCCC2=CC=CC=C2OC	23 (57)
AD9/ AD33		CC(=CCOC1=CC2=C(C=C1)C(=O)C(=CC3=CC=CC=C3)O2)C	52 (26)
AD10/ AD34		C1CC(C1)(CNC(=O)C2=CC3=C(C=C2)C(=O)NC(=S)N3)C4=CC=CC=C4	0 (23)
AD11/ AD35		COC1=C(C=C(C=C1)[N+](=O)[O-])C(=O)N2CCN(CC2)C3=CC=CC=C3F	0 (0)
AD12/ AD36		CCCOCC1=NC2=C(C(=O)N1)SC(=C2)C3=CC=CC=C3	30 (30)
AD13/ AD37		CN(C)C1=NC(=NC(=N1)N)CN(C)CCOC2=CC=CC=C2Cl	55 (22)
AD14/ AD38		CC1CCCCC1NC(=O)C2=CC(=C(C=C2)NC)[N+](=O)[O-]	15 (27)
AD15/ AD39		C1=CC=C(C(=C1)C(F)(F)F)NC(=O)C2=CC(=NN2)C3=C(C=CC(=C3)Cl)O	27 (59)
AD16/ AD40		CCS(=O)(=O)C1=NC=C(C(=N1)C(=O)NC2=CC=CC=C2C(F)(F)F)Cl	64 (95)
AD17/ AD41		C1=CC=C(C=C1)CN2N=C3C=CC=CC3=N2	97 (97)

AD18/ AD42		CCN(CC1=CC=CC=C1OCC)C(=O)CC2=CC=C(C=C2)N3C(=NN=N3)C	98 (88)
AD19/ AD43		COC1=CC=CC=C1OCCN2C3=CC=CC=C3N(C2=N)CC(=O)N	90 (95)
AD20/ AD44		CC1=CC=CC=C1CSC2=NNC(=N2)C3=CC=NC=C3	91 (89)
AD21/ AD45		CC1=C(N=C2N(CN(CN2C1=O)CCC3=CC=CC=C3)C4=CC=CC=C4)C	35 (58)
AD22/ AD46		C1=CC=C(C(=C1)NC(=O)C2=CC=C(C=C2)Cl)NC(=O)C3=CC=NN3	19 (26)
AD23/ AD47		CC1=CC2=C(C=C1)NC3=C2CCCC3NCC(CC4=CC=CC=C4)O	23 (73)
AD24/ AD48		COC1=CC=CC=C1NC(=O)C2=CC3=C(CCC3)C=C2	27 (97)
AE1/ AE25		C1=CC=C(C=C1)C2=C(N=NC(=N2)Cl)C3=CC=CC=C3	12 (26)
AE2/ AE26		CCNC(=O)C1=CC=CC=C1NC(=O)C2=CC=CC=C2	32 (30)
AE3/ AE27		C1=CC=C(C=C1)CSC2=NC=NC(=C2)C3=CC=CC=C3	36 (27)
AE4/ AE28		CC1=CC=CC=C1C(=O)N2CCC(CC2)C3=NN4C(=NN=C4S3)C(C)C	21 (45)

AE5/ AE29		C1CCC(C1)C2=NN=C3N2N=C(S3)CN4C=CN=C4C5=CC=CC=C5	13 (28)
AE6/ AE30		C1C2C(=O)N(C(=O)N2C(S1)C3=CC=CC=C3F)C4=CC=CC5=CC=CC=C54	83 (90)
AE7/ AE31		C1C2=C(C=CC3=C2OC(=CC4=CC=CC=C4)C3=O)OCN1CC5=CN=CC=C5	93 (91)
AE8/ AE32		C1CCN(C1)C2=NC(=NC3=C2SC=C3)C4=CC=CC=C4	89 (94)
AE9/ AE33		CC1CC(CN(C1)C(=O)C2=CC(=CC=C2)S(=O)(=O)N(C)C3=CC=CC=C3)C	24 (21)
AE10/ AE34		CC1=NN(C2=C1SC(=N2)N(C)CC3=CC=CC=C3CN(C)C)C	10 (12)
AE11/ AE35		CC1=CC=CC=C1C(=O)NC2=NN(C=N2)CC3=CC=CC=C3	18 (25)
AE12/ AE36		CC1=NN2C(=C1)N=C(C=C2N3CCCN(CC3)C(=O)C)C4=CC=CC=C4	22 (36)
AE13/ AE37		CC1=CC=C(C=C1)NC(=O)C2=CC=CC=C2OC(=O)C	0 (7)
AE14/ AE38		CC(OC1=CC=C2C(OC(C)=C(C2=O)C3=CC4=C(OCCCO4)C=C3)=C1)=O	23 (25)
AE15/ AE39		CCN(CC)CCOC(=O)C(C1=CC=CC=C1)C2=CC=CC=C2	44 (54)

AE16/ AE40		C1CCN(CC1)CCC(C2=CC=CC=C2)(C3=CC=CC=C3)O	35 (92)
AE17/ AE41		C1=CC=C2C(=C1)C(=C3C=CC=CC3=N2)N	35 (62)
AE18/ AE42		CCCNC(C)C(=O)NC1=CC=CC=C1C	59 (88)
AE19/ AE43		CCN(CC)C(=O)C1=CC=CC(=C1)C	51 (72)
AE20/ AE44		CC(C)NCC(COC1=CC=C(C=C1)CC(=O)N)O	21 (54)
AE21/ AE45		CN(C(OC(C)(C)C)=O)CCCC12CCC(C3=CC=CC=C23)C4=CC=CC=C41	90 (97)
AE22/ AE46		CC(C1=CC=C(C=C1)N2CC3=CC=CC=C3C2=O)C(=O)O	60 (71)
AE23/ AE47		CC(C1=CC(=C(C=C1)C2=CC=CC=C2)F)C(=O)O	26 (40)
AE24/ AE48		CC(C1=CC=CC=C1)C2=C(O)C=C(O)C=C2	85 (97)
AF1/ AF25		CC(C)(C)C1=CC=C(C=C1)CN(C)CC2=CC=CC3=CC=CC=C32	41 (88)
AF2/ AF26		CC(C1=CC=CC2=CC=CC=C21)NCCCC3=CC(=CC=C3)C(F)(F)F	92 (97)

AF3/ AF27		CN(C)CCC(C1=CC=CC=C1)C2=CC=CC=N2	0 (24)
AF4/ AF28		CC(C1=CC=CC=C1)(C2=CC=CC=N2)OCCN(C)C	92 (92)
AF5/ AF29		CC(C)(C)C(C(=O)NC(CC1=CC=CC=C1)C(CN(CC2=CC=C(C=C2)C3=CC=CC=N3)NC(=O)C(C(C)(C)C)NC(=O)OC)O)NC(=O)OC	91 (92)
AF6/ AF30		CCN(CC1=CC=NC=C1)C(=O)C(CO)C2=CC=CC=C2	33 (75)
AF7/ AF31		CC(C1=CC(=CC=C1)C(=O)C2=CC=CC=C2)C(=O)O	17 (24)
AF8/ AF32		CC(C1=CC2=C(C=C1)C3=CC=CC=C3C2)C(=O)O	36 (69)
AF9/ AF33		O=C([C@H](C1=CC2=CC=C(OC)C=C2C=C1)C)OC	27 (40)
AF10/ AF34		CC(C1=CC=C(C=C1)C2=CC=CC=C2)C(=O)O	17 (13)
AF11/ AF35		C1CNC(C2=CC=CC=C21)C3=CC=CC=C3	20 (23)
AF12/ AF36		CC(CC1=CC(=CC=C1)C(F)(F)F)NCCOC(=O)C2=CC=CC=C2	16 (0)
AF13/ AF37		CC1=CC(=C(C=C1)C)OCCCC(C)(C)C(=O)O	93 (96)

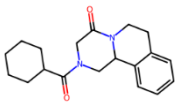
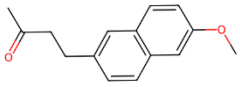
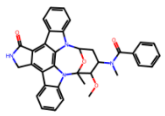
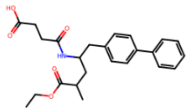
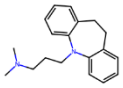
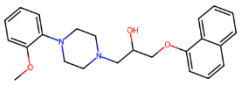
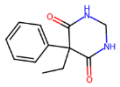
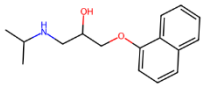
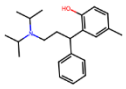
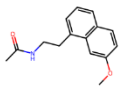
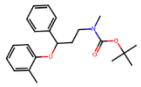
AF14/ AF38		C1CCC(CC1)C(=O)N2CC3C4=CC=CC=C4CCN3C(=O)C2	71 (95)
AF15/ AF39		CC(=O)CCC1=CC2=C(C=C1)C=C(C=C2)OC	89 (94)
AF16/ AF40		CC12C(C(CC(O1)N3C4=CC=CC=C4C5=C6C(=C7C8=CC=CC=C8N2C7=C53)CNC6=O)N(C)C(=O)C9=CC=CC=C9)OC	53 (62)
AF17/ AF41		CCOC(=O)C(C)CC(CC1=CC=C(C=C1)C2=CC=CC=C2)NC(=O)CCC(=O)O	10 (24)
AF18/ AF42		CN(C)CCCN1C2=CC=CC=C2CCC3=CC=CC=C31	20 (49)
AF19/ AF43		COC1=CC=CC=C1N2CCN(CC2)CC(COC3=CC=CC4=CC=CC=C43)O	65 (96)
AF20/ AF44		CCC1(C(=O)NCNC1=O)C2=CC=CC=C2	93 (90)
AF21/ AF45		CC(C)NCC(COC1=CC=CC2=CC=CC=C21)O	92 (21)
AF22/ AF46		CC1=CC(=C(C=C1)O)C(CCN(C(C)C)C(C)C)C2=CC=CC=C2	96 (95)
AF23/ AF47		CC(=O)NCCC1=CC=CC2=C1C=C(C=C2)OC	92 (97)
AF24/ AF48		CC1=CC=CC=C1OC(C2=CC=CC=C2)CCN(C(OC(C)(C)C)=O)C	12 (15)

Table 2-3 SMILES strings and yields for all substrates used in 1,536-well LSS screen across both 3.5 equivalents and 7.0 equivalents of reductant

2.5.4 ***Procedure for Microsomal Stability Assay***

General setup and execution of the high-throughput experiment to be coupled directly into the microsomal stability assay remains the same as outlined in the above section "Procedure for Arene Reduction Comparison Screen." Stock solutions, or suspensions, of the appropriate reagents were prepared, under inert atmosphere, as detailed in the heatmap preparation table below. A 24-well aluminum microvial plate (Analytical Sales & Services #24253) was equipped with oven-dried shell vials (Analytical Sales & Services cat. no. 884001) and parylene-coated stir dowels were added to each vial (Analytical Sales & Services #13258). All stock solutions were prepared in EtOH and dosed into the appropriate well locations using single or multichannel micropipetters. Sequence of addition is as follows: substrate addition, $B_2(OH)_4$ addition, and finally $[Rh(COD)OH]_2$ addition to reach the final reaction volume (100 µL). The microvial plate was quickly sealed, removed from the glove box, and stirred on a tumble stirrer with heating to 50 ºC for 24 hours.

The reactions were quenched by opening the reaction block and adding 100 µL saturated aqueous $NaHCO_3$ solution, then the reaction plate was allowed to stir for 15 minutes. Following, approximately 3 mg (0.63 mmol/g loading, >5.0 equiv relative to Rh loading) of SiliaMetS DMT metal scavenging resin (SiliCycle #R79030B) was added to each well and stirred for another 60 minutes to sequester remaining rhodium catalyst. From each reaction, a 20 µL aliquot of the quenched reaction mixture was transferred to a separate vial containing 80 µL of acetonitrile to reach a final concentration of 10 mM for each crude reaction mixture to be tested in the metabolism assay.

Briefly, 197.5 µL pre-warmed potassium phosphate buffer (0.1 M, pH 7.4) was added to a 96-well plate (Greiner # Z667234) via multichannel micropipettor and incubated for 5 minutes at 37°C. Then, NADPH generating system (25 µL, 10 mM, XenoTech # K5100) was added to all wells (using the buffer as a substitute for the negative control). Then, stock solutions of the test compounds (2.5 µL, 10 mM) were added to the assay plate. Finally, each well was charged with thawed mixed gender human liver microsomes (12.5 µL, 20 mg/mL, XenoTech # H0604). The final solutions were gently mixed by pipetting up and down two to three times. Immediately, 50 µL of each sample for the 0-minute time point was withdrawn and transfered to a quench solution of 100 µL ice-cold acetonitrile with internal standard (100 mg/L, caffeine). The well plate was incubated at 37°C for 60 minutes with additional aliquots taken from the

corresponding wells at the 15-, 30-, and 60-minute marks to be quenched. The quenched acetonitrile plate was then centrifuged for 5 minutes at 3500 × g. Finally, 100 µl of the quenched supernatant fraction was transferred into a 96-well polypropylene collection plate for analysis. Samples were stored at -20 °C until analyzed by UPLC-MS. Percent remaining of each substrate was determined by comparing the ratio of MS ionization peak area of each substrate/caffeine relative to the substrate/caffeine area at the 0-minute time point. Additionally, the pure unsaturated starting materials for each substrate were analyzed by the same assay procedure to determine the percent change in metabolism over 60 minutes between the unsaturated drug and it reduced congener. Data for the 20 of 24 substrates that were detected at quantitatable concentrations following LSS and subseqeuent microsome exposure are shown in the below tables and figures.

Reagents	C_{stock} (M)	V_{dose} (µL)	Wells
Gemfibrozil	0.3	33	A1
(±)-Propranolol	0.3	33	A2
Aminacrine	0.3	33	A3
Ketoprofen	0.3	33	A4
Atorvastatin Calcium	0.3	33	A5
Atenolol	0.3	33	A6
Diethyltoluamide	0.3	33	B1
Praziquantel	0.3	33	B2
Prilocaine	0.3	33	B3
Indoprofen	0.3	33	B4
Flurbiprofen	0.3	33	B5
Nabumetone	0.3	33	B6
Naftopidil	0.3	33	C1
Sacubitril	0.3	33	C2
Atazanavir	0.3	33	C3
Tropicamide	0.3	33	C4
Imipramine	0.3	33	C5
(*S)*-Naproxen-OMe	0.3	33	C6
Butenafine	0.3	33	D1
Boc-Maprolitine	0.3	33	D2
Primidone	0.3	33	D3
Benfluorex	0.3	33	D4
(*R*)-Cinacalcet	0.3	33	D5
Phenethyl Resorcinol	0.3	33	D6
$B_2(OH)_4$ (5.0 equiv)	1.5	33	All
$[Rh(COD)OH]_2$	0.012	33	All

Table 2-4 Recipe for 24-Well LSS Screen for Microsomal Stability Studies

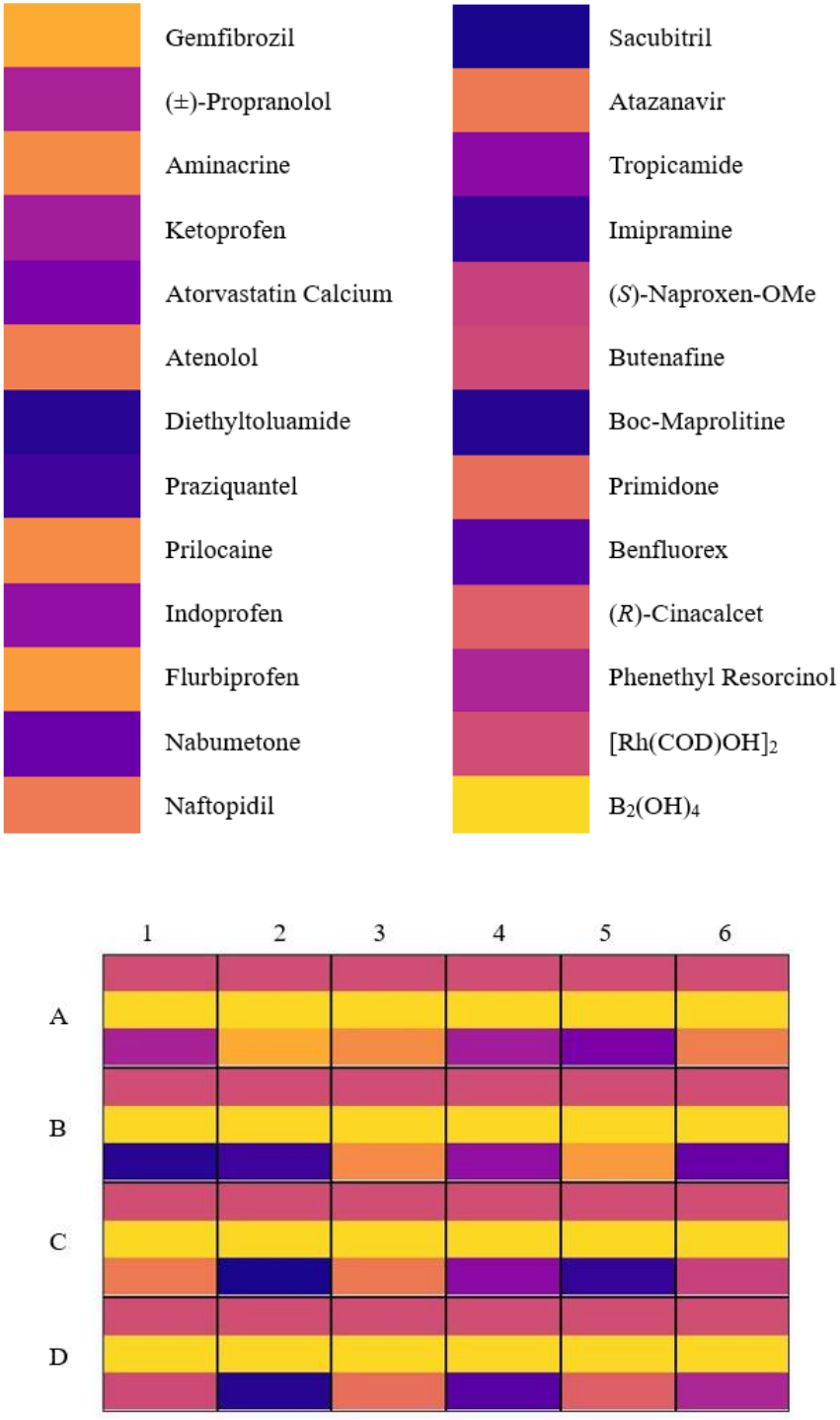


Figure 2-19 Reagents and Grid of Screen for Microsomal Stability Studies

Compound ID	%Remaining Before LSS				%Remaining After LSS				%Change After 60 min
	0 min	15 min	30 min	60 min	0 min	15 min	30 min	60 min	
Gemfibrozil	N.D.	N.D.	N.D.	**N.D.**	N.D.	N.D.	N.D.	**N.D.**	-
(±)-Propranolol	100	95.73	92.97	**90.62**	100	92.51	85.76	**81.28**	**-9.35**
Aminacrine	100	83.65	75.11	**66.24**	100	81.54	68.51	**53.85**	**-12.39**
Ketoprofen	100	61.21	39.88	**30.47**	100	60.22	37.09	**28.25**	**-2.22**
Atorvastatin Calcium	100	96.55	93.76	**91.69**	100	91.03	83.61	**78.58**	**-13.1**
Atenolol	100	90.62	82.55	**75.78**	100	89.79	82.82	**77.49**	**1.71**
Diethyltoluamide	100	89.01	81.69	**75.45**	100	89.66	82.06	**76.26**	**0.82**
Praziquantel	100	62.99	31.78	**15.26**	100	60.01	27.08	**0**	**-15.26**
Prilocaine	100	86.01	75.01	**67.4**	100	78.04	64.04	**53.63**	**-13.77**
Indoprofen	100	97.61	99.05	**101.53**	100	95.1	91.05	**87.49**	**-14.04**
Flurbiprofen	100	50.08	25.06	**9.28**	100	65.01	29.01	**16.41**	**7.13**
Nabumetone	100	58.01	40.66	**21.73**	100	57.53	37.99	**26.97**	**5.23**
Naftopidil	100	72.22	58.9	**47.01**	100	69.53	39.56	**21.37**	**-25.63**
Sacubitril	100	60.16	34.05	**22.58**	100	58.76	33.78	**20.67**	**-1.91**
Atazanavir	100	84.65	72.9	**65.29**	100	81.14	68.89	**59.92**	**-5.37**
Tropicamide	100	95.19	91.88	**88.12**	100	93.81	89.56	**85.51**	**-2.61**
Imipramine	100	76.13	62.51	**53.47**	100	74.77	59.61	**48.1**	**-5.36**
(*S*)-Naproxen-OMe	N.D.	N.D.	N.D.	**N.D.**	100	N.D.	N.D.	**N.D.**	-
Butenafine	100	97.75	95.61	**94.86**	100	96.73	93.97	**92.17**	**-2.69**
Boc-Maprolitine	100	71.56	59.39	**45.29**	100	69.65	46.83	**38.05**	**-7.24**
Primidone	100	71.03	43.6	**27.78**	100	70.43	44.65	**29.94**	**2.16**
Benfluorex	100	N.D.	N.D.	**N.D.**	N.D.	N.D.	N.D.	**N.D.**	-
(*R*)-Cinacalcet	100	67.41	49.02	**35.4**	100	63.72	45.98	**33.7**	**-1.7**
Phenethyl Resorcinol	N.D.	N.D.	N.D.	**N.D.**	N.D.	N.D.	N.D.	**N.D.**	-

Table 2-5 Comparison of %remaining of parent arene compounds after 60 minutes of exposure to human liver microsomes. Determined by LC-MS integration of parent compound relative to caffeine internal standard.

N.D. = Not determined

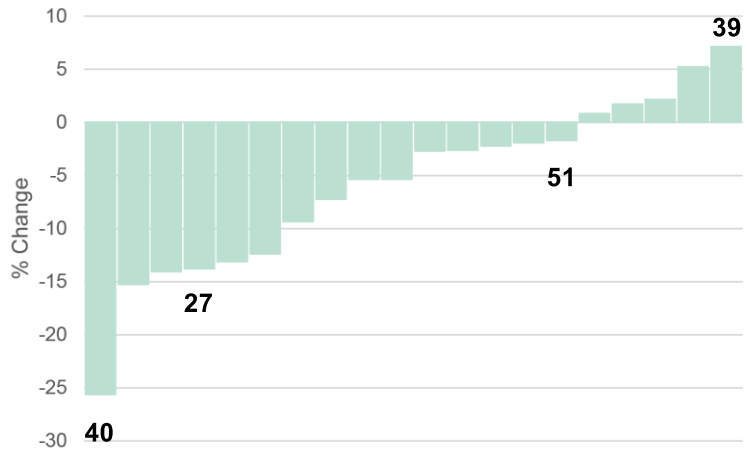


Figure 2-20 Difference in metabolic stability of 20 drugs determined before and after late-stage saturation. Ordered by increasing metabolic stability of saturated congener relative to its unsaturated parent material

2.5.5 Measurement of $LogP_{o/w}$

General procedure

1). Preparation of standard solutions for compound.

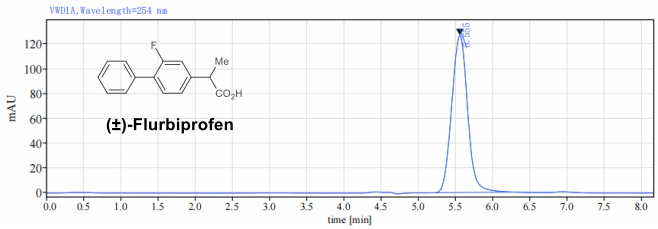
The compound (5.00 mg) was weighed precisely, placed in a 10 mL volumetric flask, added with acetonitrile and dissolved by ultrasonication, fixed volume, and shaken well to obtain a solution of the compound with a mass concentration of 0.5 mg/mL.

2). Establishment of standard curve.

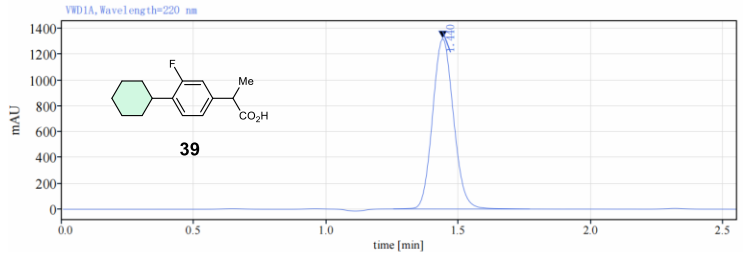
To acetonitrile (1.0 ml) 10, 20, 30, 40, 50, 60, 70 μl of the solution were added to obtain 7 sets of standard solutions of A1 to A7 with different mass concentrations. The samples (A1 - A7) were filtered through 0.22 μm microporous filter membrane and injected into Reversed-phase HPLC (RP-HPLC) for determination and the peak areas (Y1 - Y7) were recorded. The regression equation in table S26 was derived by linear regression analysis using the mass concentration (X, mg/mL) of the compounds as the horizontal coordinate and the peak area value (Y) as the vertical coordinate. (linear regression equation: Y＝a•X + b; a, b are fit coefficients)

Compound	Wavelength (nm)	MeCN/H_2O	Flow Rate (mL/min)	T_r (min)
(±)-Flurbiprofen	254	80 : 20	0.2	5.555
27	220	90 : 10	1.0	1.440
(±)-Indoprofen	210	90 : 10	0.2	5.384
37	210	90 : 10	0.2	5.755
(*2S*,*4R*)-Sacubitril	210	90 : 10	0.2	5.708
70	220	90 : 10	0.2	6.799
Chromatographic conditions: Agilent Ltd Poroshell 120 (EC-C18, 4.6 × 100 mm, 2.7 μm), MeCN/H_2O, 40 °C				

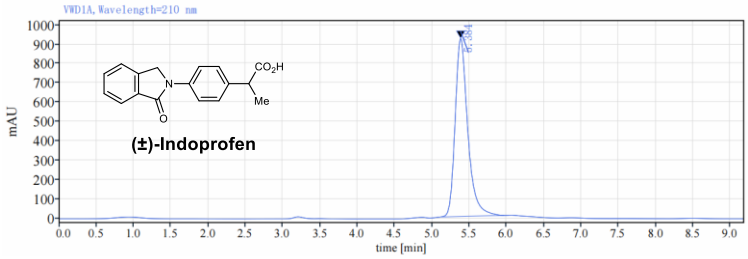
Table 2-6 RP-HPLC separation conditions of compounds



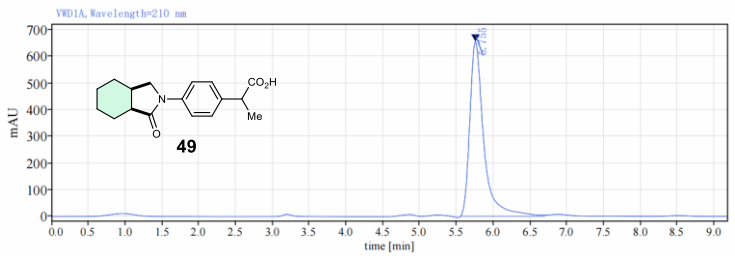
rettime [min]	type	width [min]	area	height	area%
5.555	MM m	1.06	1883.73	126.63	100.00



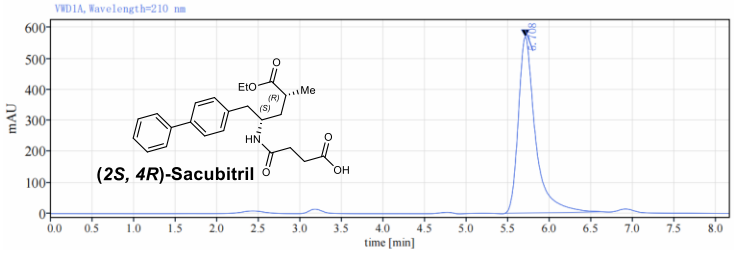
rettime [min]	type	width [min]	area	height	area%
1.440	MM m	0.52	7247.36	1321.62	100.00



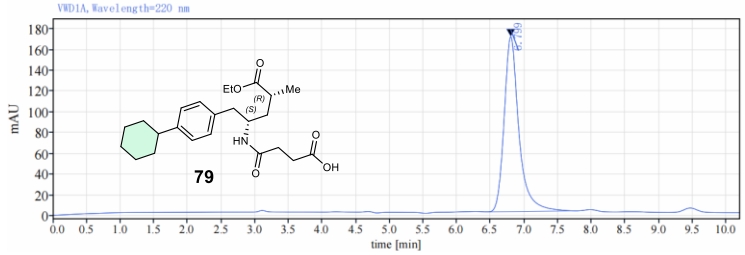
rettime [min]	type	width [min]	area	height	area%
5.384	MM m	0.86	10815.79	918.06	100.00



rettime [min]	type	width [min]	area	height	area%
5.755	MM m	1.14	8677.62	654.85	100.00



rettime [min]	type	width [min]	area	height	area%
5.708	MM m	1.18	8113.46	568.71	100.00

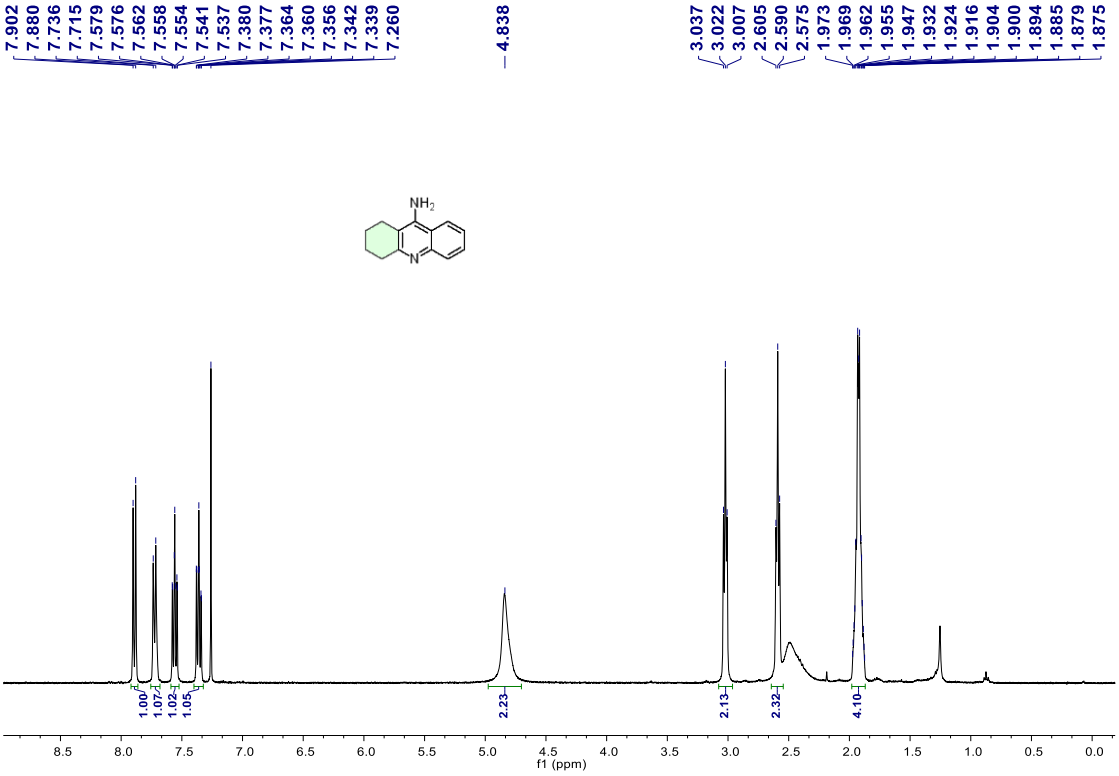


rettime [min]	type	width [min]	area	height	area%
6.799	MM m	1.39	2560.11	168.21	100.00

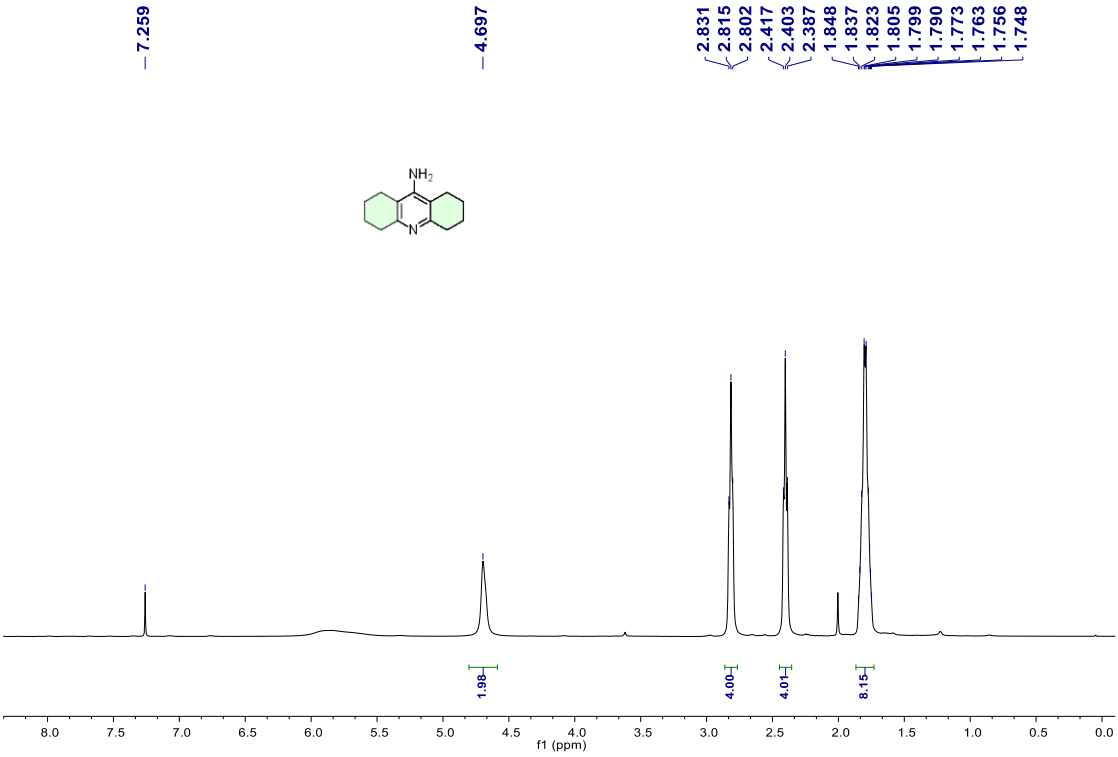
Compound	**Linear Regression Equation**	***R*²**	**Linearity Range** (mg/mL)
(±)-Flurbiprofen	Y = 197293.665•X − 59.181	0.99917	0.005 - 0.033
39	Y = 15834.360•X − 16.576	0.99908	0.010 - 0.041
(±)-Indoprofen	Y = 334318.323•X − 172.298	0.99977	0.005 - 0.033
49	Y = 262994.605•X + 131.012	0.99942	0.005 - 0.033
(2S,4R)-Sacubitril	Y = 326954.136•X + 263.693	0.99946	0.005 - 0.033
79	Y = 113686.699•X + 93.459	0.99957	0.005 - 0.033

Table 2-7 Standard equation and linearity of compounds (n = 7)

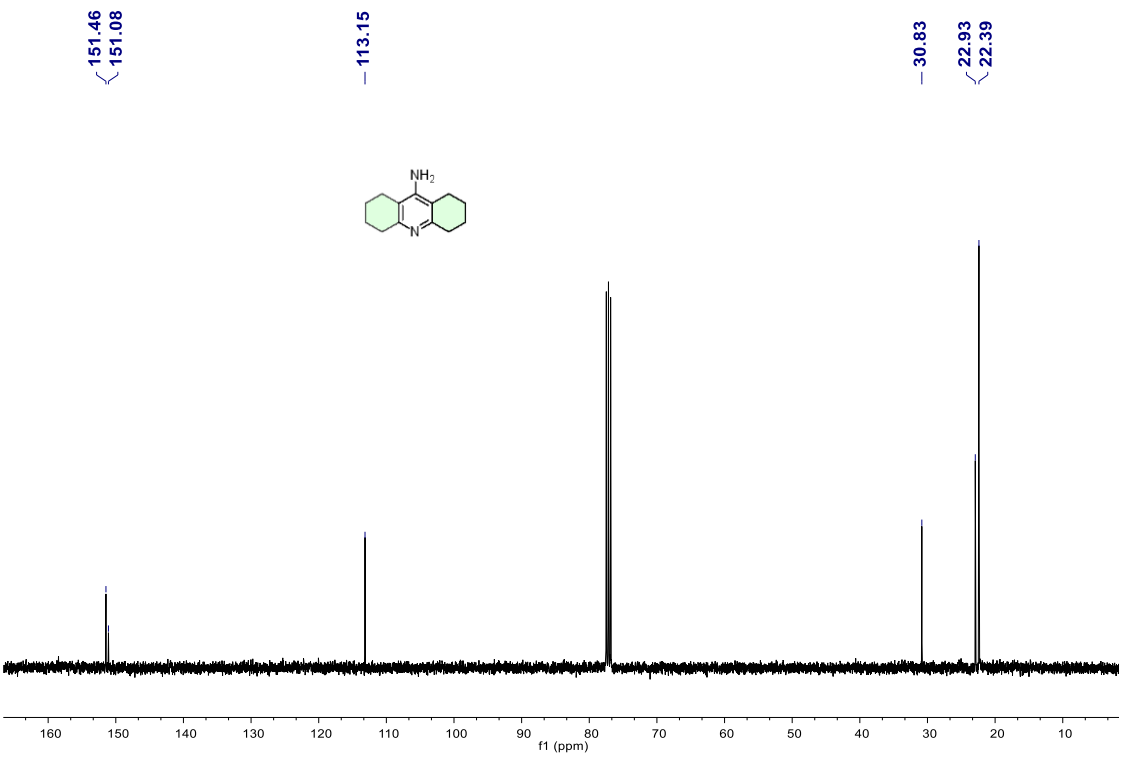
2.6 **Spectra**



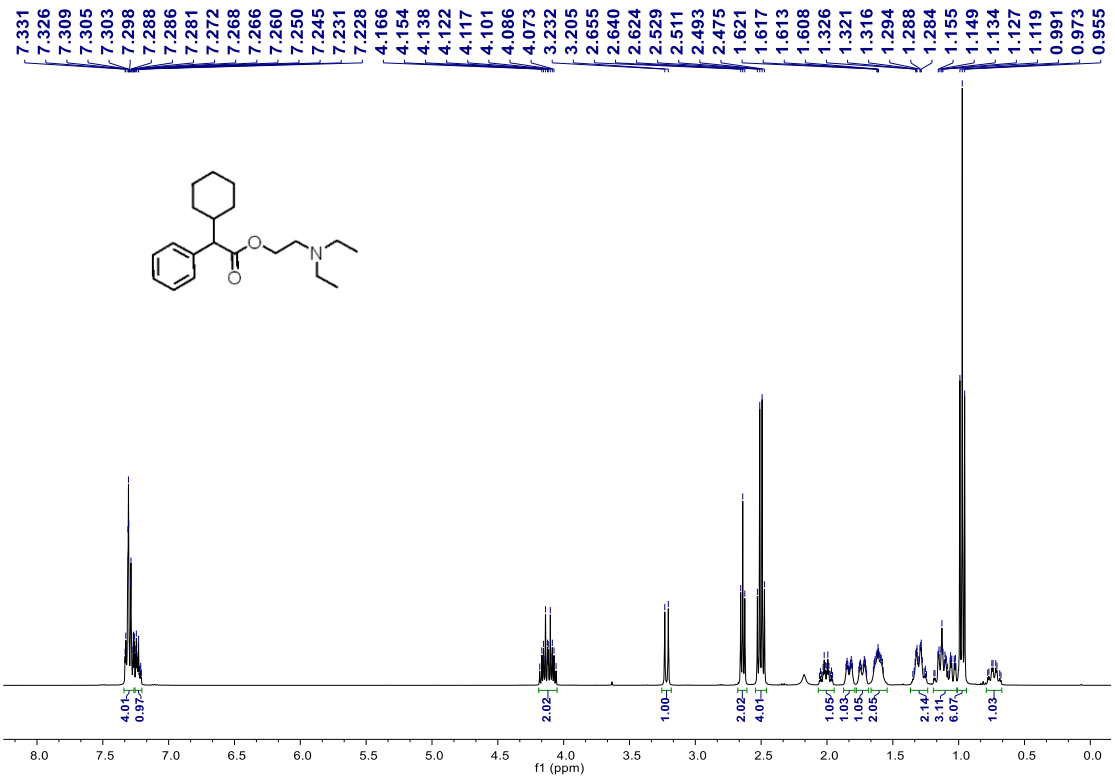
Spectrum 2-1 ^{1}H NMR of compound 20



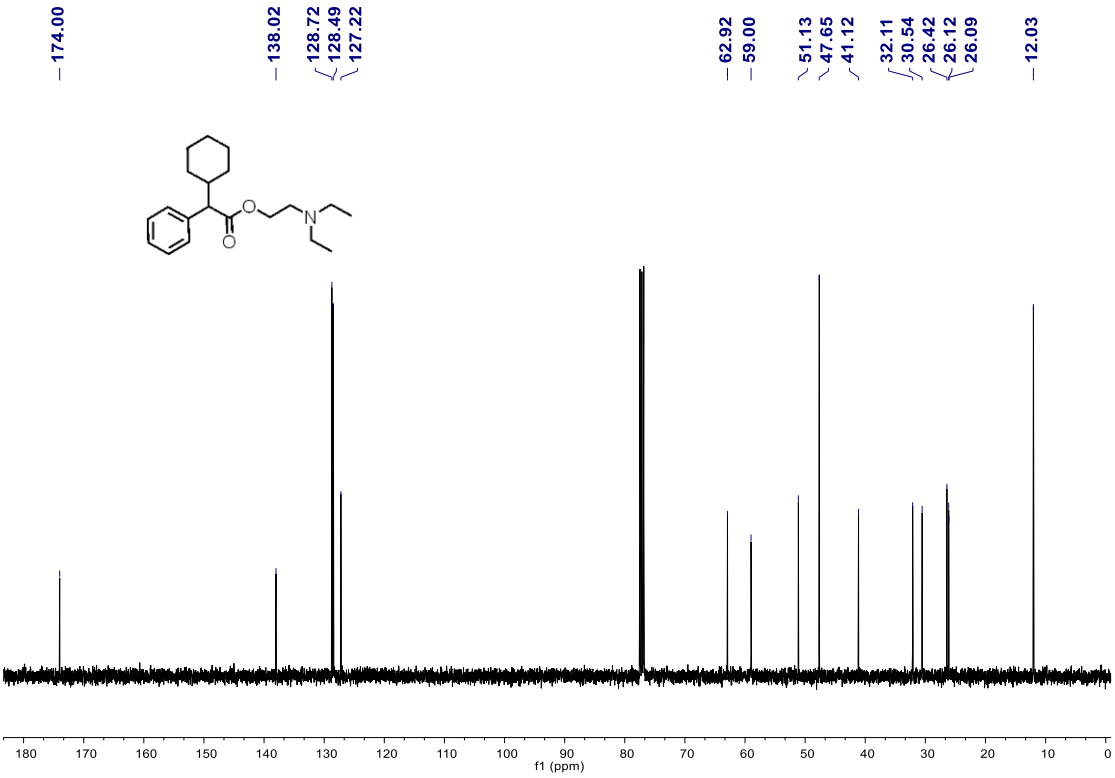
Spectrum 2-2 ^{1}H NMR of compound 21



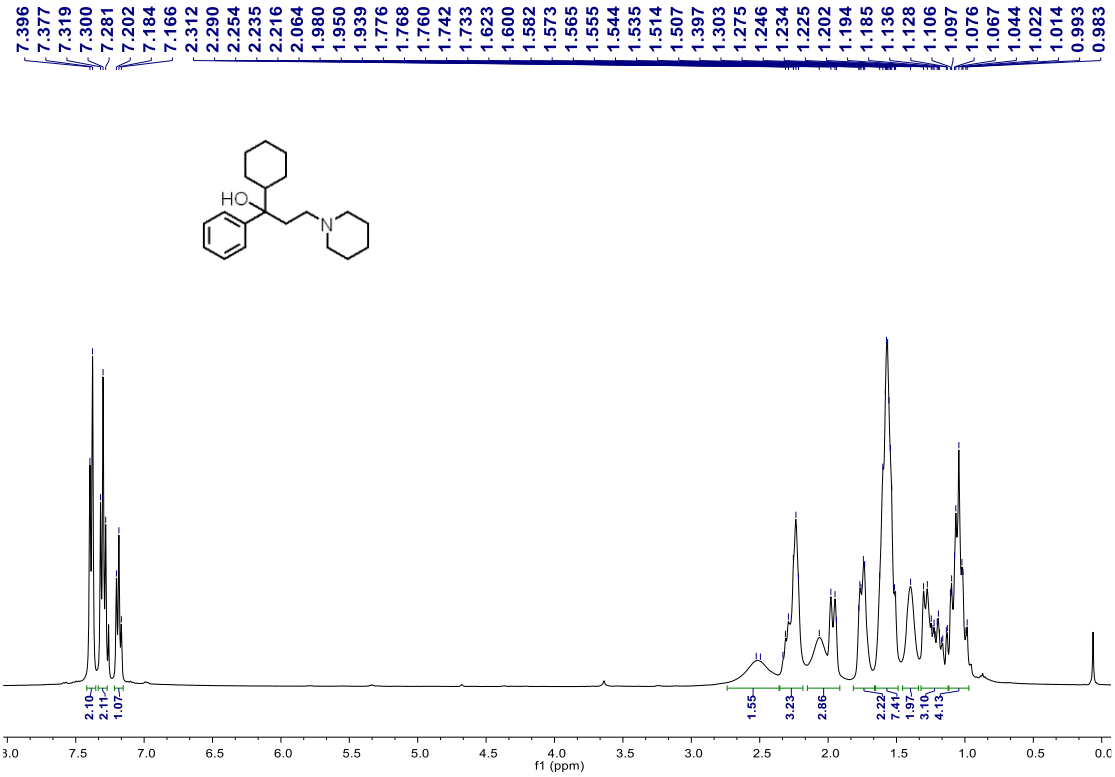
Spectrum 2-3 ^{13}C NMR of compound 21



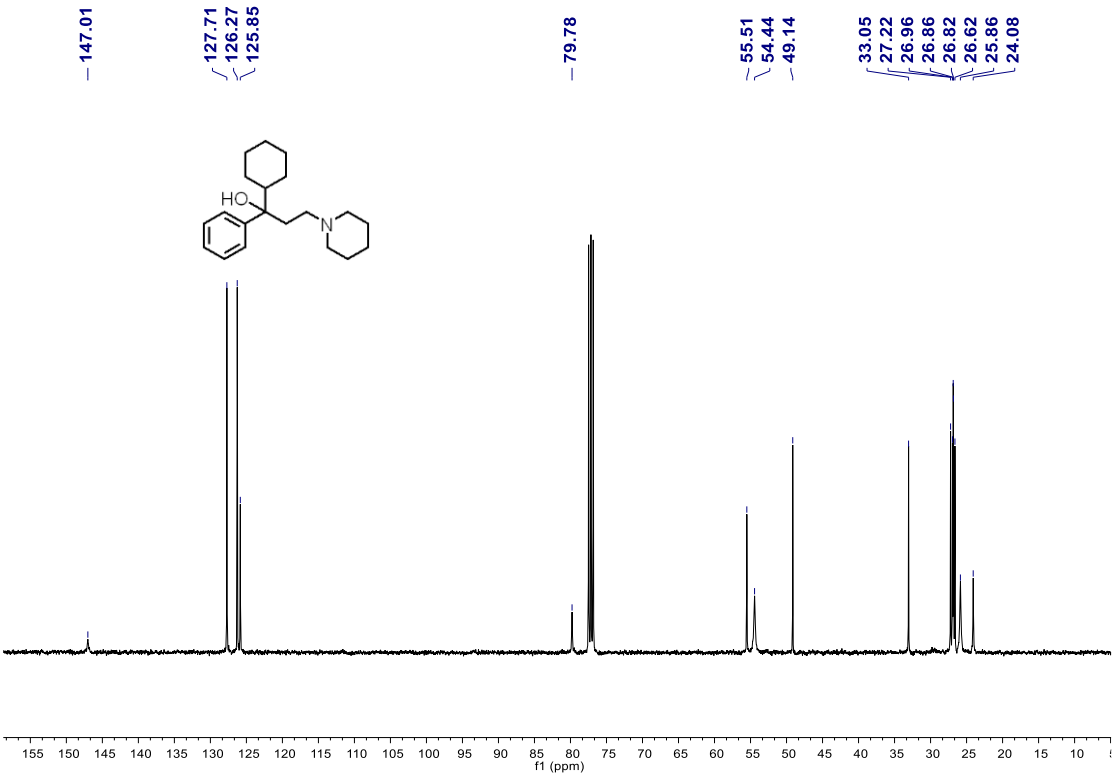
Spectrum 2-4 ^{1}H NMR of compound 23



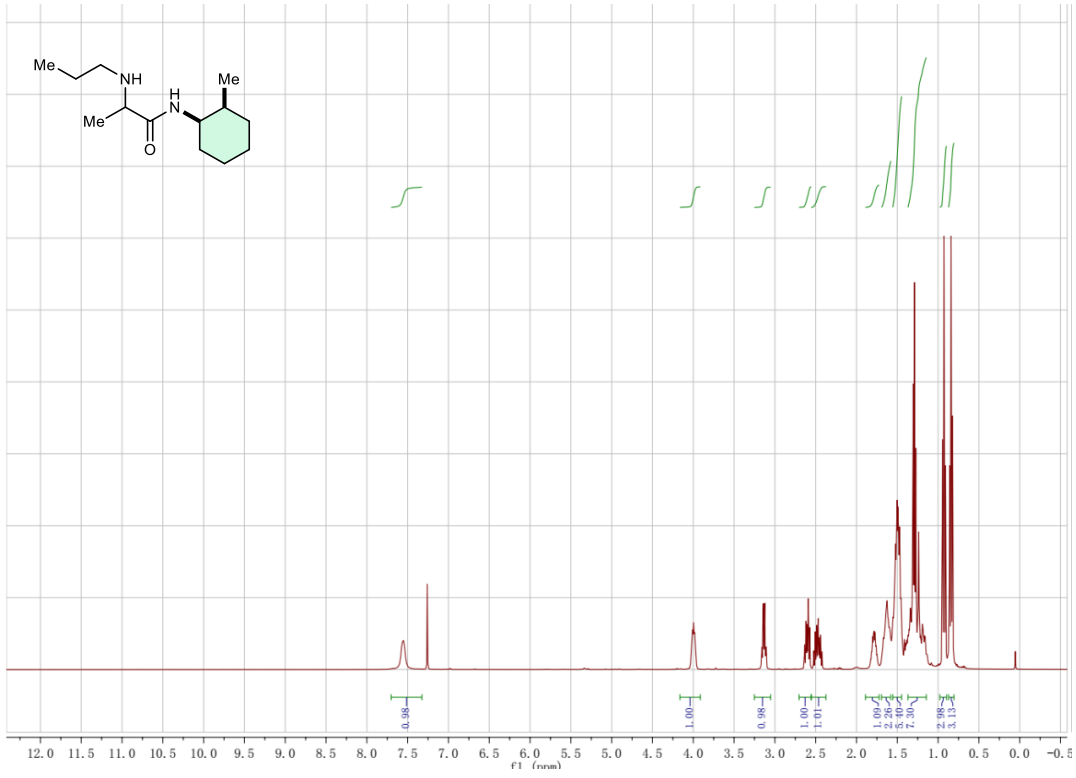
Spectrum 2-5 ^{13}C NMR of compound 23



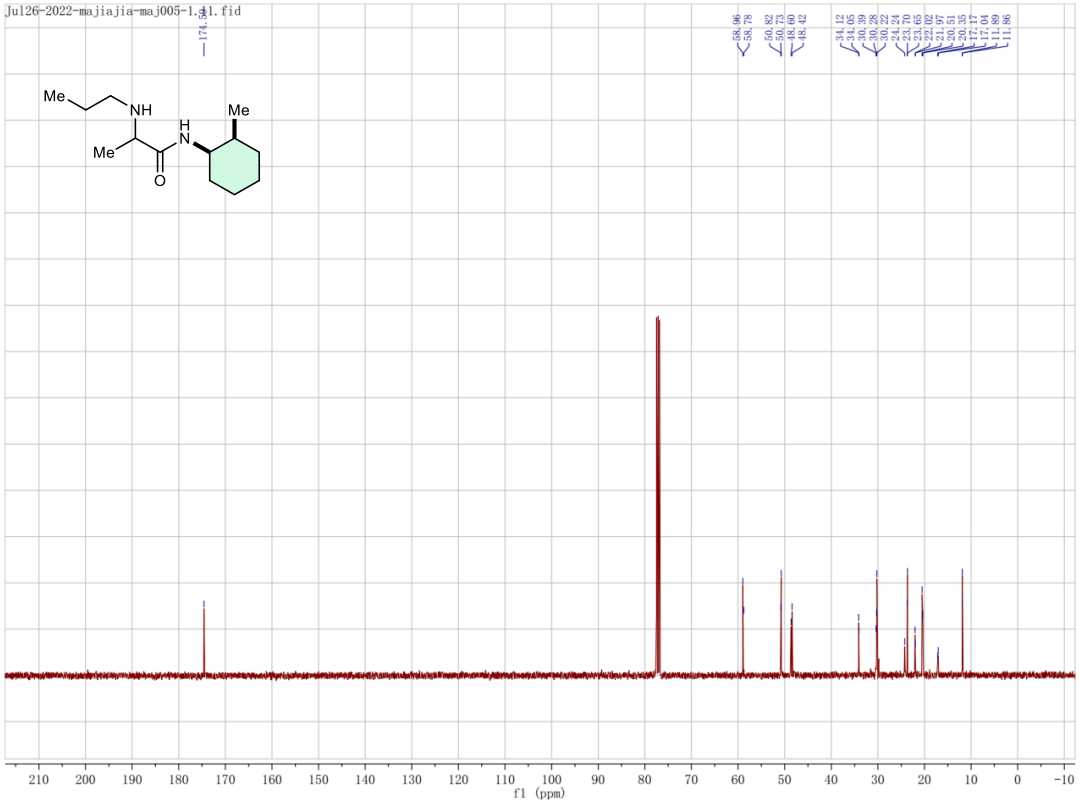
Spectrum 2-6 ^{1}H NMR of compound 25



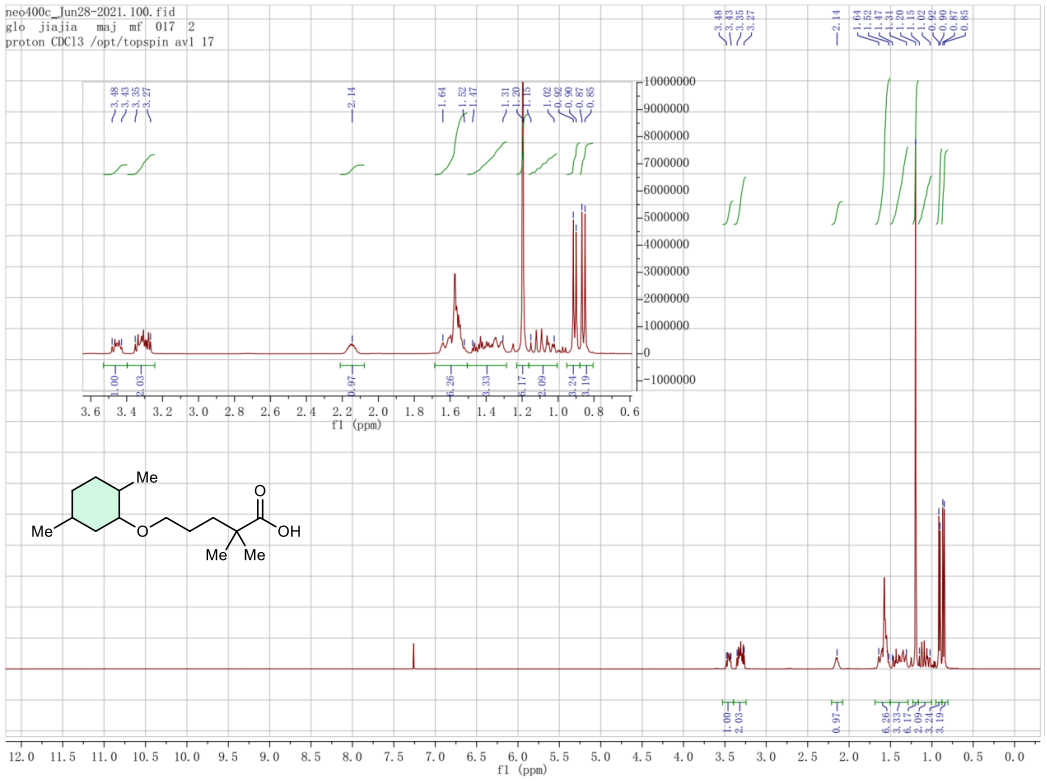
Spectrum 2-7 ^{13}C NMR of compound 25



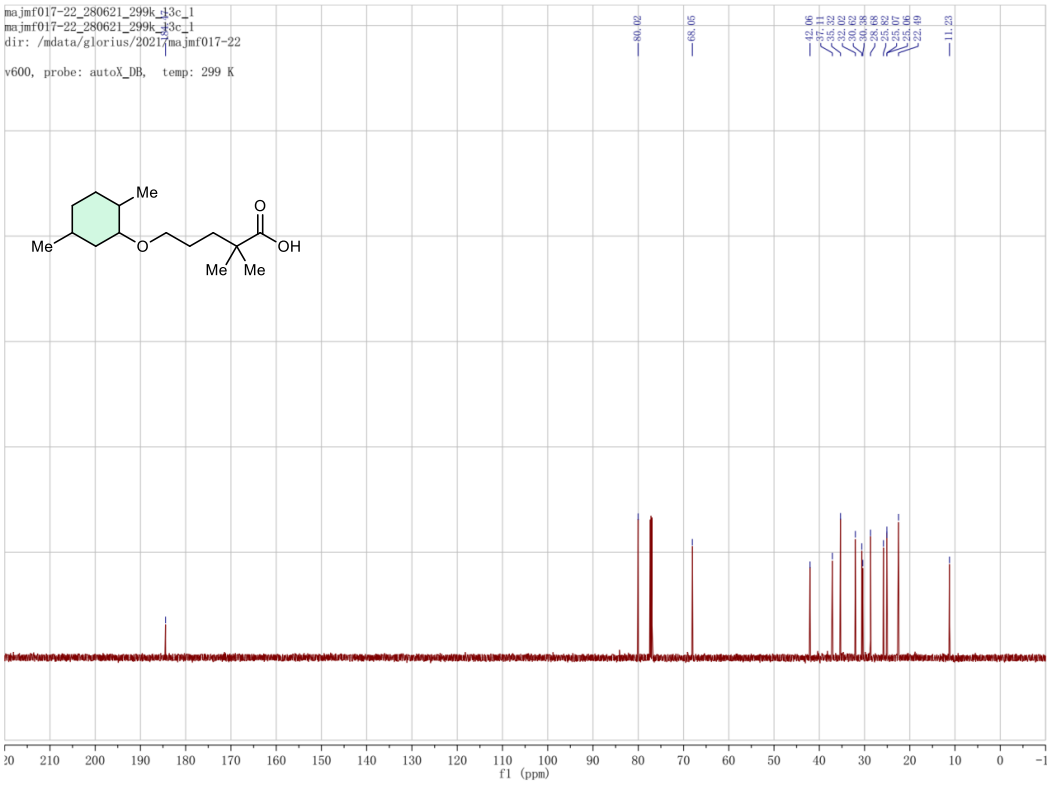
Spectrum 2-8 ^{1}H NMR of compound 27



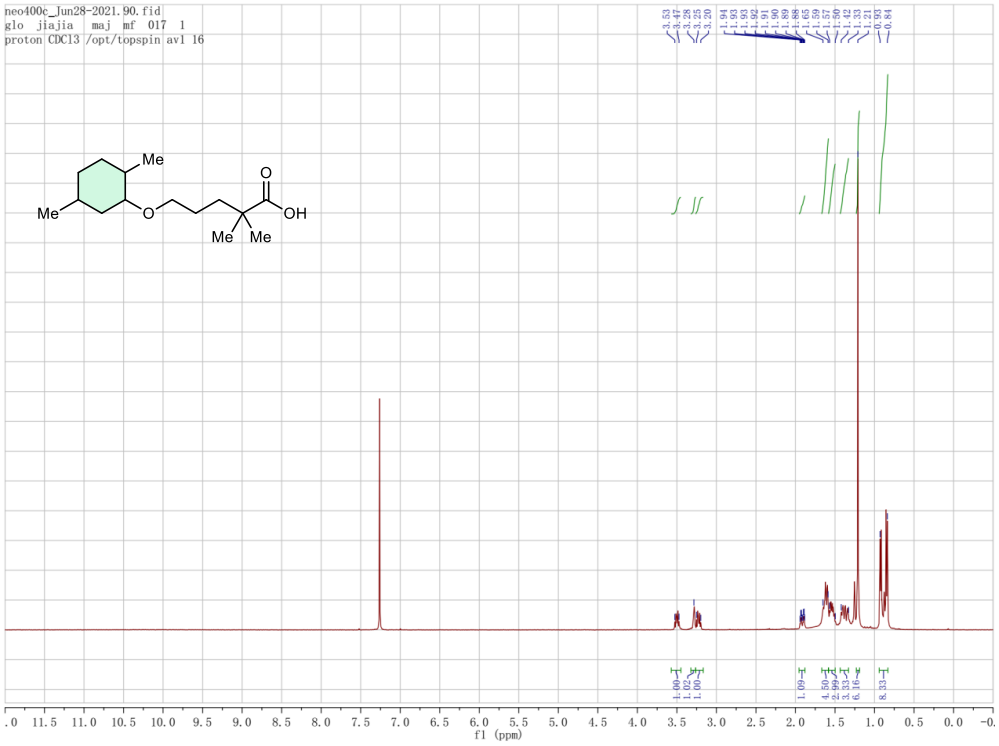
Spectrum 2-9 ^{13}C NMR of compound 27



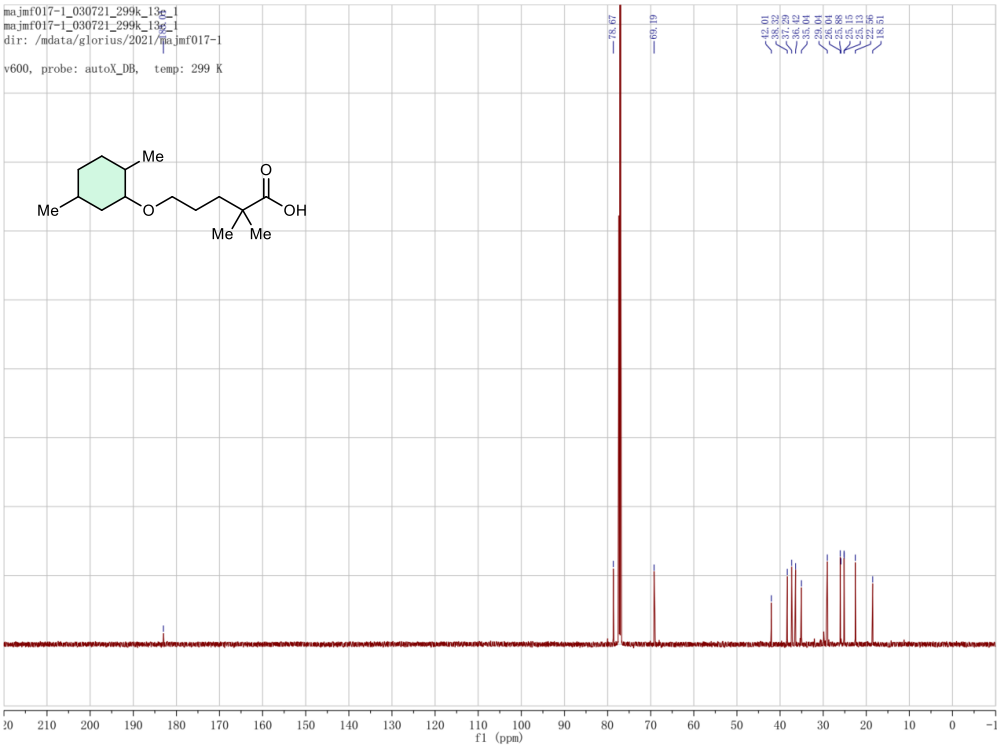
Spectrum 2-10 ^{1}H NMR of compound 29a



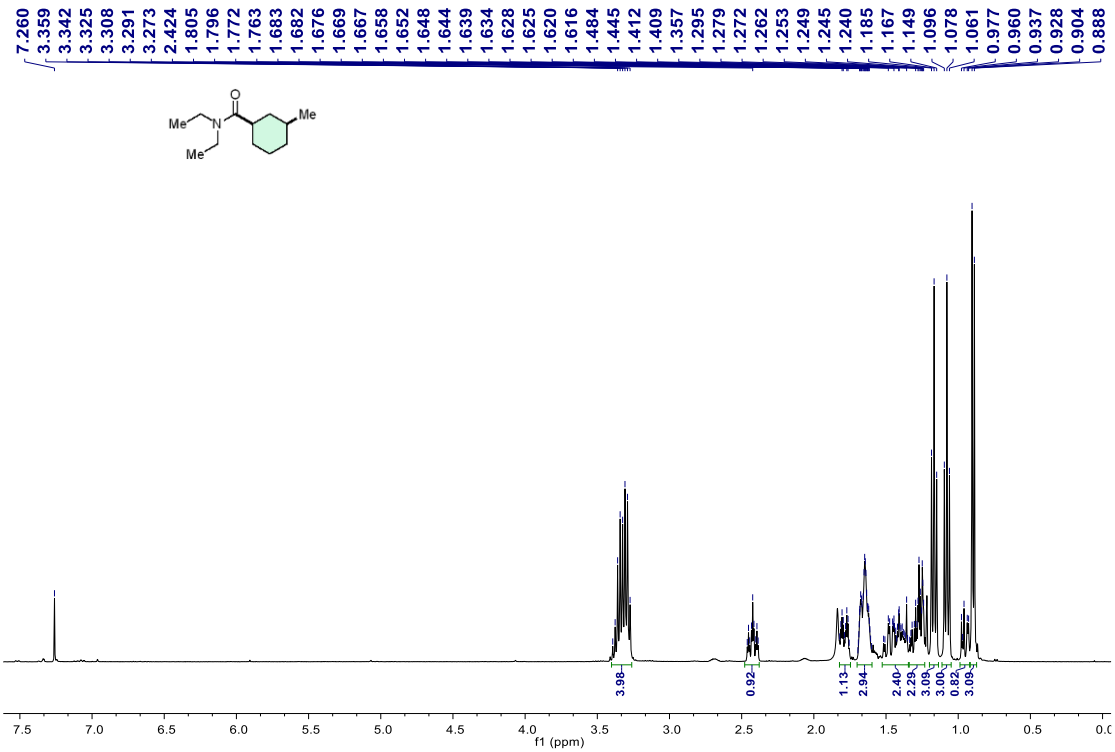
Spectrum 2-11 ^{13}C NMR of compound 29a



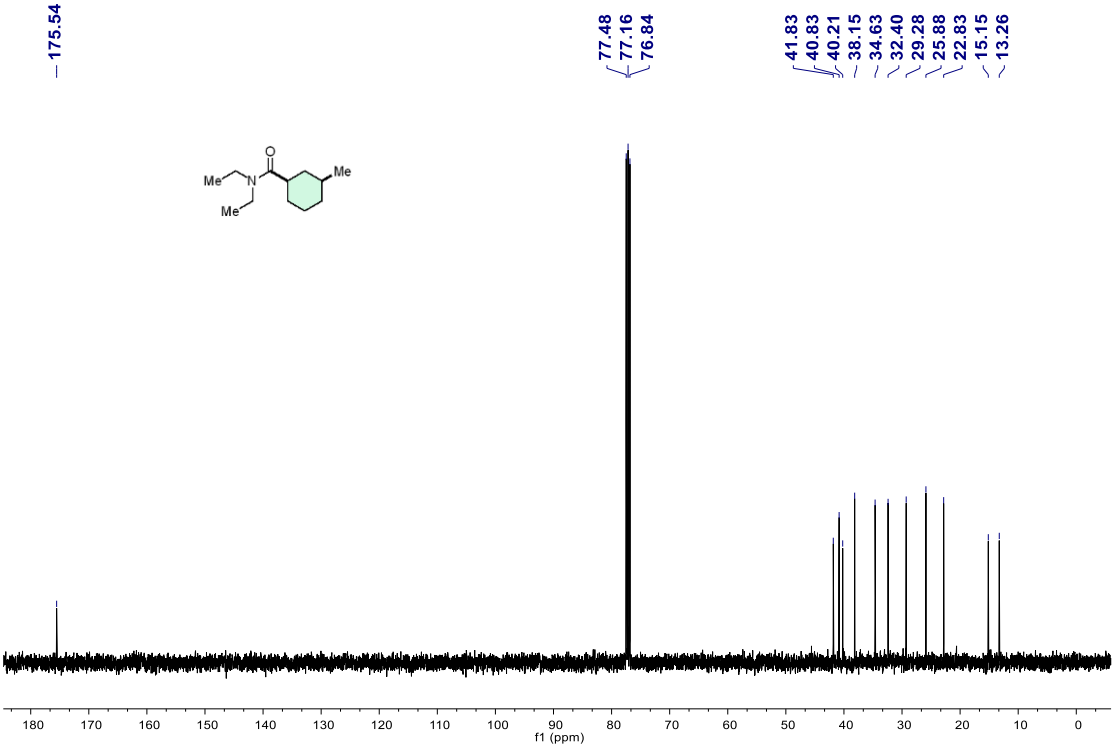
Spectrum 2-12 ^{1}H NMR of compound 29b



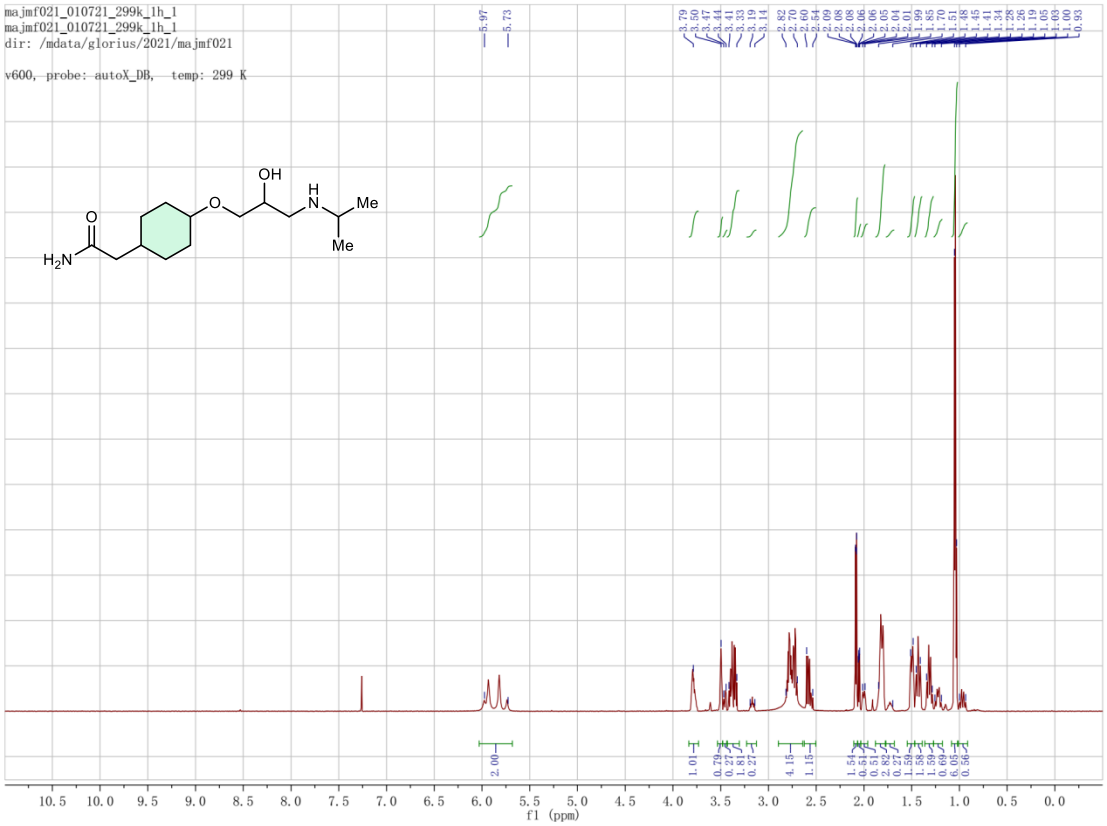
Spectrum 2-13 ^{13}C NMR of compound 29b



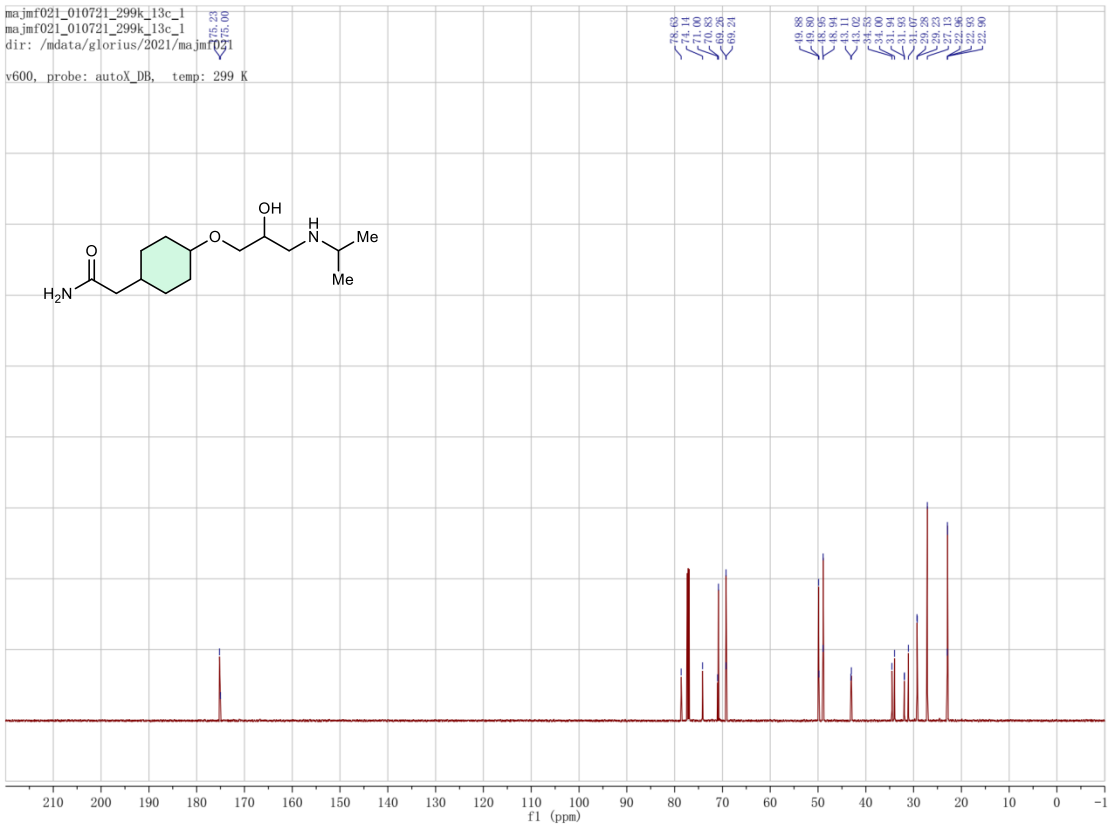
Spectrum 2-14 ^{1}H NMR of compound 31



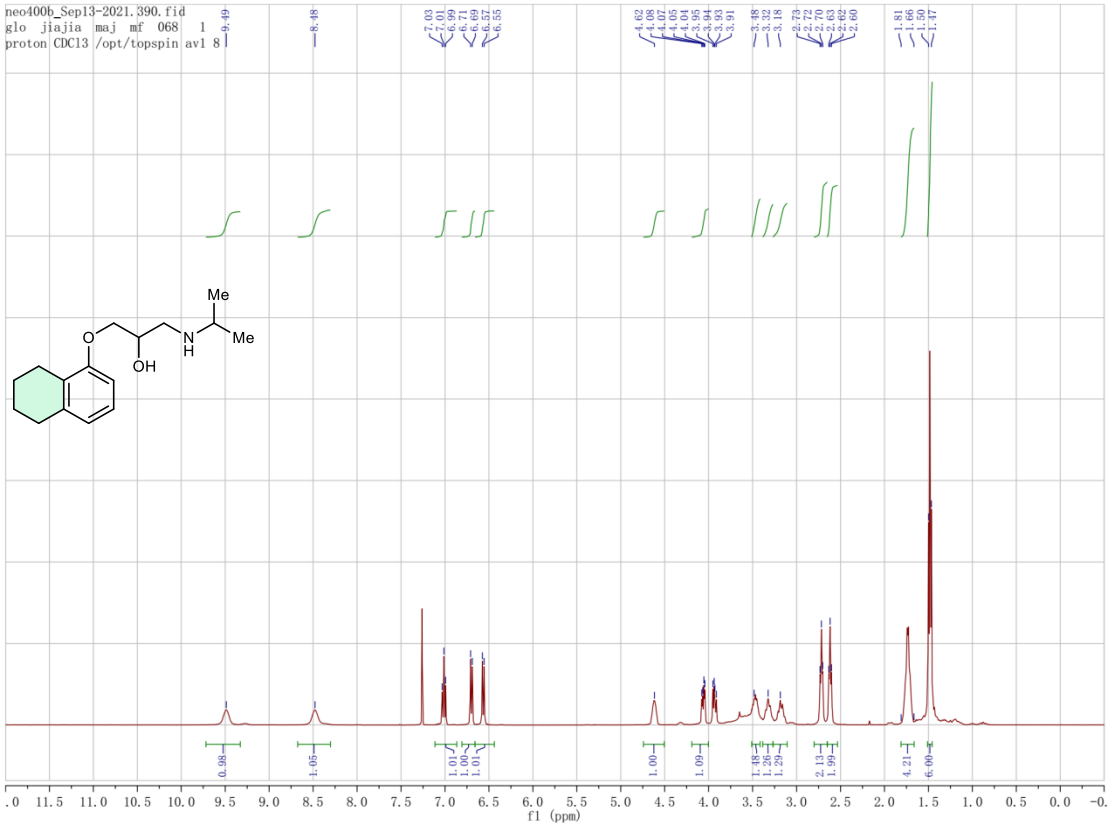
Spectrum 2-15 ^{13}C NMR of compound 31



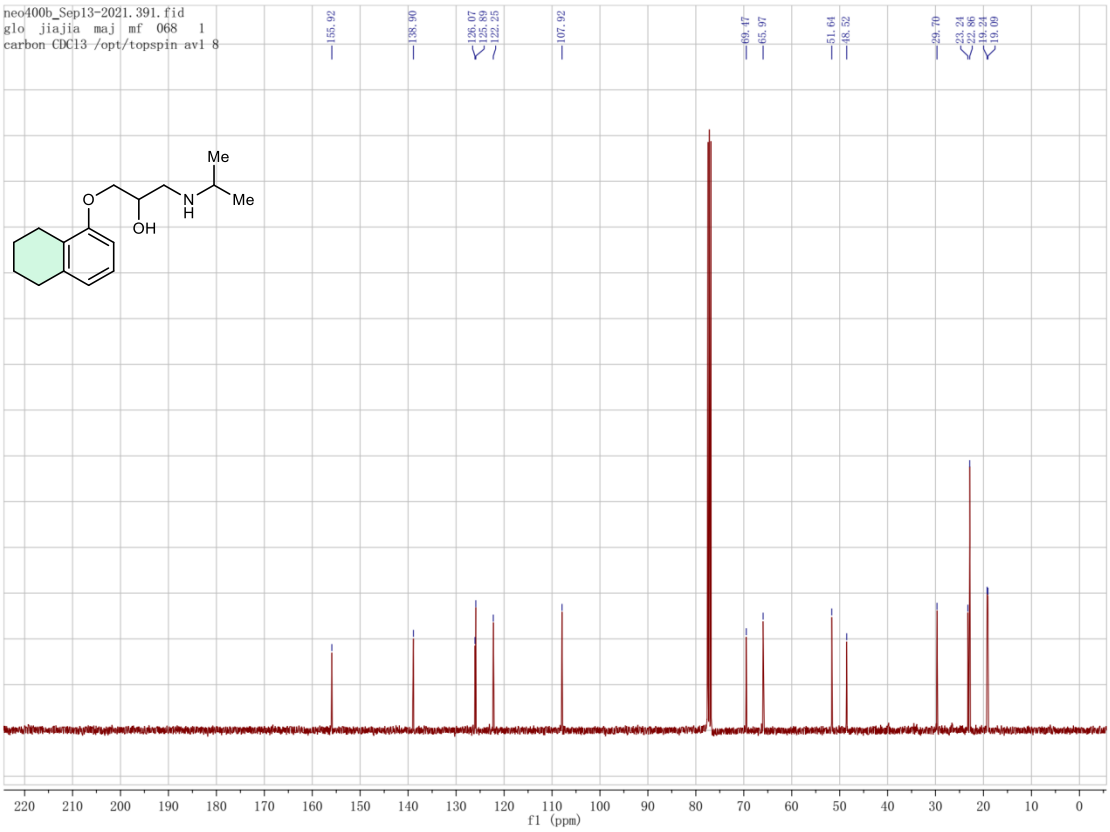
Spectrum 2-16 ^{1}H NMR of compound 33



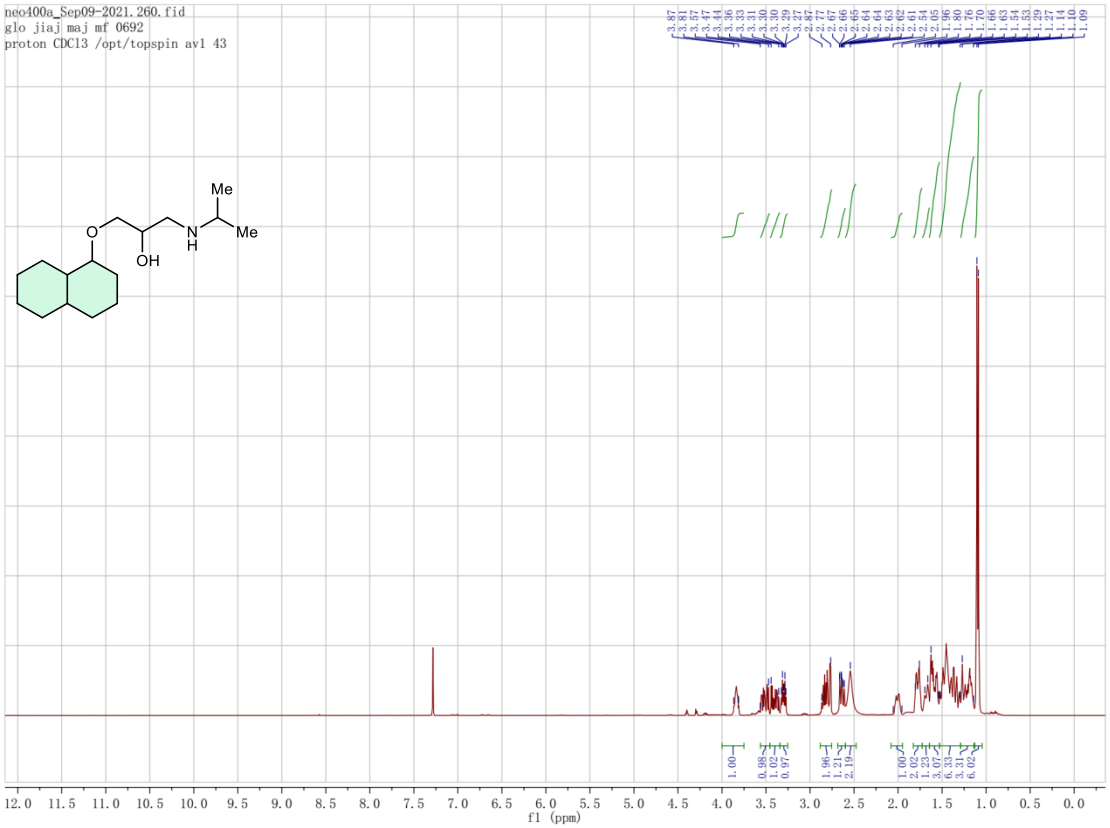
Spectrum 2-17 ^{13}C NMR of compound 33



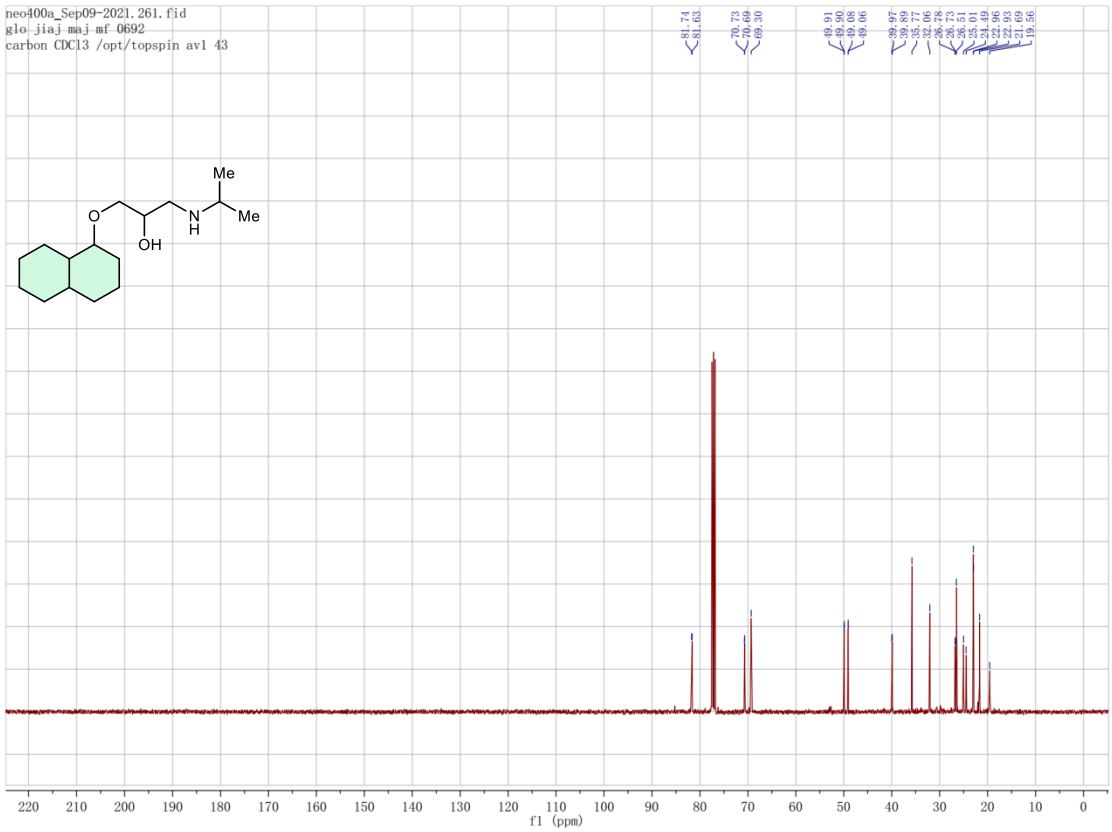
Spectrum 2-18 ^{1}H NMR of compound 35



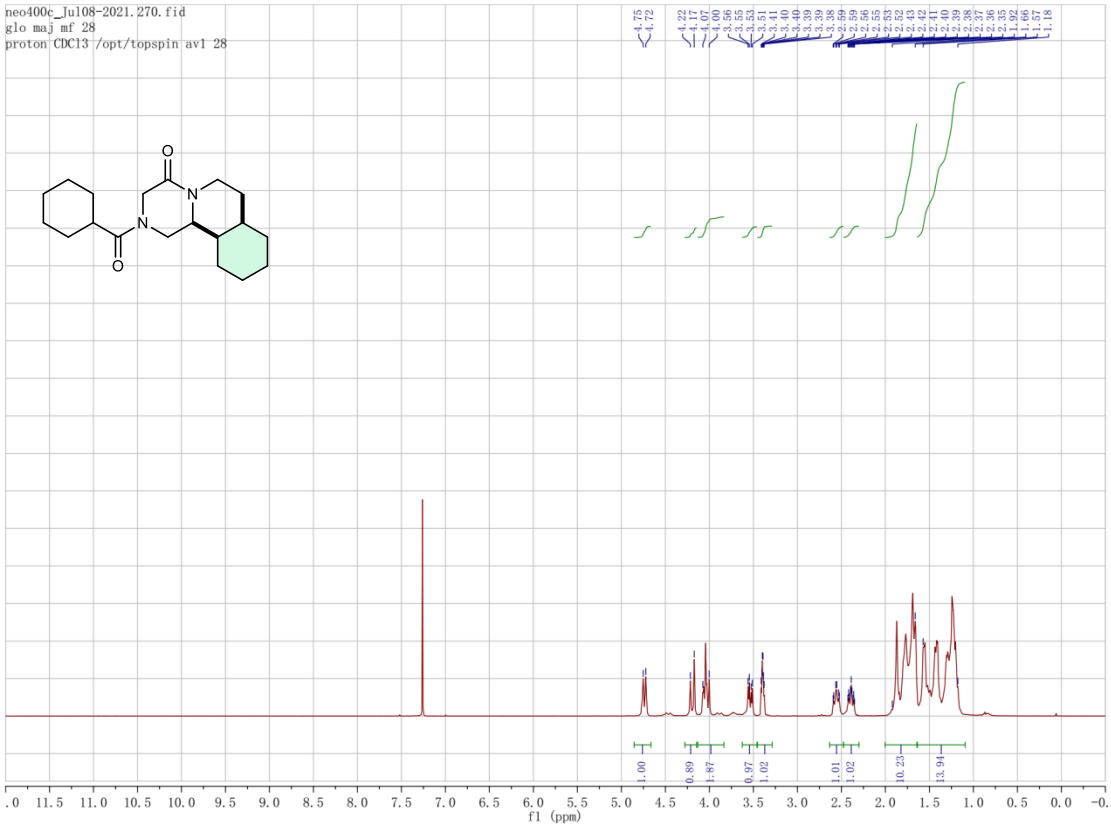
Spectrum 2-19 ^{13}C NMR of compound 35



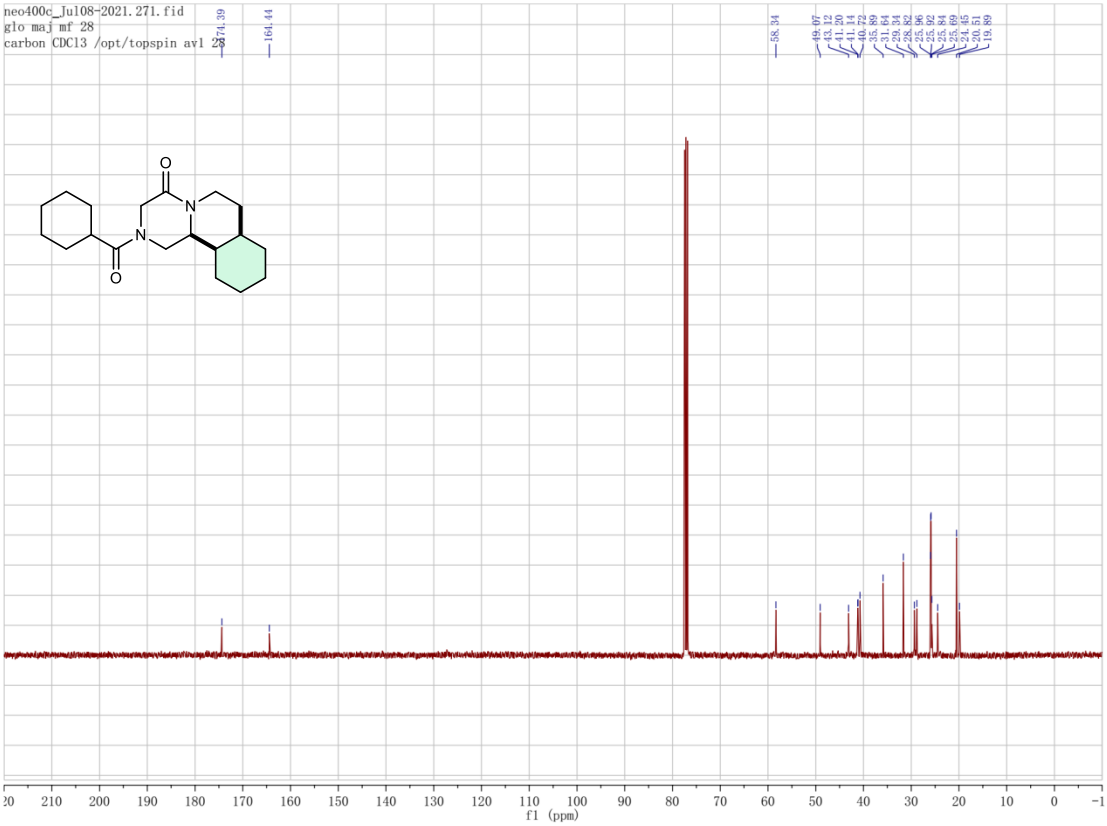
Spectrum 2-20 ^{1}H NMR of compound 35’



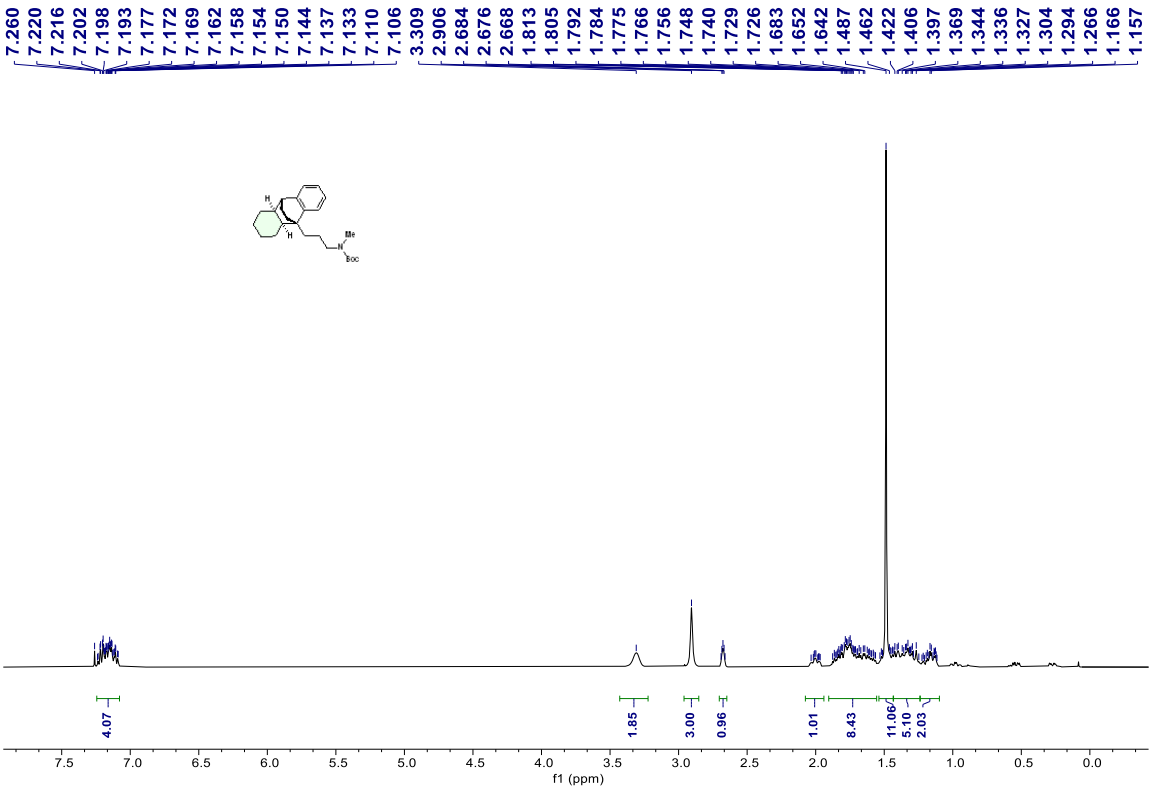
Spectrum 2-21 ^{13}C NMR of compound 35'



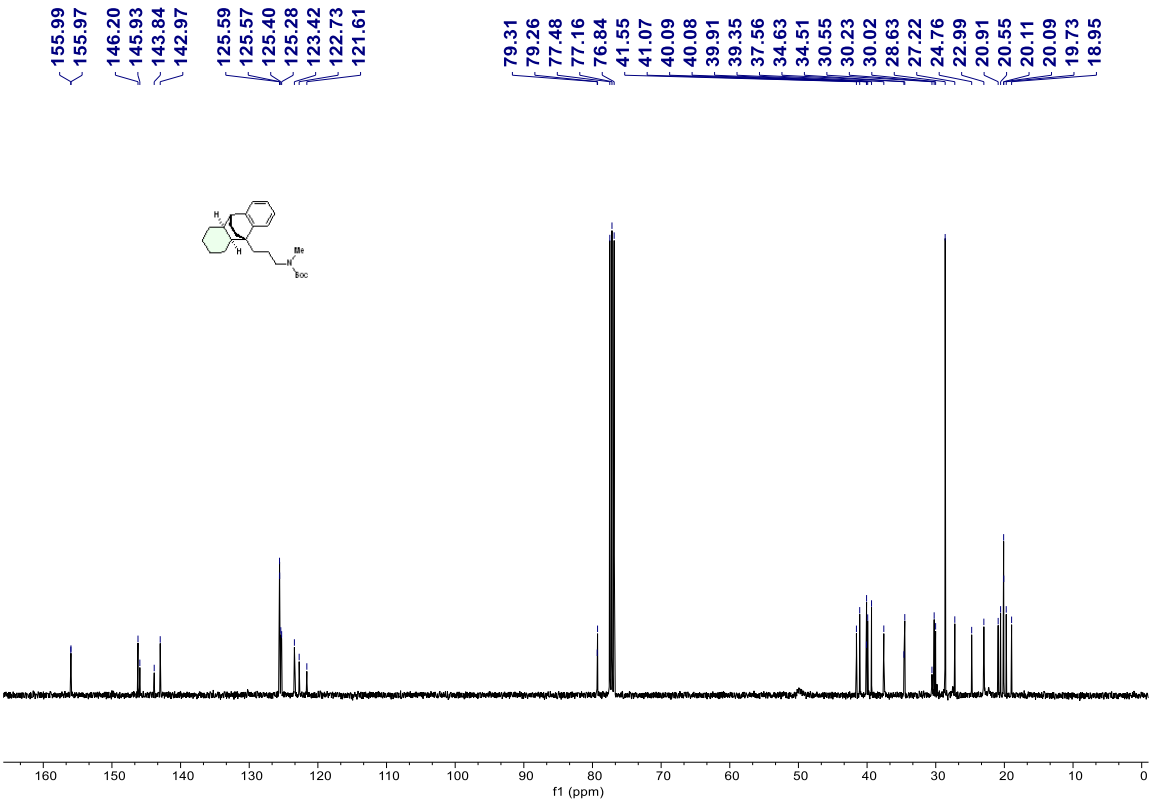
Spectrum 2-22 ^{1}H NMR of compound 37



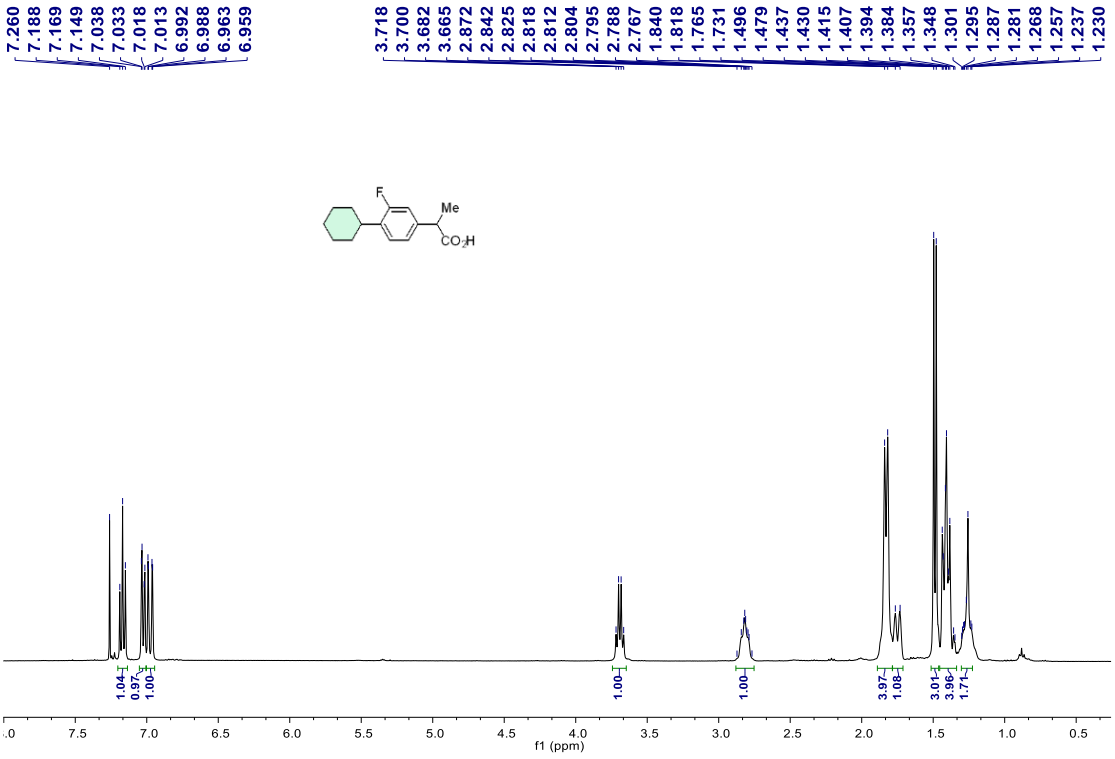
Spectrum 2-23 ^{13}C NMR of compound 37



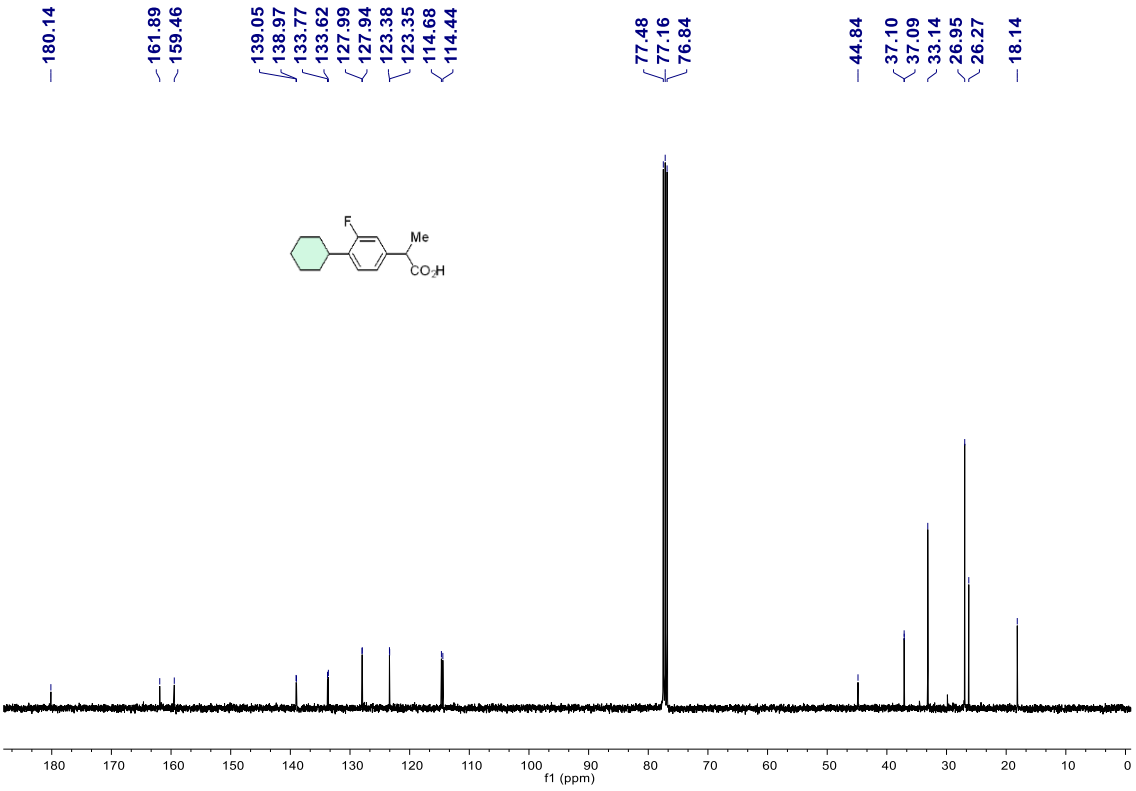
Spectrum 2-24 ^{1}H NMR of compound 38



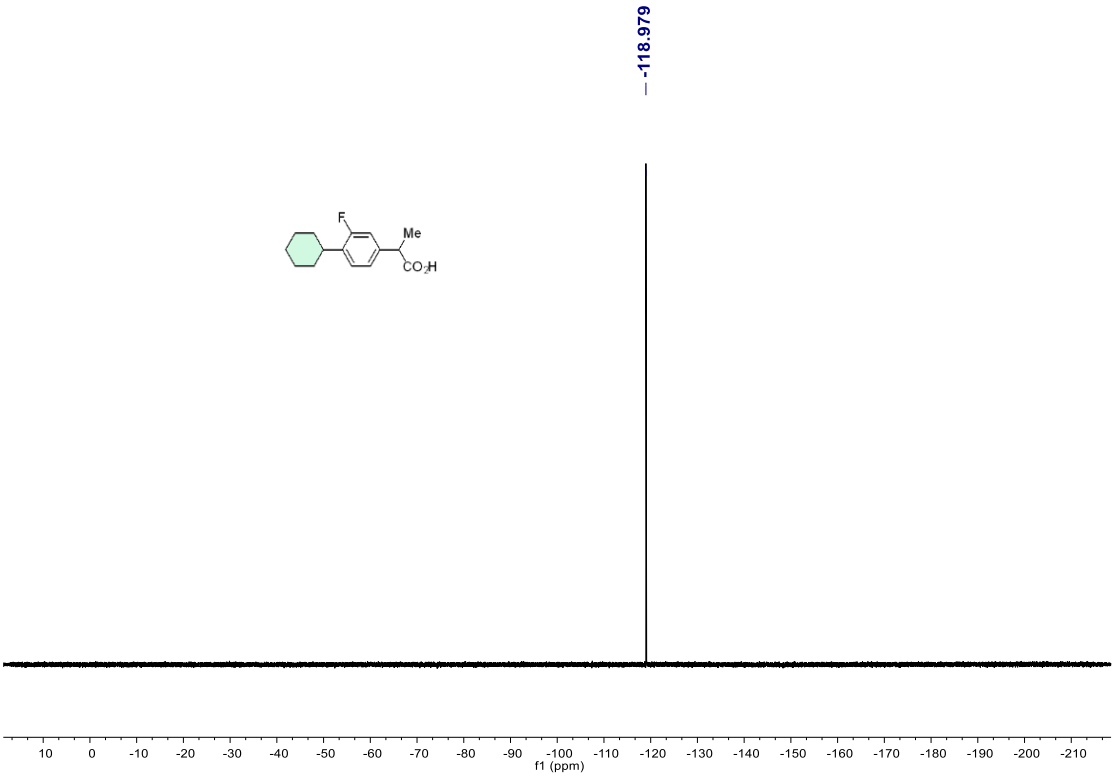
Spectrum 2-25 ^{13}C NMR of compound 38



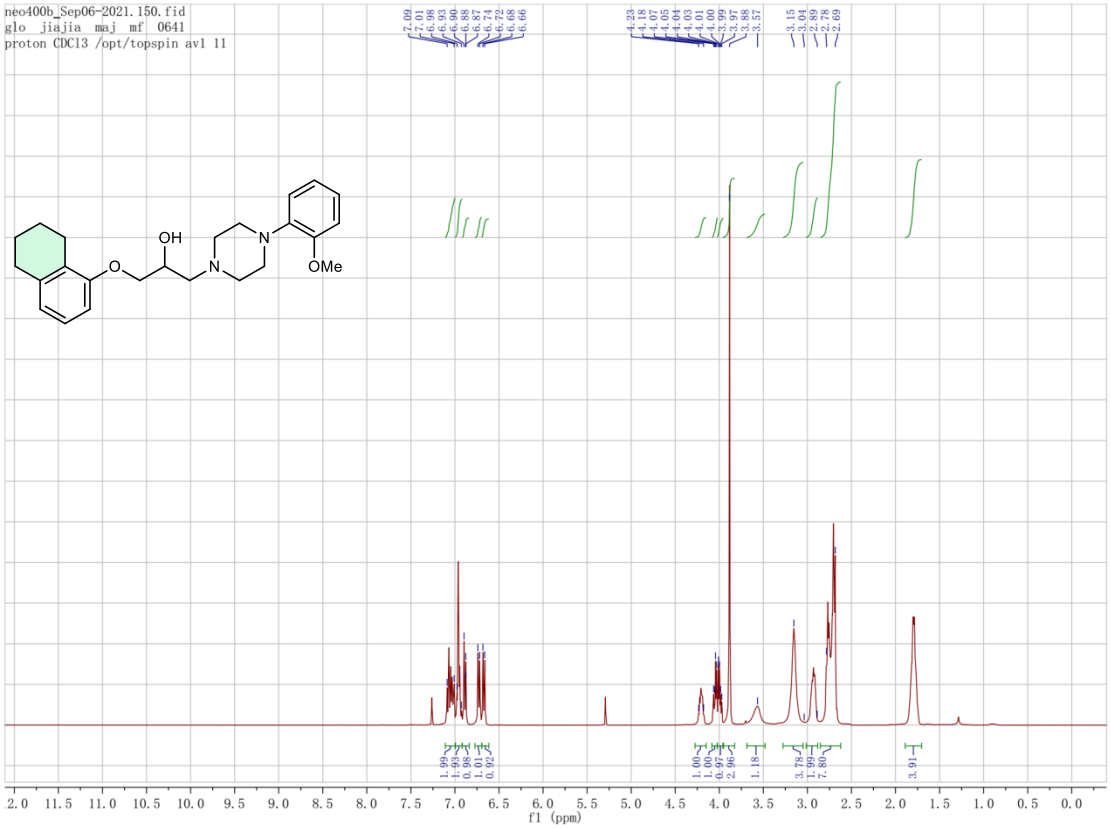
Spectrum 2-26 ^{1}H NMR of compound 39



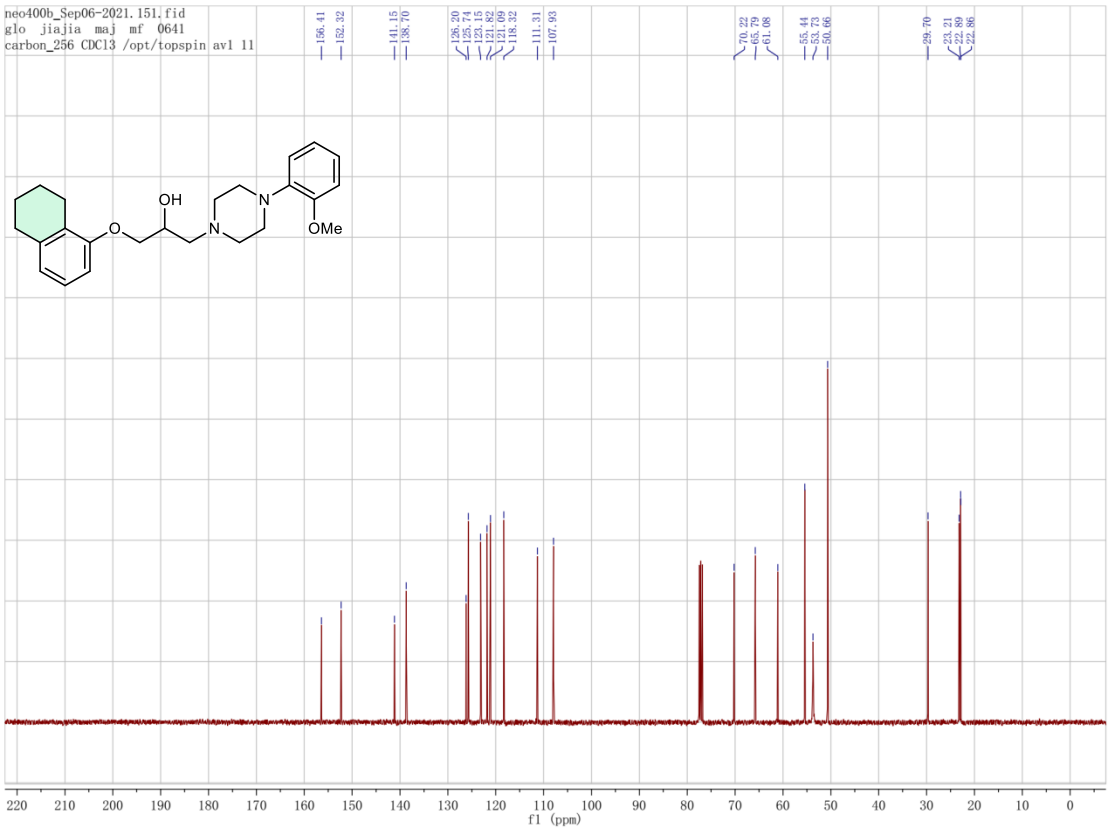
Spectrum 2-27 ^{13}C NMR of compound 39



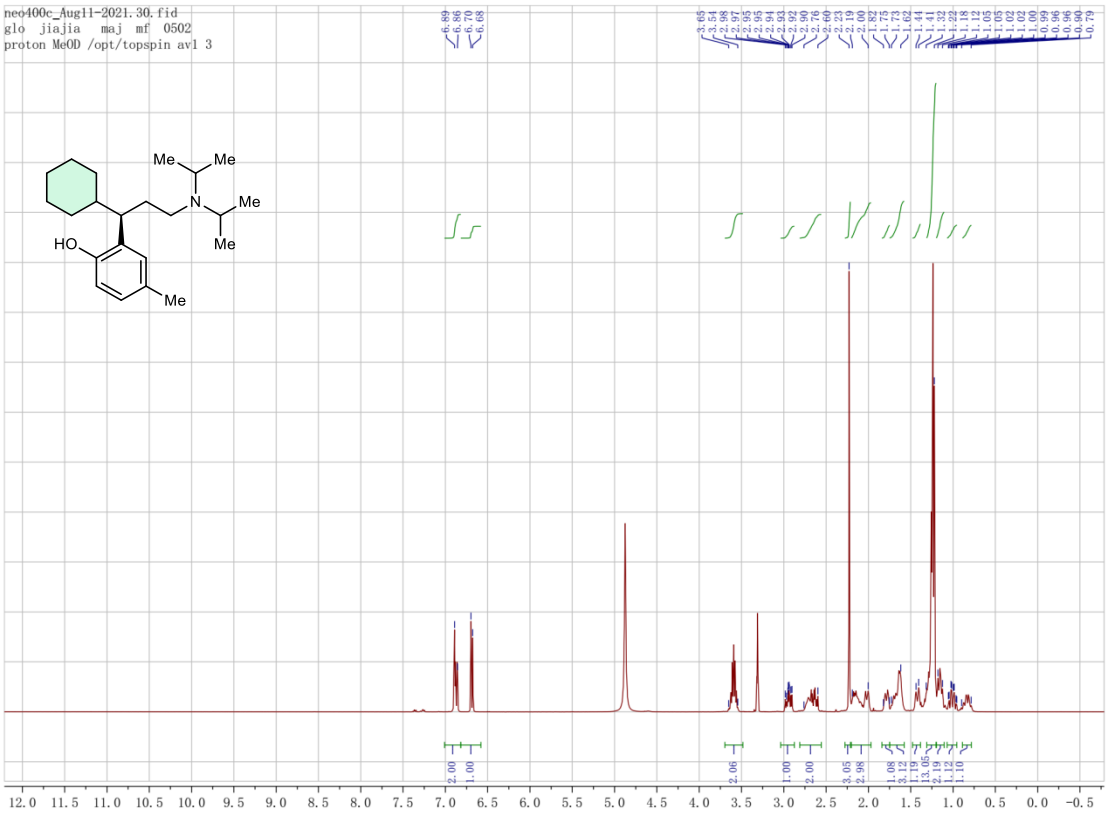
Spectrum 2-28 ^{19}F NMR of compound 39



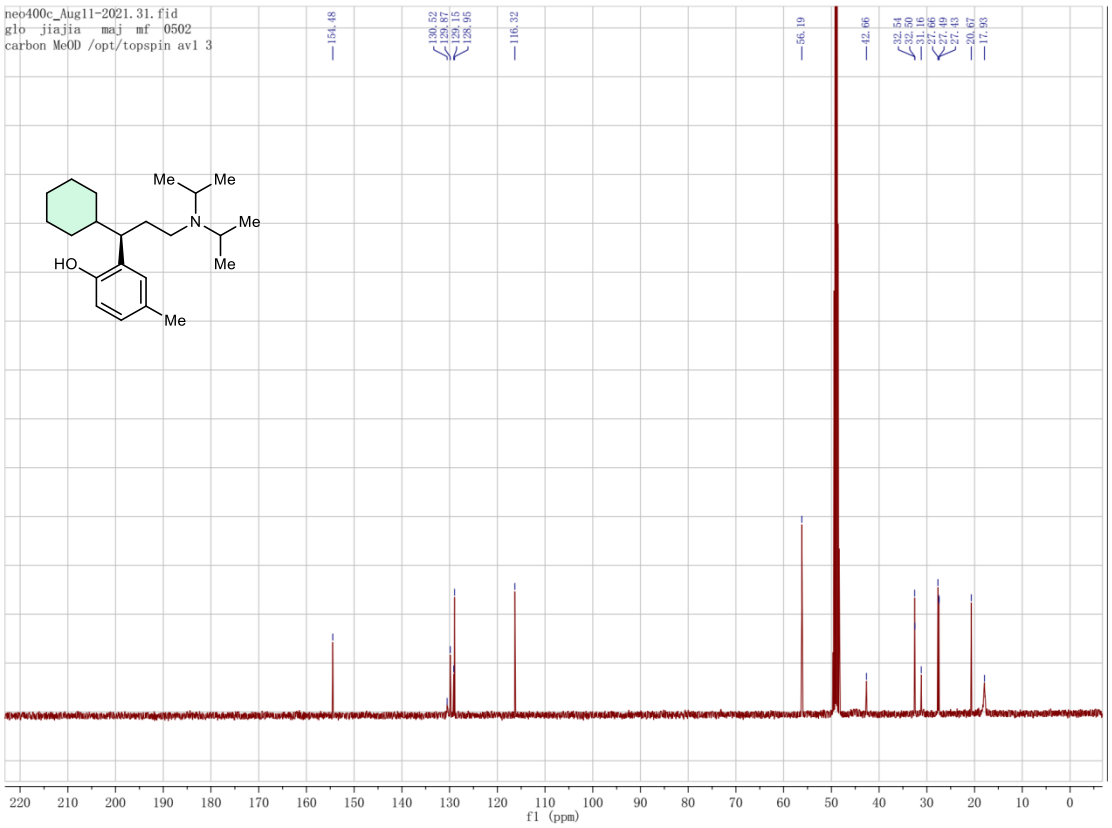
Spectrum 2-29 ^{1}H NMR of compound 40



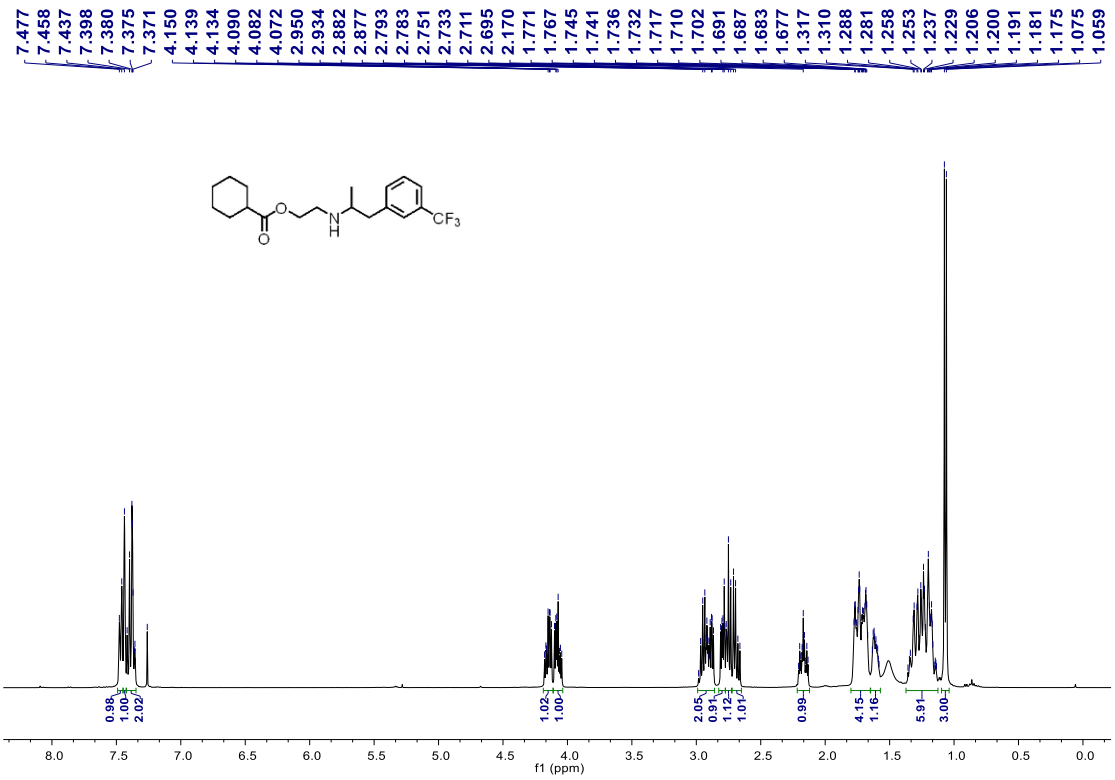
Spectrum 2-30 ^{13}C NMR of compound 40



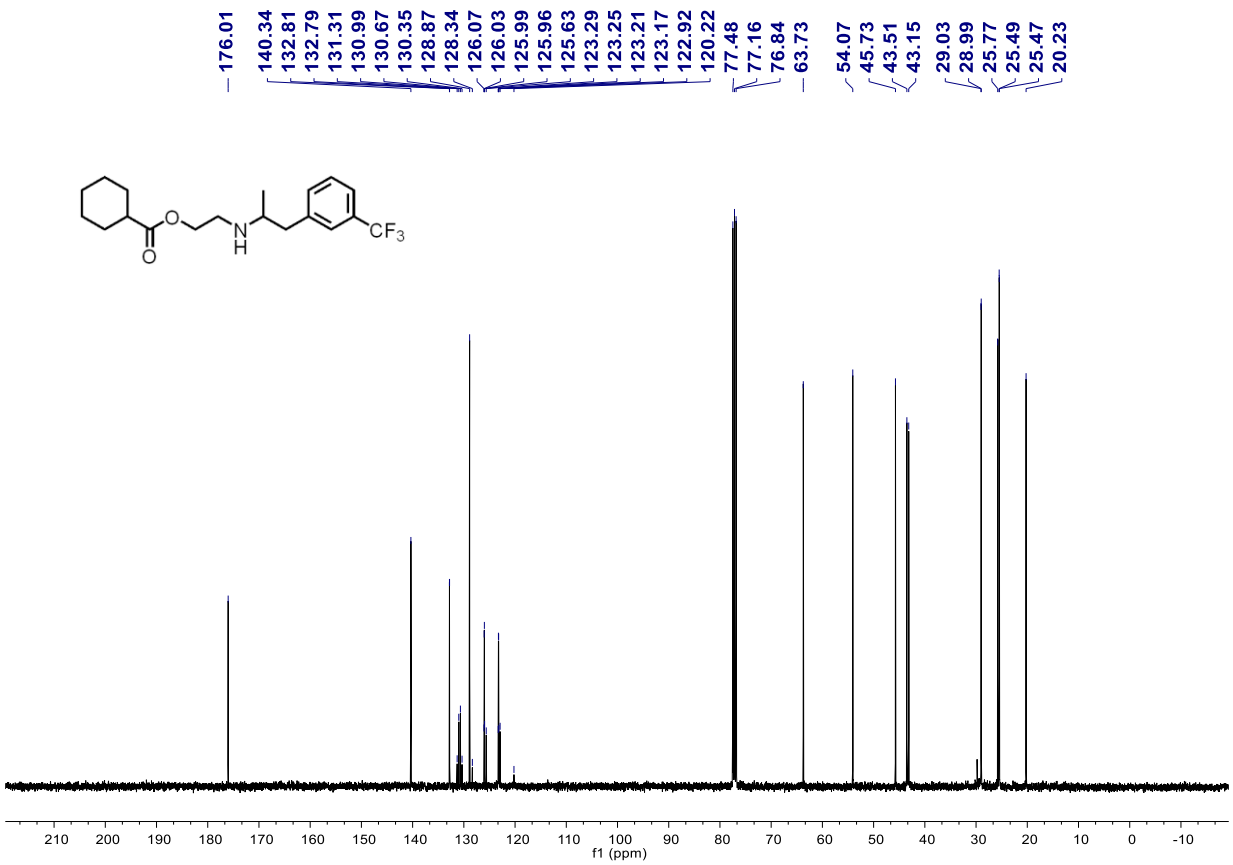
Spectrum 2-31 ^{1}H NMR of compound 41



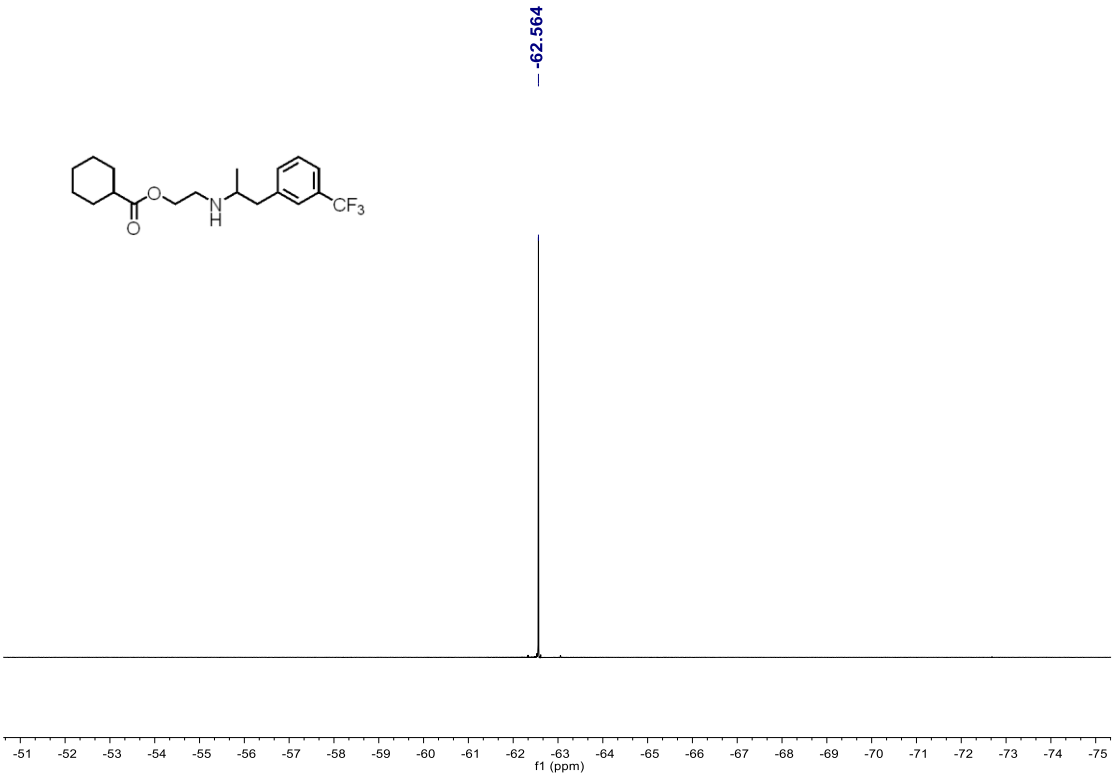
Spectrum 2-32 ^{13}C NMR of compound 41



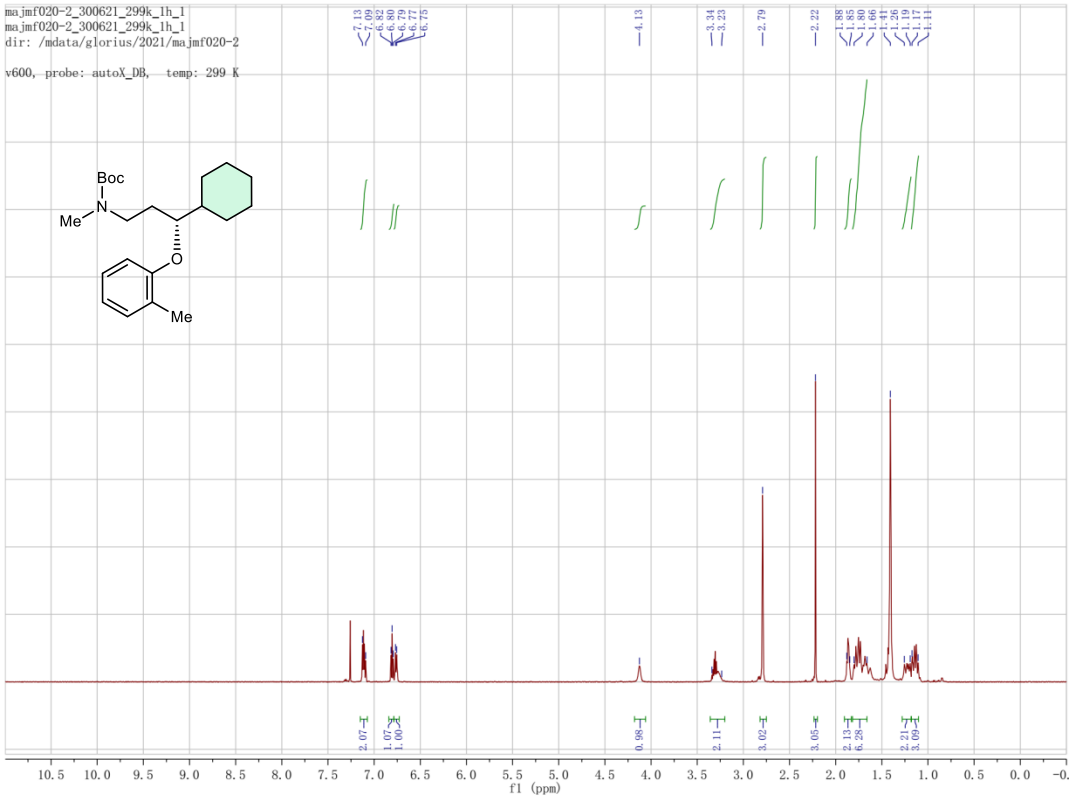
Spectrum 2-33 ^{1}H NMR of compound 42



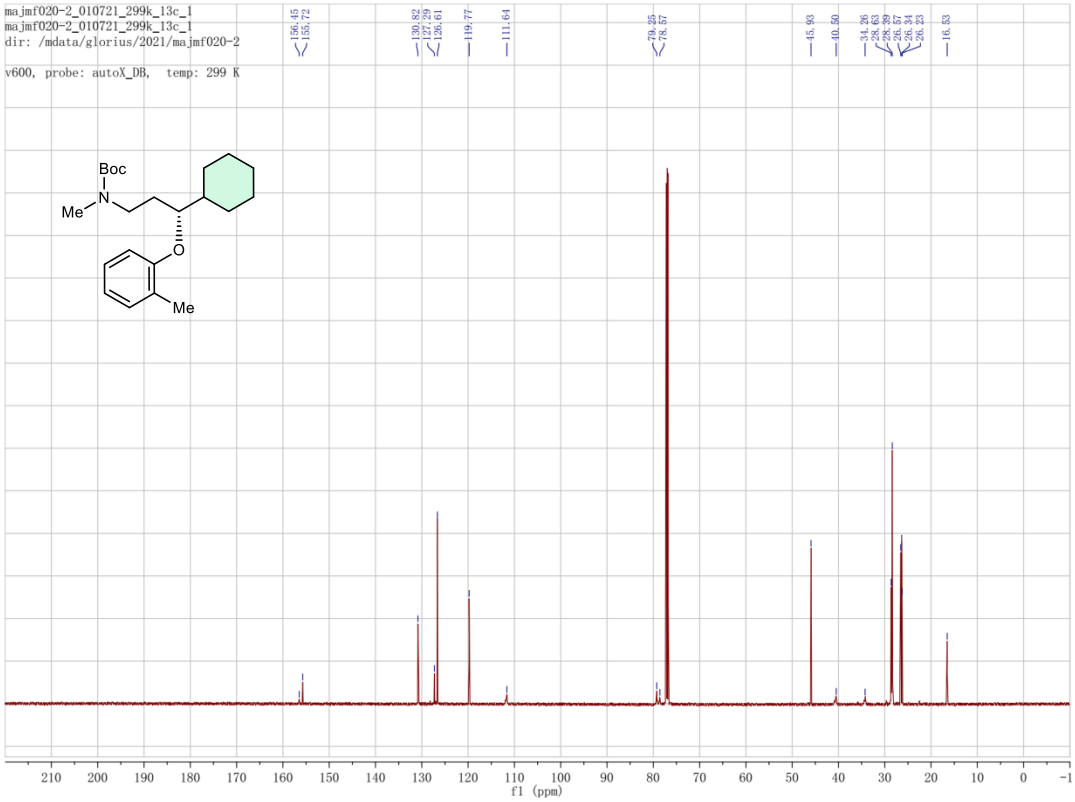
Spectrum 2-34 ^{13}C NMR of compound 42



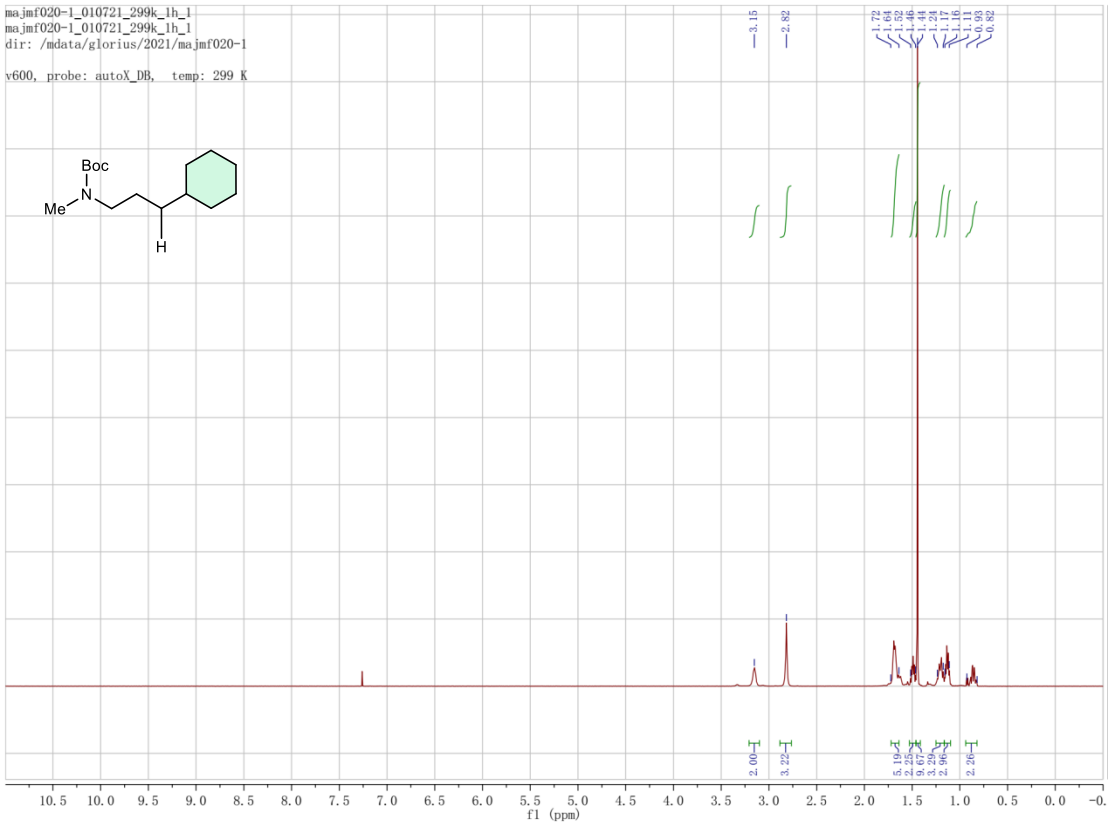
Spectrum 2-35 ^{19}F NMR of compound 42



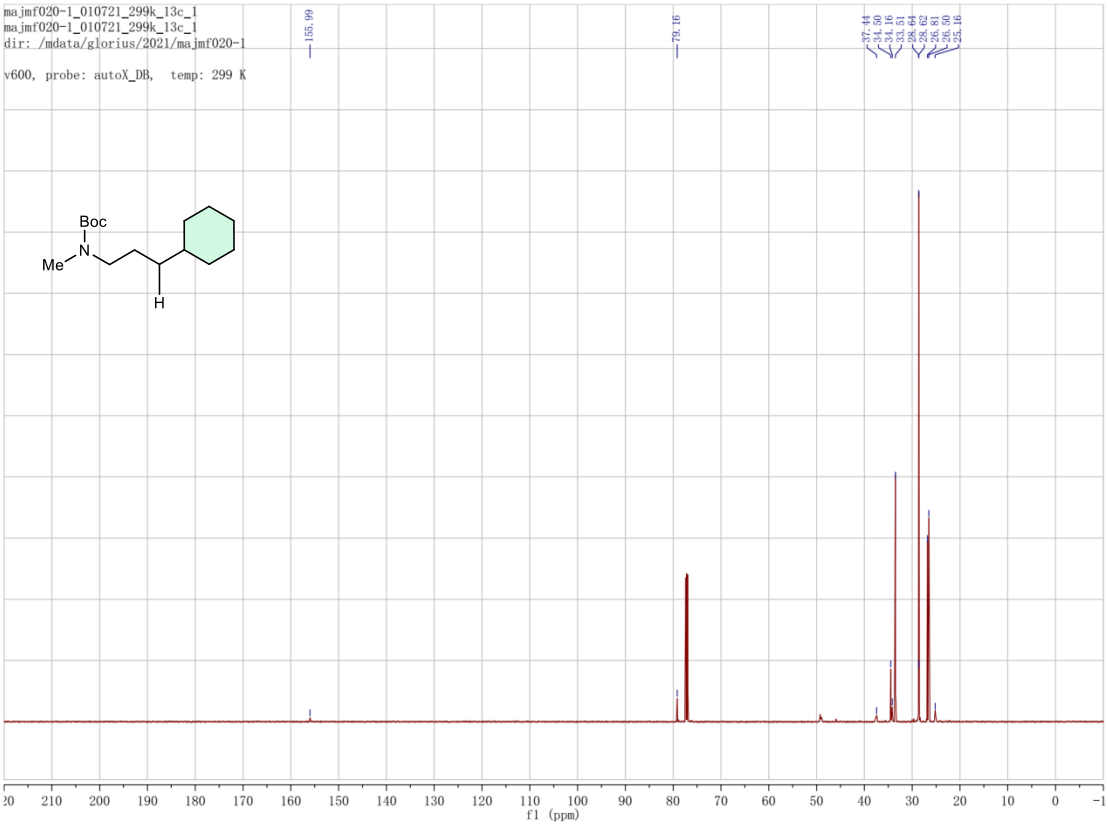
Spectrum 2-36 ^{1}H NMR of compound 43



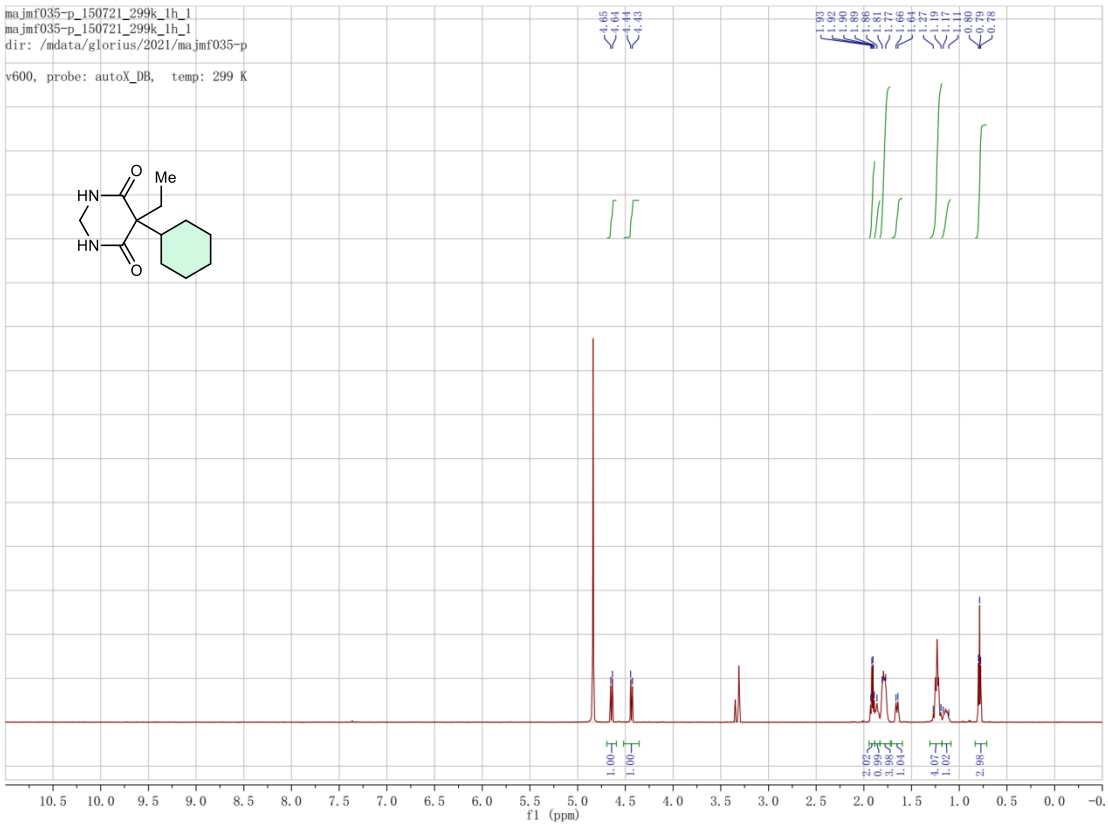
Spectrum 2-37 ^{13}C NMR of compound 43



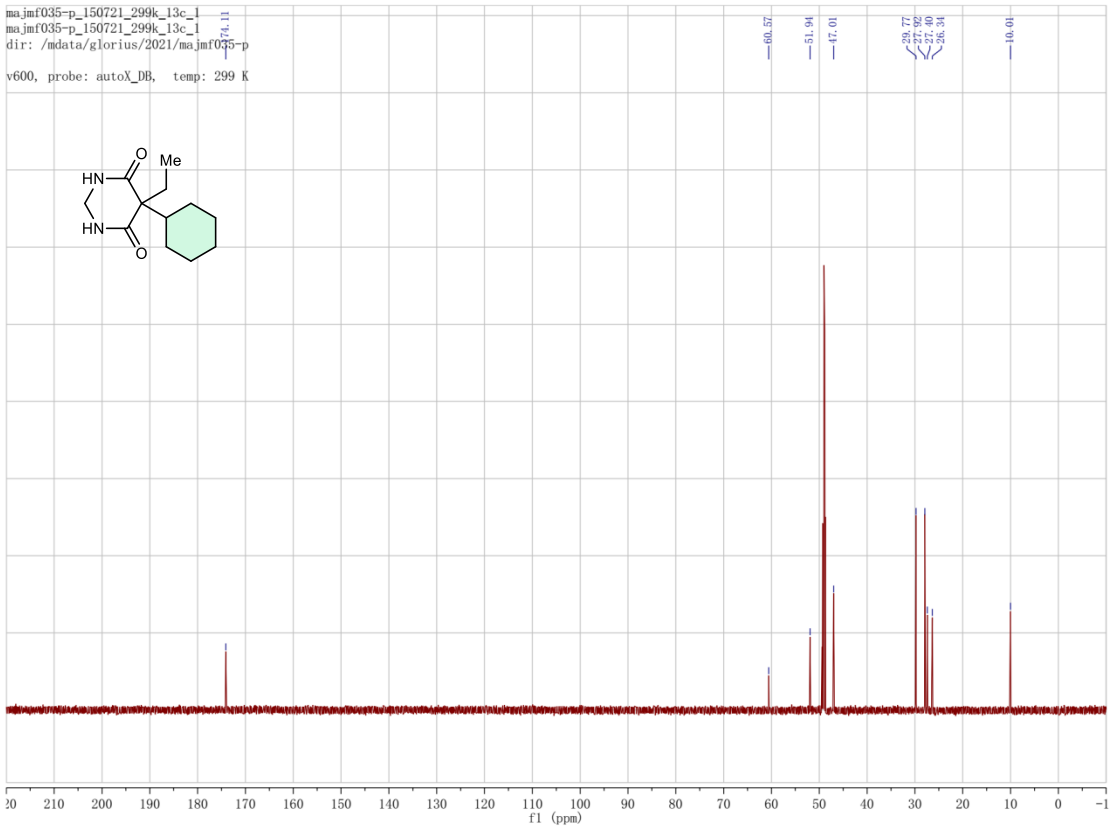
Spectrum 2-38 ^{1}H NMR of compound 43’



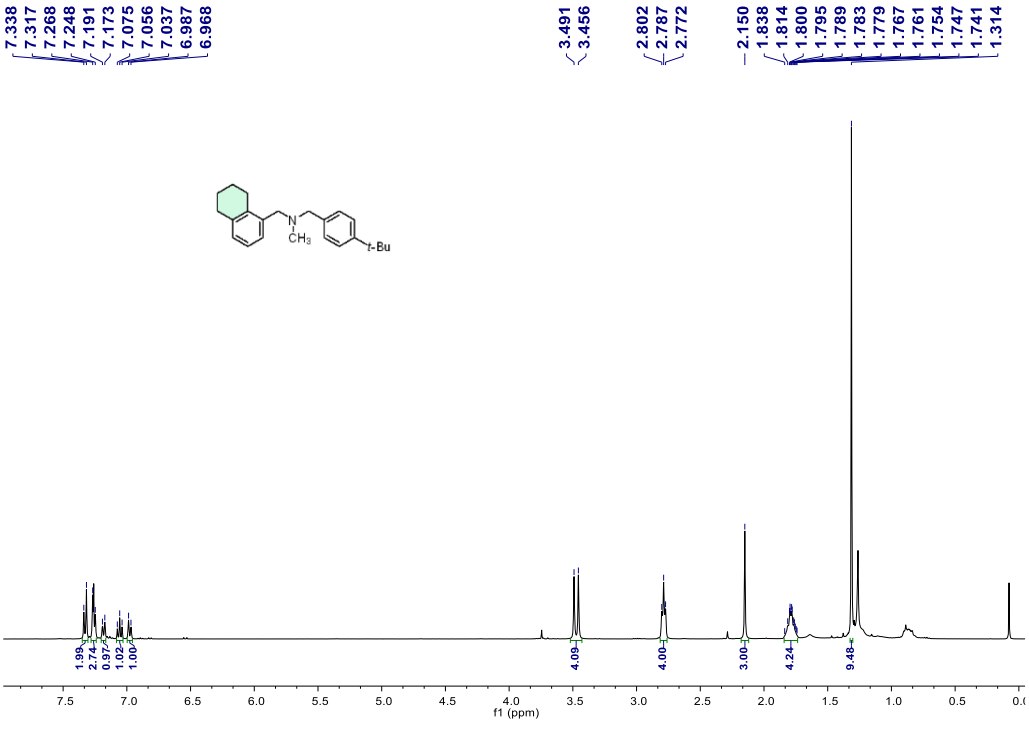
Spectrum 2-39 ^{13}C NMR of compound 43’



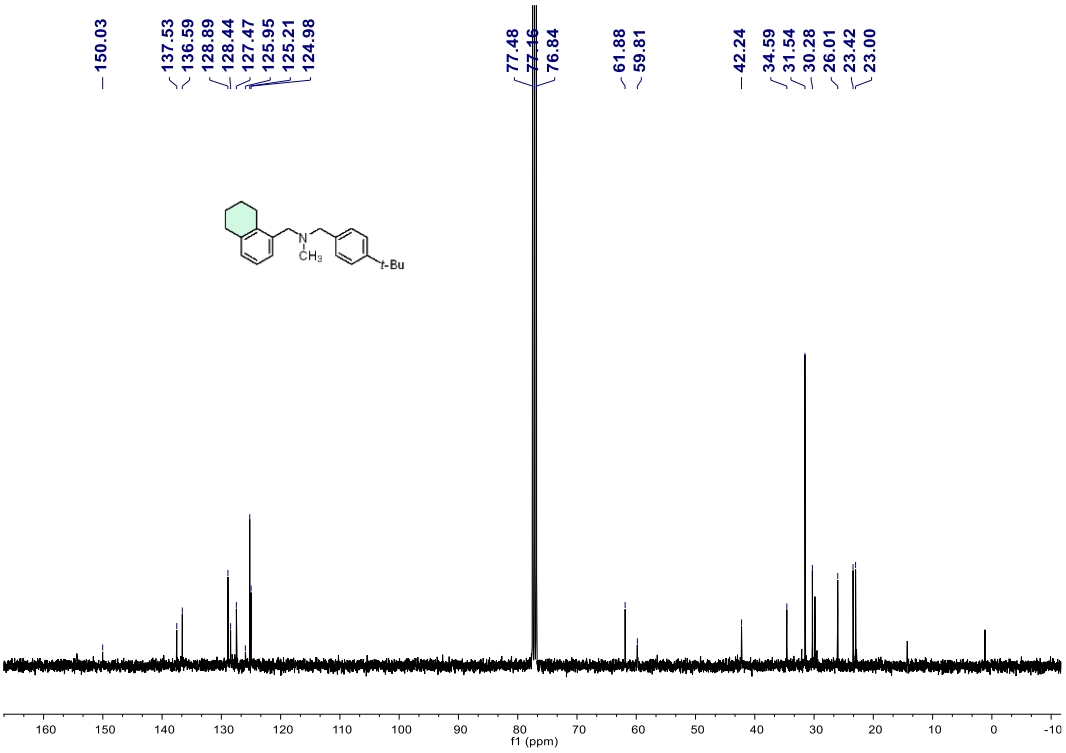
Spectrum 2-40 ^{1}H NMR of compound 44



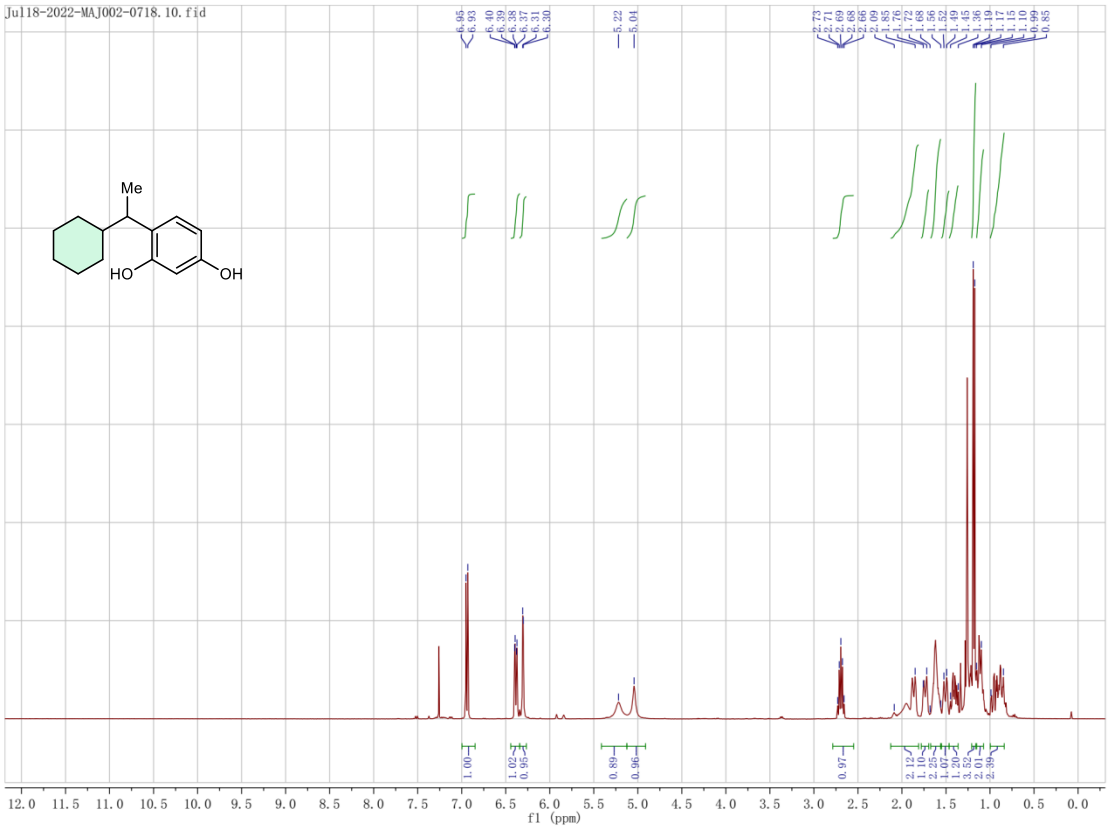
Spectrum 2-41 ^{13}C NMR of compound 44



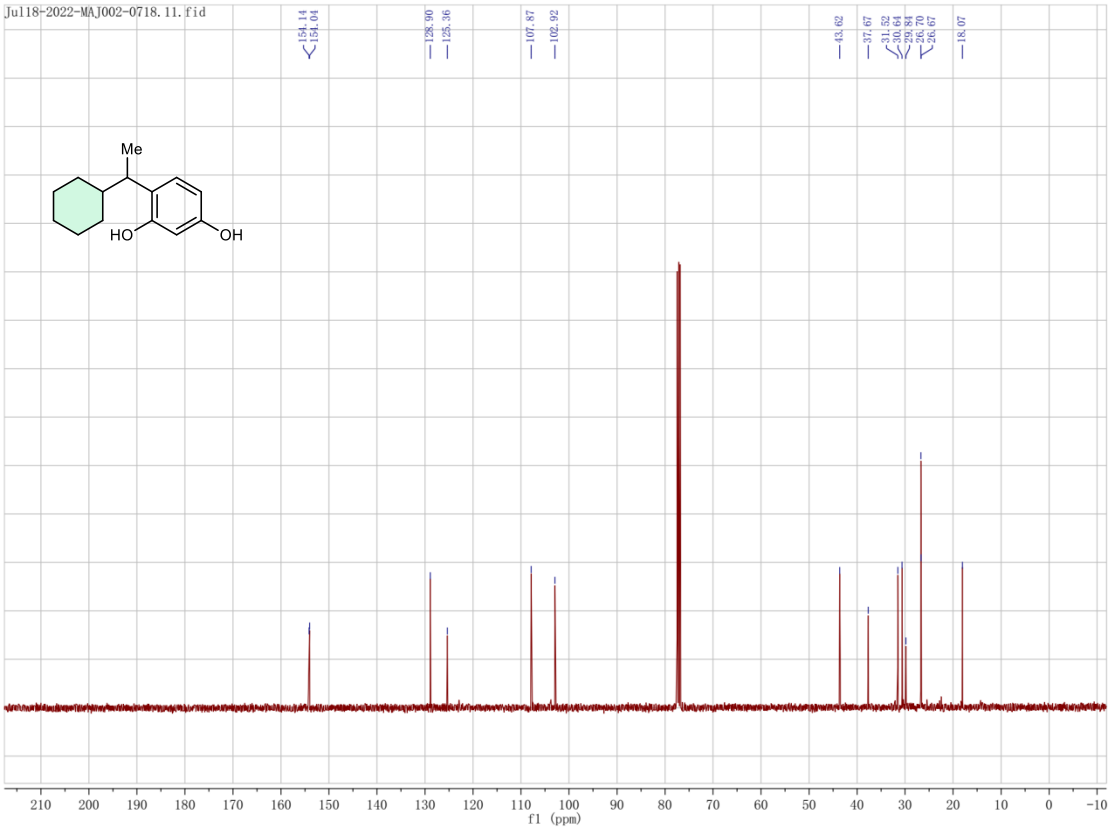
Spectrum 2-42 ^{1}H NMR of compound 45



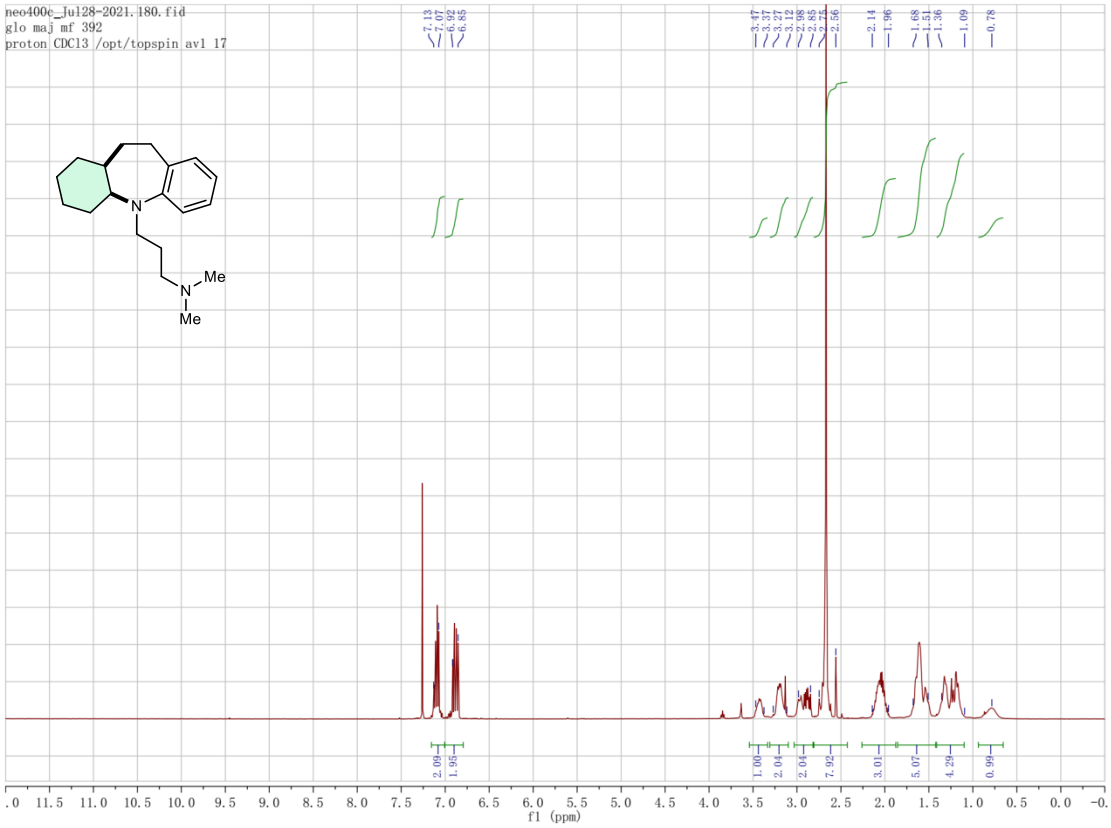
Spectrum 2-43 ^{13}C NMR of compound 45



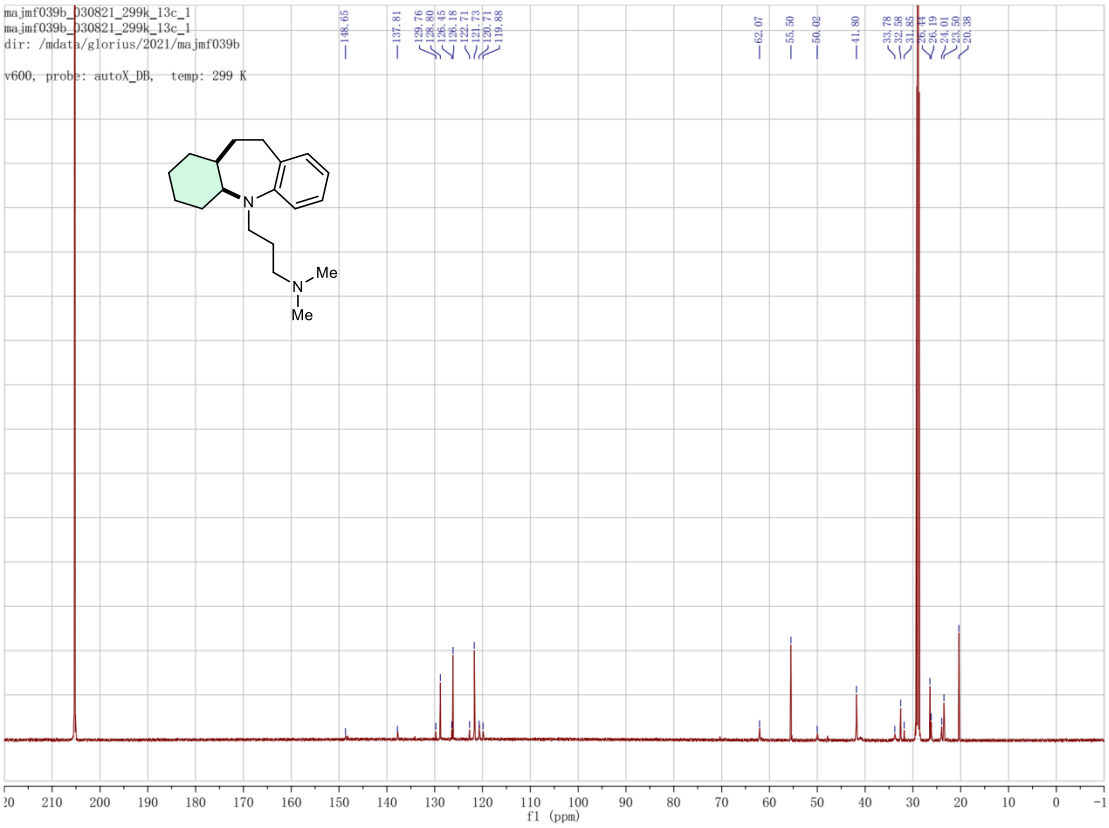
Spectrum 2-44 ^{1}H NMR of compound 46



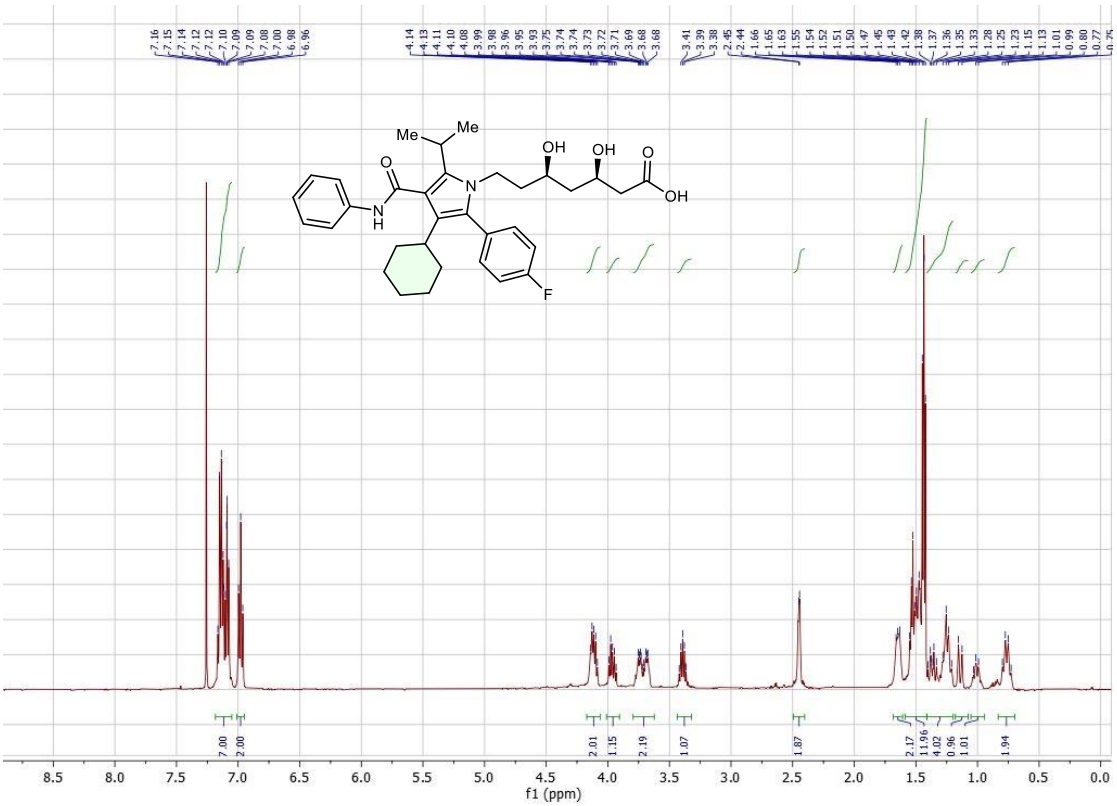
Spectrum 2-45 ^{13}C NMR of compound 46



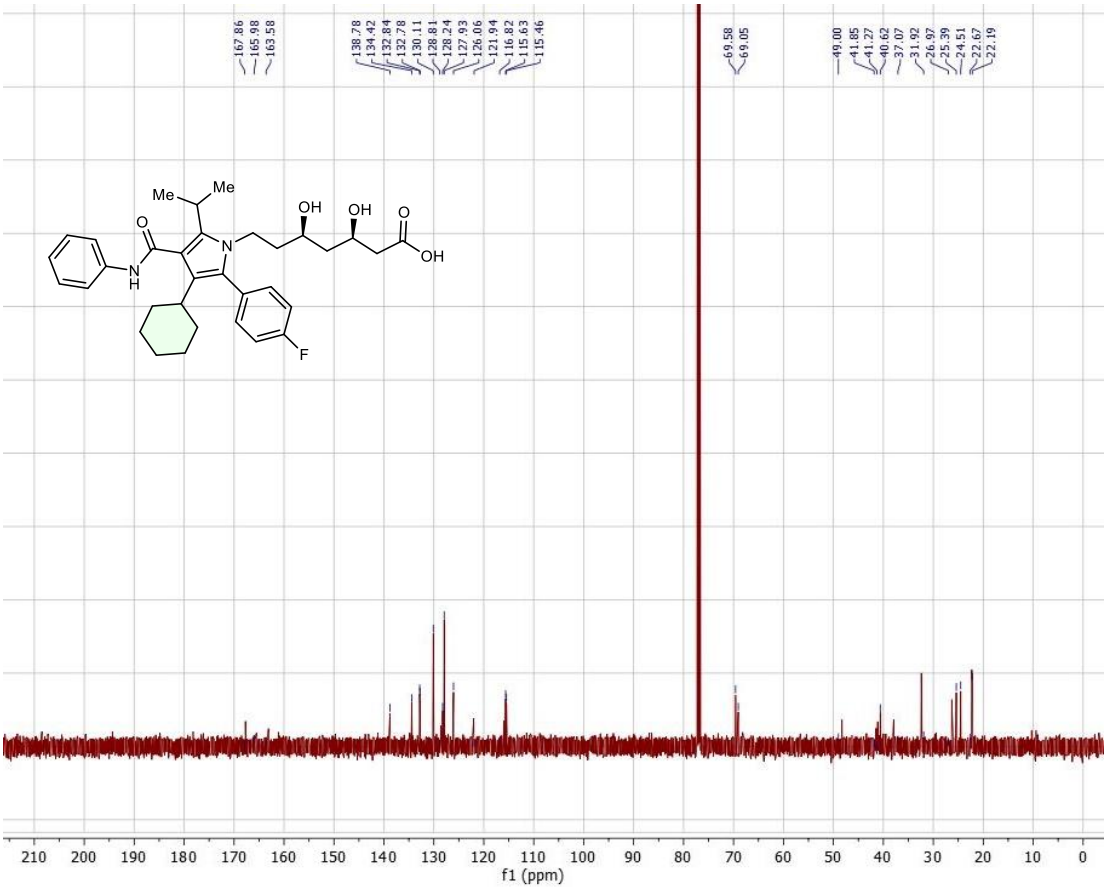
Spectrum 2-46 ^{1}H NMR of compound 47



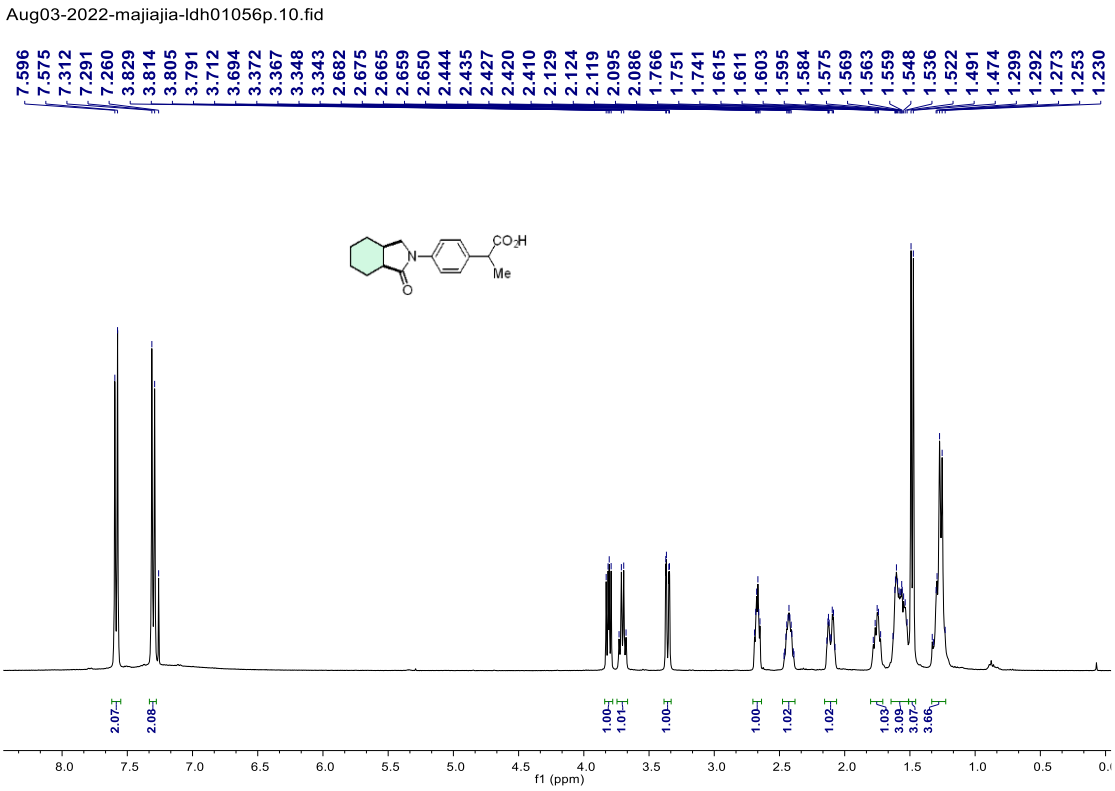
Spectrum 2-47 ^{13}C NMR of compound 47



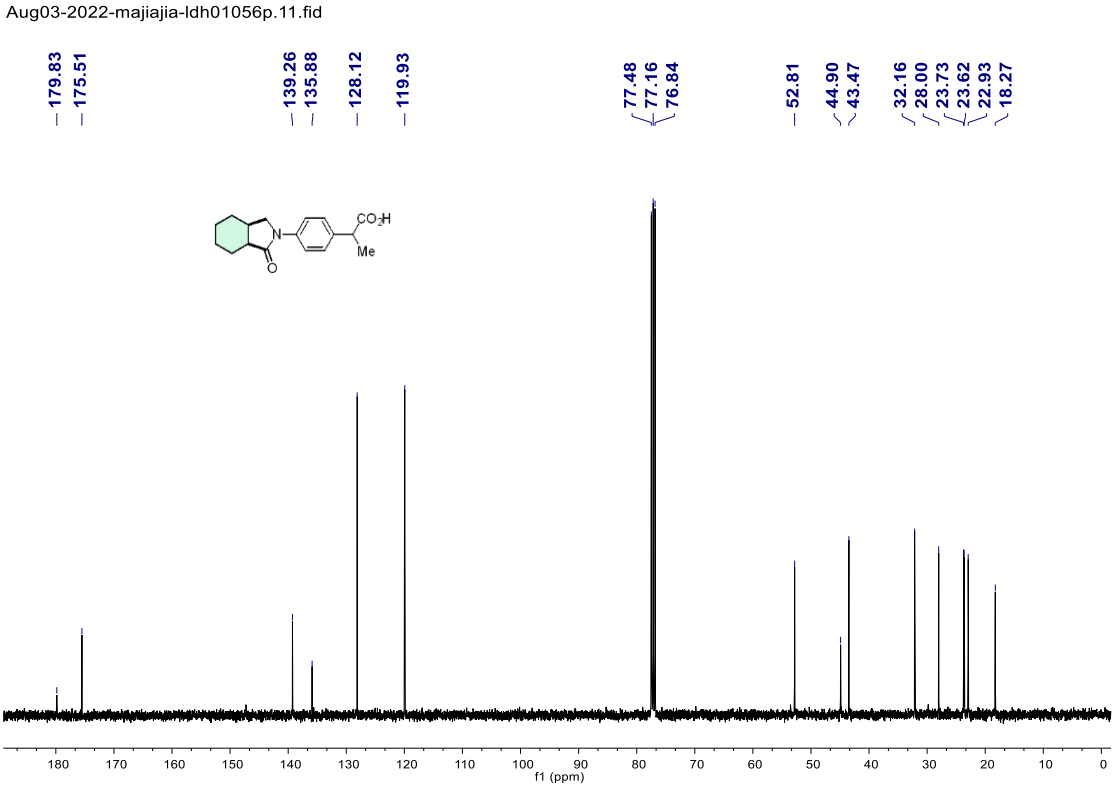
Spectrum 2-48 ^{1}H NMR of compound 48



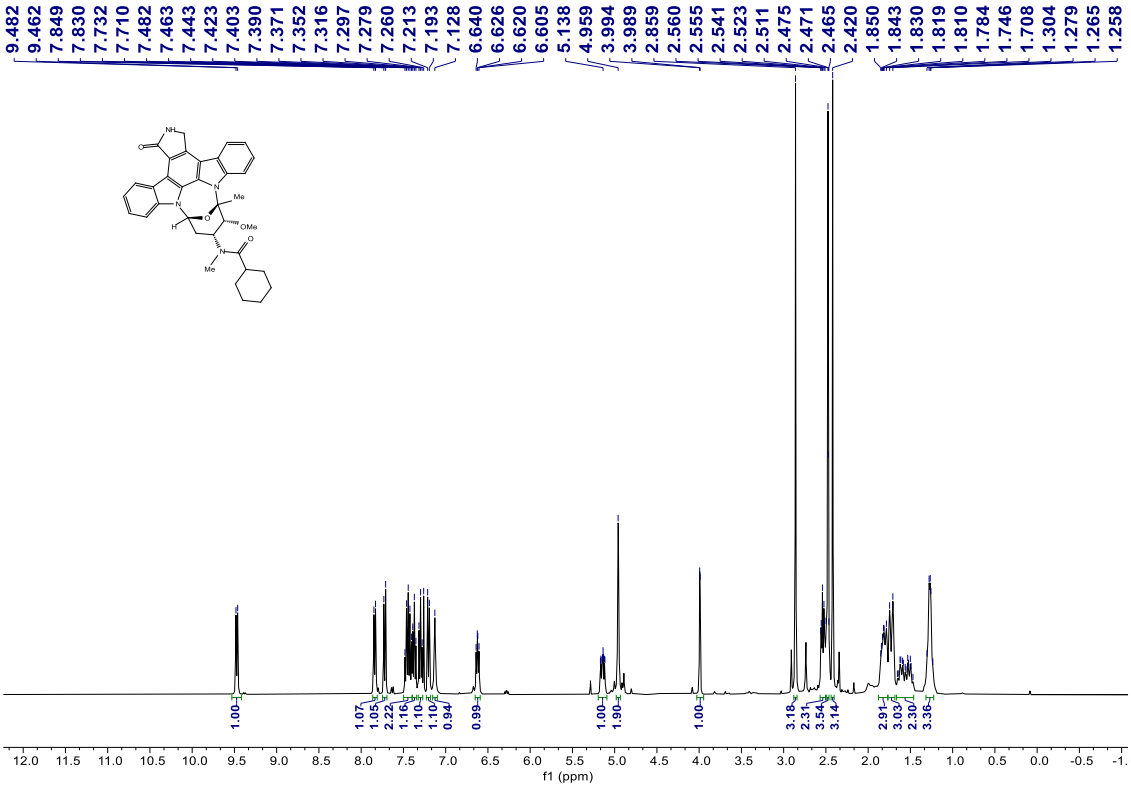
Spectrum 2-49 ^{13}C NMR of compound 48



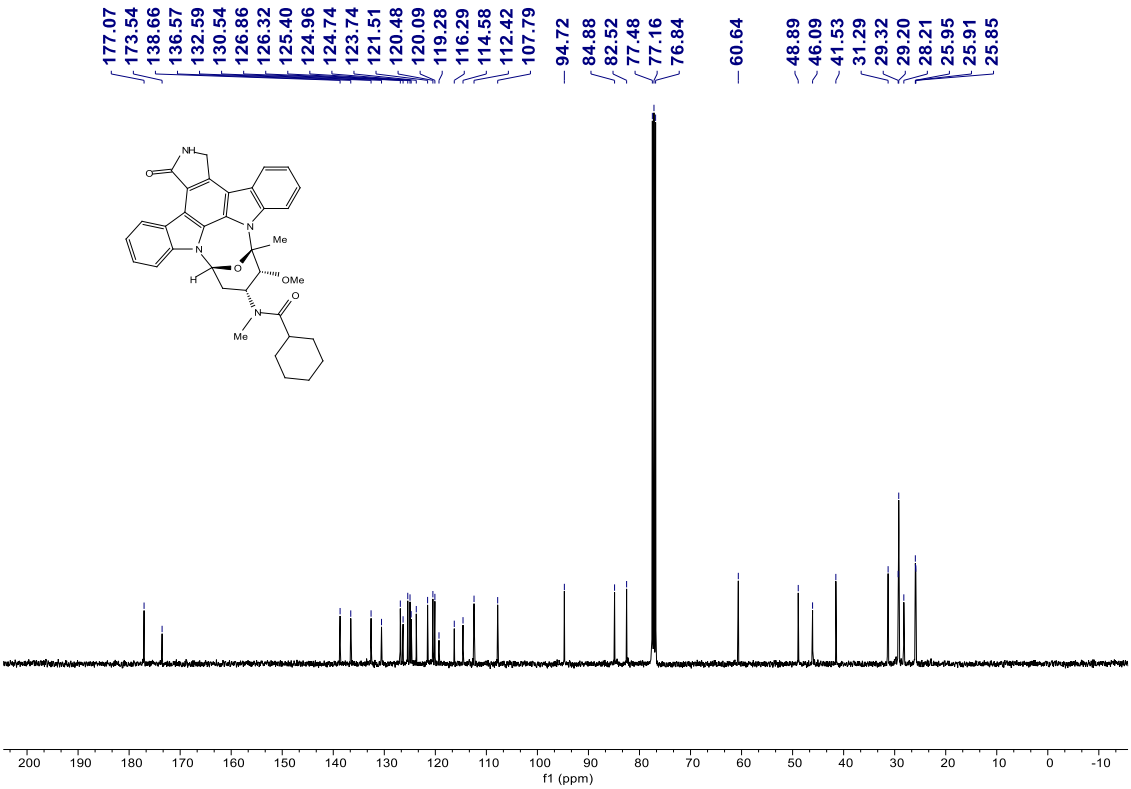
Spectrum 2-50 ^{1}H NMR of compound 49



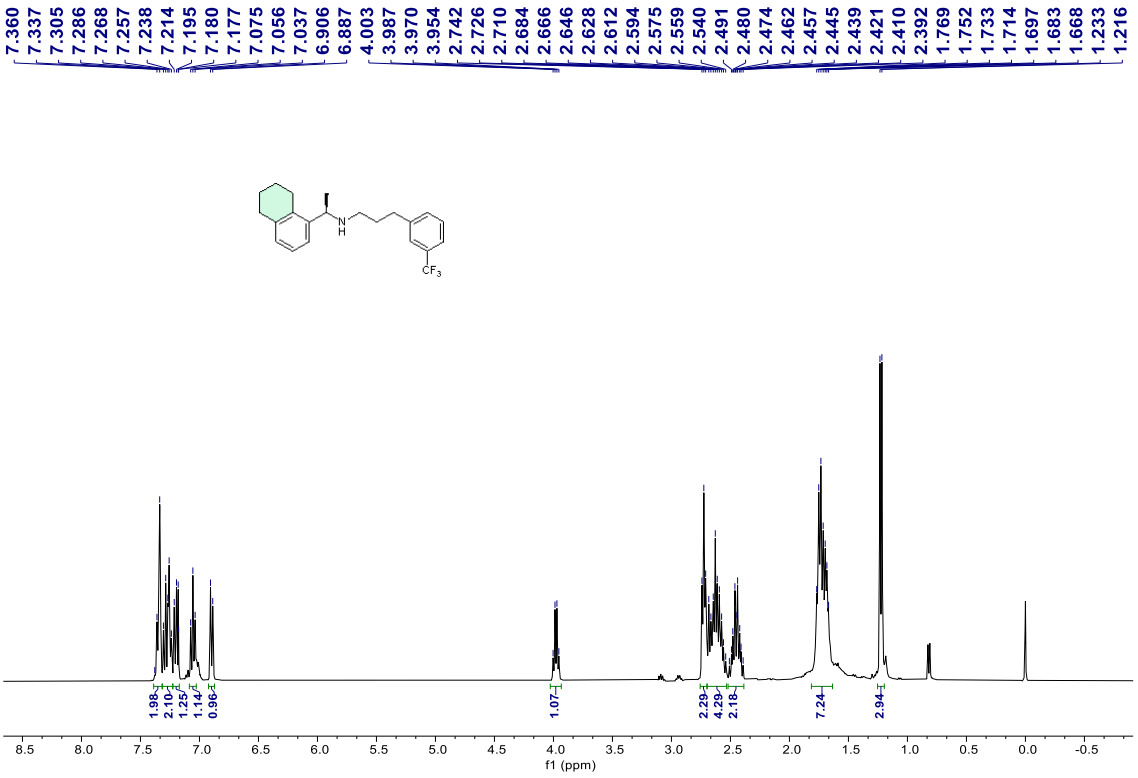
Spectrum 2-51 ^{13}C NMR of compound 49



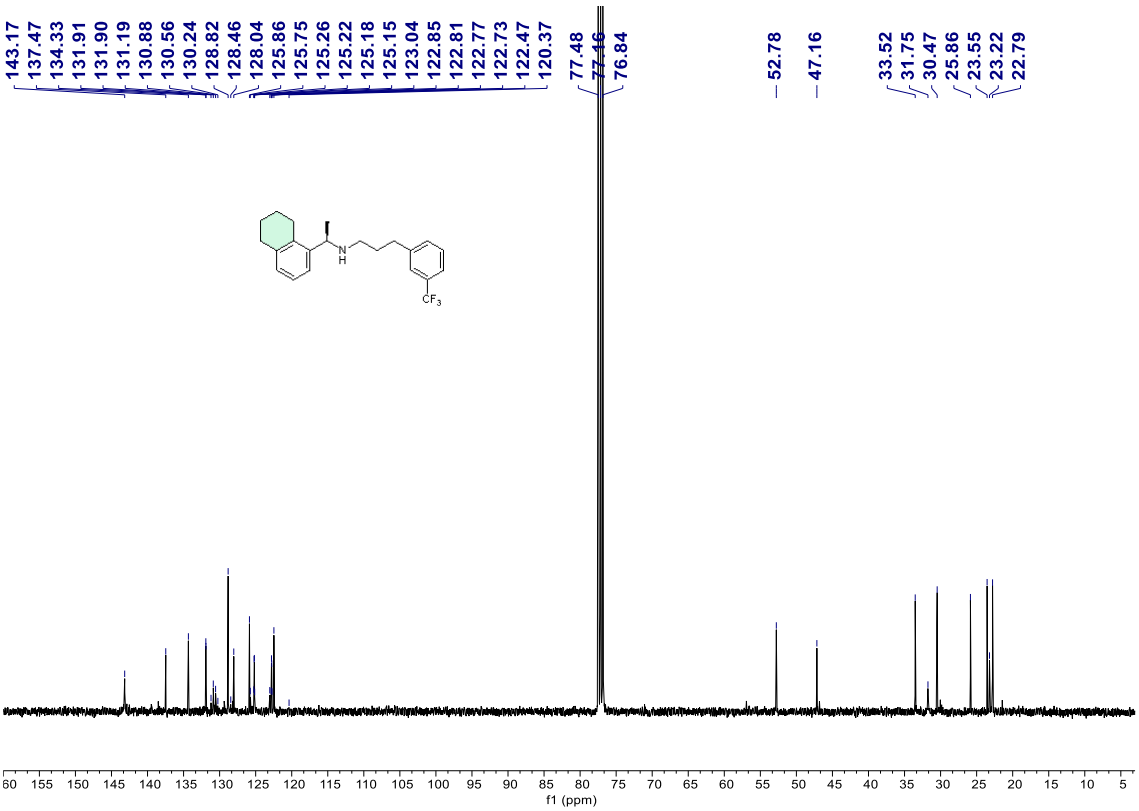
Spectrum 2-52 ^{1}H NMR of compound 50



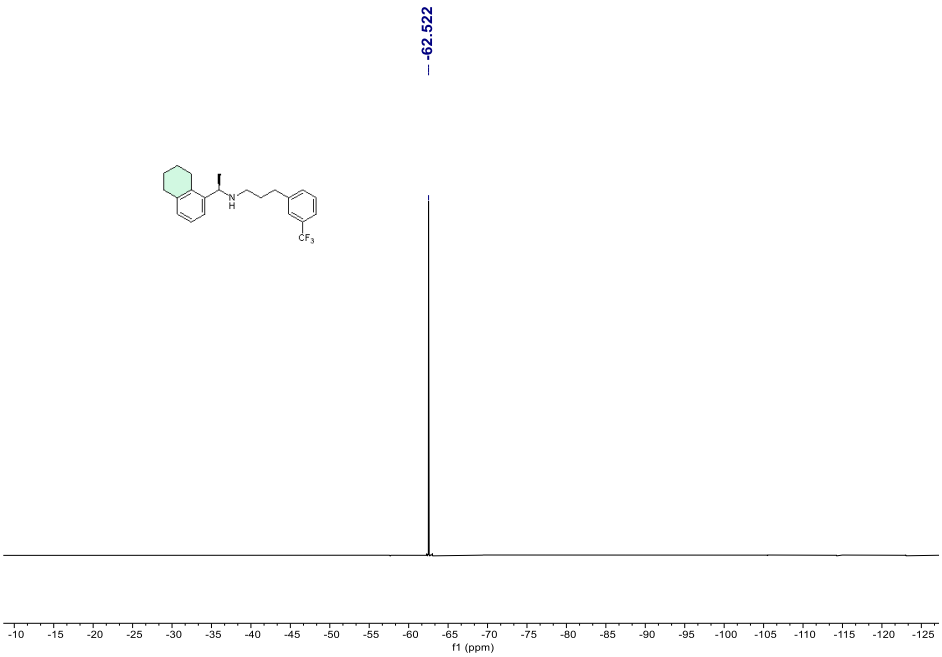
Spectrum 2-53 ^{13}C NMR of compound 50



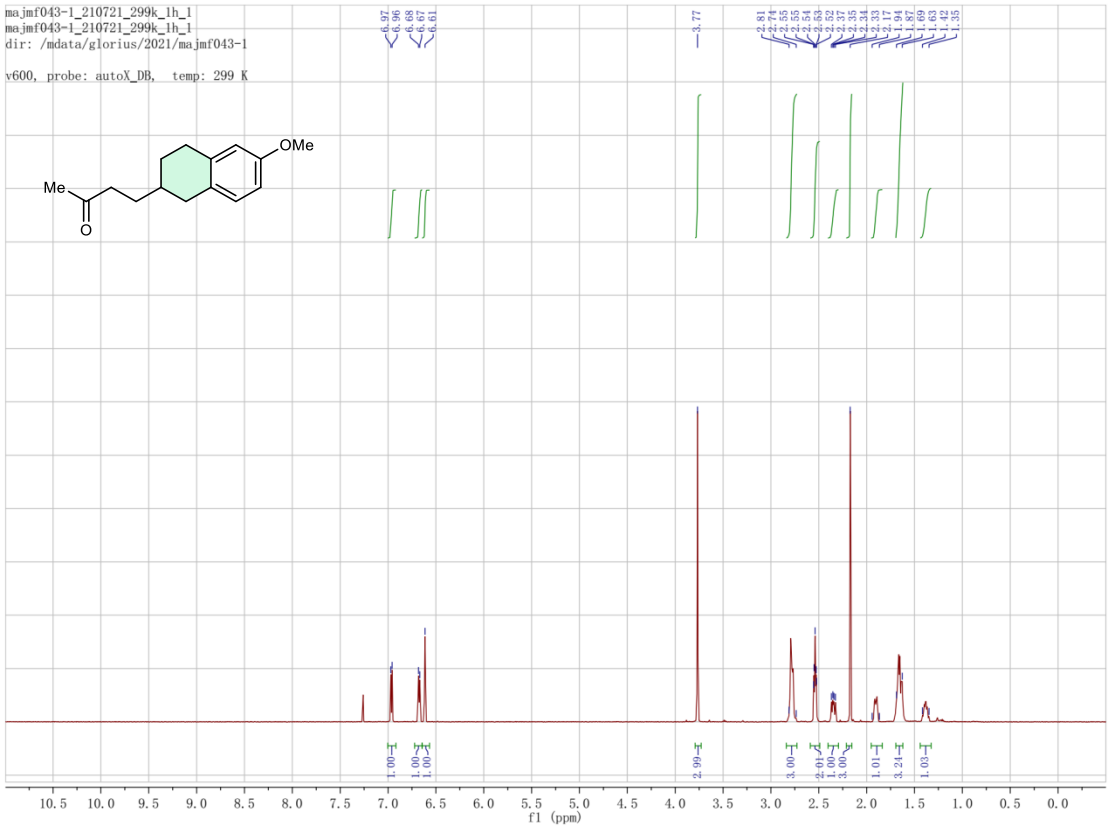
Spectrum 2-54 ^{1}H NMR of compound 51



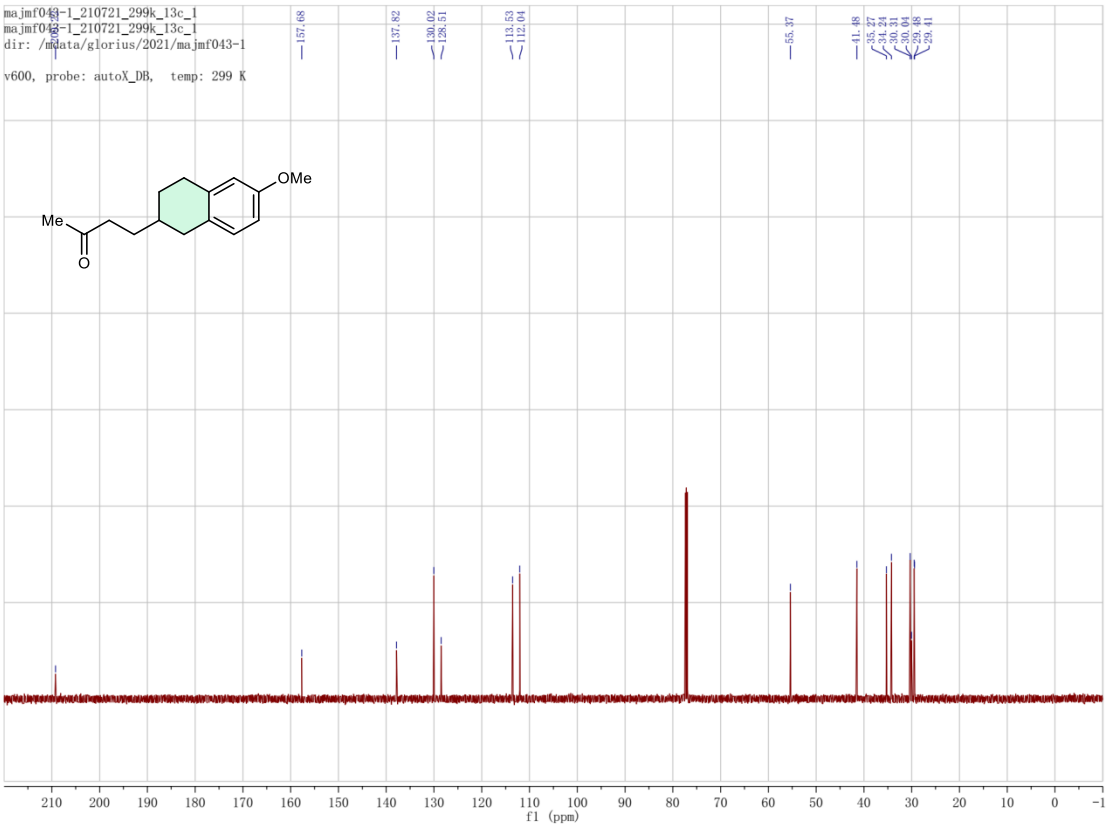
Spectrum 2-55 ^{13}C NMR of compound 51



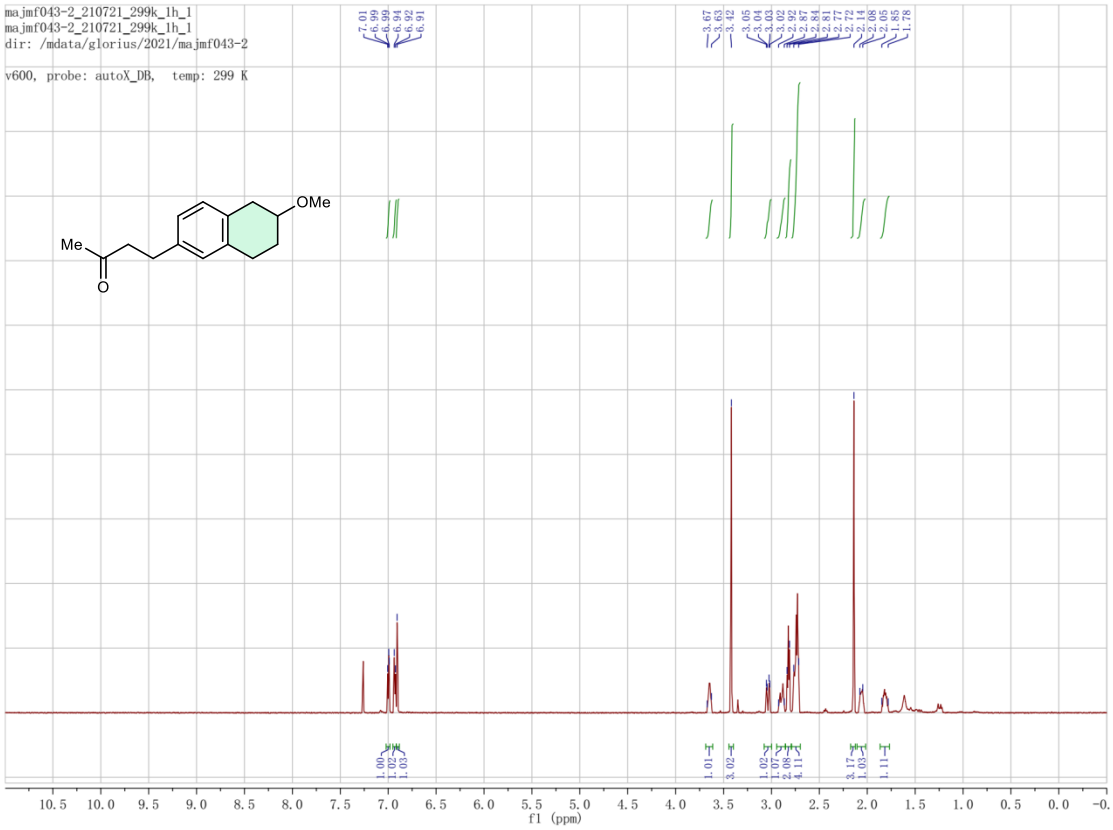
Spectrum 2-56 ^{19}F NMR of compound 51



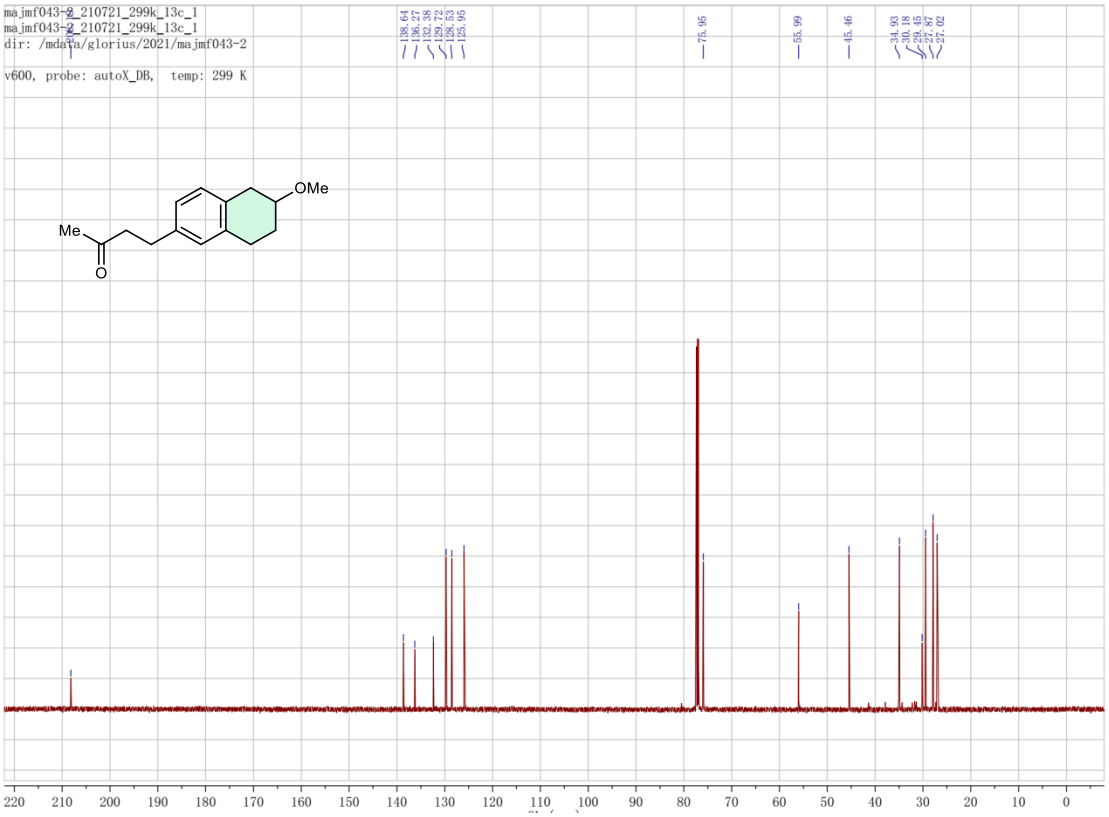
Spectrum 2-57 ^{1}H NMR of compound 53



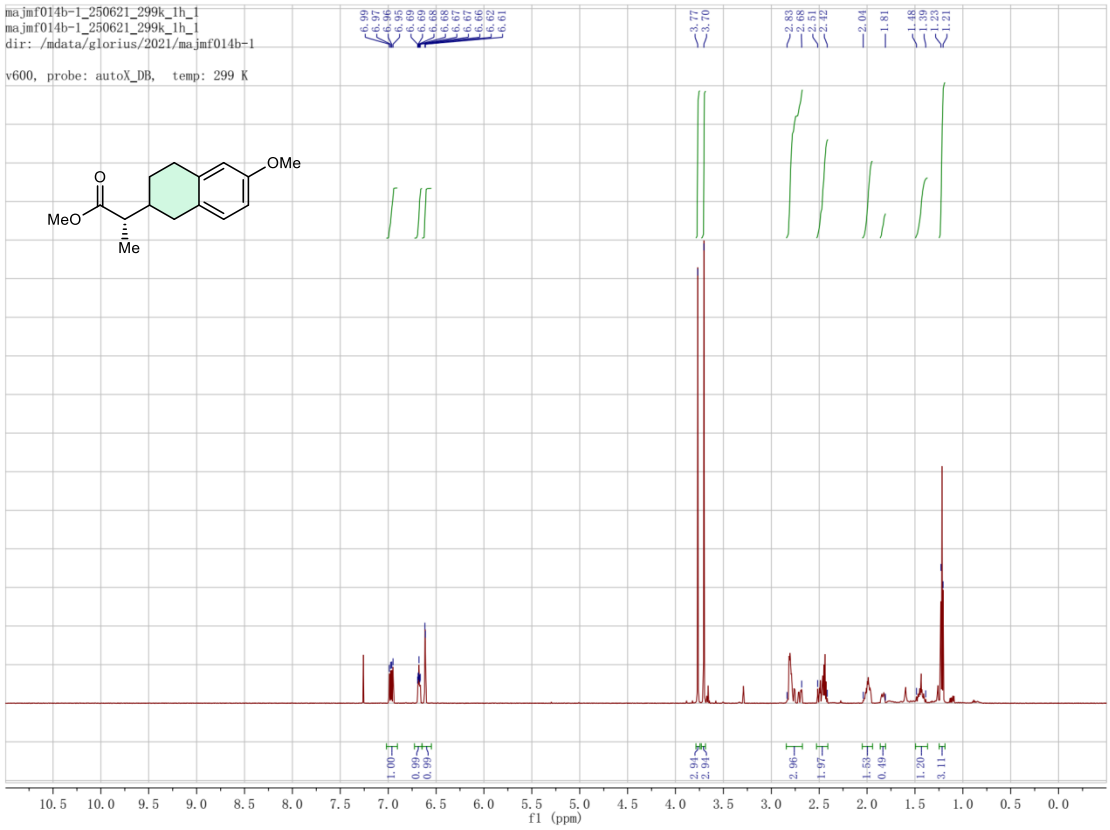
Spectrum 2-58 ^{13}C NMR of compound 53



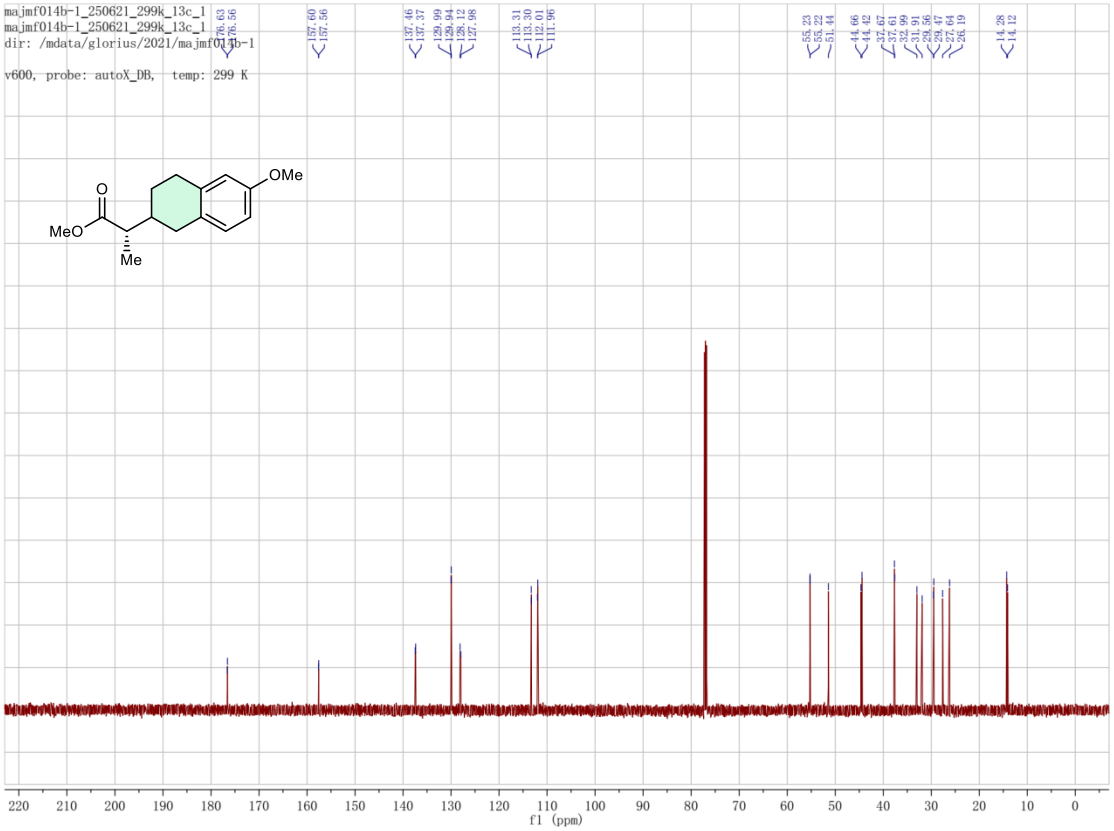
Spectrum 2-59 ^{1}H NMR of compound 54



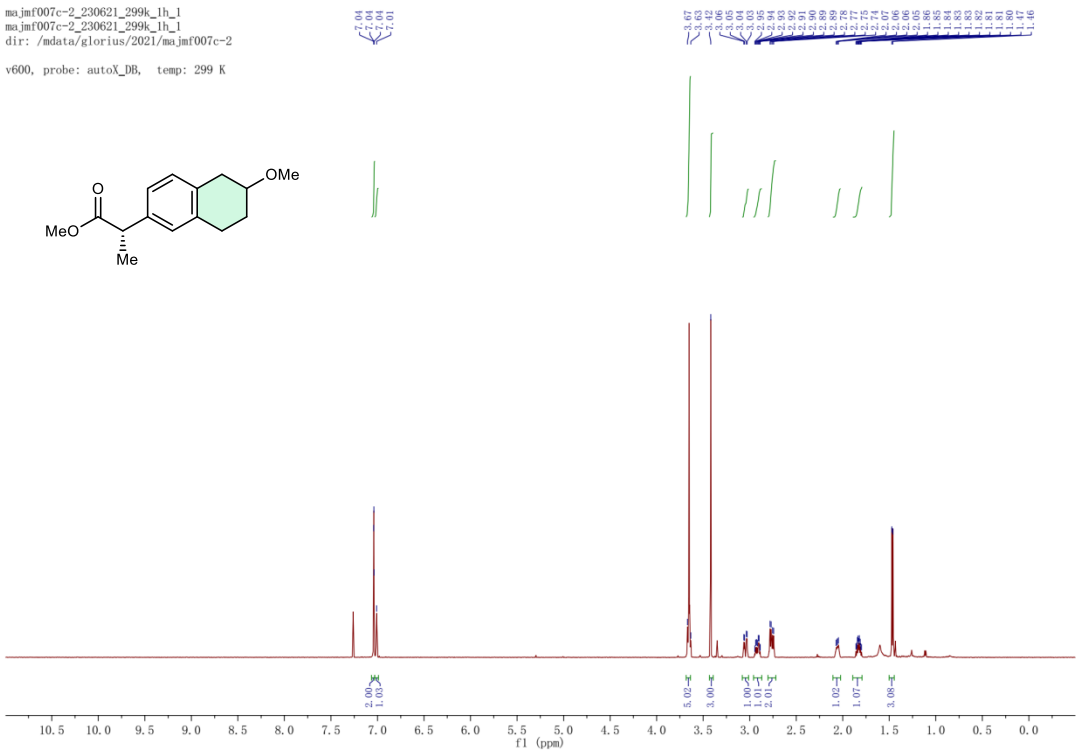
Spectrum 2-60 ^{13}C NMR of compound 54



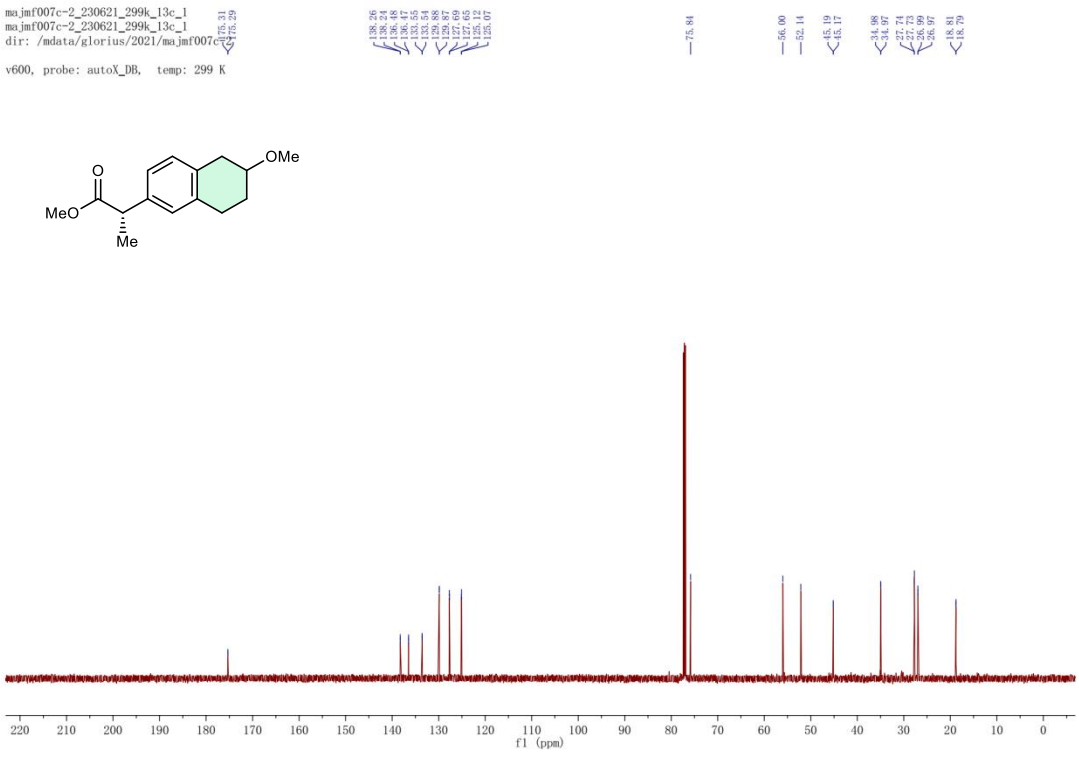
Spectrum 2-61 ^{1}H NMR of compound 56



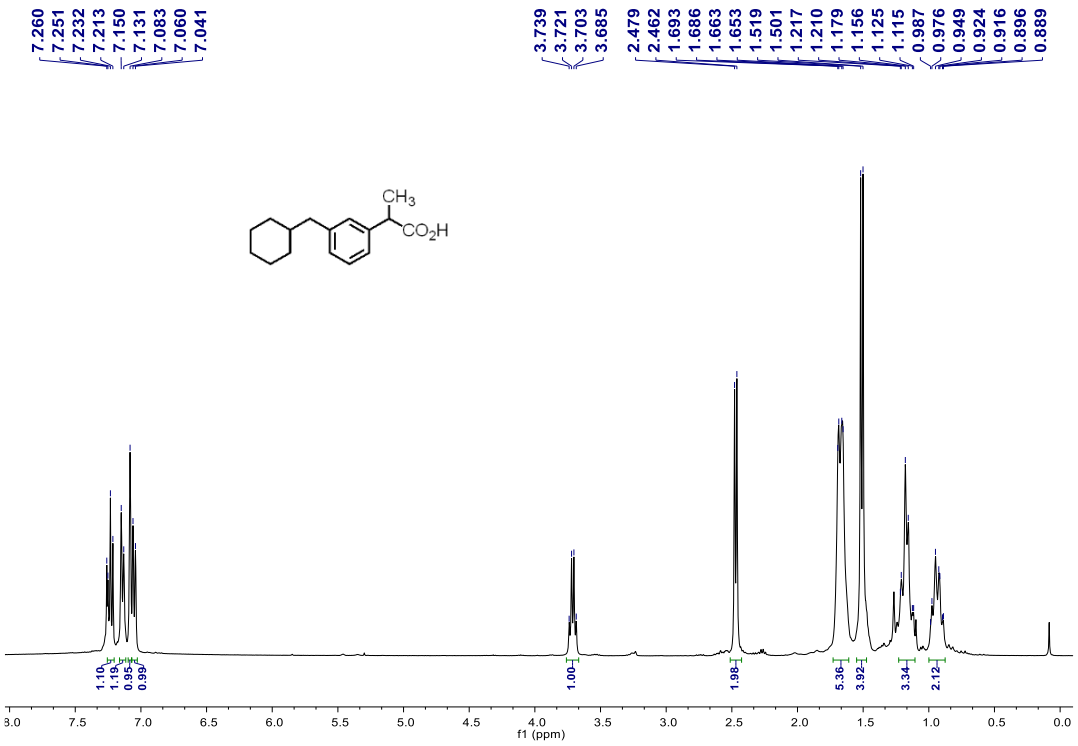
Spectrum 2-62 ^{13}C NMR of compound 56



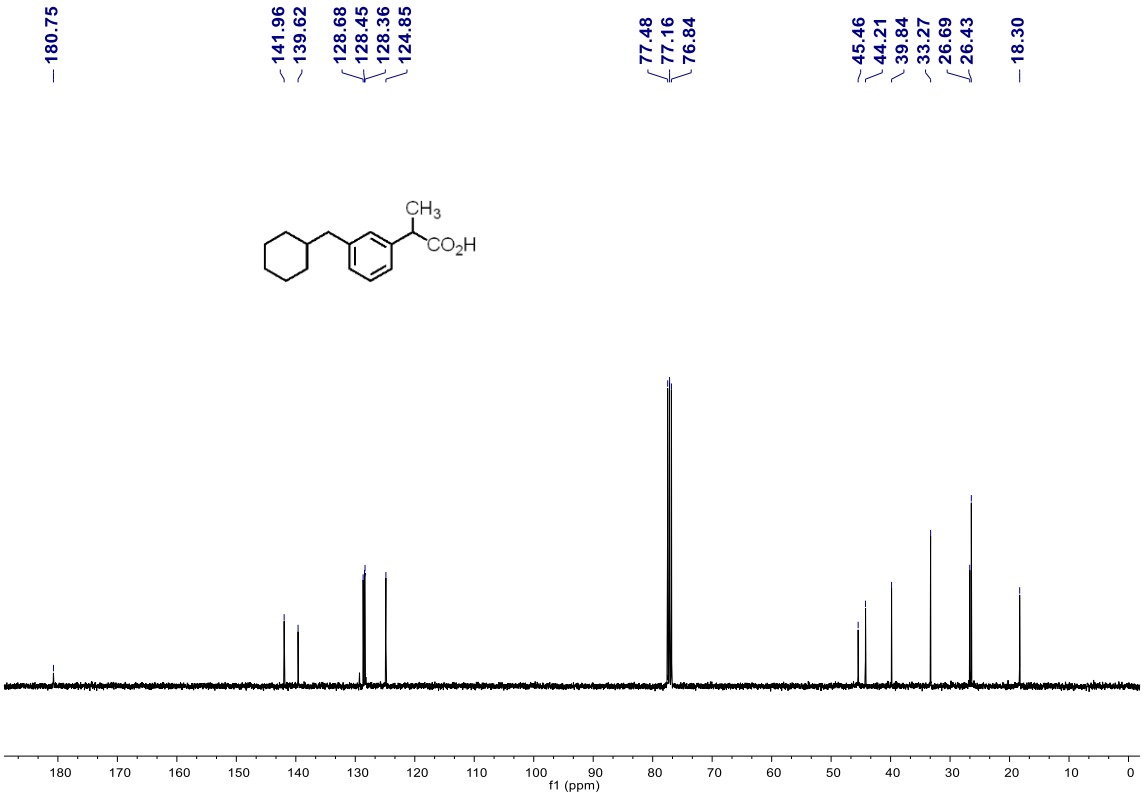
Spectrum 2-63 ^{1}H NMR of compound 57



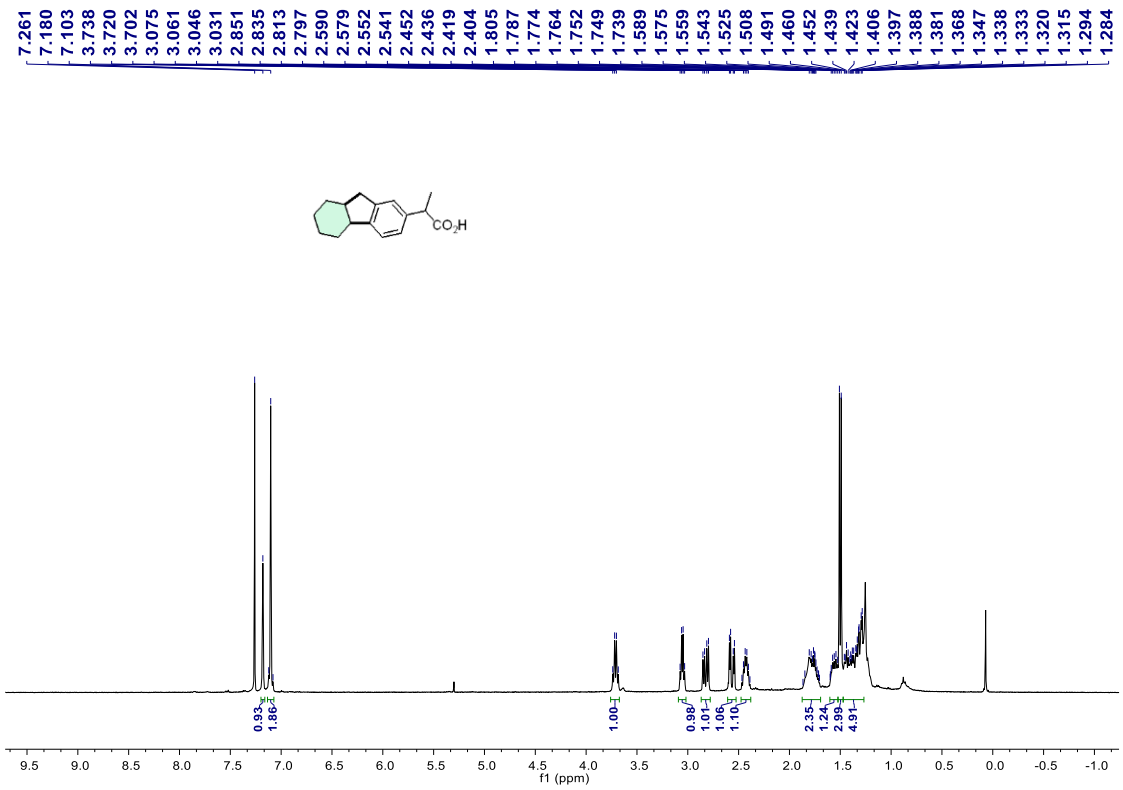
Spectrum 2-64 ^{13}C NMR of compound 57



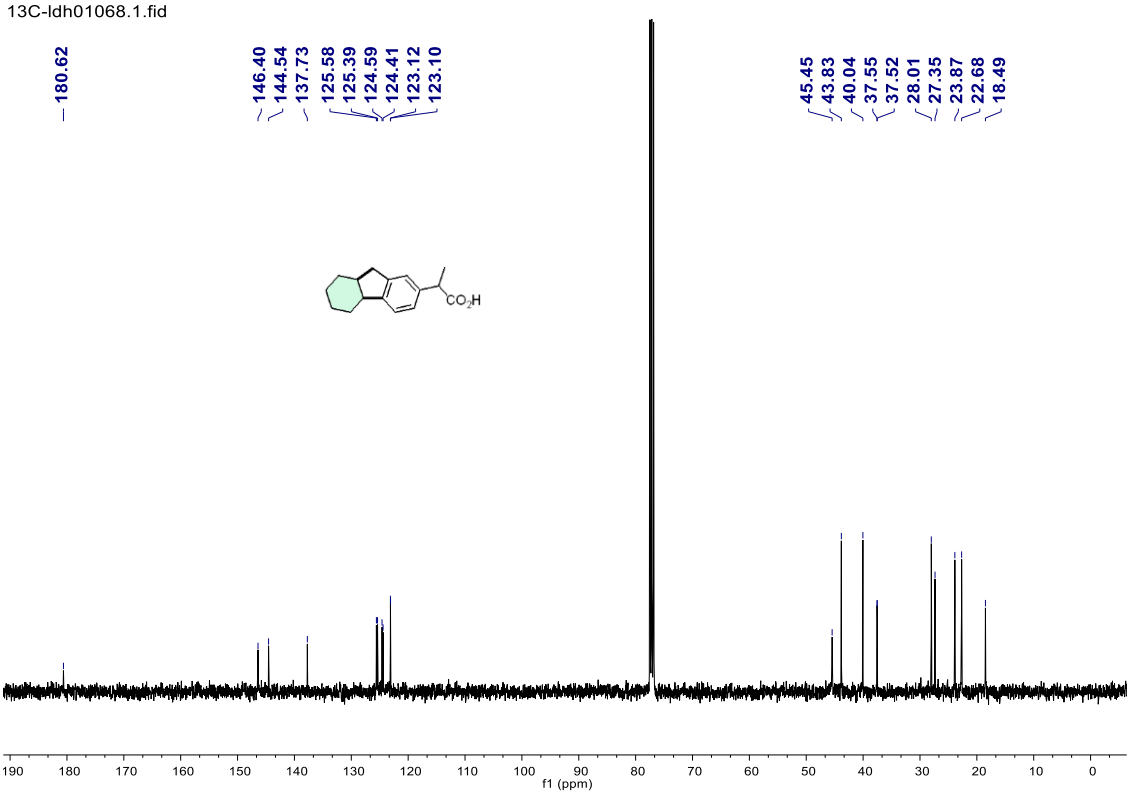
Spectrum 2-65 ^{1}H NMR of compound 59



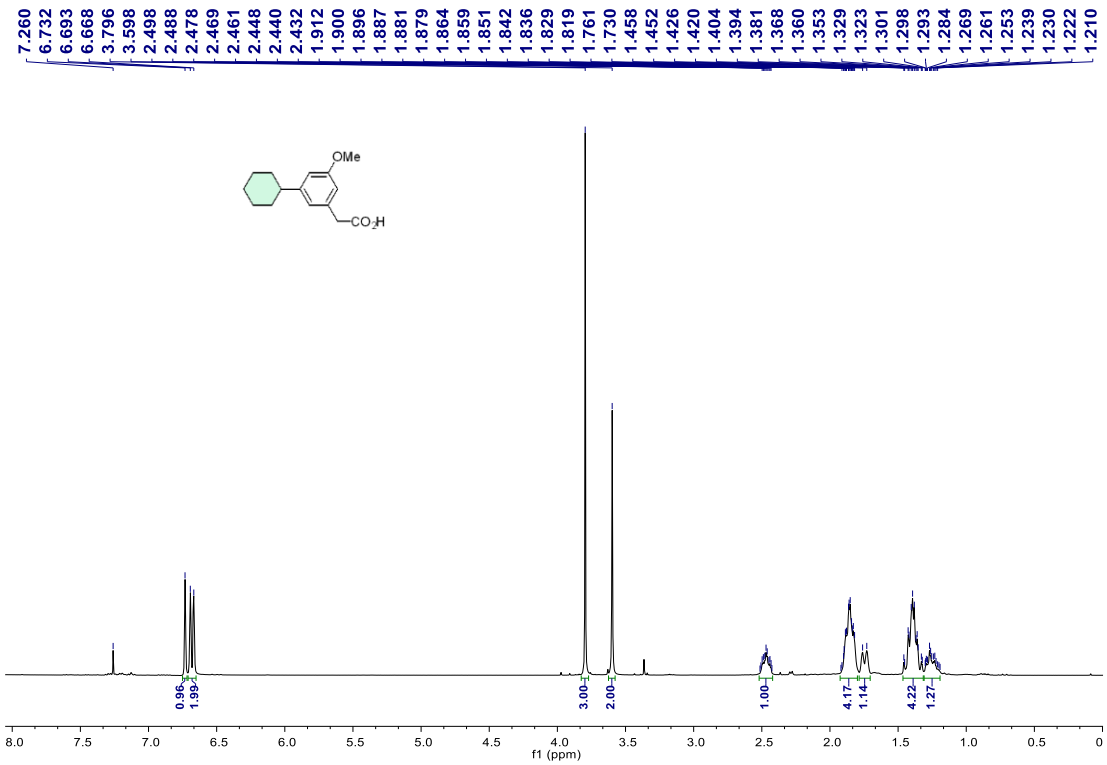
Spectrum 2-66 ^{13}C NMR of compound 59



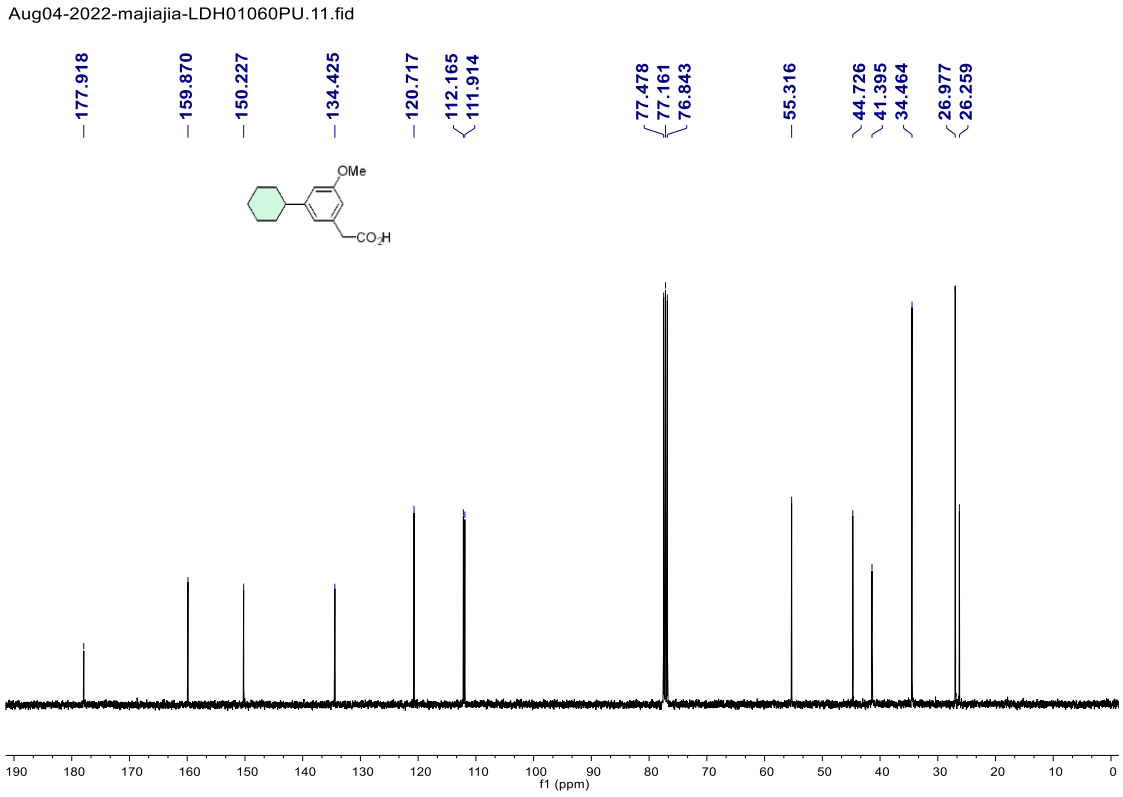
Spectrum 2-67 ^{1}H NMR of compound 62



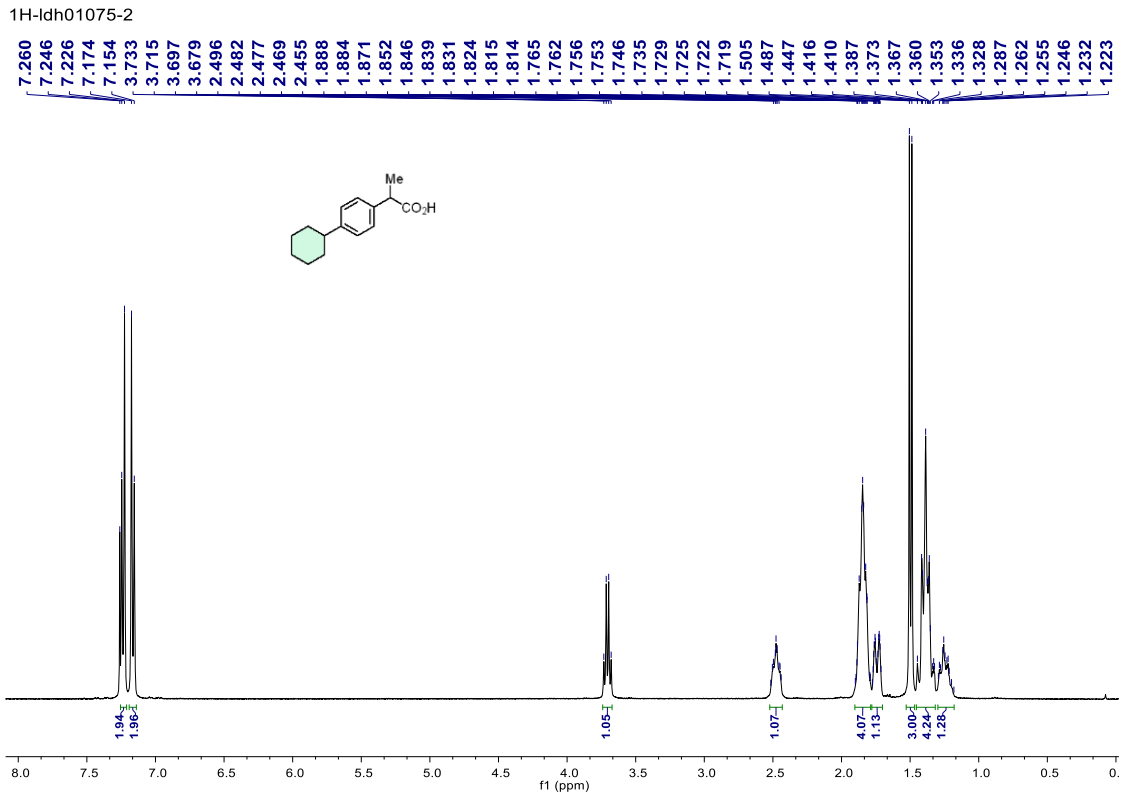
Spectrum 2-68 ^{13}C NMR of compound 62



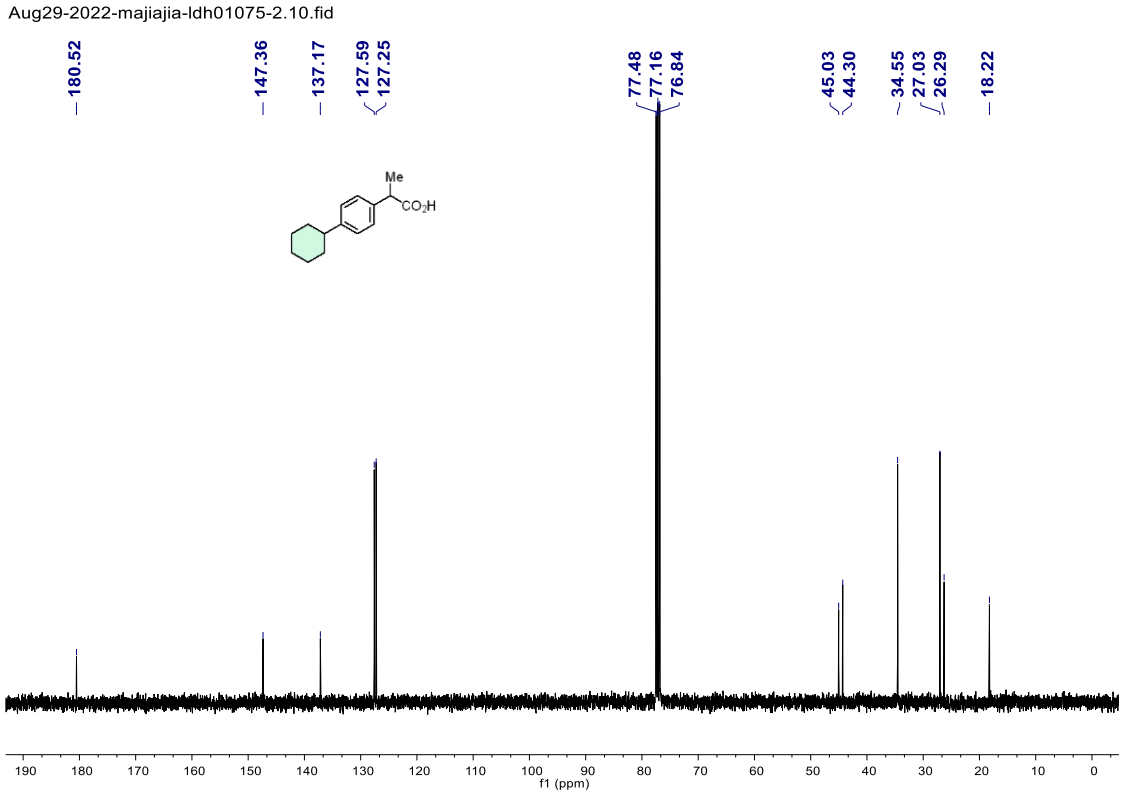
Spectrum 2-69 ^{1}H NMR of compound 67



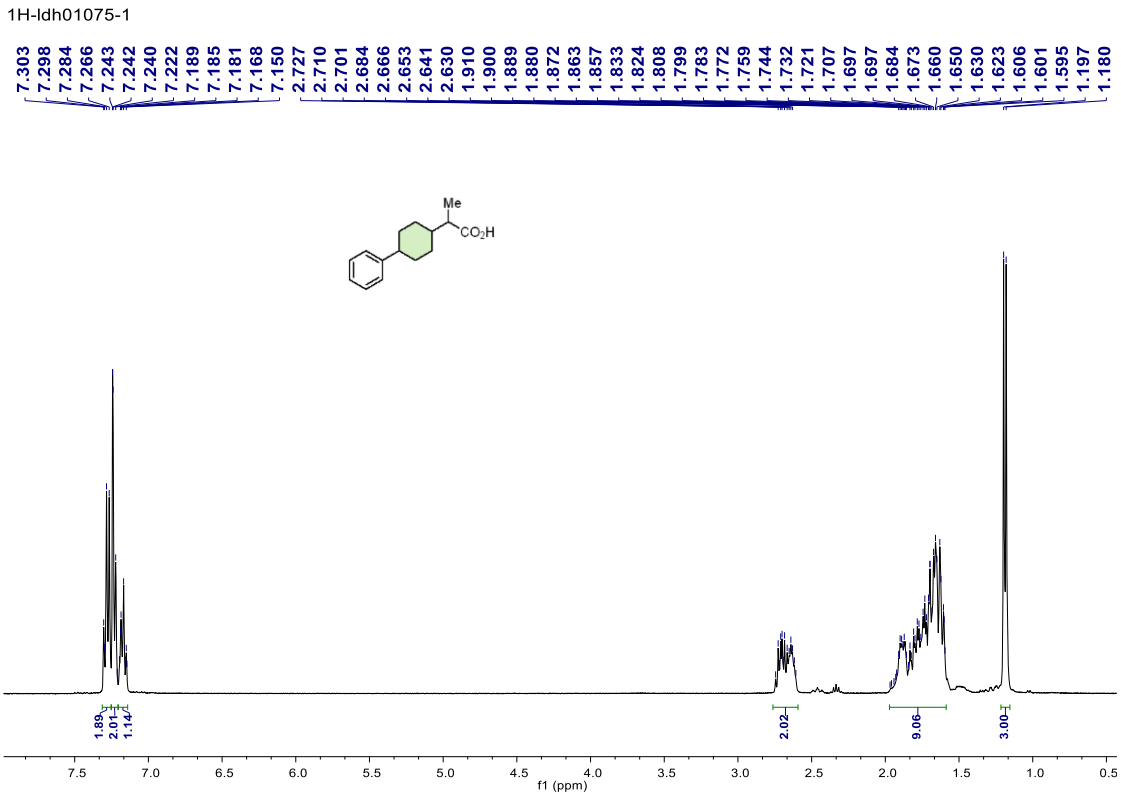
Spectrum 2-70 ^{13}C NMR of compound 67



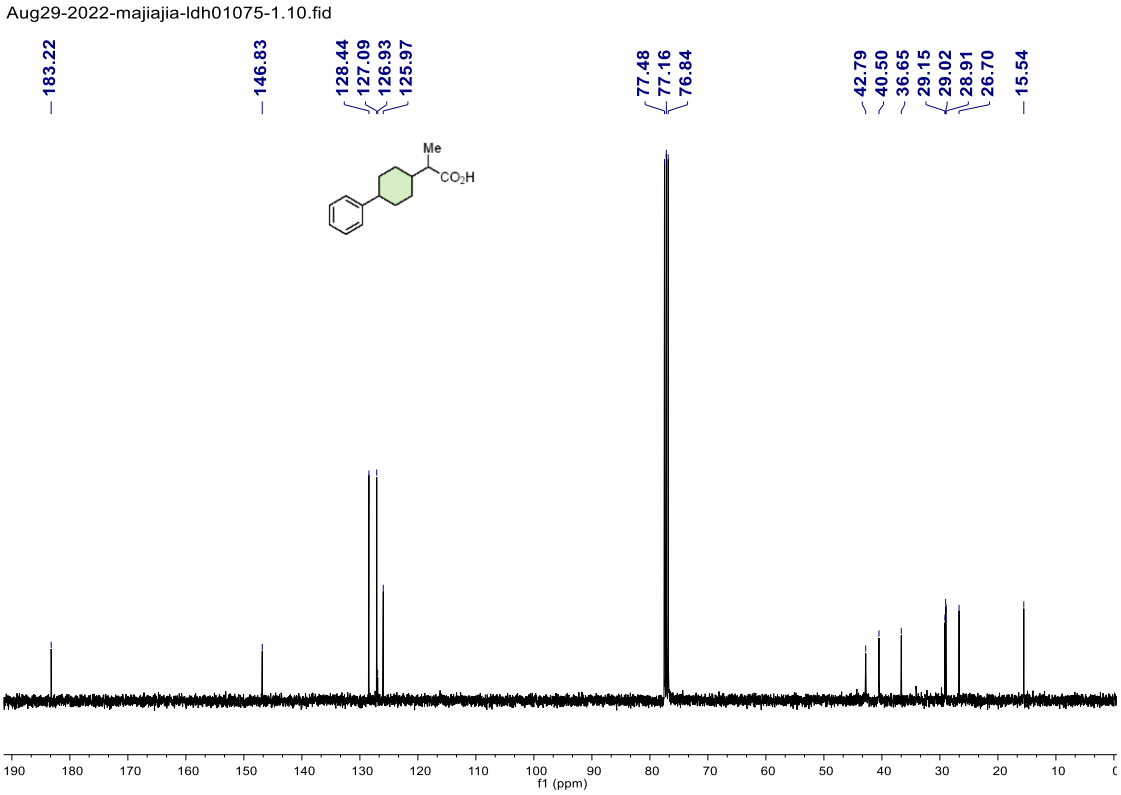
Spectrum 2-71 ^{1}H NMR of compound 69



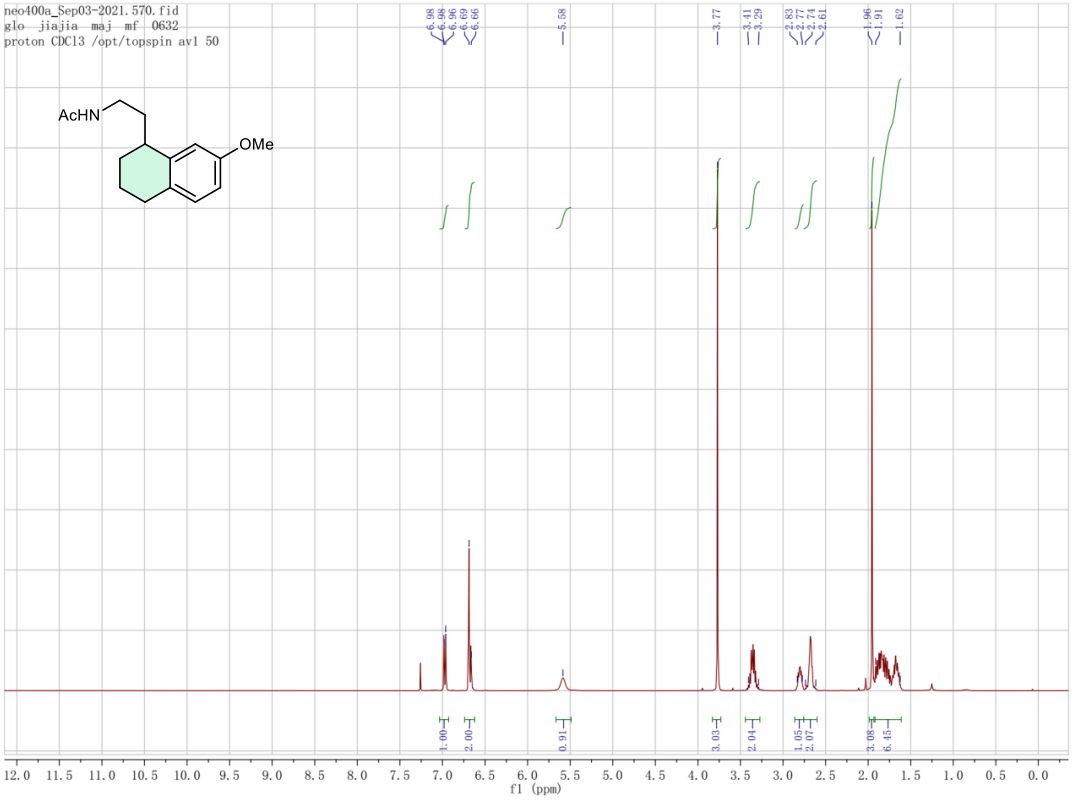
Spectrum 2-72 ^{13}C NMR of compound 69



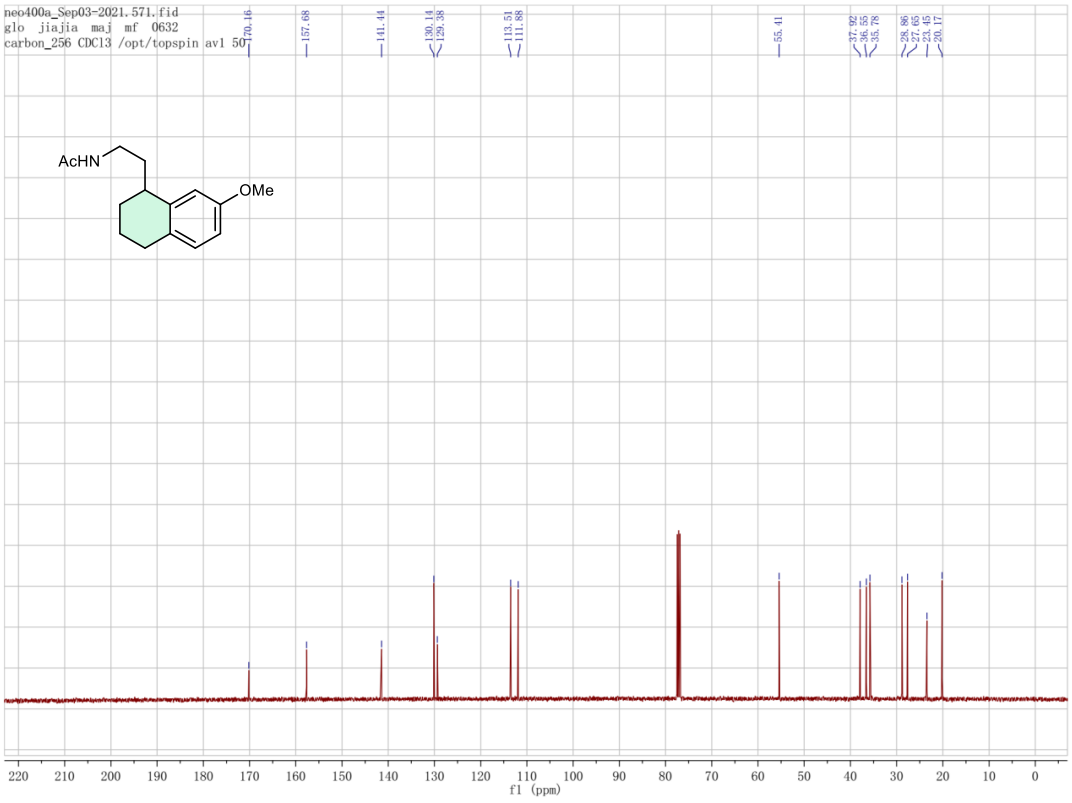
Spectrum 2-73 ^{1}H NMR of compound 71



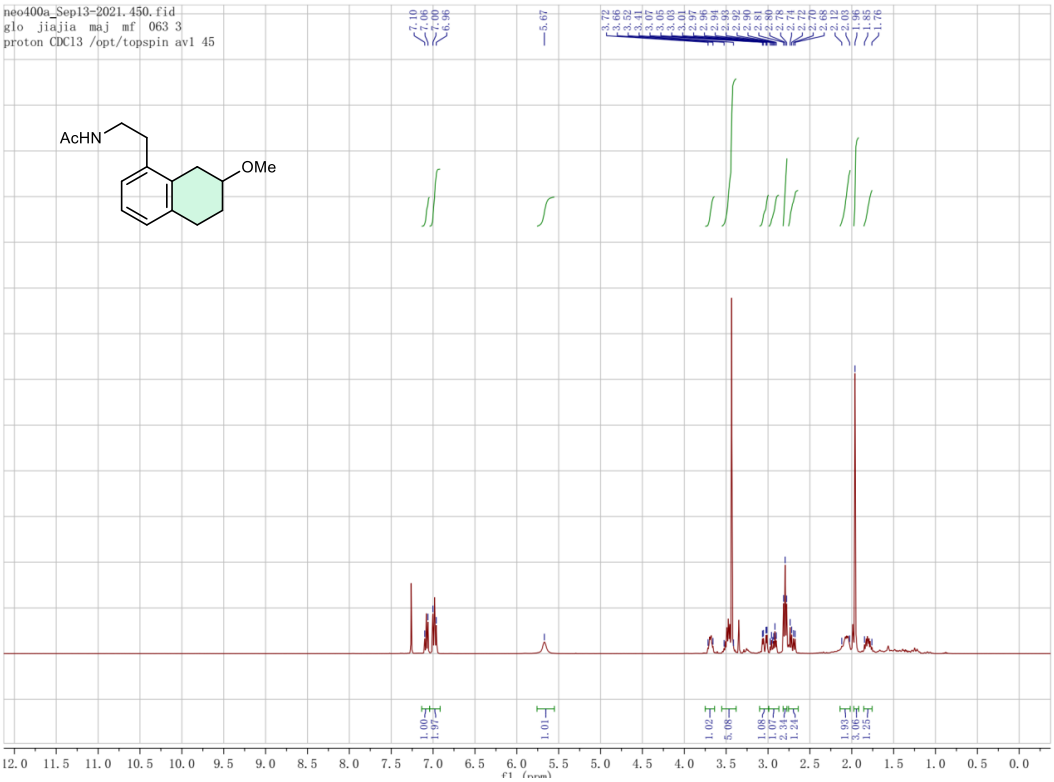
Spectrum 2-74 ^{1}H NMR of compound 71



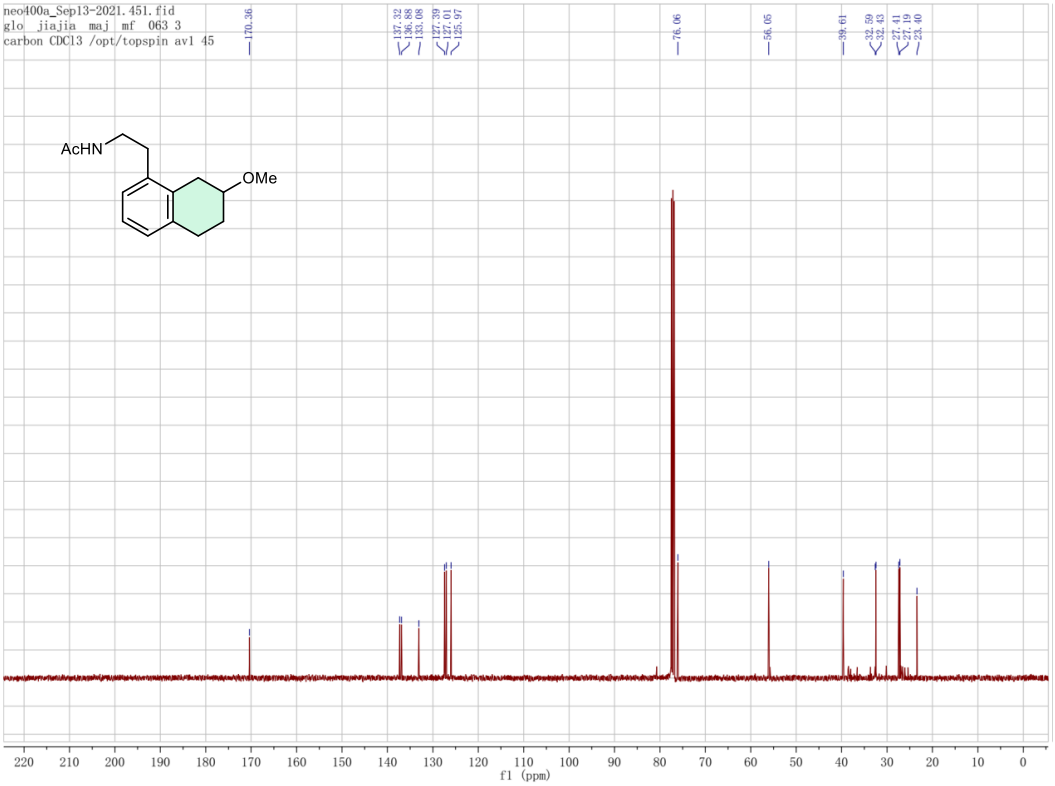
Spectrum 2-75 ^{1}H NMR of compound 74



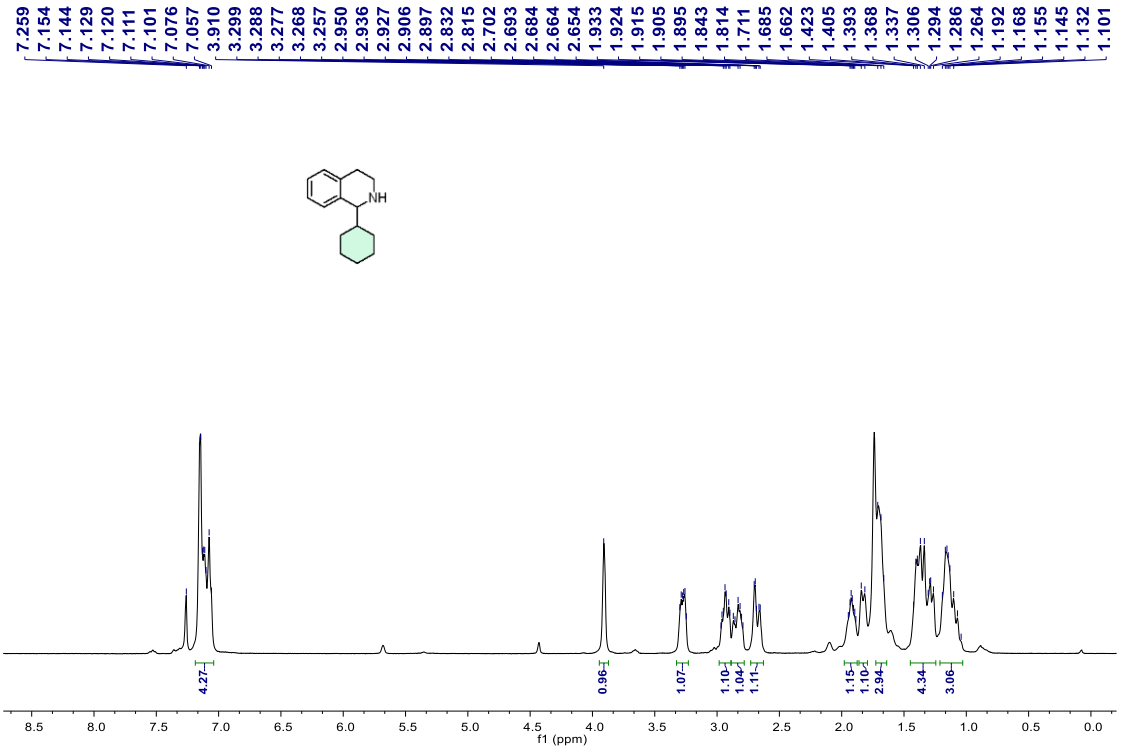
Spectrum 2-76 ^{13}C NMR of compound 74



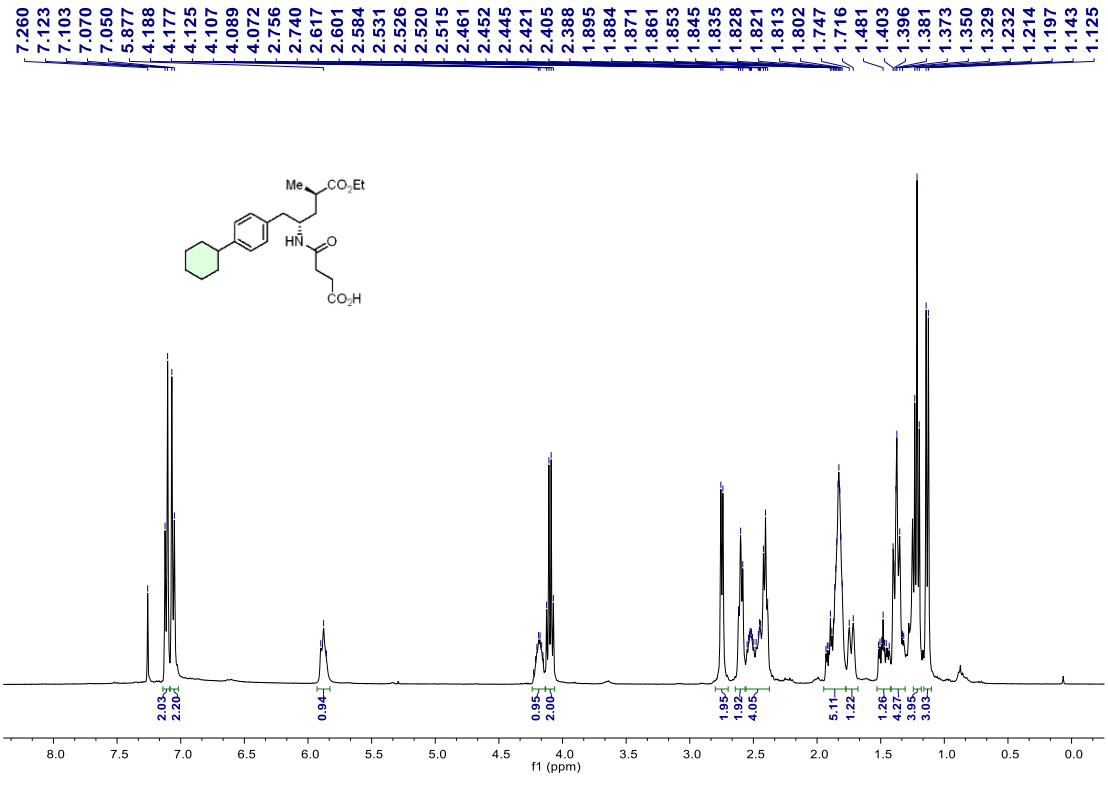
Spectrum 2-77 ^{1}H NMR of compound 74'



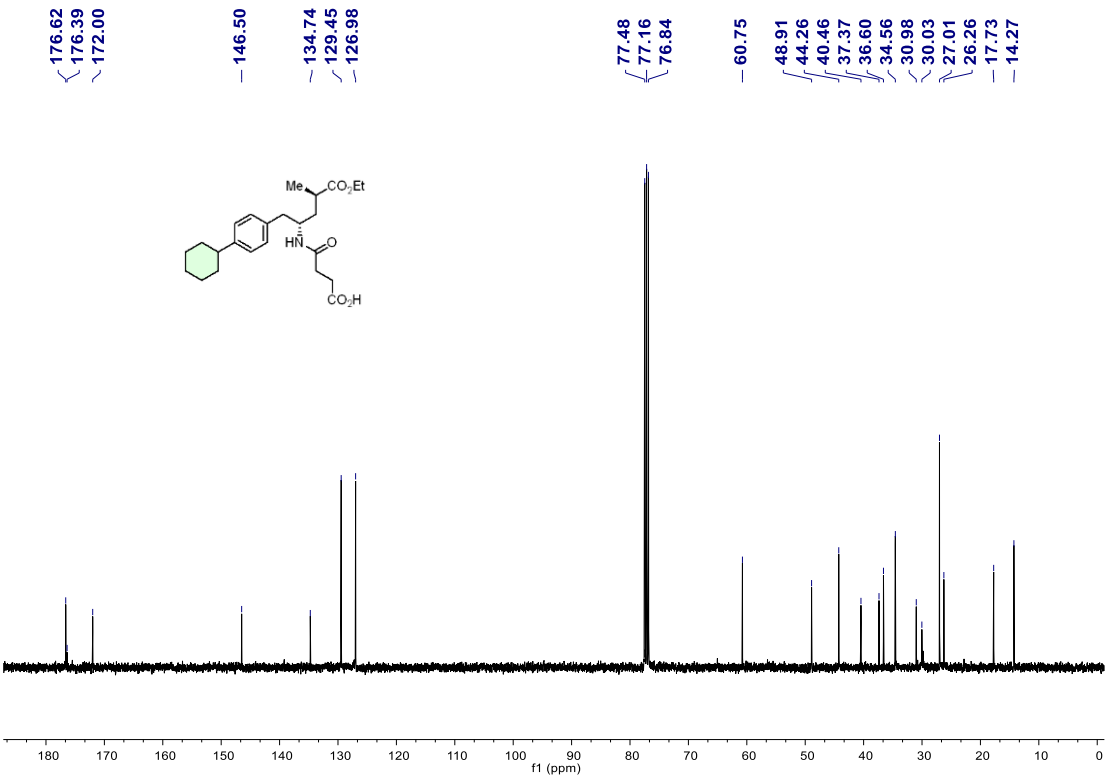
Spectrum 2-78 ^{13}C NMR of compound 74'



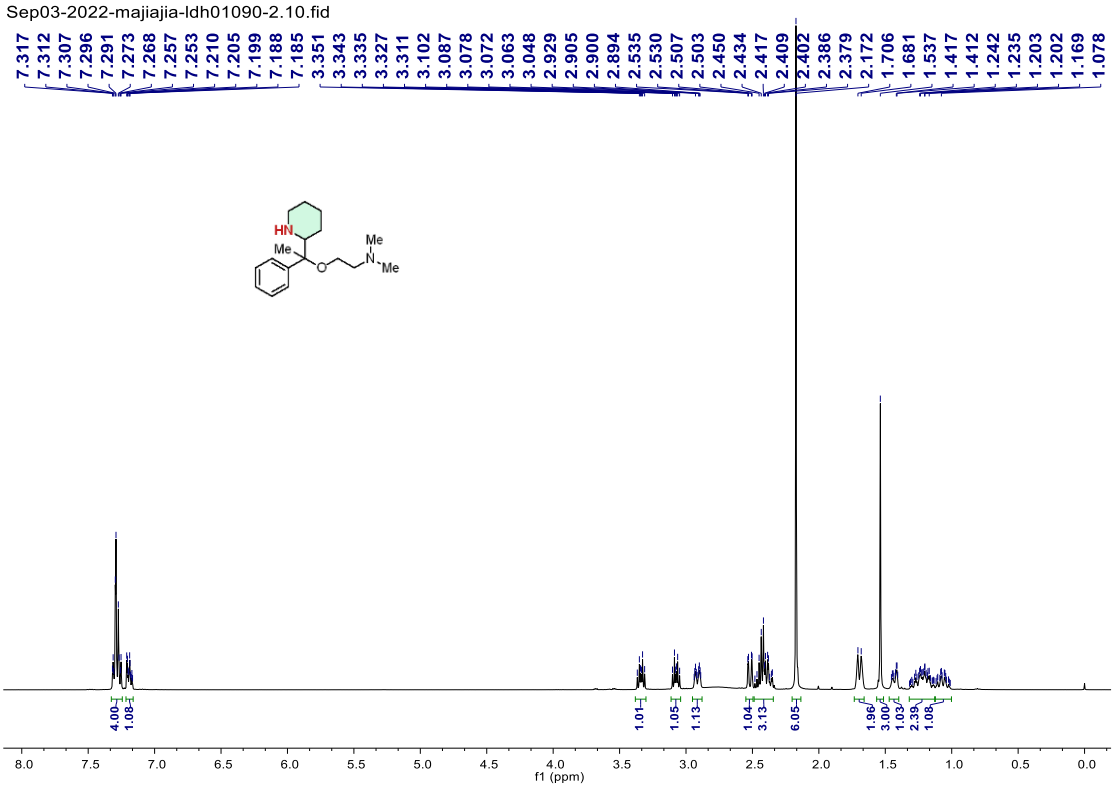
Spectrum 2-79 ^{1}H NMR of compound 77



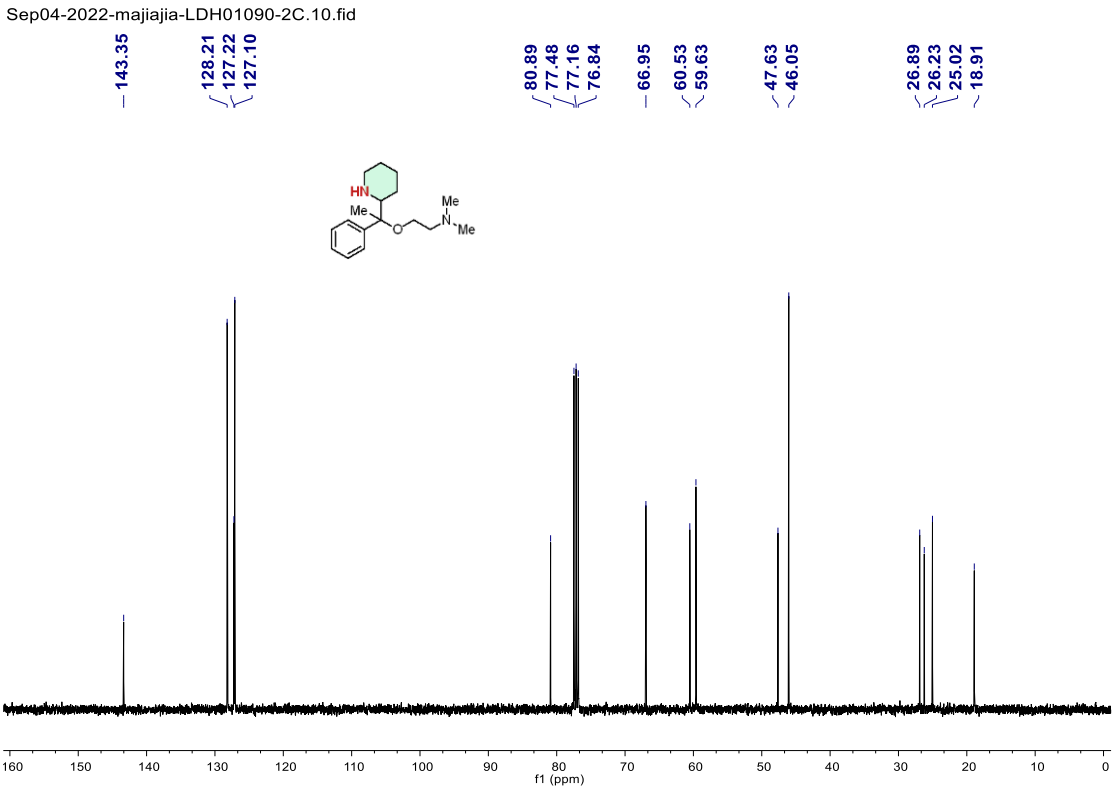
Spectrum 2-80 ^{1}H NMR of compound 79



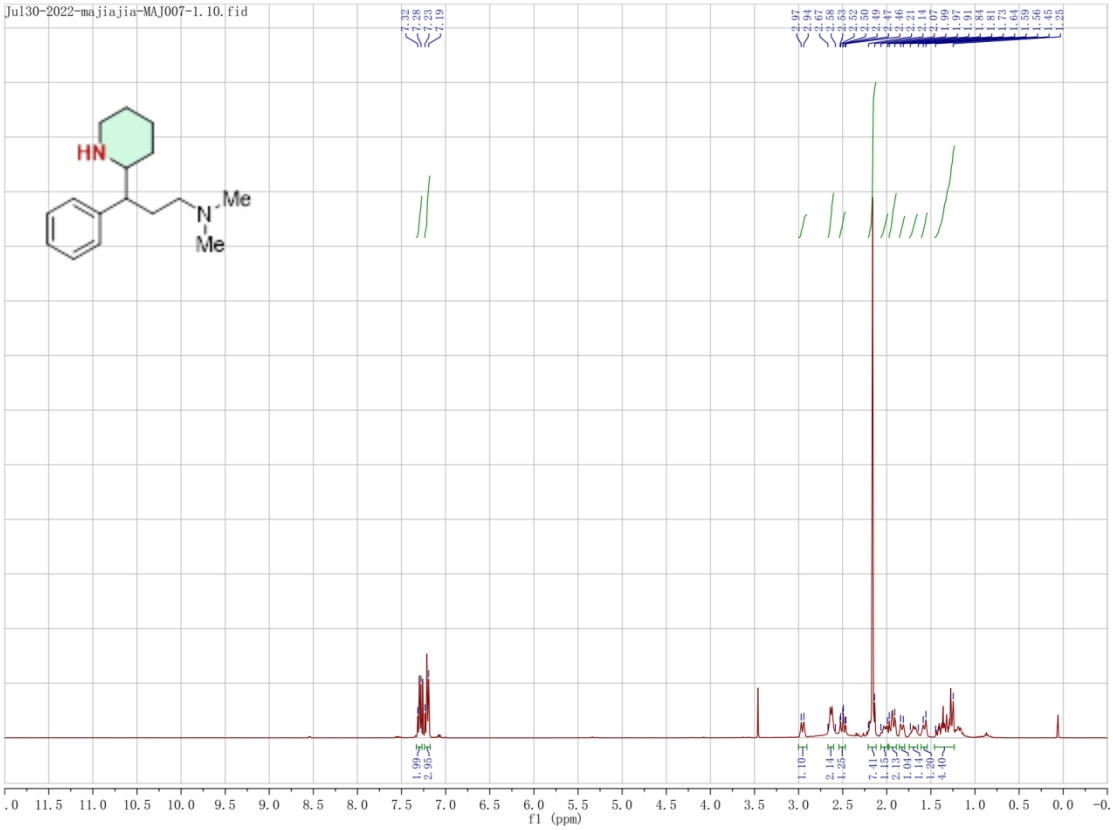
Spectrum 2-81 ^{13}C NMR of compound 79



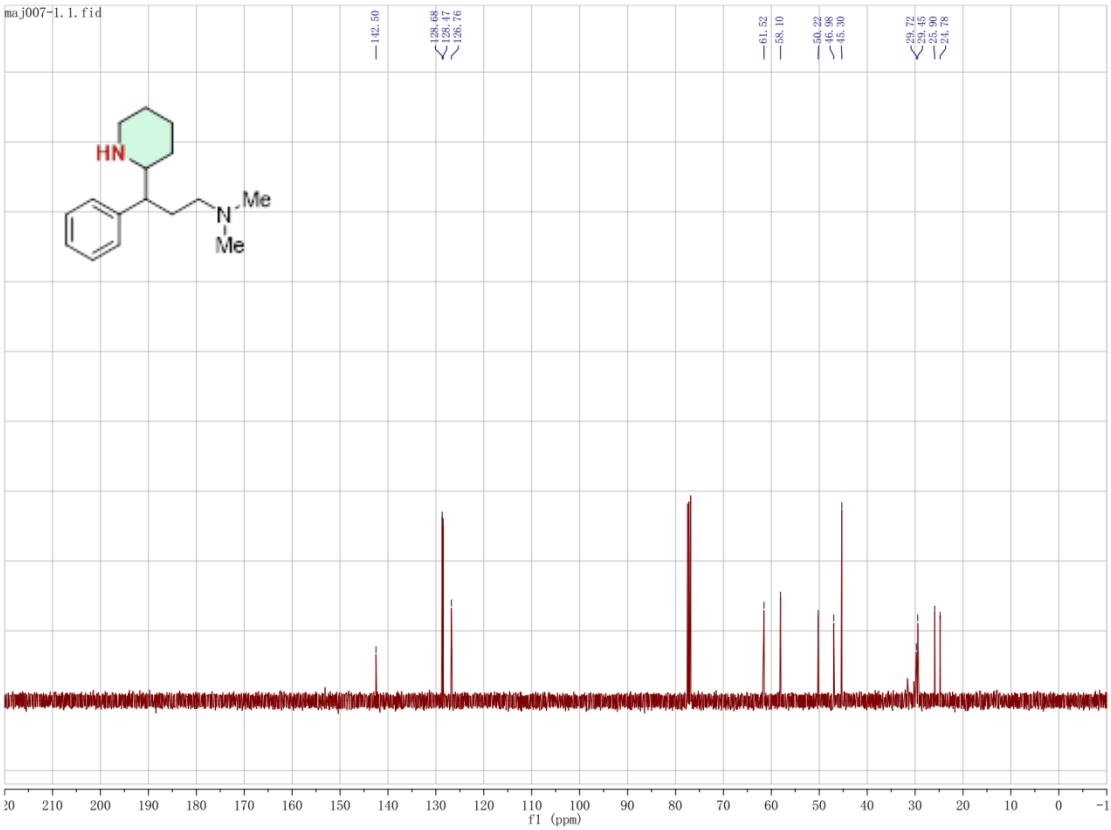
Spectrum 2-82 ^{1}H NMR of compound 80



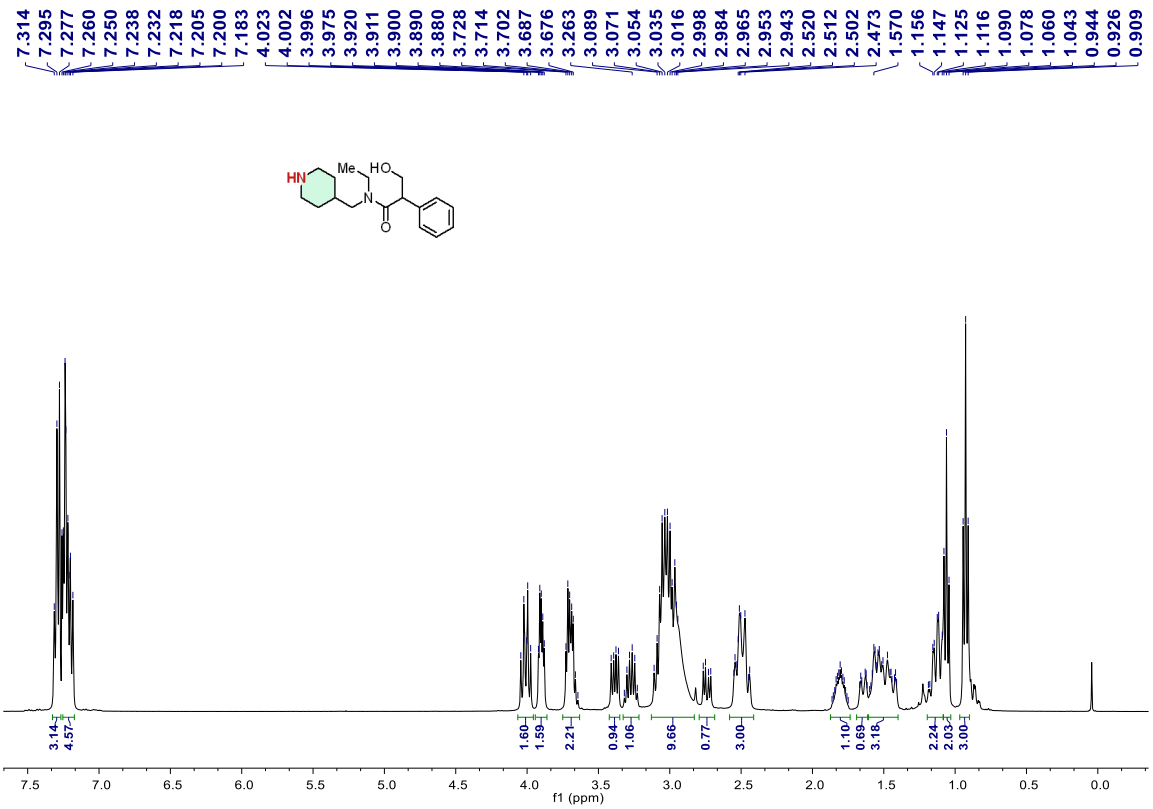
Spectrum 2-83 ^{13}C NMR of compound 80



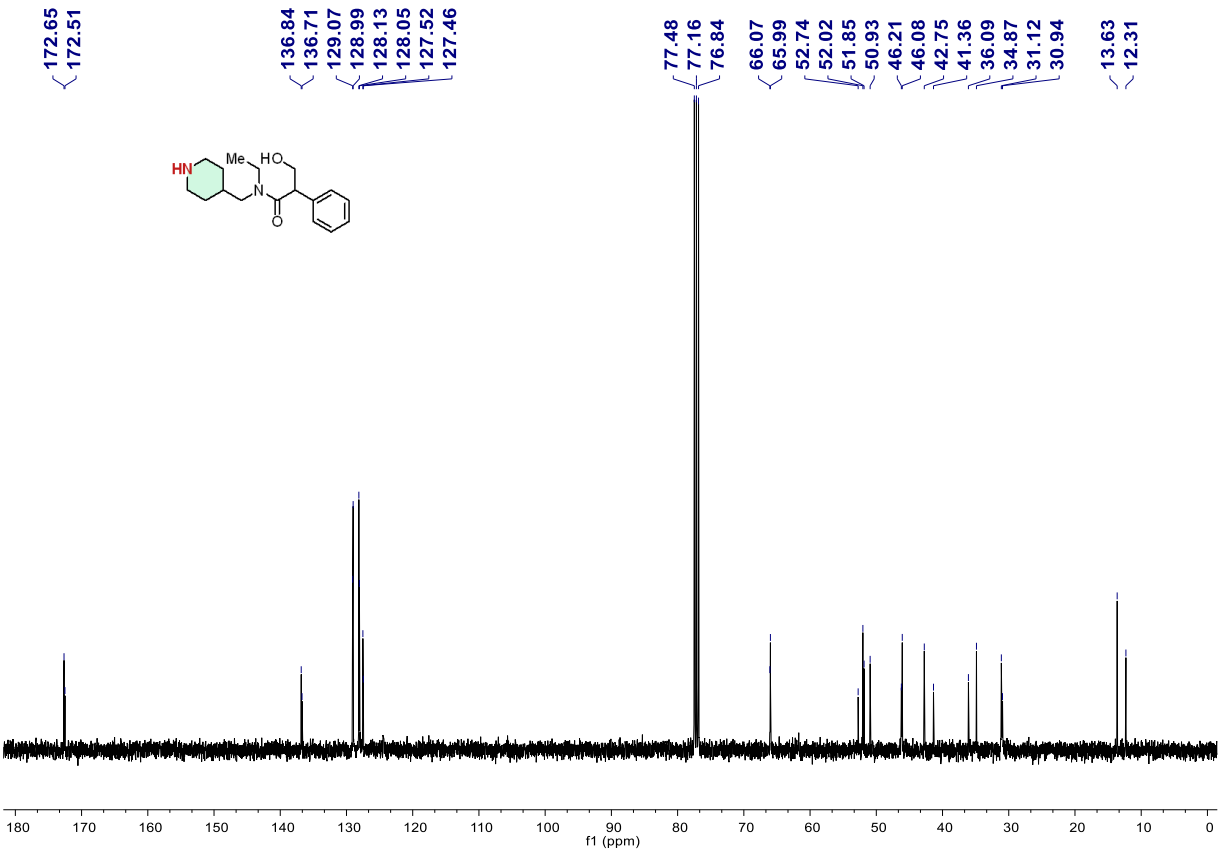
Spectrum 2-84 ^{1}H NMR of compound 81



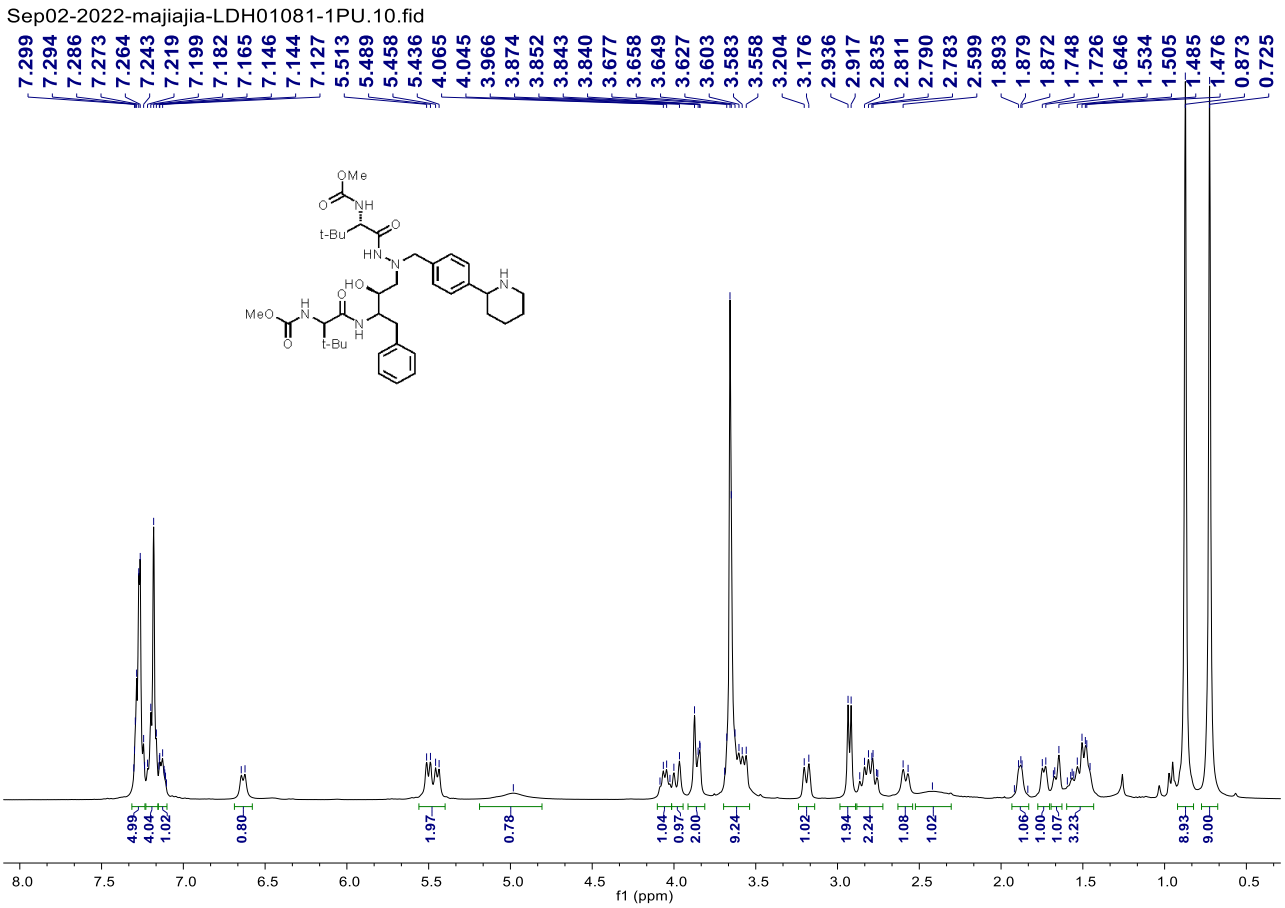
Spectrum 2-85 ^{13}C NMR of compound 81



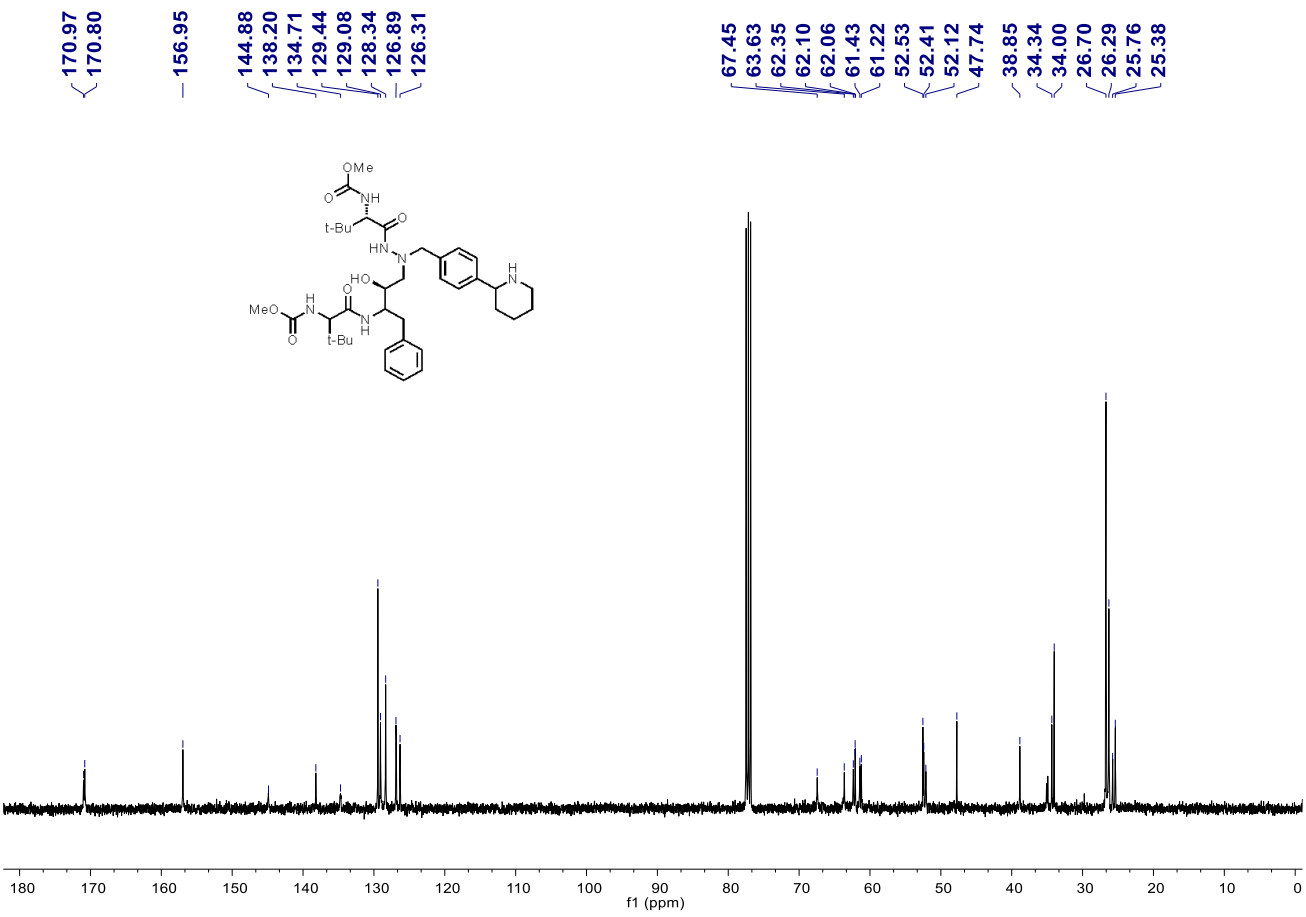
Spectrum 2-86 ^{1}H NMR of compound 82



Spectrum 2-87 ^{13}C NMR of compound 82



Spectrum 2-88 ^{1}H NMR of compound 83



Spectrum 2-89 ^{13}C NMR of compound 83

2.7 **References**

(87) Sabatier, P.; Senderens, J. Hydrogenations Directes Rdalis6es En Presence Du Nickel Reduit; Preparation de l'hexahydrobenzene. *Comptes Rendus* **1901**, *132*, 210–212.

(88) Wiesenfeldt, M. P.; Nairoukh, Z.; Li, W.; Glorius, F. Hydrogenation of Fluoroarenes: Direct Access to All-Cis-(Multi)Fluorinated Cycloalkanes. *Science* **2017**, *357* (6354), 908–912. https://doi.org/10.1126/science.aao0270.

(89) Nairoukh, Z.; Wollenburg, M.; Schlepphorst, C.; Bergander, K.; Glorius, F. The Formation of All-Cis-(Multi)Fluorinated Piperidines by a Dearomatization–Hydrogenation Process. *Nat. Chem.* **2019**, *11* (3), 264–270. https://doi.org/10.1038/s41557-018-0197-2.

(90) Gelis, C.; Heusler, A.; Nairoukh, Z.; Glorius, F. Catalytic Transfer Hydrogenation of Arenes and Heteroarenes. *Chem. – Eur. J.* **2020**, *26* (62), 14090–14094. https://doi.org/10.1002/chem.202002777.

(91) Huck, C. J.; Sarlah, D. Shaping Molecular Landscapes: Recent Advances, Opportunities, and Challenges in Dearomatization. *Chem* **2020**, *6* (7), 1589–1603. https://doi.org/10.1016/j.chempr.2020.06.015.

(92) Lückemeier, L.; Pierau, M.; Glorius, F. Asymmetric Arene Hydrogenation: Towards Sustainability and Application. *Chem. Soc. Rev.* **2023**, *52* (15), 4996–5012. https://doi.org/10.1039/D3CS00329A.

(93) Burrows, J.; Kamo, S.; Koide, K. Scalable Birch Reduction with Lithium and Ethylenediamine in Tetrahydrofuran. *Science* **2021**, *374* (6568), 741–746. https://doi.org/10.1126/science.abk3099.

(94) Ungarean, C. N.; Galer, P.; Zhang, Y.; Lee, K. S.; Ngai, J. M.; Lee, S.; Liu, P.; Sarlah, D. Synthesis of (+)-Ribostamycin by Catalytic, Enantioselective Hydroamination of Benzene. *Nat. Synth.* **2022**, *1* (7), 542–547. https://doi.org/10.1038/s44160-022-00080-x.

(95) Wang, Y.; Chang, Z.; Hu, Y.; Lin, X.; Dou, X. Mild and Selective Rhodium-Catalyzed Transfer Hydrogenation of Functionalized Arenes. *Org. Lett.* **2021**, *23* (5), 1910–1914. https://doi.org/10.1021/acs.orglett.1c00341.

(96) Zhou, Q.; Zhang, L.; Meng, W.; Feng, X.; Yang, J.; Du, H. Borane-Catalyzed Transfer Hydrogenations of Pyridines with Ammonia Borane. *Org. Lett.* **2016**, *18* (20), 5189–5191. https://doi.org/10.1021/acs.orglett.6b02610.

(97) Lovering, F.; Bikker, J.; Humblet, C. Escape from Flatland: Increasing Saturation as an Approach to Improving Clinical Success. *J. Med. Chem.* **2009**, *52* (21), 6752–6756. https://doi.org/10.1021/jm901241e.

(98) Ritchie, T. J.; Macdonald, S. J. F. The Impact of Aromatic Ring Count on Compound Developability – Are Too Many Aromatic Rings a Liability in Drug Design? *Drug Discov. Today* **2009**, *14* (21–22), 1011–1020. https://doi.org/10.1016/j.drudis.2009.07.014.

(99) Chu, J. C. K.; Rovis, T. Complementary Strategies for Directed C(Sp^3)−H Functionalization: A Comparison of Transition-Metal-Catalyzed Activation, Hydrogen Atom Transfer, and Carbene/Nitrene Transfer. *Angew. Chem. Int. Ed.* **2018**, *57* (1), 62–101. https://doi.org/10.1002/anie.201703743.

(100) Choi, J.; Fu, G. C. Transition Metal–Catalyzed Alkyl-Alkyl Bond Formation: Another Dimension in Cross-Coupling Chemistry. *Science* **2017**, *356* (6334), eaaf7230. https://doi.org/10.1126/science.aaf7230.

(101) Cernak, T.; Dykstra, K. D.; Tyagarajan, S.; Vachal, P.; Krska, S. W. The Medicinal Chemist's Toolbox for Late Stage Functionalization of Drug-like Molecules. *Chem. Soc. Rev.* **2016**, *45* (3), 546–576. https://doi.org/10.1039/C5CS00628G.

(102) Campos, K. R.; Coleman, P. J.; Alvarez, J. C.; Dreher, S. D.; Garbaccio, R. M.; Terrett, N. K.; Tillyer, R. D.; Truppo, M. D.; Parmee, E. R. The Importance of Synthetic Chemistry in the Pharmaceutical Industry. *Science* **2019**, *363* (6424), eaat0805. https://doi.org/10.1126/science.aat0805.

(103) Börgel, J.; Ritter, T. Late-Stage Functionalization. *Chem* **2020**, *6* (8), 1877–1887. https://doi.org/10.1016/j.chempr.2020.07.007.

(104) Moir, M.; Danon, J. J.; Reekie, T. A.; Kassiou, M. An Overview of Late-Stage Functionalization in Today's Drug Discovery. *Expert Opin. Drug Discov.* **2019**, *14* (11), 1137–1149. https://doi.org/10.1080/17460441.2019.1653850.

(105) Guillemard, L.; Kaplaneris, N.; Ackermann, L.; Johansson, M. J. Late-Stage C–H Functionalization Offers New Opportunities in Drug Discovery. *Nat. Rev. Chem.* **2021**, *5* (8), 522–545. https://doi.org/10.1038/s41570-021-00300-6.

(106) Kim, S.; Chen, J.; Cheng, T.; Gindulyte, A.; He, J.; He, S.; Li, Q.; Shoemaker, B. A.; Thiessen, P. A.; Yu, B.; Zaslavsky, L.; Zhang, J.; Bolton, E. E. PubChem in 2021: New Data Content and Improved Web Interfaces. *Nucleic Acids Res.* **2021**, *49* (D1), D1388–D1395. https://doi.org/10.1093/nar/gkaa971.

(107) Ishikawa, M.; Hashimoto, Y. Improvement in Aqueous Solubility in Small Molecule Drug Discovery Programs by Disruption of Molecular Planarity and Symmetry. *J. Med. Chem.* **2011**, *54* (6), 1539–1554. https://doi.org/10.1021/jm101356p.

(108) Krzyzanowski, A.; Pahl, A.; Grigalunas, M.; Waldmann, H. Spacial Score─A Comprehensive Topological Indicator for Small-Molecule Complexity. *J. Med. Chem.* **2023**, *66* (18), 12739–12750. https://doi.org/10.1021/acs.jmedchem.3c00689.

(109) Brown, D. G.; Boström, J. Analysis of Past and Present Synthetic Methodologies on Medicinal Chemistry: Where Have All the New Reactions Gone?: Miniperspective. *J. Med. Chem.* **2016**, *59* (10), 4443–4458. https://doi.org/10.1021/acs.jmedchem.5b01409.

(110) Zhang, L.; Lin, D.; Kusov, Y.; Nian, Y.; Ma, Q.; Wang, J.; Von Brunn, A.; Leyssen, P.; Lanko, K.; Neyts, J.; De Wilde, A.; Snijder, E. J.; Liu, H.; Hilgenfeld, R. α-Ketoamides as Broad-Spectrum Inhibitors of Coronavirus and Enterovirus Replication: Structure-Based

Design, Synthesis, and Activity Assessment. *J. Med. Chem.* **2020**, *63* (9), 4562–4578. https://doi.org/10.1021/acs.jmedchem.9b01828.

(111) Dai, W.; Zhang, B.; Jiang, X.-M.; Su, H.; Li, J.; Zhao, Y.; Xie, X.; Jin, Z.; Peng, J.; Liu, F.; Li, C.; Li, Y.; Bai, F.; Wang, H.; Cheng, X.; Cen, X.; Hu, S.; Yang, X.; Wang, J.; Liu, X.; Xiao, G.; Jiang, H.; Rao, Z.; Zhang, L.-K.; Xu, Y.; Yang, H.; Liu, H. Structure-Based Design of Antiviral Drug Candidates Targeting the SARS-CoV-2 Main Protease. *Science* **2020**, *368* (6497), 1331–1335. https://doi.org/10.1126/science.abb4489.

(112) Bregman, H.; Chakka, N.; Guzman-Perez, A.; Gunaydin, H.; Gu, Y.; Huang, X.; Berry, V.; Liu, J.; Teffera, Y.; Huang, L.; Egge, B.; Mullady, E. L.; Schneider, S.; Andrews, P. S.; Mishra, A.; Newcomb, J.; Serafino, R.; Strathdee, C. A.; Turci, S. M.; Wilson, C.; DiMauro, E. F. Discovery of Novel, Induced-Pocket Binding Oxazolidinones as Potent, Selective, and Orally Bioavailable Tankyrase Inhibitors. *J. Med. Chem.* **2013**, *56* (11), 4320–4342. https://doi.org/10.1021/jm4000038.

(113) Mendez, D.; Gaulton, A.; Bento, A. P.; Chambers, J.; De Veij, M.; Félix, E.; Magariños, M. P.; Mosquera, J. F.; Mutowo, P.; Nowotka, M.; Gordillo-Marañón, M.; Hunter, F.; Junco, L.; Mugumbate, G.; Rodriguez-Lopez, M.; Atkinson, F.; Bosc, N.; Radoux, C. J.; Segura-Cabrera, A.; Hersey, A.; Leach, A. R. ChEMBL: Towards Direct Deposition of Bioassay Data. *Nucleic Acids Res.* **2019**, *47* (D1), D930–D940. https://doi.org/10.1093/nar/gky1075.

(114) Ling, Y.; Hao, Z.-Y.; Liang, D.; Zhang, C.-L.; Liu, Y.-F.; Wang, Y. The Expanding Role of Pyridine and Dihydropyridine Scaffolds in Drug Design. *Drug Des. Devel. Ther.* **2021**, *Volume 15*, 4289–4338. https://doi.org/10.2147/DDDT.S329547.

(115) Sadybekov, A. V.; Katritch, V. Computational Approaches Streamlining Drug Discovery. *Nature* **2023**, *616* (7958), 673–685. https://doi.org/10.1038/s41586-023-05905-z.

(116) Buitrago Santanilla, A.; Regalado, E. L.; Pereira, T.; Shevlin, M.; Bateman, K.; Campeau, L.-C.; Schneeweis, J.; Berritt, S.; Shi, Z.-C.; Nantermet, P.; Liu, Y.; Helmy, R.; Welch, C. J.; Vachal, P.; Davies, I. W.; Cernak, T.; Dreher, S. D. Nanomole-Scale High-Throughput Chemistry for the Synthesis of Complex Molecules. *Science* **2015**, *347* (6217), 49–53. https://doi.org/10.1126/science.1259203.

(117) Gesmundo, N. J.; Sauvagnat, B.; Curran, P. J.; Richards, M. P.; Andrews, C. L.; Dandliker, P. J.; Cernak, T. Nanoscale Synthesis and Affinity Ranking. *Nature* **2018**, *557* (7704), 228–232. https://doi.org/10.1038/s41586-018-0056-8.

(118) Gesmundo, N.; Dykstra, K.; Douthwaite, J. L.; Kao, Y.-T.; Zhao, R.; Mahjour, B.; Ferguson, R.; Dreher, S.; Sauvagnat, B.; Saurí, J.; Cernak, T. Miniaturization of Popular Reactions from the Medicinal Chemists' Toolbox for Ultrahigh-Throughput Experimentation. *Nat. Synth.* **2023**, *2* (11), 1082–1091. https://doi.org/10.1038/s44160-023-00351-1.

(119) Allegretti, M.; Cesta, M. C.; Bertini, R.; Bizzarri, C.; Colotta, F. 2-Aryl-Propionic Acids and Pharmaceutical Compositions Containing Them. WO2003043625A1, May 30, 2003. https://patents.google.com/patent/WO2003043625A1/en?oq=WO2003043625A1 (accessed 2025-10-27).

(120) Sprague, P. W.; Heikes, J. E. Synthesis and Antiinflammatory Activity of Cis-4,5,6,7,8,8a,9-Hexahydro-.Alpha.-Methyl-5H-Fluorene-2-Acetic Acid. *J. Med. Chem.* **1977**, *20* (5), 726–728. https://doi.org/10.1021/jm00215a023.

(121) Tamura, Y.; Yoshimoto, Y.; Kunimoto, K.; Tada, S.; Tomita, T.; Wada, T.; Seto, E.; Murayama, M.; Shibata, Y. Nonsteroidal Antiinflammatory Agents. 1. 5-Alkoxy-3-Biphenylylacetic Acids and Related Compounds as New Potential Antiinflammatory Agents. *J. Med. Chem.* **1977**, *20* (5), 709–714. https://doi.org/10.1021/jm00215a018.

(122) Moriconi, A.; Cesta, M. C.; Cervellera, M. N.; Aramini, A.; Coniglio, S.; Colagioia, S.; Beccari, A. R.; Bizzarri, C.; Cavicchia, M. R.; Locati, M.; Galliera, E.; Di Benedetto, P.; Vigilante, P.; Bertini, R.; Allegretti, M. Design of Noncompetitive Interleukin-8 Inhibitors Acting on CXCR1 and CXCR2. *J. Med. Chem.* **2007**, *50* (17), 3984–4002. https://doi.org/10.1021/jm061469t.

(123) Fourmaintraux, E.; Depreux, P.; Lesieur, D.; Guardiola-Lemaître, B.; Bennejean, C.; Delagrange, P.; Howell, H. E. Tetrahydronaphthalenic Derivatives as New Agonist and Antagonist Ligands for Melatonin Receptors. *Bioorg. Med. Chem.* **1998**, *6* (1), 9–13. https://doi.org/10.1016/S0968-0896(97)00175-2.

(124) Abe, M.; Munakata, H.; Abe, K.; Saito, T.; Horiguchi, Y.; Nojima, H.; Taguchi, K. Effects of 1-Cyclohexyl- and 1-Cyclohexyl-N-Propargyl-1,2,3,4-Tetrahydroisoquinoline on Dopaminergic Spontaneous Discharge in Nigral Neurons of Rats. *Brain Res. Bull.* **2016**, *121*, 201–208. https://doi.org/10.1016/j.brainresbull.2016.02.007.

Chapter 3 FRET for Reaction Development

3.1 **Introduction**

As detailed in the prior discussion in Chapter 1, HTE is a rapidly expanding field with new technologies and applications emerging all the time. The continuous development of new automation platforms has allowed chemists to set up hundreds or thousands of reactions in a single day with relative ease.[29,116,118] On the contrary, only modest headway has been made in improving analytical turn-around times for extracting data from these increasingly large HTE datasets. The most frequently employed analytical technique in HTE, liquid chromatography-mass spectrometry (LC–MS), still requires upwards of several minutes of instrument runtime per sample.

MALDI–TOF–MS (Matrix-Assisted Laser Desorption/Ionization Time-Of-Flight Mass Spectrometry)[76] and NL–ADE–MS (Neutral Loss Acoustic Droplet Ejection Mass Spectrometry)[77] cut analytical runtimes down to ~1 to 2 seconds per sample but require expensive and specialized equipment or limit the breadth of data that can be retrieved from each sample. Additionally, the time required for manual deconvolution and identification of the materials in each reaction mixture remains time intensive. Hartwig's "Snap Deconvolution" approach[79] helps to accelerate deconvolution at the expense of increasing the number of samples that must be analyzed. When scaled to the analysis of several thousand complex reaction mixtures, this approach becomes unfeasible. As such, we sought to develop a high-throughput analytical platform capable of addressing these issues.

3.2 **Reaction Deconvolution with FRET**

Towards this goal, we began exploring alternate techniques to help alleviate the slow analytical turnaround times in HTE. Native to the field of molecular biology, we envisioned Fluorescence Resonance Energy Transfer (FRET) would make an appealing reaction analysis platform for ultra miniaturized chemistry. Traditionally, FRET is used to detect fluorescent proteins and small molecules in close spatial proximity to one another in high-throughput biological assays.[125–128] Hartwig's work in the early 2000's provides an early showcase of FRET

in the analysis of 96-well chemical reactions[84–86] which inspired us towards the potential of FRET for 1,536-well plate HTE.

Tagging of reaction substrates with inert fluorescent labels would enable generation of fluorescence data on 1,536 reactions in a matter of minutes and an immediate green light on reaction success for follow-up analysis of hits. Quantification of the gain and loss of fluorescence by either fluorophore can be used to inform conversion from starting material to product, akin to an LC–MS assay yield. Additionally, the stringent requirements for FRET between two fluorophores also helps ensure selective detection of covalently coupled substrates. Requiring <10 nanometer separation distance between appropriately oriented fluorophores with overlapping spectral absorption and emission profiles ensures only covalently coupled substrates are capable of FRET interaction (Figure 3-1).

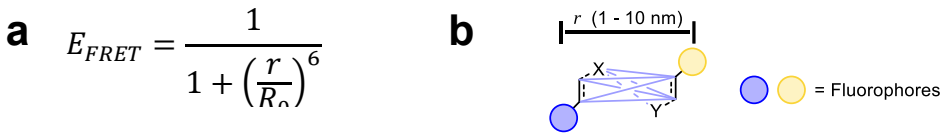


Figure 3-1 A) Equation for efficiency of FRET energy transfer, E_{FRET}. Inter-dye separation distance is represented by **r**. Förster distance, R_0, is proportional to the overlap of the emission band of one dye and the absorption band of the second dye as well as the molecular orientation between the two dyes. B) FRET is observable between the fluorescently labelled substrates when their with reaction handles, **X** and **Y**, couple together.

3.3 **Development of FRET Pairs**

While there are a substantial number of functional FRET pairs in the scientific literature,[125,126,129] our goal was to identify an inert FRET pair agnostic to the presence of common reaction conditions and additives. Compatibility of the dyes with a diverse range of appended functional groups is also an important consideration for FRET to be applicable to reaction development. In this venture, we identified the Perylene (**84**) and 4,4-difluoro-4-bora-3a,4a-diaza-s-indacene (BODIPY, **85**) scaffolds as a potential FRET pair of interest (Figure 3-2).

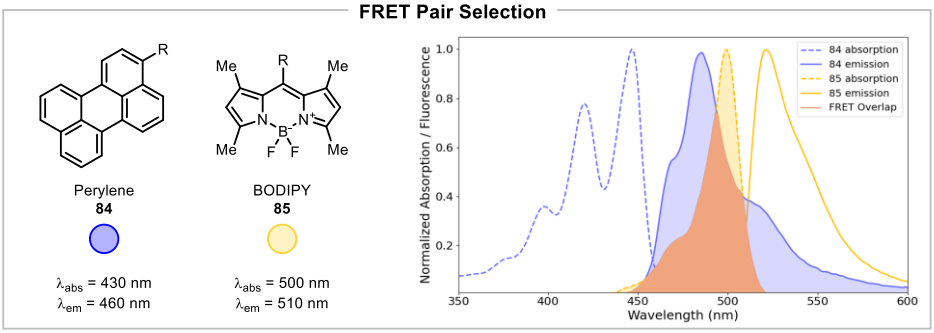


Figure 3-2 Depiction of the Perylene **84** and BODIPY **85** fluorophores. Normalized absorption and emission spectra of the two fluorophores are shown along with the spectral overlap required for FRET shaded as the orange curve.

Both the Perylene and BODIPY fluorophores can reportedly withstand a variety of diverse reaction conditions while also having been directly used in previous FRET applications.[130–135] As such, we undertook the development of several Perylene–BODIPY FRET pairs with a range of sp^2 and sp^3 tags to validate our proposed FRET system. As a starting point to begin development of our FRET platform, we chose an amine and carboxylic acid as representative functional groups for facile coupling to the resulting amide.

3.3.1 ***Perylene–BODIPY (sp^2-sp^3) Amine-Acid Pair***

Based on our prior successes in employing activated sp^2-amines as activated diazonium salts,[69,136] we first sought to develop an sp^2-amine and sp^3-acid dye pair to enable reaction development on diazonium-based amines. We employed a straightforward synthesis of aniline appended Perylene **87** via direct formylation of Perylene **84** followed by Wittig coupling with (4-nitrobenzyl)triphenylphosphonium bromide and subsequent Pd/C hydrogenation. Carboxylic acid-appended BODIPY **88** was synthesized in a one-step procedure from condensation and cyclization of glutaric anhydride with 2,4-dimethyl pyrrole, in the presence of boron trifluoride diethyl etherate (Figure 3-3).

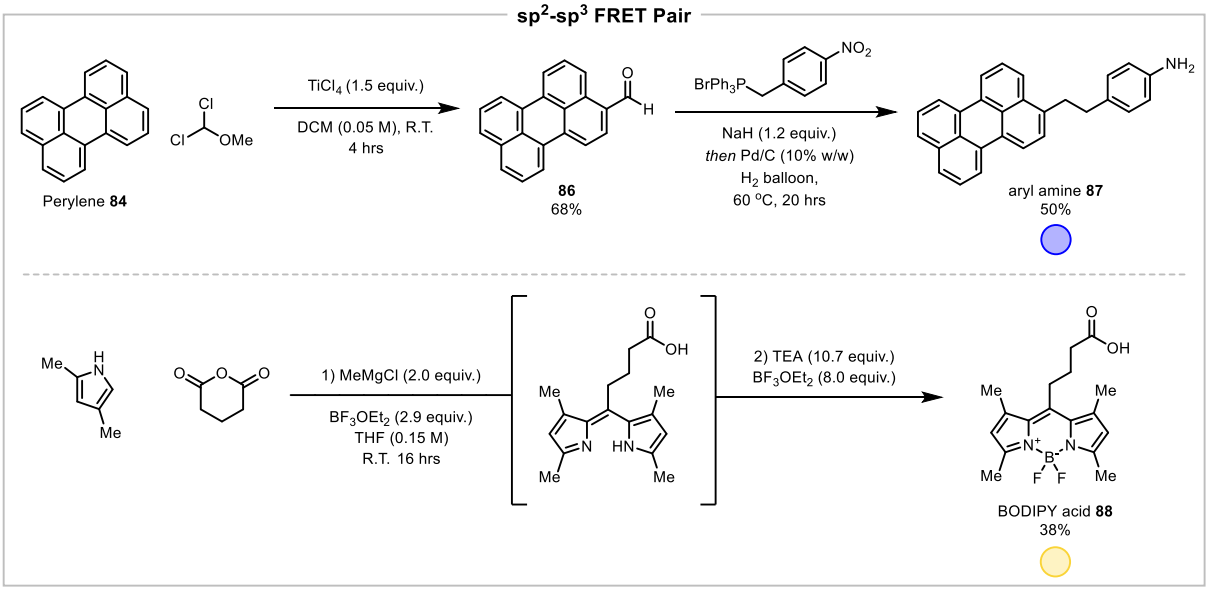


Figure 3-3 Two-step synthesis formylation and coupling step to synthesize Perylene aryl amine **87**. One-step synthesis of BODIPY acid **88** from dimethyl pyrrole and glutaric anhydride.

We conducted our initial studies to confirm FRET between Perylene **87** and BODIPY **88** via amide coupling of their sp^2-amine and sp^3-acid functionalities. Amide **89** revealed a 9.1-times increase in signal-to-noise (S/N), measured as the ratio of fluorescence measured at 510 nm and 460 nm for the coupled amide **89** compared to uncoupled **87** and **88** (Figure 3-4).

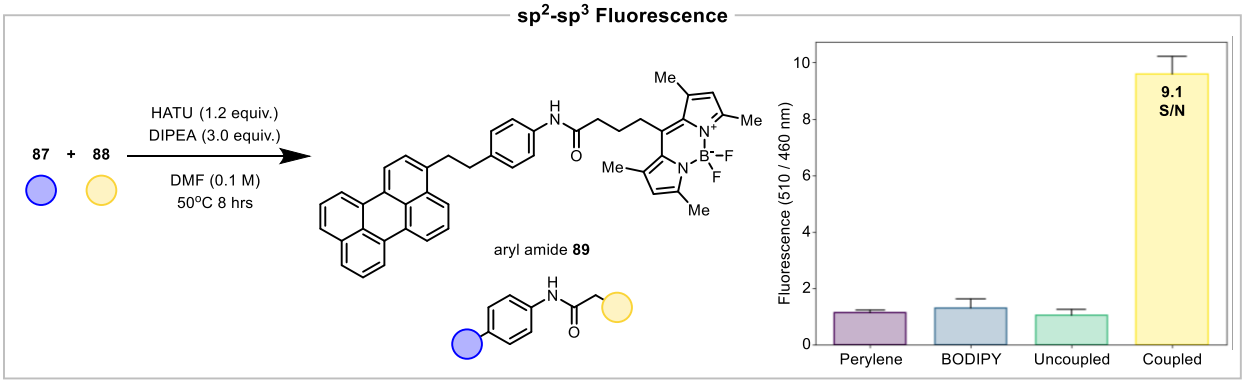


Figure 3-4 Coupling of sp^2 Perylene amine **87** with sp^3 BODIPY acid **88** to FRET-active amide **89**. The ratio of fluorescence at 510 / 460 nm reveals a 9.1-fold increase in fluorescence for the amide coupled dyes over the uncoupled dyes. All dyes are 10 μM in DMSO. Uncoupled fluorescence is reported from well containing 10 μM of both free amine and acid present. Excitation λ = 430 nm.

While these results demonstrated preliminary evidence towards our proposed Perylene-BODIPY FRET system, we also noted solubility issues with the sp^2-rich Perylene scaffold. Particularly when tailoring on the pendant aryl amine functionality, a substantial decrease in organic solubility was noted compared to the free Perylene dye. We reasoned that the increased lipophilicity and potential π-stacking interaction of the adjacent aniline is responsible for the evident insolubility. At this point, we turned towards an sp^3–sp^3 system to alleviate this issue.

3.3.2 Perylene-BODIPY (sp^3-sp^3) Amine-Acid Pair

Following common literature proceedings, we began synthesis of our sp^3-amine appended Perylene dye via NBS bromination and Sonogashira coupling with N-Boc-propargylamine. While bromination to **90** and the subsequent alkyne coupling steps proceeded smoothly, the propargylamine coupling introduced a conjugated alkyne that proved difficult to fully hydrogenate to the desired alkyl amine **91**. Even in the case of heating the reaction mixture to 60°C and using the more reactive $Pd(OH)_2$ in place of Pd/C only improved yields up to 19% across hydrogenation and the subsequent Boc-deprotection.

We then explored an alternate Pd-catalyzed Mizoroki–Heck coupling of **90** with acrylonitrile which afforded vinyl nitrile **92**. Initial screening of reductive conditions revealed sodium borohydride in the presence of 20 mol% of cobalt(II) chloride capable of trace nitrile reduction to the free amine. We reasoned that increased cobalt equivalents may help overcome any sequestration by the free amine product to allow the reaction to proceed in higher yield. A super stoichiometric 2.0 equivalents of cobalt(II) chloride gratifyingly afforded reduction of vinyl nitrile **92** to the alkyl amine **91** in a 72% yield over both coupling and reduction steps

(Figure 3-5). Additionally, alkylamine analogue **91** proved to be much better behaved in THF and MeOH reaction solvents compared to the prior aryl amine **87**.

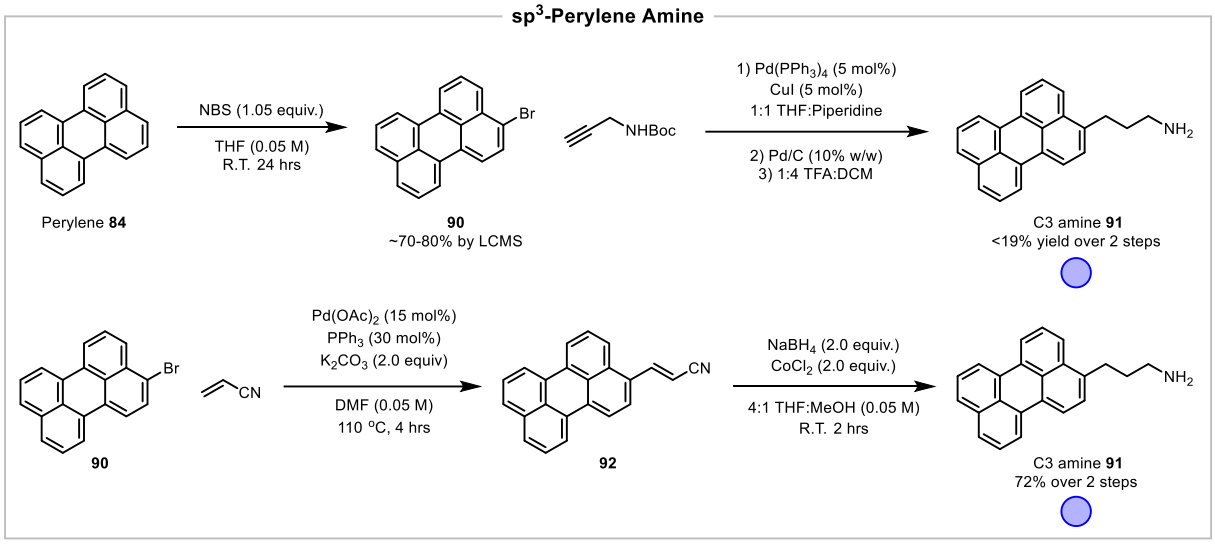


Figure 3-5 Synthesis of Perylene alkyl amine **91**. Initial attempts at Sonogashira coupling and reduction failed to fully reduce the appended alkyne in appreciable yields. Alternate Mizoroki-Heck coupling followed by cobalt-assisted nitrile reduction enabled synthesis of **91** on multi-gram scale.

Photochemical measurements revealed moderately improved FRET efficiency for the new dye system. Compared to the prior sp^2-sp^3 dyes' 9.1-fold signal-to-noise ratio, the newer sp^3-sp^3 system reported a modestly increased 11.6-fold signal-to-noise ratio for the coupled dyes and improved solubility properties (Figure 3-6). Additionally, poisoning studies revealed the high chemical stability of our new C3 amide **93** (see Figure **3-23** to **3-25**). We posited further improvement in FRET efficiency could be drawn from optimizing the inter-dye separation distance, which may be too constrained by the short linker of amide **93**.

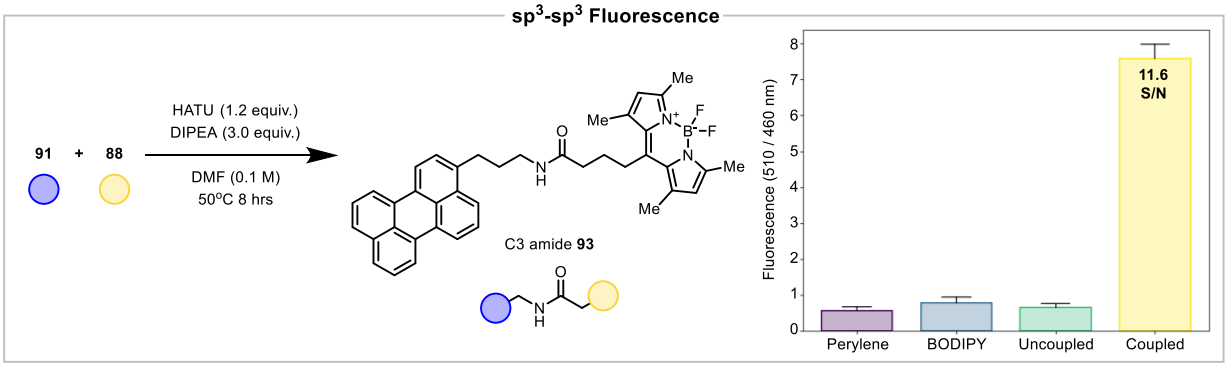


Figure 3-6 Coupling of sp^3 Perylene amine **91** with sp^3 BODIPY acid **88** to alkyl amide **93**. The Fluorescence ratio at 510 / 460 nm gives an 11.6-fold increase for the amide over the uncoupled dyes. All dyes are 10 μM in DMSO. Uncoupled fluorescence is from well containing 10 μM of both free amine and acid present. Excitation λ = 430 nm.

3.3.3 ***Effects of Linker Length***

To probe the impact of linker length on FRET efficiency, we designed several Perylene derivatives with iteratively longer linker lengths between the Perylene fluorophore and the terminal alkyl amine handle. Friedel Crafts acylation allowed for facile attachment of FMOC-protected amines directly onto the Perylene core. Acylation of Perylene with the acid chlorides of Fmoc-protected hexanoic acid, octanoic acid, and undecanoic acid gave benzylic ketones **94a-c**. Immediate FMOC-deprotection with excess piperidine followed by reductive deoxygenation with trifluoroacetic acid and triethylsilane gave the six-carbon amine **95a** in 62% yield, 8-carbon amine **95b** in 51% yield, and 11-carbon amine **95c** and 44% yield (Figure 3-7).

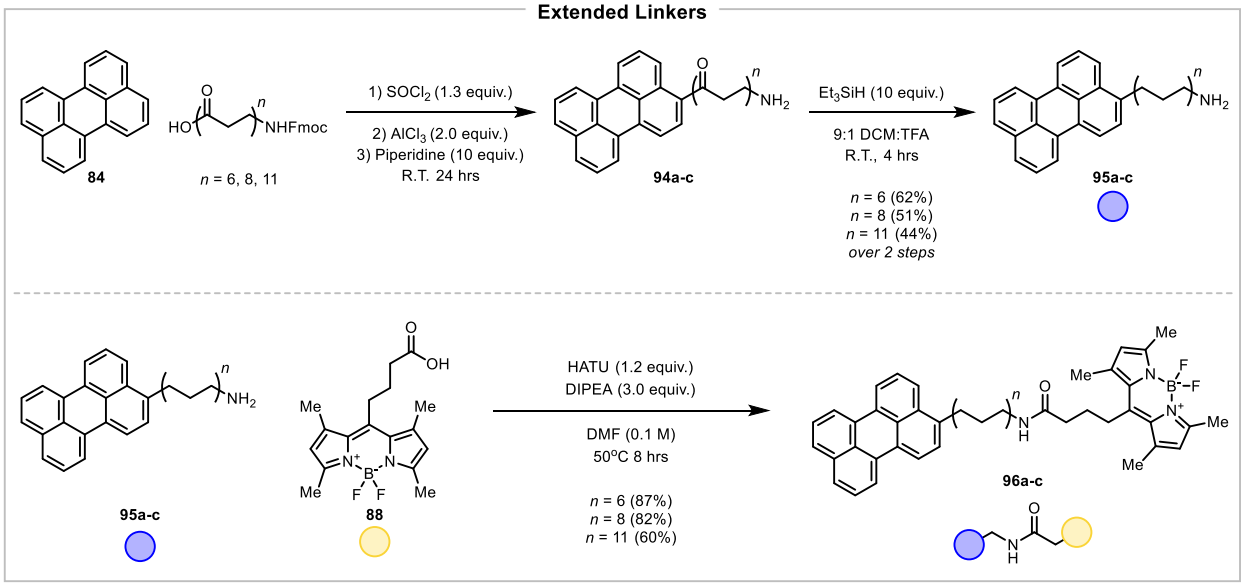


Figure 3-7 Synthesis of Perylene amines with extended linkers through Friedel-Crafts Acylation and reduction steps. Newly synthesized amines coupling with BODIPY **88** towards new FRET pairs **96a-c**.

Subsequent amide coupling of the newly synthesized amines **95a-c** with BODIPY **88** directly gave the final FRET pairs **96a-c** in yields from 60% to 87%. Relative to the prior 11.6-fold S/N for C3 amide **93**, the extended linker derivatives **96a-c** revealed a considerable 94.2-fold S/N for the C6 amide **96a** along with an 11.6 and 7.2-fold S/N for C8 amide **96b** and C11 amide **96c**, respectively. These results support the hypothesis that the constrained geometry of the C3 analogue was indeed impacting FRET efficiency. However, extension to 8 and 11-carbon linked perylene dyes extends beyond the optimal separation distance where FRET efficiency begins to fall off.

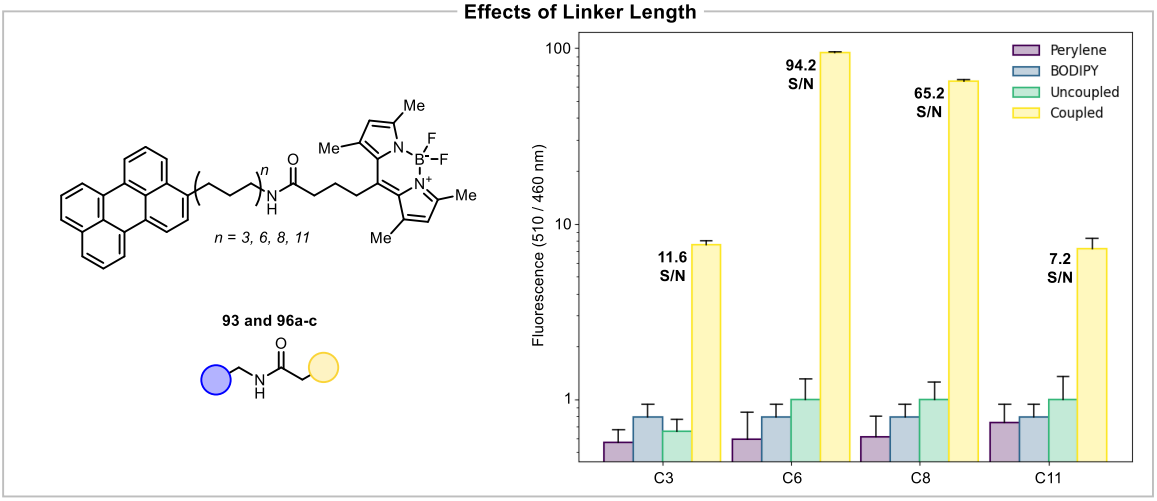


Figure 3-8 Fluorescence for extended-linker amides **96a-c** compared to previous 3-carbon amide **93**. Maximal 94.2 signal-to-noise of coupled amide relative to uncoupled amine/acid pair is reported from the 6-carbon linker of amide **96a**. Longer linker distances decrease FRET efficiency. All dyes are 10 μM in DMSO. Uncoupled fluorescence is reported from well containing 10 μM of both free amine and acid present. Excitation λ = 430 nm. Y-axis is plotted on a logarithmic scale.

3.4 **Comparison of UPLC–MS and FRET Analysis Platforms**

With our optimal FRET pair in hand, we sought to conduct a series of head-to-head tests on the efficacy of our FRET platform compared to traditional LC-MS reaction analysis. We first evaluated the titration of pure amide **96a** into solutions containing decreasing amounts of uncoupled amine **95a** and acid **88**. Increasing the mole fraction of amide in solution from 0 to 1.0 resulted in a 41-fold decrease in perylene's fluorescence at 460 nm (Figure 3-9 A). A calibration curve from Perylene's loss of fluorescence at 460 nm enabled us to derive assay yields from fluorescence intensity.

Following, we sought to validate the direct fluorescence analysis of crude reaction mixtures. Screening of the amide coupling between amine **95a** and acid **88** enabled direct comparison of FRET assay yields to LC–MS assay yields. Ranging from 0.0 to 1.5 equivalents of amide coupling reagent, HATU, strong correlation between both methods was evident. Both methods start and end within 3% of each other with lower FRET assay yields at the intermediate points of 0.50-1.25 equivalents HATU (Figure 3-9 B). We reason this can be attributed to variations in the aliquots taken for diluting the 0.1 M reaction wells down to 10 μM for fluorescence imaging.

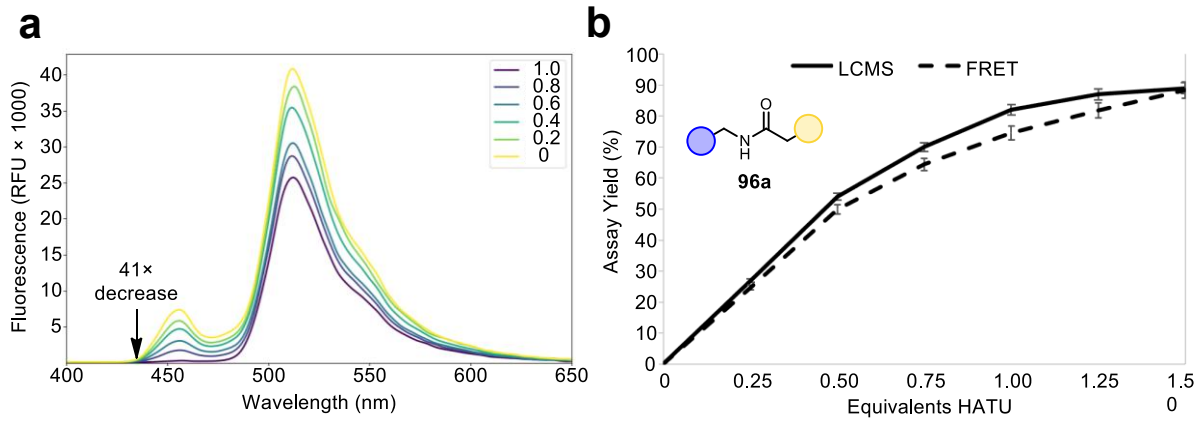


Figure 3-9 a) Trends in decreasing fluorescence at 460 nm with increasing mole fraction of amide **96a**. A constant final concentration of 10 μM of amine+acid+amide is maintained while mole fraction of amide increases relative to decreasing mole fraction of amine+acid. b) Comparison of LCMS and FRET assay yields in the amide coupling of **95a** and **88** across varied equivalents of amide-coupling reagent HATU.

From these results, we next tested FRET in a higher-throughput workflow. We designed a more diverse amide coupling screen of our Perylene and BODIPY dyes in miniaturized 1,536-well plate format. Across quadruplicate reactions screening 7 amide coupling reagents, 8 bases, 3 solvents (DMF, DMSO, Diglyme), DMAP and HOBT additives, we sought to test the limits of our FRET platform. After execution of the experiment, dilution of our reaction plates to produce typical 384-well plate LC-MS-ready samples, an additional dilution step to 10 μM provided the final 384-well fluorescence plates for FRET imaging. Of particular note, UPLC-MS analysis of these 1,536 samples took 3 days of instrument runtime while the FRET plates were immediately imaged in 10 minutes, following completion of the dilution protocol.

Initial attempts at generating FRET assay yields from loss of fluorescence at 460 nm like in Figure 3-9 B, gave modest correlation to LC-MS assay yields. However, using the ratiometric fluorescence of 510 nm / 460 nm as a proxy for yield gave much closer correlation to the LC–MS analysis (Figure 3-10). We attribute this difference to the more profound impact that slight variations in transfer and dilution volumes can have on ultra miniaturized scale, compared to a more traditional benchtop experiment like Figure 3-9 B. Though not a true determination of assay yield, determining ratiometric fluorescence of 510 nm / 460 nm helps normalize fluorescence values for an approximation of reaction yield in ultra miniaturized experiments.

Reassuringly, we identified similar reaction trends in both our ratiometric FRET analysis and LC–MS analysis. Both methods identified the same combination of EDC HCl with DMF as

the highest yielding combination of coupling reagent and solvent with an average yield of 77% by UPLC–MS and a 110% increase in fluorescence ratio, relative to negative control wells.

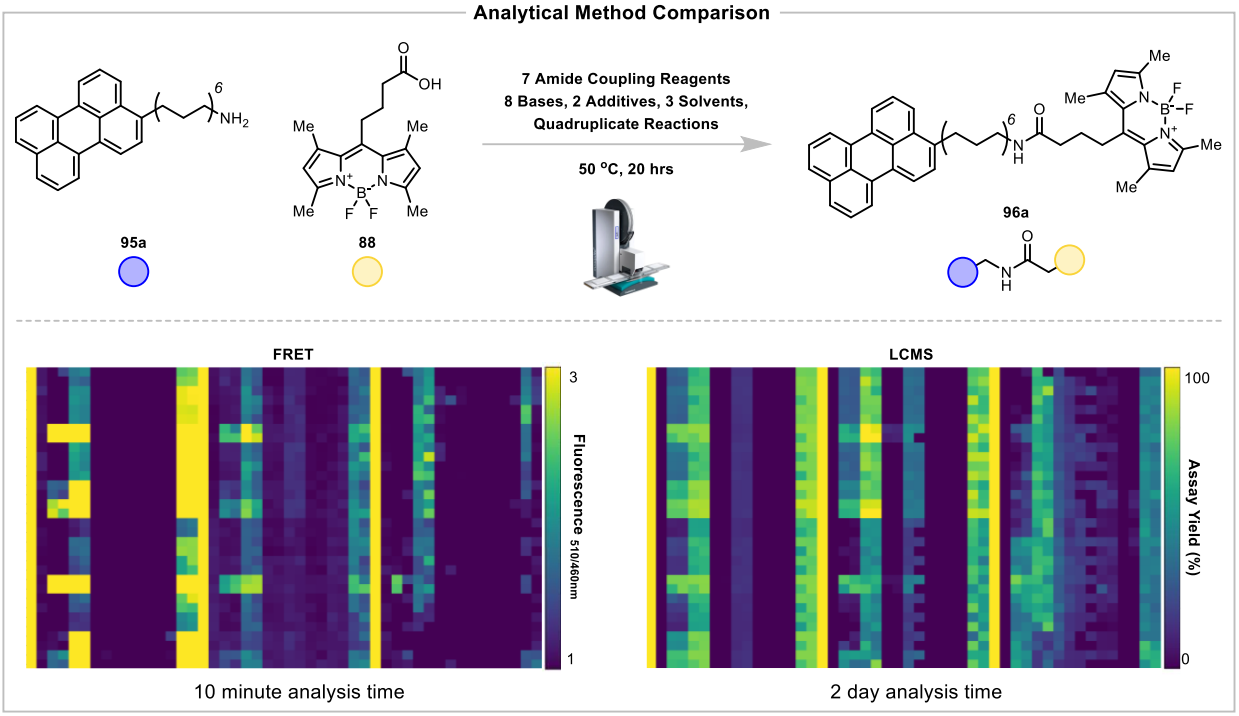


Figure 3-10 High-throughput 1,536-well plate screen of amide coupling conditions on optimized FRET dyes. Comparison of FRET platform relative to traditional UPLC–MS assay yields.

Also, general performance trends between lower performing combinations of reagents are generally good. HATU and DCC are the next best performing coupling reagents and reactions in DMF generally outperform DMSO or diglyme according to both analytical methods. Importantly, good analytical correlation can also be drawn from wells with potentially confounding UV-emissive reagents such as PyBOP, HATU, and DMTMM. Considering the reproducibility of the data, average variations of reactions run in quadruplicate were 16.8% and 16.5% by LC–MS and FRET methods, respectively. Plotting LC–MS assay yields versus ratiometric fluorescence for each well gives a modest linear trend for yields above ~20%. While there is little variation in the fluorescence of lower yielding reactions, FRET can identify yields above ~40% consistently (Figure 3-11). In summation, ratiometric fluorescence as a proxy for reaction yield does perform worse than assay yield derived from loss of fluorescence at 460 nm alone. However, we have shown that ratiometric fluorescence for 1,536-well experiments is still very capable of elucidating general reaction trends between higher and lower performing pockets of reaction space. Collectively, these results demonstrate the ability of FRET to produce reliable

HTE reaction data in a matter of 10 minutes by fluorescence plate reading, compared to the current regime of multiday LC-MS runtimes.

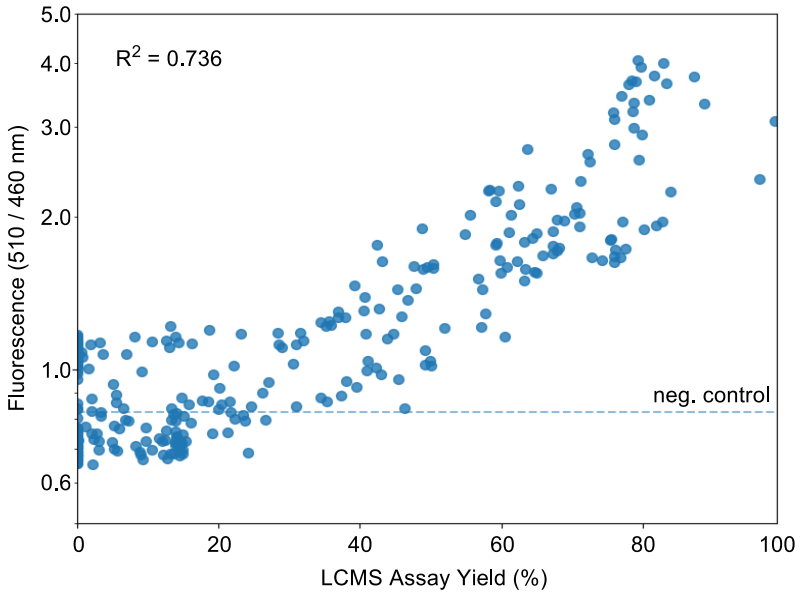


Figure 3-11 Comparison of LC–MS Assay Yields vs Ratiometric FRET analysis of 1,536-well amide coupling experiment. Each set of quadruplicate wells is averaged and displayed as a single point. The y-axis is displayed on a logarithmic scale with the average of negative controls displayed as the horizontal blue line at y = 0.826. Coefficient of determination of the log-scaled data is additionally displayed.

As a final measure of our platform's ability to enable rapid discovery of novel reactivity, we conducted an expansive screening of 7,680 unique coupling conditions beyond that of the traditional amide coupling. Sampling across 120 different transition metal catalysts and 16 nitrogen, oxygen, and phosphine-based ligands under either acidic, basic, oxidative, or reductive additives, we sought to rapidly probe and identify unique coupling modes between amine **95a**, activated as its corresponding pyridinium salt, and free acid **88** (see Figures **3-32** to **3-38** in experimental section). While first pass analysis via FRET didn't reveal any novel reactivity once hits were then analyzed via LC–MS, we successfully identified a previously unreported Pummerer-type rearrangement between acid **88** and DMSO solvent under reductive iridium-catalyzed conditions. While these results lay outside the initial scope of the screen, they still pose an interesting case-study in reaction discovery.

3.5 **Conclusions and Future Work**

Here, we present the results on the development of a FRET-based analytical platform for high-throughput reaction analysis. Notably, our platform is the first to demonstrate the application of FRET towards the analysis of reactions in ultra-miniaturized 1,536-well plate

format. These results are a considerable improvement upon previous fluorometric techniques that have only been applied to the analysis of 96-well plate experiments at best. This work provides the foundation for overcoming the current analytical bottleneck in high-throughput chemistry, and the potential of fluorescence plate reading as a viable alternative to chromatographic reaction analysis.

While considerable work has been done to overcome the limitations of our FRET platform, there are still notable areas of improvement that may improve user-friendliness and help further validate FRET on more complex reaction systems. First speaking to the synthesis of the reported dyes, solubility is certainly an area of improvement for many of the perylene dyes. While synthesis of the final alkyl amine dyes is manageable with significantly dilute reaction volumes, dilution is often undesirable for investigation of novel chemistry due to decreased reaction rates. Appending pendant alkyl groups to the perylene core is an existing strategy for improving solubility. However, complicating regioisomeric products that result from unselective alkylation reactions tend to hinder the viability of this approach. Potential modification of the alkyl linker with PEG-like functionalities may help improve solubility properties without complicating the synthesis these dyes. As well, simplified dye synthesis and tagging to a functional group of interest may help to further expand the utility of this approach as the laborious multistep planning and synthesis to make new dyes with varying functionalities is another current limitation.

Additionally, further validation of FRET across a broader range of reaction conditions and reagents may help strengthen the appeal of the platform for those looking to explore more diverse chemistry. We envision our Perylene and BODIPY dyes can be extended to a wide range of functional groups and applications beyond that of amine-acid coupling. Our preliminary results to synthesize the ester analogue of an earlier FRET system provided that alternative functionalities are tolerated without major perturbations to the fluorescence performance. We hope that further development of this FRET platform and its application towards reaction analysis may reinforce its viability across diverse chemical systems.

A particular application that may benefit from FRET analysis is the determination of reaction kinetics. While typical kinetic experiments require extensive collection and analysis of reaction data across systematically varied reagent stoichiometries, FRET is conveniently poised to facilitate the rapid collection of reactant and product ratios in the form of fluorescence

endpoints. While we have already demonstrated linear fluorescence that result from the coupling of perylene **95a** and BODIPY **88** to coupled amide **96a** on benchtop scale, it would be a straightforward endeavor to determine kinetic profiles directly from such fluorescence data.

It is my hope that this research helps encourage further development of high-throughput reaction analysis techniques. As the field continues to advance, we may soon realize the capability for real-time reaction monitoring of high-throughput chemistry. While robotics platforms may soon enable the autonomous setup and execution of experiments, the development of fully in-line analytical systems to collect and analyze massive libraries of reaction data may prove equally important in pushing the limits of how quickly we can make new molecules.

3.6 **Experimental Section for the FRET Platform**

3.6.1 ***General Methods***

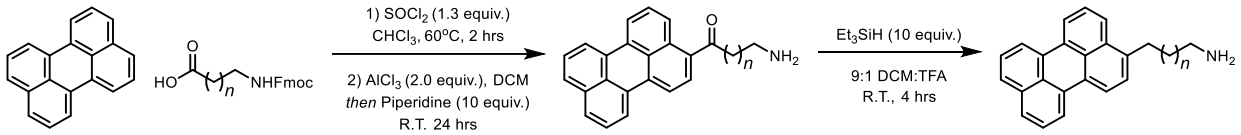
Unless otherwise noted, all reactions were carried out under an atmosphere of argon or nitrogen in dried glassware. Dry solvents were either purchased from Fisher Scientific or Sigma-Aldrich, stored under activated molecular sieves, withdrawn under positive nitrogen pressure or purified using a custom-made SPS purification system (activated alumina columns) and transferred under nitrogen. Solvents for flash column chromatography (Hexanes, EtOAc, CH_2Cl_2, MeOH) were used without additional purification. The aqueous ammonium hydroxide referenced in purification protocols is a concentrated 28% aqueous solution. Reagents were purchased from Sigma-Aldrich, ACROS Organics, TCI, Ambeed, Fisher Scientific and used without additional purification, unless otherwise stated.

Absorbance and fluorescence data were obtained using a BioTek Synergy H1 Multimode Reader with adjustable monochromator and Gen5 version 1.11 software for protocol design and data collection. Full absorption and fluorescence spectra of purified dyes were collected in 96-well plates containing well volumes of 200 μL of 10 μM dye solutions in DMSO. All 384-well imaging was conducted using 50 μL of 10 μM dyes or crude reaction solutions diluted to 10 μM in DMSO. Instrument parameters: top plate imaging, 8 mm read height, gain calibrated to 40,000 RFU for the well with greatest fluorescence at 510 nm in each experiment. Each fluorescence data point represents the average of 5 data points collected 100 ms apart.

Transferring and dosing of 384 and 1,536-well plates was conducted using an SPT Labtech Mosquito liquid handling robot and the corresponding mosquito software to develop dosing and mixing procedures. Glass 1-dram (Fisherbrand™ parts No. 03-339-21B) or 2-dram vials (Fisherbrand™ parts No. 03-339-21D) were used as reaction vessels, fitted with screwcaps with Teflon-coated silicone septa (CG-4910-02), and magnetic stir bars (Fisher Scientific #14-513-93 or #14-513-65). Microtiter plate evaporation was performed using a Genevac HT-4X Series II centrifugal evaporator with vacuum pump controller (Genevac #70-0938), BOC Edwards XDS-5 dry scroll pump (Edwards #A724-01-104), and side-bridge swing attachments for well plate evaporation. Vacuum plot capacity: 2.3 L. Vacuum control range: 1-1000 mbar. Standard evaporation method listed below: 40°C internal chamber temperature, 1 mbar chamber vacuum, very low rotor speed, 2 hours runtime.

3.6.2 ***Procedures for Synthesis of FRET Dyes***

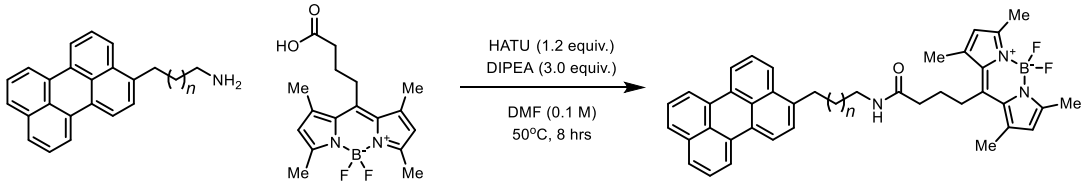
General Procedure for Friedel–Crafts Acylation of Perylene



To a dry scintillation vial was added a magnetic stir bar and carboxylic acid (4.756 mmol, 1.2 equiv.). Following, $CHCl_3$ (9.5 mL, 0.5 M) and thionyl chloride (376 µL, 5.152 mmol, 1.3 equiv.) were added sequentially. The vial was capped and heated to 60°C for 2 hours, then solvent was evaporated *in vacuo*. The crude residue was redissolved in DCM (19 mL) and added to a flask containing Perylene (1.000 g, 3.963 mmol, 1.0 equiv.) and $AlCl_3$ (1.057 g, 7.926 mmol, 2.0 equiv.) in DCM (60 mL). The reaction was stirred at room temperature for 20 hours, then piperidine (10.91 mL, 39.63 mmol, 10 equiv.) was added and the flask left to stir for another 4 hours at room temperature. The reaction was quenched by addition of water (30 mL) and the contents were extracted in triplicate with DCM (3 x 30 mL). The crude extracts were dried with sodium sulfate, then solvent was removed *in vacuo*.

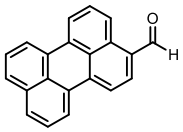
The residue taken up in 9:1 DCM:TFA (39.6 mL, 0.1 M) and triethylsilane (6.33 mL, 39.63 mmol, 10 equiv.) was added dropwise. The reaction was stirred for 4 hours, then cooled to 0°C and quenched with aqueous potassium carbonate. After extraction with DCM, drying of extracts with sodium sulfate, and solvent evaporation, the Perylene alkyl amine product was purified by silica chromatography.

General Procedure for Amide Coupling of Perylene and BODIPY Dyes



A dry 2-dram vial was prepared with Perylene amine (62 µmol, 1.0 equiv.), BODIPY acid **88** (21 mg, 62 µmol, 1.0 equiv.), HATU (28 mg, 74 µmol, 1.2 equiv.), and a magnetic stir bar. The vial was placed under an atmosphere of nitrogen, then dry DMF (620 µL, 0.1 M) was added. Finally, N,N-diisopropylethylamine (32 µL, 190 µmol, 3.0 equiv.) was added and the reaction was heated

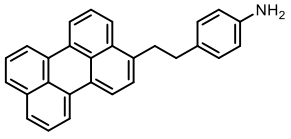
to 50°C for 8 hours. The reaction was stopped by addition of water and extracted with ethyl acetate (3 x 5 mL). The combined extracts were dried with sodium sulfate and solvent was removed *in vacuo*. Pure amide product was retrieved by silica chromatography.



86

Perylene-3-carbaldehyde (86)

To a dry 100 mL flask, Perylene (800 mg, 3.17 mmol, 1.0 equiv.) and a magnetic stir bar was added. The flask was sealed and flushed with dry nitrogen. Following, dry DCM (63.4 mL, 0.05 M) was added and the flask was cooled to 0°C. In one portion, dichloro(methoxy)methane (315 µL, 3.49 mmol, 1.1 equiv.) was added to the reaction solution, then a solution of titanium tetrachloride in DCM (4.76 mL, 4.76 mmol, 1 M, 1.5 equiv.) was added over the course of 5 minutes. The reaction was allowed to stir at room temperature for 4 hours, then quenched by addition of aq. HCl (30 mL, 0.5 M) and extracted in triplicate with DCM (3 x 20 mL). The combined extracts were dried with anhydrous sodium sulfate and solvent was evaporated *in vacuo*. The product was purified by silica chromatography (3:1 DCM:Hexanes) to yield aldehyde **86** as an orange powder (601 mg, 68% yield). Rf = 0.46 in 3:1 DCM:Hexanes.
^{1}H NMR (499 MHz, dmso) δ 10.28 (s, 1H), 9.04 (d, *J* = 8.4 Hz, 1H), 8.48 (d, *J* = 7.7 Hz, 2H), 8.44 (d, *J* = 7.7 Hz, 1H), 8.41 (d, *J* = 7.6 Hz, 1H), 8.08 (d, *J* = 7.8 Hz, 1H), 7.92 (d, *J* = 8.0 Hz, 1H), 7.85 (d, *J* = 8.0 Hz, 1H), 7.71 (t, *J* = 7.9 Hz, 1H), 7.58 (dt, *J* = 9.8, 7.8 Hz, 2H). ^{13}C NMR (126 MHz, dmso) δ 193.90, 137.72, 137.15, 134.37, 131.97, 131.21, 130.58, 130.29, 129.95, 129.87, 129.55, 129.13, 128.51, 127.75, 127.62, 127.45, 124.41, 123.95, 122.52, 121.89, 120.35.



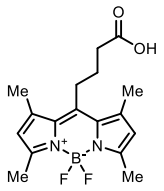
87

4-(2-(perylen-3-yl)ethyl)aniline (aryl amine, 87)

A dry 50 mL flask was charged with bromo(4-nitrobenzyl)triphenyl-l5-phosphane (410 mg, 0.856 mmol, 1.2 equiv.) and 60% sodium hydride in mineral oil (34.2 mg, 0.856 mmol, 1.2

equiv.) along with a stir bar. The flask was placed under an atmosphere of nitrogen gas and dry THF was added (7.1 mL). Ylide formation was allowed to occur over 30 minutes, stirring at room temperature. Following, a solution of **86** (200 mg, 0.713 mmol, 1.0 equiv.) in THF (7.1 mL) was added and the reaction was heated to 60ºC for the following 20 hours. To the reaction flask, palladium on carbon (10 mg, 10% Pd by weight) was added and the flask was sparged with hydrogen gas for 15 minutes. The flask was then attached to a balloon of hydrogen to continue stirring for another 8 hours at room temperature. The reaction was stopped by filtering through a pad of celite and the filtrate extracted with water (30 mL) and DCM (3 x 10 mL). The combined extracts were dried with sodium sulfate and evaporated *in vacuo*. Product was isolated by silica chromatography using DCM to yield **87** as an orange powder (132 mg, 50% yield). Rf = 0.33 in 100% DCM.

^{1}H NMR (499 MHz, dmso) δ 8.37 (dd, *J* = 16.0, 7.7 Hz, 1H), 8.30 (d, *J* = 6.6 Hz, 0H), 8.26 (d, *J* = 7.8 Hz, 1H), 8.00 (d, *J* = 8.3 Hz, 0H), 7.80 – 7.73 (t, 1H), 7.62 – 7.57 (t, 1H), 7.53 (q, *J* = 7.8 Hz, 1H), 7.36 (d, *J* = 7.7 Hz, 1H), 6.95 (d, *J* = 8.4 Hz, 1H), 6.50 (d, *J* = 8.4 Hz, 1H), 4.85 (s, 1H), 3.25 – 3.13 (t, 1H), 2.84 – 2.76 (t, 1H). ^{13}C NMR (126 MHz, dmso) δ 147.07, 138.67, 134.75, 133.00, 131.46, 131.19, 131.17, 129.23, 129.17, 128.96, 128.74, 128.30, 128.17, 127.93, 127.66, 127.38, 127.35, 127.28, 124.42, 121.10, 121.06, 120.98, 120.66, 114.45, 36.01, 35.62.



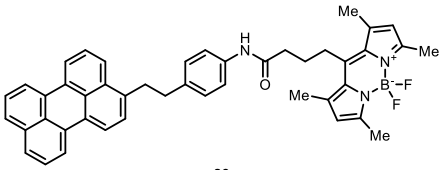
88

4-(5,5-difluoro-1,3,7,9-tetramethyl-5H-4l4,5l4-dipyrrolo[1,2-c:2',1'-f][1,3,2]diazaborinin-10-yl)butanoic acid (BODIPY acid, 88)

A dry 150 mL flask containing a stir bar was charged with 30 mL of dry THF and 2,4-dimethyl-1H-pyrrole (2.53 mL, 24.54 mmol, 2.0 equiv.). Methylmagnesium chloride in THF (8.180 mL, 3 M, 24.54 mmol, 2.0 equiv.) was added dropwise and the vial was left to stir at room temperature for 30 minutes. Following, sequential dropwise addition of glutaric anhydride (1400 mg, 12.27 mmol, 1.0 equiv.) in 30 mL THF then boron trifluoride diethyl etherate (9.762 mL, 46% Wt, 35.44 mmol, 2.88 equiv.) in THF was carried out. The vial was left to stir at room temperature for 16 hours. To the dark brown solution, triethylamine (18.3 mL, 131.3 mmol, 10.7 equiv.) then

additional boron trifluoride diethyl etherate (27.11 mL, 46% Wt, 98.40 mmol, 8.02 equiv.) in THF were added. The flask was heated to 50ºC for 4 more hours, then quenched with addition of 30 mL saturated aq. NH_4Cl. The reaction mixture was extracted with DCM in triplicate (3 x 15 mL). The extracts were combined, dried with sodium sulfate and solvent evaporated *in vacuo*. The crude product was first eluted through a silica plug with 100% DCM, then adsorbed to silica for further purification. Pure product **88** was isolated via gradient elution (1:2 EtOAc:Hexanes with 1% AcOH) as a red solid (1.556 mg, 38% yield).

^{1}H NMR (499 MHz, cdcl$_3$) δ 6.05 (s, 2H), 3.05 – 2.98 (m, 2H), 2.54 (t, *J* = 7.2 Hz, 2H), 2.51 (s, 6H), 2.42 (s, 6H), 2.02 – 1.92 (m, 2H). ^{13}C NMR (126 MHz, cdcl$_3$) δ 178.03, 154.30, 144.62, 140.34, 131.44, 121.86, 33.89, 27.36, 26.48, 16.33, 14.50, 14.48, 14.46. ^{19}F NMR (470 MHz, cdcl$_3$) δ -146.45, -146.55, -146.65, -146.77.

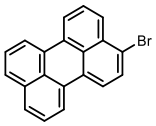


89

4-(5,5-difluoro-1,3,7,9-tetramethyl-5H-4l4,5l4-dipyrrolo[1,2-c:2',1'-f][1,3,2]diazaborinin-10-yl)-N-(4-(2-(perylen-3-yl)ethyl)phenyl)butanamide (aryl amide, 89)

Amide product **x** was synthesized by the general method for Amide Coupling of Perylene and BODIPY Dyes from C6 amine and BODIPY acid. Silica chromatography (95:5 DCM:EtOAc) afforded pure amide **89** as a red-orange solid in 70% yield. Rf = 0.63 in 90:10:1 DCM:EtOAc Pure product was retrieved by silica chromatography (95:5 DCM:EtOAc) as a red-orange solid (43 mg, 70% yield). Rf = 0.63 in 95:5 DCM:EtOAc.

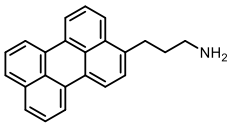
^{1}H NMR (499 MHz, dmso) δ 9.95 (s, 1H), 8.38 (d, *J* = 7.5 Hz, 1H), 8.34 (d, *J* = 7.5 Hz, 1H), 8.29 (d, *J* = 7.5 Hz, 1H), 8.24 (d, *J* = 7.5 Hz, 1H), 8.01 (d, *J* = 8.4 Hz, 1H), 7.76 (t, *J* = 9.0 Hz, 2H), 7.59 (t, *J* = 8.0 Hz, 1H), 7.54 – 7.48 (m, 4H), 7.35 (d, *J* = 7.6 Hz, 1H), 7.22 (d, *J* = 8.6 Hz, 2H), 6.21 (s, 2H), 3.27 (t, *J* = 8.1 Hz, 2H), 3.06 – 2.92 (m, 6H), 2.41 (s, 6H), 2.40 (s, 6H), 1.91 – 1.84 (m, 2H). ^{13}C NMR (126 MHz, dmso) δ 170.57, 153.62, 146.66, 141.42, 138.25, 137.57, 136.68, 134.74, 133.00, 131.47, 131.22, 131.14, 129.29, 129.09, 128.75, 128.32, 128.16, 127.97, 127.69, 127.37, 127.35, 127.32, 124.39, 122.19, 121.12, 120.93, 120.69, 119.63, 36.83, 36.02, 34.99, 27.85, 27.59, 16.31, 14.55.



90

3-bromoperylene (90)

A dry 150 mL flask was charged with Perylene (1.200 g, 4.756 mmol, 1.0 equiv.), N-Bromosuccinimide (888.8 mg, 4.994 mmol, 1.05 equiv.), and a magnetic stirbar. The flask was placed under an atmosphere of nitrogen, and dry THF (95.12 mL, 0.05M) was added. The reaction was allowed to stir at room temperature for 24 hours, then quenched by addition of 10 mL saturated aqueous sodium thiosulfate and 30 mL brine. The reaction mixture was extracted with DCM in triplicate (3 x 30 mL) and solvent evaporated *in vacuo*. The crude mixture was then directly used in later reactions. Yields were routinely in the 70-80% range based on LC-MS conversion.

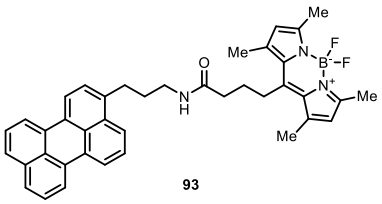


91

3-(perylen-3-yl)propan-1-amine (C3 amine, 91)

A dry 150 mL flask was charged with 3-bromoperylene (1.000 g, 3.019 mmol, 1.0 equiv.), palladium(II) acetate (101.7 mg, 0.453 mmol, 0.15 equiv.), triphenylphosphine (237.6 mg, 0.906 mmol, 0.30 equiv.), and potassium carbonate (834.5 mg, 6.038 mmol, 2.0 equiv.). To this flask, dry DMF (60.4 mL, 0.05 M) and acrylonitrile (989 µL, 15.10 mmol, 5.0 equiv.) were sequentially added via syringe. The reaction was then heated to 110ºC for 4 hours to achieve full conversion. Addition of 20 mL saturated aqueous lithium chloride was used to quench the reaction. Following extraction with DCM (3 x 20 mL), the combined extracts were dried with anhydrous sodium sulfate and solvent was evaporated *in vacuo*. The crude product was then redissolved in 4:1 THF:MeOH (30 mL) and addition of solid cobalt(II) chloride (784.0 mg, 6.038 mmol, 2.0 equiv.) and sodium borohydride (228.4 mg, 6.038 mmol, 2.0 equiv.) was carried out. The mixture was stirred at room temperature for 2 hours, then quenched by addition of brine. The reaction mixture was extracted with DCM (3 x 20 mL), dried with anhydrous sodium sulfate and evaporated *in vacuo*. Pure product **91** was retrieved by silica chromatography (95:5:1 DCM:MeOH:NH_4OH to 85:15:1 DCM:MeOH:NH_4OH) as an orange solid (671 mg, 71.8%

yield). ^{1}H NMR (499 MHz, cdcl$_3$) δ 8.21 (d, *J* = 7.6 Hz, 1H), 8.18 (d, *J* = 7.6 Hz, 1H), 8.16 (d, *J* = 7.6 Hz, 1H), 8.12 (d, *J* = 7.7 Hz, 1H), 7.89 (d, *J* = 8.4 Hz, 1H), 7.67 (t, *J* = 7.9 Hz, 2H), 7.54 – 7.50 (t, *J* = 7.9 Hz, 1H), 7.47 (td, *J* = 7.8, 2.5 Hz, 2H), 7.34 (d, *J* = 7.7 Hz, 1H), 3.07 (t, *J* = 7.8 Hz, 2H), 2.86 (t, *J* = 7.0 Hz, 2H), 1.92 (p, *J* = 7.4 Hz, 2H), 1.25 (s, 2H). ^{13}C NMR (126 MHz, cdcl$_3$) δ 138.24, 134.67, 133.02, 131.81, 131.45, 129.58, 129.12, 128.52, 127.73, 127.36, 126.77, 126.58, 126.53, 126.33, 123.73, 120.15, 120.13, 120.06, 119.72, 42.23, 34.50, 30.71.

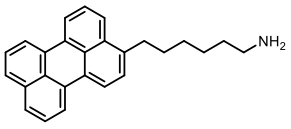


93

4-(5,5-difluoro-1,3,7,9-tetramethyl-5H-4l4,5l4-dipyrrolo[1,2-c:2',1'-f][1,3,2]diazaborinin-10-yl)-N-(3-(perylen-3-yl)propyl)butanamide (C3 amide, 93)

Amide product **x** was synthesized by the general method for Amide Coupling of Perylene and BODIPY Dyes from C3 amine and BODIPY acid. Silica chromatography (100:1 DCM:AcOH to 90:10:1 DCM:EtOAc:AcOH) afforded pure amide **93** as an orange powder in 75% yield. Rf = 0.35 in 90:10:1 DCM:EtOAc:AcOH.

^{1}H NMR (499 MHz, dmso) δ 8.36 – 8.31 (m, 2H), 8.30 (d, *J* = 7.5 Hz, 1H), 8.27 (d, *J* = 7.7 Hz, 1H), 8.06 (t, *J* = 5.6 Hz, 1H), 7.92 (d, *J* = 8.4 Hz, 1H), 7.76 (t, *J* = 8.3 Hz, 2H), 7.57 – 7.48 (m, 3H), 7.42 (d, *J* = 7.6 Hz, 1H), 6.19 (s, 2H), 3.19 (q, *J* = 6.7 Hz, 2H), 3.01 (t, *J* = 7.7 Hz, 2H), 2.95 – 2.90 (m, 2H), 2.38 (s, 12H), 2.30 (t, *J* = 6.9 Hz, 2H), 1.87 – 1.75 (m, 4H). ^{13}C NMR (126 MHz, dmso) δ 171.62, 153.58, 146.73, 141.38, 138.56, 134.73, 132.98, 131.50, 131.19, 131.12, 131.09, 129.26, 128.79, 128.32, 128.15, 127.96, 127.50, 127.36, 127.33, 127.15, 124.32, 122.14, 121.11, 121.06, 120.99, 120.67, 38.93, 35.96, 30.42, 30.38, 28.13, 27.66, 16.27, 14.54.

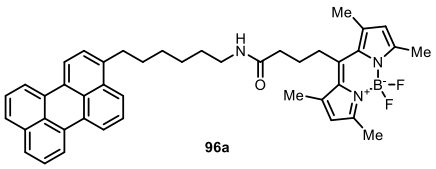


95a

6-(perylen-3-yl)hexan-1-amine (C6 amine, 95a)

The general method for Friedel-Crafts Acylation of Perylene was applied to 6-((((9*H*-fluoren-9 yl)methoxy)carbonyl)amino)hexanoic acid (1.681 g, 4.756 mmol, 1.2 equiv.). Pure product **95a**

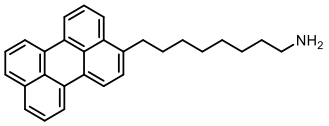
was obtained by silica chromatography (90:10:1 DCM:MeOH:NH_4OH to 80:20:1 DCM:MeOH:NH_4OH) as an orange powder in 62% yield. Rf = 0.60 in 80:20:1 DCM:MeOH:NH_4OH. ^1H NMR (499 MHz, dmso) δ 8.29 (dd, *J* = 10.0, 7.5 Hz, 2H), 8.22 (d, *J* = 7.5 Hz, 1H), 8.17 (d, *J* = 7.7 Hz, 1H), 7.85 (d, *J* = 8.4 Hz, 1H), 7.72 (t, *J* = 8.6 Hz, 2H), 7.55 – 7.44 (m, 3H), 7.29 (d, *J* = 7.6 Hz, 1H), 2.90 (t, *J* = 7.7 Hz, 2H), 2.72 (s, 2H), 2.50 (t, *J* = 6.3 Hz, 2H), 1.60 (p, *J* = 7.2 Hz, 2H), 1.30 (m, 6H). ^{13}C NMR (126 MHz, dmso) δ 139.20, 134.74, 133.00, 131.44, 131.20, 131.17, 129.07, 128.75, 128.24, 128.17, 127.85, 127.36, 127.32, 127.28, 127.10, 124.37, 121.02, 120.99, 120.92, 120.53, 41.82, 33.19, 32.89, 30.62, 29.48, 26.73.



4-(5,5-difluoro-1,3,7,9-tetramethyl-5H-4l4,5l4-dipyrrolo[1,2-c:2',1'-f][1,3,2]diazaborinin-10-yl)-N-(6-(perylen-3-yl)hexyl)butanamide (C6 amide, 96a)

Amide product **x** was synthesized by the general method for Amide Coupling of Perylene and BODIPY Dyes from C6 amine and BODIPY acid. Silica chromatography (100:1 DCM:AcOH to 90:10:1 DCM:EtOAc:AcOH) afforded pure amide **96a** as an orange powder in 87% yield. Rf = 0.45 in 90:10:1 DCM:EtOAc:AcOH.

^1H NMR (499 MHz, $cdcl_3$) δ 8.20 (dd, *J* = 11.6, 7.5 Hz, 2H), 8.16 (d, *J* = 7.5 Hz, 1H), 8.12 (d, *J* = 7.7 Hz, 1H), 7.87 (d, *J* = 8.5 Hz, 1H), 7.67 (t, *J* = 8.0 Hz, 2H), 7.54 – 7.45 (m, 3H), 7.33 (d, *J* = 7.7 Hz, 1H), 6.03 (s, 2H), 5.43 (s, 1H), 3.24 (q, *J* = 6.9 Hz, 2H), 3.02 (t, *J* = 7.7 Hz, 2H), 2.99 – 2.93 (m, 2H), 2.52 (s, 6H), 2.39 (s, 6H), 2.27 (t, *J* = 7.0 Hz, 2H), 1.98 – 1.88 (m, 2H), 1.77 (p, *J* = 7.7 Hz, 2H), 1.49 (dp, *J* = 15.2, 7.3 Hz, 4H), 1.42 – 1.36 (m, 2H). ^{13}C NMR (126 MHz, $cdcl_3$) δ 171.41, 154.03, 145.36, 140.50, 138.63, 134.69, 133.04, 131.81, 131.51, 131.46, 131.44, 129.50, 129.12, 128.52, 127.75, 127.38, 126.83, 126.61, 126.56, 126.31, 123.74, 121.75, 120.17, 120.12, 120.05, 119.71, 39.63, 36.32, 33.28, 30.35, 29.58, 29.35, 27.52, 27.44, 26.86, 16.39, 14.47.

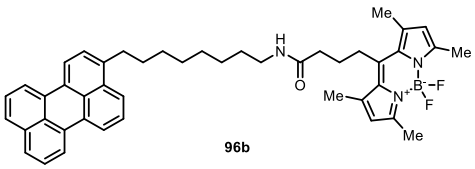


95b

8-(perylen-3-yl)octan-1-amine (C8 amine, 95b)

The general method for Friedel-Crafts Acylation of Perylene was applied to 8-((((9*H*-fluoren-9 yl)methoxy)carbonyl)amino)octanoic acid (1.814 g, 4.756 mmol, 1.2 equiv.). Pure product **95b** was obtained by silica chromatography (90:10:1 DCM:MeOH:NH_4OH to 80:20:1 DCM:MeOH:NH_4OH) as an orange powder in 51% yield. Rf = 0.64 in 80:20:1 DCM:MeOH:NH_4OH

^1H NMR (499 MHz, dmso) δ 8.35 (dd, *J* = 12.2, 7.5 Hz, 2H), 8.29 (d, 1H), 8.25 (d, 1H), 8.00 (s, 2H), 7.90 (d, *J* = 8.4 Hz, 1H), 7.75 (t, *J* = 8.7 Hz, 2H), 7.56 (t, *J* = 7.9 Hz, 1H), 7.51 (td, *J* = 7.8, 3.8 Hz, 2H), 7.37 (d, *J* = 7.7 Hz, 1H), 2.96 (t, *J* = 7.7 Hz, 2H), 2.75 – 2.68 (t, *J* = 7.7 Hz, 2H), 1.65 (p, *J* = 7.5 Hz, 2H), 1.53 (p, *J* = 7.4 Hz, 2H), 1.37 (p, *J* = 7.6 Hz, 2H), 1.28 (m, *J* = 5.4 Hz, 6H). ^{13}C NMR (126 MHz, dmso) δ 139.22, 134.74, 133.01, 131.46, 131.18, 131.14, 129.10, 128.77, 128.30, 128.16, 127.91, 127.46, 127.38, 127.34, 127.18, 124.41, 121.09, 121.05, 120.99, 120.60, 32.94, 30.62, 29.46, 29.20, 29.00, 27.38, 26.31, 25.51.



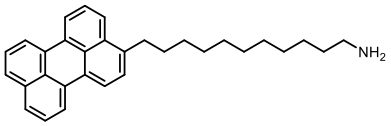
96b

4-(5,5-difluoro-1,3,7,9-tetramethyl-5H-4l4,5l4-dipyrrolo[1,2-c:2',1'-f][1,3,2]diazaborinin-10-yl)-N-(8-(perylen-3-yl)octyl)butanamide (C8 amide, 96b)

Amide product **x** was synthesized by the general method for Amide Coupling of Perylene and BODIPY Dyes from C8 amine and BODIPY acid. Silica chromatography (100:1 DCM:AcOH to 95:5:1 DCM:EtOAc:AcOH) afforded pure amide **96b** as an orange powder in 82% yield. Rf = 0.40 in 95:5:1 DCM:EtOAc:AcOH.

^1H NMR (499 MHz, $cdcl_3$) δ 8.22 (d, *J* = 7.4 Hz, 1H), 8.19 (d, *J* = 7.5 Hz, 1H), 8.16 (d, *J* = 7.5 Hz, 1H), 8.13 (d, *J* = 7.7 Hz, 1H), 7.88 (d, *J* = 8.4 Hz, 1H), 7.67 (t, *J* = 8.3 Hz, 2H), 7.52 (t, *J* = 7.9 Hz, 1H), 7.47 (td, *J* = 7.8, 2.9 Hz, 2H), 7.33 (d, *J* = 7.7 Hz, 1H), 6.04 (s, 2H), 5.39 (t, *J* = 5.8 Hz, 1H), 3.26 – 3.20 (q, *J* = 6.7 Hz, 2H), 3.05 – 2.96 (m, 4H), 2.52 (s, 6H), 2.41 (s, 6H), 2.29 (t, *J* = 7.1 Hz, 2H), 2.00 – 1.90 (m, 2H), 1.76 (p, *J* = 7.7 Hz, 2H), 1.47 (m, 4H), 1.41 – 1.29 (m,

6H). ^{13}C NMR (126 MHz, cdcl$_3$) δ 171.37, 154.05, 145.34, 140.49, 138.89, 134.68, 133.06, 131.78, 131.50, 131.47, 129.41, 129.10, 128.52, 127.72, 127.33, 126.81, 126.60, 126.54, 126.25, 123.82, 121.74, 120.13, 120.08, 119.67, 39.66, 36.35, 33.37, 30.49, 29.65, 29.61, 29.40, 29.21, 27.53, 27.44, 26.88, 16.42, 14.47.

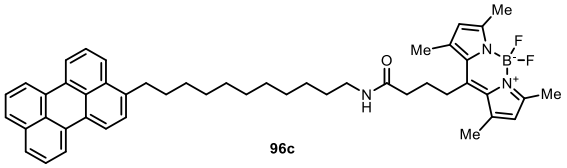


95c

11-(perylen-3-yl)undecan-1-amine (C11 amine, 95c)

The general method for Friedel-Crafts Acylation of Perylene was applied to 11-((((9H-fluoren-9-yl)methoxy)carbonyl)amino)undecanoic acid (2.014 g, 4.756 mmol, 1.2 equiv.). Pure product **95c** was obtained by silica chromatography (90:10:1 DCM:MeOH:NH$_4$OH to 80:20:1 DCM:MeOH:NH$_4$OH) as an orange powder in 44% yield.

^{1}H NMR (400 MHz, dmso) δ 8.32 (dd, *J* = 10.2, 7.5 Hz, 2H), 8.26 (d, *J* = 7.5 Hz, 1H), 8.23 (d, *J* = 7.7 Hz, 1H), 7.90 (d, *J* = 8.4 Hz, 1H), 7.74 (t, *J* = 7.8 Hz, 2H), 7.54 (t, *J* = 9.1 Hz, 1H), 7.50 (dt, *J* = 7.7, 3.8 Hz, 2H), 7.36 (d, *J* = 7.6 Hz, 1H), 2.97 (t, *J* = 7.7 Hz, 2H), 2.70 (t, *J* = 7.5 Hz, 2H), 1.67 (p, *J* = 7.2 Hz, 2H), 1.52 (p, *J* = 7.4 Hz, 2H), 1.37 (p, *J* = 7.5 Hz, 2H), 1.34 – 1.20 (m, 12H). ^{13}C NMR (101 MHz, dmso) δ 139.25, 134.78, 133.09, 131.51, 131.25, 131.22, 129.13, 128.84, 128.24, 127.83, 127.44, 127.30, 127.11, 127.05, 124.33, 121.03, 121.01, 120.96, 120.90, 120.53, 32.88, 30.54, 29.47, 29.40, 29.31, 29.23, 28.95, 27.65, 26.33.



96c

4-(5,5-difluoro-1,3,7,9-tetramethyl-5H-4l4,5l4-dipyrrolo[1,2-c:2',1'-f][1,3,2]diazaborinin-10-yl)-N-(11-(perylen-3-yl)undecyl)butanamide (C11 amide, 96c)

Amide product **x** was synthesized by the general method for Amide Coupling of Perylene and BODIPY Dyes from C11 amine and BODIPY acid. Silica chromatography (100:1 DCM:AcOH to 95:5:1 DCM:EtOAc:AcOH) afforded pure amide **96c** as an orange powder in 60% yield.

^{1}H NMR (499 MHz, cdcl$_3$) δ 8.21 (d, *J* = 7.5 Hz, 1H), 8.18 (d, *J* = 7.5 Hz, 1H), 8.15 (d, *J* = 7.5 Hz, 1H), 8.12 (d, *J* = 7.8 Hz, 1H), 7.88 (d, *J* = 8.4 Hz, 1H), 7.65 (t, *J* = 8.4 Hz, 2H), 7.53 – 7.48

(t, *J* = 7.9 Hz, 1H), 7.46 (td, *J* = 7.8, 2.8 Hz, 2H), 7.33 (d, *J* = 7.7 Hz, 1H), 6.03 (s, 2H), 3.21 (q, *J* = 7.0 Hz, 2H), 3.04 – 2.95 (m, 4H), 2.51 (s, 6H), 2.41 (s, 6H), 2.29 (t, *J* = 7.1 Hz, 2H), 1.99 – 1.90 (m, 2H), 1.75 (p, *J* = 7.7 Hz, 2H), 1.45 (m, 4H), 1.36 (m, 2H), 1.26 (m, 12H). ^{13}C NMR (126 MHz, cdcl$_3$) δ 171.33, 154.04, 145.34, 140.47, 139.01, 134.68, 133.07, 131.75, 131.52, 131.49, 129.36, 129.10, 128.53, 127.67, 127.28, 126.76, 126.57, 126.52, 126.21, 123.84, 121.72, 120.09, 120.06, 119.63, 39.68, 36.33, 33.38, 30.53, 29.75, 29.61, 29.51, 29.49, 29.46, 29.23, 27.52, 27.43, 26.89, 16.40, 14.44.

3.6.3 ***Photophysical Studies on Perylene and BODIPY Dyes***

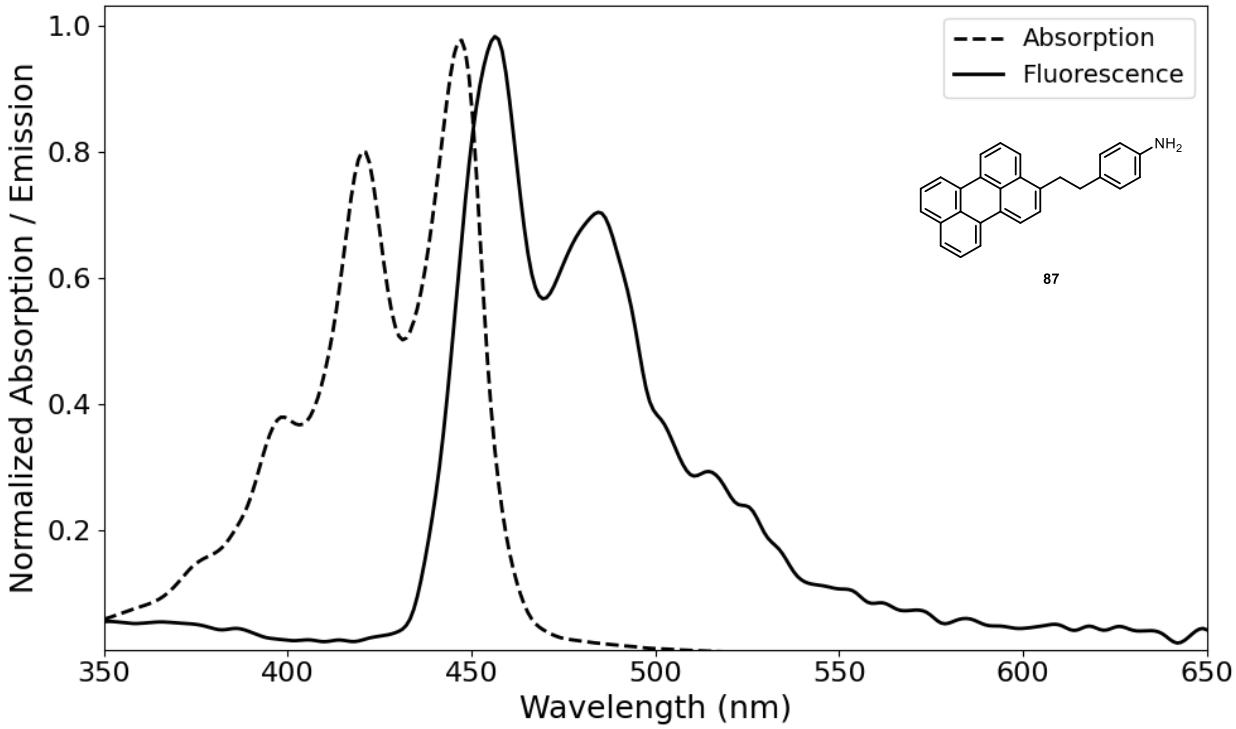


Figure 3-12 Normalized absorption and emission spectra of 10 μM **87** in DMSO. Excitation λ = 300 nm, λ max abs. = 447 nm, λ max em. = 455 nm

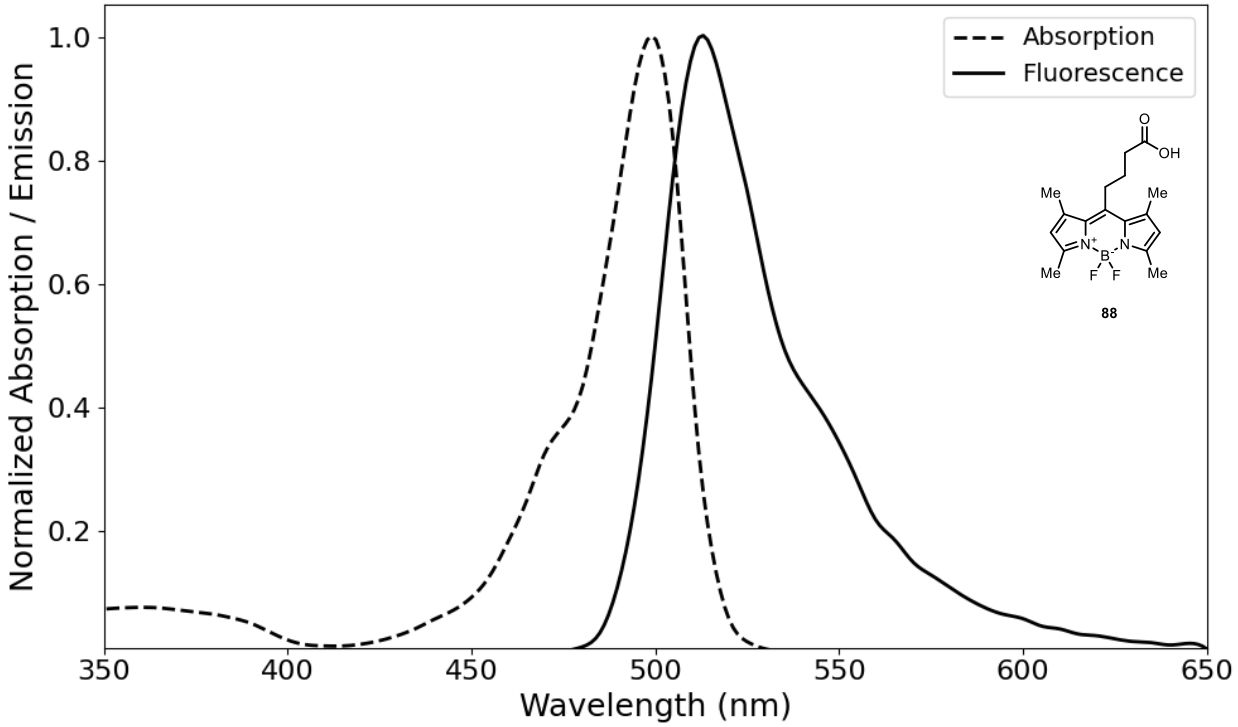


Figure 3-13 Normalized absorption and emission spectra of 10 μM **88** in DMSO. Excitation λ = 300 nm, λ max abs. = 499 nm, λ max em. = 512 nm

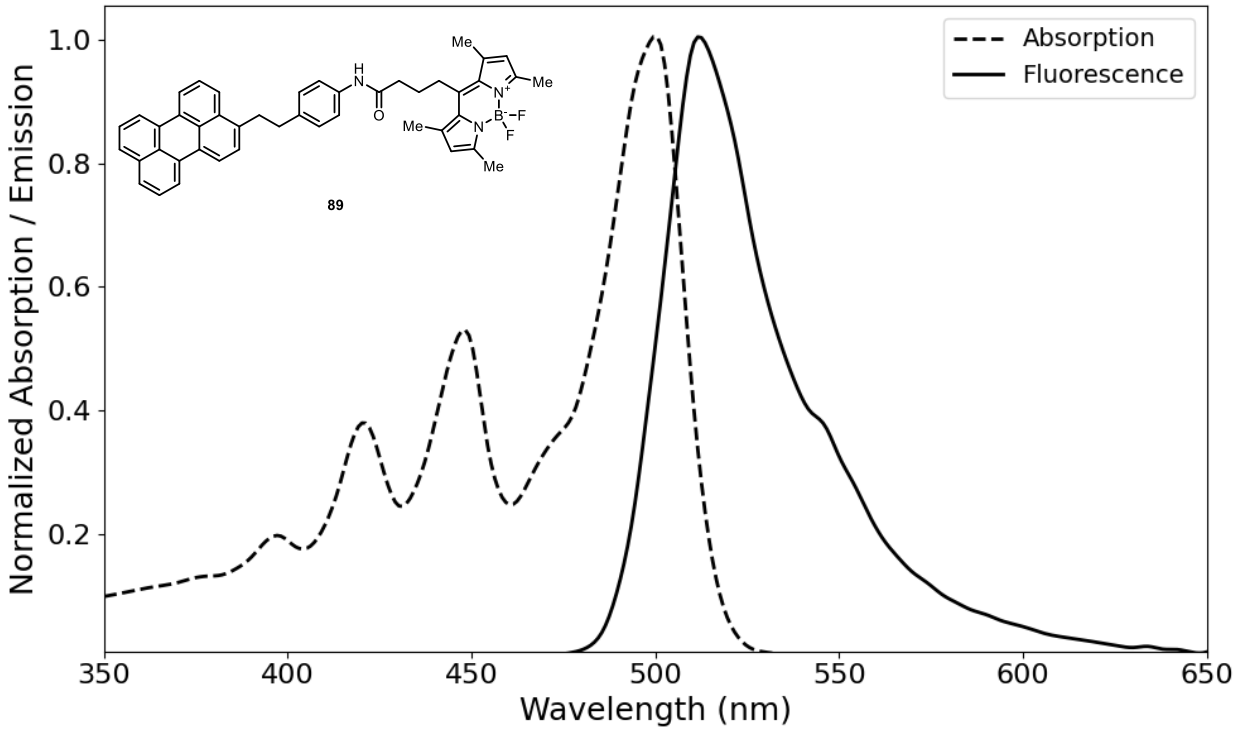


Figure 3-14 Normalized absorption and emission spectra of 10 μM **89** in DMSO. Excitation λ = 300 nm, λ max abs. = 498 nm, λ max em. = 512 nm

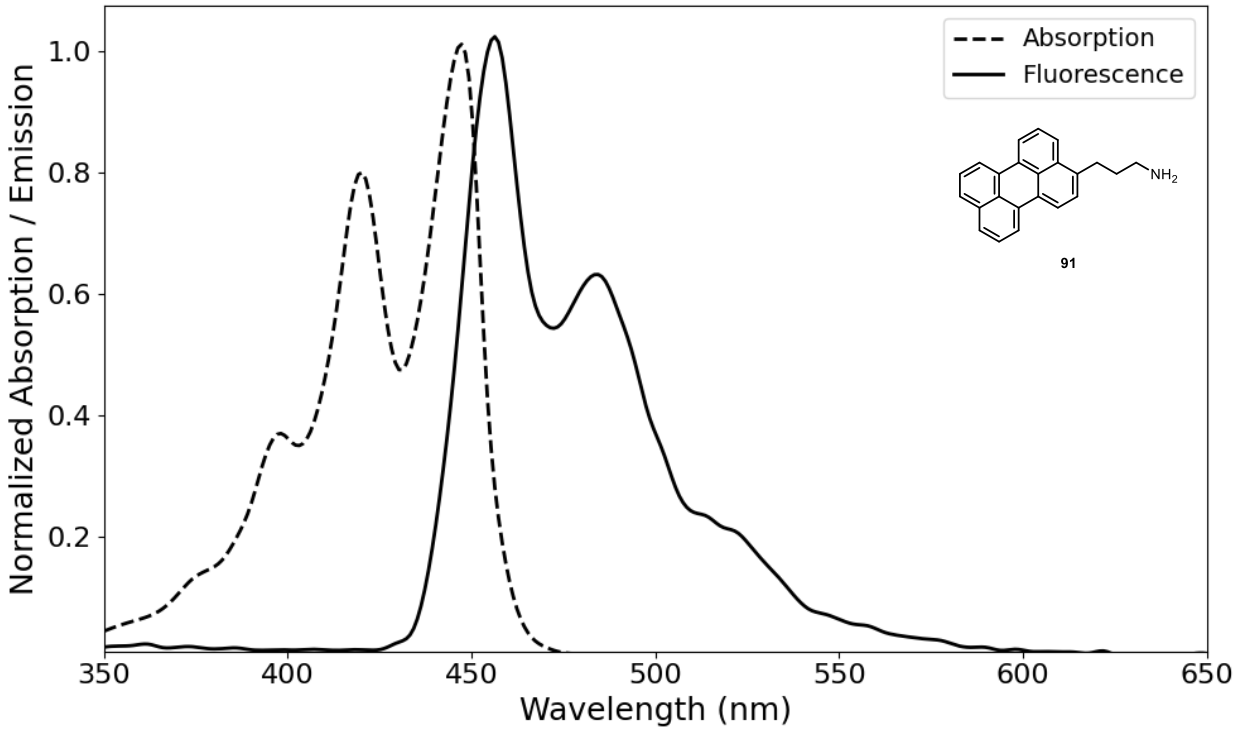


Figure 3-15 Normalized absorption and emission spectra of 10 µM **91** in DMSO. Excitation λ = 300 nm, λ max abs. = 447 nm, λ max em. = 456 nm

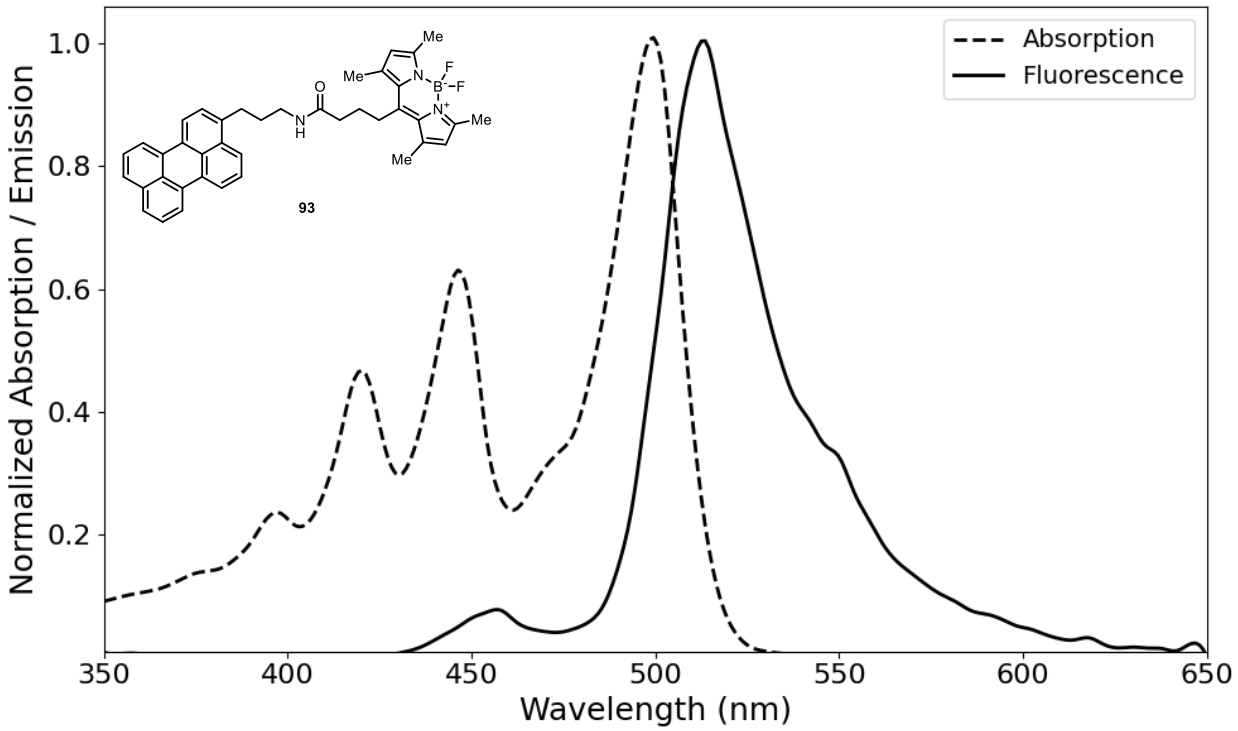


Figure 3-16 Normalized absorption and emission spectra of 10 µM **93** in DMSO. Excitation λ = 300 nm, λ max abs. = 499 nm, λ max em. = 512 nm

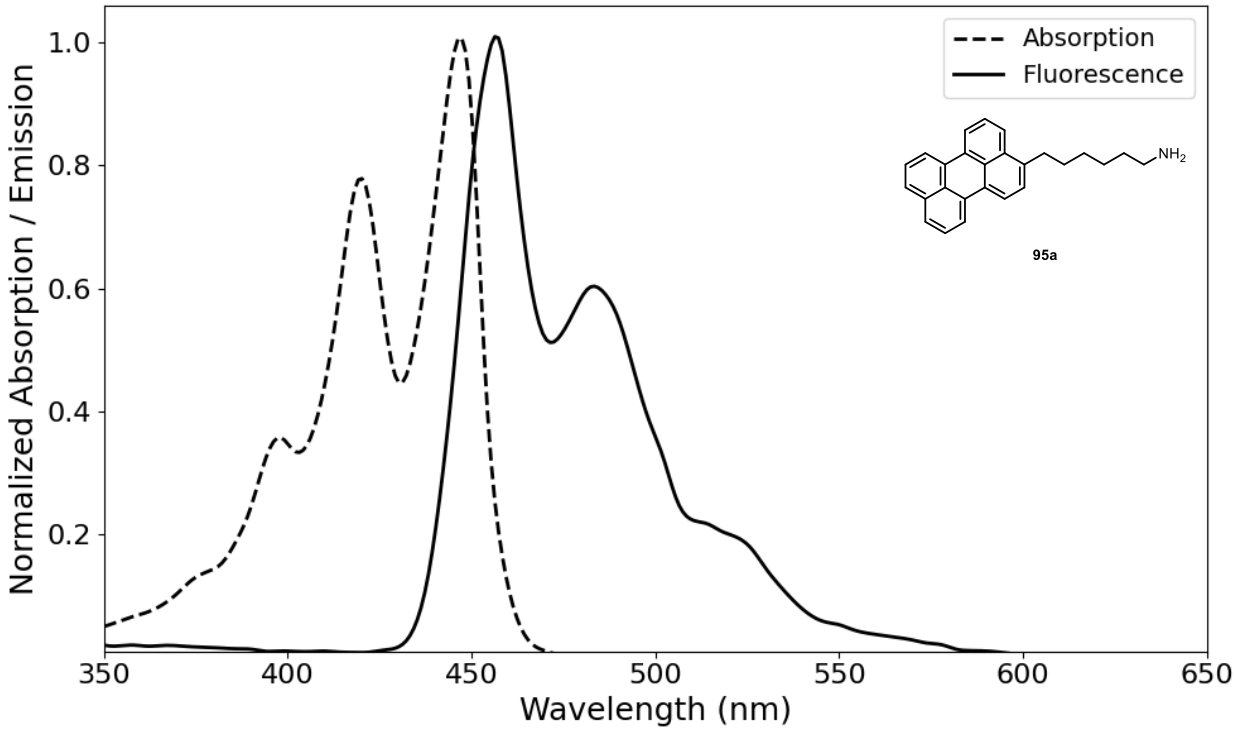


Figure 3-17 Normalized absorption and emission spectra of 10 μM **95a** in DMSO. Excitation λ = 300 nm, λ max abs. = 447 nm, λ max em. = 457 nm

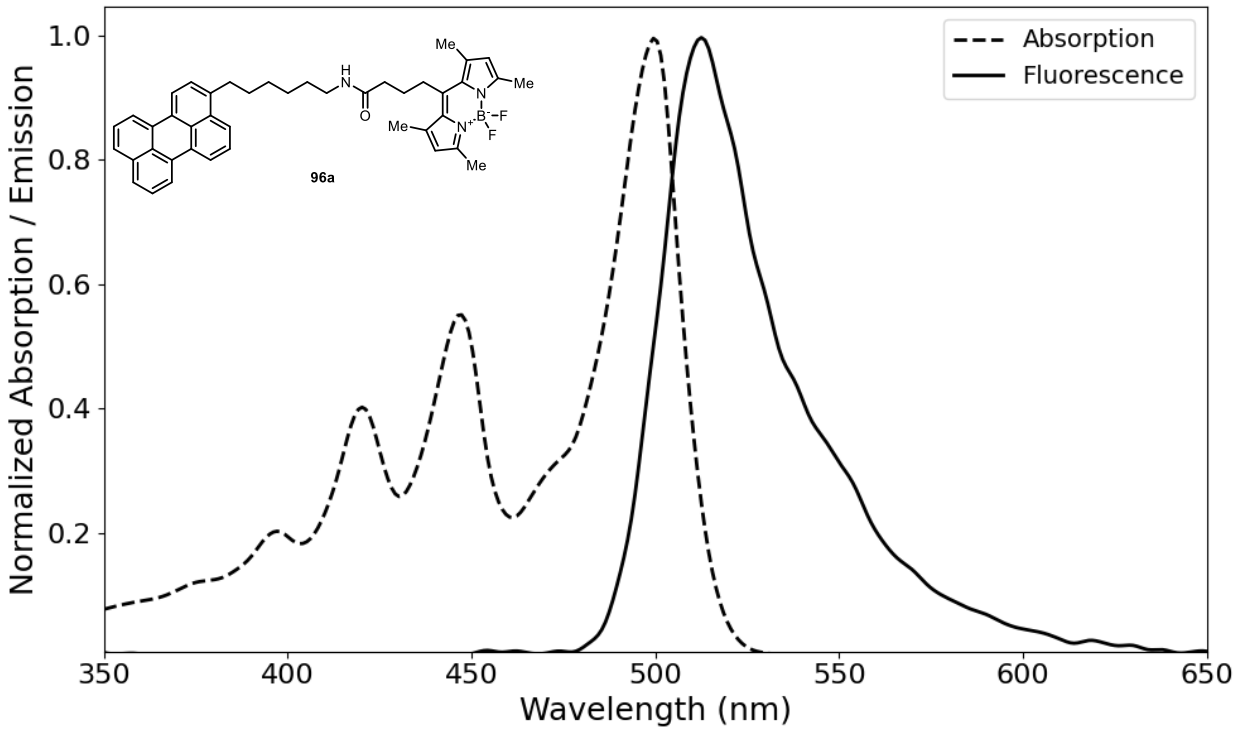


Figure 3-18 Normalized absorption and emission spectra of 10 μM **96a** in DMSO. Excitation λ = 300 nm, λ max abs. = 500 nm, λ max em. = 512 nm

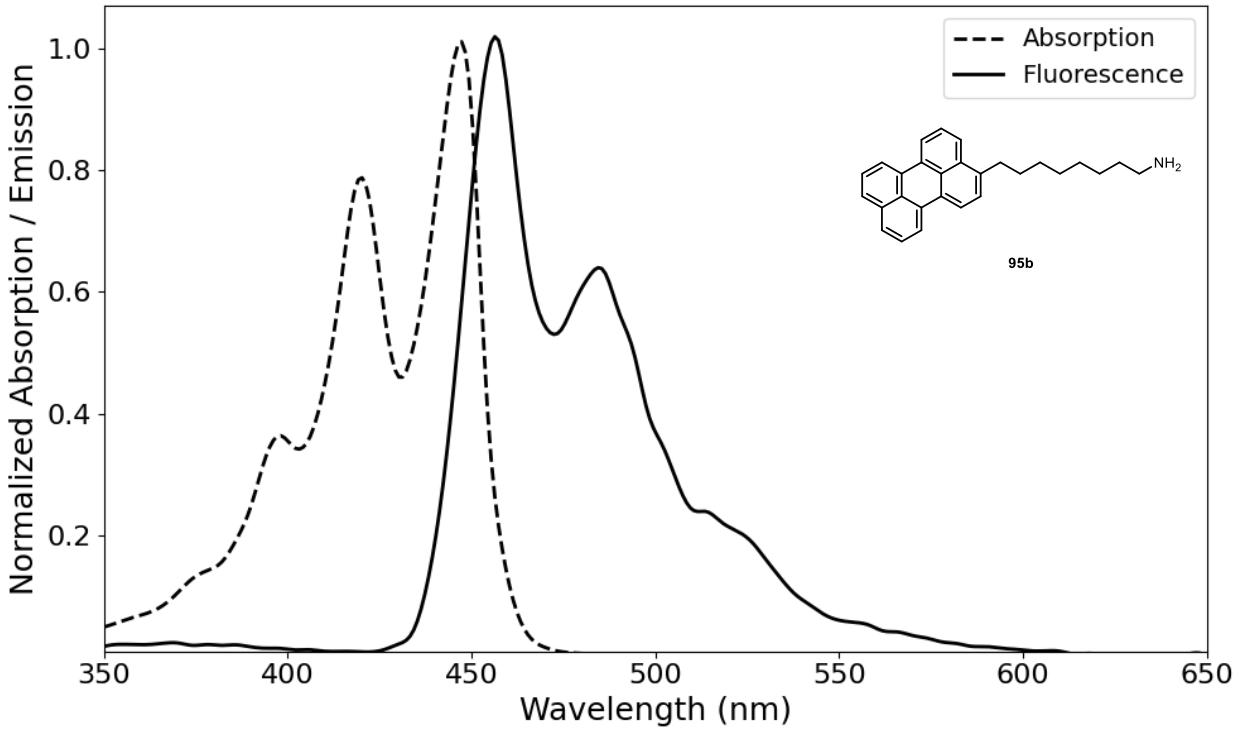


Figure 3-19 Normalized absorption and emission spectra of 10 μM **95b** in DMSO. Excitation λ = 300 nm, λ max abs. = 447 nm, λ max em. = 458 nm

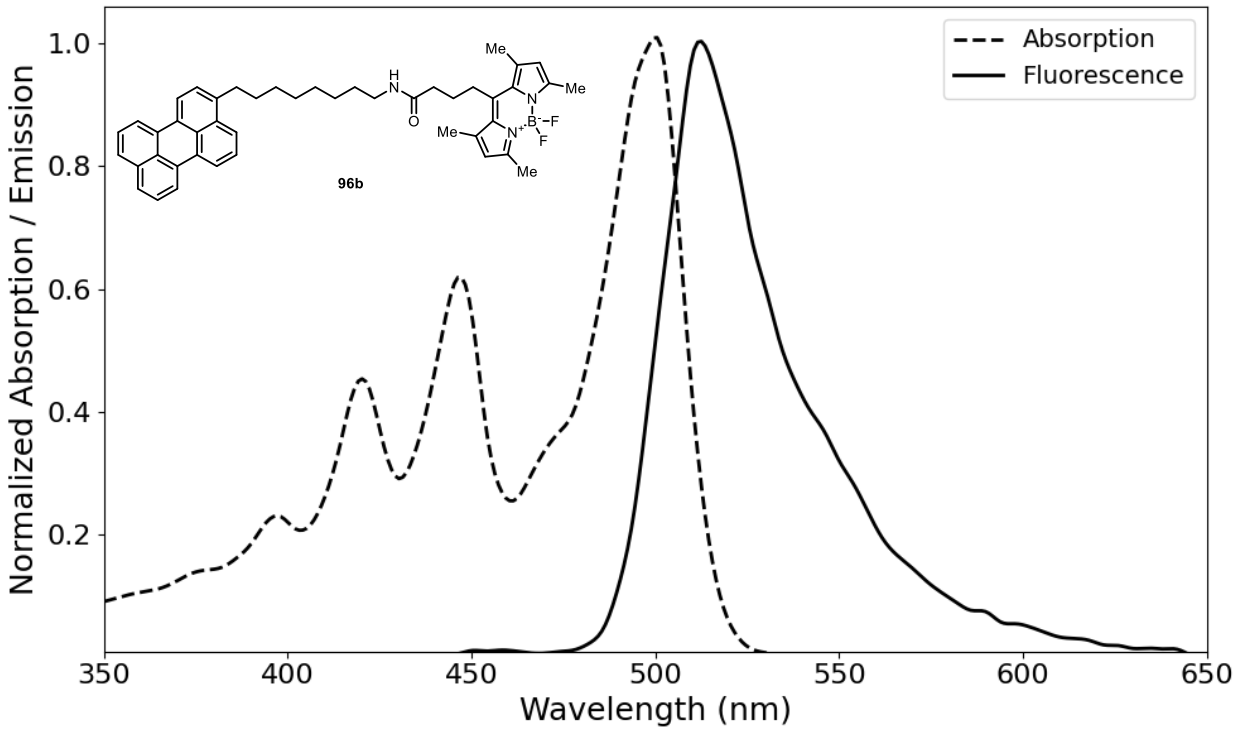


Figure 3-20 Normalized absorption and emission spectra of 10 μM **96b** in DMSO. Excitation λ = 300 nm, λ max abs. = 499 nm, λ max em. = 512 nm

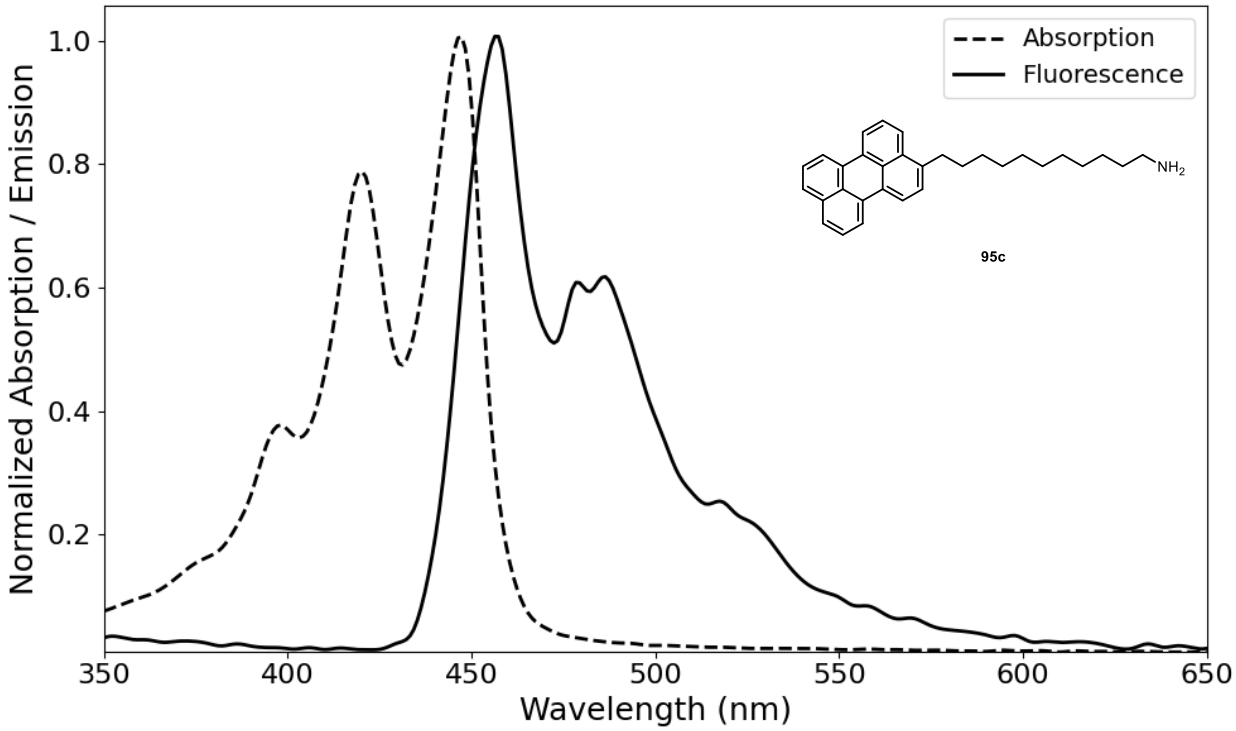


Figure 3-21 Normalized absorption and emission spectra of 10 μM **95c** in DMSO. Excitation λ = 300 nm, λ max abs. = 447 nm, λ max em. = 457 nm

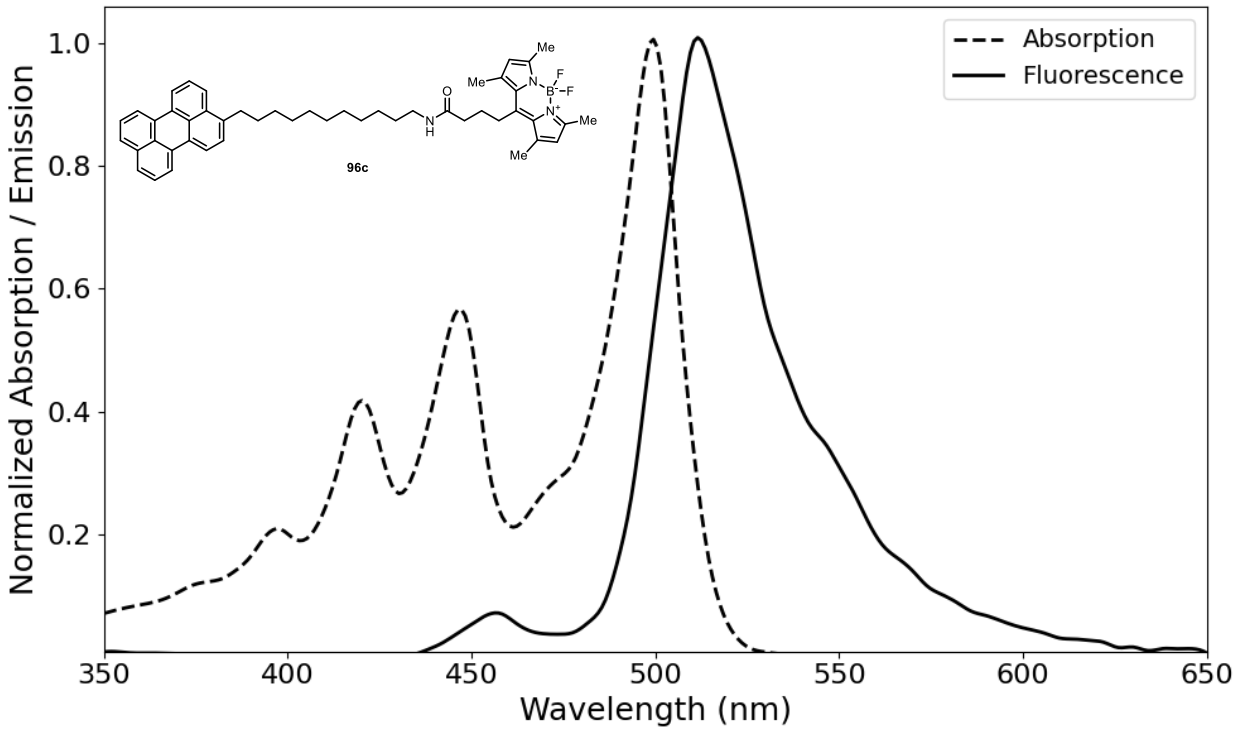


Figure 3-22 Normalized absorption and emission spectra of 10 μM **96c** in DMSO. Excitation λ = 300 nm, λ max abs. = 499 nm, λ max em. = 512 nm

Fluorescence Poisoning Study

A 96-well plate was dosed uniformly with C3 amide **93** in anhydrous DMSO, along with varying combinations of metals, ligands, and chemical additives. The bottom two rows are free from metal while the rightmost two columns are free from any ligands. The identity and quantity of stock solutions prepared in DMSO are noted in the table below. Each well was dosed with reagents to a final volume of 100 μL and blank solvent added as needed to wells with fewer components. Following dosing of each well with their corresponding mixture of metal, ligand, and/or additive, the plate was briefly stirred for 5 minutes, then a 10 μL aliquot was taken from each well and diluted to 10 μM in a separate fluorescence plate to gauge the initial fluorescence intensity when exciting at 430 nm and detecting at 510 nm. The reaction plate was sealed and allowed to stir at room temperature for 24 hours, then each well was diluted with DMSO to a final concentration of 100 μM. A final 10-fold dilution was carried out into a separate 96-well fluorescence plate containing DMSO to determine the fluorescence of each well following exposure to chemical additives. The before and after fluorescence heatmaps are shown below.

Reagents	**C_{stock} (M)**	**V_{dose} (nL)**	**Wells**
C3 amide **93**	0.4	25	All
$Pd(dba)_2$	0.4	25	Rows A and D
$NiBr_2$ glyme	0.4	25	Rows B and E
$RuCl_3$	0.4	25	Rows C and F
Brettphos	0.4	25	Columns 1 and 6
Xantphos	0.2	25	Columns 2 and 7
PPh_3	0.4	25	Columns 3 and 8
4-4′-Dimethoxy-2-2′-bipyridine	0.2	25	Columns 4 and 9
Phenanthroline	0.2	25	Columns 5 and 10
DIPEA	0.4	25	A1-5, B1-5, C1-5, G11
Acetic acid	0.4	25	D1-5, E1-5, F1-5, H11
Triethyl silane	0.4	25	A6-10, B6-10, C6-10, G12
Dess-Martin periodinane	0.4	25	D6-10, E6-10, F6-10, H12

Table 3-1 Concentrations of reagent stock solutions prepared for the 96-well fluorescence poisoning experiment and the volumes they are dosed into the appropriate reaction wells.

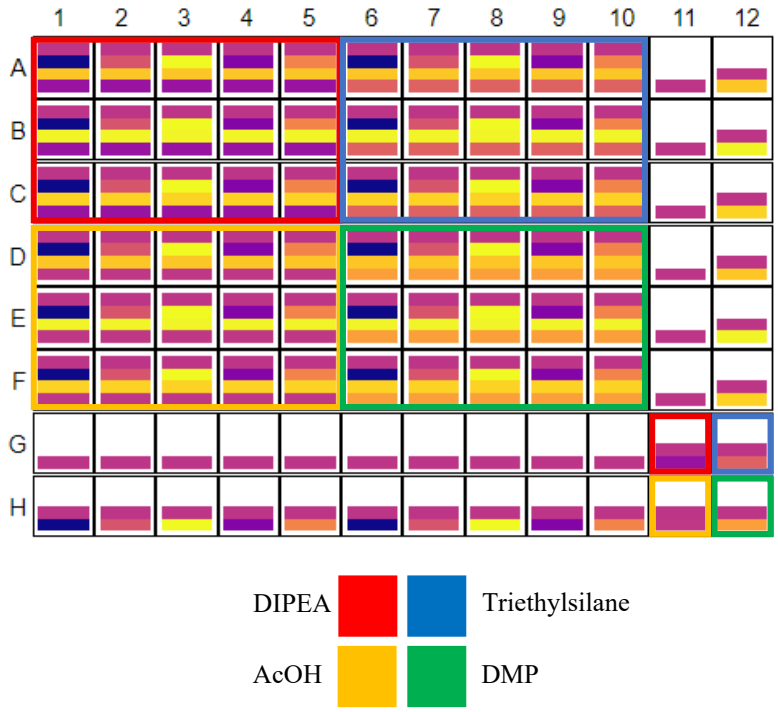


Figure 3-23 Grid of 96-well screen subjecting pure C3 amide **93** to various transition metal catalyzed conditions. Metals are allocated by row and ligands by column. Colored well outlines correlates to one of four different acid/base/reductant/oxidant additives.

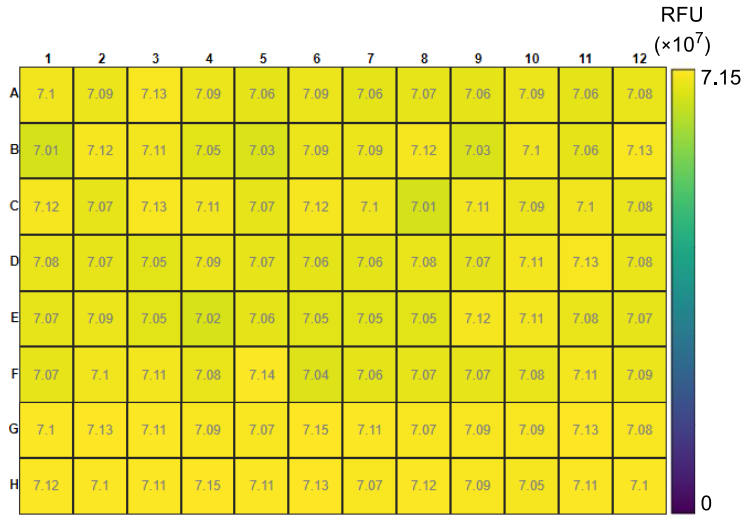


Figure 3-24 Initial fluorescence of 96-well poisoning study taken at t = 0 hrs. Excitation λ = 430 nm, emission λ = 510 nm.

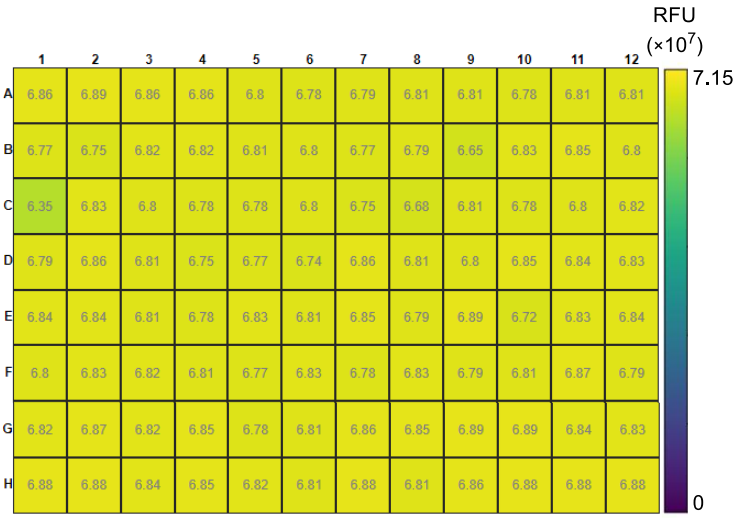


Figure 3-25 Final fluorescence of 96-well poisoning study taken at t = 24 hrs. Excitation λ = 430 nm, emission λ = 510 nm. 4% decrease in average plate fluorescence was noted relative to the initial data.

Fluorescence Calibration Curve

To determine fluorescence trends between the uncoupled amine **95a** and acid **88** relative to the amide coupled analogue **96a**, a calibration curve was produced by measuring the fluorescence response factor of stock solutions containing varied percentages of purified amide product **96a** to uncoupled amine **95a** and acid **88**. The loss of fluorescence at 460 nanometers was used as indication of the Perylene dye undergoing FRET in the amide coupled system while the uncoupled Perylene dye remains fluorescent.

Two standard solutions were freshly prepared in DMSO. One of pure amide (**96a**, 100 mM) and one containing a mixture of amine (**95a**, 100 mM) and acid (**88**, 100 mM). Six wells in a black Corning 96-well plate (part no. #3915) containing 180 µL DMSO were then prepared and various volumes of amide and amine/acid stock solutions were added to a final volume of 200 µL in each vial. The volume of amide stock solution added to each vial is as follows: 20 µL, 16 µL, 12 µL, 8 µL, 4µL, or 0 µL, respectively. The volume of amine and acid stock solution added to these same vials is as follows: 0 µL, 4 µL, 8 µL, 12 µL, 16 µL, and 20 µL. Each well was pipette mixed three times to ensure homogeneity then imaged on a fluorescence plate reader in triplicate. Fluorescence values were recorded using a 430 nm excitation wavelength and 460 nm emission wavelength. The RFU value for each sample was averaged for three runs and plotted against the mole fraction of amide in each sample, relative to the mole fraction of uncoupled amine and acid. The resulting calibration curves, with error bars from the triplicate imaging, are

shown in Figures 3-24 and 3-25. The linear regression formula from fluorescence at 460 nm was used to determine assay yields for low throughput screening experiments while the ratio of fluorescence at 510 / 460 nm was used to gauge relative conversion in high-throughput 1,536-well experiments where minor variations in dilution factor can drastically impact assay yield determined from a single fluorescence endpoint.

$$\text{RFU (460 nm)} = \text{-46851} * \text{assay yield (\%)} + 47503.$$

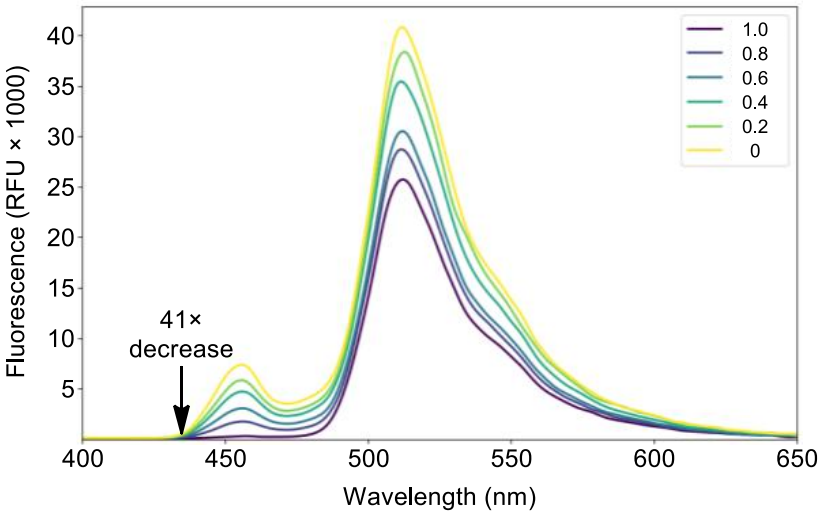


Figure 3-26 Titration of increasing mole fraction of FRET-active amide **96a** (0 to 1.0 mole fraction). Decreasing fluorescence at 460 nm was used to plot the resulting linear trend line below.

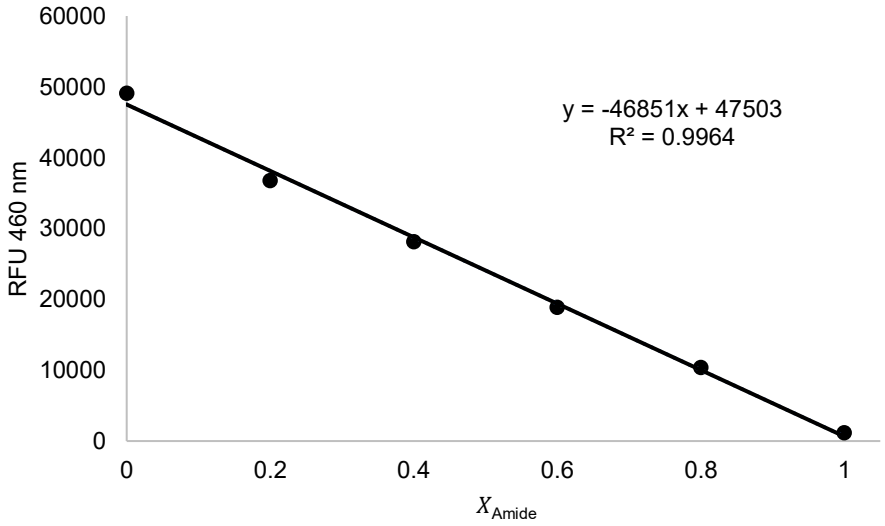
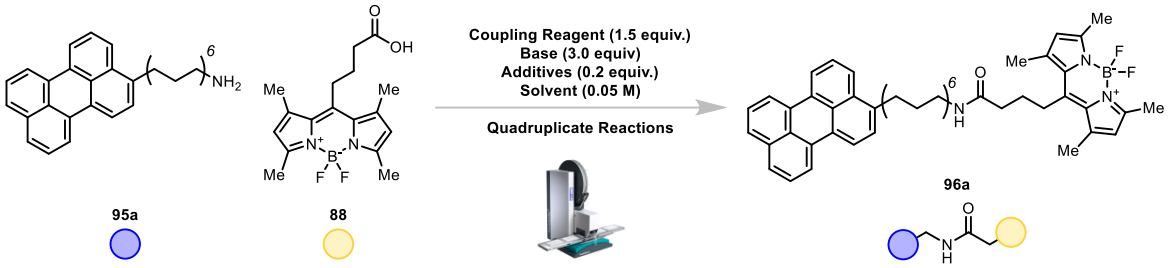


Figure 3-27 Titration of uncoupled amine **95a** and acid **88** with increasing mole fraction of amide **96a**. The lower fluorescence at 460 nanometers for amide **96a** results from energy transfer between the linked Perylene and BODIPY dyes.

3.6.4 ***Procedure for Nanoscale Amine-Acid Screen***



The 1,536-well plate (Corning part no. #4560) for the amide coupling of FRET dyes was initially prepared by dosing 1 µL of a 0.05 M DMSO solution of both Perylene amine **95a** and BODIPY acid **88** to all wells except columns 1, 17, and 33. The DMSO contents were evaporated over a 2-hour cycle using a Genevac centrifugal evaporator. Following, appropriate reagent stock solutions in the corresponding solvent were dosed as listed in the table below. The final 1,536-well plate is divided into thirds by solvent and each stock solution listed in the table is prepared in triplicate, only varying by solvent each time. Stock solutions in DMF were dosed to the left third of the plate, DMSO solutions dosed to the middle third, and diglyme solutions to the right third of the plate. Positive control was first dosed as 1 µL of pure amide **96a**, to columns 1, 17, and 33. The amine and acid previously dosed to columns 2, 18, and 34 were reconstituted in 1 µL of the appropriate solvent to act as negative controls. Subsequent reagent dosing is as follows: 333 µL of the appropriate base was dosed across an entire row, 333 µL of DMAP stock solution was dosed to the top half of the plate, 333 µL of HOBT was dosed to the bottom half of the plate, and finally 333 µL of the appropriate coupling reagent was dosed to an entire column in each third of the plate, only swapping from DMF to DMSO to diglyme between each third of the plate.

Once dosing was complete and final well volumes of 1 µL were achieved, the reaction plate was sealed with foil sealing tape (ThermoFisher part No. 232699) and centrifuged (Fisher Scientific Mini Plate Spinner) on full speed for ~1 minute. The reaction plate was then placed inside the plate heating apparatus (Eppendorf ThermoMixer C with Eppendorf ThermoTop attachment) to heat at 50°C for 20 hours. The foil seal was removed, and the reaction wells were quenched by addition of 1 µL of caffeine (0.05 M) in DMSO and the reaction plate centrifuged. Reaction aliquots of 600 nL were then transferred into four 384-well microtiter plates (Analytical sales part no. #38120) pre-filled with 29.4 µL of HPLC-grade DMSO per well for UPLC–MS

analysis. From the LC–MS plates, 1 μL was taken and further diluted into fluorescence imaging plates (Greiner part no. #781209) containing 49 μL DMSO for a final concentration of 10 μM. Fluorescence data collection was executed with 430 nm excitation wavelength and dual emission detection at 460 nm and 510 nm (8 mm read height, negative control wells set to 40,000 RFU at 510 nm). The LC–MS plates were subsequently analyzed and product ratios relative to the caffeine internal standard were used to generate assay yield values using the trendline equation of Figure 3-25:

Assay Yield (%) = 24.836 * (Product integration / Caffeine integration)

Reagents	C_{stock} (M)	V_{dose} (nL)	Wells
Amine **95a** and acid **88**	0.05	1000	All but columns 1, 17, 33
Pure amide **96a** (+ control)	0.05	1000	Columns 1, 17, 33
Blank base	N/A	333	Rows 1, 2, 17, 18
DIPEA	0.45	333	Rows 3, 4, 19, 20
Triethylamine	0.45	333	Rows 5, 6, 21, 22
N-Methyl imidazole	0.45	333	Rows 7, 8, 23, 24
N-Methyl morpholine	0.45	333	Rows 9, 10, 25, 26
Pyridine	0.45	333	Rows 11, 12, 27, 28
2,6-Lutidine	0.45	333	Rows 13, 14, 29, 30
2,4,6-Collidine	0.45	333	Rows 15, 16, 31, 32
4-Dimethylaminopyridine	0.03	333	Rows 1-16
1-Hydroxybenzotriazole	0.03	333	Rows 17-32
HATU	0.225	333	Columns 3, 4, 19, 20, 35, 36
DCC	0.225	333	Columns 5, 6, 21, 22, 37, 38
PyBOP	0.225	333	Columns 7, 8, 23, 24, 39, 40
DMTMM	0.225	333	Columns 9, 10, 25, 26, 41, 42
COMU	0.225	333	Columns 11, 12, 27, 28, 43, 44
CDI	0.225	333	Columns 13, 14, 29, 30, 45, 46
EDC HCl	0.225	333	Columns 15, 16, 31, 32, 47, 48

Table 3-2 Concentrations of reagent stock solutions prepared for 1,536-well plate amide coupling experiment and the volumes they are dosed into the appropriate reaction wells. Each stock solution is made in triplicate at the same concentration and dosed at the same volume, only differing by solvent (one in DMF, DMSO, and diglyme).

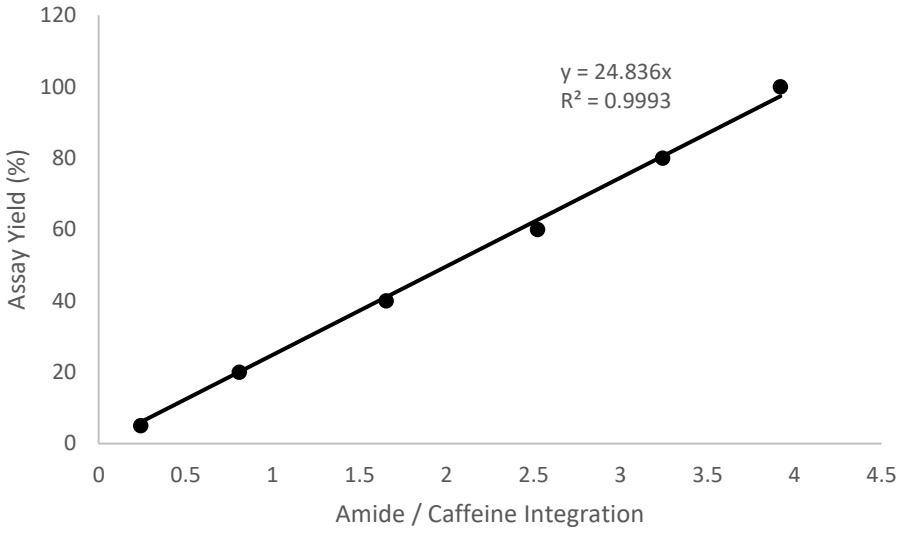


Figure 3-28 Calibration Curve for Assay yield determination of amide coupling yields by LC–MS.

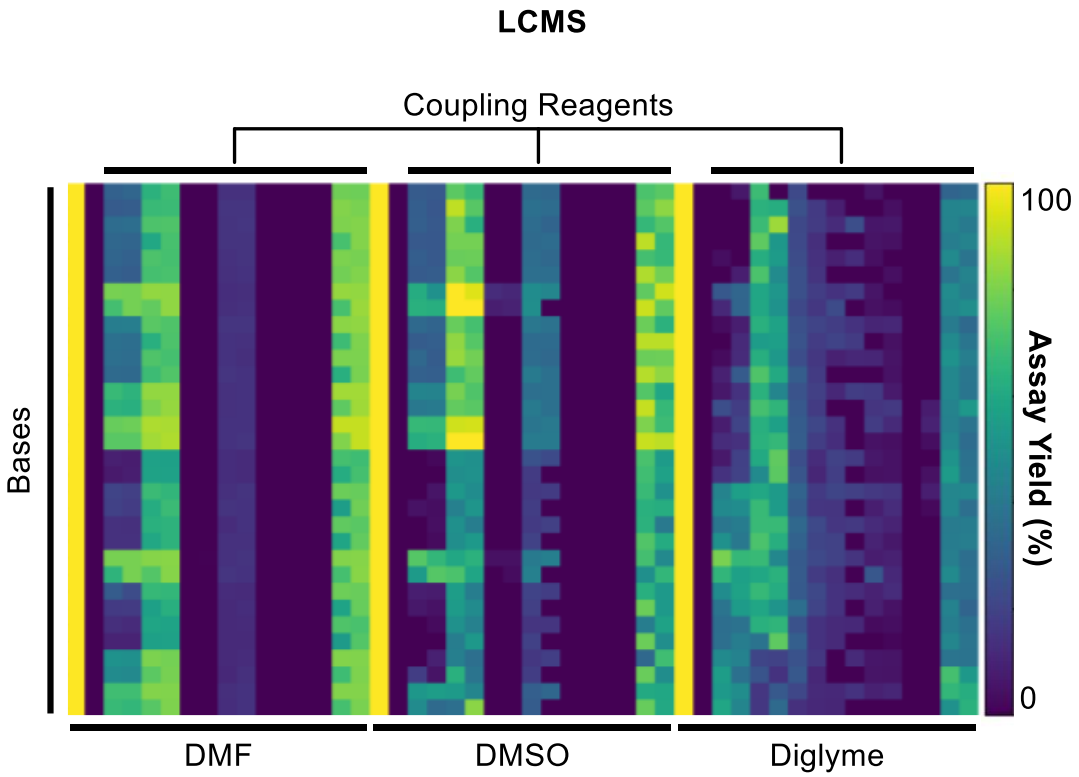


Figure 3-29 Heatmap from LC–MS analysis of the 1,536-well amide coupling of FRET dyes. Colored by increasing assay yield. Columns 1, 2, 17, 18, 33, and 34 are positive and negative controls.

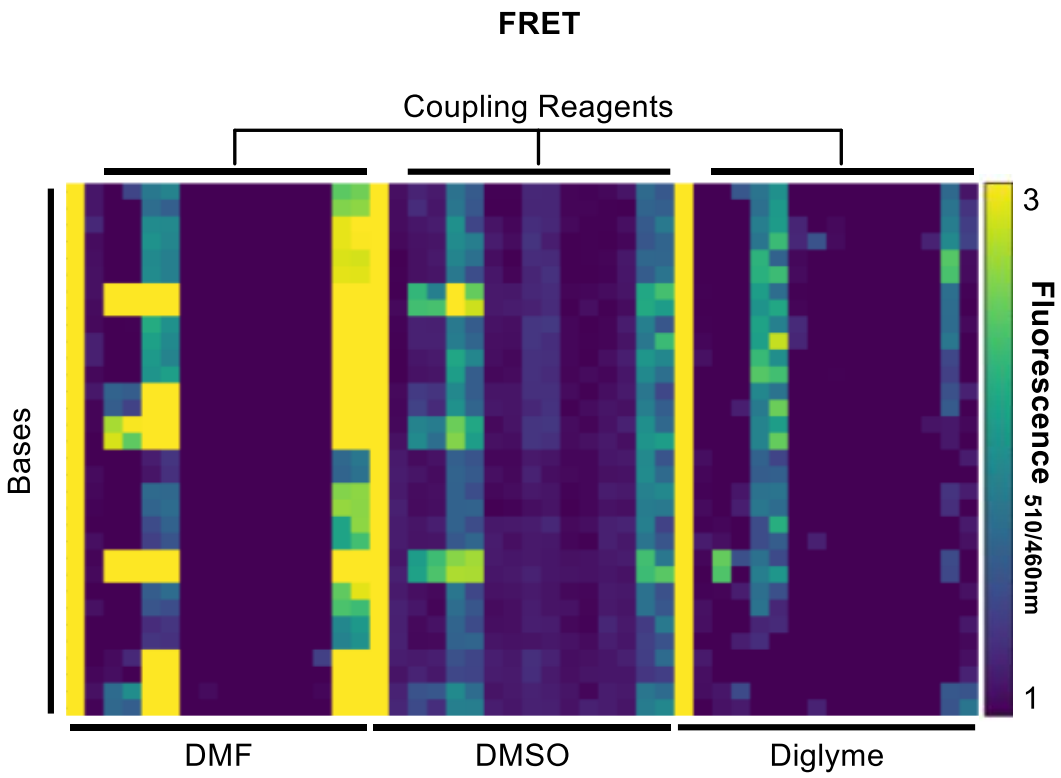


Figure 3-30 Heatmap from fluorescence analysis of the 1,536-well amide coupling of FRET dyes. Colored by the increasing fluorescence ratio at 510 nm / 460 nm. Columns 1, 2, 17, 18, 33, and 34 are positive and negative controls.

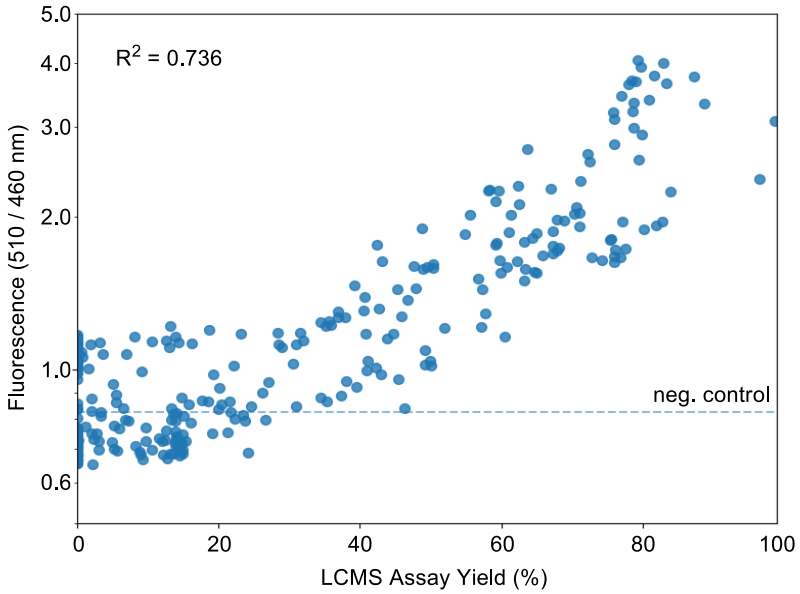
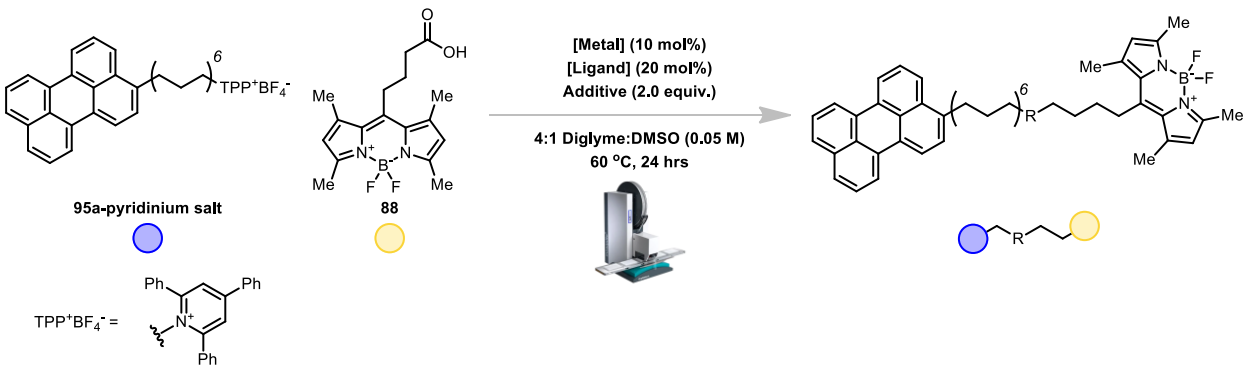


Figure 3-31 Comparison of LC–MS Assay Yields vs Ratiometric FRET analysis of 1,536-well amide coupling experiment. The y-axis is displayed on a logarithmic scale and R^2 value is representative of fitting the log-value data to a linear trend.

3.6.5 ***Procedure for Nanoscale Pyridinium Salt-Acid Screen***



Each of the five 1,536-well reaction plates (Corning part no. #4560) was initially dosed with 1 uL of 0.05 M DMSO stock solution containing both uncoupled dyes to all wells except for column 1 which served as a positive control. Centrifugal evaporation was carried out to remove the dosed DMSO, then dosing of the corresponding reaction components was done in the following order: positive control (amide **96a**), ligand, metal, then additives. Appropriate stock solutions made up in 4:1 diglyme:DMSO solvent were dosed as is listed in the table below. The reaction plate was centrifuged between additions of different components.

Once dosing was complete and final well volumes of 1 µL were achieved, the reaction plates were sealed with foil sealing tape (ThermoFisher part No. 232699) and centrifuged (Fisher Scientific Mini Plate Spinner) on full speed for ~1 minute. The reaction plates were then placed inside the plate heating apparatus (Eppendorf ThermoMixer C with Eppendorf ThermoTop attachment) to heat at 60°C for 24 hours. The foil seal was removed, and the reaction wells were quenched by addition of 1 µL of caffeine (0.05 M) in DMSO and the reaction plates centrifuged. Reaction aliquots of 600 nL were then transferred into four 384-well microtiter plates (Analytical sales part no. #38120) pre-filled with 29.4 µL of HPLC-grade DMSO per well for UPLC–MS analysis. From the LC–MS plates, 1 µL was taken and further diluted into fluorescence imaging plates (Greiner part no. #781209) containing 49 µL DMSO for a final concentration of 10 µM. Fluorescence data collection was executed with 430 nm excitation wavelength and dual emission detection at 460 nm and 510 nm (8 mm read height, negative control wells set to 40,000 RFU at 510 nm). Initial hits, as gauged by >1.5-fold fluorescence signal at 510 nm / 460 nm, were validated by LC–MS analysis. The identified Pummerer-type rearrangement from several wells

containing BODIPY acid **88,** DMSO, $[Ir(cod)Cl]_2$ and triethyl silane was scaled up on model substrates as shown in **Figure 3-38**.

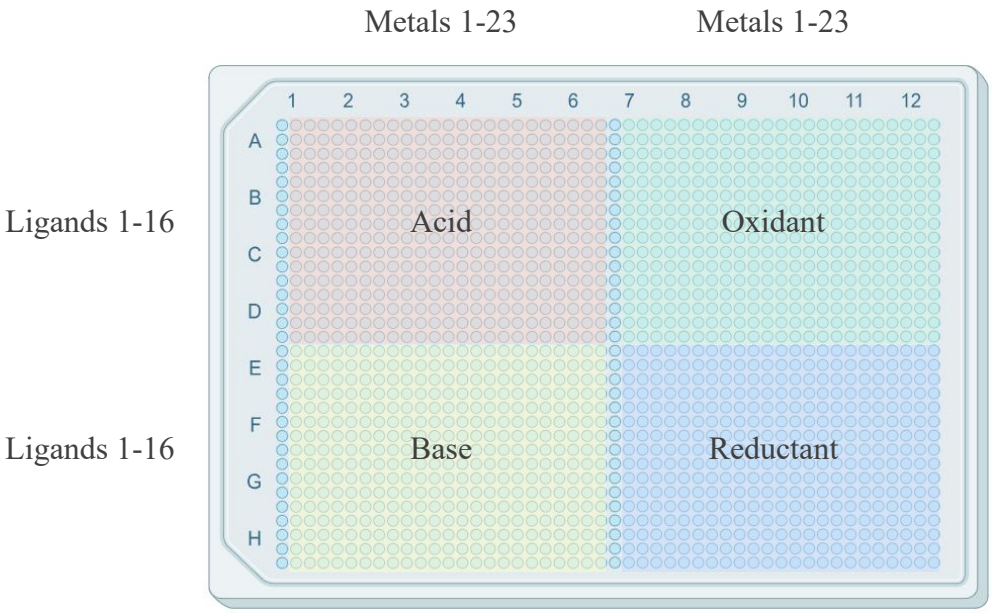


Figure 3-32 Layout for each of the five 1,536-well reaction plates in the nanoscale pyridinium salt-acid screening campaign. In each plate the substrate, control, ligand, and additives dosed are identical between plates. The only variable is the identity of metals dosed to each column of each plate. Columns 1 and 25 represent positive and negative controls, respectively, which only received amide **96a** (+ control) or uncoupled dyes **95a-pyridinium salt** and **88** (- neg control).

Reagents	**C_{stock} (M)**	**V_{dose} (nL)**	**Wells**
Pyridinium salt of **95a** and acid **88**	0.05	1000	All but column 1
Pure amide **96a** (+ control)	0.05	1000	Column 1
Acetic acid	0.15	333	Rows: A – P, Columns: 2-24
DIPEA	0.15	333	Rows: Q – AF, Columns: 2-24
Tetra-n-butylammonium iodide	0.15	333	Rows: A – P, Columns: 26-48
Triethyl silane	0.15	333	Rows: Q – AF, Columns: 26-48
2,2'-bipyridine	0.015	333	Rows: A, Q
4,4'-bis(trifluoromethyl)-2,2'-bipyridine	0.015	333	Rows: B, R
4-4'-Dimethoxy-2-2'-bipyridine	0.015	333	Rows: C, S
Phenanthroline	0.015	333	Rows: D, T

Salicylaldoxime	0.015	333	Rows: E, U
N^1,N^2-Bis(1-naphthalenylmethyl)ethanediamide	0.015	333	Rows: F, V
2,3,4,5,6-Pentafluoroanilino(oxo)acetic acid	0.015	333	Rows: G, W
2,6-Dimethoxyanilino(oxo)acetic acid	0.015	333	Rows: H, X
2,6-Dimethylanilino(oxo)acetic acid	0.015	333	Rows: I, Y
Triphenylphospine	0.030	333	Rows: J, Z
1,3-Bis(diphenylphosphino)propane	0.015	333	Rows: K, AA
1,1'-Bis(diphenylphosphino)ferrocene	0.015	333	Rows: L, AB
tBuXphos	0.030	333	Rows: M, AC
Triethyl phosphite	0.030	333	Rows: N, AD
Tri-o-tolyl Phosphite	0.030	333	Rows: O, AE
No Ligand	-	333	Rows: P, AF
Metals	0.015	333	Columns 2-24, 26-48

Table 3-3 List of reagents that are dosed to all five 1,536 plates in the same locations per plate.

Metals in Plate 1	
Metal	**Wells**
Titanium(IV) ethoxide	Columns: 2, 26
Bis(cyclopentadienyl)titanium(IV) dichloride	Columns: 3, 27
Titanium hydride	Columns: 4, 28
(Pentamethylcyclopentadienyl)titanium(IV) Trichloride	Columns: 5, 29
Titanium tetrafluoride	Columns: 6, 30
Titanium(IV) oxide bis(acetylacetonate)	Columns: 7, 31
Vanadium(III) chloride	Columns: 8, 32
Vanadium(IV) oxide bis(2,4-pentanedionate)	Columns: 9, 33
Vanadium(III) acetylacetonate	Columns: 10, 34
Vanadium(II) chloride	Columns: 11, 35
Vanadium(III) fluoride	Columns: 12, 36
Chromium(III) chloride	Columns: 13, 37
SODIUM BIS(2-HYDROXY-2-METHYLBUTYRATO)OXOCHROMATE(V)	Columns: 14, 38
MANGANESE(II) CARBONATE	Columns: 15, 39
CYCLOPENTADIENYLMANGANESE TRICARBONYL	Columns: 16, 40
Manganese(II) nitrate hydrate	Columns: 17, 41
Gallium(III) bromide	Columns: 18, 42

Gallium(III) trifluoromethanesulfonate	Columns: 19, 43
Gallium(III) 2,4-pentanedionate	Columns: 20, 44
Gallium Iodide	Columns: 21, 45
Zirconium fluoride	Columns: 22, 46
BIS(CYCLOPENTADIENYL)ZIRCONIUM CHLORIDE HYDRIDE	Columns: 23, 47
ZIRCONOCENE DICHLORIDE	Columns: 24, 48

Table 3-4 Metals used in the first of five 1,536 well reaction plates in the pyridinium salt-acid screening campaign.

Metals in Plate 2	
Metal	**Wells**
ZIRCONIUM(IV) CHLORIDE	Columns: 2, 26
Triruthenium dodecacarbonyl	Columns: 3, 27
Dichloro(1,5-cyclooctadiene)ruthenium(II)	Columns: 4, 28
Ruthenium(III) Chloride	Columns: 5, 29
CHLORO(CYCLOPENTADIENYL)BIS(TRIPHENYLPHOSPHINE)RUTHENIUM(II)	Columns: 6, 30
Tris(acetonitrile)cyclopentadienylruthenium(II) hexafluorophosphate	Columns: 7, 31
TRIS(TRIPHENYLPHOSPHINE)RHODIUM(I) CHLORIDE	Columns: 8, 32
BIS(1,5-CYCLOOCTADIENE)RHODIUM(I) TETRAFLUOROBORATE	Columns: 9, 33
PENTAMETHYLCYCLOPENTADIENYLRHODIUM(III) CHLORIDE DIMER	Columns: 10, 34
Hydroxy(1,5-cyclooctadiene)rhodium(I) dimer	Columns: 11, 35
Chloro(1,5-cyclooctadiene)rhodium(I)dimer	Columns: 12, 36
SILVER(I) FLUORIDE	Columns: 13, 37
SILVER CARBONATE	Columns: 14, 38
SILVER TRIFLUOROMETHANESULFONATE	Columns: 15, 39
SILVER ACETATE	Columns: 16, 40
SILVER(I) OXIDE	Columns: 17, 41
SILVER CARBONATE	Columns: 18, 42
SILVER HEXAFLUOROPHOSPHATE	Columns: 19, 43
SILVER(II) FLUORIDE	Columns: 20, 44
Indium(III) chloride	Columns: 21, 45
INDIUM(III) BROMIDE	Columns: 22, 46
INDIUM(III) TRIFLUOROMETHANESULFONATE	Columns: 23, 47
Lanthanum(III) chloride	Columns: 24, 48

Table 3-5 Metals used in the second of five 1,536 well reaction plates in the pyridinium salt-acid screening campaign.

Metals in Plate 3	
Metal	**Wells**
Pentamethylcyclopentadienyliridium(III) chloride,dimer	Columns: 2, 26
BIS(1,5-CYCLOOCTADIENE)DIIRIDIUM(I) DICHLORIDE	Columns: 3, 27
(1,5-CYCLOOCTADIENE)(METHOXY)IRIDIUM(I) DIMER	Columns: 4, 28
(1,5-Cyclooctadiene)(pyridine)(tricyclohexylphosphine)-iridium(I) hexafluorophosphate	Columns: 5, 29
Carbonylchloro bis(triphenylphosphine)iridium(I)	Columns: 6, 30
(1,5-Cyclooctadiene)(hexafluoroacetylacetonato)iridium(I)	Columns: 7, 31
(Acetylacetonato)dicarbonyliridium(I)	Columns: 8, 32
PLATINUM(II) CHLORIDE	Columns: 9, 33
(1,5-CYCLOOCTADIENE)DIMETHYLPLATINUM(II)	Columns: 10, 34
GOLD(III) CHLORIDE	Columns: 11, 35
GOLD(I) CHLORIDE	Columns: 12, 36
Gold(III) bromide	Columns: 13, 37
Gold(iii)hydroxide	Columns: 14, 38
Aluminum fluoride	Columns: 15, 39
Aluminum trifluoromethanesulfonate	Columns: 16, 40
Aluminum 2,4-pentanedionate	Columns: 17, 41
Chromium(III) acetate	Columns: 18, 42
Ammonium hexachlororuthenate(IV)	Columns: 19, 43
Bis(2,2,6,6-tetramethyl-3,5-heptanedionato)zinc	Columns: 20, 44
Bis(2-methylallyl)(1,5-cyclooctadiene)ruthenium(II)	Columns: 21, 45
Bis(cyclopentadienyl)ruthenium(II)	Columns: 22, 46
cis-Dichlorobis(diethylsulfide)platinum(II)	Columns: 23, 47
cis-Dichlorobis(pyridine)platinum(II)	Columns: 24, 48

Table 3-6 Metals used in the third of five 1,536 well reaction plates in the pyridinium salt-acid screening campaign.

Metals in Plate 4	
Metal	**Wells**
Dichlorobis(benzonitrile)platinum(II)	Columns: 2, 26
Dichlorotricarbonylruthenium(II) dimer	Columns: 3, 27
Indium(III) acetylacetonate	Columns: 4, 28
Iridium(III) acetylacetonate	Columns: 5, 29
Manganese bis(trifluoromethanesulfonate)	Columns: 6, 30

Manganese carbonyl	Columns: 7, 31
Manganese(II) acetate	Columns: 8, 32
Manganese(II) bromide	Columns: 9, 33
Tetrakis(triphenylphosphine)platinum(0)	Columns: 10, 34
Molybdenum(VI) dioxide bis(acetylacetonate)	Columns: 11, 35
Molybdenum(V) chloride	Columns: 12, 36
Ammonium dimolybdate	Columns: 13, 37
Platinum(II) acetylacetonate	Columns: 14, 38
Platinum(iv)iodide	Columns: 15, 39
Rhodium(III) acetylacetonate	Columns: 16, 40
Rhodium(III) iodide	Columns: 17, 41
Ruthenium(III) acetate	Columns: 18, 42
Ruthenium(III) acetylacetonate	Columns: 19, 43
Ruthenium(III) iodide	Columns: 20, 44
Terbium(III) fluoride	Columns: 21, 45
Tris(2,2,6,6-tetramethyl-3,5-heptanedionato)yttrium(III)	Columns: 22, 46
Yttrium(III) fluoride	Columns: 23, 47
Yttrium(III) trifluoromethanesulfonate	Columns: 24, 48

Table 3-7 Metals used in the fourth of five 1,536 well reaction plates in the pyridinium salt-acid screening campaign.

Metals in Plate 5	
Metal	**Wells**
Zinc diethyldithiocarbamate	Columns: 2, 26
Zinc bis(trifluoromethylsulfonyl)imide	Columns: 3, 27
Manganese(ii)hexafluoroacetylacetonate	Columns: 4, 28
Manganese(II) sulfide	Columns: 5, 29
Manganocene	Columns: 6, 30
Tris(2,2,6,6-tetramethyl-3,5-heptanedionato)manganese(III)	Columns: 7, 31
Manganese(III) acetylacetonate	Columns: 8, 32
Niobium(V) ethoxide	Columns: 9, 33
Yttrium(III) nitrate hexahydrate	Columns: 10, 34
Chromium carbonyl	Columns: 11, 35
Chromium(II) chloride	Columns: 12, 36
Chromium(III) acetylacetonate	Columns: 13, 37
Chromium(III) fluoride tetrahydrate	Columns: 14, 38

Hafnium(IV) chloride	Columns: 15, 39
Iridium (III) chloride	Columns: 16, 40
Niobium(V) chloride	Columns: 17, 41
Tantalum(V) chloride	Columns: 18, 42
Tantalum(V) fluoride	Columns: 19, 43
Bis(cyclopentadienyl)hafnium dichloride	Columns: 20, 44
Hafnium(IV) acetylacetonate	Columns: 21, 45
Yttrium(III) hexafluoroacetylacetonate	Columns: 22, 46
Zirconium(IV) acetylacetonate	Columns: 23, 47
METHYLTRIOXORHENIUM(VII)	Columns: 24, 48

Table 3-8 Metals used in the fifth of five 1,536 well reaction plates in the pyridinium salt-acid screening campaign.

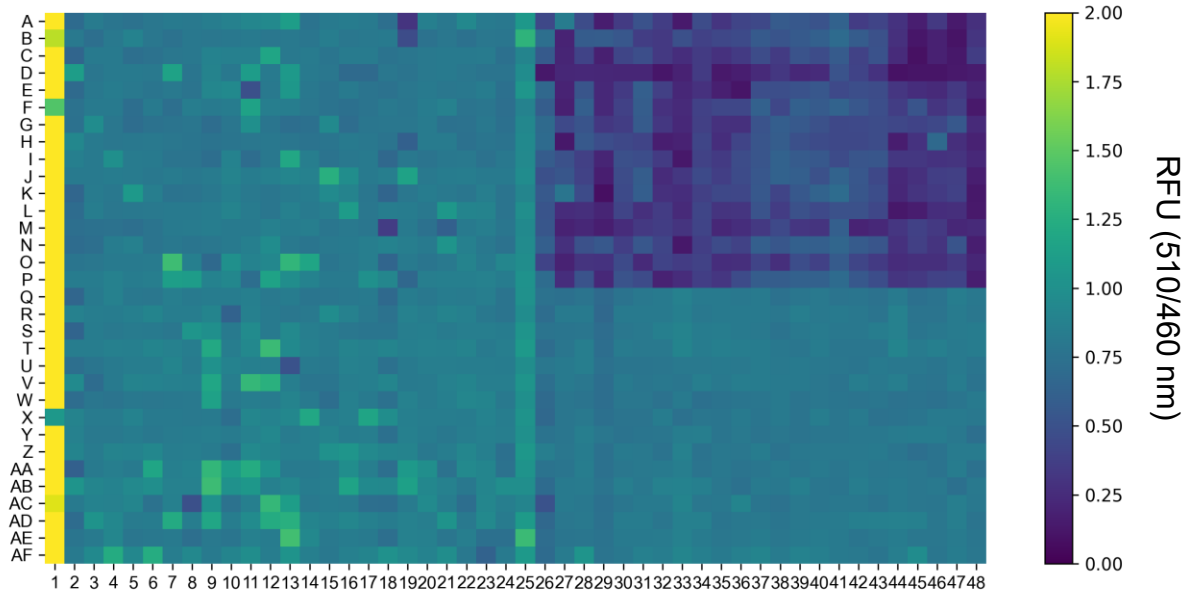


Figure 3-33 Heatmap of Fluorescence detected at at 510nm / 460 nm for Plate 1 from the nanoscale pyridinium salt-acid FRET screen. Excitation λ = 430 nm.

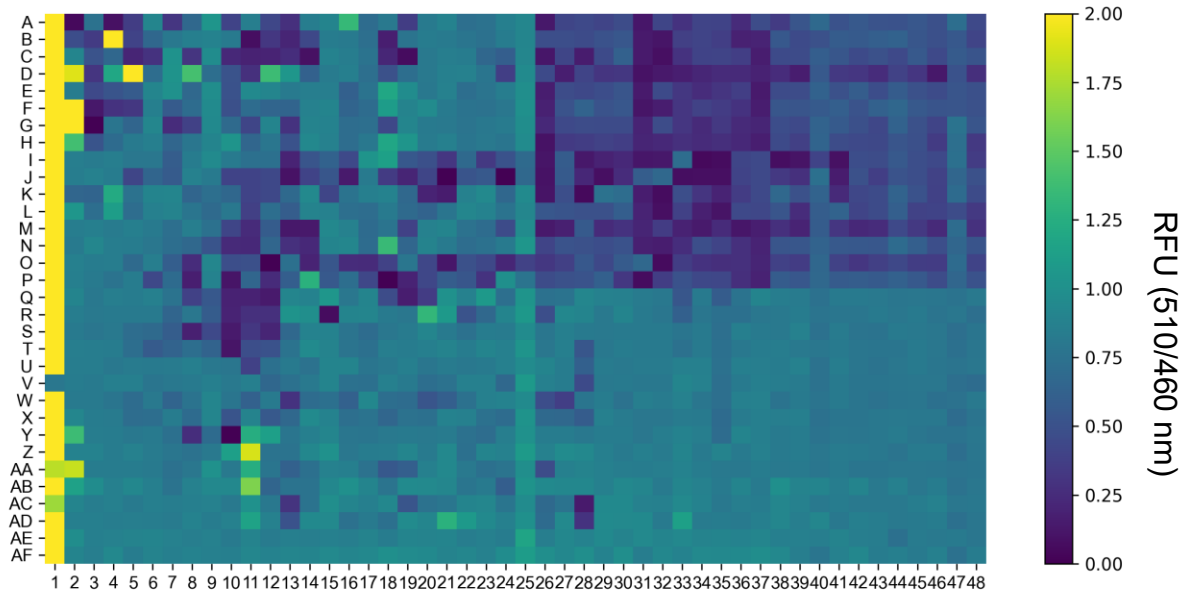


Figure 3-34 Heatmap of Fluorescence detected at at 510nm / 460 nm for Plate 2 from the nanoscale pyridinium salt-acid FRET screen. Excitation λ = 430 nm.

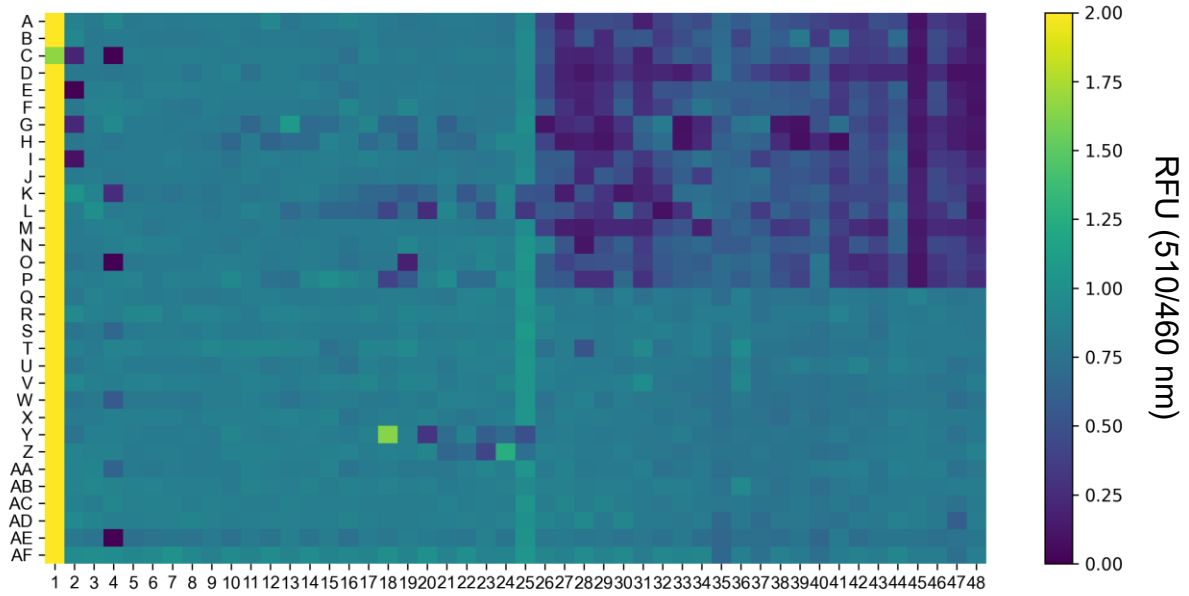


Figure 3-35 Heatmap of Fluorescence detected at at 510nm / 460 nm for Plate 3 from the nanoscale pyridinium salt-acid FRET screen. Excitation λ = 430 nm.

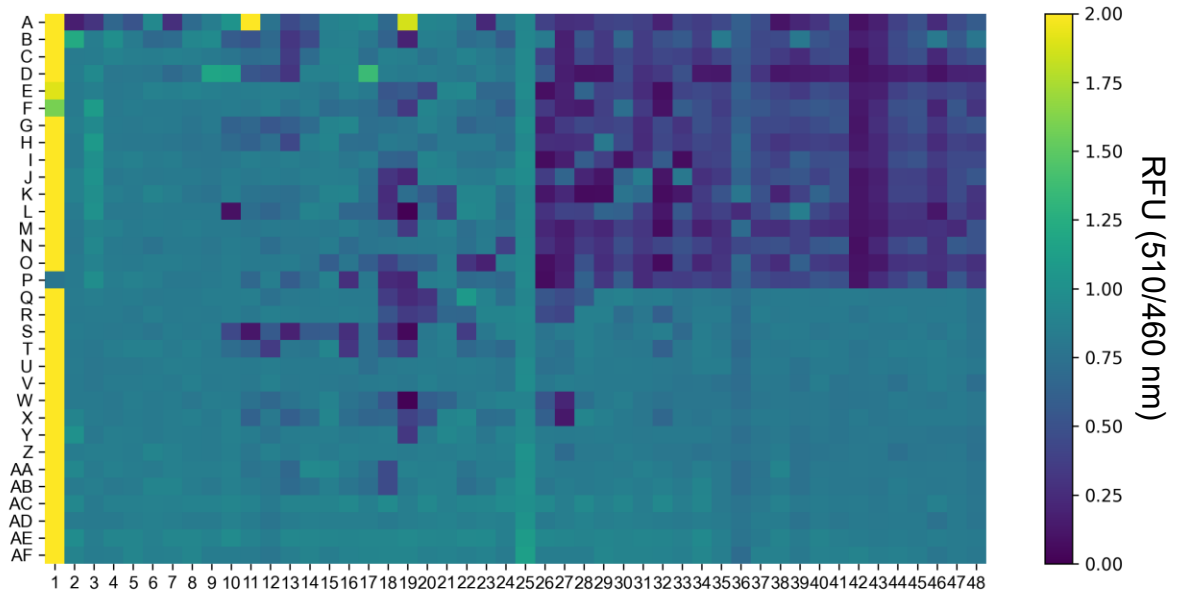


Figure 3-36 Heatmap of Fluorescence detected at at 510nm / 460 nm for Plate 4 from the nanoscale pyridinium salt-acid FRET screen. Excitation λ = 430 nm.

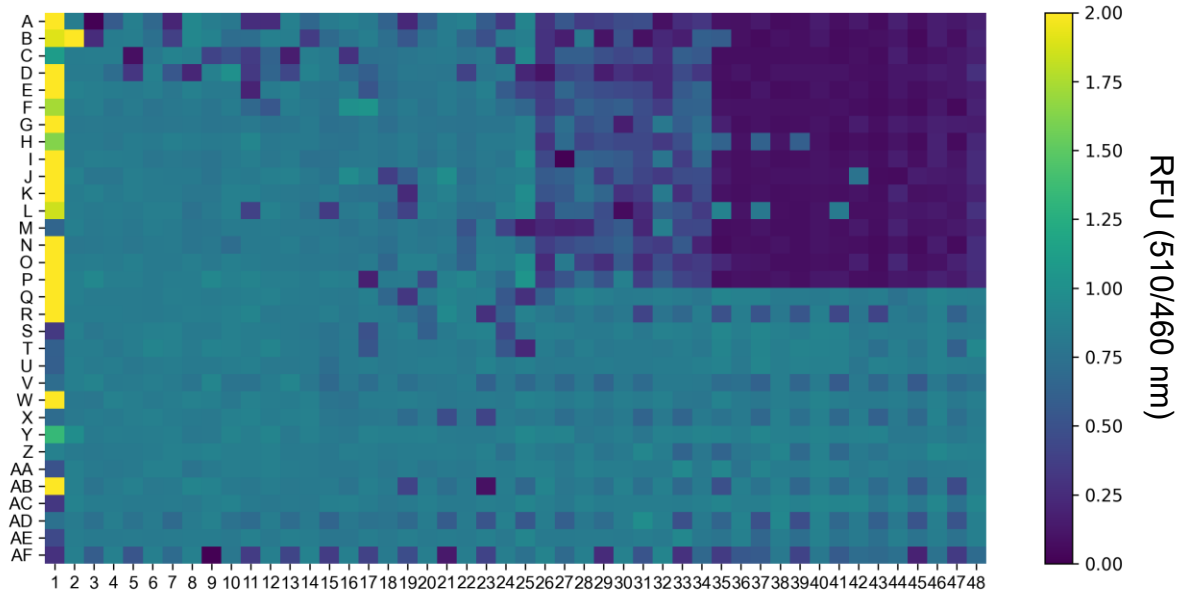


Figure 3-37 Heatmap of Fluorescence detected at at 510nm / 460 nm for Plate 5 from the nanoscale pyridinium salt-acid FRET screen. Excitation λ = 430 nm.

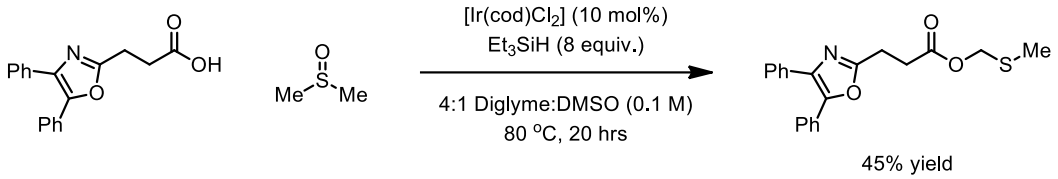
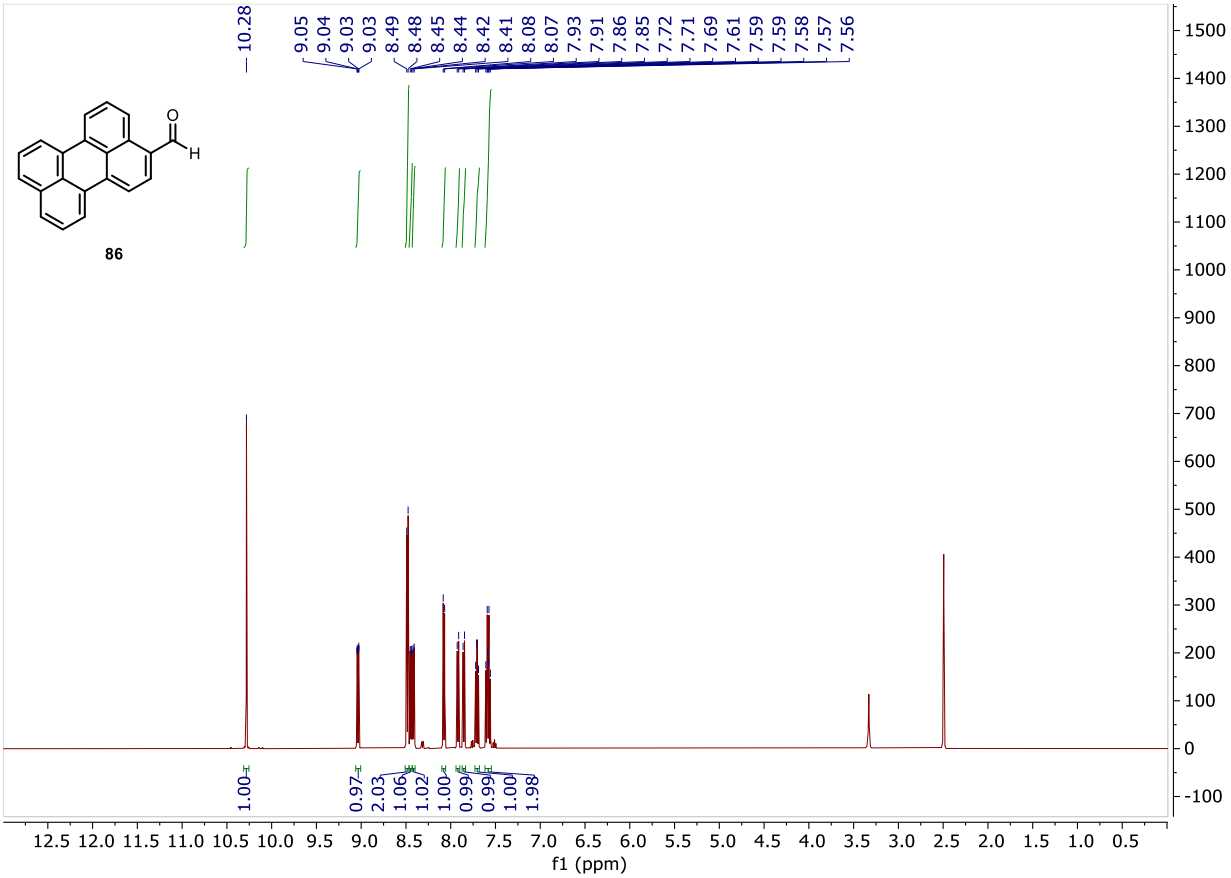
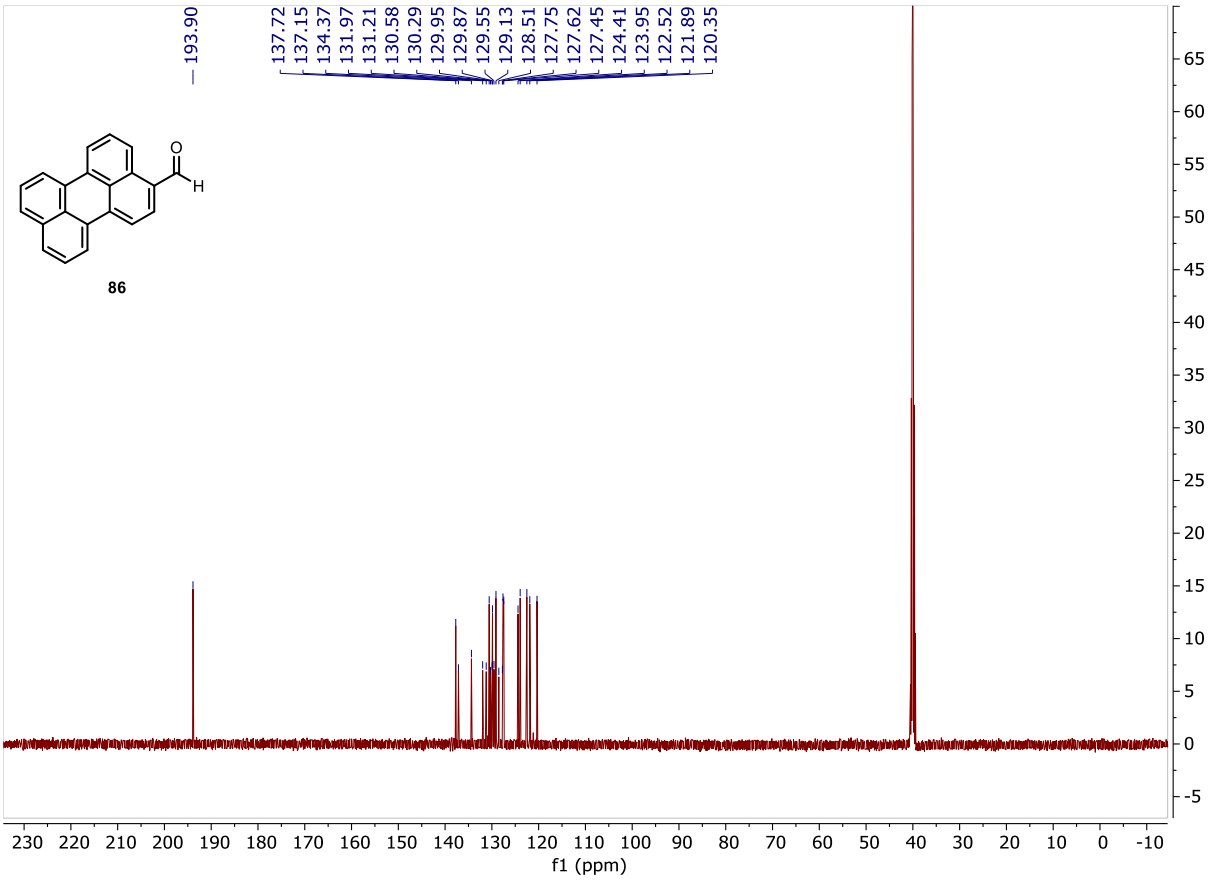


Figure 3-38 Identified Pummerer-type rearrangement from wells containing [Ir(cod)Cl_2] and triethyl silane. Showcased on a model acid substrate.

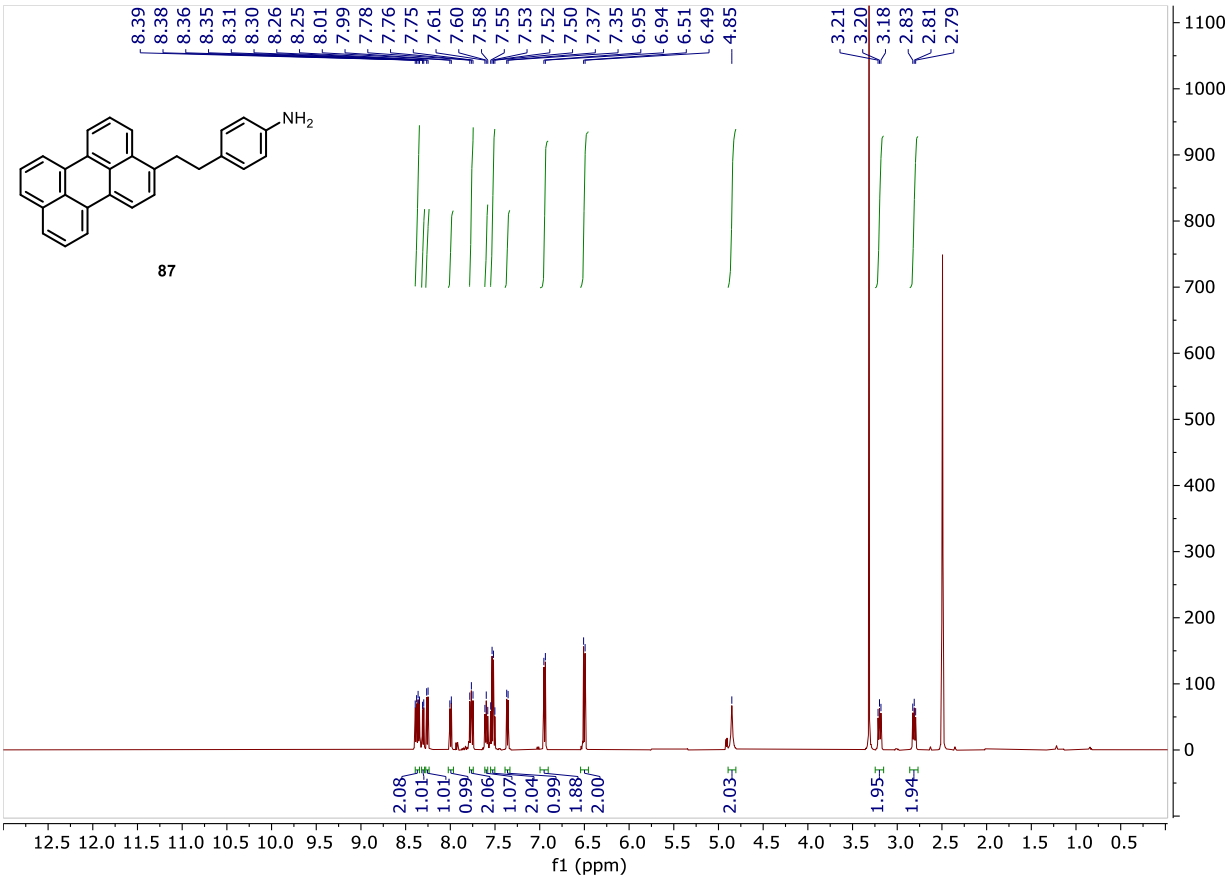
3.7 **Spectra**



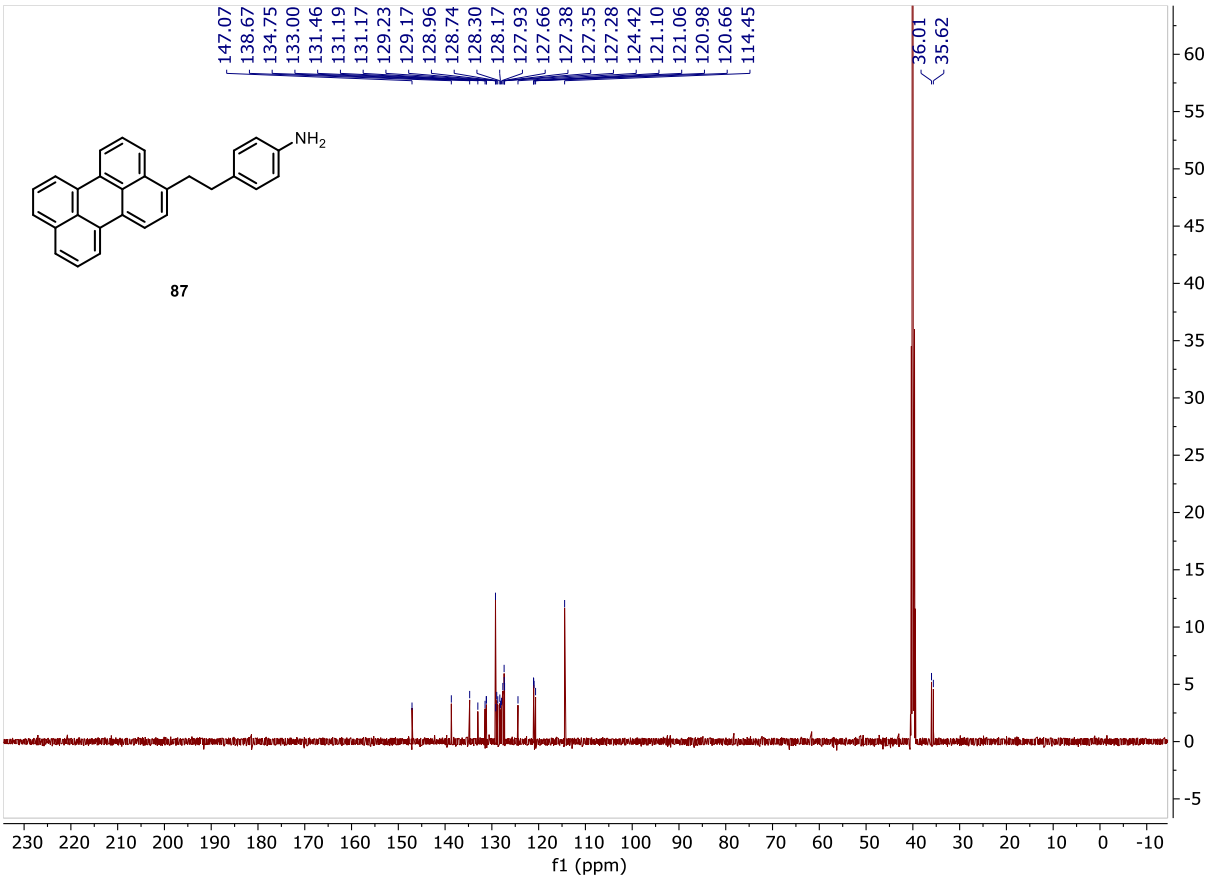
Spectrum 3-1 ^{1}H NMR of compound 86



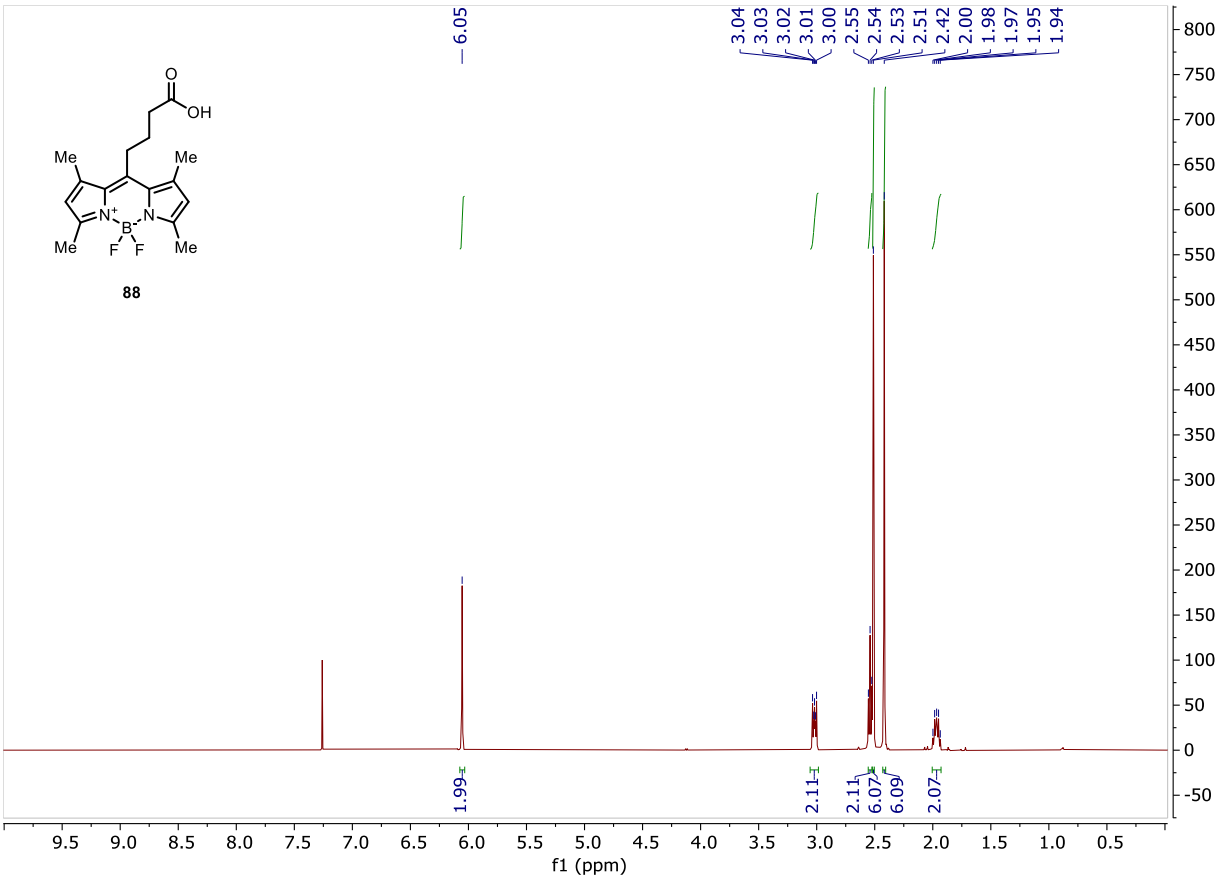
Spectrum 3-2 ^{13}C NMR of compound 86



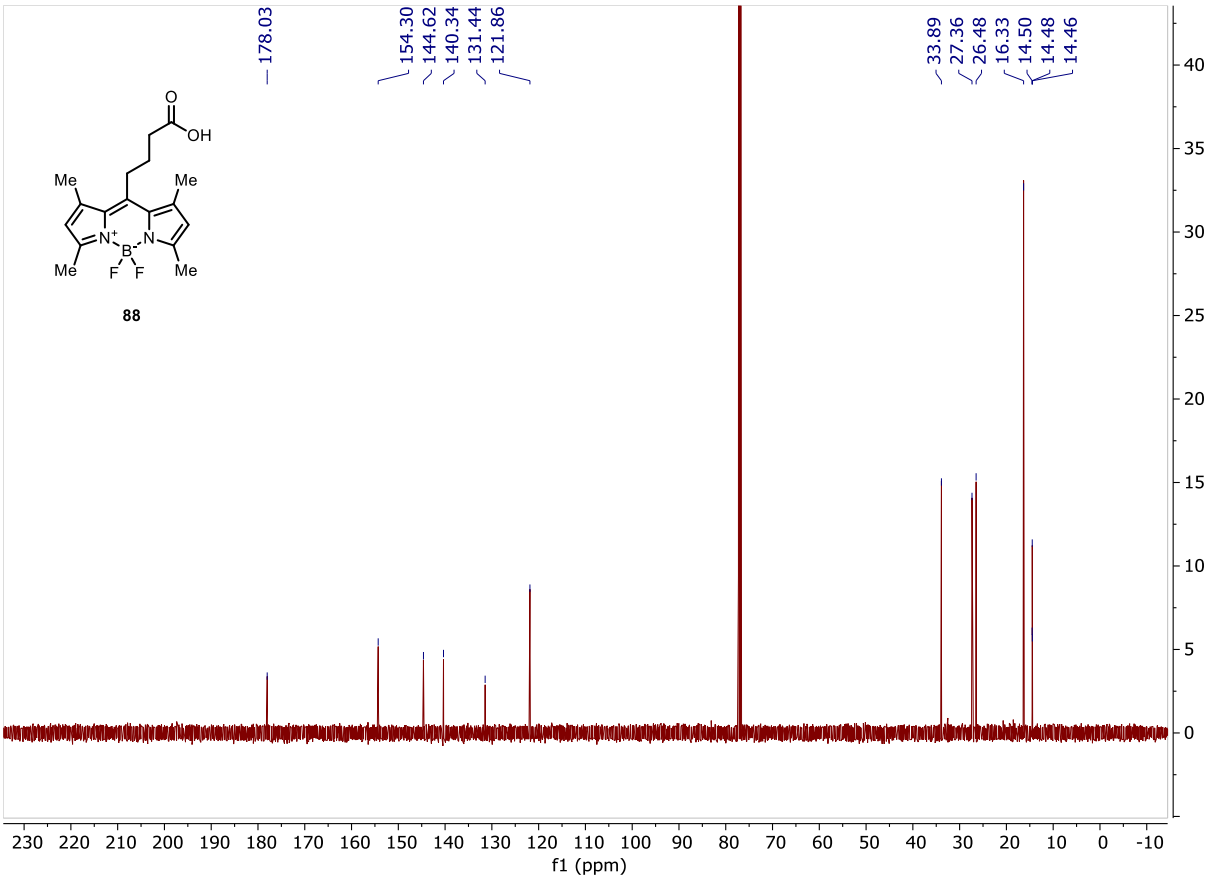
Spectrum 3-3 ^{1}H NMR of compound 87



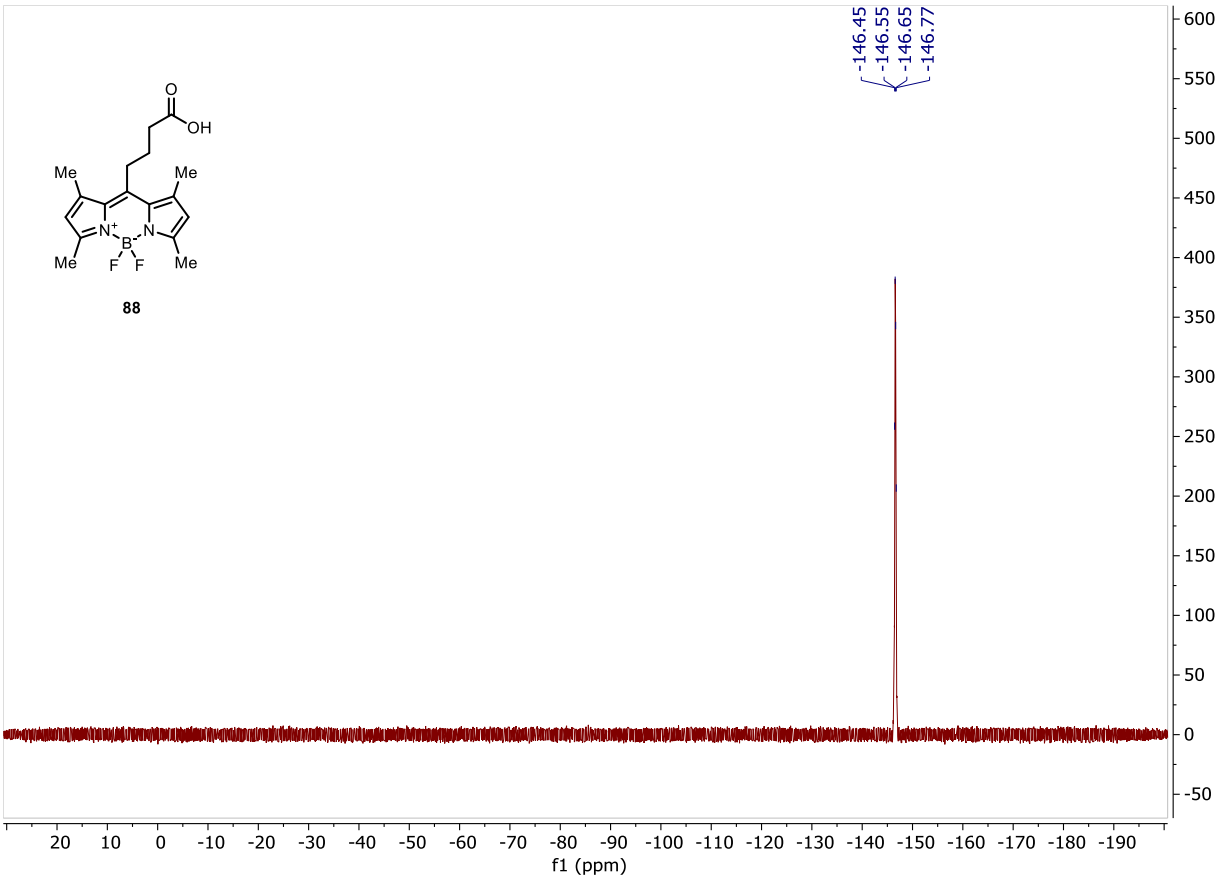
Spectrum 3-4 ^{13}C NMR of compound 87



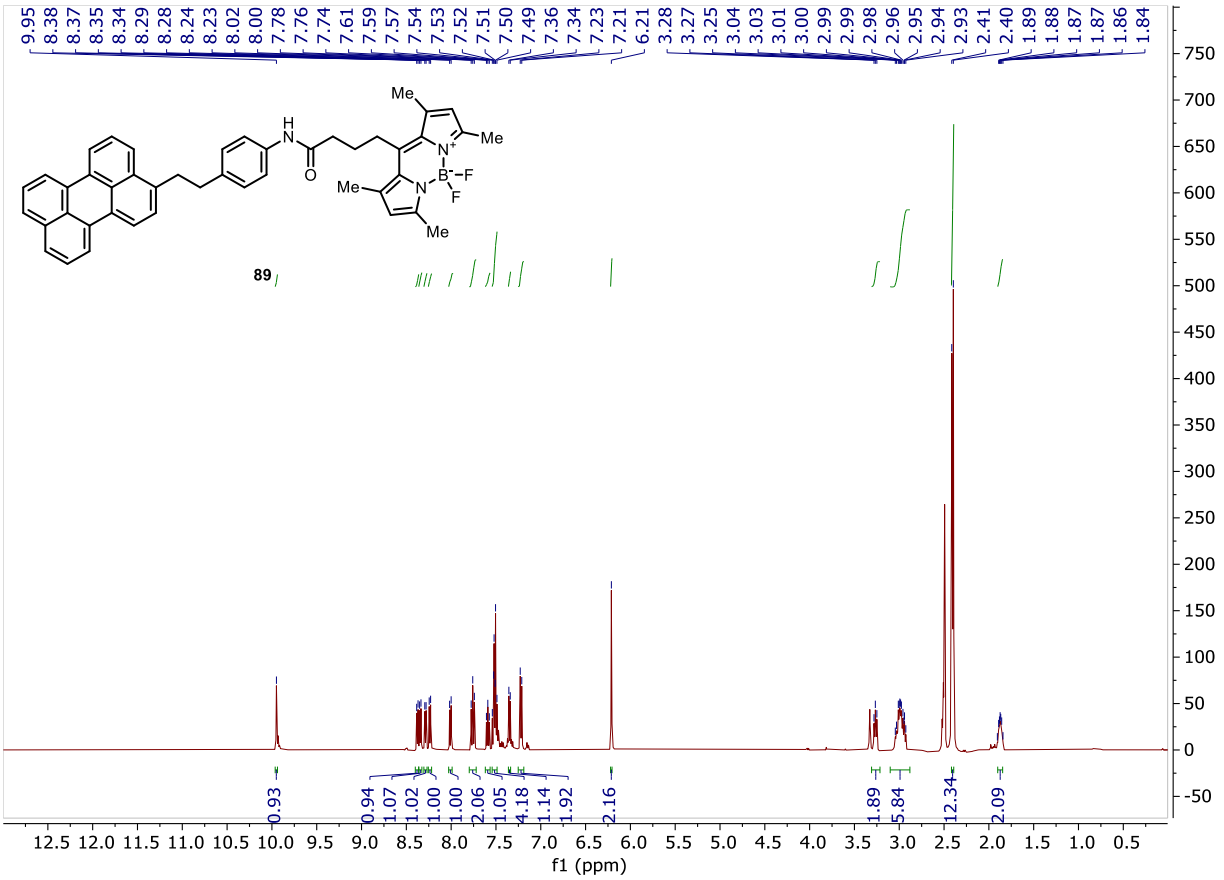
Spectrum 3-5 ^{1}H NMR of compound 88



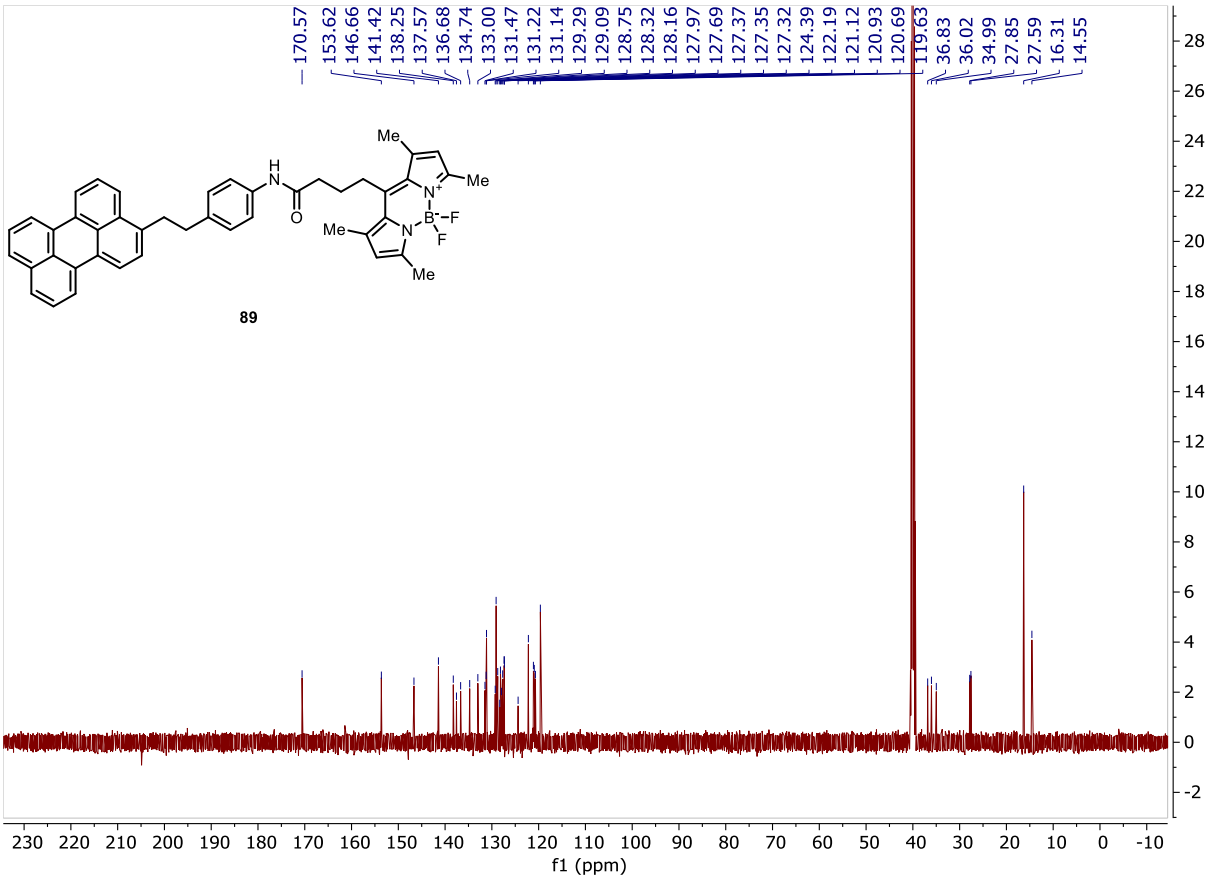
Spectrum 3-6 ^{13}C NMR of compound 88



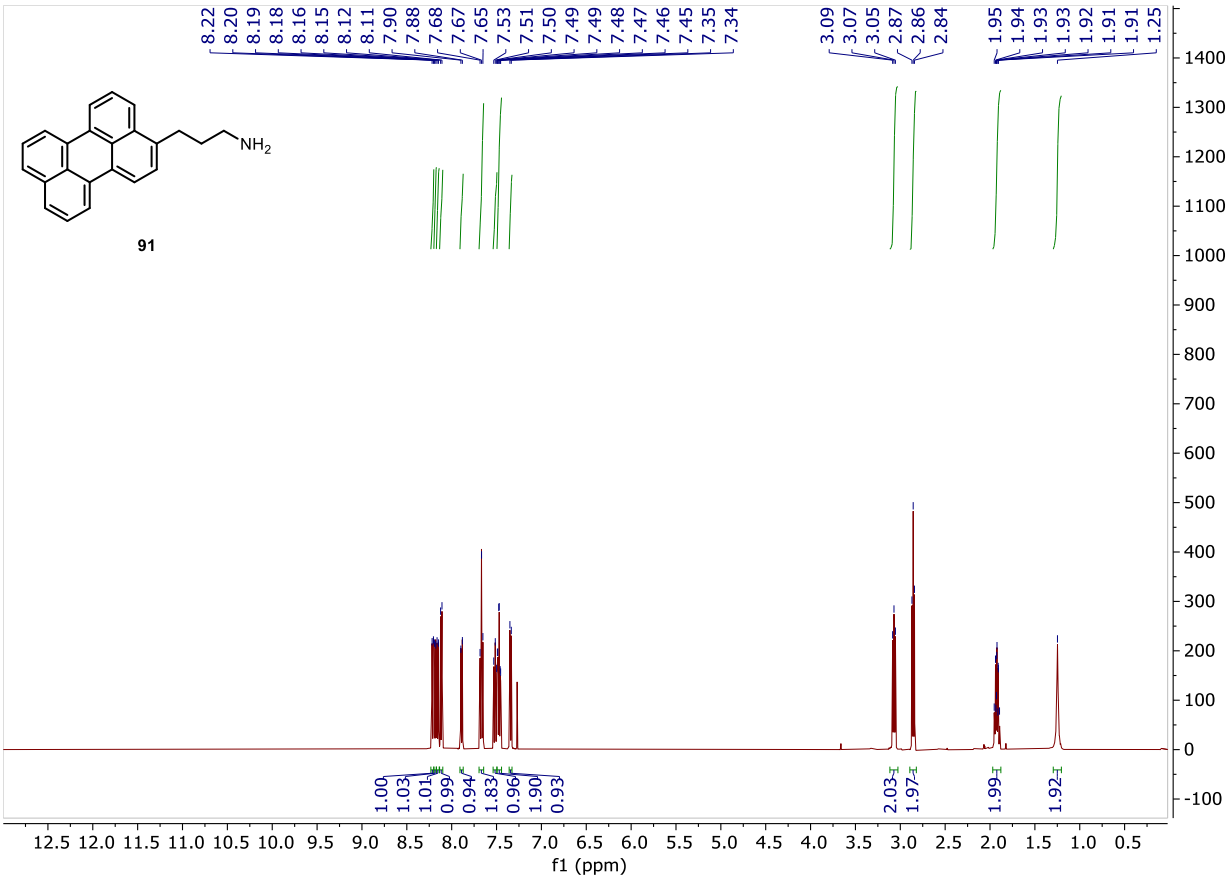
Spectrum 3-7 ^{19}F NMR of compound 88



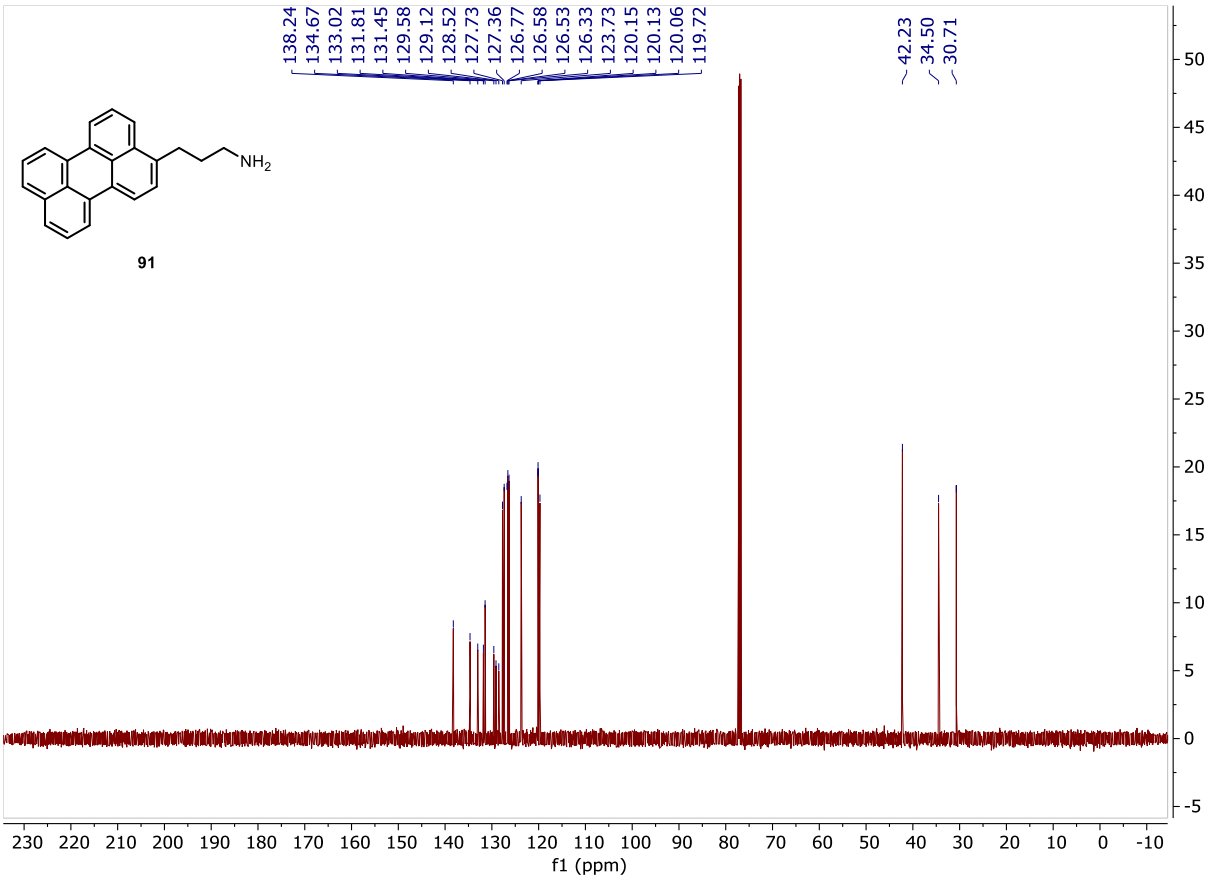
Spectrum 3-8 ^{1}H NMR of compound 89



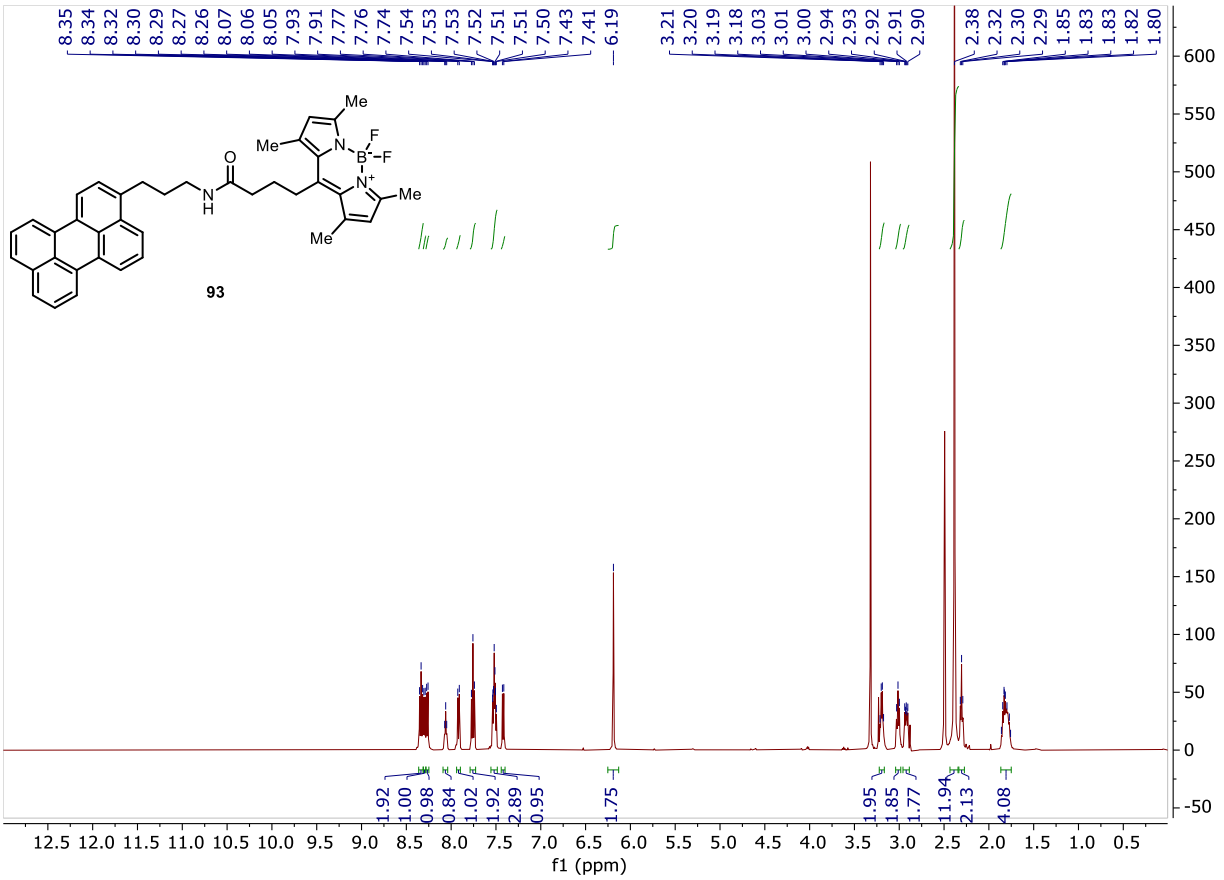
Spectrum 3-9 ^{13}C NMR of compound 89



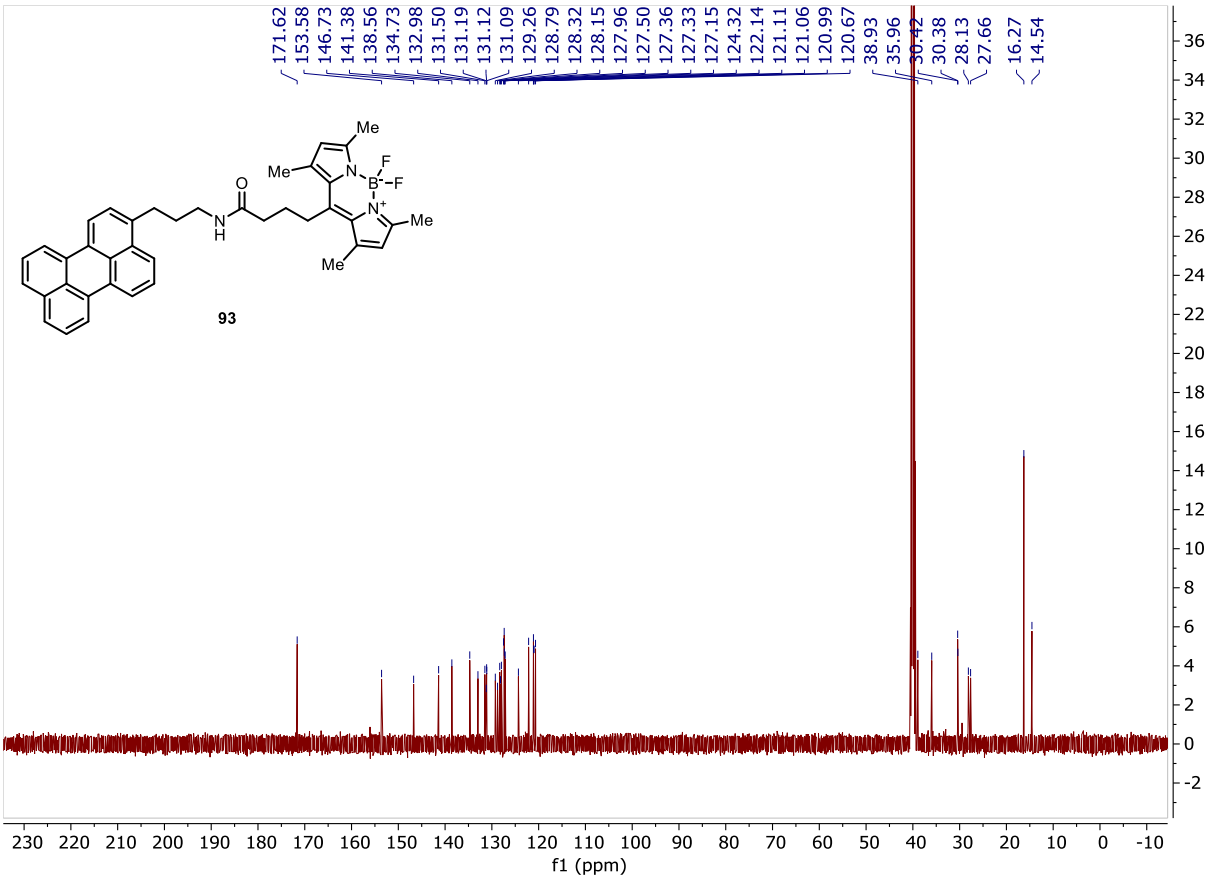
Spectrum 3-10 ^{1}H NMR of compound 91



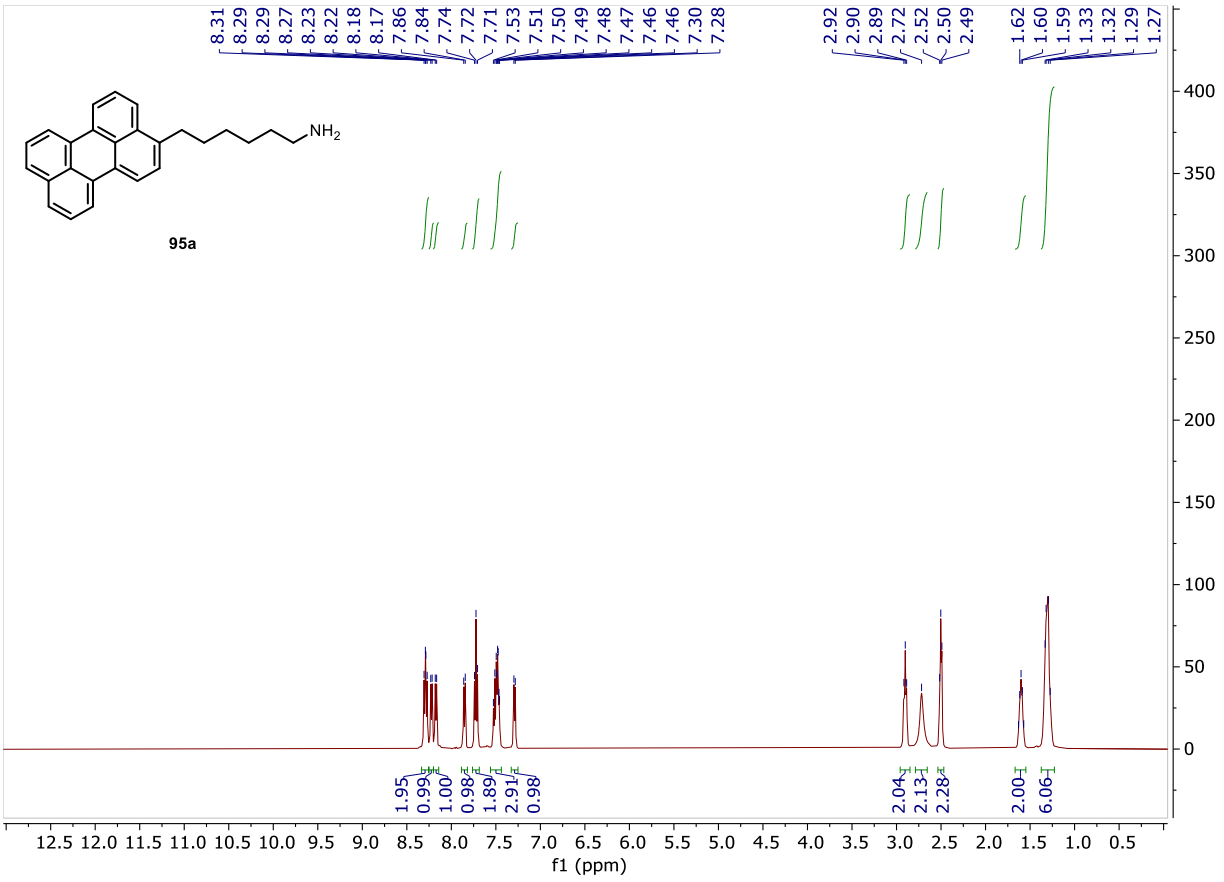
Spectrum 3-11 ^{13}C NMR of compound 91



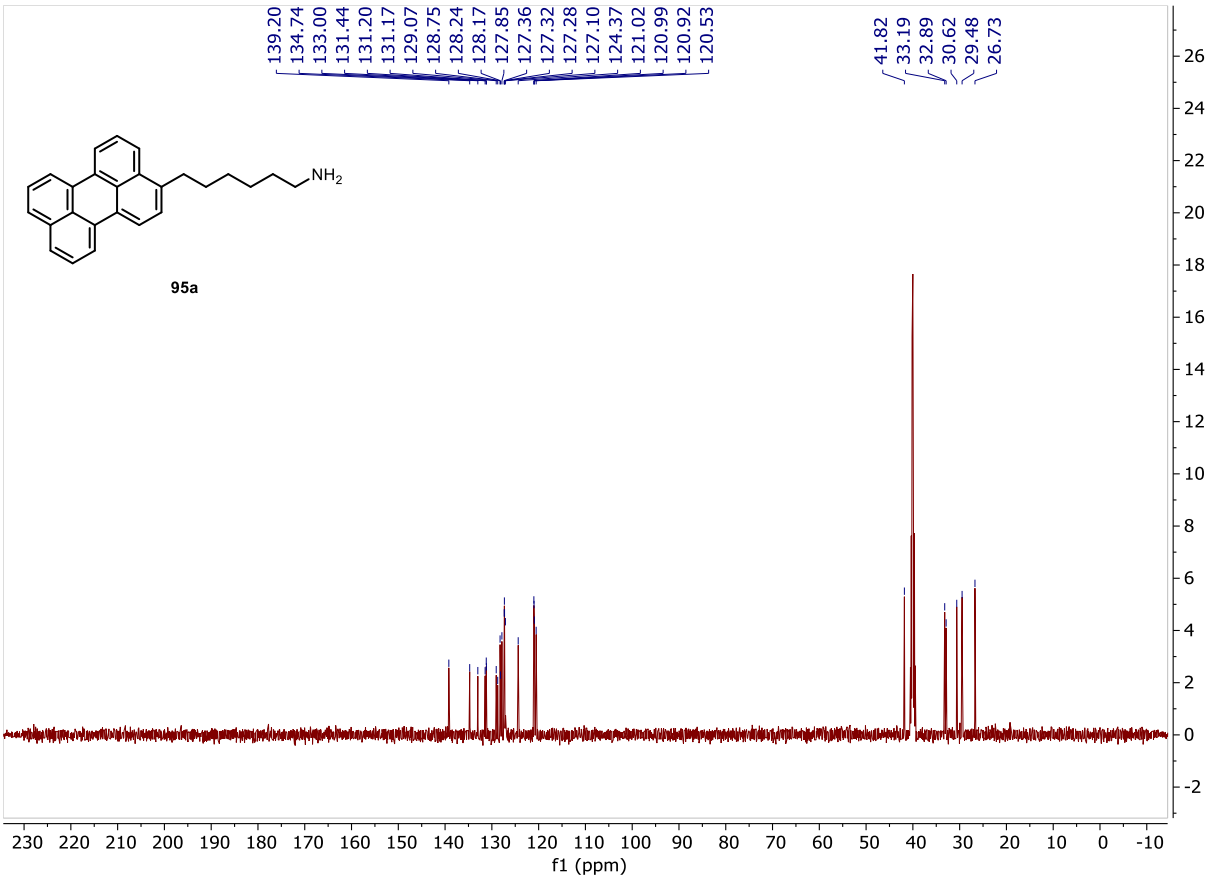
Spectrum 3-12 ^{1}H NMR of compound 93



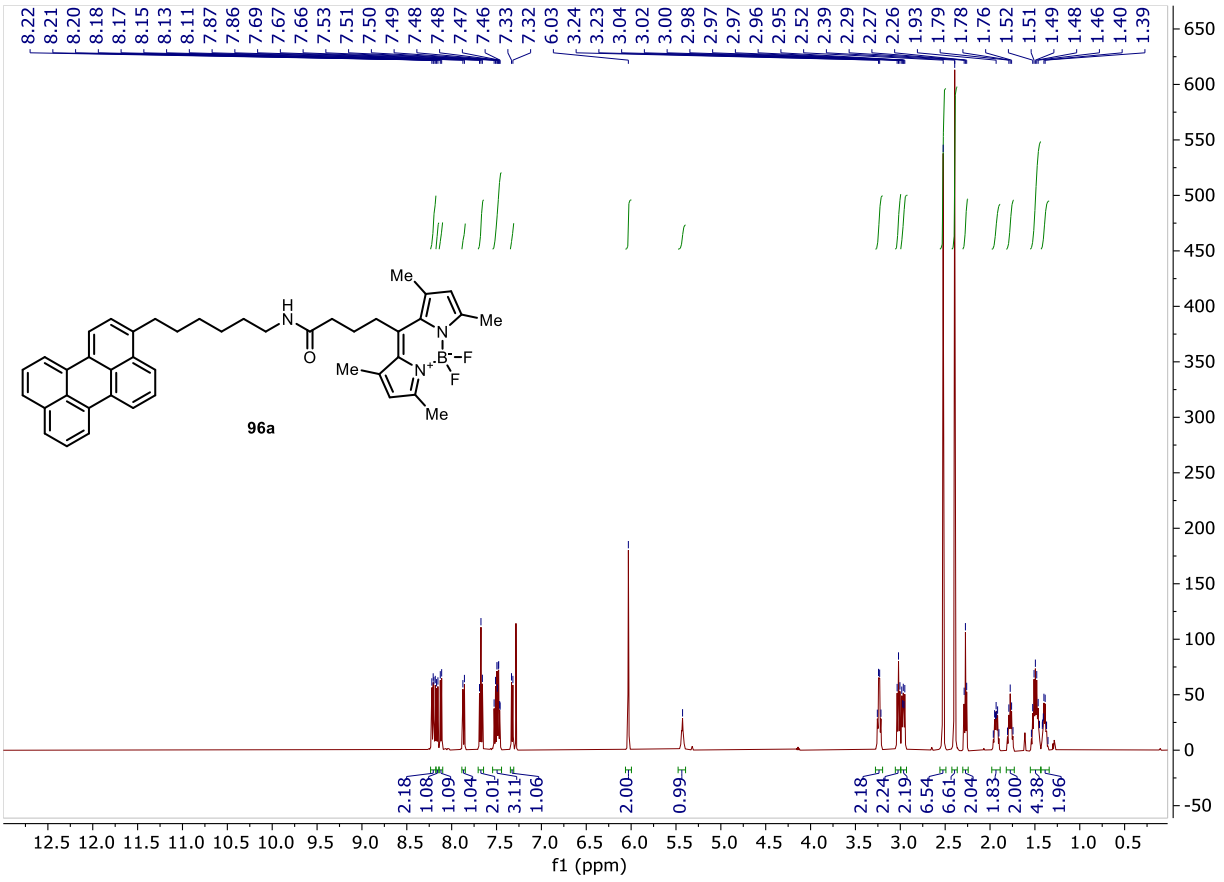
Spectrum 3-13 ^{13}C NMR of compound 93



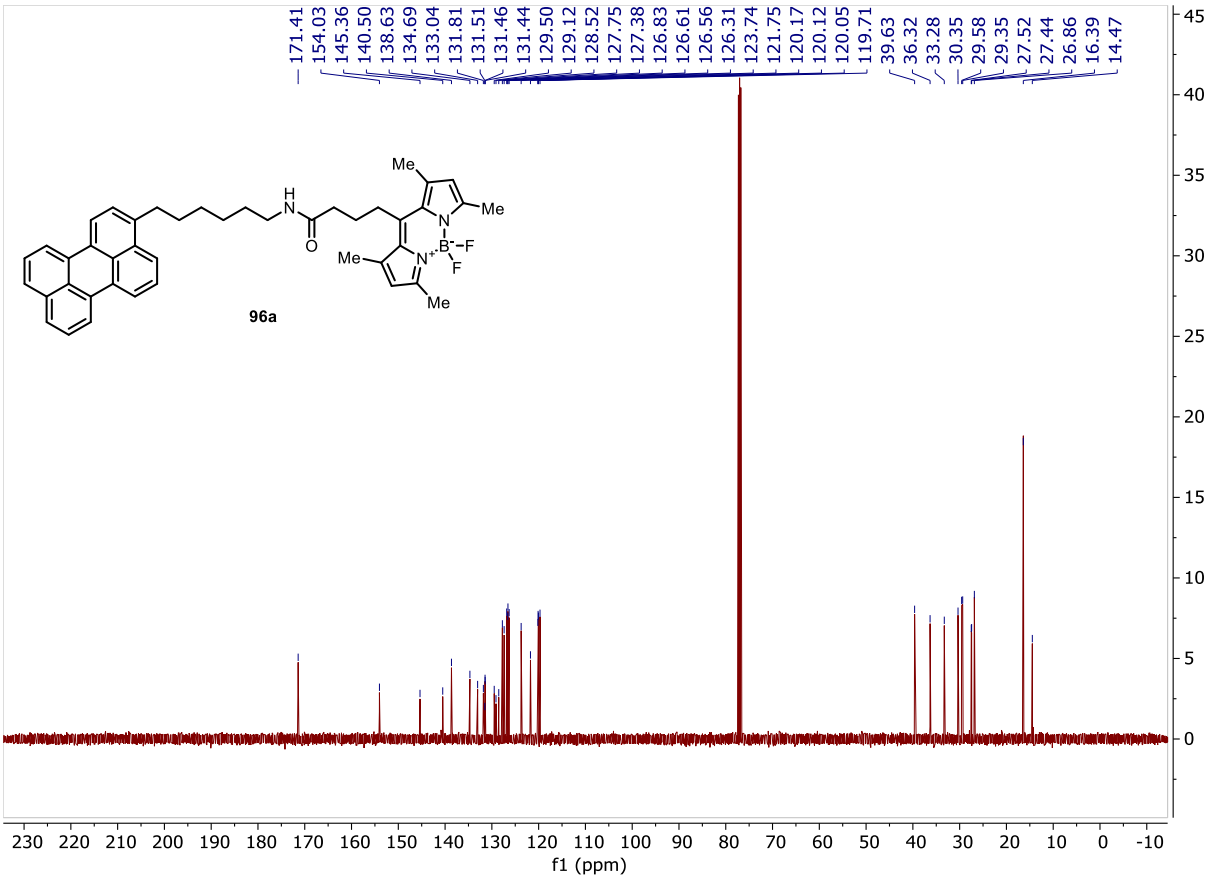
Spectrum 3-14 ^{1}H NMR of compound 95a



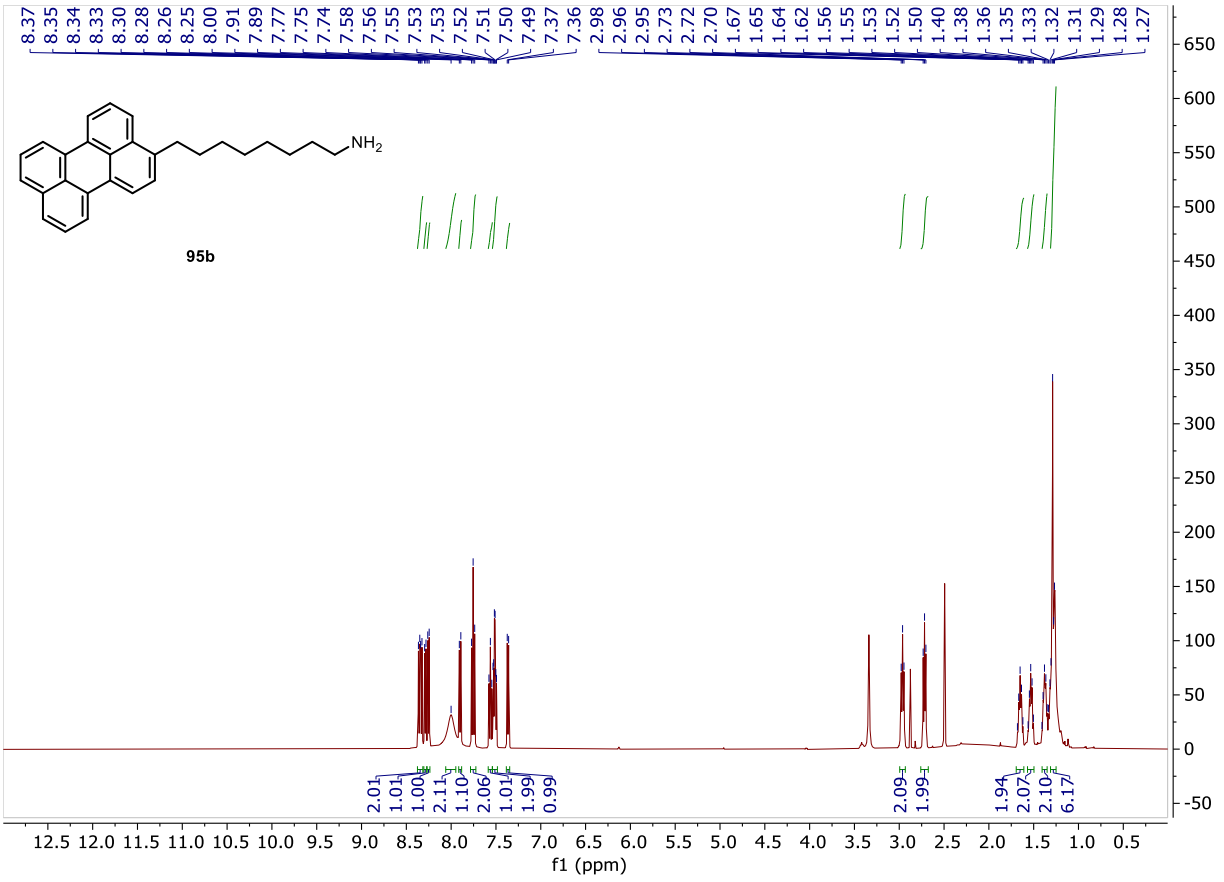
Spectrum 3-15 ^{13}C NMR of compound 95a



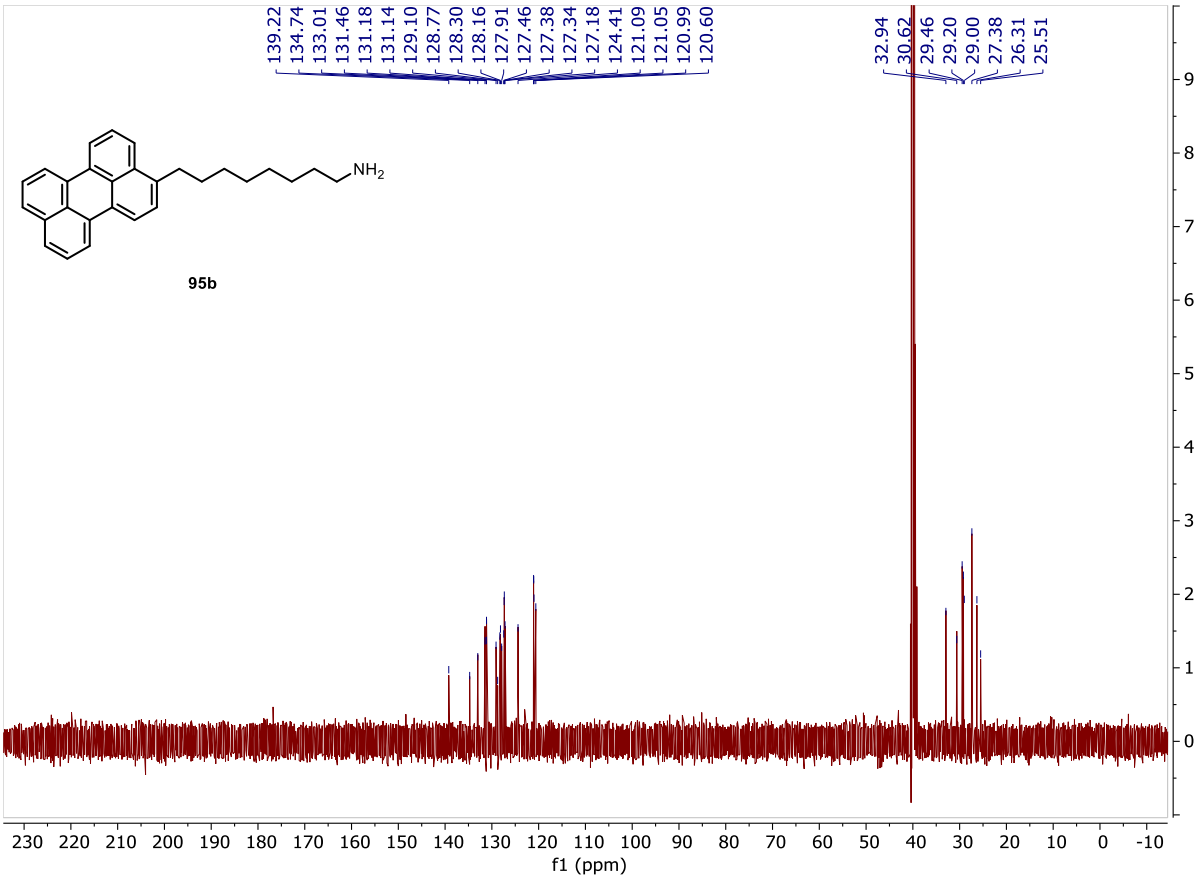
Spectrum 3-16 ^{1}H NMR of compound 96a



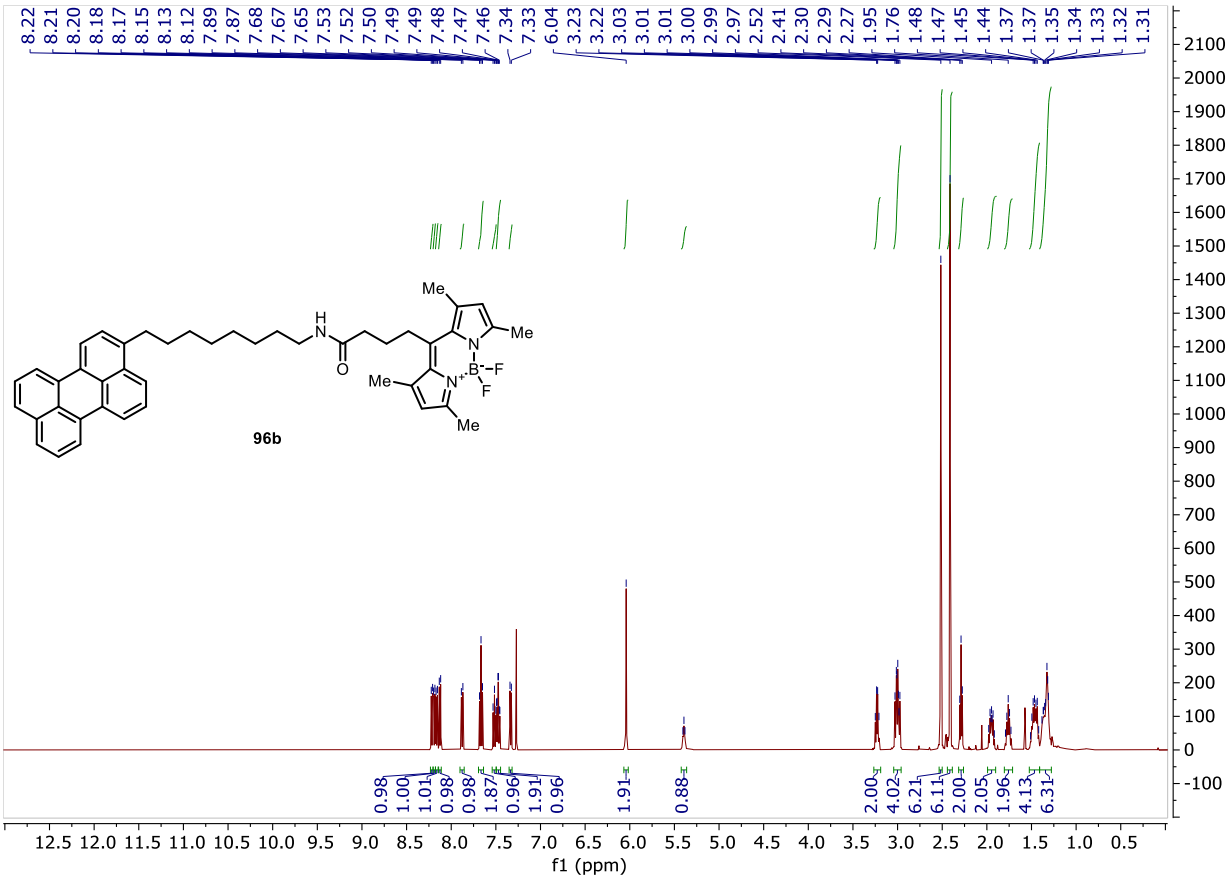
Spectrum 3-17 ^{1}H NMR of compound 96a



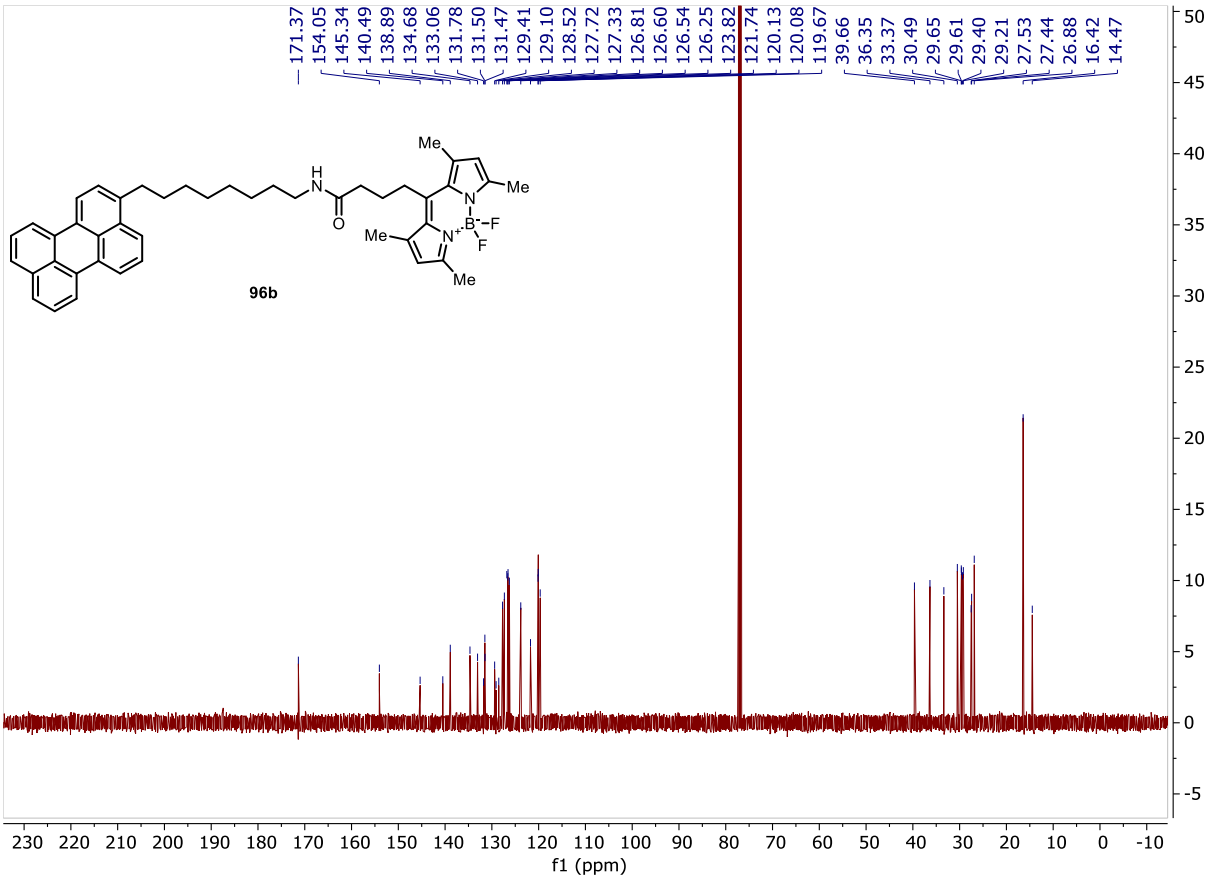
Spectrum 3-18 ^{13}C NMR of compound 95b



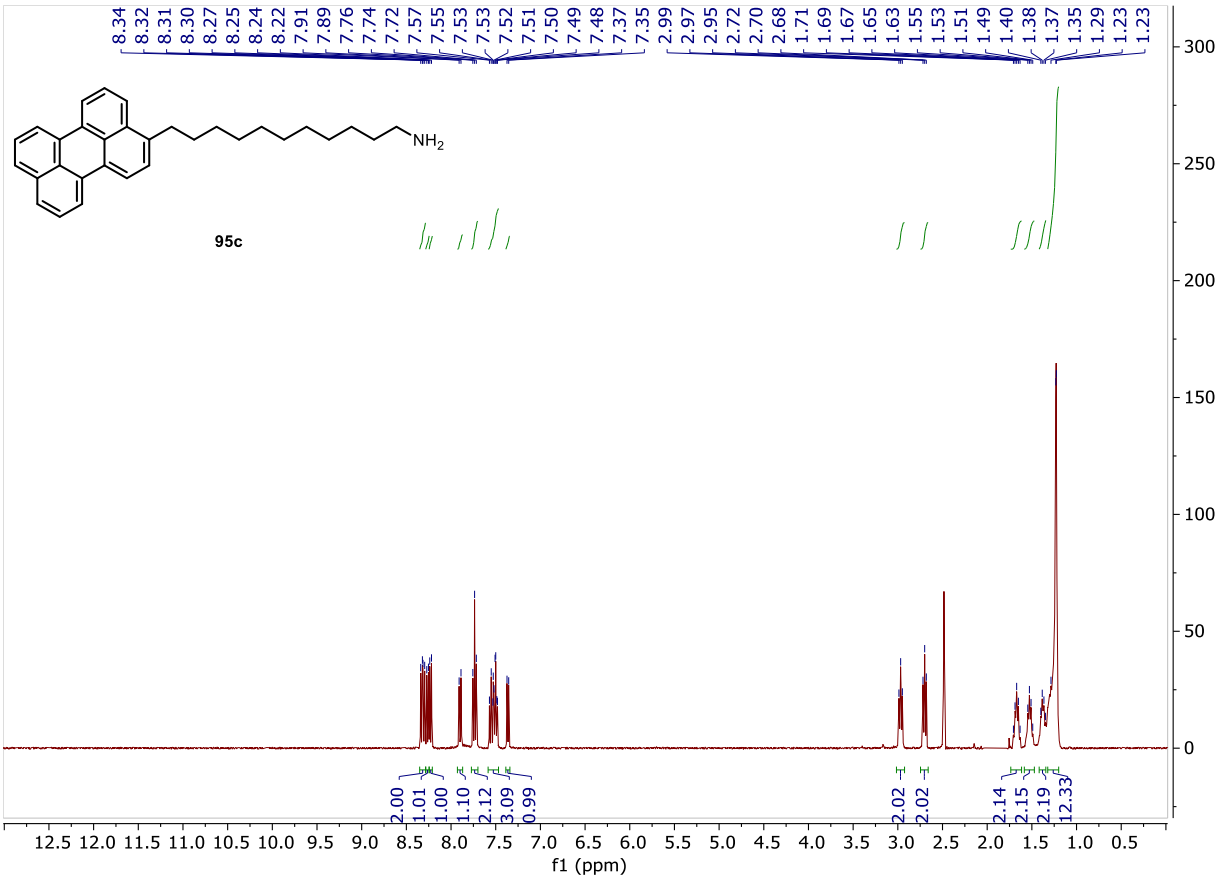
Spectrum 3-19 ^{13}C NMR of compound 95b



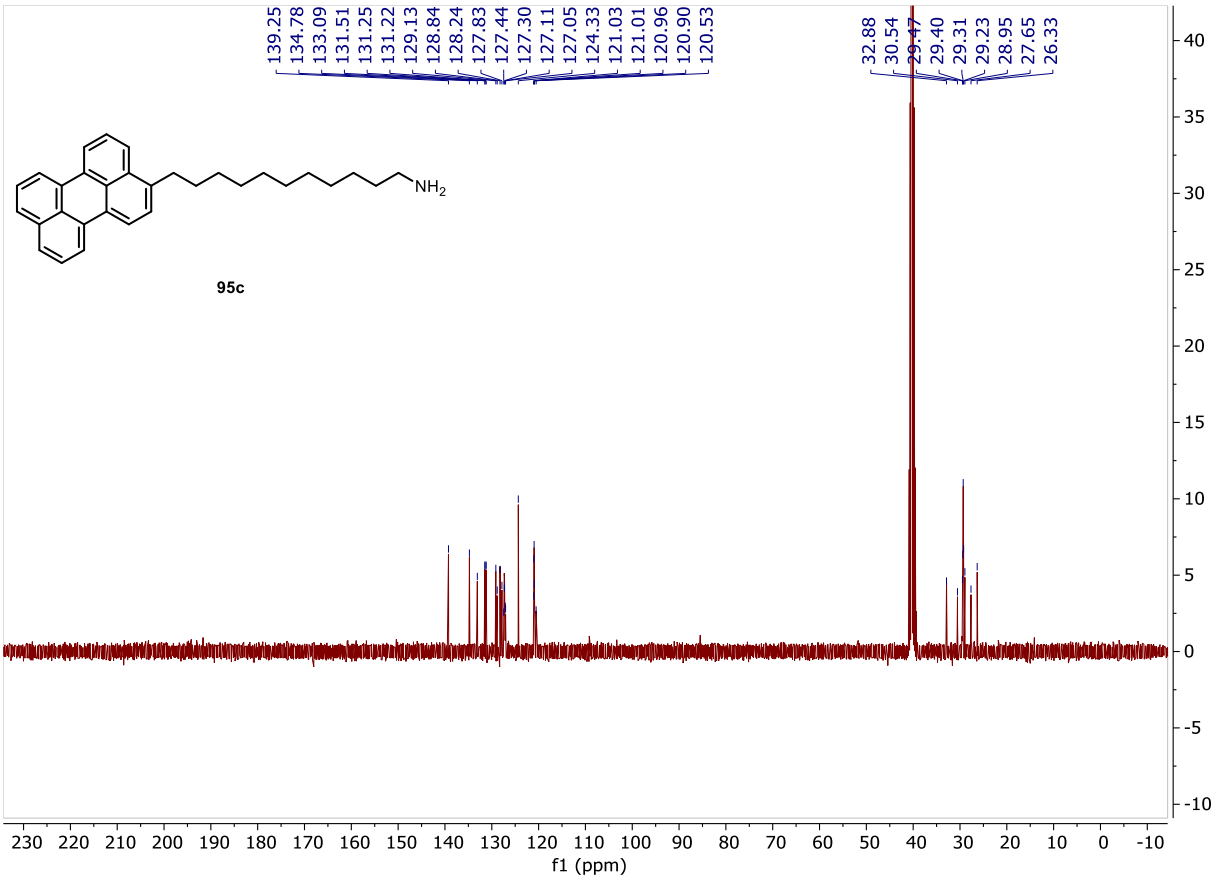
Spectrum 3-20 ^{1}H NMR of compound 96b



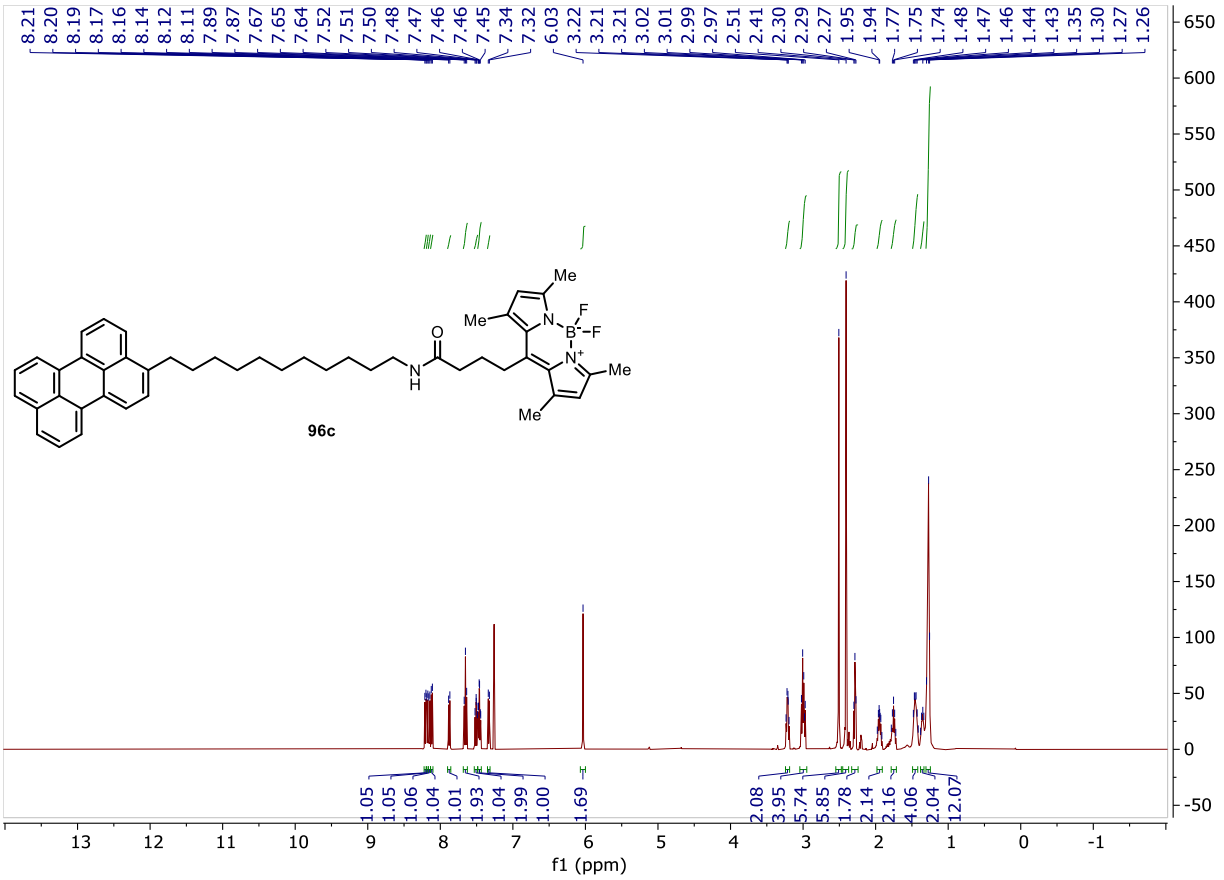
Spectrum 3-21 ^{13}C NMR of compound 96b



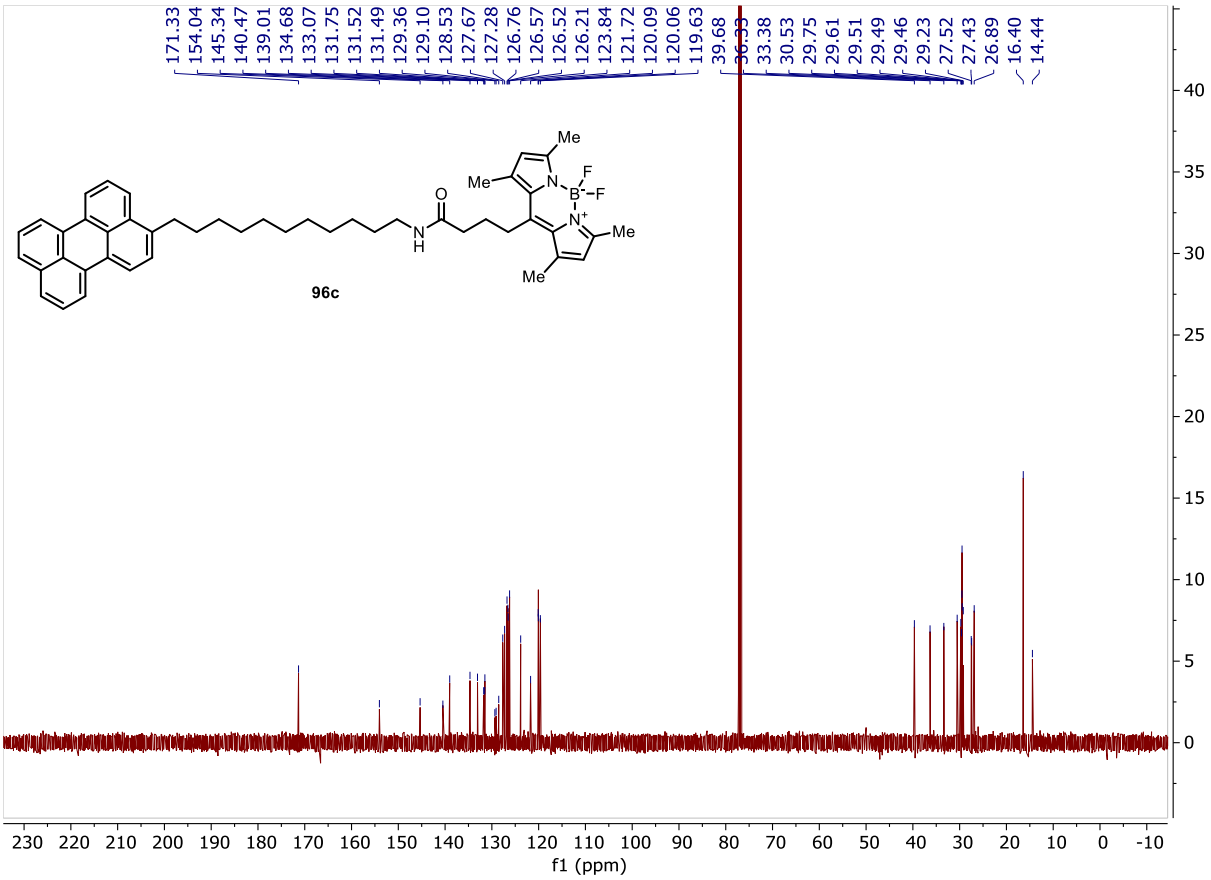
Spectrum 3-22 ^{1}H NMR of compound 95c



Spectrum 3-23 ^{13}C NMR of compound 95c



Spectrum 3-24 ^{1}H NMR of compound 96c



Spectrum 3-25 ^{13}C NMR of compound 96c

3.8 **References**

(125) Yuan, L.; Lin, W.; Zheng, K.; Zhu, S. FRET-Based Small-Molecule Fluorescent Probes: Rational Design and Bioimaging Applications. *Acc. Chem. Res.* **2013**, *46* (7), 1462–1473. https://doi.org/10.1021/ar300273v.

(126) Wu, L.; Huang, C.; Emery, B. P.; Sedgwick, A. C.; Bull, S. D.; He, X.-P.; Tian, H.; Yoon, J.; Sessler, J. L.; James, T. D. Förster Resonance Energy Transfer (FRET)-Based Small-Molecule Sensors and Imaging Agents. *Chem. Soc. Rev.* **2020**, *49* (15), 5110–5139. https://doi.org/10.1039/C9CS00318E.

(127) Jia, X.; Chen, Q.; Yang, Y.; Tang, Y.; Wang, R.; Xu, Y.; Zhu, W.; Qian, X. FRET-Based Mito-Specific Fluorescent Probe for Ratiometric Detection and Imaging of Endogenous Peroxynitrite: Dyad of Cy3 and Cy5. *J. Am. Chem. Soc.* **2016**, *138* (34), 10778–10781. https://doi.org/10.1021/jacs.6b06398.

(128) Lee, M. M.; Peterson, B. R. Quantification of Small Molecule–Protein Interactions Using FRET between Tryptophan and the Pacific Blue Fluorophore. *ACS Omega* **2016**, *1* (6), 1266–1276. https://doi.org/10.1021/acsomega.6b00356.

(129) Fang, B.; Shen, Y.; Peng, B.; Bai, H.; Wang, L.; Zhang, J.; Hu, W.; Fu, L.; Zhang, W.; Li, L.; Huang, W. Small-Molecule Quenchers for Förster Resonance Energy Transfer: Structure, Mechanism, and Applications. *Angew. Chem. Int. Ed.* **2022**, *61* (41), e202207188. https://doi.org/10.1002/anie.202207188.

(130) Wang, M.; Vicente, M. G. H.; Mason, D.; Bobadova-Parvanova, P. Stability of a Series of BODIPYs in Acidic Conditions: An Experimental and Computational Study into the Role of the Substituents at Boron. *ACS Omega* **2018**, *3* (5), 5502–5510. https://doi.org/10.1021/acsomega.8b00404.

(131) Goze, C.; Ulrich, G.; Ziessel, R. Tetrahedral Boron Chemistry for the Preparation of Highly Efficient "Cascatelle" Devices. *J. Org. Chem.* **2007**, *72* (2), 313–322. https://doi.org/10.1021/jo060984w.

(132) Uriel, C.; Permingeat, C.; Ventura, J.; Avellanal-Zaballa, E.; Bañuelos, J.; García-Moreno, I.; Gómez, A. M.; Lopez, J. C. BODIPYs as Chemically Stable Fluorescent Tags for Synthetic Glycosylation Strategies towards Fluorescently Labeled Saccharides. *Chem. – Eur. J.* **2020**, *26* (24), 5388–5399. https://doi.org/10.1002/chem.201905780.

(133) Rybczynski, P.; Smolarkiewicz-Wyczachowski, A.; Piskorz, J.; Bocian, S.; Ziegler-Borowska, M.; Kędziera, D.; Kaczmarek-Kędziera, A. Photochemical Properties and Stability of BODIPY Dyes. *Int. J. Mol. Sci.* **2021**, *22* (13), 6735. https://doi.org/10.3390/ijms22136735.

(134) Rani, K.; Sengupta, S. Metal-Free FRET Macrocycles of Perylenediimide and Aza-BODIPY for Multifunctional Sensing. *Chem. Commun.* **2023**, *59* (8), 1042–1045. https://doi.org/10.1039/D2CC06225A.

(135) Dou, L.; Li, Y.; Dong, L.; Zhang, S.; Wu, Y.; Gong, Y.; Yang, W.; Lu, H.; Zhu, S.; Zhou, X. Panchromatic Light-Absorbing [70]Fullerene-Perylene-BODIPY Triad with Cascade of Energy Transfer as an Efficient Singlet Oxygen Sensitizer. *Molecules* **2023**, *28* (8), 3534. https://doi.org/10.3390/molecules28083534.

(136) Shen, Y.; Mahjour, B.; Cernak, T. Development of Copper-Catalyzed Deaminative Esterification Using High-Throughput Experimentation. *Commun. Chem.* **2022**, *5* (1), 83. https://doi.org/10.1038/s42004-022-00698-0.

Chapter 4 Development of Diverse Amine-Acid Couplings

4.1 Introduction to Amine-Acid Couplings

We briefly introduced the amide coupling in the prior chapter as the traditional way to unite our FRET dyes with amines and carboxylic acid handles. This chapter however, will focus on the development of less conventional coupling modes between amines and acids.

Amidation of carboxylic acids with amines is the single most prevalent reaction in the pharmaceutical industry, comprising a quarter of reactions ran in pharma as of 2018.[137] Despite the abundance of commercially available amine and acid feedstocks, few other reactions are have been developed between amines and acids. While work by our lab[21,23,136,138,139] and others[140–143] have elucidated some of these alternate modes of C–O, C–N, and C–C coupling between amines and acids, there is still a plethora of theoretical, but currently unrealized reactions in this space.[139,144] To bridge this gap in knowledge we have engaged in the development of novel amine-acid coupling reactions and their utility towards modulating the physicochemical properties of medicinally relevant molecules.

4.2 Enabling the Functionalization of Amines

To better facilitate coupling reactions between amines and acids, pre-activation is often required to produce substrates with selective or enhanced reactivity profiles. Prevalent forms of activated carboxylic acids include esters formed from N-hydroxyphthalimide, pivalic anhydride, di-*tert*-butyl dicarbonate, and 2-hydroxypyridine to better enable oxidative addition with metal complexes.[143,145,146] Alternately, amines are often activated as diazonium salts, potassium trifluoroborate salts, or pyridinium salts to create a highly electrophilic species or generate a carbon-based radical that can undergo subsequent coupling.[136,140,145]

In particular, amines activated to their pyridinium salts have seen significant use in recent years for their ability to generate carbon-based radicals upon loss of the neutral pyridine.[147,148] Beyond these radical based approaches, we envisioned the highly electron-withdrawing pyridinium system could prove useful in stabilizing a carbanion at the pyridinium salts' α-position. Here, we report our investigation on the α-functionalization of pyridinium salts

through reaction with aldehydes as well as the indium-catalyzed deamination and rearrangement of the resulting adduct.

4.2.1 ***α-Functionalization and Rearrangement of Pyridinium Salts***

Our investigation into the of α-functionalization of amines, activated as their pyridinium salt, began with the synthesis of a model coupling partner that could sufficiently stabilize a carbanion adjacent to the pyridinium system. We hypothesized a diaryl methylene would be sufficiently acidic to allow carbanion formation, while stabilizing the resulting negative charge. From benzyl amine **97** and 2,4,6-triphenylpyrylium tetrafluoroborate **98**, we prepared our model activated amine species **99** (Figure 4-1).

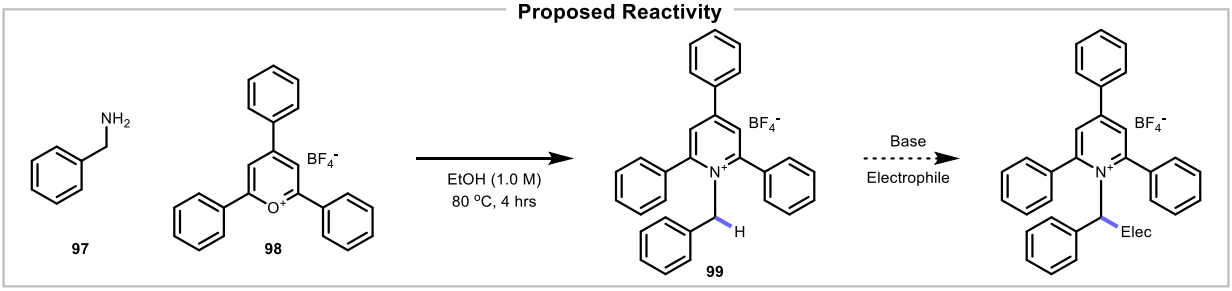


Figure 4-1 Synthesis of model pyridinium salt **99** from benzyl amine **97** and pyrylium salt **98**. The proposed reactivity would engage the α-position of the pyridinium salt via deprotonation and subsequent capture by an electrophile.

Following, we began to examine the deprotonation of **99** and its addition into a simple electrophile such as benzaldehyde **100**. The initial reaction hit provided potassium *tert*-butoxide as a capable base for the deprotonation and addition of **99** into benzaldehyde in a 35% yield of alcohol adduct **101**. As incomplete consumption of the pyridinium starting material was observed, we reasoned increasing temperature may help enable the deprotonation and subsequent addition reaction. However, the presence of such a strong base at elevated temperatures primarily led to decomposition of the pyridinium salt and only a minor improvement in yield, 42% when heated to 60 °C. From these results, we looked to identify weaker bases that could withstand higher temperatures. Screening organic bases such as triethylamine or proton sponge only produced trace yields at best, while inorganic bases such as potassium phosphate, and various carbonate bases provided workable yields. The improved solubility from potassium carbonate to cesium carbonate enabled optimization of the addition into benzaldehyde up to 70% with near total starting material consumption (Figure 4-2). Following, we sought to probe what reactivity could be accessed from such derivatized pyridinium salts.

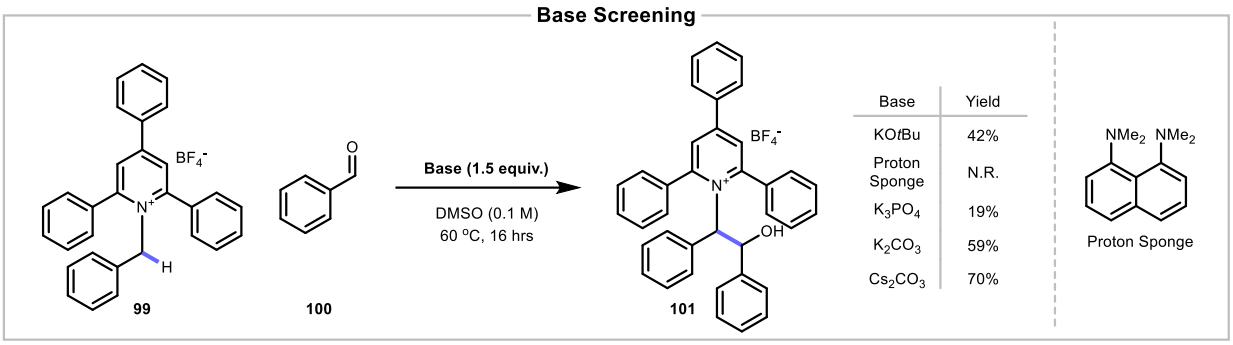


Figure 4-2 Optimization of pyridinium salt deprotonation conditions to enable C–C bond formation with benzaldehyde.

Attempts to cleave the triphenyl pyridinium salt back to its starting amine failed with hydroxide or hydrazine, likely due to the high steric hinderance of the pyridinium system in **101**. Additionally, attempts to eliminate or substitute the pyridinium salt with base, heat, or nucleophiles failed. In the vast majority of cases, the pyridinium salt likely decomposed into the corresponding alkyl radical which engaged in various unproductive pathways. However, attempting to enable reactivity from chelation of the alcohol in **101**, we identified a range of lewis acid catalysts capable of initiating a semi-pinacole type rearrangement. While the majority of lewis acids produced <20% yields of rearranged diphenylacetaldehyde **102**, indium(III) chloride and indium(III) bromide uniquely afforded greater than 60% yields in both cases (Figure 4-3).

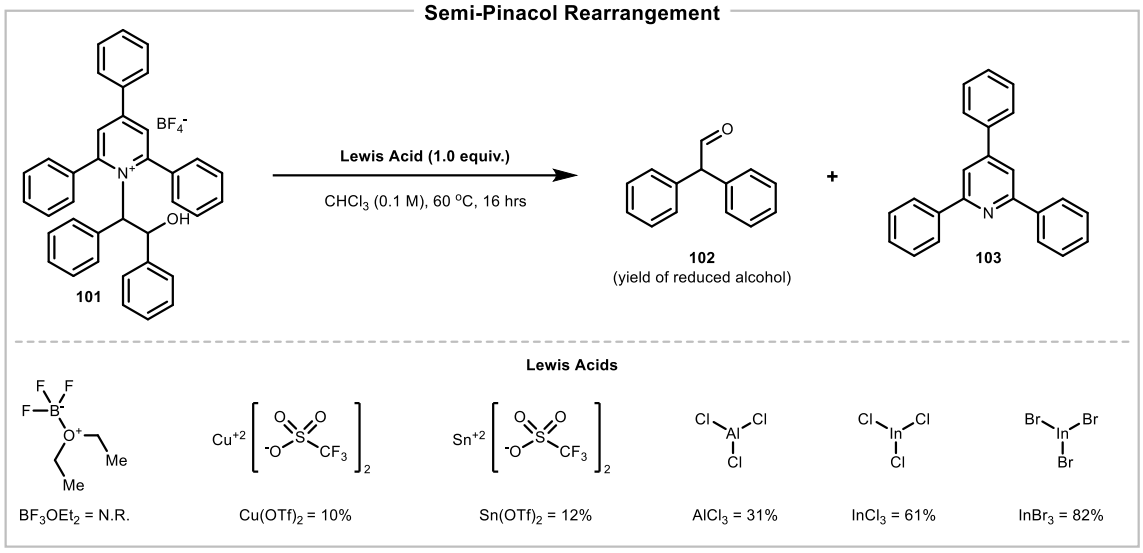


Figure 4-3 Lewis Acid screening for rearranged aldehyde product **102** that results from migration of phenyl ring and loss of triphenyl pyridine **103**. Yields of **102** are reported as the alcohol resulting from $NaBH_4$ reduction of the aldehyde.

This unexpected reactivity seems to stem from the ability to triphenylpyridine **103** to act as a good leaving group, when initiated by intramolecular phenyl migration. The steric hindrance of the triphenylpyridinium system prevents nucleophilic addition into the pyridinium ring directly but collapse of the alcohol for C=O bond formation can act as the driving force for phenyl migration and loss of triphenylpyridine. In summary, this work provides an example of the ability to functionalize amines activated as pyridinium salts and the unexpected deaminative reactivity that can arise from such structures.

4.3 **Applying Diverse Amine-Acid Couplings to Fluorescein**

To demonstrate the potential of such unconventional amine-acid couplings in drug development, we have shown the derivatization of Fluorescein **104**, a common bioimaging dye bearing a carboxylic acid, with Toluidine **105** as a model amine substrate. We sought to develop a library of Fluorescein derivatives with diversified physicochemical properties resulting from the application of unique coupling conditions on the same amine and acid building blocks (Figure 4-4). Our hypothesized library of Fluorescein analogues would vary in hydrogen-bond donor and acceptor count, lipophilicity, polar surface area, molecular weight, and fraction of sp^3 atoms based on the coupling conditions employed.

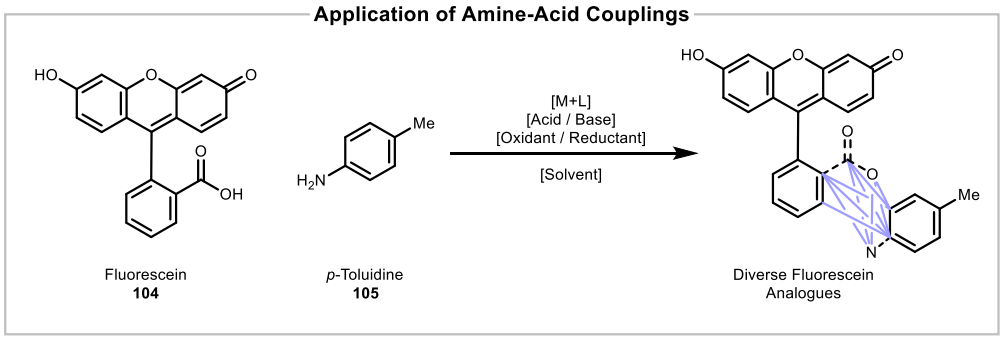


Figure 4-4 Application of diverse amine-acid couplings to the derivatization of the bioimaging dye Fluorescein **104** with *p*-toluidine **105**.

Initial attempts to engage Fluorescein's carboxylic acid moiety resulted in sluggish reactivity and low yields, even for reliable reactions like the amide coupling. We realized that Fluorescein's ability to equilibrate between a closed lactone form **106** and open carboxylic acid form **104** was significantly favoring the unreactive lactone in most cases. Fortunately, we realized the possibility of shutting off Fluorescein's ability to cyclize via acetylation and reduction of its xanthene core. This technique is typically used so Fluorescein can act as an oxidative sensor.[149,150] The reduced analogue is no longer fluorescent until contacting oxidative

species, wherein the ring will oxidize and restore fluorescein. In our case, we can use the reduced diacetylated Fluorescein **107** to shut off the undesired lactonization of the acid for more efficient amine-acid coupling. Accessing **107** from reaction with excess acetic anhydride and subsequent reduction by zinc and acetic acid directly affords us the functional acid substrate for our diverse couplings with toluidine **105** (Figure 4-5).

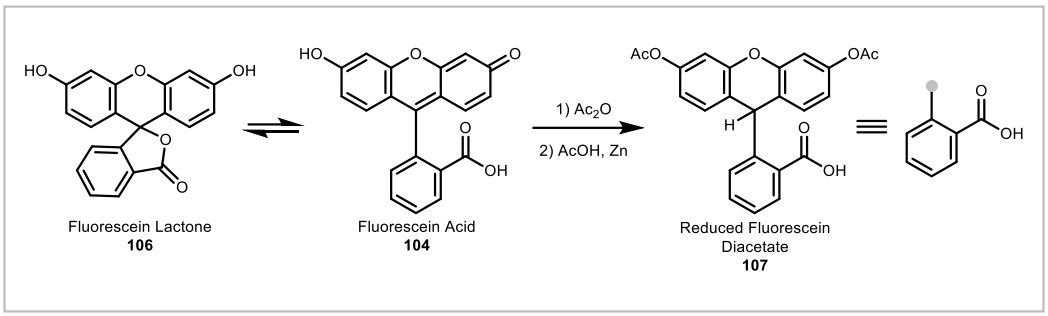


Figure 4-5 Fluorescein's equilibrium between closed **106** and open **104** forms can be shut off by protection and reduction of the tricyclic xanthene core. Reduced Fluorescein diacetate **107** can be directly used in coupling with *p*-toluidine **105**.

Here we will begin with detailing the optimization of the reductive amination of Fluorescein. From prior literature reports[151,152] and work done by our lab, reducing metal-hydride conditions were identified as a starting point for reaction optimization. Screening across a range of three platinum catalysts, six phosphine ligands, and two silane reductants, we identified the combination of platinum(II) chloride, Brettphos, and phenylsilane as our top performers. From an assay yield of 53%, we scaled up the reductive amination for a 44% yield of diacetylated alkyl amine **108a** and a 12% yield of deacetylated product **108b**. Deprotection of the still diacetylated product with lithium hydroxide hydrate proceeded smoothly to give a final yield of 49% for alkyl amine **108b** across both coupling and deprotection steps.

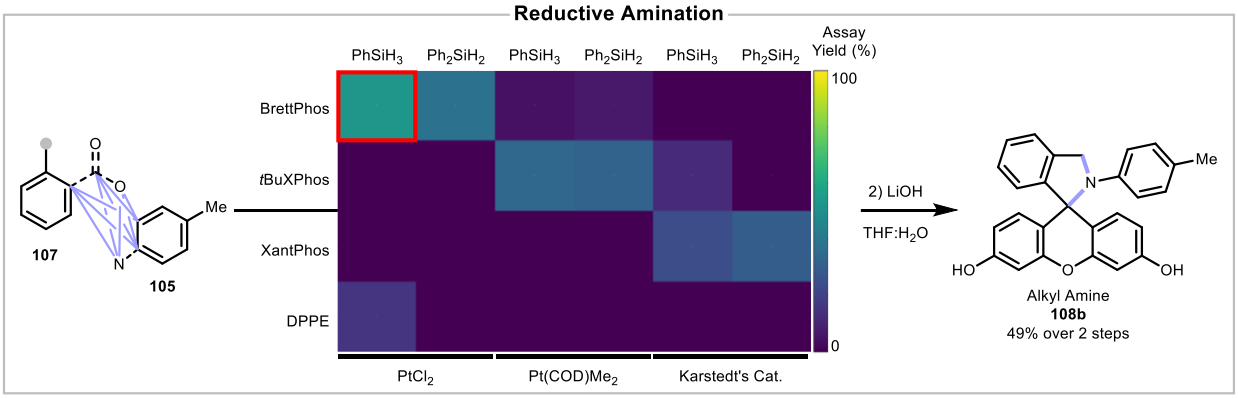


Figure 4-6 HTE Screen for Fluorescein Alkyl Amine **108**. Each row was dosed with a different phosphine ligand, every two rows a different platinum catalyst, and rows alternate between phenylsilane and diphenylsilane reductants.

Subsequent investigation of the oxidative cyclization of Fluorescein led us to investigate a two-step procedure involving the formation of Fluorescein amide **109**, followed by cyclization of the amide to a proposed Fluorescein benzoxazole **110** structure. As no reports currently exist on the direct coupling of an amine and a carboxylic acid into a benzoxazole, we elected to do a discreet first step to synthesize and isolate amide **109** before proceeding into screening of cyclization conditions (Figure 4-7).

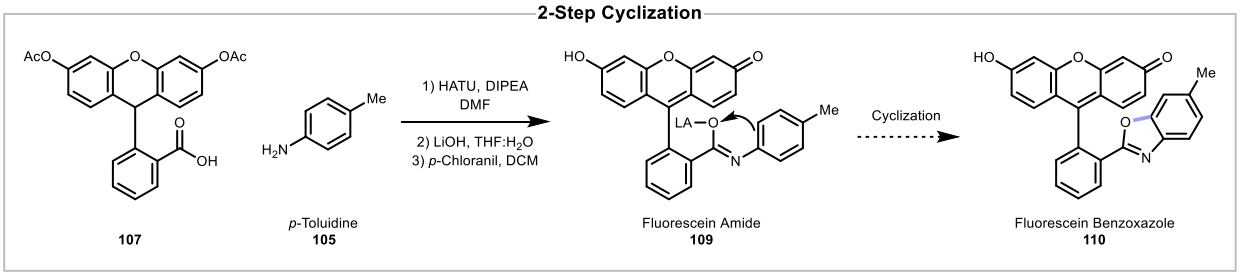


Figure 4-7 Proposed scheme for amidation of Fluorescein followed by oxidative cyclization of its amide motif.

A prior literature report on the cyclization of amides into benzoxazoles using triflic acid, oxone, and 1-iodo-4-nitrobenzene served as our starting point.[153] The proposed reaction conditions are hypothesized to enable the cyclization through *in situ* formation of a hypervalent iodide species that enables arene addition into the amide carbonyl.

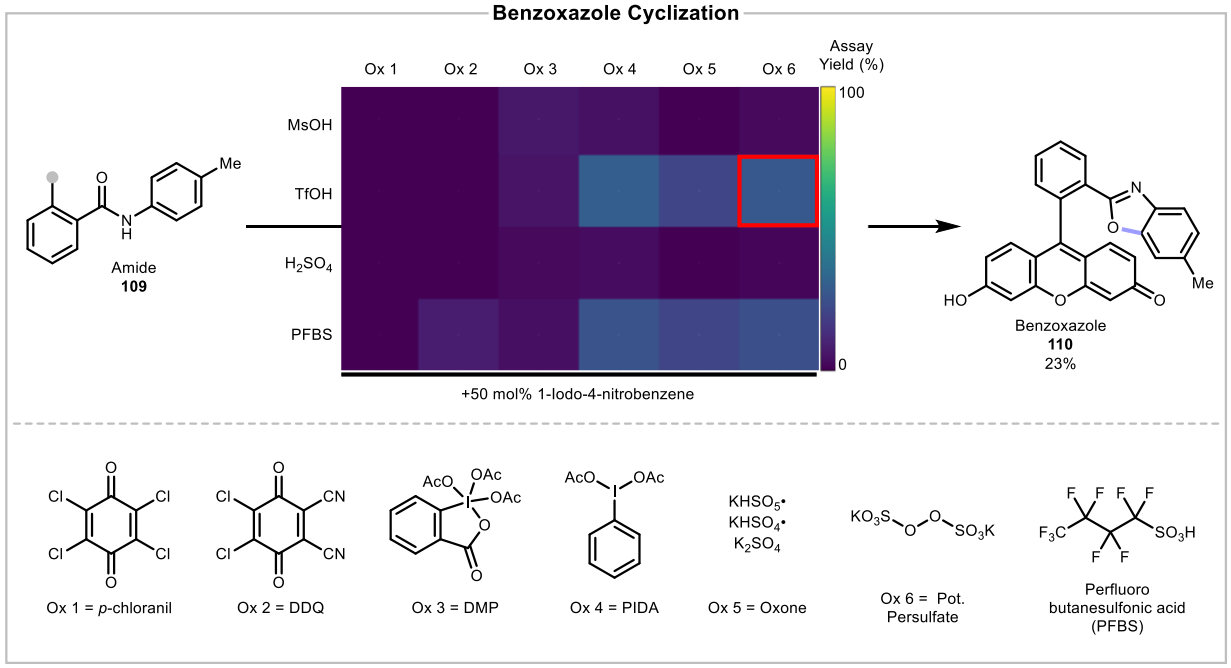


Figure 4-8 HTE Screen for Fluorescein Benzoxazole **110** from Fluorescein Amide **109**. Each row was dosed with a different acid, each column with a different oxidant, and all wells received 50 mol% 1-iodo-4-nitrobenzene additive.

On first pass, the harsh reaction conditions primarily served to deprotect and oxidize the Fluorescein starting material, with only trace product formation. Increasing equivalents of acid and iodide did little to improve reaction yields as reaction on the Fluorescein scaffold appeared to be too slow for productive reaction before decomposing. Elevating reaction temperatures from room temperature to 70 ^{o}C while limiting reaction time to four hours provided 13% reaction yield as a starting point for further HTE screening. Exploring a range of six different oxidants and four different acids, we identified the combination of triflic acid with potassium persulfate as the top hit which afforded a 27% assay yield (Figure 4-8). Scale up of these conditions afforded a final 23% isolated yield for the challenging cyclization of amide **109** to benzoxazole **110**.

Along with a host of 10 other derivatives synthesized by our lab, the analogues **108b** and **110** complete our foray into unique amine-acid couplings applied to Fluorescein. The complete library is shown in Figure 4-9. The full library hosts a range of functionalities derived from the transmutation of the initial amine and acid groups.

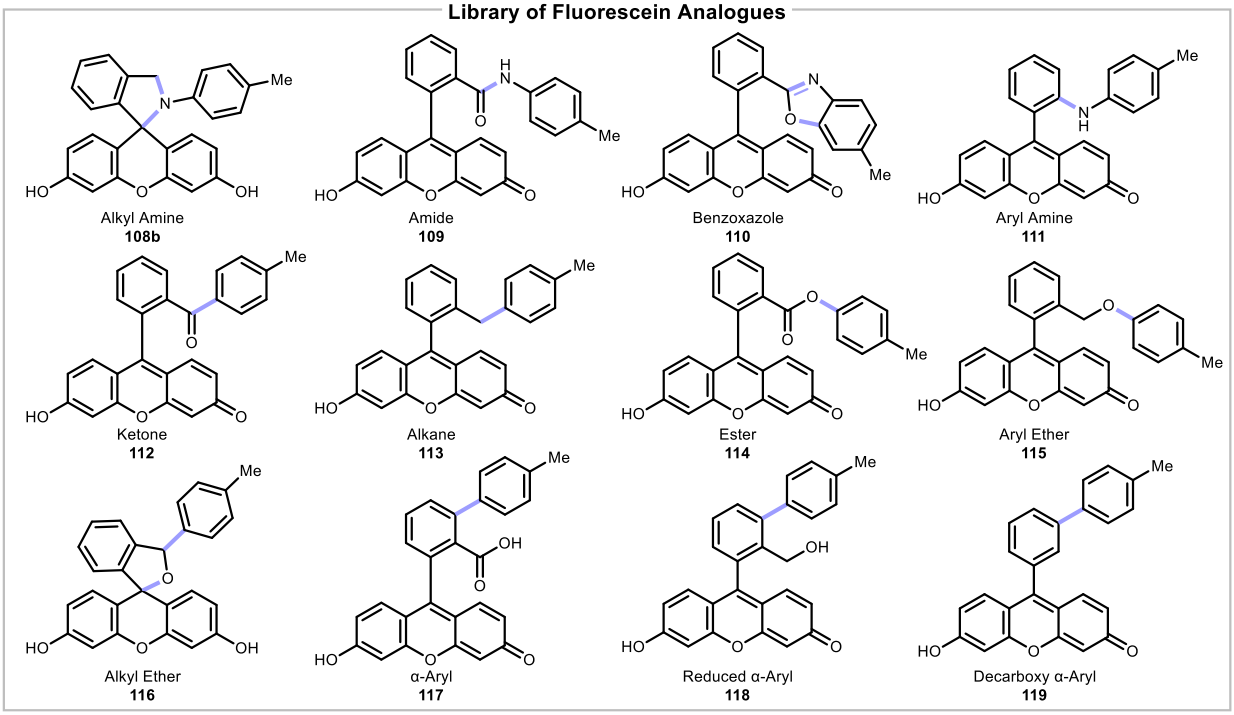


Figure 4-9 Complete library of 12 Fluorescein analogues accessed from coupling of Fluorescein **104** or reduced Fluorescein diacetate **107** with *p*-toluidine **105**.

In addition to amine and amide derivatives **108b**-**110**, diaryl amine **111** was afforded through decarboxylative coupling of fluorescein. Alternatively, deaminative protocols enabled access to structures **112**-**119**, which host a range of sp^2 and sp^3 motifs with stemming from

reductive coupling of the starting carboxylic acid. For instance ketone **112**, ester **114**, and α-arylated acid **117** still retain their carbonyl functionalities. Further reduction to alkane **113**, ethers **116** and **117**, as well as reduced α-arylated variants **118** and **119** provide further deviation of the Fluorescein scaffold with a higher fraction of sp^3 atoms. To visualize the range of physicochemical properties accessed by these analogues, we created kernel density estimate plots for these twelve analogues (Figure 4-10).

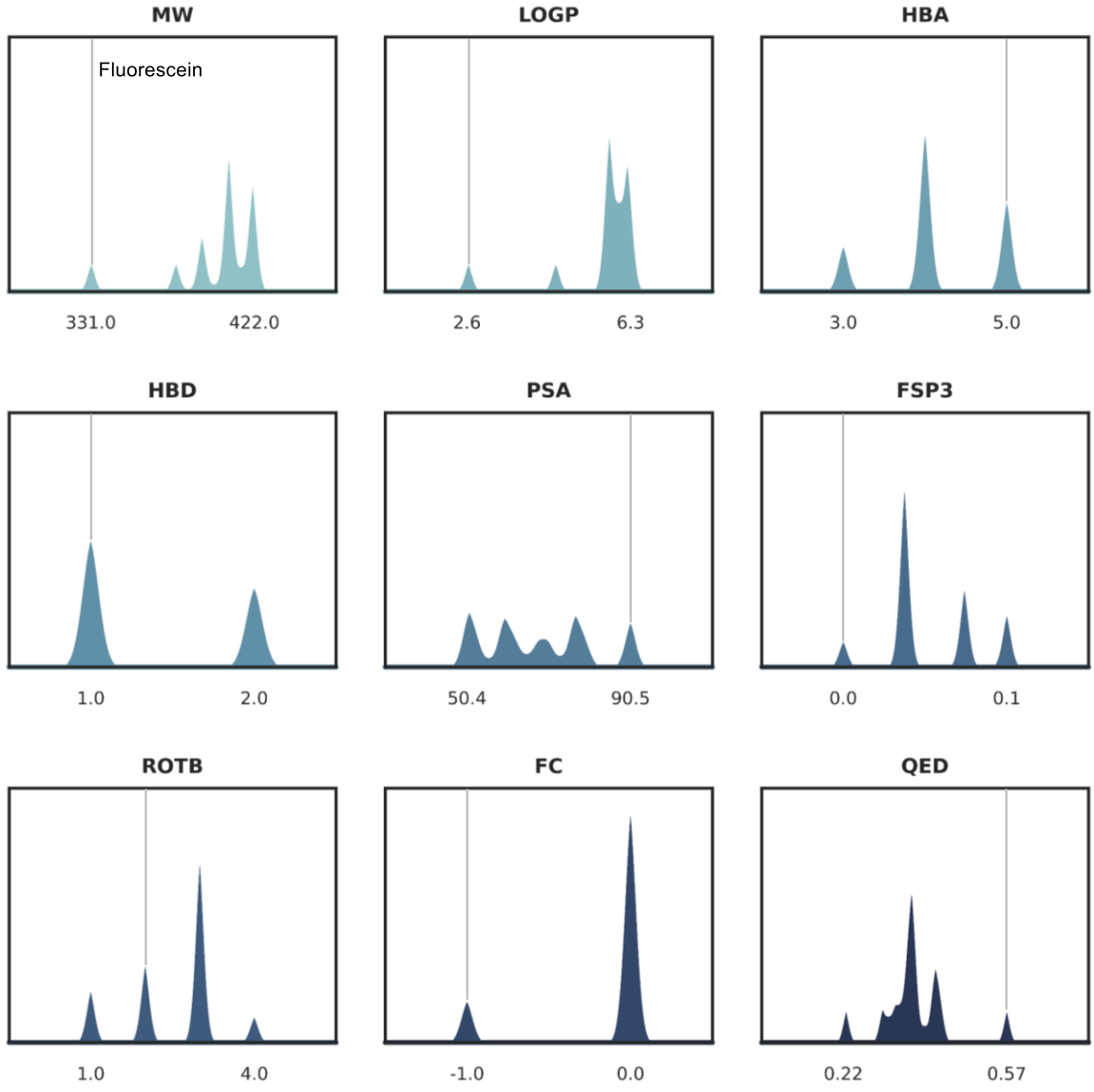


Figure 4-10 Kernel Density Estimate plots showing the range of physicochemical properties of the Fluorescein analogue library. The grey line in each plot indicates the value of Fluorescein carboxylic acid. Height of each peak represents the frequency of occurrence for each value. MW = molecular weight, LOGP = calculated log(partition coefficient), HBA/D = h-bond acceptor/donor count, PSA = polar surface area, ROTB = rotatable bond count, FC = formal charge at pH 7.4, QED = quantitative estimate of drug likeness. Values are computed using RDKit.

While the goal of driving directly towards optimized physicochemical properties is not a core focus of this work, KDE plots help to visualize the range of properties accessible through such unique coupling regimes. Beyond these twelve coupling modes, we envision many more may potentially be accessible through further development of unorthodox amine-acid couplings.

4.4 **Conclusions and Future Work**

In summary, these works serve as important case studies demonstrating the potential of transforming simple amine and acid feedstocks into structurally complex molecules. While the examples presented here represent only a fraction of what is theoretically achievable, they underscore the potential of what reactivity is still waiting to be explored. It is our hope that this work will encourage continued investigation and discovery in this expanding field.

Regarding future directions, much of this work has highlighted the importance of activating groups for developing novel amine-acid couplings. Whether in the case of α-functionalizing amines or many of the reactions on Fluorescein, employing the appropriate activating group has enabled us to access highly unorthodox reactivity patterns. A prominent area of interest that may find use in developing new amine-acid couplings is that of recently emerging skeletal editing techniques. These methods enable facile incorporation or deletion of oxygen and nitrogen atoms in highly complex molecules through *in situ* substrate activation. Many of these techniques can likely find great utility in amine-acid coupling and help enable access to even more diverse molecular frameworks as the field of skeletal editing grows.

4.5 **Experimental Section for Amine-Acid Couplings**

4.5.1 ***General Methods***

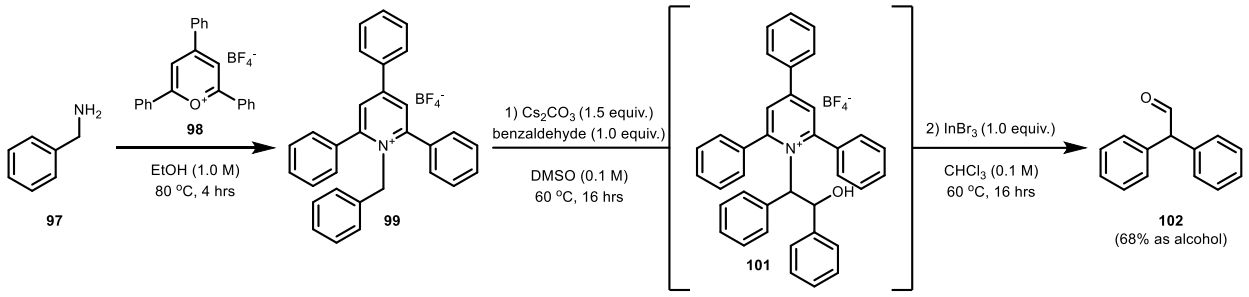
Unless otherwise noted, all reactions were carried out under an atmosphere of argon or nitrogen in dried glassware. Dry solvents were either purchased from Fisher Scientific or Sigma-Aldrich, stored under activated molecular sieves, withdrawn under positive nitrogen pressure or purified using a custom-made SPS purification system (activated alumina columns) and transferred under nitrogen. Solvents for flash column chromatography (Hexanes, EtOAc, CH_2Cl_2, MeOH) were used without additional purification. Reagents were purchased from Sigma-Aldrich, ACROS Organics, TCI, Ambeed, Fisher Scientific and used without additional purification, unless otherwise stated. Glass 1-dram (Fisherbrand™ parts No. 03-339-21B) or 2-dram vials (Fisherbrand™ parts No. 03-339-21D) were used as reaction vessels, fitted with screwcaps with Teflon-coated silicone septa (CG-4910-02), and magnetic stir bars (Fisher

Scientific #14-513-93 or #14-513-65). 24-well HTE screens were conducted using aluminum reaction blocks (Analytical sales #24249) equipped with oven-dried shell vials (Analytical sales #884001) and parylene-coated stir dowels (Analytical sales #13258)

Proton nuclear magnetic resonance (^{1}H NMR) spectra were recorded on a Varian MR-500 MHz, or Varian MR-400 MHz spectrometer and chemical shifts are reported in parts per million (ppm) using the solvent residual peak as an internal standard ($CDCl_3$ at 7.26 ppm, DMSO-d_6 at 2.50 ppm, D_2O at 4.80). Data are reported using the abbreviations: app = apparent, s = singlet, d = doublet, t = triplet, q = quartet, m = multiplet, comp = complex, br = broad. Coupling constant(s) are reported in Hz. Proton-decoupled carbon nuclear magnetic resonance spectra (^{13}C NMR) spectra were recorded on a Varian MR-500 MHz or Varian MR-400 MHz spectrometer and chemical shifts are reported in ppm using the solvent as an internal standard ($CDCl_3$ at 77.16 ppm, DMSO-d_6 at 39.52 ppm). High resolution mass spectrometry data (HRMS) was obtained on a Micromass AutoSpec Ultima Magnetic Sector instrument. Reaction analysis was typically performed by thin-layer chromatography (TLC) on silica gel 60 F_{254} glass plates (Fisher Scientific #S07876) and visualized using ultraviolet light (254 nm) or potassium permanganate ($KMnO_4$) stain; or using a Waters I-class ACQUITY UPLC-MS (Waters Corporation, Milford, MA, USA) equipped with in-line photodiode array detector (PDA) and QDa mass detector (ESI positive ionization mode). 0.1 µL sample injections were taken from acetonitrile solutions of reaction mixtures or products (~1 mg/mL). A partial loop injection mode was used with the needle placement at 1.0 mm from bottom of the wells and a 0.2 µL air gap at pre-aspiration and post-aspiration. Column used: Waters Cortecs UPLC C18+ column, 2.1mm · 50 mm with (Waters #186007114) with Waters Cortecs UPLC C18+ VanGuard Pre-column 2.1mm · 5 mm (Waters #186007125), Mobile Phase A: 0.1 % formic acid in Optima LC/MS grade water, Mobile Phase B: 0.1% formic acid in Optima LC/MS-grade MeCN. Flow rate: 0.8 mL/min. Column temperature: 45 °C. The PDA sampling rate was 20 points/sec. The QDa detector monitored m/z 150-750 with a scan time of 0.06 seconds and a cone voltage of 30 V. The PDA detector range was between 210 nm – 400 nm with a resolution of 1.2 nm. 1-minute and 2-minute methods were used. The method gradients are as follows: 0 min: 0.8 mL/ min, 95% 0.1% formic acid in water/ 5% 0.1% formic acid in acetonitrile; 1.5 min: 0.8 mL/ min, 0.1% 0.1% formic acid in water/ 99.9% 0.1% formic acid in acetonitrile; 1.91 min: 0.8 mL/min, 95%

0.1% formic acid in water/ 5% 0.1% formic acid in acetonitrile. Flash chromatography was performed on silica gel (230 – 400 Mesh, Grade 60) under a positive pressure of air.

4.5.2 ***Procedures for the Synthesis and Reaction of Pyridinium Salts***



To a solution of 2,4,6-triphenylpyrylium tetrafluoroborate **98** (352.1 mg, 0.889 mmol, 1.0 equiv) in anhydrous ethanol (0.889 mL) was added benzylamine **97** (102 µL, 0.933 mmol, 1.05 equiv) at room temperature. The solution was then stirred at 80 °C for 4 h. The reaction mixture was cooled to room temperature, then triturated into a flask containing 10 mL diethyl ether to precipitate the pyridinium salt. Vacuum filtration was used to retrieve the analytically pure salt **99** that matches all prior characterization data.

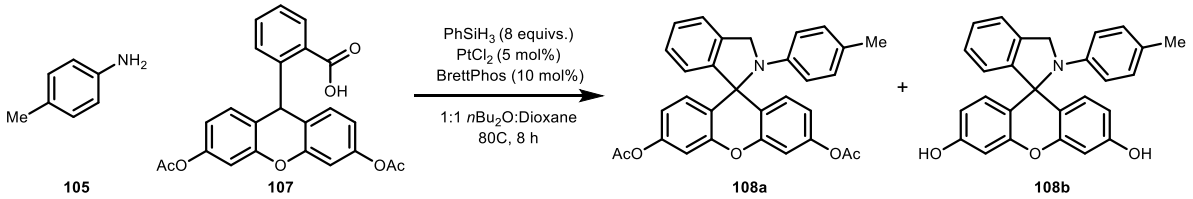
Solid cesium carbonate (434.4 mg, 1.333 mmol, 1.5 equiv) was then added to **99**, along with a stir bar. The reaction vial was capped and flushed with nitrogen gas, then anhydrous DMSO (8.89 mL) was added followed by benzaldehyde (90 µL, 0.889 mmol, 1.0 equiv). The reaction was stirred at 60 °C for 16 h. The mixture was diluted with water (30.0 mL) and extracted with DCM (3 x 10 mL). The combined organic layers were dried over anhydrous Na2SO4, filtered, and concentrated in vacuo. To the crude residue, solid indium (III) bromide (315.1 mg, 0.889 mmol, 1.0 equiv) was added along with chloroform (8.89 mL). The reaction mixture was heated to 60 °C for 16 h. After dilution with brine (10.0 mL) and extraction with DCM (3 x 5.0 mL), the combined organic layers were dried over anhydrous Na2SO4, filtered, and concentrated in vacuo to give the crude aldehyde product **102**.

For isolation, the crude mixture containing aldehyde **102**, was dissolved in anhydrous ethanol (8.89 mL) and solid portions of $NaBH_4$ (33.6 mg, 0.889 mmol, 1.0 equiv) were added at room temperature. The solution was stirred at room temperature for 2 hours, cooled to 0 °C, and quenched with aqueous acetic acid (1.0 M, 15 mL). Extraction with DCM (3 x 5 mL), drying of the combined organic layers with Na2SO¬4, and removal of solvent in vacuo yielded the

corresponding reduced alcohol product. The crude alcohol was purified by flash chromatography (silica gel, eluent: 10-20% EtOAc/hexanes) to afford 2,2-diphenylethanol (119.9 mg, 68% yield) as a white solid.

1H NMR (500 MHz, CDCl3) ∂ 7.36-7.33 (m, 4H), 7.31–7.22 (m, 6H), 4.25-4.22 (m, 1H), 4.20 – 4.18 (m, 2H). 13C NMR (125 MHz, CDCl3) ∂ 141.37, 128.74, 128.32, 128.32, 126.84, 66.16, 53.66. HRMS (ESI): calculated C14H15O+ [M + H]+: 199.1117, found: 199.1124.

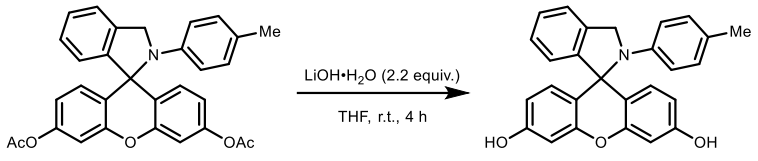
4.5.3 ***Procedures for Fluorescein Couplings***



To an oven dried 2-dram vial charged with a stir bar in a glovebox was added Dihydrofluorescein diacetate **107** (105 mg, 0.25 mmol, 2.5 equiv) and p-toluidine **105** (10.7 mg, 0.10 mmol, 1.0 equiv). These were suspended in 500 µL of dibutyl ether. Simultaneously, Platinum(II) chloride (1.33mg, 5 µmol, 0.05 equiv) and BrettPhos (5.37 mg, 10 µmol, 0.10 equiv) were stirred in 500 µL of 1,4-Dioxane for 15 minutes. Following, Phenylsilane (98.6 µL, 0.80 mmol, 8.0 equiv) was added to the platinum/ligand solution. This solution was stirred for 30 seconds, then transferred to the fluorescein solution, the vial capped and removed from the glovebox. This vial was heated at 80 °C for 8 hours. After cooling to room temperature, the reaction was quenched with dropwise addition of 0.5 mL methanol and 0.5 mL saturated aq. $CuSO_4$. The vial was allowed to stir at room temperature for 1 hour, then the crude mixture was diluted with ethyl acetate and poured into a separatory funnel containing 15 mL of 1M aqueous $NaHCO_3$. The aqueous layer was extracted with 3x15 mL of ethyl acetate, the organic layers combined, dried over sodium sulfate, and evaporated. The crude mixture was loaded onto a column and purified with 20-50% ethyl acetate in hexanes to retrieve 21.4 mg diacetate alkyl amine product **108a** as a colorless solid (44% yield) along with 5.8 mg of deprotected alkyl amine **108b**. R_f = 0.45 in 3:7 EtOAc:Hexanes.

108a: ^{1}**H NMR** (499 MHz, $CDCl_3$) δ 7.41 (d, *J* = 7.6 Hz, 1H), 7.24 (t, *J* = 7.4 Hz, 1H), 7.14 (t, *J* = 7.5 Hz, 1H), 6.87 (d, *J* = 8.5 Hz, 2H), 6.84 (d, *J* = 7.7 Hz, 1H), 6.76 (d, *J* = 8.5 Hz, 2H), 6.68 (d, *J* = 2.5 Hz, 2H), 6.52 – 6.45 (m, 2H), 6.36 (dd, *J* = 8.5, 2.5 Hz, 2H), 5.08 (s, 2H), 2.14 (s, 3H),

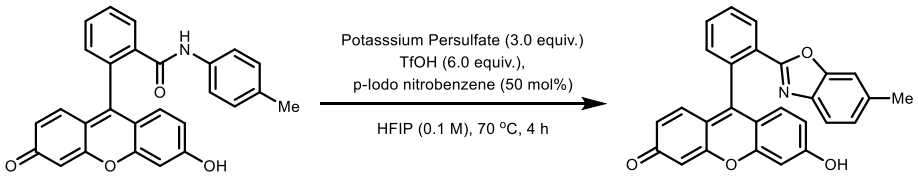
2.02 (s, 2H). **^{13}C NMR** (126 MHz, cdcl3) δ 168.9, 150.6, 150.5, 132.4, 129.4, 128.4, 128.3, 127.7, 123.8, 123.6, 122.3, 117.4, 113.9, 109.9, 55.4, 22.2, 21.2, 20.2.; **HRMS**: Calcd. for $C_{31}H_{26}NO_5$ $[M+H]^+$ = 492.1806 m/z, found = 492.1801 m/z.



108a **108b**

To deprotect, diacetate alkyl amine **108a** (20.0 mg, 39.6 µmol, 1.0 equiv) was dissolved in 1 mL THF. Followed by dropwise addition of lithium hydroxide monohydrate (3.65 mg, 87.0 µmol, 2.2 equiv) in 0.5 mL water, the mixture was stirred at room temperature for 4 hours. The vial was diluted with 10 mL ethyl acetate and poured into a separatory funnel containing 15 mL of 1M aqueous $NaHCO_3$. The aqueous layer was extracted with 3x15 mL of ethyl acetate, organic layers combined, dried over sodium sulfate, and solvent evaporated. The residue was characterized without further purification yielding 14.6 mg deprotected alkyl amine **108b** (88% yield) as an orange solid. R_f = 0.63 in 1:1 EtOAc:Hexanes.

108b: ^{1}H NMR (499 MHz, dmso) δ 9.63 (s, 2H), 7.47 (d, *J* = 7.6 Hz, 1H), 7.23 (t, *J* = 7.4 Hz, 1H), 7.13 (t, *J* = 7.5 Hz, 1H), 6.76 (d, *J* = 8.4 Hz, 2H), 6.65 (d, *J* = 7.7 Hz, 1H), 6.62 (d, *J* = 8.5 Hz, 2H), 6.56 (d, *J* = 2.4 Hz, 2H), 6.38 (d, *J* = 8.5 Hz, 2H), 6.32 (dd, *J* = 8.5, 2.4 Hz, 2H), 5.02 (s, 2H), 2.04 (s, 3H). **^{13}C NMR** (126 MHz, dmso) δ 158.0, 151.1, 150.8, 142.0, 133.3, 129.4, 129.0, 128.4, 127.6, 124.6, 123.6, 123.0, 117.2, 113.7, 112.3, 102.6, 67.0, 55.1, 20.3; **HRMS**: Calcd. for $C_{27}H_{22}NO_3$ $[M+H]^+$ = 408.1594 m/z, found = 408.1583 m/z



109 **110**

To an oven dried 2-dram vial charged with a stir bar was added Fluorescein amide **109** (42.1 mg, 0.10 mmol, 1.0 equiv) and 1-Iodo-4-nitrobenzene (12.5 mg, 0.05 mmol, 0.5 equiv). Following, 1.0 mL of HFIP was added, then triflic acid (53 µL, 0.6 mmol, 6.0 equiv). To the stirring solution, potassium persulfate (81.1 mg, 0.3 mmol, 3.0 equiv) was quickly added. The vial was

capped under oxygen atmosphere and stirred at 70 °C for 4 hours. After reaction completion, dropwise addition of 0.1 mL of 1M aqueous sodium thiosulfate was carried out to quench residual oxidant. The crude mixture was then diluted with ethyl acetate and poured into a separatory funnel containing 15 mL of 1M aqueous $NaHCO_3$. The aqueous layer was extracted with 3x15 mL of ethyl acetate, the organic layers combined, dried over sodium sulfate, and evaporated. The crude mixture was loaded onto a column and purified with 30-70% Acetone in Ethyl Acetate to retrieve 9.4 mg cyclized benzoxazole **110** as a red solid (23% yield). R_f = 0.30 in 1:1 Acetone:EtOAc.

^{1}H NMR (500 MHz, DMSO-d6) δ 8.45 – 8.38 (m, 1H), 7.60 – 7.53 (m, 1H), 7.42 (d, *J* = 8.2 Hz, 1H), 7.30 (s, 1H), 6.85 (d, *J* = 9.3 Hz, 2H), 2.35 (s, 1H). **^{13}C NMR** (126 MHz, dmso) δ 160.6, 150.5, 149.9, 139.3, 136.5, 132.7, 132.1, 131.6, 130.6, 130.3, 130.1, 126.5, 126.5, 119.9, 114.9, 111.0, 103.9, 21.6.; **HRMS**: Calcd. for $C_{27}H_{18}NO_4$ $[M+H]^+$ = 420.1230 m/z, found = 420.1251 m/z.

4.5.4 ***HTE Screening for Fluorescein Alkyl Amine***

Stock solutions, or suspensions, were prepared as shown in the heatmap preparation table. In an inert atmosphere glovebox, reagents were weighed and dissolved or suspended in anhydrous solvent to achieve their listed concentrations in the associated table. Stock solutions of reagents were stirred until either a clear solution or a uniform slurry was achieved. All stock solutions were prepared in a 1:1 mixture of *n*-BuOH:Dioxane to the concentration listed in the table below. A 24-well aluminum microvial plate was equipped with oven-dried shell vials and parylene-coated stir dowels and then moved into the glovebox. Prestirring of metals with ligands was carried out by dosing 20 µL each of the appropriate metal and ligand stock solutions into the 24-well plate via single channel micropipetter. The 24-well block was then stirred at room temperature for 15 minutes, followed by addition of Dihydrofluorescein diacetate, p-toluidine, and finally silane stock solutions to achieve a final reaction volume of 100 µL per well. The microvial plate was sealed, removed from the glove box, and stirred with heating to 80 ºC for 8 hours.

Finally, the reaction block was opened and quenched by addition of 25 µL MeOH then 25 µL aqueous LiOH monohydrate (1M) was added to deprotect remaining acetylated product. The block was allowed to stir at room temperature for 1 hour, then 100 µL 0.1M caffeine in acetonitrile was added to each well. After pipetting the contents of each well up and down, a 100

μL aliquot of the quenched reaction mixture was added into a 96-well polypropylene collection plate (Analytical Sales & Services cat. no. 17P687). The solvent was evaporated by blowing nitrogen down on the analytical plate. LCMS grade acetonitrile (600 μL) was added and the reactions were then analyzed by UPLC-MS. The assay yields were produced by measuring the UV absorbance peak area of exclusively the deprotected alkyl amine product relative caffeine internal standard.

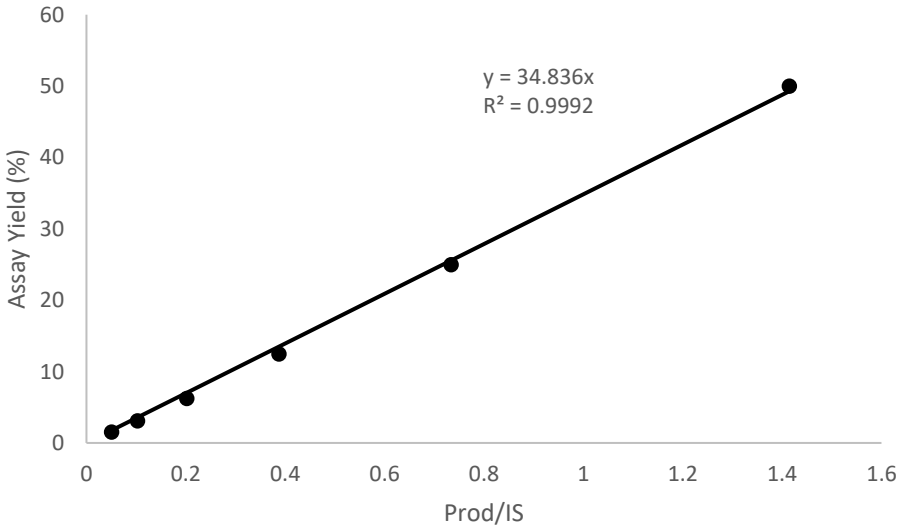


Figure 4-11 Calibration Curve for Fluorescein Alkyl Amine

Reagent	Solvent	C_{stock} (M)	Vdose (µL)	Wells	Order added
Fluorescein **107**	*n*Bu_2O, Dioxane	1.25	20	All	3
Toluidine **105**	*n*Bu_2O, Dioxane	0.5	20	All	4
$PtCl_2$	*n*Bu_2O, Dioxane	0.05	20	['A1', 'A2', 'B1', 'B2', 'C1', 'C2', 'D1', 'D2']	1
Me_2(COD)Pt	*n*Bu_2O, Dioxane	0.05	20	['A3', 'A4', 'B3', 'B4', 'C3', 'C4', 'D3', 'D4']	1
Karstedt's Catalyst	*n*Bu_2O, Dioxane	0.05	20	['A5', 'A6', 'B5', 'B6', 'C5', 'C6', 'D5', 'D6']	1
Brettphos	*n*Bu_2O, Dioxane	0.025	20	['A1', 'A2', 'A3', 'A4', 'A5', 'A6']	2
tBuXphos	*n*Bu_2O, Dioxane	0.025	20	['B1', 'B2', 'B3', 'B4', 'B5', 'B6']	2
Xantphos	*n*Bu_2O, Dioxane	0.025	20	['C1', 'C2', 'C3', 'C4', 'C5', 'C6']	2
Dppe	*n*Bu_2O, Dioxane	0.025	20	['D1', 'D2', 'D3', 'D4', 'D5', 'D6']	2
Phenylsilane	*n*Bu_2O, Dioxane	4.0	20	['A1', 'A3', 'A5', 'B1', 'B3', 'B5', 'C1', 'C3', 'C5', 'D1', 'D3', 'D5']	5
Diphenylsilane	*n*Bu_2O, Dioxane	4.0	20	['A2', 'A4', 'A6', 'B2', 'B4', 'B6', 'C2', 'C4', 'C6', 'D2', 'D4', 'D6']	5

Table 4-1 Reagents used in Fluorescein Alkyl Amine Screen.

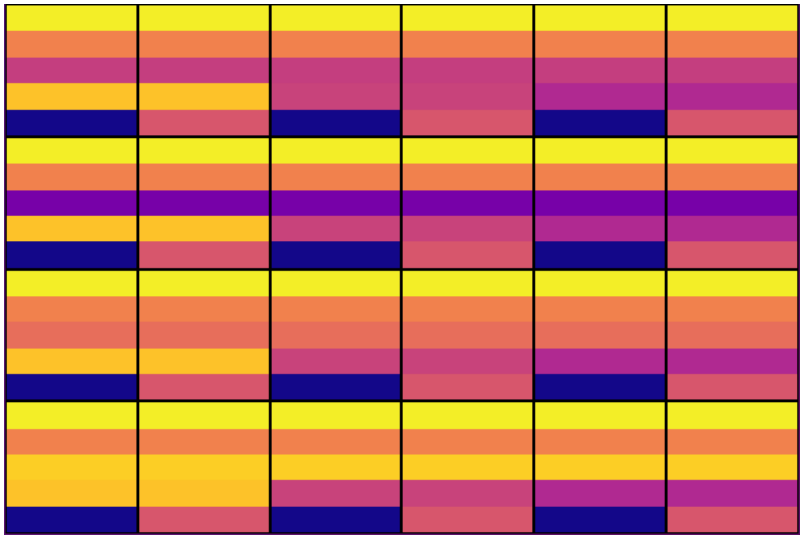


Figure 4-12 Grid of 24-Well Fluorescein Alkyl Amine Screen

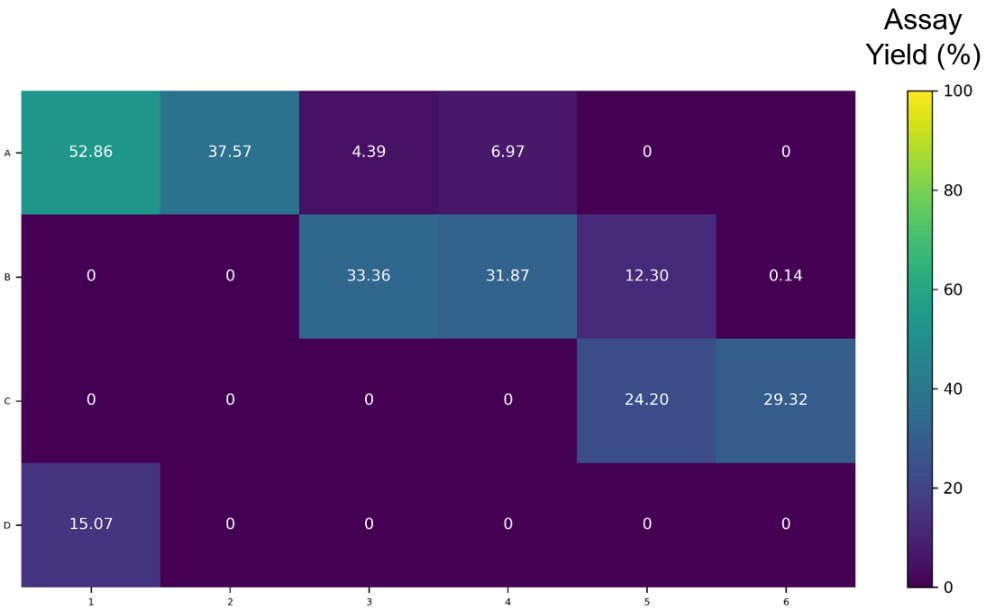


Figure 4-13 Heatmap for Fluorescein Alkyl Amine Screen

4.5.5 ***HTE Screening for Fluorescein Benzoxazole***

Stock solutions, or suspensions, were prepared as shown in the heatmap preparation table. Reagents were weighed and dissolved or suspended in solvent under air to achieve their listed concentrations in the associated table. The 24-well aluminum microvial plate was first equipped with oven-dried shell vials and parylene-coated stir dowels. Stock solutions were then prepared in hexafluoro-2-propanol (HFIP) to the concentration listed in the table below. To wells with potassium persulfate or oxone salts, solid doses of the respective oxidant were instead directly weighed into the corresponding wellplate vials. Dosing of all oxidant solutions was first carried out, with an additional 25 µL of HFIP was added to wells previously portioned with solid potassium persulfate or oxone. Following dosing of oxidant solutions, stock solutions of fluorescein amide, aryl iodide, and finally acid were dosed into the appropriate wells. The 24-well block was sealed and stirred at 70 °C for 4 hours.

The reaction wells were quenched by opening the reaction block and adding 100 µL of 1M aqueous sodium thiosulfate and 100 µL 0.1M caffeine in acetonitrile was added to each well. After pipetting the contents of each well up and down, a 100 µL aliquot of the quenched reaction mixture was added into a 96-well polypropylene collection plate (Analytical Sales & Services cat. no. 17P687). LCMS grade acetonitrile (600 µL) was added and the reactions were then analyzed by UPLC-MS. The assay yields were produced by measuring the UV absorbance peak area of the desired product relative caffeine internal standard.

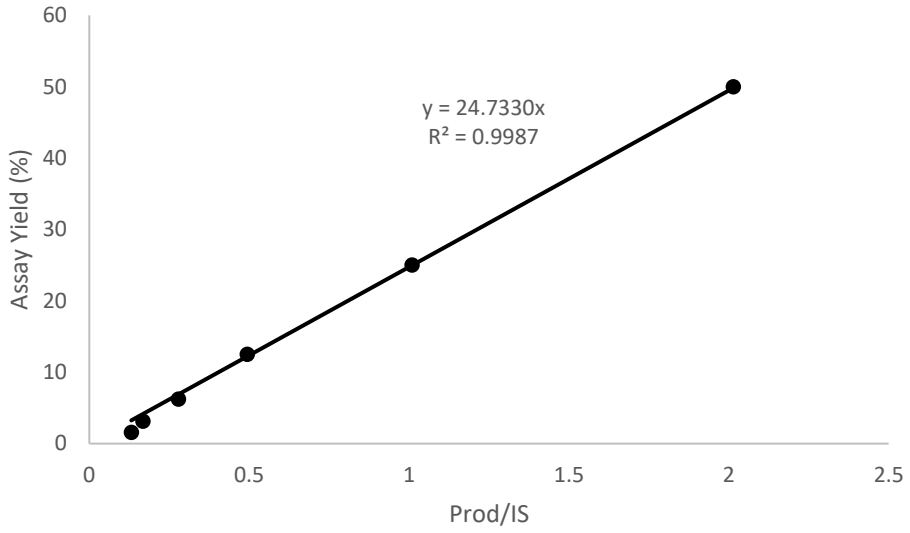


Figure 4-14 Calibration Curve for Fluorescein Benzoxazole

Reagent	Solvent	C_{stock} (M)	Vdose (μL)	Wells	Order added
Fluorescein Amide **109**	HFIP	0.4	25	All	3
p-Iodo Nitrobenzene	HFIP	0.2	25	All	2
Chloranil	HFIP	1.2	25	['A1', 'B1', 'C1', 'D1']	1
DDQ	HFIP	1.2	25	['A2', 'B2', 'C2', 'D2']	1
DMP	HFIP	1.2	25	['A3', 'B3', 'C3', 'D3']	1
PIDA	HFIP	1.2	25	['A4', 'B4', 'C4', 'D4']	1
Oxone	HFIP	N/A	25*	['A5', 'B5', 'C5', 'D5']	1
Potassium Persulfate	HFIP	N/A	25*	['A6', 'B6', 'C6', 'D6']	1
Mesylic Acid	HFIP	2.4	25	['A1', 'A2', 'A3', 'A4', 'A5', 'A6']	4
Triflic Acid	HFIP	2.4	25	['B1', 'B2', 'B3', 'B4', 'B5', 'B6']	4
Sulfuric Acid	HFIP	2.4	25	['C1', 'C2', 'C3', 'C4', 'C5', 'C6']	4
Perfluorobutane sulfonic acid	HFIP	2.4	25	['D1', 'D2', 'D3', 'D4', 'D5', 'D6']	4

Table 4-2 Reagents used in Fluorescein Benzoxazole Screen.

* = Solid powder weighed directly into wells, then diluted with blank solvent

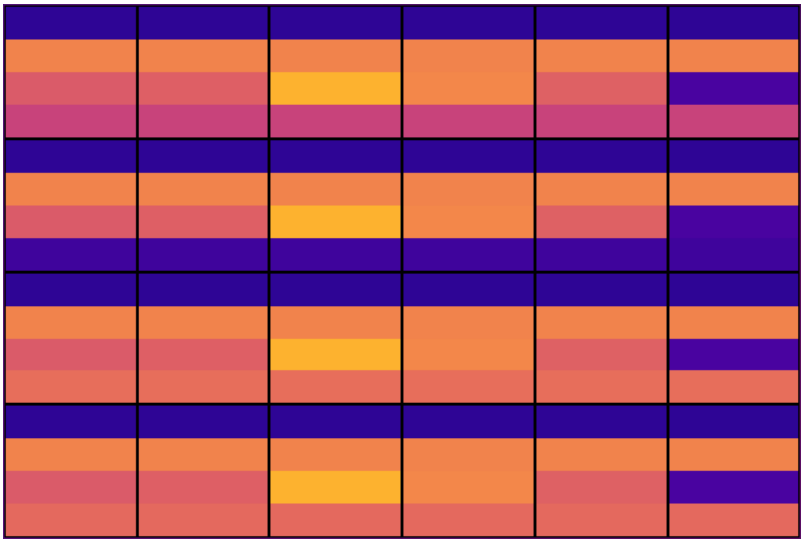


Figure 4-15 Grid of 24-Well Fluorescein Biaryl Ether Screen

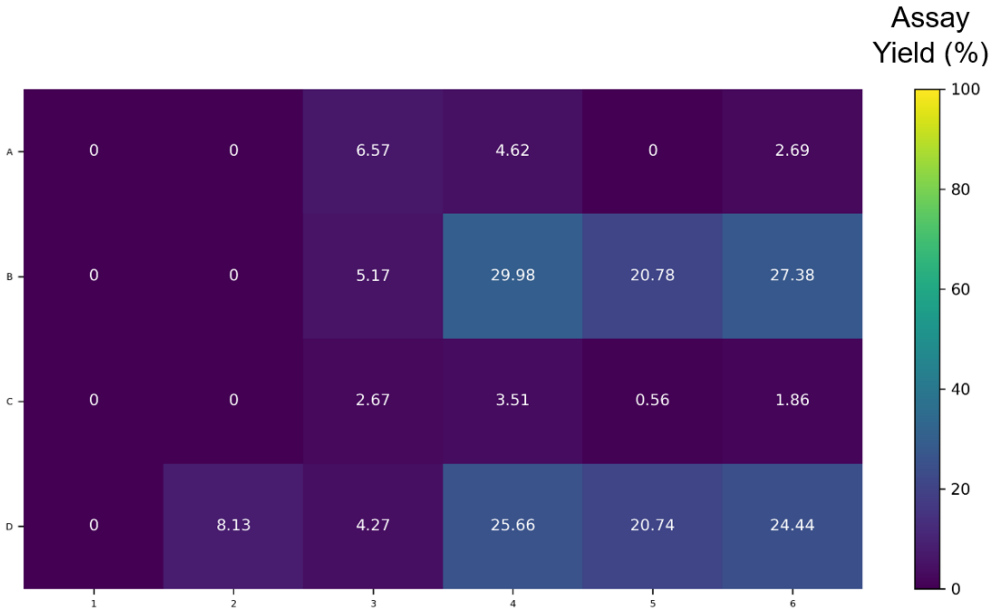
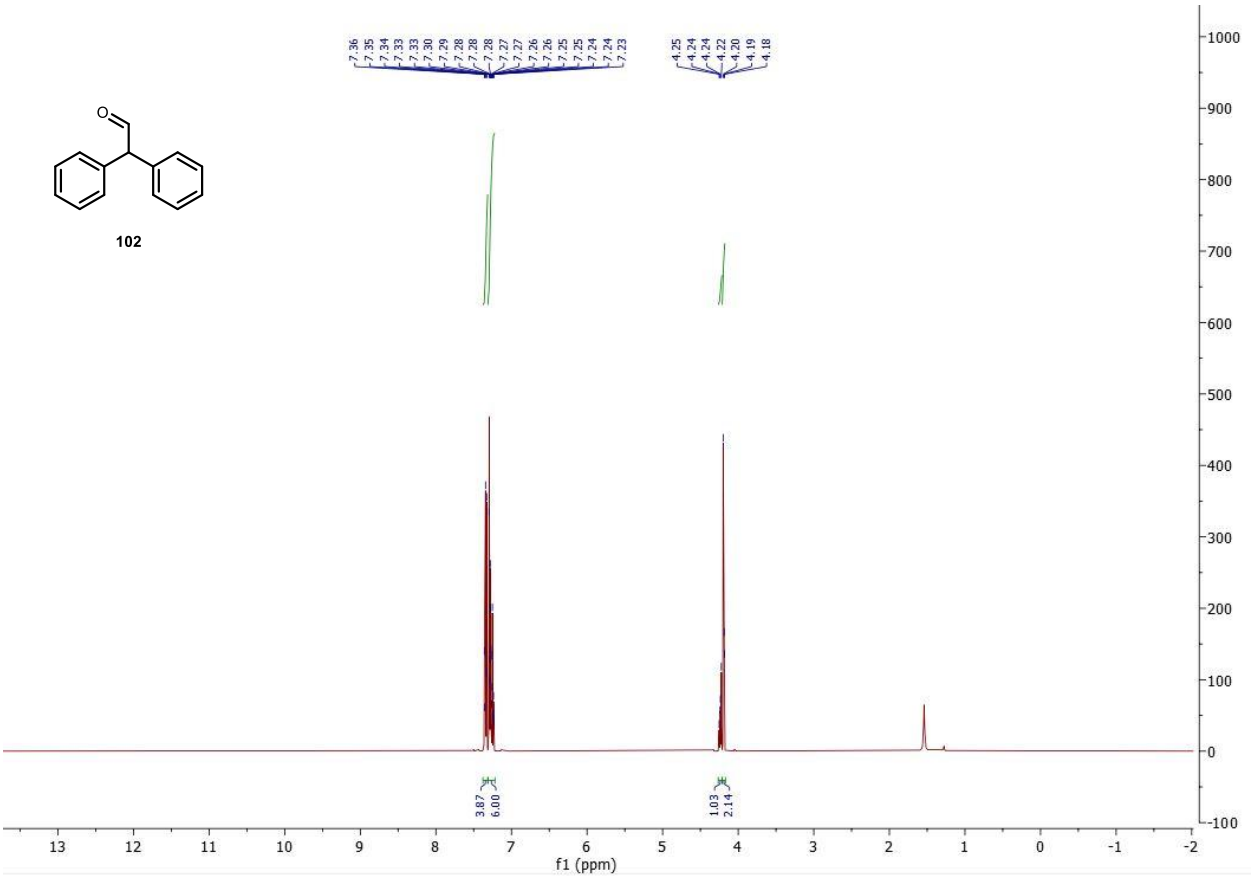
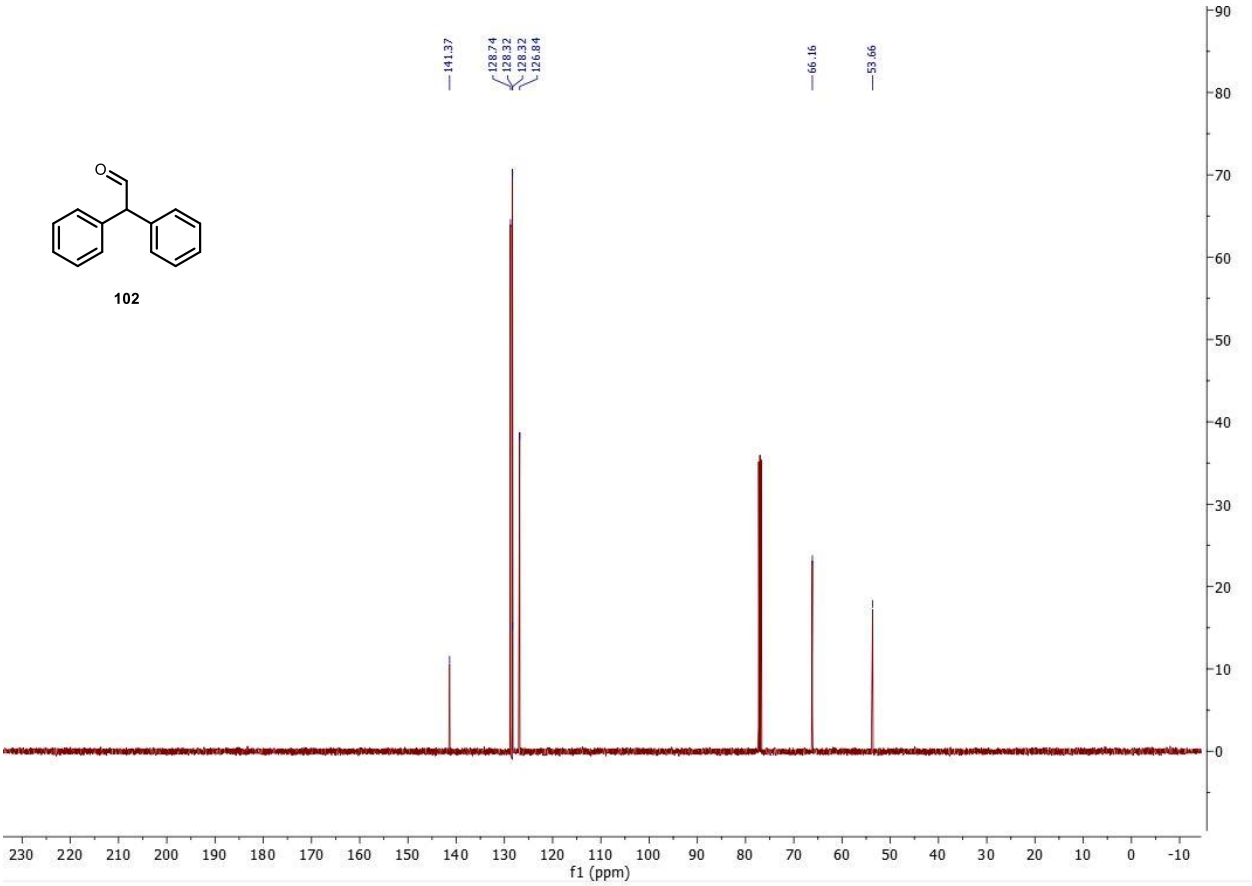


Figure 4-16 Heatmap for Fluorescein Benzoxazole Screen

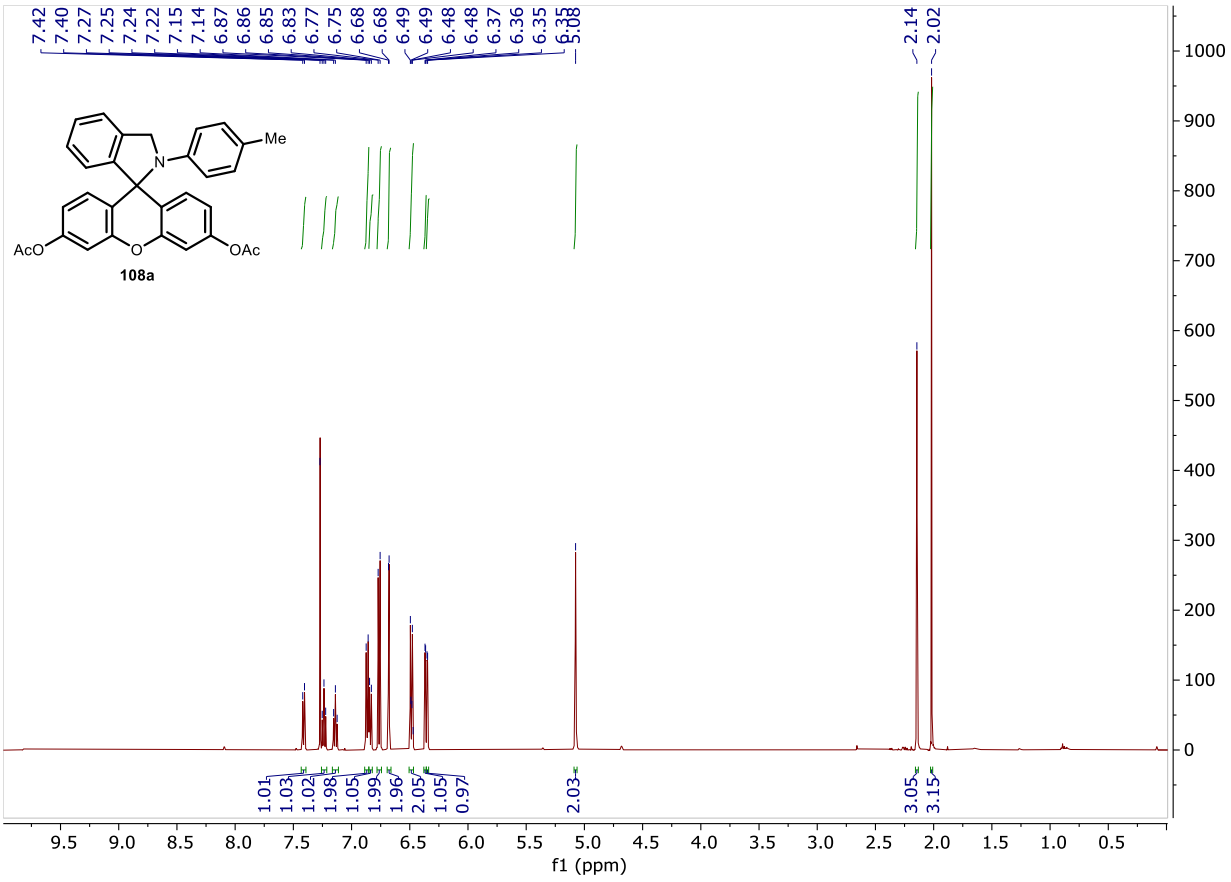
4.6 **Spectra**



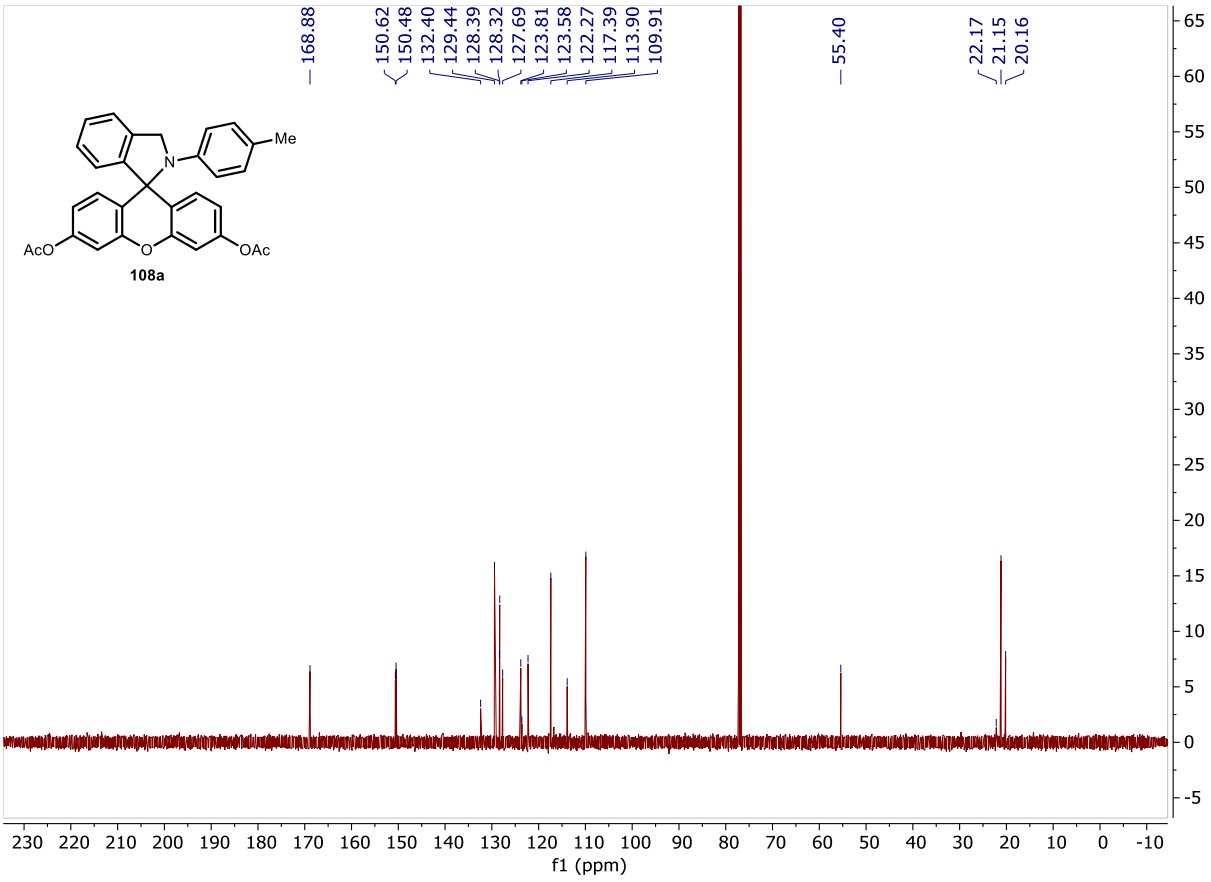
Spectrum 4-1 ^{1}H NMR of compound 102



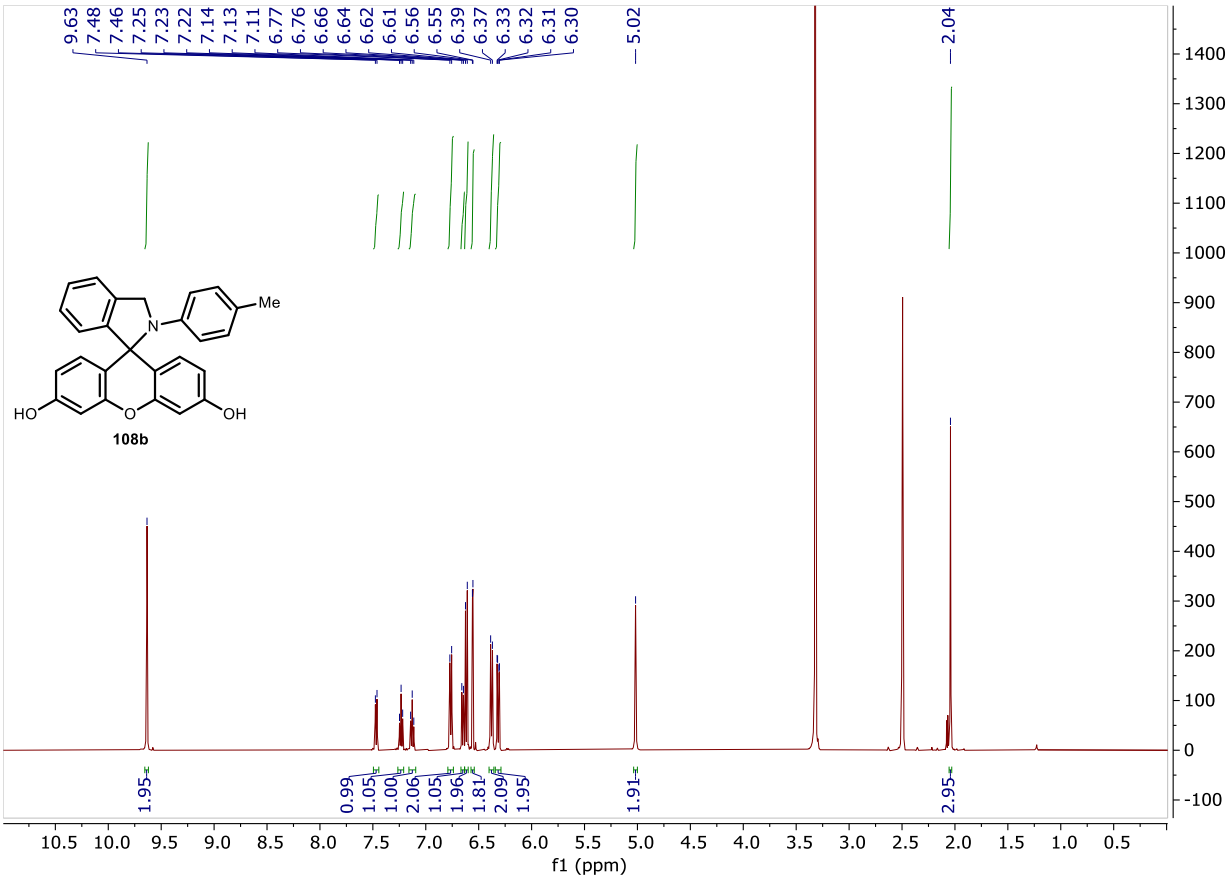
Spectrum 4-2 ^{13}C NMR of compound 102



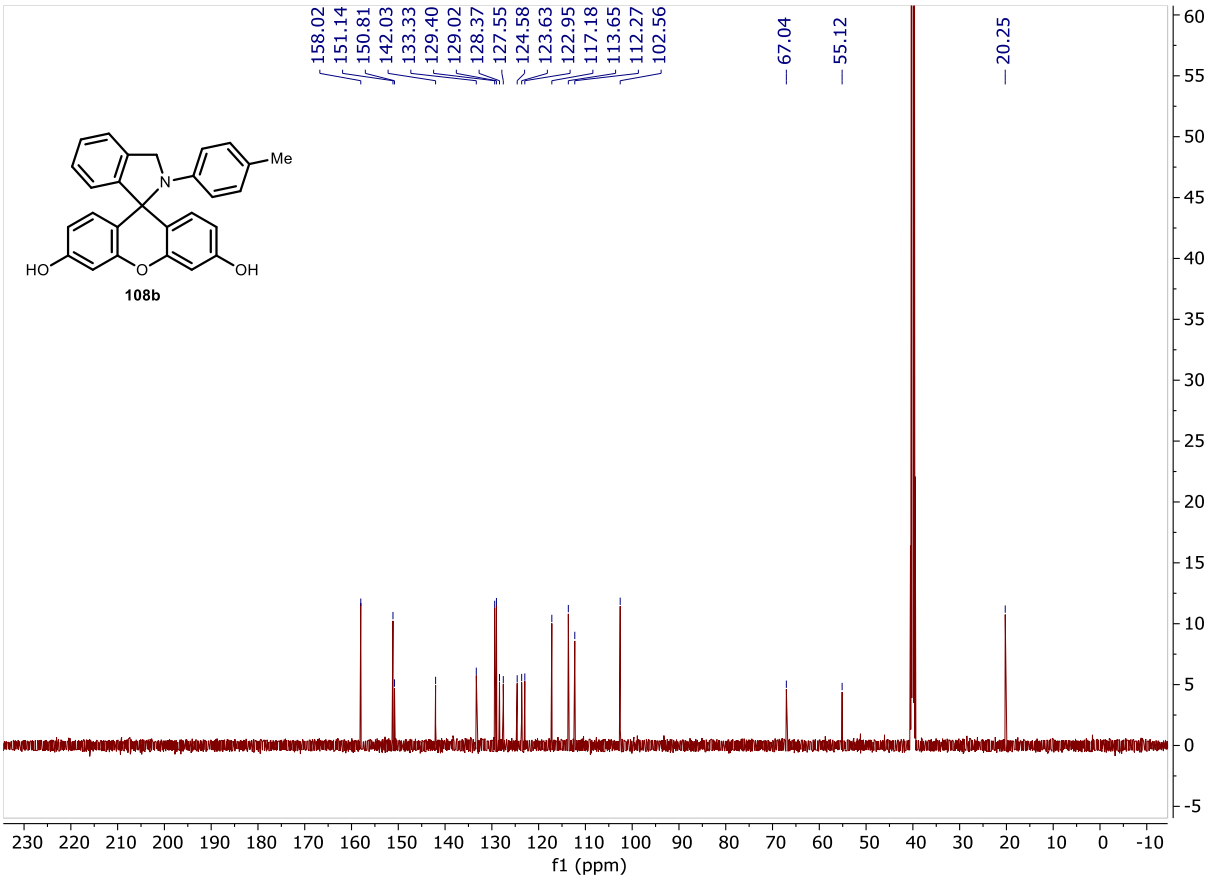
Spectrum 4-3 ^{1}H NMR of compound 108a



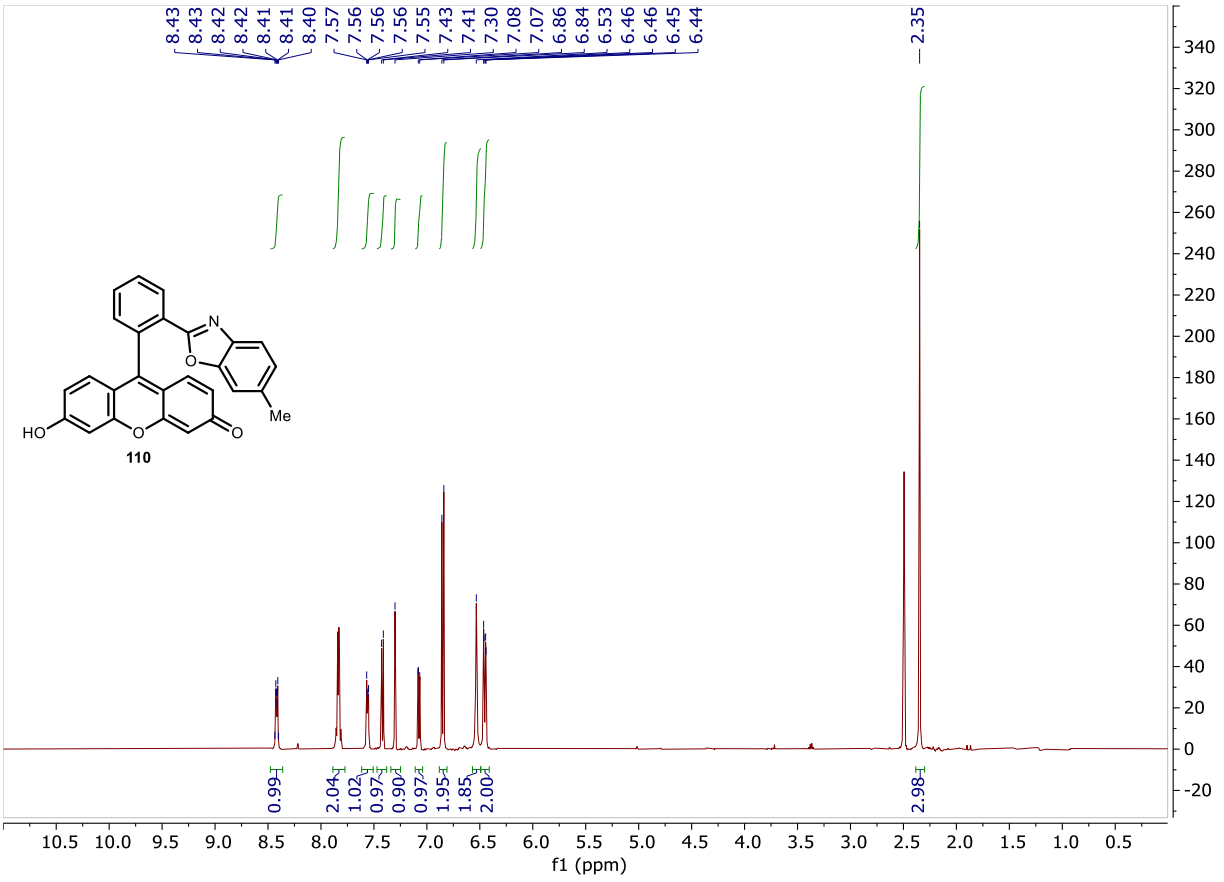
Spectrum 4-4 ^{13}C NMR of compound 108a



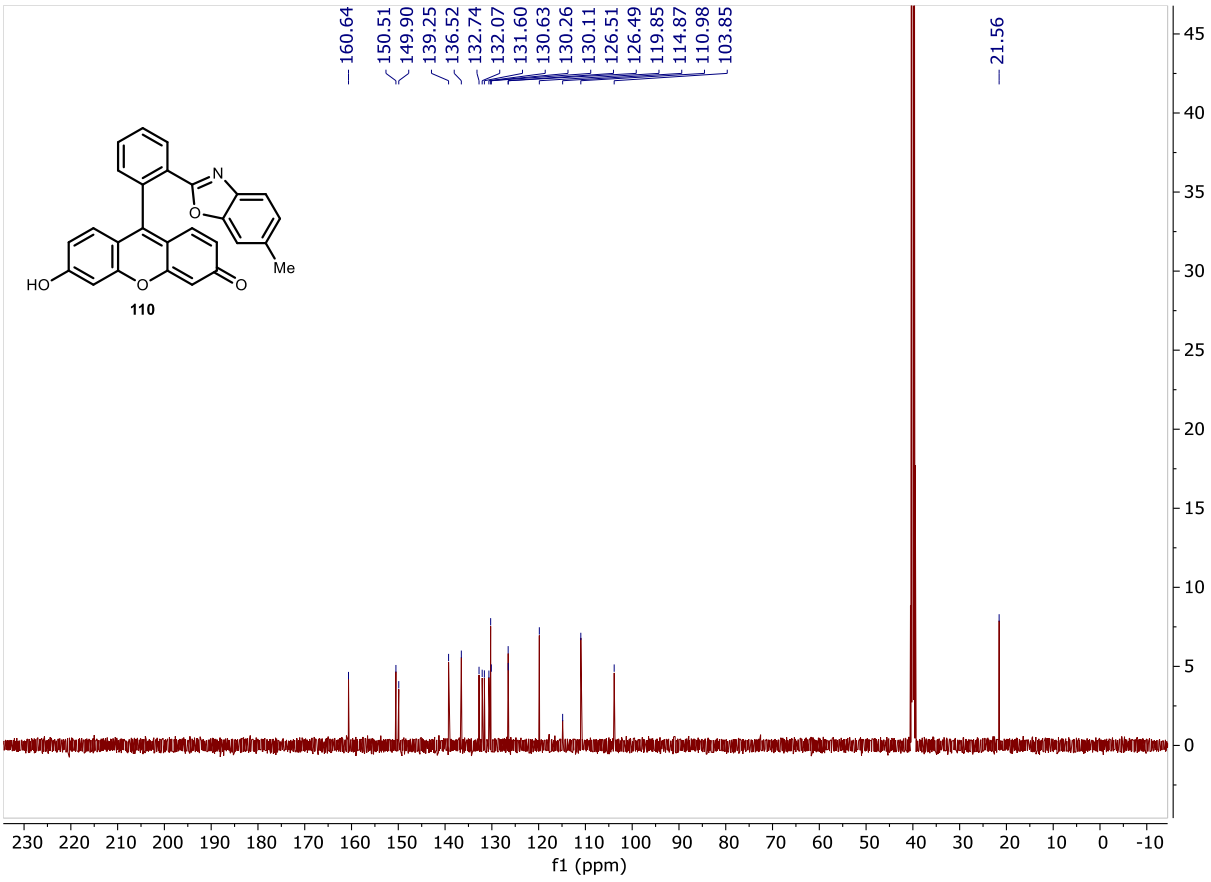
Spectrum 4-5 ^{1}H NMR of compound 108b



Spectrum 4-6 ^{13}C NMR of compound 108b



Spectrum 4-7 ^{1}H NMR of compound 110



Spectrum 4-8 ^{13}C NMR of compound 110

4.7 **References**

(137) Boström, J.; Brown, D. G.; Young, R. J.; Keserü, G. M. Expanding the Medicinal Chemistry Synthetic Toolbox. *Nat. Rev. Drug Discov.* **2018**, *17* (10), 709–727. https://doi.org/10.1038/nrd.2018.116.

(138) McGrath, A.; Zhang, R.; Shafiq, K.; Cernak, T. Repurposing Amine and Carboxylic Acid Building Blocks with an Automatable Esterification Reaction. *Chem. Commun.* **2023**, *59* (8), 1026–1029. https://doi.org/10.1039/D2CC05670D.

(139) Mahjour, B.; Shen, Y.; Liu, W.; Cernak, T. A Map of the Amine–Carboxylic Acid Coupling System. *Nature* **2020**, *580* (7801), 71–75. https://doi.org/10.1038/s41586-020-2142-y.

(140) Liu, K.; Ding, D.; Xing, W.; Liu, L.; Zhang, S.; Meng, Q.; Chen, T. Palladium-Catalysed Deaminative/Decarboxylative Cross-Coupling of Organoammonium Salts with Carboxylic

Acids. *Org. Biomol. Chem.* **2023**, *21* (7), 1384–1388. https://doi.org/10.1039/D2OB02251F.

(141) Sheng, T.; Zhang, H.-J.; Shang, M.; He, C.; Vantourout, Julien. C.; Baran, Phil. S. Electrochemical Decarboxylative N-Alkylation of Heterocycles. *Org. Lett.* **2020**, *22* (19), 7594–7598. https://doi.org/10.1021/acs.orglett.0c02799.

(142) Stoll, E. L.; Tongue, T.; Andrews, K. G.; Valette, D.; Hirst, D. J.; Denton, R. M. A Practical Catalytic Reductive Amination of Carboxylic Acids. *Chem. Sci.* **2020**, *11* (35), 9494–9500. https://doi.org/10.1039/D0SC02271C.

(143) Wang, J.; Ehehalt, L. E.; Huang, Z.; Beleh, O. M.; Guzei, I. A.; Weix, D. J. Formation of C(Sp2)–C(Sp3) Bonds Instead of Amide C–N Bonds from Carboxylic Acid and Amine Substrate Pools by Decarbonylative Cross-Electrophile Coupling. *J. Am. Chem. Soc.* **2023**, *145* (18), 9951–9958. https://doi.org/10.1021/jacs.2c11552.

(144) Zhang, R.; Mahjour, B.; Outlaw, A.; McGrath, A.; Hopper, T.; Kelley, B.; Walters, W. P.; Cernak, T. Exploring the Combinatorial Explosion of Amine–Acid Reaction Space via Graph Editing. *Commun. Chem.* **2024**, *7* (1), 22. https://doi.org/10.1038/s42004-024-01101-w.

(145) Boit, T. B.; Bulger, A. S.; Dander, J. E.; Garg, N. K. Activation of C–O and C–N Bonds Using Non-Precious-Metal Catalysis. *ACS Catal.* **2020**, *10* (20), 12109–12126. https://doi.org/10.1021/acscatal.0c03334.

(146) Malapit, C. A.; Borrell, M.; Milbauer, M. W.; Brigham, C. E.; Sanford, M. S. Nickel-Catalyzed Decarbonylative Amination of Carboxylic Acid Esters. *J. Am. Chem. Soc.* **2020**, *142* (13), 5918–5923. https://doi.org/10.1021/jacs.9b13531.

(147) Liao, J.; Basch, C. H.; Hoerrner, M. E.; Talley, M. R.; Boscoe, B. P.; Tucker, J. W.; Garnsey, M. R.; Watson, M. P. Deaminative Reductive Cross-Electrophile Couplings of Alkylpyridinium Salts and Aryl Bromides. *Org. Lett.* **2019**, *21* (8), 2941–2946. https://doi.org/10.1021/acs.orglett.9b01014.

(148) Baker, K. M.; Tallon, A.; Loach, R. P.; Bercher, O. P.; Perry, M. A.; Watson, M. P. α-Chiral Amines via Thermally Promoted Deaminative Addition of Alkylpyridinium Salts to Sulfinimines. *Org. Lett.* **2021**, *23* (20), 7735–7739. https://doi.org/10.1021/acs.orglett.1c02708.

(149) Reiniers, M. J.; van Golen, R. F.; Bonnet, S.; Broekgaarden, M.; van Gulik, T. M.; Egmond, M. R.; Heger, M. Preparation and Practical Applications of 2′,7′-Dichlorodihydrofluorescein in Redox Assays. *Anal. Chem.* **2017**, *89* (7), 3853–3857. https://doi.org/10.1021/acs.analchem.7b00043.

(150) Hempel, S. L.; Buettner, G. R.; O'Malley, Y. Q.; Wessels, D. A.; Flaherty, D. M. Dihydrofluorescein Diacetate Is Superior for Detecting Intracellular Oxidants: Comparison with 2',7'-Dichlorodihydrofluorescein Diacetate, 5(and 6)-Carboxy-2',7'-Dichlorodihydrofluorescein Diacetate, and Dihydrorhodamine 123. *Free Radic. Biol. Med.* **1999**, *27* (1–2), 146–159. https://doi.org/10.1016/s0891-5849(99)00061-1.

(151) Lee, G.; Bae, J.; Ali, K.; Cho, E. J. Reductive Amination of Carboxylic Acids via Nickel(II) Catalysis: A Ligand-Tuned Strategy for C–N Bond Formation. *J. Org. Chem.* **2025**, *90* (40), 14141–14145. https://doi.org/10.1021/acs.joc.5c01592.

(152) Sorribes, I.; Junge, K.; Beller, M. General Catalytic Methylation of Amines with Formic Acid under Mild Reaction Conditions. *Chem. – Eur. J.* **2014**, *20* (26), 7878–7883. https://doi.org/10.1002/chem.201402124.

(153) Alla, S. K.; Sadhu, P.; Punniyamurthy, T. Organocatalytic Syntheses of Benzoxazoles and Benzothiazoles Using Aryl Iodide and Oxone via C–H Functionalization and C–O/S Bond Formation. *J. Org. Chem.* **2014**, *79* (16), 7502–7511. https://doi.org/10.1021/jo501216h.